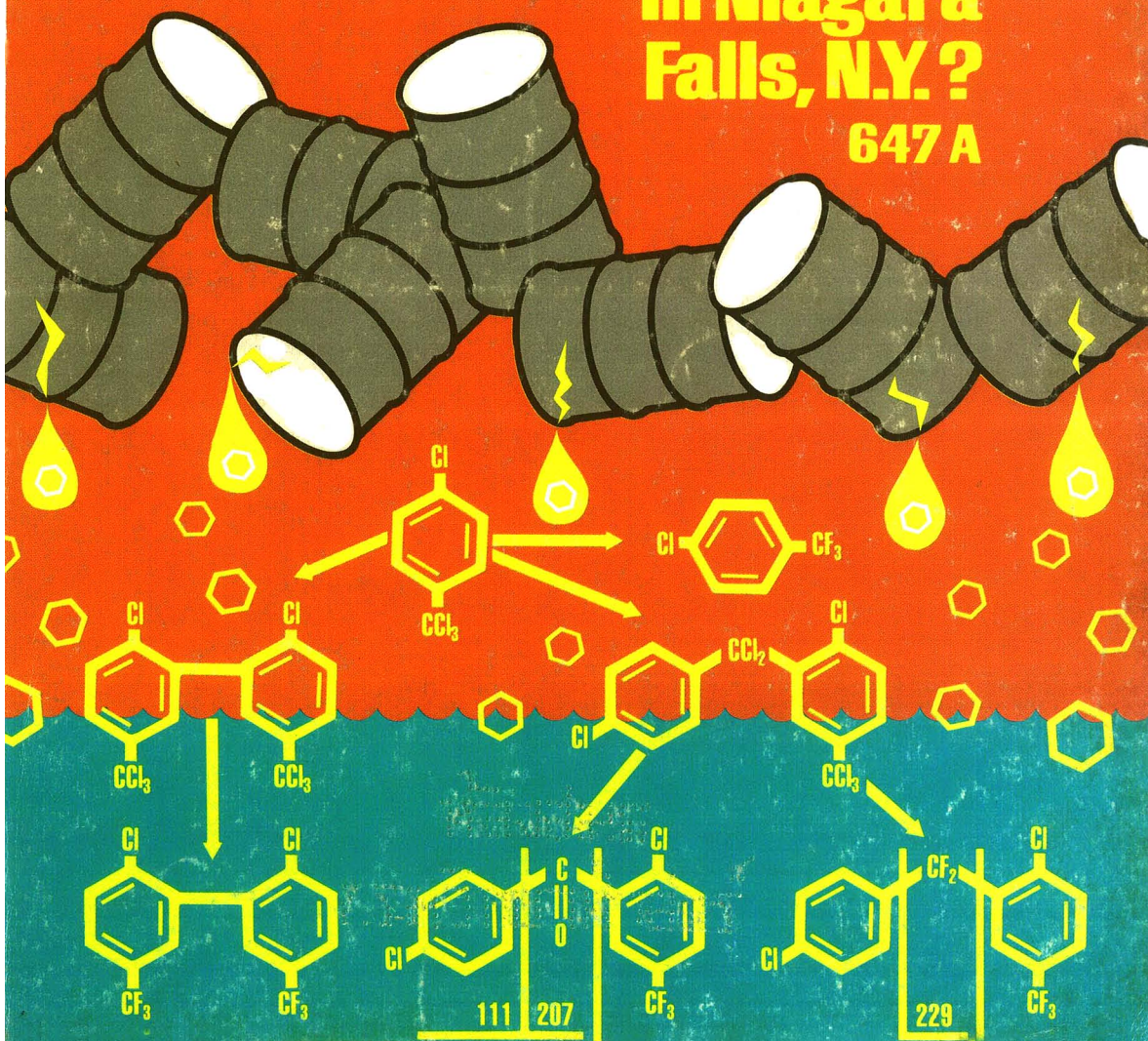


# Analytical

## CHEMISTRY

### What was Leaking from a Hazardous-Waste Dump in Niagara Falls, N.Y.?

647 A



# Automated Ion Analysis for Priority Pollutants

## Formally approved by the USEPA for NPDES and NIPDWR compliance monitoring

The QuikChem® Automated Ion Analyzer from Lachat Instruments offers unmatched productivity for the environmental laboratory. Here are just a few of the features that can help make your laboratory more efficient and profitable:

**High sample throughput** with 90-240 samples processed every hour.

**Complete inter-sample washout** eliminates carryover between samples to enhance accuracy and precision.

**Automatic in-line dilution** provides accurate determination of concentration ranges up to 3 decades in a single run.

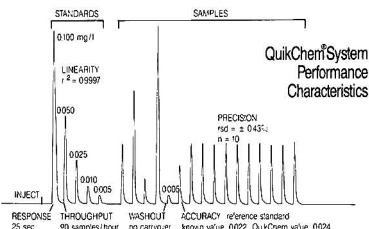
**Multi-channel analysis** permits up to 4 analytes to be determined simultaneously in each sample in completely independent concentration ranges.

**Short analysis times** provide results within 1 minute following sample introduction.

**Simple method switching** makes it easy and quick—less than 10 minutes—to change from one method to another.

**Real-time reporting** eliminates waiting for results. All computations are made immediately after each sample is processed, including corrections for baseline and sensitivity drifts and calculations for dilution factors, weight factors, inter-channel relationships and user-programmed functions.

**Random access sampling** facilitates replicate sampling, data quality monitoring and automatic recalibration.



Determination of nitrate in discharge water

## QuikChem methods approved for NPDES monitoring

Alkalinity  
Ammonia  
Chloride\*  
Chromium  
Conductivity  
Cyanide  
Fluoride\*  
Hardness

Kjeldahl Nitrogen, Total  
Nitrate/Nitrite\*  
ortho-Phosphate  
Phenolics  
Phosphorus, Total  
Silica  
Sulfate\*

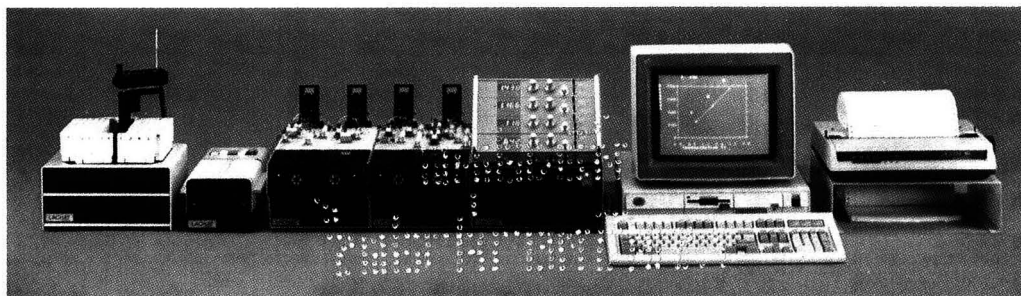
\*Also approved for NIPDWR

## Free handbook

To receive a free copy of *The Compendium of QuikChem Methods Approved by the USEPA for NPDES and NIPDWR Compliance Monitoring*, call our Environmental Applications Group toll free at (800) 247-7613 or write us today.

LACHAT  
INSTRUMENTS

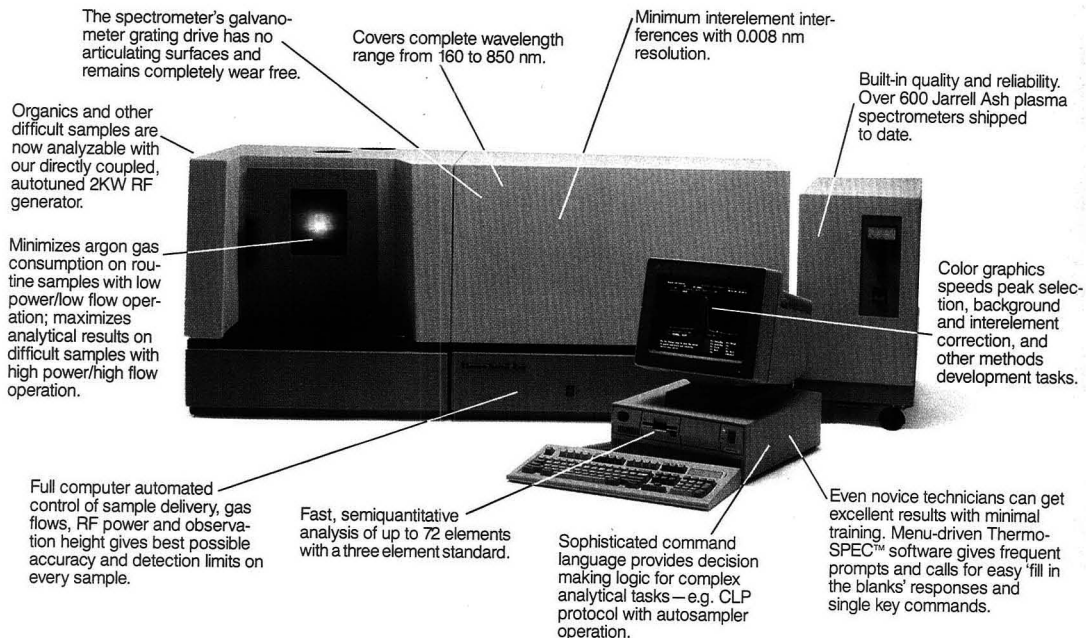
10500 N. Port Washington Road • Mequon, Wisconsin 53092  
414-241-3872 / 800-247-7613, toll free/telex: 26-9681



CIRCLE 84 ON READER SERVICE CARD



# If You're Shopping For A Sequential Plasma Spectrometer, Tear Out This Ad & Take It With You.



In the words of our chief engineer, our *AtomScan™* 25 Spectrometer is "everything anyone ever wanted in a sequential ICP instrument."

It's the culmination of more than three decades of developmental work, incorporating the best features—RF generator, monochromator, sample delivery and excitation, data system and software—of all previous generations of Jarrell Ash plasma spectrometers.

And whether you are a research spectroscopist or an occasional user, that simply means you are going to get better accuracy and detection limits on every

element in any sample matrix with the AtomScan 25 than with instruments costing twice as much.

Don't take our word for it.

Tear out this ad and take it with you on your trip to see brand X. See if they offer you anywhere near as much for so little.

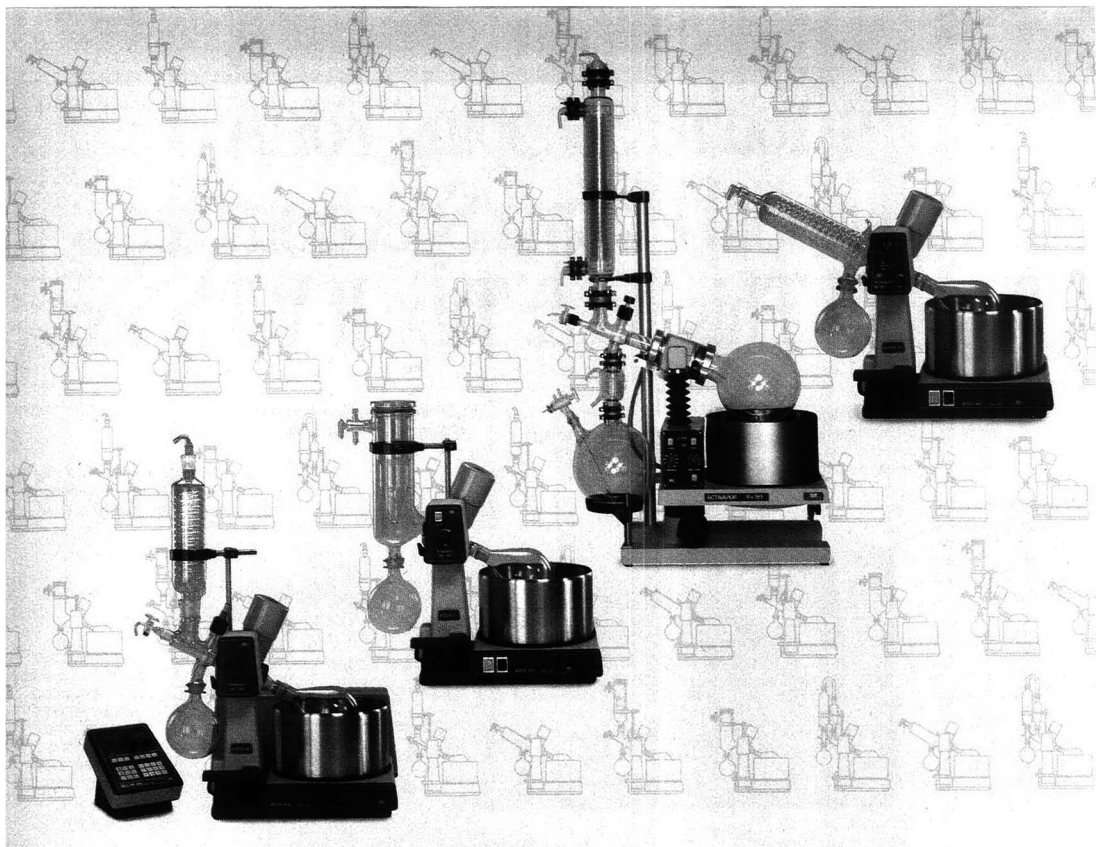
We think we'll make you a believer.

For literature or a demonstration of the AtomScan 25, call (617) 520-1880. Or write Thermo Jarrell Ash Corp., 8 East Forge Parkway, Franklin, MA 02038-9101.

**Thermo Jarrell Ash Corporation**

A Division of Thermo Instrument Systems, Inc.

CIRCLE 156 ON READER SERVICE CARD



# Büchi gives you more.

Rotary evaporators to meet more needs,  
giving you more value.

Move up to Büchi. Whether it's a fully automated evaporation system with microprocessor control or a basic rotary evaporator, there's a Büchi Rotavapor<sup>®</sup> designed to fit your needs.

**More versatility and reliability.** Büchi rotary evaporators handle volumes as low as 5 mL and up to 50 L or more. A wide range of models and glassware assemblies lets you choose a system for most any solvent, any application, any need. Büchi rotary evaporators are built to give you years of reliable service.

**More convenience and efficiency.** Büchi rotary evaporators have constant high-torque drives for efficient evaporation regardless of load. The improved quick-action Servo-Jack<sup>™</sup> makes it easier than ever to lower and raise the evaporator into and out of the bath. And vertical condensers such as the cold trap increase condensation efficiency and save valuable bench space.

**More safety.** Büchi rotary evaporators feature variable speed sparkless induction motors. Plastic nozzles on condensers provide safer tube connections. And heating baths have low-liquid-level protection and over-temperature safety shutoff.

**More value for you.** Move up to Büchi for the widest equipment range, intelligent design, and reliable performance. Move up for versatility, convenience, efficiency, and safety—for outstanding value that has made Büchi the world's best seller.

For more information: call 800-645-3050; in New York, 516-334-7500. Or write Brinkmann Instruments, Inc., Cantiague Road, Westbury, NY 11590. (In Canada: 416-675-7911; 50 Galaxy Blvd., Rexdale, Ont. M9W 4Y5)

<sup>®</sup>Rotavapor<sup>®</sup> is a registered trademark of Büchi Laboratoriums-Technik AG.

## Büchi

Shaping the future. **Brinkmann**  
INSTRUMENTS, INC.



**MAY 15, 1988**

**VOLUME 60**

**NUMBER 10**



ANCHAM  
60(10) 605A-656A/961-1088 (1988)  
ISSN 0003-2700

Registered in U.S. Patent and Trademark Office;  
Copyright 1988 by the American Chemical Society

ANALYTICAL CHEMISTRY (ISSN 0003-2700) is published semimonthly by the American Chemical Society at 1155 16th St., N.W., Washington, D.C. 20036. Editorial offices are located at the same ACS address (202-872-4600; TDD 202-872-8733). Second-class postage paid at Washington, D.C., and additional mailing offices. Postmaster: Send address changes to ANALYTICAL CHEMISTRY Membership & Subscription Services, P.O. Box 3337, Columbus, Ohio 43210.

**Claims for missing numbers** will not be allowed if loss was due to failure of notice of change of address to be received in the time specified; if claim is dated (a) North America: more than 90 days beyond issue date, (b) all other foreign: more than one year beyond issue date, or if the reason given is "missing from files."

**Copyright Permission:** An individual may make a single reprographic copy of an article in this publication for personal use. Reprographic copying beyond that permitted by Section 107 or 108 of the U.S. Copyright Law is allowed, provided that the appropriate per-copy fee is paid through the Copyright Clearance Center, Inc., 27 Congress St., Salem, Mass. 01970. For reprint permission, write Copyright Administrator, B&J Division, ACS, 1155 16th St., N.W., Washington, D.C. 20036.

**Registered names and trademarks, etc.,** used in this publication, even without specific indication thereof, are not to be considered unprotected by law.

**Advertising Management:** Centcom, Ltd., 500 Post Rd. East, Westport, Conn. 06880 (203-226-7131)

**1988 subscription rates include air delivery outside the U.S., Canada, and Mexico**

	1 yr	2 yr
<b>Members</b>		
Domestic	\$ 25	\$ 42
Canada and Mexico	50	92
Europe	78	148
All Other Countries	113	218
<b>Nonmembers</b>		
Domestic	38	64
Canada and Mexico	63	114
Europe	133	242
All Other Countries	168	312

Three-year and other rates contact: Membership & Subscription Services, ACS, P.O. Box 3337, Columbus, Ohio 43210 (614-421-3776).

**Subscription orders by phone** may be charged to Visa, MasterCard, Barclay card, Access, or American Express. Call toll free at (800) ACS-5558 from anywhere in the continental United States; from Washington, D.C., call 872-8065. Mail orders for new and renewal subscriptions should be sent with payment to the Business Management Division, ACS, P.O. Box 57136, West End Station, Washington, D.C. 20037.

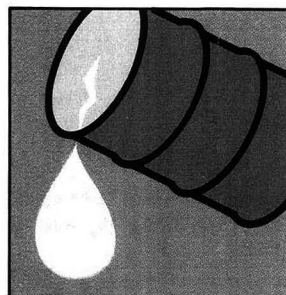
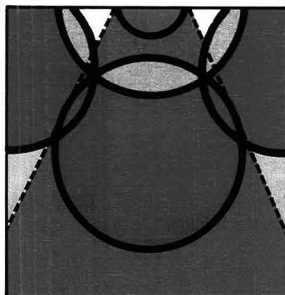
**Subscription service inquiries and changes of address** (include both old and new addresses with ZIP code and recent mailing label) should be directed to the ACS Columbus address noted above. Please allow six weeks for change of address to become effective.

**ACS membership information:** Lorraine Bowlin (202-872-4567).

**Single issues,** current year, \$6.00 except review issue and LabGuide, \$10.00; **back issues and volumes and microform editions** available by single volume or back issue collection. For information or to order, call (800) ACS-5558 or write the Microform & Back Issues Office at the Washington address.

**Nonmembers rates in Japan:** Rates above do not apply to nonmember subscribers in Japan, who must enter subscription orders with Maruzen Company Ltd., 3-10 Nihonbashi 2-chome, Chuo-ku, Tokyo 103, Japan. Tel: (03) 272-7211.

# Analytical<sup>®</sup> CHEMISTRY



## REPORT

**623 A**

**The teaching of analytical chemistry in Europe.** Ernő Pungor and Robert Kellner of the Technical Universities in Budapest and Vienna, respectively, discuss the analytical chemistry curriculum in Europe today

## ANALYTICAL APPROACH

**647 A**

**On the cover.** What was leaking from a hazardous-waste dump in Niagara Falls, N.Y.? Ronald A. Hites of Indiana University outlines the steps taken to identify the structures of organic compounds leaking from the Hyde Park dump

## BRIEFS

**610 A**

## NEWS

**621 A**

This year's recipients of the **Society for Analytical Chemists of Pittsburgh Starter Grant Awards** are Leonidas G. Bachas and Denley B. Jacobson. ▶ **Frederick Kavanagh** has been selected to receive the 1988 **Harvey W. Wiley Award**. ▶ Scientists have developed a new imaging technique to determine the structure of molecules

## BOOKS

**630 A**

**Critical reviews.** Books on two-dimensional NMR spectroscopy and separation and spectrophotometric determination of elements are reviewed by Jerry P. Heeschen and M. S. Epstein

## FOCUS

**635 A**

**Thirty-nine years of analytical chemistry.** The Society for Analytical Chemists of Pittsburgh honors its 1988 award winner with a retrospective of analytical chemistry

## NEW PRODUCTS & MANUFACTURERS' LITERATURE

**642 A**

## AUTHOR INDEX

**961**

## Capillary Supercritical Fluid Chromatography—Mass Spectrometry Using a "High Mass" Quadrupole and Splitless Injection 962

Ammonium adduct ions of polysiloxanes and of derivatized oligosaccharides are observed up to the 3000-dalton mass limit of the instrument. Conventional capillary hardware is used for splitless injection.

**J. David Pinkston\***, Grover D. Owens, Leisa J. Burkes, and Thomas E. Delaney, The Procter & Gamble Co., Miami Valley Laboratories, P.O. Box 398707, Cincinnati, Ohio 45239-8707, and David S. Millington and David A. Maltby, Duke University Medical Center, Division of Pediatric Genetics and Metabolism, Box 3028, Durham, N.C. 27710 *Anal. Chem.*, 60 (1988)

## Average Mass Approach to the Isotopic Analyses of Compounds Exhibiting Significant Interfering Ions 966

The average mass method is applied to the isotopic analysis of materials exhibiting molecular ion groups distorted by overlapping ions. The method may be more general and accurate than conventional methodologies.

**Karl F. Blom**, E. I. du Pont de Nemours & Company, Medical Products Department, Experimental Station, E336/29A, Wilmington, Del. 19898 *Anal. Chem.*, 60 (1988)

## Inductively Coupled Plasma Mass Spectrometric Analysis of Ultrapuric Acids 971

An ICP/MS is used for analysis of distilled water and five ultrapuric reagent acids at impurity levels ranging from ng/g to <1 pg/g. Both isotope dilution and external standardization methods are used.

**Paul J. Paulsen**, Eilyn S. Beary, Diane S. Bushee, and John R. Moody\*, Center for Analytical Chemistry, National Bureau of Standards, Gaithersburg, Md. 20899 *Anal. Chem.*, 60 (1988)

## Quantitation of Ethyl Carbamate in Whiskey, Sherry, Port, and Wine by Gas Chromatography/Tandem Mass Spectrometry Using a Triple Quadrupole Mass Spectrometer 975

Ethyl carbamate is quantitated down to a level of 3 ppb in alcoholic beverages using GC/MS/MS and a stable isotope-labeled internal standard. The precision of replicate injections of the final solution is  $\pm 1\%$ , and the variability of the extraction-isolation procedure is 3% by GC/N/TEA.

**William C. Brumley\***, Benjamin J. Canas, Gracia A. Perfetti, Magdi M. Mossoba, James A. Sphon, and Paul E. Corneliusen, Division of Contaminants Chemistry and Division of Food Chemistry and Technology, Food and Drug Administration, Washington, D.C. 20204 *Anal. Chem.*, 60 (1988)

## Computer-Assisted Prediction of Gas Chromatographic Retention Times of Polychlorinated Biphenyls 978 ■

Retention times of polychlorinated biphenyls are predicted using molecular structure descriptors. A five-variable regression equation with an  $R^2$  of 0.997 and an RSD of 1.7% is developed.

**Mohamed Noor Hasan and Peter C. Jurs\***, Department of Chemistry, 152 Davey Laboratory, The Pennsylvania State University, University Park, Pa. 16802 *Anal. Chem.*, 60 (1988)

## Prediction of Gas Chromatographic Retention Characteristic of Polychlorinated Biphenyls 982

Two models based on structural descriptors are developed for the prediction of relative retention times and retention indexes of polychlorinated biphenyls by linear temperature-programmed GC on SE-54 and DB-5 stationary phases, respectively.

**Albert Robbat, Jr.\***, George Xyrafas, and Durwood Marshall, Department of Chemistry, Tufts University, Medford, Mass. 02155 *Anal. Chem.*, 60 (1988)

## Ligand-Accelerated Coupled Transport of Metals across a Liquid Membrane Containing a General Complexing Agent 986

A 15-fold enrichment of Zn(II) into 0.1 M HCl is achieved by using a dithizone-containing membrane and a 10-mM concentration of thiosulfate in the sample.

**James A. Cox\*** and Atul Bhatnagar, Department of Chemistry, Miami University, Oxford, Ohio 45056 *Anal. Chem.*, 60 (1988)

## Simultaneous Determination of Uronic Acids and Aldoses in Plankton, Plant Tissues, and Sediment by Capillary Gas Chromatography of *N*-Hexylaldonamide and Alditol Acetates 988

Aldoses and uronic acids from natural samples are determined simultaneously. Hydrolysis and derivatization efficiencies are quantitated with recovery standards. Acidic polysaccharides are hydrolyzed with 40% yields and 20% mean deviations.

**Jeffrey S. Walters and John I. Hedges\***, School of Oceanography, WB-10, University of Washington, Seattle, Wash. 98195 *Anal. Chem.*, 60 (1988)

\* Corresponding author

■ Supplementary material available



Our ICP instruments now feature  
IBM® Personal System/2™ computers.

# Good things come in small packages.

Now...JY brings you the advantages of full-featured ICP analysis in our smallest package.

Just starting spectroanalysis? Converting elemental analysis from AA to ICP? Adding more ICP capacity? The JY 24 was made for you!

The JY 24 packs everything that has made JY the ICP of choice into a single compact space-saving unit — including some not-so-small things like a 40 MHz RF generator!

The JY 24 complements JY's versatile line of ICP units, both sequential and simultaneous, for all your spectroanalytical problems. For information on the complete spectrum of JY spectroanalytical instruments, use the reader service card, or write or call today.



## The New JY 24 Sequential ICP is reasonably priced too!

**JOBIN  
YVON**



**J-Y Optical Systems**  
**Instruments SA, Inc.**

6 Olsen Avenue, Edison, NJ 08820-2419 Tel. (201) 494-8660, Telex 844516 FAX (201) 494-8796  
(In Europe:) Jobin Yvon, 16-18 Rue du Canal 91163 Longjumeau, France, Tel. (33) 1.69.09.34.93

IBM and Personal System/2 are registered trademarks of IBM Corporation.

CIRCLE 70 ON READER SERVICE CARD

## Universal Detection of Ions by Replacement-Ion Chromatography Employing an Anion-Replacement Method and an Ultraviolet-Visible Spectrophotometric Detector 995

The method and detection system are described. Good precision (<5% RSD) and detection limits (1–15 ng) are observed for monovalent cations. Universal calibration is also possible. Limitations of the method are discussed.

Leonard J. Galante and Gary M. Hieftje\*, Department of Chemistry, Indiana University, Bloomington, Ind. 47405

*Anal. Chem.*, 60 (1988)

## Computer Simulation of Differential Scanning Calorimetry: Influence of Thermal Resistance Factors and Simplex Optimization of Peak Resolution 1003

An equivalent-circuit model for a DSC of the heat-flux type and computer simulations are used to probe the influence of thermal resistances on peak area, amplitude, onset temperature, and resolution.

Guang-Way Jang and Krishnan Rajeshwar\*, Department of Chemistry, The University of Texas at Arlington, Arlington, Tex. 76019

*Anal. Chem.*, 60 (1988)

## The Vinland Map 1009

Anatase  $\text{TiO}_2$ , a modern pigment, is determined in 20 representative ink samples from the Vinland Map. Ultramicroanalytical techniques used include polarized light microscopy, X-ray diffraction, scanning electron microscopy with selected-area electron diffraction, electron microprobes, and ion microprobes.

Walter C. McCrone, McCrone Research Institute, 2820 South Michigan Avenue, Chicago, Ill. 60616

*Anal. Chem.*, 60 (1988)

## Plasticized Poly(vinyl chloride) Properties and Characteristics of Valinomycin Electrodes. Current-Time Responses to Voltage Steps 1018

Short- and long-time solutions are described for the current-time responses of carrier membranes under mass transport control (plateau voltages, limiting steady-state currents). For DNA plasticized membranes,  $D_{\text{val}} = 1.3 \times 10^{-8} \text{ cm}^2$  for short-time behavior and  $1.5 \times 10^{-6} \text{ cm}^2$  for long-time behavior.

Michael L. Iglehart and Richard P. Buck\*, Department of Chemistry, University of North Carolina, Chapel Hill, N.C. 27514, and György Horvai and Ernő Pungor, Technical University of Budapest, Gellért tér 4, 1111 Budapest XI, Hungary

*Anal. Chem.*, 60 (1988)

## Analytical and Mechanistic Aspects of the Electrochemical Oxidation of Keto Steroids Derivatized with Phenylhydrazine, (4-Nitrophenyl)hydrazine, and (2,4-Dinitrophenyl)hydrazine 1023

Derivatization with (4-nitrophenyl)hydrazine is used for determination of 3- and 17-keto steroids in nonmammalian biological fluids using HPLC with electrochemical detection. Derivatization is shown to be quantitative, and the response is linear with a detection limit of 1–5 ng for injection volumes of 20  $\mu\text{L}$ . The oxidation mechanism is discussed.

Thompson, Division of Chemical and Physical Sciences, Deakin University, Waurn Ponds, Victoria 3217, Australia, and Anthony R. Bourne, Peter A. Huf, and Thomas G. Watson\*, Division of Biological and Health Sciences, Deakin University, Waurn Ponds, Victoria 3217, Australia

*Anal. Chem.*, 60 (1988)

## Design, Characterization, and Applications of a Photoacoustic Cell for Temperature and Atmosphere Control 1027

The construction and performance characteristics of a photoacoustic cell with elevated temperature (up to 500 °C) and atmosphere control are described. Application to the study of thermal decomposition reactions, phase transitions, and solid-gas reactions is demonstrated.

Meg M. Thompson and Richard A. Palmer\*, P. M. Gross Chemical Laboratory, Duke University, Durham, N.C. 27706

*Anal. Chem.*, 60 (1988)

## Simultaneous Multielemental Analysis of Some Environmental and Biological Samples by Inductively Coupled Plasma Atomic Emission Spectrometry 1033

The samples are digested sequentially in Parr bombs and analyzed using ICP-AES. Thirty-four elements are accurately determined using modified  $k$  values and the carbon content.

Shane S. Que Hee\* and James R. Boyle, Department of Environmental Health, University of Cincinnati Medical Center, 3223 Eden Avenue, Cincinnati, Ohio 45267-0056

*Anal. Chem.*, 60 (1988)

## Effects of Metal Cations on the Fluorescence Intensity of Polycyclic Aromatic Hydrocarbons in Sodium Taurocholate Micellar Solutions 1043

Metal cations enhance the fluorescence of some PAHs in sodium taurocholate micellar solutions, improving detection limits by as much as an order of magnitude. Largest enhancements are observed for PAHs with very low aqueous solubility, whereas relatively soluble PAHs are quenched.

Kasem Nithipatikom and Linda B. McGowan\*, Department of Chemistry, P. M. Gross Chemical Laboratory, Duke University, Durham, N.C. 27706

*Anal. Chem.*, 60 (1988)

## Nondestructive Depth Profiling of Rare-Earth and Actinide Zeolites via Rutherford Backscattering Methods 1046

Results show that Rutherford backscattering methods can be used to distinguish surface and bulk compositions in ion-exchanged zeolites via theoretical depth profile calculations.

Scott A. Baumann and Michael D. Strathman, Charles Evans and Associates, Redwood City, Calif. 94063, and Steven L. Suib\*, Departments of Chemistry, Chemical Engineering, and Institute of Materials Science, University of Connecticut, Storrs, Conn. 06268

*Anal. Chem.*, 60 (1988)

## Effects of Surface on the Atomization of Lead by Graphite Furnace 1051

Effects attributable to magnesium chloride are similar with either coated or uncoated platforms. Condensed-phase decomposition of magnesium chloride is slightly enhanced with the uncoated surface, but this effect does not entirely account for differences observed between surfaces with wall atomization.

William G. Brumbaugh\*, National Fisheries Contaminant Research Center, U.S. Fish and Wildlife Service, Route 1, Columbia, Mo. 65201, and Samuel R. Koirtyohann, Department of Chemistry, University of Missouri, Columbia, Mo. 65211

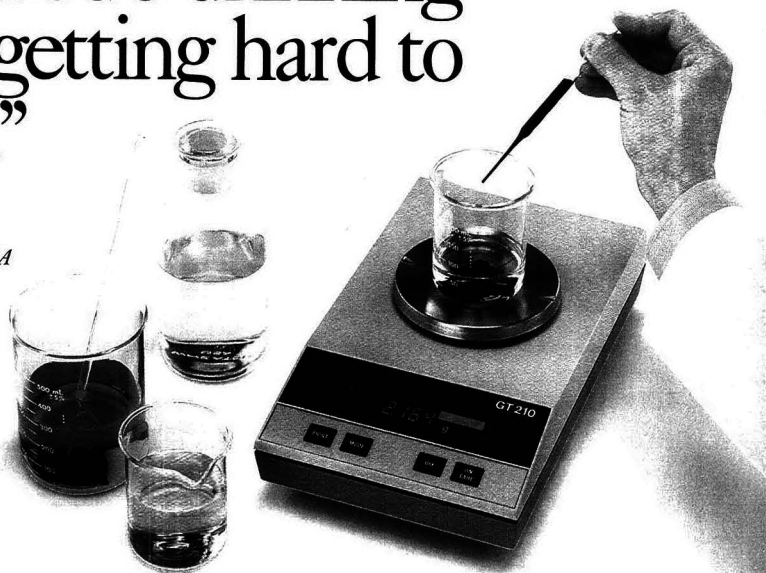
*Anal. Chem.*, 60 (1988)





"I switched to Ohaus  
because their easy-to-use  
FillGuide™ helps me determine  
if Cape Cod's drinking  
water is getting hard to  
swallow."

*Gordon Rice  
Lab Director  
Aqua Test  
W. Chatham, MA*



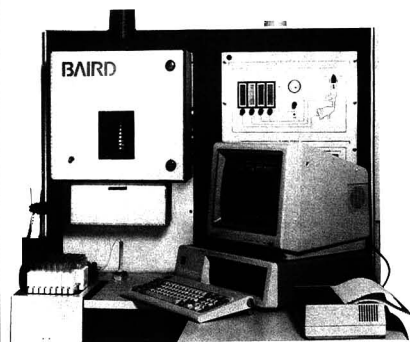
Easy-to-use Ohaus FillGuide™ speeds the measuring of reagents for testing contaminant levels in drinking water. Just press a button to tare out the container's weight and weigh in each component. The FillGuide™ indicates target weight or capacity used. The GT210, equipped with Ohaus FillGuide™, is one of nine toploaders ranging in capacity from 210 g to 8000 g with readabilities of 0.001 g to 0.1 g. For more information, call or write Ohaus, Hanover Road, Florham Park, NJ 07932, (800) 672-7722.

*Solid, sensible balances & scales.*

**OHAUS**★

CIRCLE 120 ON READER SERVICE CARD

Before you  
choose an ICP,  
Examine our  
family tree.



Only BAIRD offers a complete line of ICP emission spectrometers designed and built to meet the demands of every industry and every application — **WITHOUT COMPROMISE.** Innovative ICP technology. Outstanding technical and service support. Become part of BAIRD's family of satisfied customers. Call us today.

BAIRD CORPORATION  
An Imco Delaval Company  
125 Middlesex Turnpike  
Bedford, Massachusetts 01730  
617/276-6096

**BAIRD**  
The Spectroscopy People

## BRIEFS

### Direct Mixture Analysis Using Carbon-Proton *J*-Resolved Nuclear Magnetic Resonance 1055

Long-range *J*-resolved C-H NMR experiments combined with carbon NMR spectral library search procedures are used for analysis of unseparated mixtures.

Charles L. Wilkins\*, Steven T. K. Ha, and Robert W. K. Lee, Department of Chemistry, University of California, Riverside, Calif. 92521  
*Anal. Chem.*, 60 (1988)

### Ionization of Alkylbenzenes Studied by Gas Chromatography/Laser Ionization Mass Spectrometry 1060

A series of singly and multiply substituted alkylbenzenes are investigated by GC/MS. Relative ionization efficiencies and mass spectra are recorded for these compounds.

Richard B. Opsal and James P. Reilly\*, Department of Chemistry, Indiana University, Bloomington, Ind. 47405  
*Anal. Chem.*, 60 (1988)

### Waveguide Capillary Flow Cell for Fluorometry 1065

A detection limit of <1 pg/mL of perylene is obtained with the 12-m fiber. The experimental and theoretical behavior of the hollow fiber as a fluorescence cell are described.

Kitao Fujiwara, J. B. Simeonsson, B. W. Smith, and J. D. Winefordner\*, Department of Chemistry, University of Florida, Gainesville, Fla. 32611  
*Anal. Chem.*, 60 (1988)

### Laser-Excited Time-Resolved Solid-Phase Fluoroimmunoassays with the New Europium Chelate 4,7-Bis(chlorosulfonylphenyl)-1,10-phenanthroline-2,9-dicarboxylic Acid as Label 1069

The europium chelate 4,7-bis(chlorosulfonylphenyl)-1,10-phenanthroline-2,9-dicarboxylic acid is introduced indirectly into antibodies. The labeled antibodies are used successfully for solid-phase time-resolved fluoroimmunoassays.

Esther Reichstein, Yehezkel Shami, Mohabir Ramjeesingh, and Eleftherios P. Diamandis\*, CyberFluor, Inc., 179 John Street, Toronto, Ontario M5T 1X4, Canada  
*Anal. Chem.*, 60 (1988)

### Automated Fluorometric Determination of Formaldehyde in Air 1074

The system strips formaldehyde vapor from air into water by means of a glass coil through which air and water flow concurrently. The aqueous formaldehyde is then oxidized by NAD<sup>+</sup> to produce NADH, which is measured fluorometrically. The detection limit is 120 pptv, with an RSD of 2.0% at 20 ppbv formaldehyde.

Allan L. Lazrus\*, Karen L. Fong, and John A. Lind, National Center for Atmospheric Research, Boulder, Colo. 80307  
*Anal. Chem.*, 60 (1988)



# CONSISTENCY

## *The Solid Gold Standard*

If you want your calibration gas mixtures to provide consistent accuracy, move up to the Gold Standard... Matheson Primary Standards.

Our Primary Standard mixtures should be used whenever you need the most accurate instrument calibrations, or in those applications where the knowledge of the component concentration is critical.

Primary Standards improve your accuracy because our preparation process and quality control procedures are designed to provide each cylinder with a consistent, high quality product. We build accuracy by:

- Using the latest in high load, high sensitivity analytical gas mixing balances, built to our specifications.
- Using NBS certified weights as reference standards.
- Using only the purest gases that have been completely analyzed for impurities for all mixture components.
- Taking into account the weight of all impurities in component gases - not only the major gases.
- Instrument QC after blending to ensure no gross error.

### **A Word Of Caution!**

All of this careful preparation is wasted if you do not use a suitable gas transfer system between cylinder and instrument. We strongly recommend our 3104 regulator. Dubbed the GC regulator, it is ultrasonically cleaned, has an impermeable stainless steel diaphragm, packless outlet control valve and is designed to pass an inboard helium leak test up to  $2 \times 10^{-8}$  sccs.

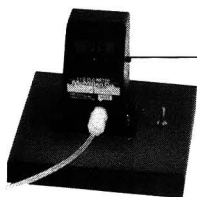
Accurate gas mixtures, proper regulators and experienced technique assure consistency.

If you would like some useful information about gas mixtures, send for a copy of "Gas Mixtures, Facts and Fables". Use the Reader Service No., or contact us.

**Matheson®**  
Gas Products

World Leader in Specialty Gases & Equipment

30 Seaview Drive, Secaucus, NJ 07096-1587



**FINALLY!**

**An economical  
alternative to the  
Gas Rotameter!**

## Electronic Gas Flowmeter

3½ Digit LCD Digital Display\*  
Linear 0-5VDC Output

From **\$199.00** (List Price)

\*Bar Graph Display Available

## Gas Flo - Sensor

0-5VDC Linear Output

Flow ranges from  
20ml/min to 20L/min

From **\$99.00** (List Price)



**McMillan**  
C · O · M · P · A · N · Y

**McMillan Company**

1301 Sparrow Trail Copperas Cove, Texas 76522  
(512) 473-6912 FAX: 817-547-5805

CIRCLE 104 ON READER SERVICE CARD

## Graphics for Chemical Structures

This exciting book presents the latest information from recognized experts in the field of chemical structure handling on microcomputers... and includes the newest developments in related systems on both mini- and mainframe computers. The book begins with an excellent overview of the evolution of computer graphics—and will introduce you to the four general types of software packages currently available • scientific word processing packages • packages that allow graphics entry of chemical structures but do not allow substructure searching or interfacing with other systems • packages that allow graphics structure entry and substructure searching and interfacing with other systems • packages designed to act as front ends to molecular modeling systems. This volume continues with discussions and comparisons of various software packages for the chemist. Information managers, information scientists, systems analysts, bench chemists, physical chemists, and PC enthusiasts will find this book a vital, necessary reference.

Wendy A. Warr, Editor

ACS Symposium Series No. 341  
LC 87-3575 ISBN 0-8412-1401-8

176 pages (1987) Clothbound  
US & Canada \$44.95 Export \$53.95

Order from: American Chemical Society, Distribution Office Dept. 58  
1155 Sixteenth St., N.W., Washington, DC 20036

or CALL TOLL FREE **800-227-5558** and use your credit card!

## BRIEFS

### Correspondence

#### Fabrication of an Oxygen Electrode Using Semiconductor Technology 1078

Hiroaki Suzuki, Fujitsu Laboratories, Ltd., 10-1 Morinosato-Wakamiya, Atsugi 243-01, Japan, and Eiichi Tamiya and Isao Karube\*, Research Laboratory of Resources Utilization, Tokyo Institute of Technology, 4259 Nagatsuta-cho, Midori-ku, Yokohama 227, Japan  
*Anal. Chem.*, 60 (1988)

#### Fiber-Optic Biosensors Based on the Fluorometric Detection of Reduced Nicotinamide Adenine Dinucleotide 1080

Julie Wangsa and Mark A. Arnold\*, Department of Chemistry, University of Iowa, Iowa City, Iowa 52242  
*Anal. Chem.*, 60 (1988)

#### Comment on Rigorous Convergence Algorithm for Fitting a Monoexponential Function with a Background Term Using the Least-Squares Method 1083

Harald Gampp, Marcel Maeder\*, and Andreas D. Zuberbühler\*, Institute of Inorganic Chemistry, University of Basel, CH-4056 Basel, Switzerland  
*Anal. Chem.*, 60 (1988)

### Technical Notes

#### Fluorination of Sulfur Tetrafluoride, Pentafluorosulfur Chloride, and Disulfur Decafluoride to Sulfur Hexafluoride for Mass Spectrometric Isotope Ratio Analysis 1084

Swroop K. Bains-Sahota and Mark H. Thieme\*, Department of Chemistry, B-017, University of California—San Diego, La Jolla, Calif. 92093  
*Anal. Chem.*, 60 (1988)

#### Plasma Desorption Mass Spectrometry of Peptides Adsorbed on Nitrocellulose from a Glutathione Matrix 1086

Ian Jardine\*, Gale F. Scanlan, and Anthony Tsarbopoulos, Department of Pharmacology, Mayo Clinic, Rochester, Minn. 55905, and Daniel J. Liberato, Department of Drug Metabolism, Hoffmann-La Roche, Inc., Nutley, N.J. 07110

*Anal. Chem.*, 60 (1988)

# The productive investment.



Today's affordable data networking system from Waters.

Waters new 860 Networking System combines the productivity of Waters own Expert™ Ease chromatography software with the power of the Digital® VAX® family of computers, for an affordable data solution. Lab managers can monitor multiple users, compare results and generate presentation quality reports. Chromatographers get virtually instantaneous data reduction, faster throughput, high resolution A/D conversion and access to resources such as laser printers and plotters.

**digital**  
Cooperative Marketing  
Program

The 860 System is also a wise investment because it lets you tie your existing Waters 840, Maxima™ or Baseline™ workstations right into the network. Or our new LAC/E™ and SAT/IN™ Modules let you acquire analog signals directly from any LC, GC or IC chromatograph without using a data workstation, for even greater flexibility and efficiency.

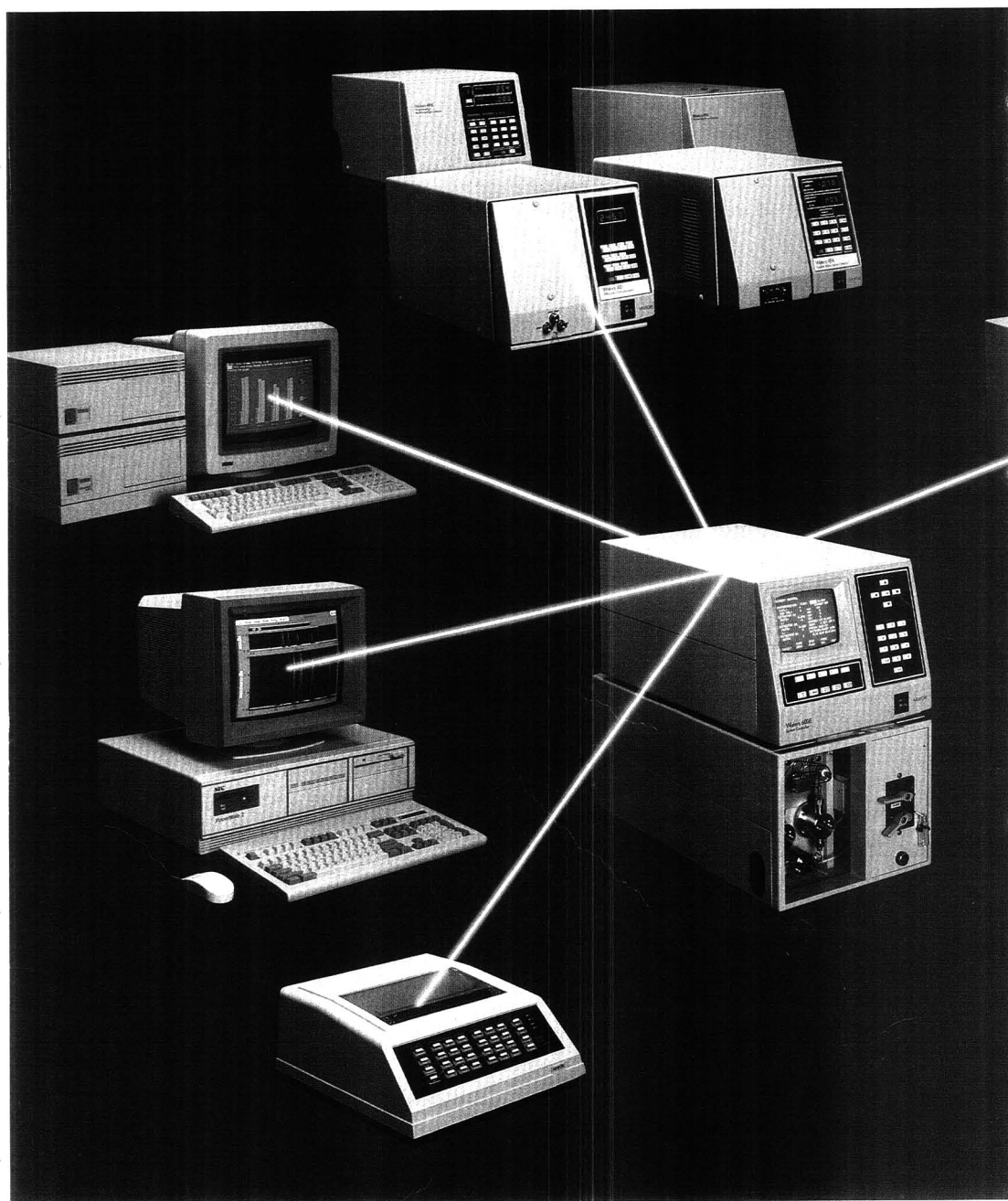
Knowing that Waters is a Digital Equipment System Cooperative Marketing Partner means you can count on a networking strategy that provides the flexibility to configure new systems without obsoleting current systems.



Let us help you configure the best data system for your current needs, while planning for future growth. Call your local Waters Data Specialist or phone \*16171 478-2000 x3006.

**Waters**  
Division of MILLIPORE





# Power is communication.

## Waters PowerLine™ HPLC modules provide the essential link.

If you're looking for the most advanced HPLC technology, shouldn't you expect:

- **Documentation** of sample injection, solvent delivery and detection parameters on an integrator, PC or MicroVAX™ station?
- **Single keyboard control** of individual modules or a complete system—with or without a separate PC?
- **Method storage** and recall of all parameters for each module in a system for error-free chromatographic set up?
- **Upgradability from a wide choice** of autosamplers, detectors, and data—with the same modules offered in a component system or in integrated cabinets?
- **Maximum uptime** with proven hardware design and the world's most comprehensive application development and technical support that ensures your uptime is productive time?

Waters PowerLine HPLC modules fulfill all of your expectations. Once you've tapped into Waters PowerLine, you'll receive all the above advantages of intermodule communication, plus a choice of free standing modules or integrated systems. And you'll get free installation of every system, user training and the comprehensive support that ensures your chromatographic success. *This is the Waters difference.*

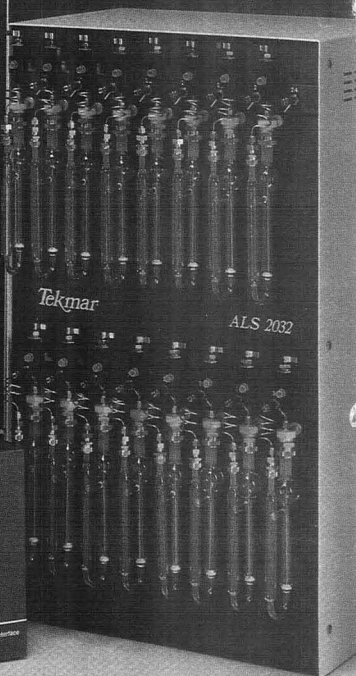
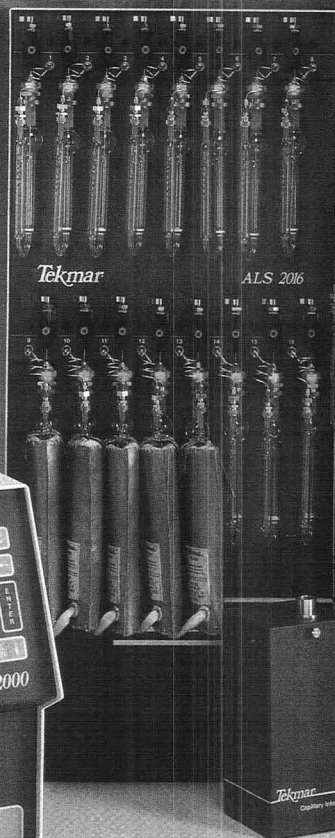
Call (617) 478-2000 and ask for extension 2255.

Waters  
Division of MILLIPORE



MicroVAX is a trademark of Digital Equipment Corporation.  
PowerLine is a trademark of Millipore Corporation.  
© 1988 Millipore Corporation.

From the World's Leader  
in Purge and Trap  
Technology



## THE 2000 SERIES CONCENTRATOR SYSTEMS by Tekmar®

In 1975, the first commercial Purge & Trap Concentrator was built. It was a Tekmar. Since that first instrument, we have listened carefully to our customers' suggestions and responded to their needs. Considering this valuable input, it's no wonder that the 2000 Series is the most advanced technology available for Purge and Trap/Dynamic Headspace Analysis.

- LSC 2000 Concentrator features glass-lined stainless steel tubing and menu-driven programming with four method storage
- Cryofocusing accessory features on-column trapping
- Automated Samplers for 16, 32 and 50 samples allow for ease of operation
- Automated Sample Heaters for ALS 2016 and 2032 enable soils analysis and DHA



# Tekmar®

Our 4th Generation  
of Purge & Trap  
Automated Systems

CALL NOW FOR MORE INFORMATION (800) 543-4461, or in Ohio (800) 344-8569, Telex #21-4221, Telefax (513) 761-5183

Tekmar Company, 10 Knollcrest Drive, P.O. Box 371856, Cincinnati, Ohio 45222-1856

CIRCLE 158 ON READER SERVICE CARD

## Bachas and Jacobson Receive Starter Grant Awards

Leonidas G. Bachas of the University of Kentucky and Denley B. Jacobson of North Dakota State University have been selected as the 1988 recipients of the Society for Analytical Chemists of Pittsburgh Starter Grant Awards. The \$10,000 awards are given to encourage high-quality innovative research by new professors in the field of analytical chemistry, as well as to promote the development and training of graduate students in the field.

**Bachas** received a Ph.D. degree from the University of Michigan under the guidance of Mark Meyerhoff. Upon completion of his postdoctoral work, he joined the faculty of the chemistry department at the University of Kentucky in 1986. His research interests include the development of ion-selective fiber-optic sensors employing fluorophores.

**Jacobson** is currently studying the chemistry of discrete transition-metal cluster ion complexes in the gas phase using Fourier transform mass spectrometry. He received a Ph.D. degree from Purdue University under the direction of Ben Freiser. In 1986 he joined the chemistry department faculty at North Dakota State University after completing postdoctoral work at the California Institute of Technology with Jesse Beauchamp.

## Kavanagh Wins the Wiley Award



Frederick Kavanagh will receive the 1988 Association of Official Analytical Chemists (AOAC) Harvey W. Wiley Award at the 102nd AOAC Annual International Meeting in September. Kavanagh, who was employed by Eli Lilly & Co. from 1953 until his retirement in 1973, is cited for his contributions to the field of analytical microbiology. He is well known for the development of microbiological turbidimetric assays used for several antibiotics in agriculture and for the design of new scientific instruments.

The \$2500 award is given annually to a scientist who has made outstanding contributions to the development of analytical methods for foods, drugs, cosmetics, pesticides, feeds, fertilizers, and environmental contaminants. Established in 1956, the award honors Harvey W. Wiley, the "father" of the 1906 Pure Food and Drug Act and a founder of the AOAC.

Kavanagh earned A.B. and A.M. degrees in chemistry from the University of Missouri in 1931 and 1933, respectively. He received a Ph.D. degree in chemistry from Columbia University and worked at the New York Botanical Gardens, where he isolated and characterized antibiotics produced by *Basidiomycetes*. At Lilly, he codeveloped the AutoTurb system, an automated microbiological assay

widely used in the pharmaceutical industry for antibiotic, vitamin, and feed assays.

## New Imaging System Discloses Molecular Structures

Scientists at the Argonne National Laboratory (ANL) in collaboration with the Weizmann Institute of Science in Israel have discovered a new way to determine the orientation of atoms in small molecules. According to Elliot Kanter and Zeev Vager of ANL, the new imaging technique, known as Multi-Particle Position and Time Sensitive (MUPPATS) detection, can provide three-dimensional images of small molecules. Using the MUPPATS detector, one can directly measure the geometry of a molecule and determine the positions and energies of several atoms at once using state-of-the-art techniques borrowed from nuclear and high-energy physics.

The MUPPATS detector uses a phenomenon known as the "Coulomb explosion," a force that causes particles with similar charges to repel one another while opposites attract. Using the new detector, scientists can gain a better understanding of how atoms and molecules interact to form new molecules, as well as how chemical reactions occur. Possible applications include studying the causes of acid rain, determining the chemical evolution of life on Earth, and understanding the formation of molecules in interstellar dust clouds.

## For Your Information

**Finnigan MAT** has announced the establishment of an analytical biochemistry group to be directed by **Ian Jardine**, professor of pharmacology at the Mayo Clinic and the Mayo Medical School. The group will develop methods and products for the application of mass spectrometry to analytical biochemistry. According to John Hearn, executive vice-president of Finnigan MAT, "The addition of this new group marks another significant step in our serious commitment to the biochemical industry."

A new inductively coupled plasma/mass spectrometry bibliography is available from **Perkin-Elmer**. The references are annotated and include information on subject matter, analyte elements, sample matrices, and physical performance criteria. To obtain a copy of the bibliography, contact The Perkin-Elmer Corp., 761 Main Avenue, Norwalk, Conn. 06859-0082 (800-762-4000).

A portable device used to detect and identify toxic gases in the work place or environment has been designed by the Argonne National Laboratory. The **Chemical Parameter Spectrometer 100** weighs 15 lbs and can detect 40 common industrial gases. In less than three minutes, the instrument can detect and identify the gas and sound an alarm if the concentration exceeds safe levels. For more information, contact David Baurac at 312-972-5584.





## The first step in successful amino acid analysis.

First, we need to talk. But not about model numbers and purchase orders.

We need to talk about what you want and need. About how you prefer to run your laboratory — philosophies, methodologies and procedures.

At first, you'll do most of the talking, while we listen. And learn. Then — and not until then — we'll recommend the best answer for your particular analysis needs.

You may need the superior quantitation and reproducibility of the classical ion exchange technique. Or the speed and sensi-

tivity of reversed phase. We offer them both.

For the flexibility of HPLC, we offer System Gold,<sup>™</sup> the Personal<sup>™</sup> Chromatograph. And the System 6300 dedicated ion exchange analyzer for physiological and diagnostic applications.

Whichever your choice, we provide proven methods, too. Complete and *guaranteed*.

You see, we've been involved in automated amino acid analysis since Moore, Stein and Spackman pioneered it in 1958. So you can rely on us for in-depth applications and technical support. Anytime.

All the time.

That's why you can trust our recommendation. But we won't recommend a thing until we sit down and talk. And listen.

Take the first step in successful amino acid analysis. Contact your local Beckman office in major cities worldwide. In the US, call 800/742-2345.

Beckman Instruments, Inc., Altex Division, 2350 Camino Ramon, P.O. Box 5101, San Ramon, California 94583.

# BECKMAN

A SMITHKLINE BECKMAN COMPANY

# The Teaching of Analytical Chemistry in Europe

**Ernö Pungor**

Institute of General and  
Analytical Chemistry  
Technical University  
Budapest, Hungary

**Robert Kellner**

Institute of Analytical Chemistry  
Technical University  
Vienna, Austria

Analytical chemistry began to develop in the Middle Ages, continued to grow during the so-called Phlogiston Era, and enjoyed a golden age of progress and acceptance during the past century (1). The foundations of numerous fields of modern analytical chemistry were laid in various European scientific schools during the 1800s. The theory of classical analytical chemistry, which essentially is based on the work of Ostwald, began to flourish following the activities of Kolthoff, and the first independent journal devoted to analytical chemistry was initiated during the past century by Fresenius.

Because of the advances of the chemical industry in Germany at the end of the nineteenth century, chemical synthesis became a prime interest to



has changed drastically. When using classical methods, the analyst had direct contact with the sample, and his or her laboratory skill was the most important factor in the procedure. As shown in Figure 1, this relationship has changed because of the increasing use of automated analysis and robotics. Today, in addition to being skillful in the laboratory, it is important for the analyst to understand what physical phenomena cause signal production and how the data collected can be treated mathematically so as to afford meaningful information.

The activities of analytical chemists are wide ranging. In addition to producing reliable results using traditional methods, analytical chemists have to devise new techniques, apply them, and automate them. This range of activities requires skills that are entirely different from those that characterized a good analytical chemist in the nineteenth or early twentieth centuries.

## New curricula respond to modern demands

As in the United States, analytical chemists in Europe have confronted modern demands by making basic

## REPORT

chemists in Europe and organic chemistry developed. In the early part of the twentieth century, physical chemistry developed and analytical chemistry assumed the role of maidservant in the realm of chemistry (in Latin, *ancilla chemiae*). At European universities, analytical chemistry was a discipline associated with other sciences; and departments of inorganic and analytical chemistry, organic and analytical chemistry, and physical and analytical chemistry were established.

## New societal demands boost analytical chemistry

The recent increasing societal demands for greater amounts of analytical data have lifted analytical chemistry from the subordinate position it held in the early part of the twentieth century. Such demands are associated

with many aspects of modern life. This need for data has placed analytical chemistry on many new tracks. A steadily growing number of papers authored by American scientists have appeared in ANALYTICAL CHEMISTRY, and a steadily growing number of papers authored predominantly by European chemists have appeared in numerous European analytical chemistry journals.

Given the growing regard and need for analytical chemistry, it has become imperative to enhance the reliability of analytical methods and to reduce the effects of subjective error. New, rapid, and automated methods of laboratory analysis have made possible sophisticated process control, which has led to the introduction of monitors. Consequently, the relationship between the analyst and the sample to be analyzed

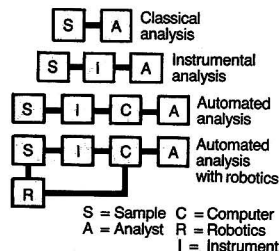


**Figure 1.** As analytical procedures have become more automated, direct interaction between analyst and sample has diminished.

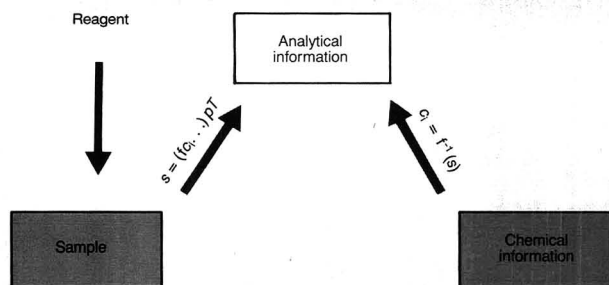


Figure 2. Once obtained from the sample and reagent, analytical information must be translated into chemical information (qualitative and quantitative data).

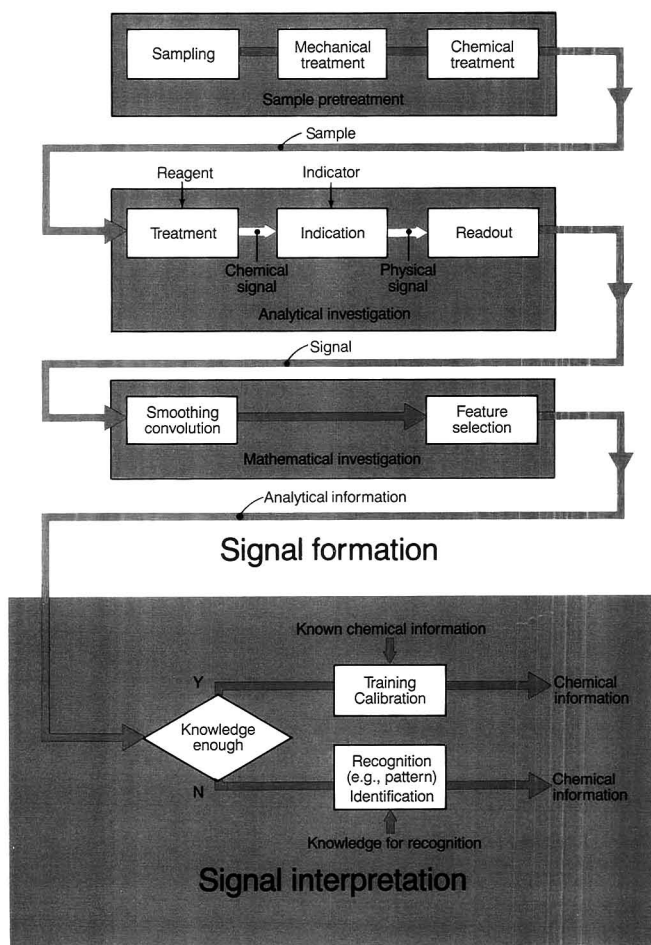


Figure 3. A detailed diagram of the analytical process shows the chemist's role in signal interpretation.

changes in the techniques developed during the nineteenth century. This process also greatly influenced the teaching of analytical chemistry.

University courses have been constructed to provide chemists with the basic knowledge needed to attain the skills that will be applied in modern laboratories. As the scientific requirements have changed, the academic system has been revised. In a 1979 special issue, *Fresenius' Zeitschrift für Analytische Chemie* focused on teaching analytical chemistry in different countries (2), and in 1981 an issue was devoted to the challenges in, and effects of, teaching (3).

The Working Party for Analytical Chemistry (WPAC) of the Federation of European Chemical Societies (FECS) conducted a study of how analytical chemistry was taught in Europe in 1983/1984. This study, published in 1985 (4, 5), included more than 200 universities. Before examining the results and conclusions of the study, let us pose some important questions: What is the definition of analytical chemistry? How broad is the field? On what background information should analytical chemistry rely?

#### Philosophical aspects of analytical chemistry

A good definition of analytical chemistry has been the topic of extensive discussion by analytical chemists in Europe. One acceptable definition is the following: the science of signal production and interpretation necessary for the qualitative and quantitative characterizations of materials. According to the general concept formulated by Malissa, in which an analytical signal is seen to be the result of an interaction between sample and reagent (generally, any source of energy), signal production can be described by the simple relationship  $M + R \rightarrow S$ , where  $M$  is the sample,  $R$  is the reagent, and  $S$  is the signal (6).

A resulting complex of signals is called *analytical information*. Signals may be processed by mathematical methods—for example, transformations or derivations—to yield data smoothing, feature selection, and other results. The choice of mathematical methods used to process data depends on the conditions of the analytical measurement. To translate analytical information as defined above into chemical information (qualitative and quantitative data), a decoding procedure must be applied (see Figure 2). The reliability of the decoding procedure depends on the knowledge of the analytical chemist, which, in turn, depends on the way the chemist was taught and trained. During their studies, university students today must acquire the basic knowledge that enables them to de-

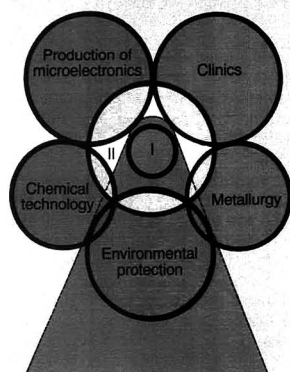


Figure 4. The relationships among fundamentals of analytical chemistry (I), analytical knowledge of a specific field (II), and knowledge required for a specialist (pie-shaped area).

code analytical information correctly. The position of analytical knowledge in the overall scheme of analysis is shown in Figure 3.

In contrast to the earlier times, when the practice of analytical chemistry required knowledge of inorganic chemistry and some organic and physical chemistries, modern analytical re-

search and development requires a broad knowledge of inorganic, organic, and physical chemistries, some physics, modern electronics and digital systems, and a thorough knowledge of the specific field in which the work is conducted (see Figure 4).

Obviously, this specialized knowledge of a field cannot be acquired during the first years of academic study; therefore, the old European system, in which analytical chemistry was merely a subject dealt with early in the curriculum, has been changed. Almost everyone involved in university teaching believes that academic study only provides the fundamentals of knowledge and impetus for the development of independent thinking. These can then be applied to research in a special field. This is especially true of analytical chemistry because of the vast background that is required. For these reasons, some European universities now emphasize fundamentals of analytical chemistry and present specific analytical subjects in specialized and post-graduate programs.

#### Analytical training in Europe

Results of the WPAC/FECS survey, published in 1985 (4, 5), are shown in Figures 5 and 6. Of the participating countries (listed in the box), 229 institutions responded to the question-

#### Participants in the FECS/WPAC study

Country	No. of institutions <sup>a</sup>
Austria	4
Belgium	7
Bulgaria	8
Czechoslovakia	2
Cyprus	—
Denmark	7
Finland	9
France	6
Federal Republic of Germany	42
Greece	3
Hungary	7
Ireland	6
Italy	23
Netherlands	6
Norway	1
Poland	9
Portugal	1
Spain	8
Soviet Union	2
Sweden	5
Switzerland	6
Turkey	2
United Kingdom	45
Yugoslavia	20
Total responses	229

<sup>a</sup> Questionnaires were evaluated from each of these institutions.

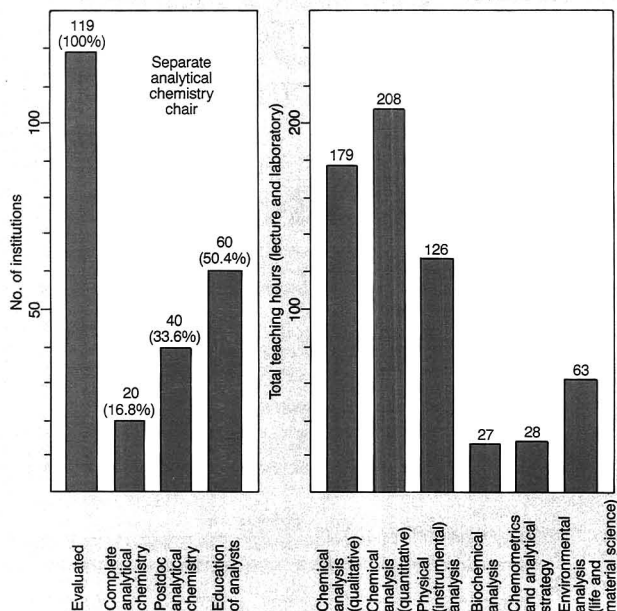


Figure 5. Survey results for European institutions with separate chairs for analytical chemistry. (Adapted with permission from Reference 4.)

naire. It is notable that 119 of them have a separate department or chair of analytical chemistry; the remaining 110 do not. As might be expected, institutions that have separate analytical departments or chairs appear to provide a broader education in the field. In many universities in Europe, the undergraduate and graduate years are not implicitly differentiated; thus, the data presented in Figures 5 and 6 refer to the "complete curriculum" during the undergraduate and graduate years.

In addition, to obtain a Ph.D. degree in analytical chemistry in Europe, the candidate must prepare a thesis under the supervision of a senior scientist. This thesis is refereed by two experts. However, this differs from country to country and from university to university. Some universities have a supervisor who is also a referee; others have two referees from outside the university. At some universities an oral debate is a prerequisite, whereas at others the acceptance of the thesis by the referees is sufficient for granting the Ph.D. degree. In all cases, the Ph.D. candidate must pass a special examination that requires a broad knowledge of analytical chemistry.

The percentages of institutions offering a complete curriculum in analytical chemistry were 16.8% in schools with separate chairs and 4.5% in



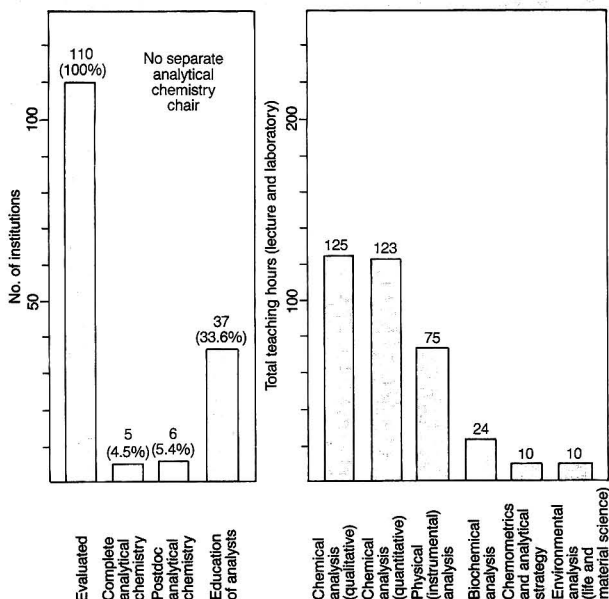


Figure 6. Survey results for European institutions without separate chairs for analytical chemistry. (Adapted with permission from Reference 4.)

schools without separate chairs. A complete curriculum includes all six of the following courses: qualitative chemical analysis, quantitative chemical analysis, physical (instrumental) analysis, biochemical analysis, chemometrics and analytical strategies, and environmental analysis (life and material sciences).

A number of conclusions can be drawn from the data presented in Figures 5 and 6. A comparison of teaching hours devoted to analytical chemistry in the two types of institutions (with and without separate chairs) reveals the benefit of having a separate chair. For institutions offering complete curricula, schools with separate chairs have a total of 632 hours of lecture and laboratory, whereas schools without separate chairs have a total of 367 hours of lecture and laboratory. In addition, the breakdown of hours devoted to the six analytical branches reveals that schools with separate chairs are more flexible and can better incorporate new programs. New fields are underrepresented at schools without chairs, and classical subjects appear to have been cut back without being replaced. Subjects incorporated into analysis courses at universities with separate chairs now include extraction chromatography, ion-selective electrodes, flow analysis, and chemome-



## XR300

### EDXRF SPECTROMETER

Super Fast

## The waiting is over...

Energy Dispersive X-Ray Fluorescence spectrometry (EDXRF) is one of the fastest and most reliable techniques for making chemical analyses of a wide range of sample types.

The all new XR300 EDXRF from Link Analytical offers accurate, precise and extremely rapid multielement analyses for all elements from Na to U in the periodic table. The wide dynamic range of XRF, from low PPM concentrations to high weight % levels, often without the need to dilute the sample ensures that a minimum of sample pretreatment is necessary.

As a qualitative elemental tool EDXRF has no equal. A clear easily interpreted spectrum display indicates the element present and a computer aided peak identification routine rapidly completes the process.

To capitalise on the inherent speed of the technique, the XR300 software operates within a powerful multiground environment thus ensuring that the pace of the analysis is not compromised by the need to suspend spectrum acquisition during data reduction operations.

From single analyses to fully automated runs, the XR300 has a potential answer to all of your elemental analysis problems. To find out how this powerful instrument can help you why not call us today?



**Link**  
ANALYTICAL

**XR300**  
*Super Fast* ENERGY DISPERSIVE X-RAY FLUORESCENCE SPECTROMETERS

Link Analytical Inc.  
240 Twin Dolphin Drive,  
Suite D  
Redwood City,  
California 94065 USA  
Tel: (415) 595-5465  
Fax: (415) 595-5589

Link Analytical Limited,  
Hullfax Road, High Wycombe  
Bucks HP12 3SE,  
England  
Tel: 0494 442255  
Telex: 837542 LINK HWG  
Fax: 0494 24129

Link Analytical (France) S.A.R.L.  
9 Rue Fernand Leger,  
Centre Val Courcelle,  
91190 Gif Sur Yvette, France  
Tel: (1) 6907 7802  
Telex: 803848S LINK  
Fax: (1) 6907 4469

Link Nordiska AB  
Box 153,  
181 22 Lindinge,  
Sweden  
Tel: 08-767 9170  
Telex: 12645 SPECTAB  
Fax: 02-4841667

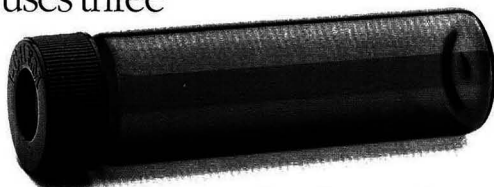
Link Analytical, (Aus) Pty. Ltd.  
P.O. Box 7,  
Pennant Hills,  
N.S.W. 2120,  
Sydney, Australia.  
Tel: 2-6753130  
Fax: 02-4841667

CIRCLE 90 ON READER SERVICE CARD

# Good chemistry begins with contaminant-free sample containers.

That's why I-Chem uses three different Protocols™ to prepare containers.

One for glass bottles and jars. One for polyethylene and Nalgene products. And a third one for vials. In fact, our vials are prepared at a totally separate facility, in a chemical free environment.



To give you that extra assurance, all I-Chem containers come with heavy duty .030 Teflon® lined closures. Vials and

septum bottles are supplied with our quality Teflon®-silicone septa.

We put our containers to the test before you do. Using trace analytical techniques

such as graphite furnace AA, ICP and

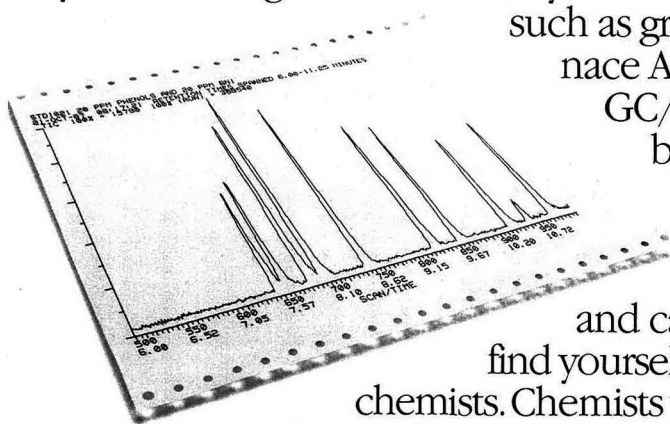
GC/MS, we profile each batch of containers before they go to your lab.



Pick up the phone and call I-Chem today. You'll find yourself talking to other chemists. Chemists who understand what

it takes to do good chemistry.

Chemists in the container business.



## I-CHEM

I-CHEM RESEARCH

Hayward, CA (800) 443-1689 (800) 262-5006 In Calif.

New Castle, DE (800) 553-3696

Houston, Texas Naperville, Illinois Atlanta, Georgia

Protocol and Protocols are trademarks of I-Chem Research. Teflon is a registered trademark of DuPont.

CIRCLE 75 ON READER SERVICE CARD

# Stable Isotopes: The Source

Isotec Inc. offers a large selection of enriched stable isotopes and labelled compounds available for research and industry.

**Deuterium** — A wide variety with enrichments to 99.99%.

**Carbon-13** — Organics, inorganics, sugars, amino acids, etc. . .

**Nitrogen-15** — Ammonia, urea and other fertilizers — enrichments 10 to 99%

**Oxygen-18** — Gas, water, multi-labelled compounds . . .

**Metal stable isotopes** — A comprehensive range from atomic number 12 to 82.

**Custom synthesis capability** — Just call us!

Send for our latest catalog. **ISOTEC** is THE source of stable isotopes for industry and research.

**ISOTEC INC.**  
A Matheson, USA Company

3858 Benner Road  
Miamisburg, OH 45342  
(513) 859-1808  
(800) 448-9760

**Table I. Analytical chemistry courses at the Technical University, Vienna (5 years or 10 terms diploma study)**

Course	Term	Lectures	Labs	Seminars
		(hours per week)	(hours per week)	
Chemical Analysis I	1	4	—	—
Chemical Analysis II	2	2	9	—
Chemical Analysis III	3	—	12	—
Physical Analysis I	3	3	—	—
Physical Analysis II	7	3	5	—
Automatic Analysis	8	3	—	—
Organic Analysis	6	3	—	—
Environmental Analysis	6	3	2	—
Seminar Modern AC	9	—	—	5
Diploma Thesis	10	—	30	—

**Table II. Specialization in analytical chemistry**

Methods	Problems
Separation methods	Environmental analysis
Mass spectrometry	Food analysis
Atomic spectroscopy	Biochemical analysis
Molecular spectroscopy	Pharmaceutical analysis
Structure elucidation	Clinical analysis
Chemometrics	Material science
Trace analysis	Automated analysis
Micro analysis	Toxicology
Surface analysis	Forensic analysis
Electroanalysis	Geochemical analysis
Thermal analysis	Extraterrestrial analysis

trics, to name a few.

Today at the Technical University, Vienna, the ideal curriculum, proposed by Kellner and Malissa (7) and shown in Figure 7, is closely approximated. Tables I and II indicate the curriculum for the first five years and the specializations the candidates may choose from for the analytical chemistry methods and problems in Figure 7.

## Conclusions

Analytical chemistry should not be intertwined with other branches of chemistry; it should be a separate discipline. Analytical education should have the following aim: to create graduates who not only have the required knowledge and skills in analytical chemistry, enabling them to compete on an international level, but who also are aware of their responsibility to society and to nature.

We have not made a rigorous study such as the one conducted by the ACS four years ago, which revealed that the majority of chemists consider organic and analytical chemistries to be

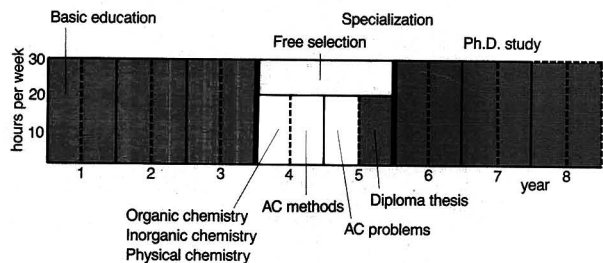


**Figure 7. Model curriculum for a technical university, including basic education, specialization, and Ph.D. thesis work.**  
(Adapted with permission from Reference 7.)

the most important subjects taught at universities—and the subjects most needed in the course of their practices (8). However, we believe that analytical chemistry enjoys a similar status in Europe. According to a survey done in West Germany and Austria, 20% of chemists claimed that they dealt predominantly with analytical questions in their daily work. We believe that analytical chemistry is one of the most, if not *the* most, important subjects taught worldwide.

#### References

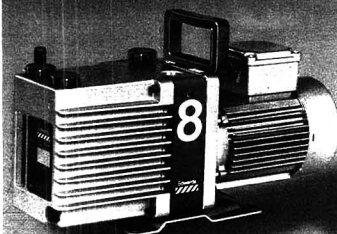
- (1) Szabadvary, F. *History of Analytical Chemistry*; Pergamon Press: New York, 1966.
- (2) *Fresenius Z. Anal. Chem.* 1979, 297, 2.
- (3) *Fresenius Z. Anal. Chem.* 1981, 305, 2.
- (4) Pungor, E.; Kellner, R. *Education of Analytical Chemistry in Europe*; Österreichische Gesellschaft für Mikrochemie und Analytische Chemie: Wien, Austria, 1985.
- (5) Kellner, R.; Pungor, E. *Modern Analytical Chemistry Education in Europe at University Level TRAC 1985*, 4(5).
- (6) Malissa, H. *Fresenius Z. Anal. Chem.* 1974, 271, 97.
- (7) Kellner, R.; Malissa, H. *Fresenius Z. Anal. Chem.* 1984, 319, 1.
- (8) *Chem. Eng. News* 1984, 62(43), 30.



**Ernő Pungor** (left) received his Ph.D. in chemistry from the Pázmány Péter University (Budapest, Hungary) in 1949. Since 1970 he has been professor and head of the Institute for General and Analytical Chemistry of the Technical University of Budapest. In 1976 he became a full member of the Hungarian Academy of Sciences, and he is a member of the advisory or editorial boards of 10 international analytical journals. He has received medals and awards for his achievements in analytical chemistry and has authored or co-authored more than 500 scientific articles.

**Robert Kellner** is a professor of analytical chemistry at the Technical University, Vienna, Austria. He received his Ph.D. from the university in 1971. His research interests include extreme applications of FT-IR spectroscopy to micro-, surface, and trace analysis. In addition, he has published more than 80 papers on solid-liquid interface phenomena, microcontaminations, metal chelates, and flavor analysis.

## The Ideal Lab Vacuum Pump



Model E2M8 Rotary Vane Pump

**Edwards**

*First with ideas. Last to quit.*

Edwards High Vacuum  
3279 Grand Island Blvd.  
Grand Island, NY 14072  
(716) 773-7552

CIRCLE 40 ON READER SERVICE CARD

## Plenum Books

### COMPUTER-ENHANCED ANALYTICAL SPECTROSCOPY

edited by **Henk L. C. Meuzelaar** and **Thomas L. Isenhour**

A broad overview of advances in computerized optimization, data exploration, and spectral interpretation methods in mass spectrometry, infrared spectroscopy, and nuclear magnetic resonance spectroscopy. A volume in the series *Modern Analytical Chemistry*.  
0-306-42644-7/288 pp./ill./1987/\$52.50

### MASS SPECTROMETRY IN BIOTECHNOLOGICAL PROCESS ANALYSIS AND CONTROL

edited by **Elmar Heinze** and **Matthias Reuss**

A summary of the current state of mass spectrometry applications in biotechnological process analysis and control, with reports on instrumentation and gas analysis, membrane inlet systems, applications and computer control, and pyrolysis-MS and HPLC-MS interfacing.  
0-306-42777-X/proceedings/254 pp./ill. 1987/\$59.50

### VIBRATIONAL SPECTROSCOPY OF MOLECULES ON SURFACES

edited by **John T. Yates, Jr.**, and **Theodore E. Madey**

Chapters cover the basic theoretical aspects of vibrational spectroscopy on surfaces, normal modes and excitation mechanisms in vibrational spectroscopy, various methods used to observe surface vibrations, and relatively new techniques that permit vibrational studies to be made on single-crystal substrates. Volume 1 in the series *Methods of Surface Characterization*.

0-306-42505-X/484 pp./ill./1987/\$75.00



**PLENUM PUBLISHING CORPORATION**  
233 Spring Street  
New York, NY 10013-1578  
Telephone orders:  
(212) 620-8000/1-800-221-9369

CIRCLE 125 ON READER SERVICE CARD



## Applications of 2-D NMR

**Two-Dimensional NMR Spectroscopy. Applications for Chemists and Biochemists.** William R. Croasmun and Robert M. K. Carlson. 511 pp. VCH Publishers, 220 East 23rd St., Suite 909, New York, N.Y. 10010. 1987. \$95

*Reviewed by Jerry P. Heeschen, The Dow Chemical Company, Analytical Sciences, 1897 Building, Midland, Mich. 48667*

Two-dimensional nuclear magnetic resonance spectroscopy (2-D NMR) has become a very powerful class of experiments (in the hands of an adept scientist) with broad adaptability to new situations. It is the product of a happy marriage between modern pulse FT-NMR technology, with its large memory and high-speed computers, and the physicists and chemists who love to manipulate spin systems. Basic 2-D experiments are now a standard capability of modern NMR spectrometers, and this timely book intends to make 2-D NMR users of those who are familiar with normal 1-D NMR.

“... recommended  
for NMR-knowledgeable  
beginners in 2-D  
NMR.”

The 2-D NMR goal is correlation of the lines of the observed NMR spectrum with other properties of the system. This book deals with applications to high-resolution spectrum analysis, utilizing either coupling between the NMR-active nuclei or chemical exchange to perform the correlation. The coupling can be scalar (through bonds) or direct through space (within 5 Å). The coupling may be homonuclear (between like nuclei) or heteronuclear.

Most often, the 2-D technique is used to analyze 1-D spectra. The major successes of 2-D NMR have been achieved with very large molecules, where there is so much overlapping detail in the normal 1-D spectrum that

analysis can be performed only by spreading this detail over two directions. The most appropriate large molecules thus far have been those of biological origin. Of course, the techniques are applicable to all NMR-active molecules.

Three introductory chapters (Gray, Hull, Bernstein) are followed by chapters on cyclosporin A (Kessler, Oschkinat, and Loosli), DNA (Kearns), complex carbohydrates (Dabrowski), steroids (Croasmun and Carlson), organic compounds (Rinaldi), and natural products (Martin). All chapters were written to teach the fundamentals of applying 2-D NMR, and they contain many examples. The role of 2-D NMR in overall schemes for solving problems is thoroughly discussed throughout the book.

Many useful illustrations and tables are included, and all chapters but the first offer large bibliographies. The glossary of acronyms is useful, and the index is thorough. In addition, the editing job is superb. Chapter organization is uniform; each chapter contains an introduction, text, and conclusions. Each author was aware of the others' contributions and, to a large extent, avoided duplicating introductory arguments.

The heart of this book is William Hull's chapter on experimental aspects of 2-D NMR. He offers a "shopping list" of necessary instrument capabilities, then discusses in detail the design of experiments and analysis of results. Many tables of pulse and phase sequences are provided.

The one obvious omission is a rigorous presentation of 2-D NMR theory. This omission is acceptable because the book's goal is applications, but it would have been helpful to have recommended general source material within the several pages of good descriptive theory in Chapter 1. As it stands, the reader must glean many theoretical details from brief discussions and individual references.

The book should retain its timely character for several years. All of the current basic experiments are covered, so that new variations will be understandable. The recently introduced

spin-lock-based experiment CAMEL-SPIN is treated briefly.

In conclusion, the book is strongly recommended for NMR-knowledgeable beginners in 2-D NMR. It should serve also as a useful desktop reference for review and planning.

**Separation and Spectrophotometric Determination of Elements.** Zygmunt Marczenko. 708 pp. John Wiley & Sons, 605 Third Ave., New York, N.Y. 10016. 1986. \$166

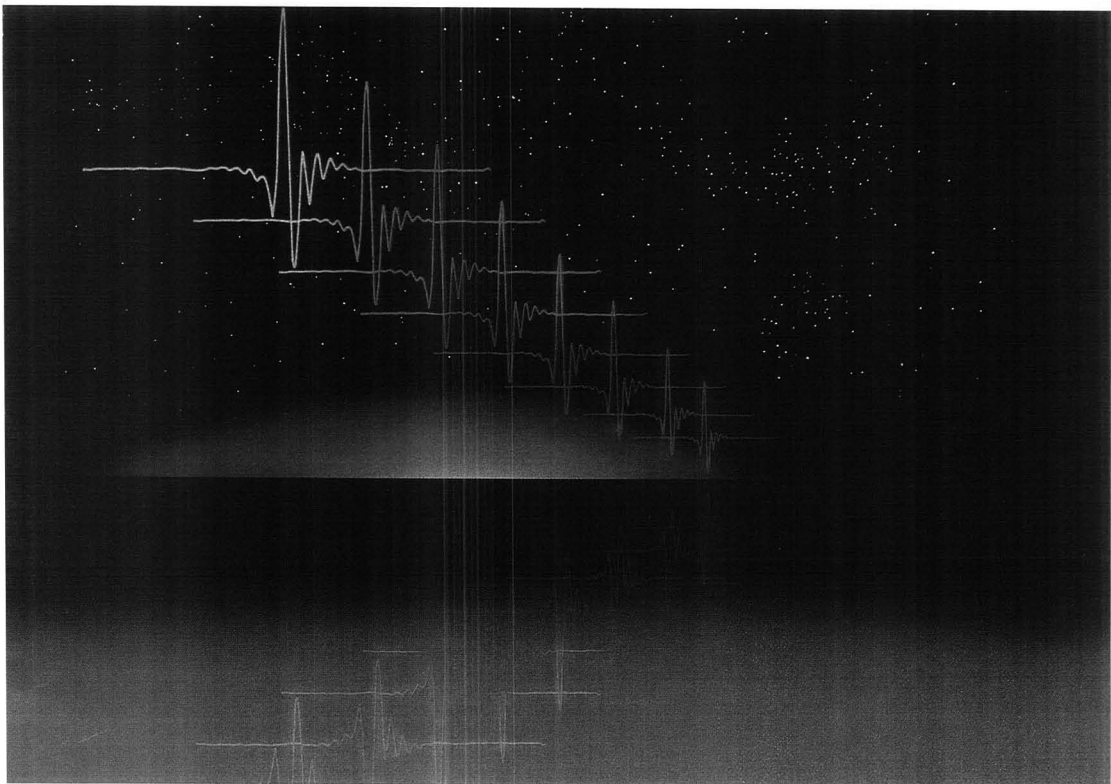
*Reviewed by M. S. Epstein, Center for Analytical Chemistry, National Bureau of Standards, Gaithersburg, Md. 20899*

This book is a useful text intended as a reference for the laboratory that is either involved in spectrophotometric analysis or requires separations prior to analysis by any method. It attempts to cover a diverse series of topics in fewer than 700 pages. The difficulty of that task is most obvious in Part I of the book, which covers general topics such as separation schemes (solvent extraction, precipitation, volatility, ion exchange), principles and instrumentation used for spectrophotometry, and color reagents in only 119 pages. Entire books have been written on each of those subjects. The author must therefore resort to extensive referencing to cover each subject adequately.

The decision to either place detailed information in the text or to reference that information is based on factors that may be out of the author's control. However, I find it rather frustrating to consult a "reference" text and then be unable to find the information or be directed to other references that may be difficult to obtain or hard to understand. When general subjects are covered, it is far more valuable to have the book author's interpretation and explanations of the technical matter than to be referred to other references. The lack of such explanations in this text is a serious omission.

Any text dealing with spectrophotometric methods must be compared with the classic series *Photometric De-*

**Incomparable value:  
Low-cost, high-performance FT-IR.  
Only from Perkin-Elmer.**



Presenting the 1600 Series FT-IR Spectrophotometer—the first complete FT-IR system that dramatically extends price-performance value. The 1600 blends advanced electronics, optics and software into a compact, bench-top system.

**UNMATCHED EASE OF USE**

The press of a single key puts you in control of all functions. Powerful graphics let you instantly manipulate spectra, rescale or rerange displays and activate five spectroscopic functions. Plus, our exclusive purge-free optical design gives you fast start-up.

**EXCLUSIVE MULTITASKING CAPABILITY**

The 1600's special multitasking capability saves you time by letting you scan, acquire spectra and plot simultaneously. Also, the 1600 interfaces easily with an IBM® PC or fully compatible computer.

**ALL FOR LESS**

If price has kept you away from FT-IR, the 1600 is your sensible solution. To find out more, talk to your Perkin-Elmer Technical Representative.

IBM is a registered trademark of International Business Machines Corporation.

Or for literature in the U.S., please call 1-800-762-4000 or write:

Perkin-Elmer Corp., 761 Main Ave., Norwalk, CT 06859-0012 U.S.A. Tel: (203) 762-1000. Telex 965-954.  
Bodenseewerk Perkin-Elmer & Co., GmbH, Postfach 1120, 7770 Ueberlingen, Federal Republic of Germany. Tel: (07551) 810.  
Perkin-Elmer Ltd., Post Office Lane, Beaconsfield, Bucks HP9 1QA, England. Tel: Beaconsfield (04946) 6161.



**PERKIN ELMER**

CIRCLE 127 ON READER SERVICE CARD

# WHEATON Centrifuges

## Do not disturb

- Micro to macro, a full range of bench top centrifuges precision engineered for rapid acceleration and extremely quiet operation
- Gentle, turbulence-free electronic braking system prevents resuspension of separated sample
- Electronic interlock safety feature prevents lid from being opened before rotor stops
- Wheaton quality construction for long, service-free operation

For more information call  
609/825-1400 or write:



**WHEATON  
INSTRUMENTS**

Manufacturers Since 1888  
1301 N. Tenth Street  
Millville, NJ 08332, USA  
Call Toll-Free: 1-800/225-1437  
Ext. 2527

## BOOKS

*termination of Traces of Metals.* The fourth edition of this text has most recently appeared in two volumes covering "General Aspects" (1085 pp.; Sandell and Onishi; John Wiley & Sons, 1978), and "Individual Metals, Aluminum to Lithium" (885 pp.; Onishi; John Wiley & Sons, 1986). The subject matter covered in Part I of *Separation and Spectrophotometric Determination of Elements* is similar to that of the "General Aspects" text, except that the latter covers the subject in 10 times as many pages and provides valuable information on sample preparation and contamination control, which is lacking from this text. There have been no major developments in the general aspects of spectrophotometric measurements in the eight years that separate these texts. One example of the difference in depth of subject matter is illustrated by the discussion of accuracy and precision. The reviewed text covers the subject in three pages with 11 references. The Sandell and Onishi "General Aspects" text covers the subject in 30 pages with 26 notes that are actually references with descriptive text. It is perhaps like comparing a two-volume desk encyclopedia with the *Encyclopedia Britannica*.

Part II, "Methods for Separation and Determination of Individual Elements," although still much condensed compared with the extensive compilation of Onishi, is much more acceptable. The experimental details of a separation or a spectrophotometric procedure must usually be obtained from the original referenced work, so that a detailed description in the text of the reference book is useful but not necessary. More importantly, all elements—both nonmetals and metals—are discussed in the text, and major procedures for the separation and spectrophotometric determination of each element are adequately covered. However, at least one case of what might be described as the author's bias toward his own research appears in the extensive citation of Eriochrome Cyanine R as a color reagent.

I have mixed feelings about this text. The general section, Part I, is useful only as a very cursory introduction to the subject matter and is not a good reference. The real value of this book is Part II, where methods are compiled. Until further editions of *Photometric Determination of Traces of Metals* covering other elements become available, the reviewed text must be considered the most complete compilation, although certainly not the most comprehensive for specific elements. In general, the text is cumbersome at

times but is still quite readable. There were more than 150 printing errors listed on the errata sheet provided with the book. However, I believe this text would be a useful addition to any chemical library because the comprehensive compilation of methods will save hours of library searches.

## Books Received

**Fundamentals of Chemistry. General, Organic, and Biological.** Joseph D. DeLeo. 793 pp. Scott, Foresman/Little, Brown College Division, 1900 East Lake Ave., Glenview, Ill. 60025. 1988. \$33.56

**Handbook of Laboratory Management.** Virginia P. White. 240 pp. ISI Press, 3501 Market St., Philadelphia, Pa. 19104. 1988. \$49.95

**Inductively Coupled Plasma Emission Spectroscopy. Part II: Applications and Fundamentals.** P.W.J.M. Boumans, Ed. xii + 486 pp. John Wiley & Sons, 605 Third Ave., New York, N.Y. 10016. 1987. \$70

**Industrial Applications of the Mössbauer Effect.** G. J. Long and J. G. Stevens, Eds. x + 796 pp. Plenum Press, 233 Spring St., New York, N.Y. 10013. 1986. \$115

**Methods for Analytical Atomic Spectroscopy.** 8th ed. xxiii + 1123 pp. American Society for Testing and Materials, 1916 Race St., Philadelphia, Pa. 19103. 1987. \$74

**Applications of Mass Spectrometry in Food Science.** J. Gilbert, Ed. xxii + 440 pp. Elsevier Science Publishers, 52 Vanderbilt Ave., New York, N.Y. 10017. 1987. \$108

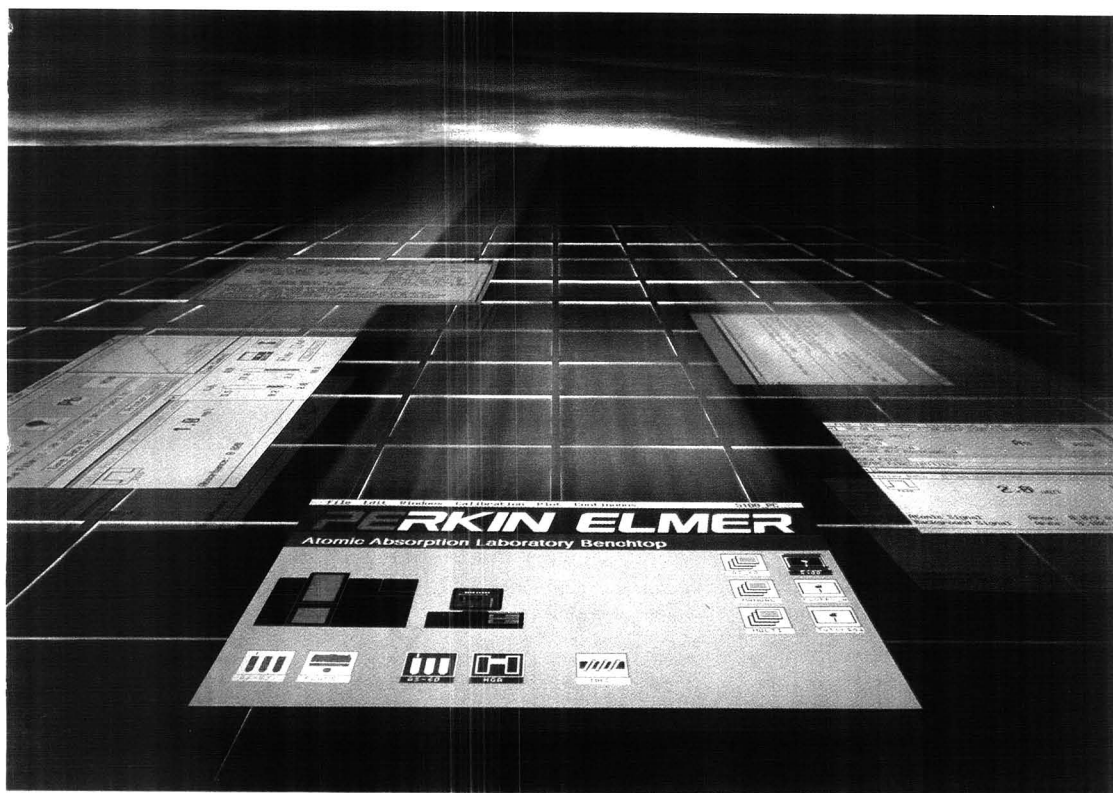
**Radionuclide Tracers: Their Detection and Measurement.** M. F. L'Annunziata. xvii + 505 pp. Academic Press, 111 Fifth Ave., New York, N.Y. 10003. 1987. \$96

**Introduction to Nondestructive Testing: A Training Guide.** P. E. Mix. xiv + 406 pp. John Wiley & Sons, 605 Third Ave., New York, N.Y. 10016. 1987. \$54.95

**Physical Methods of Chemistry, 2nd. ed. Vol. III A: Determination of Chemical Composition and Molecular Structure—Part A.** B. W. Rossiter and J. F. Hamilton, Eds. ix + 624 pp. John Wiley & Sons, 605 Third Ave., New York, N.Y. 10016. 1987. \$110

CIRCLE 175 ON READER SERVICE CARD

# The ultimate in AA. The Perkin-Elmer 5100 PC.



This is the only Atomic Absorption Spectrometer that can combine all major sampling and background correction techniques plus PS/2™ or PC control into a single system. The Perkin-Elmer 5100 PC gives you unsurpassed performance in one fully automated instrument, and it's exclusively yours from the world leader in AA technology.

#### UNMATCHED FLEXIBILITY

A twist-of-a-knob lets you switch between flame AA and Zeeman graphite furnace analyses. Or, equip your 5100 PC with full range continuum background correction, conventional graphite

furnace or Mercury/Hydride systems. Whatever your needs, you get superb AA automation with the capability of determining up to 12 elements with one method.

#### SIMPLY SUPERIOR SOFTWARE

Powerful software, coupled with a unique user interface tailored specifically for AA, drives the 5100 PC. It's dynamic and highly visual, with high-resolution color graphics, windows, drop-down menus and dialog boxes. You get an interface that's remarkably powerful and truly easy to use.

#### VERSATILITY FOR TOMORROW

The Model 5100 PC defies

obsolescence. Start with the basics. Expand at your own pace into Zeeman, graphite furnace or Mercury/Hydride. It's versatility with a future. And it's our best, so you know there's nothing better. Your Perkin-Elmer Technical Representative has complete information. Or, for literature in the U.S., please call 1-800-762-4000.

Perkin-Elmer Corp., 761 Main Ave., Norwalk, CT  
06859-0012 U.S.A. Tel: (203) 762-1000.  
Telex 965-954.

Bodenseewerk Perkin-Elmer & Co., GmbH,  
Postfach 1120, 7770 Ueberlingen,  
Federal Republic of Germany.  
Tel: (07551) 810.

Perkin-Elmer Ltd., Post Office Lane, Beaconsfield,  
Bucks HP9 1QA, England.  
Tel: Beaconsfield (04946) 6161.

PS/2 is a registered trademark of International Business Machines Corporation.

## PERKIN ELMER

CIRCLE 128 ON READER SERVICE CARD

## If distilled water is so reliable, why don't stills come with these?



### Introducing the new lonpure-12 Lab Water System from Millipore.

There are two things you can't get from a still.

The first is consistent water quality. As a still is used, it gets dirty. And so does your lab water. The lonpure-12 system, utilizing continuous deionization (CDI) technology, eliminates the problem of purity degradation.

The second is a guarantee. For one full year, we guarantee the water produced by our lonpure-12 system will be greater than 1.0 megohm-cm. We even built in a resistivity meter, to alert you if the water quality falls below that level.

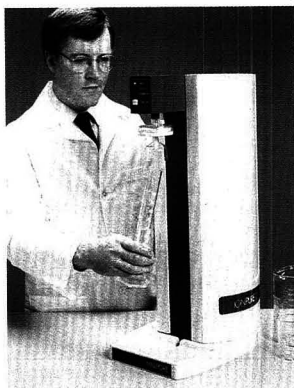
#### Never needs cleaning.

Get rid of your rubber gloves, your brushes, your acids, and anything else you use to clean your still. With the lonpure-12 system, you won't need them. Depending on the quality of your feed water, the lonpure-12 system will run 1 to 2 years without a module change.

### A big difference in performance. No difference in price.

The lonpure-12 system not only gives you consistency and freedom from maintenance, it also gives you more for your money.

Initial cost of the 12 liter per hour lonpure-12 system is about the same as a 3-6 liter per hour still. But the energy cost to operate it is considerably less. And since you won't waste energy cleaning and maintaining the system, you can also reduce labor costs and downtime.



CIRCLE 100 ON READER SERVICE CARD

### How CDI works.

CDI technology, pioneered by Millipore, employs a combination of ion exchange resin and selectively permeable membranes to remove ions from feed water. But unlike conventional DI systems, our continuous deionization system uses an electric current to drive off retained ions from the resins, keeping them constantly regenerated. And a Millipak® 0.22 µm final filter keeps bacteria levels below 10 cfu/ml.

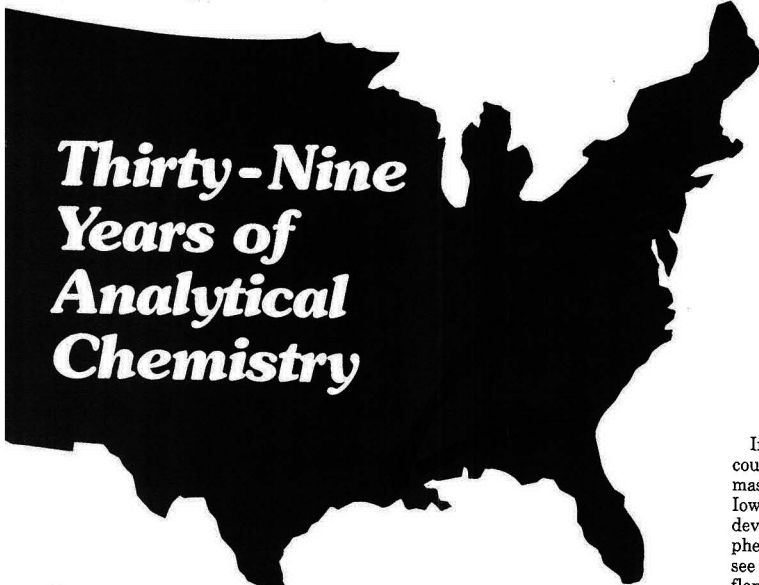
All of this makes the lonpure-12 system an ideal alternative to stills for qualitative and general instrument analyses, producing buffers and reagents, or rinsing and washing glassware.

#### Make a clean break from stills.

For more information on the new lonpure-12 system, contact your Millipore Applications Specialist. Or call (800) 225-1380, in Massachusetts (617) 275-9200. Millipore Corporation, 80 Ashby Road, Bedford, MA 01730.

# MILLIPORE





# Thirty-Nine Years of Analytical Chemistry

*The Society for  
Analytical Chemists  
of Pittsburgh  
honors its 1988  
award winner with  
a retrospective of  
analytical chemistry*

In the 39 years since the Pittsburgh Conference was founded, analytical chemistry, like the conference itself, has made tremendous progress. These advances were showcased at the annual Society for Analytical Chemists of Pittsburgh (SACP) award symposium, held at this year's conference to honor Henry Freiser, the 1988 winner of the Pittsburgh Analytical Chemistry Award. Because Freiser was involved in the beginnings of the Pittsburgh Conference as a member of the SACP, the organizers of the award symposium felt that a retrospective of the last 39 years of analytical chemistry would be especially appropriate.

Velmer Fassel, professor emeritus at Iowa State University and a well-known fixture at the Pittsburgh Conference (he was on the program for 36 consecutive years), led off the symposium with a discussion of the decline and revival of analytical atomic spectroscopy between 1949 and 1988. The early years of this period, said Fassel, saw primarily evolutionary developments in emission spectroscopy for elemental analysis, followed by a period of stagnation in the early 1950s.

Starting in 1955, however, atomic absorption spectrometry (AAS) began to make its mark. In 1961 a carbon furnace was developed to augment flame atomization, and by the mid-1960s AA was growing so fast that John Willis (CSIRO-Australia) at one time indicated that if the growth rate were to continue at the same pace, the entire surface of the earth would soon be covered with AA spectrometers!

By 1966, said Fassel, it had become clear that what was needed was one analytical technique that could replace the myriad of methods used for elemental analysis, which included gravimetry, titration, and AAS. Atomic emission spectrometry (AES) looked to some researchers as if it could fulfill this role, he continued, but it was generally dismissed for three reasons: AAS was so popular that it overwhelmed AES, the detection limits for AES weren't as good as those for other methods, and the measurement of ab-

## FOCUS

sorption rather than emission was thought at the time to have a natural advantage. But in the mid-1960s, T. B. Reed developed techniques for stabilizing the previously unstable inductively coupled plasma torch, which led to the development of inductively coupled plasma atomic emission spectroscopy (ICP-AES) by two independent research groups, one led by S. Greenfield at Albright and Wilson (Oldburg, England) and the other led by Fassel at the Ames Laboratory. This new technique allowed simultaneous determination of several elements for the first time, and its success is evident in the number of instruments now in use. The first commercially available ICP-AES instrument appeared in 1975, and such instruments are now in virtually every laboratory involved in elemental analysis.

In 1980, said Fassel, an inductively coupled plasma was combined with a mass spectrometer by R. S. Houk at Iowa State, launching the next phase of development in elemental analysis: hyphenated techniques. Fassel expects to see further development of traditional flame and furnace AAS methods and ICP-AES as well as development of various hyphenated techniques such as ICP/MS, GC/MIP-AES, and GC/helium afterglow-AES.

Fred McLafferty of Cornell University then spoke about the past and future of mass spectrometry (MS). The pioneering work of J. J. Thomson (whose first parabola design has been used for a mass spectrometer with a 27-m radius) showed many attributes of MS that are basic to its present capabilities for structure elucidation of a variety of organic compounds, said McLafferty.

"In many ways," he continued, "the varied scientific developments that have kept analytical MS expanding dramatically reflect the revolutionary growth in analytical chemistry as a whole. Its then-unique sensitivity for submilligram samples has now been extended to subpicogram levels. Its then-unusual information content, with scores of possible peaks at hundreds of possible masses, has been extended to hundreds of possible peaks at even more masses by a corresponding increase in resolution." In the early 1950s, a low-resolution spectrum required a 20-30-min scan time, said McLafferty, whereas modern data-handling and computer techniques can collect several spectra per second.

Equally exciting developments have increased the upper limit of sample molecular weight by 100 times compared with the instruments of the early 1950s. The direct probe for introducing samples into the high-vacuum ion source, pioneered by O'Neal and Reed in the late 1950s, provided the first dramatic lowering of vapor pressure re-

quirements for MS samples, and the development of field desorption and  $^{252}\text{Cf}$  plasma desorption in the early 1970s has sparked a whole range of techniques, the most common of which is fast atom bombardment, said McLafferty.

Parallel developments in interfacing liquid chromatography (LC) to MS have now made the growth of LC/MS reminiscent of that of GC/MS two decades ago, continued McLafferty. In addition, the use of the mass spectrometer as a separation as well as an identification device, as in tandem mass spectrometry (MS/MS), can greatly increase the speed of separation and dramatically improve the signal-to-noise ratio for critical analyses. GC/MS/MS, and now even LC/MS/MS, have proven especially valuable for routine analysis of complex mixtures such as drug metabolites in blood or synthetic fuels.

"The future of MS also looks bright," said McLafferty. "Several groups are making dramatic contributions to the fundamental chemistry of gaseous ions and relating this to solution-phase ionic reactions. Neutralization-reionization techniques allow unique studies of unusual metastable neutral species as well as reducing rearrangements that have always been the bane of the mass spectrometrists. Probably the most encouraging sign, however, said McLafferty, is the productivity of young mass spectrometrists who are discovering new principles, instrumentation, methodology, and applications at a surprising rate. "And," he said, "you ain't seen nothing yet!"

Jim Shoolery of Varian Associates covered NMR in a talk entitled "High Resolution NMR—37 Years—and Still Exploding?" According to Shoolery, the commercial development of increasingly powerful and versatile NMR spectrometers has been going on for nearly four decades. "This process has fueled an explosion of applications that has spread from chemistry to medicine and promises to continue with unabated momentum for the foreseeable future," he said. "The range of capabilities provided by today's instruments is all the more amazing when the comparatively brief history of the technique is considered."

Following World War II, said Shoolery, two physicists, Felix Bloch and Edward Purcell, were interested in detecting and precisely measuring the magnetic moments of atomic nuclei. In 1946 each succeeded in detecting the precession of protons in a magnetic field using a radio frequency oscillator to excite the resonance as the field was

swept through the correct value, and NMR spectrometry was born. As the magnets available for the instruments improved, they discovered that the value they obtained for the magnetogyric ratio seemed to depend on the compound that contained the nucleus. This "chemical shift" was originally regarded as a terrible nuisance, but in 1951 three of Bloch's co-workers—Arnold, Dharmatti, and Packard—put a sample of ethanol in the instrument and the resulting three peaks revealed that nuclei could be used to probe the structures of molecules.

Russell Varian, founder of Varian Associates, recognized the significance of this discovery, and in 1953 the first commercial NMR instrument entered the market. This early instrument, said Shoolery, could detect chemical shifts but was too insensitive and unstable to solve any real chemical problems. These difficulties were overcome through the development of higher magnetic fields, better magnetic materials, and improved techniques for stabilizing the field and adjusting its homogeneity. In 1955 Shoolery, who was involved in development of these early instruments, made a scouting expedition to the Pittsburgh Conference, and in 1956 the first Varian high-resolution NMR instrument joined the exposition. Over the next 30 years instrumental improvements, superconducting magnets, and powerful computers led to increases of 3–4 orders of magnitude in sensitivity and stability. New techniques such as multipulse Fourier transform NMR and two-dimensional NMR, said Shoolery, allow even more information to be determined.

L. B. Rogers of the University of Georgia described the work done in separations by chemical engineers, synthetic chemists, physical chemists, biochemists, and analytical chemists during the past 39 years. In the late 1940s and early 1950s, said Rogers, GC and multidimensional thin-layer chromatography were developed, and major advances in electronics, instrumentation, and automation were achieved. It was during this period, he continued, that a broader, unified approach to separations started to develop in the chemical community. For example, in the area of chromatography, the van Deemter equation played a major role that continued through the 1960s, and the high resolution achievable today for fractionation of oligomers and optical isomers is a direct result of those studies.

The period starting in the late 1960s, said Rogers, has brought two major advances: the concept of field flow frac-

tionation proposed by Giddings, which is today gaining momentum and broadening the capabilities for rapid fractionation of species ranging from small ions and molecules to large proteins and discrete particles; and the advent of affordable digital computers for the laboratory.

Henry Freiser wound up the symposium with a retrospective describing the "parallel paths of progress" of the SACP and his teaching career. Freiser started his academic career as a physical chemist teaching analytical chemistry at the University of Pittsburgh in 1945. At the time, said Freiser, he was studying the use of dipole moments as a method of structure elucidation. He was transformed by association with the SACP into a card-carrying analytical chemist and was lucky, he said, to have landed in such a hotbed of analytical chemistry activity.

The SACP, said Freiser, held its first analytical chemistry symposium in 1946 and was a cosponsor, along with the Spectroscopy Society of Pittsburgh, of the first Pittsburgh Conference in 1950. Because he was one of the junior members of the SACP, he was originally slated to be the hotel liaison at that first conference but ended up as exposition chairman instead when no one else wanted the job. The exposition in 1950 had only 10 booths (compared with 2300 in 1988), but the job was challenging nevertheless, said Freiser.

He continued his work on the Pittsburgh Conference in 1951, serving as copresident with John J. McGovern. This association with the Pittsburgh Conference was valuable training, said Freiser, for serving as a department chairman, and it also led to exposure for his graduate students and their research. He also met George Morrison, now Editor of ANALYTICAL CHEMISTRY, through the Pittsburgh Conference, and the resulting collaboration led to their classic textbook on solvent extraction. Freiser is especially proud of the fact that four of his former students from the University of Pittsburgh—Laben Melnick, Bruce LaRue, James McKaveney, and Robert Mainier—were elected presidents of subsequent Pittsburgh Conferences.

Freiser closed with his idea of the secret of the phenomenal growth of the Pittsburgh Conference: a multitude of energetic people all striving for a better conference. The Pittsburgh Conference has grown from a small local meeting to a large international one, and, said Freiser, based on his knowledge of the dedicated people involved, it can only continue to get bigger and better in the future.

Mary Warner



## Is your GC/MS prepared for the unexpected?

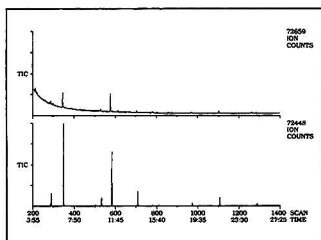


Figure 1. EI (top) and NICI (bottom) total ion chromatograms from the fish extract demonstrate the lower background interference and greater sensitivity with negative ion chemical ionization.

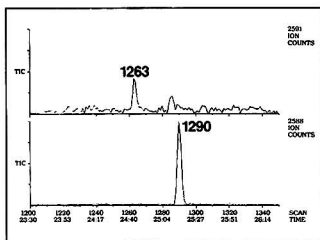


Figure 2. EI (top) and NICI (bottom) chromatograms from scan 1200 to 1360 are compared. The component at 1263 in the EI chromatogram is a phthalate ester. The component at 1290 in the NICI chromatogram is mirex ( $C_{10}Cl_{12}$ ).

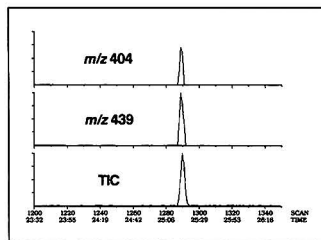


Figure 3. Mass chromatograms of  $m/z$  404 (top) and  $m/z$  439 (middle), the most intense peaks of the  $[M-4Cl]^-$  and  $[M-3Cl]^-$  isotopic clusters in mirex's mass spectrum, are shown. At the bottom is the NICI total ion chromatogram from scan 1200 to 1360.

Perhaps you depend on your GC/MS for meeting regulatory protocols. Maybe you need it for quality control or general analysis. The fact is, tough analytical problems are a way of life in the mass spec lab. And you never know what's in store for tomorrow.

One of our customers asked for assistance in identifying halogenated organic contaminants in a fish extract. We used the Finnigan MAT INCOS<sup>™</sup> 50 equipped with both electron ionization (EI) and negative ion chemical ionization (NICI). The results are shown in the figures here.

The negative ion chromatogram revealed a startling component: mirex, an insecticide and fire retardant. The presence of mirex was confirmed both by comparison with a standard's retention time and NICI mass spectrum.

NICI's greater sensitivity for good electron capture molecules such as mirex provided the answer that EI alone could not deliver.

The INCOS 50. The only GC/MS within its price range to offer the full repertoire of ionization techniques for your most challenging samples. Read our Applications Report, "Evaluation

of Different Ionization and Inlet Techniques on the INCOS 50." Ask for a demonstration. And never miss an important component again.



U.S.A., 355 River Oaks Parkway, San Jose, CA 95134, (408) 433-4800  
 Benelux, Landjweel 7, 3805 PE Veenendaal, The Netherlands 08385 27266  
 France, 69, rue de Paris, F-91400 Orsay (1) 69 28 52 53  
 Italy, Via Valadier, 37B, 00193 Rome, (06) 8578067  
 Japan, Shinjoh 1546, 2-7-1 Hiramawara-cho, Chiyoda-ku, Tokyo 102 (03) 221-1001  
 Sweden, Årstadsgatan 1C, 1 117 43 Stockholm, (08) 190480  
 U.K., Paradise, Hemel Hempstead, Herts HP2 4TG (0442) 233555  
 W. Germany, Postfach 14 40 62, D-2800 Bremen 14 (0421) 54 93 0

Get ready with the INCOS 50.

# New Wiley Books—Now on 15-Day Free Exam

## INORGANIC MASS SPECTROMETRY

Edited by F. ADAMS, R. GIJBELS, and R. VAN GRIEKEN

Leading experts discuss the entire field of inorganic mass spectrometry, including the steps along the way from historical beginning to the current techniques using lasers as ion sources. The instrumentation and its analytical characteristics are outlined. 404 pp. (1-82364-3) 1988 \$65.00

## ON-LINE PROCESS ANALYZERS

GARY D. NICHOLS

This book is a practical, plant-level handbook and guide to the selection, development, engineering, installation, operation, and maintenance of on-line process analytical instrumentation. approx. 300 pp. (1-86608-3) 1988 \$50.00

## CHROMATOGRAPHIC SEPARATIONS

(Analytical Chemistry by Open Learning Series)

PETER A. SEWELL and BRIAN CLARKE

This unit introduces chromatography and covers the theory and practice which are common to all forms of the technique. 335 pp. (1-91371-5) 1988 \$29.95

## KINETIC ASPECTS OF ANALYTICAL CHEMISTRY

(Chemical Analysis Series)

HORACIO A. MOTTOLA

Focuses on the role of kinetics in contemporary analytical chemistry including practical applications. Thoroughly investigates all chemical rapid rate processes, rapid reactions and heterogeneous and homogeneous catalysis. Mathematical basis of different aspects of kinetics is presented consistently and succinctly.

approx. 275 pp. (1-83676-1) 1988 \$69.95

## TWO-DIMENSIONAL NMR SPECTROSCOPY

JAN SCHRAML and JON M. BELLAMA

Two-dimensional NMR is an exciting new technique which brings information that is usually not accessible by any other means. This book explains the fundamentals of two-dimensional NMR to such an extent that the practicing chemist will be able to run an experiment in his own lab.

approx. 525 pp. (1-60178-0) May 1988 \$79.95

## CHROMATOGRAPHIC ENANTIO-SEPARATION

STIG ALLENMARK

Describes the theory and practice of separation of optical antipodes and enantiomers by means of chromatography. Provides the reader with a thorough treatment of the principles and ideas behind various chiral stationary phases used in gas and liquid chromatography, and gives a comprehensive account of the many areas under development.

approx. 230 pp. (0-21080-X) May 1988 \$64.95

## SILICON CHEMISTRY

E.R. COREY, J.Y. COREY, and P.P. GASPAR

Introduces the important industrial uses of organo-silicon chemistry which includes the application of silicon as an agent for the alloying and de-oxidizing of metals, the production of silanes and organo-metallic compounds, and its uses as a semiconductor.

565 pp. (0-21081-8) 1988 \$99.95

## MOLECULAR LUMINESCENCE SPECTROSCOPY

Methods and Applications, Part Two  
(Chemical Analysis Series)

STEPHEN G. SCHULMAN

Considers various aspects of the analysis of solids and solid solutions. Describes analysis based on the temporal and phase characteristics of luminescence spectra and the application of these forms of analysis to the evaluation of very fast chemical reactions.

574 pp. (1-63684-3) May 1988 \$65.00

## VISIBLE AND ULTRAVIOLET SPECTROSCOPY

(Analytical Chemistry by Open Learning Series)

RONALD C. DENNEY and ROY SINCLAIR

This volume in the ACOL series covers the theory and practice of UV/visible spectrometry for both quantitative and qualitative chemical analysis.

197 pp. (1-91379-0) 1988 \$21.95

## LASER RAMAN SPECTROMETRY

Analytical Applications

(Ellis Horwood Series)

HALINA BARAŃSKA, ANNA LABUDZIŃSKA, and

JACEK TERPIŃSKI

This straightforward introduction to analytical Raman spectrometry explains the fundamentals of the theory of Raman scattering, and gives practical examples of identifications and quantitative analyses.

271 pp. (0-20829-5) 1988 \$64.95

## STATISTICS FOR ANALYTICAL CHEMISTRY, 2nd Ed.

(Ellis Horwood Series)

J.C. MILLER and J.N. MILLER

The second edition shows some of the important new advances which have taken place recently. An entirely new chapter has been introduced to give extended coverage of sampling and of control charts.

227 pp. (0-20902-X) 1988 \$39.95

Order through your bookstore or write to Jules Kazimir,  
Dept. 9-0400.

FOR FREE 15-DAY EXAM CALL TOLL-FREE

**1-800-526-5368**

In New Jersey, call collect (201) 342-6707.

Order Code # 9-0400



WILEY

## WILEY-INTERSCIENCE

John Wiley & Sons, Inc.

605 Third Avenue, New York, NY 10158

IN CANADA:

22 Worcester Road, Rexdale, Ontario M9W 1L1

Prices subject to change and higher in Canada.

092-90400

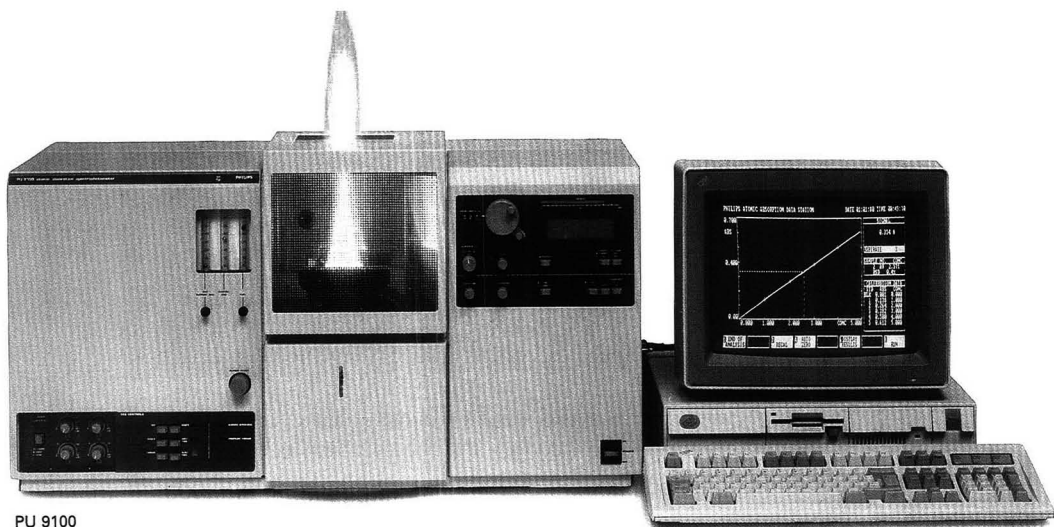
CIRCLE 180 ON READER SERVICE CARD



# PHILIPS

*Philips Analytical*

*Only one thing in AA  
could improve on the famous SP9.*



PU 9100

*Its successor.*

Our SP9 was one of the most popular AA instruments ever.

The PU9100 series is a worthy successor. Of course, it has the qualities you've come to expect from Philips Analytical: versatility, superb performance and high reliability.

Add IBM compatible software, featuring the Philips Analytical Intuitive User Interface – and system control and data handling have never been easier.

Write or 'phone now for more details of the new PU9100.



**BIGGER IDEAS FOR BETTER ANALYSIS**

**Philips Scientific Analytical Division**

York Street, Cambridge Great Britain CB1 2PX

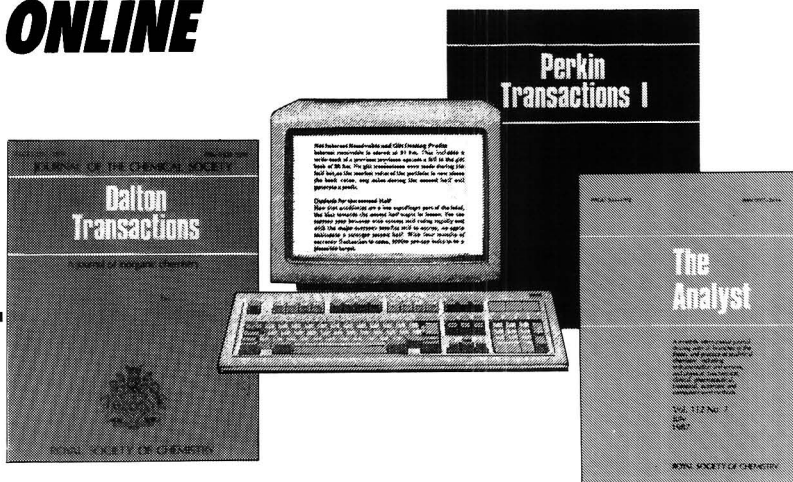
Tel: 0223 358866 Telex: 817331 Fax: 0223 312764

CIRCLE 130 ON READER SERVICE CARD

AA 23 a



# NOW YOU CAN SEARCH RSC JOURNALS ONLINE



The main primary journals published by the Royal Society of Chemistry (RSC) are now searchable online via **CHEMICAL JOURNALS ONLINE (CJO)** – a family of new online files produced by the American Chemical Society and available through STN International.

The RSC journals file (**CJRSC**) includes Chemical Communications, Dalton Transactions, Faraday Transactions (I\* & II), Perkin Transactions (I & II), The Analyst, Journal of Chemical Research,\* Journal of Analytical Atomic Spectrometry, Faraday Discussions.  
\*Available from 1988

**CJRSC** may be searched alone or in conjunction with other components of the **CJO** database which includes ACS journals and polymer journals published by Wiley.

The unique Crossover facility from STN enables you to perform the same search on **CJRSC** and **CAS ONLINE** thereby combining the breadth of coverage of Chemical Abstracts with the depth of coverage of RSC journals.

Online access to the RSC journals provides you with a convenient, rapid and economical means of keeping up with the latest significant research in the chemical sciences.

*For more information, call (614) 421-3600, or return the form below to: STN International, c/o Chemical Abstracts Service, 2540 Olentangy River Road, P.O. Box 02228, Columbus, OH 43210.*

Please send me more information on CJRSC and the Chemical Journals Online data base.

Name .....

Address .....

.....  
.....

**CHEMICAL JOURNALS  
ONLINE**

# IMPOSSIBLE TO CHANGE A FILTER DURING ANALYSIS WITHIN TWO MINUTES?



WITH THE CHROMPACK GAS CLEAN SYSTEM IT CAN BE ACHIEVED

 **CHROMPACK**

FROM CHROMATOGRAPHERS - FOR CHROMATOGRAPHERS

Chrompack International, P.O. Box 8033, 4330 EA Middelburg The Netherlands. Tel. 31 1180-27352 Telex chrom nl 37852 Fax 31 1180-33118 Subsidiaries: Middelburg, The Netherlands; Antwerp, Belgium; Paris, France; Frankfurt, West Germany; London, U.K.; Bienenheim, Canada; Bridgewater, USA; Milano, Italy



## Fluka High-Purity Water

Fluka offers 3 types of high-purity water for various applications requiring stringent quality standards.

In most water purification systems the main quality criterion is the specific resistance of the produced water. However, this parameter reflects only the ionic impurities. Thus, water with a resistivity of  $1.8 \times 10^7 \Omega\text{cm}$  may not

be suitable for many applications in inorganic trace analysis, HPLC, UV spectroscopy, or in cell and tissue cultures, biochemistry and microbiology.

That is why Fluka has included additional quality criteria for its high-purity water: trace analysis, UV absorbance at wavelengths down to 200 nm, HPLC gradient and microbiological tests.

The specific limits which have to be fulfilled by our high-purity water are listed under the corresponding product descriptions. In order to maintain a constant high quality during storage, Water for UV spectroscopy and Water for HPLC are bottled in glass. Water for inorganic trace analysis is supplied in polyethylene containers to prevent contamination with metal ions.

### 95303

#### Water

H<sub>2</sub>O M<sub>r</sub> 18.02 [7732-18-5]

for UV spectroscopy

d<sub>20</sub><sup>20</sup> 1.00

Fluka Guarantee:

Absorption:

Wave length in nm:

Max. absorption:

1 l sFr. 20.- 2.5 l sFr. 46.-

Reference cell: air

200 220 240 260 280 300  
0.07 0.05 0.04 0.04 0.04 0.04

### 95304

#### Water

H<sub>2</sub>O M<sub>r</sub> 18.02 [7732-18-5]

for HPLC

filtered through a 0.2 µm membrane filter

d<sub>20</sub><sup>20</sup> 1.00

further specification: specific resistance at 25°C:  $1.8 \times 10^7 \Omega\text{cm}$ , measured during production

Absorption:

Wave length in nm:

Max. absorption:

1 l sFr. 14.- 2.5 l sFr. 29.-

200

0.01

### 95305

#### Water

H<sub>2</sub>O M<sub>r</sub> 18.02 [7732-18-5]

for inorganic trace analysis

filtered through a 0.2 µm membrane filter

d<sub>20</sub><sup>20</sup> 1.00

further specification: specific resistance at 25°C:  $1.8 \times 10^7 \Omega\text{cm}$ , measured during production

Fluka Guarantee:

Residue on evaporation:

Residue on ignition:

KMnO<sub>4</sub>-reducing matter (as O):

Al < 0.0000005 %

Ba < 0.0000005 %

Bi < 0.0000005 %

Ca < 0.000001 %

Cd < 0.0000005 %

Co < 0.0000005 %

Cr < 0.0000005 %

Cu < 0.0000005 %

Fe < 0.0000005 %

K < 0.000001 %

1 l sFr. 18.-

< 0.001 %

< 0.0005 %

< 0.000003 %

Li < 0.0000005 %

Mg < 0.0000005 %

Mn < 0.0000005 %

Mo < 0.0000005 %

Na < 0.000001 %

NH<sub>4</sub> < 0.000005 %

Ni < 0.0000005 %

Pb < 0.0000005 %

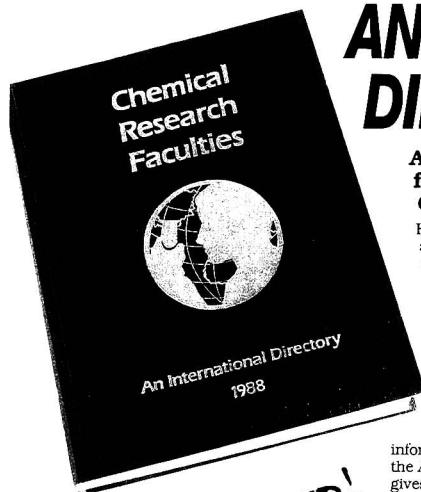
Sr < 0.0000005 %

Zn < 0.0000005 %

# CHEMICAL RESEARCH FACULTIES

## AN INTERNATIONAL DIRECTORY, 1988

More than a third ALL-NEW! information!



UPDATED!

**\$159.95** in the U.S. and Canada  
**\$191.95** in all other countries

### An invaluable resource from the American Chemical Society.

Here it is—all the information you need about chemical research and researchers at universities around the world, gathered into one volume.

*Chemical Research Faculties: An International Directory* contains a wealth of facts on more than 11,500 faculty members and 1922 departments in 107 countries. And it's a book no academic institution or chemically oriented business can afford to be without.

Designed to provide the same type of information on an international scale that the *ACS Directory of Graduate Research* gives for U.S. and Canadian schools, *Chemical Research Faculties: An International Directory* includes listings for chemistry, chemical engineering, biochemistry, pharmaceutical/medicinal chemistry, and toxicology.

It offers informative statistical tables on graduate programs worldwide. Organizes data on 72 chemical and chemical engineering societies in 54 nations. And is

cross-referenced three ways—by faculty, institution, and research subject—for easy use.

The 1988 edition has been expanded by a full third—and includes listings for toxicology departments and chemical engineering societies.

### Indispensable for industry and academia alike.

If you're involved in chemical research, *Chemical Research Faculties: An International Directory* can keep you abreast of the latest developments in your area of specialization.

If you advise graduate students, it can help you steer them toward the programs they're seeking.

And if you're in a business even remotely related to chemical research, just one of the thousands of leads this book contains could pay for the purchase price many times over.

Why not fill out the attached order form right now? Or call 800/227-5558 and charge your VISA, MasterCard, American Express, or Diners Club/Carte Blanche.

And let *Chemical Research Faculties: An International Directory* open up a whole new world of professional possibilities.

### ORDER FORM

☐ **YES! Please rush me my copy of the new international directory!**

**Chemical Research Faculties: An International Directory, 1988 Edition**

QTY. U.S./ CANADA EXPORT TOTAL

**\$159.95 \$191.95**  
AMOUNT ENCLOSED

☐ I have enclosed a check for \$\_\_\_\_\_ payable to the American Chemical Society.

☐ Purchase Order #\_\_\_\_\_ enclosed.

Charge my ☐ VISA ☐ MasterCard ☐ American Express  
☐ Barclaycard ☐ Access ☐ Diners Club/  
Carte Blanche.

Name of cardholder \_\_\_\_\_

Account # \_\_\_\_\_

Expires \_\_\_\_\_

Interbank # \_\_\_\_\_

(MasterCard and Access)

Signature \_\_\_\_\_

Note: Please allow four to six weeks for delivery. Foreign payment must be made in U.S. currency by international money order, UNESCO coupons, or U.S. bank draft. Order through your local bookseller or directly from the American Chemical Society. Orders from individuals must be prepaid.

#### PLEASE SHIP BOOKS TO:

Name \_\_\_\_\_

Address \_\_\_\_\_

TO ORDER IN THE U.S., CALL (800) 227-5558.

262

MAIL THIS ORDER FORM TO: American Chemical Society

Distribution Office, Department 262

P.O. Box 57136

West End Station

Washington, D.C. 20037

☐ Please send me more information about the *ACS Directory of Graduate Research 1987*, which gives similar data for U.S. schools.

#### Departmental Information

includes address and phone number, name of department head, advanced degrees offered, and principal areas of research.

#### Guide to Chemical Research Institutions

lists all countries, universities, and departments in order of appearance, providing an overview of each section.

#### Statistical Tables

provide for each country the number of master's and doctoral degrees conferred in 1985 and 1986 as well as the number of full-time faculty, post-doctoral appointments, and students enrolled in advanced degree programs.

#### Faculty Information

includes name, year of birth, title, degrees (with years and institutions), areas of specialization, current research, and recent publications.

#### Four Organizational Sections

break down listings into chemistry, chemical engineering, biochemistry, pharmaceutical/medicinal chemistry, and toxicology.

#### Chemical Society Information

lists address, principal officer, publications, purpose, organizational structure, and number of members.

#### Faculty Index

helps you keep up with colleagues' moves and learn more about others in your area of specialization.

#### Institutional Index

provides a merged alphabetical listing that lets you find institutions known by name but not location.

#### Index of Research Subjects

helps you locate universities, departments, and individuals doing research related to your own.



FREE  
TELEPHONE  
ORDERING

**1-800-227-5558**

Washington, D.C. area residents  
call 872-8065 or 872-8066

# NEW PRODUCTS



**Model 115 variable-wavelength UV detector** features a sensitivity range of 0.001–1.0 AUFS (10-mm light path), 2% typical peak-to-peak noise levels at 0.001 AUFS, and front-panel wavelength, sensitivity, and time constant controls. Gilson Medical Electronics **401**

**SEM.** Model SX-40A scanning electron microscope operates at accelerating voltages from 1 to 30 kV and accommodates samples up to 6 in. in diameter. The microscope's evacuation system, high-voltage turn-on function, and emission setting are automated for one-touch sequencing. International Scientific Instruments **404**

**LC detector.** Model 1000S diode array detector performs spectral scans with sensitivity of 0.002 AUFS and <1% noise under flowing conditions. The detector contains four independent channels that can be programmed to monitor absorbance at different wavelengths and ranges. Applied Biosystems **405**

**X-ray spectroscopy.** X-ray micro-fluorescence spectroscopy system provides X-ray fluorescence analysis with an XY spatial resolution of 10–100  $\mu$ m. Applications include geological and biological samples, phase-separated alloys, and microelectronic components. KeveX **406**

**Mercury.** Merc 22 automated mercury analyzer, consisting of an autosampler, hydride generator, spectrofluorometer, and computer, determines mercury at levels of ~0.1 ppb and can run 40 samples per hour unattended. The software contains programs for calibration,

automatic periodic recalibration, and dilution. Questron **407**

**ICP.** Ultrasonic nebulization system permits simultaneous multielement determination of all EPA priority pollutant elements, including As, Se, Pb, Sb, and Tl, in drinking and wastewater samples. The system is composed of an ultrasonic nebulizer, spray chamber, and aerosol desolvation glassware. Baird **408**

**Particle size.** SALD-1000 laser diffraction particle size analyzer features a measurement range of 0.25–500  $\mu$ m and analysis times of <3 min per sample. Particle systems of nonuniform densities can be measured whether suspended in a flowing or stationary liquid. Shimadzu **409**

**Gas analyzer.** M200 incorporates two complete gas chromatographs that perform high-resolution analyses in one-fiftieth of the time required by conventional instruments. The analyzer, which is 10 in. wide and weighs 12 lbs, contains 4-m, 100- $\mu$ m i.d. fused-silica columns and a micro thermal conductivity detector fabricated in silicon. Microsensor Technology **410**

**Sample preparation.** MasterLab II, consisting of a five-axis articulated arm, an IBM Personal System/2 Model

30 computer, and software, automates the entire sample preparation process. A sixth axis can be added using an optional linear transport device. Perkin-Elmer **411**

**Densitometer.** Model 300A computing densitometer uses a line scanner and an integrating cylinder to analyze an entire electrophoresis gel in ~3 min. The software allows results from up to four gels to be viewed simultaneously for comparison. Molecular Dynamics **412**

**Detector.** Backscattered electron detector, designed for use in scanning electron microscope applications, is composed of four N-type silicon diffused junction diodes (1 cm<sup>2</sup> each) arranged in an annular form. The detector operates in a biased TV mode and in a zero-biased mode for quantitative analysis. Link Analytical **413**

## Software

**Educational software.** SQUALOR, Simulated Qualitative Organic Analysis, allows students to identify unknowns by choosing from 24 classification tests and 18 derivative-forming reactions for 11 different functional groups. Instructors can prepare their own data disks and edit or add new unknowns. COMPRESS **415**

**Equations.** MacEqn provides an environment for generating equations for inclusion into documents written with Macintosh word-processing programs. Constructs such as integrals, summations, products, and fractions can be introduced without having to exit the word processor. Software for Recognition Technologies **416**

---

**For more information on listed items, circle the appropriate numbers on one of our Readers' Service Cards**

---



# An Easier Link to MSDS

- Mallinckrodt's Lab-Link II® allows access to over 1400 Material Safety Data Sheets
- Lab-Link II also includes the complete 1987-88 Mallinckrodt catalog on diskette
- Lab-Link II carries all chemicals and quantity requirements detailed under SARA Title III regulations (Sections 302, 304 and 313)
- Emergency phone numbers can be customized by the user for quick access whenever needed
- On-line help answers questions, prevents problems
- Software and manual are easy to understand and use



## Mallinckrodt Lab-Link II®

CIRCLE 102 ON READER SERVICE CARD

# Metal Detection— Pure & Simple

- Mallinckrodt's AR® Select™ nitric, sulfuric and hydrochloric acids have certified lead and mercury levels of only 0.0005 ppm (0.5 ppb)
- Other metal levels have been reduced significantly to lower detection limits for critical metallic analysis
- Lead and mercury are at state-of-the-art detection levels for this purity grade, providing wider applications at lower testing ranges
- AR Select acids may be used to test trace metal levels in water, food, soil, body tissue, industrial samples, etc.
- AR Select acids are packaged in convenient 5 pt and 500 ml containers, immediately available and competitively priced

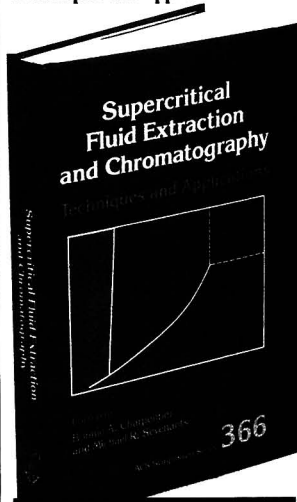


## Mallinckrodt AR® Select™

CIRCLE 103 ON READER SERVICE CARD

# Supercritical Fluid Extraction and Chromatography

## Techniques and Applications



One of the most pervasive problems in chemistry is the separation of complex materials into component parts, either to characterize a mixture or natural product or to remove a particular component from the matrix. This new book chronicles the exciting developments in supercritical fluid extraction and chromatography, particularly as applied to food systems. You'll gain in-depth knowledge on the history, current research, instrumentation, applications, and trends in this rapidly evolving field. You'll benefit from the expertise of some of the most prominent researchers working in supercritical fluids. *Supercritical Fluid Extraction and Chromatography* offers viewpoints from academia, government, and industry. Anyone working in the foods and flavors industries will find this volume a must-have resource.

Bonnie A. Charpentier and Michael R. Sevenants, Editors, *The Proctor & Gamble Company*

Developed from a symposium sponsored by the Division of Agricultural and Food Chemistry of the American Chemical Society

ACS Symposium Series No. 366  
262 pages (1988) Clothbound  
ISBN 0-8412-1469-7 LC 88-3466  
US & Canada \$59.95 Export \$71.95

Order from: American Chemical Society  
Distribution Office Dept. 84  
1155 Sixteenth St. N.W.  
Washington, DC 20036

or CALL TOLL FREE

**800-227-5558**  
and use your credit card!

## NEW PRODUCTS

### Manufacturers' Literature

**ICP newsletter.** *Leeman Letter*, No. 7, contains information on the Hildebrand grid nebulizer, tracking precious metals in wastewater, and the 1988 Winter Conference on Plasma Spectrochemistry. 6 pp. Leeman Labs 418

**GC.** Brochure highlights the Hall 1000 electrolytic conductivity detector, which features a microprocessor controller and an interactive LCD display for programming and readout of important operating parameters. 4 pp. Tracor Instruments 419

**Freeze drying.** "A Guide to Freeze Drying for the Laboratory" discusses the three steps of the freeze-drying process, a typical freeze-drying cycle and methods to facilitate the process, and suggestions for optimizing results. Labconco 420

**Newsletter.** *Focal Points* features information on micro- and ultrafiltration. Vol. I, Issue 1 contains articles on protein adsorption of filter materials, venting parameters, and cell harvesting and crossflow. 4 pp. Sartorius Filters 422

**LC.** Handbook describes the use of cyclodextrin-bonded phases in HPLC. Included is information on mobile-phase design; salt, pH, and temperature effects; regeneration; storage; and column stability. 12 pp. Advanced Separation Technologies 423

**LC/MS.** Brochure highlights the Model 201 dedicated LC/MS systems. A discussion of problem-solving capabilities and detailed descriptions of the thermospray vaporizer, ion source, controller, mass analyzer, and vacuum system are provided. 4 pp. Vestec 424

### Catalogs

**LC.** Catalog features HPLC fittings, including filters, tubing, guard columns, adapters, and unions. Products for microbore, supercritical fluid, and preparative applications are included. 88 pp. Upchurch Scientific 426

**Standards.** Catalog lists standards for environmental testing, including PCB isomers, chlorinated dioxin and furan standards, and kits required for EPA methods. The standards are available neat or in solution. 80 pp. Ultra Scientific 427

**Glassware.** Catalog features micro-scale glassware, including flasks, adapters, beakers, chromatography columns, connectors, distillation apparatus, evaporative concentrators, and NMR tubes. 48 pp. Kontes 428

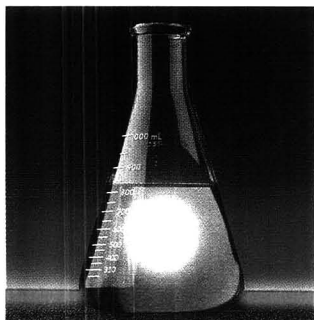
**Analytical supplies.** Catalog includes GC and LC columns; products for GC, HPLC, UV/vis, and GC/MS instruments; and laboratory robot supplies. A chromatography reference guide is also included. 248 pp. Hewlett-Packard 429



**ViscoSystem AVS 500** is a high-speed, fully automated viscosity measuring system for testing clear, opaque, and corrosive liquids. The system features a 12- or 36-position carousel that allows samples to be run continuously without supervision. Schott

402

# DIALOG. THINK OF IT AS A CATALYST.



Dialog puts ideas in motion. It's the force that changes the way you look at problems and solutions. Maybe even previous hypotheses.

We're the largest online knowledgebank in the world. Our databases have the chemical property, toxicity, regulatory and patent information you need.

We have chemical substance, substructure and identification information online. Dialog also offers other databases covering molecular formulae, ring data and properties.

But what really sets Dialog apart is how thoroughly we cover so many differ-

ent industries from chemistry to agriculture to biotechnology. We can make a big difference when a project demands more than chemical information. Since it's all on one service, you'll have what you need, quickly and easily.

With Dialog you get more than in-depth information. You get quality service and training.

We're reasonable, too. All you pay for is the time you spend using Dialog. There is no minimum usage requirement.

So when you need a catalyst to get ideas going, or to push them further, turn to Dialog. And watch how your mind reacts.

Ask your librarian or information center if your company has DIALOG. If not call 800-3-DIALOG (800-334-2564) today. Or write to us at, 3460 Hillview Ave., Palo Alto, CA 94304.

**DIALOG**<sup>®</sup> INFORMATION SERVICES, INC.  
A SUBSIDIARY OF LOCKHEED CORP

*The world's largest online knowledgebank.*

**800-3-DIALOG**

Dialog is a service mark of Dialog Services Inc. Reg. U.S. Patent and Trademark office.

CIRCLE 32 ON READER SERVICE CARD

ANALYTICAL CHEMISTRY, VOL. 60, NO. 10, MAY 15, 1988 • 645 A

# HRLC™: The new generation in HPLC.

## From Bio-Rad, new answers, new ideas, and new technology for chromatography.

High Resolution Liquid Chromatography (HRLC) combines speed, performance, and high pressure operation with three decades of Bio-Rad chromatography expertise. Whether your application requires analytical or preparative techniques, we can tailor a high resolution system designed for your individual needs. Here are some of the exciting new options you can choose from:

### New solvent delivery system

- New **dual piston pump** featuring Soft Start™ operation which provides automatic ramping to the final flow rate. This gradual build-up action protects your columns and lengthens their operating life.
- New **flow diagnostics** guide lets you pinpoint troubles that may affect your system.
- **Bio-compatible** option is a titanium-based flow system which provides an inert solvent delivery flow path.
- Optional pump configurations offer flow rates from **0.02 ml/min** to **40 ml/min** and operating pressures up to **6000 psi**.

### New IBM®-based chromatography workstation

- Choice of IBM PC, PC-XT or PC-AT computers.
- Runs up to **3 independent HPLC** systems, taking advantage of the IBM multitasking operating capability.

IBM is a trademark of International Business Machines

- Provides **complete control** of your HPLC system, including binary or ternary gradients, injectors, and samplers. Runs up to 6 pumps simultaneously.

### Sophisticated data analysis

- Up to six channels of **data collection** with super-imposable **video strip charts** and microvolt sensitivity.
- Multi-level **calibration** using linear or non-linear regression analysis.
- **Full color graphics** and on-screen baseline and data manipulations.

### Pre-assembled, pre-tested modular systems

- All Bio-Rad's modular systems are pre-assembled, pre-calibrated, and pre-plumbed, and supplied complete with **all hardware** for your application.
- All systems come with a **test column** and accompanying **test chromatogram**.

### Customized systems

- Bio-Rad takes great care in tailoring systems that meet your needs. We supply complete systems, including a variety of detectors, unparalleled selection of column chemistries and a complete line of accessories.

### It's the Chemistry that Counts™

Remember, Bio-Rad is both a **chemistry** company and an **instrument** company, which makes us unique. We are pre-eminently qualified to contribute to your HPLC requirements. Contact us today for more information.



**Chemical  
Division**

1414 Harbour Way South  
Richmond, CA 94804  
(415) 232-7000  
800-843-1412

Also in Rockville Centre, NY; Hornsby, Australia; Vienna,  
Austria; Mississauga, Canada; Watford, England; Munich,  
Germany; Milan, Italy; Tokyo, Japan; Utrecht, The Nether-  
lands; and Glatfbrugg, Switzerland.

**It's the Chemistry that Counts.™**

CIRCLE 16 ON READER SERVICE CARD

## What was Leaking from a

Ronald A. Hites

School of Public and Environmental Affairs  
and Department of Chemistry  
Indiana University  
Bloomington, Ind. 47405

The city of Niagara Falls, N.Y., is the home of several toxic waste disposal sites, the most famous of which is Love Canal. Although less well known, the Hyde Park dump is equally noxious. This hazardous-waste dump was operated by the Hooker Chemical Company from about 1953 to 1975. Approximately 55,000 tons of halogenated waste were buried at this site, which is just north of the city. The Hyde Park dump is drained by Bloody Run Creek (named for an old Indian battle).

In the early stages of a study of the impacts of hazardous-waste dumps on Lake Ontario, it was important for our research group to identify the structures of the organic compounds leaking from the Hyde Park dump. We were particularly interested in compounds with "odd" structures that could serve as long-range markers of the effluent from this particular dump. We began by sampling sediment from the Bloody Run Creek.

The sediment samples were extracted with isopropyl alcohol and dichloro-



methane in a Soxhlet apparatus, and the extracts were fractionated on a silica gel column. The resulting fractions were analyzed by gas chromatographic mass spectrometry (GC/MS) operating in the electron-impact mode. The mass spectra of several common compounds (such as chlorobenzenes, chlorotoluenes, and chlorophenols) were easily interpreted, but the spectra of two un-

usual compounds especially attracted our attention. These spectra are shown in Figures 1 and 2. In both cases, we noticed the presence of fragment ions that indicated that the molecules contained one or more fluorine atoms. What were the exact structures of these compounds?

Compound A (see Figure 1) clearly has a molecular weight of 340 and shows a two-chlorine isotope pattern; that is, the ratio of  $m/z$  340 to 342 to 344 is about 9:6:1, which is what would be predicted from the natural isotope ratios of  $^{35}\text{Cl}$  and  $^{37}\text{Cl}$ . The ion cluster at  $m/z$  321 also shows a two-chlorine isotope pattern and represents a loss of 19 daltons from the molecular ion; this must be the loss of a fluorine atom. Another important ion is at  $m/z$  305; this ion shows an isotope pattern indicative of a single chlorine atom that agrees with a 35-dalton (the mass of chlorine) loss from the molecular ion at  $m/z$  340. The ion at  $m/z$  285 has only one chlorine atom and represents a loss of 20 daltons from the ion at  $m/z$  305; this is attributable to the elimination of HF.

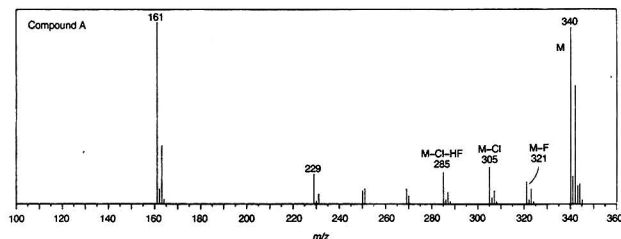


**Figure 1.** Mass spectrum of Compound A found in the sediment of Bloody Run Creek, which drains the Hyde Park dump in Niagara Falls, N.Y.



The relatively high abundance of the molecular ion suggests that Compound A is aromatic. The abundant ion at  $m/z$  161 contains one of the molecule's two chlorine atoms and about half of its mass. Based on the high abundance of this ion, we can speculate that the molecule may contain two aromatic halves, each with its own chlorine atom. To summarize, we know that the molecule contains two and only two chlorine atoms and one or more fluorine atoms and that it has an aromatic carbon skeleton consisting, perhaps, of two aromatic parts.

At this point in the interpretation, we decided to study the literature to see which aromatic compounds containing chlorine and fluorine were manufactured in the vicinity of Niagara Falls. We knew we were dealing with a dump site used by the Hooker Chemical Company, and it seemed likely that the chemicals leaking from this dump were related to this company's products. The literature and a few tactful phone calls soon told us that 4-chloro(trifluoromethyl)benzene was the only compound that met the above requirements.

Based on this hint, we returned to the mass spectrum of Compound A. We noted that 4-chloro(trifluoromethyl)benzene weighed 180 daltons and that, if we dimerized this compound by the loss of HF, we would have a molecule that weighed 340 daltons and contained two chlorine atoms. This agreed with our unknown. Unfortunately, this dimer was not listed in *Chemical Abstracts*; thus, we were on our own in confirming our tentative identification.

We realized that this dimer could have been the result of a Friedel-Crafts reaction taking place during the production of 4-chloro(trifluoromethyl)benzene, which is made by the high-pressure fluorination of 4-chloro(trichloromethyl)benzene, as indicated in the upper right of Figure 3. The reaction scheme leading to Compound A is detailed on the right-hand side of Figure 3. Two molecules of the starting material could condense to form a heptachloro intermediate (Dimer A), which, upon subsequent fluorination, would give Compound A. We carried out these reactions in our laboratory and obtained a compound that had the same mass spectrum and gas chromatographic retention time as Compound A.

The mass spectrum of Compound A (see Figure 1) shows major fragment ions at  $m/z$  161 and 229. These ions represent cleavage on either side of the central  $CF_2$  unit (see Figure 3). The  $m/z$  161 ion probably has a seven-membered ring structure substituted with one chlorine and two fluorine atoms. The ion at  $m/z$  229 is also probably a

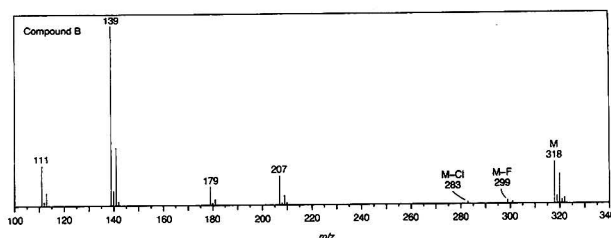


**Figure 2.** Mass spectrum of Compound B, also found in Bloody Run Creek sediment (see Figure 1).

seven-membered ring, but in this case it is substituted with one chlorine and two fluorine atoms and with a trifluoromethyl group. It is known that ions of this type (called tropylium ions) are particularly stable and thus are abundant in the mass spectra of many aromatic compounds.

Compound B, the mass spectrum of which is shown in Figure 2, was also found in the sediment of Bloody Run Creek. Clearly, this compound is aromatic (abundant molecular ion), and it contains two chlorine atoms and at least one fluorine atom (fragment ion at  $m/z$  299 from the loss of 19 daltons from the molecular ion). The molecular weight is 318 daltons, which is 22 less than that of Compound A. Because of the presence of chlorine and fluorine atoms, it was reasonable to assume that Compounds A and B were related. Thus we asked ourselves what would account for a mass difference of 22 dal-

tons. We soon realized that this is the mass difference between a  $CF_2$  group (50 daltons) and carbonyl group (28 daltons). We therefore formed the hypothesis that Compound B was a benzophenone substituted with one chlorine atom on one ring with another chlorine and a trifluoromethyl group on the other. The major fragment ions at  $m/z$  139 and 179 would be attributable to cleavage on one side of the carbonyl group, and those at  $m/z$  111 and 207 to cleavage on the other side (see Figure 3). Note that the masses of both pairs of ions add up to 318 daltons, the molecular weight.

As shown in the middle of Figure 3, this benzophenone could also have been formed during the production of 4-chloro(trifluoromethyl)benzene from the heptachloro intermediate (Dimer A). If this dimer were to have been hydrolyzed and then fluorinated, Compound B would have resulted. We veri-

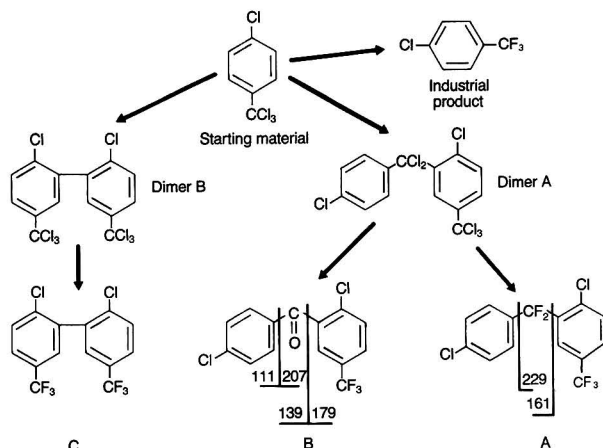
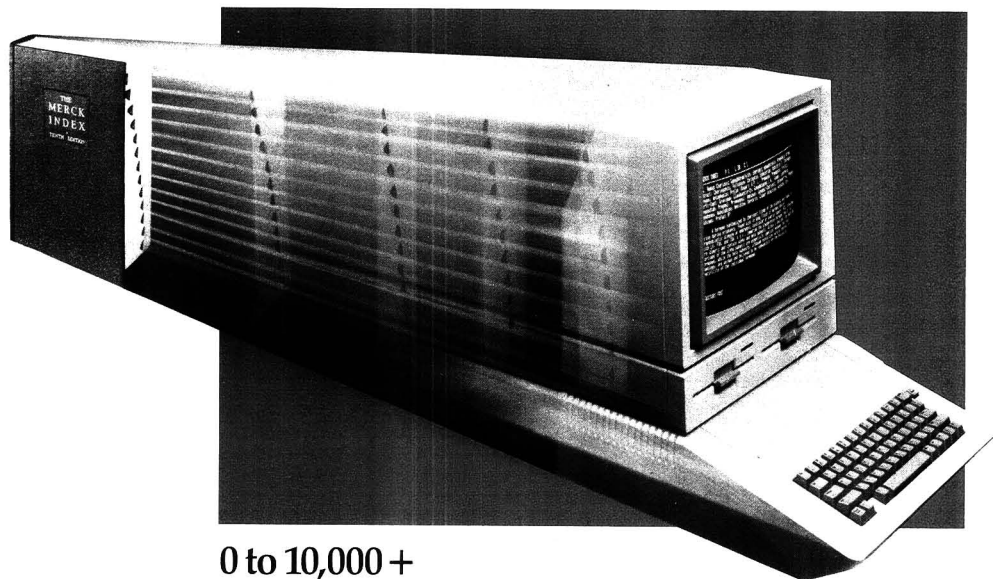


**Figure 3.** Scheme showing the genesis of Compounds A, B, and C from 4-chloro-(trichloromethyl)benzene, the precursor of 4-chloro(trifluoromethyl)benzene. The mass spectral fragmentation of Compounds A and B is indicated at the bottom.



0 to 10,000 +  
in milliseconds

# THE MERCK INDEX **ONLINE**<sup>†</sup>

## Instant access to the most widely used chemical/biomedical encyclopedia in the world

With THE MERCK INDEX ONLINE, retrieve pertinent information directly, instantly, on over 30,000 chemical, drug, and biological substances. Search for groups of compounds related by physical or chemical properties or pharmacological activity. Select records by patent assignees or trademark ownership.

Over 10,000 monographs, some not yet in print, contain information on physical and chemical properties, chemical names, trademarks, molecular formulae, literature references, toxicity data, and medical, veterinary, and commercial uses.

Semi-annual updates provide a current and convenient reference source for chemists, biologists, researchers, writers, and students.

The ideal companion to THE MERCK INDEX ONLINE:  
**THE MERCK INDEX** (10th Edition, 1983)

To order your copy, send a check or money order for \$28.50, payable to Merck & Co., Inc., to Professional Handbooks Dept., Merck & Co., Inc., P.O. Box 2000, Rahway, NJ 07065-0901.

<sup>†</sup>THE MERCK INDEX ONLINE is a mark of Merck & Co., Inc.

Merck & Co., Inc., a research-intensive company, has published THE MERCK INDEX as a non-profit service to the scientific and medical communities since 1889.



**THE MERCK INDEX **ONLINE****

Available through: BRS (800) 345-4BRS  
CIS (800) CIS-USER  
Questel (800) 424-9600  
And now, DIALOG (800) 3-DIALOG

CIRCLE 94 ON READER SERVICE CARD

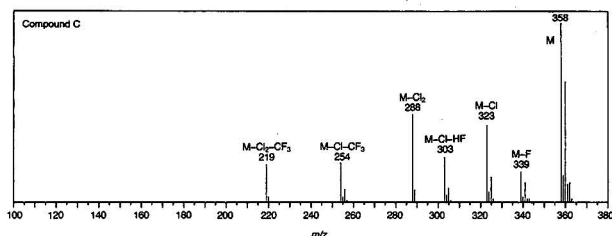


**Figure 4.** Mass spectrum of Compound C, found in fish taken from the Niagara River and Lake Ontario.

fied this reaction scheme in our laboratory and used it to synthesize an authentic sample of Compound B. The mass spectrum and gas chromatographic retention time of the synthetic product were the same as those of the unknown.

Some time after we identified Compounds A and B, we were examining GC/MS data obtained from extracts of fish caught in the Niagara River downstream from the city of Niagara Falls and from Lake Ontario itself. The mass spectrum shown in Figure 4 seemed somehow familiar. This spectrum was of a compound that contained two chlorine atoms (note the 9:6:1 isotope pattern at  $m/z$  358) and at least one fluorine atom (note the ion at  $m/z$  339, which corresponds to the loss of a fluorine atom from the molecular ion). Other ions showing the losses of chlorine and fluorine atoms were also observed at  $m/z$  303, 254, and 219. It seemed reasonable to assume that this compound was related to Compounds A and B.

The molecular weight of Compound C was 358 daltons. Remembering that two 4-chloro(trifluoromethyl)benzenes weighed 360 daltons, we noted that a simple dimerization with the loss of two hydrogen atoms would give the correct molecular weight. This dimer would be a biphenyl substituted with two chlorine atoms and two trifluoromethyl groups (see the left side of Figure 3). This compound could have resulted from the fluorination of a dimer of 4-chloro(trichloromethyl)benzene (see Dimer B in Figure 3). Compound C was synthesized, and its GC retention time and mass spectrum were identical to those of the unknown.

The identification of these three compounds was particularly fortuitous. Their structures were sufficiently unusual such that they could and did serve as tracers of material leaking from the Hyde Park dump. Unfortunately, electron-impact MS was not sensitive enough for the determination of these compounds in sediments remote from the waste disposal site. An-

other approach was necessary. We turned to electron-capture, negative ion MS. Molecules with several halogen atoms respond well using this technique. Because Compounds A to C have several fluorine and chlorine atoms, we were able to measure as few as 5 pg of Compound C in sediment from Lake Ontario using this technique. In fact, we were able to show that all of these compounds were in sediment and fish taken at distances exceeding 300 km from the source. This is another example of the ubiquity of some lipophilic, industrial organic compounds in the environment.

I thank Paul Chen, Vince Elder, Rudy Jaffe, Ray Kaminsky, and Bertha Proctor for their considerable technical contributions to various parts of this project. The work was supported by a series of three U.S. Environmental Protection Agency grants (R806350, R808865, and R808961).

#### Suggested reading

This work is part of a larger project described in detail in the following publications.

- (1) Elder, V. A.; Proctor, B. L.; Hites, R. A. *Environ. Sci. Technol.* 1981, 15, 1237.
- (2) Kaminsky, R.; Kaiser, K. L. E.; Hites, R. A. *J. Great Lakes Res.* 1983, 9, 183.
- (3) Jaffe, R.; Hites, R. A. *Environ. Sci. Technol.* 1985, 19, 736.
- (4) Jaffe, R.; Hites, R. A. *Environ. Sci. Technol.* 1986, 20, 267.
- (5) Jaffe, R.; Hites, R. A. *J. Great Lakes Res.* 1986, 12, 63.

Ronald A. Hites, professor of public and environmental affairs and professor of chemistry at Indiana University, received a B.A. degree from Oakland University, Rochester, Mich. (1964) and a Ph.D. degree in analytical chemistry (1968) from M.I.T. under the guidance of Klaus Biemann. He joined the faculty at Indiana in 1979 after serving on the faculty of chemical engineering at M.I.T. He is the president-elect of the American Society of Mass Spectrometry. His research interests include the study of toxic and organic compounds in the environment.

**Keep current on government activities  
as they affect the field of chemistry with**

## ACSWASHINGTON alert

This informative bi-weekly publication covers Federal activities as they concern science in general—and chemistry in particular. It gives timely information on: **Programs to be Funded • New Regulations • Committee Hearings, Activities • Proposed Legislation • Reference Studies, Publications • And much more!**

Based on information brought directly from Capitol Hill by ACS Washington Alert staff members and published by the American Chemical Society's Department of Government

Relations and Science Policy, this is *primary journalism at its most functional—direct, relevant, accurate.*

For information, use the coupon, write, or  
**CALL TOLL FREE  
1-800-424-6747**

American Chemical Society  
Periodicals Marketing Department  
1155 Sixteenth Street, NW  
Washington, DC 20036

**YES!** Please send me more information on the bi-weekly publication, *ACS Washington Alert*

Name

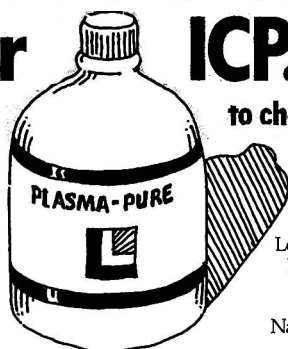
Address

City, State, Zip

# Leeman Labs' New PLASMA-PURE™ Standards for ICP...

...One MORE Reason

You need good calibration standards to get good analytical results from any technique. Inductively-Coupled Plasma (ICP), which sees light emitted by 72 elements simultaneously, demands standards of exceptional purity. Now Leeman Labs offers high-purity PLASMA-PURE ICP Standards to give you better analytical results.



to choose ICP from Leeman Labs

For a PLASMA-PURE data sheet and price list, send in the coupon, circle the reader service number, or contact Leeman Labs directly, at 600 Suffolk Street, Lowell, MA 01854, phone (617) 454-4442.

Name \_\_\_\_\_

Company \_\_\_\_\_

Address \_\_\_\_\_ Phone ( ) \_\_\_\_\_

City \_\_\_\_\_ State \_\_\_\_\_ Zip \_\_\_\_\_



LEEMAN LABS, INC.  
600 Suffolk Street  
Lowell, MA 01854  
(617) 454-4442

CIRCLE 86 ON READER SERVICE CARD

**GAIN**

## The Professional Edge

**WITH MEMBERSHIP IN THE  
AMERICAN CHEMICAL SOCIETY**

- Keep up-to-date with weekly copies of *CHEMICAL AND ENGINEERING NEWS*
- Enjoy substantial discounts on subscriptions to ACS's internationally respected, authoritative journals and publications
- Network with your fellow scientists at local, regional and national meetings
- Enhance your career opportunities with ACS employment services
- Save on insurance and retirement plans and tax deferred annuity programs
- Discover the latest advances in your discipline with a first-year-free Division membership

**... and this is just the beginning.**

Learn why 9 out of 10 ACS members renew year after year. Gain the Professional Edge: Join ACS now. For further information write or send the coupon below or call TOLL FREE 1-800-424-6747

American Chemical Society  
1155 Sixteenth St., N.W.  
Washington, DC 20036

**YES!** Please send information on the advantages of joining the ACS.

Name \_\_\_\_\_

Address \_\_\_\_\_

I am most interested in the following science(s): \_\_\_\_\_

## LABORATORY SERVICE CENTER

Amino Acids • Aminoacetal • Benzalacetophenone • Benzoic Anhydride  
Benzylthiuronium Chloride • Bromoacetal • Bromosulfonphthalein, Na  
Chloranil • 3,5-Dichlorosalicylaldehyde • Diethyl & Dimethylamine HCl  
Dimedone • Dimethylchloroacetal • 1,3-Dimethylurea • Dulcitol  
Malonic Acid • Methyl Butyrate • Methylene Iodide • o-Nitrocinnamaldehyde  
Phenetole • Potassium & Sodium m-Periodates • Sodium Catechol Disulfonate  
Sodium Diethyldithiocarbamate • Succinic Acid • a-Tetralone • Tripalmitin  
Vanillic Acid • iso-Vanillin • Veratraldehyde • Veratrole • Xylitol

Write for our Products List of over 3,000 chemicals

Tel: 516-273-0900 • TOLL FREE: 800-645-5566

Telefax: 516-273-0858 • Telex: 497-4275

**EASTERN CHEMICAL**  
A Division of UNITED-GUARDIAN, INC.

P.O. Box 2500  
DEPT. AC  
SMITHTOWN, N.Y. 11787

### WANTED: NEWLY DEVELOPED ANALYTICAL INSTRUMENTS OR MEASUREMENT CONCEPTS

#### REFINERY — PETROCHEMICAL — GAS INDUSTRIES

We are searching for new analytical instrumentation products or measurement concepts that are unique to the petrochemical/gas pipeline industry. We would like to manufacture and market these products. If you have a new instrumentation product and need help manufacturing/marketing, please contact us at: Product Search, P.O. Box 801203, Houston, TX 77280-1203, or call us at (713) 462-3941.

Use  
Laboratory  
Service Center

## FREE DATA, FAST

To quickly amass data on all of the products you need, consult the Lab Data Service section on our *Analytical Chemistry* reader reply card insert.

## CLASSIFIED HELP WANTED

### MASS SPECTROSCOPIST

The State of Connecticut Department of Environmental Protection has an anticipated opening for an Analytical Scientist to operate a GC/MS/MS and direct the operation of a mobile laboratory involved with air toxics analysis. **Requirements: General Experience:** Seven years' experience in a laboratory involving analytical work in chemistry, including mass spectral interpretation and technical program planning and development; **Special Experience:** Three years must have been in mass spectral interpretation activities; at least one year must have been in the operation of an MS/MS. A Ph.D. in organic, analytical, or physical chemistry may be substituted for the General Experience. A Bachelor's or Master's degree in those fields may be substituted for four or five years of the General Experience, respectively. **Salary Range:** \$31,911-38,771. Send resume and letter of intent to: Karen Taylor, D.E.P. Personnel, State Office Building—Room 129, 165 Capitol Avenue, Hartford, CT 06106 by June 30, 1988 or call 566-3468 for an application. EEO/AA Employer.

Use Classified  
Help Wanted Section

# MOST USED



....because  
it's the most  
useful.



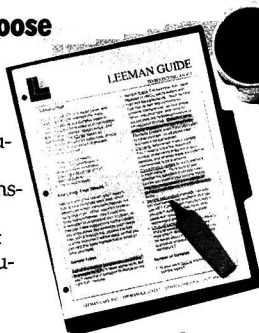
Published since 1955, the annual *LabGuide* leads all others in advertising pages and in reader usage (22,000 references daily). It's the true one-stop buying source where most manufacturers say with their ads, "Here we are. Compare our products with those of our competitors." That's why in more than six out of ten purchases by the 277,000 users it serves, the *LabGuide* is consulted before the purchase is made.



# Send for Your FREE Guide to Selecting an ICP...

...One MORE Reason to choose

If you're planning to buy an ICP spectrometer, Leeman's Guide to Selecting an ICP will help you evaluate your analytical needs and look for key ICP features. The Guide translates spectroscopic buzzwords into plain English, and an ICP Checklist leads you through a complete instrument evaluation.



ICP from Leeman Labs

Send for your FREE Guide, and learn how a Leeman ICP can work wonders in your lab. Use the coupon, circle the reader service number, or contact Leeman Labs at 600 Suffolk Street, Lowell, MA 01854, phone (617) 454-4442.



LEEMAN LABS, INC.  
600 Suffolk Street  
Lowell, MA 01854  
(617) 454-4442

Name \_\_\_\_\_

Company \_\_\_\_\_

Address \_\_\_\_\_ Phone (\_\_\_\_) \_\_\_\_\_

City \_\_\_\_\_ State \_\_\_\_\_ Zip \_\_\_\_\_

G

CIRCLE 87 ON READER SERVICE CARD

*Choosing a graduate school?  
Need to know who's doing  
research critical to yours?*

**New  
edition!**

## The ACS Directory of Graduate Research 1987

**All the information you need on chemical research and  
researchers at universities in the U.S. and Canada . . .  
in a single source.**

- Contains a wealth of facts on 668 academic departments, 11,569 faculty members, and 62,591 publication citations.
- Includes listings for chemistry, chemical engineering, pharmaceutical/medicinal chemistry, clinical chemistry, and polymer science.
- Lists universities with names and biographical information for all faculty members, their areas of specialization, titles of papers published in last two years, and telephone numbers.

1345 pages (1987) Clothbound  
Price: US & Canada \$50.00 Export \$60.00

Call toll free (800) ACS-5558 and charge your credit card.

Please send me \_\_\_\_\_ copy(ies) of the ACS Directory of Graduate Research 1987.  
Price: U.S. & Canada \$50.00, Export \$60.00

☐ Payment enclosed (make checks payable to American Chemical Society)

☐ Purchase order enclosed. P.O. # \_\_\_\_\_

Charge my: ☐ MasterCard ☐ American Express ☐ Diners Club/Carte Blanche ☐ ACCESS  
☐ Barclaycard.

Account # \_\_\_\_\_

Expires \_\_\_\_\_ Interbank # (MC and ACCESS) \_\_\_\_\_

Ship books to: \_\_\_\_\_

Name \_\_\_\_\_

Address \_\_\_\_\_

City, State, Zip \_\_\_\_\_

Orders from individuals must be prepaid. Please allow 4-6 weeks for delivery.

Mail this order form with your payment to: American Chemical Society, Distribution Office, Dept. 705,  
P.O. Box 57136, West End Station, Washington, DC 20037. 705

## ANNOUNCING

the 1988 Sessions of One of the Most Highly-Acclaimed ACS Short Courses Ever!

### THE COMPUTER- INTEGRATED LABORATORY:

**A Hands-On Experience in  
Lab Automation**

An intensive 5½-day  
laboratory-lecture course

Sunday-Friday,  
June 12-17

Sunday-Friday  
December 11-16

at Virginia Polytechnic  
Institute and State University  
Blacksburg, Virginia

**Hands-on, problem-solving experience  
that will enable you to**

- find the right laboratory information management system for your needs
- integrate your old analog systems with your new intelligent ones into a network environment
- educate your management and computing center as to why the electronic lab is fiscally and legally essential

For bench and middle-management scientists in QC, pharmaceuticals, petrochemicals, food, paper, clinical chemistry, biology, testing, materials

**Faculty:** Dr. Raymond E. Dessy, Professor of Chemistry, Virginia Polytechnic Institute and State University, Blacksburg, VA, and the Computer-Aided Research Group team.

**Call COLLECT** (202) 872-4508 for full details on these sessions. Or write: American Chemical Society, 1155 Sixteenth Street, N.W., Washington, D.C. 20036.

*A Course for  
Anyone Who Needs  
an Operational  
Knowledge of NMR*

### Modern NMR Spectrometry: PRINCIPLES AND PRACTICE

*Sunday-Friday,  
May 22-27, 1988  
Blacksburg, VA*

**An Intensive Short Course  
Sponsored by the  
American Chemical  
Society**

#### How You'll Benefit:

- ▶ Learn how to run basic and state-of-the-art 13C and 1H NMR experiments.
- ▶ Gain experience with routine instrument maintenance and troubleshooting.
- ▶ Be able to optimize and maintain an NMR spectrometer on a daily basis.
- ▶ Learn how to prepare NMR samples for data collection at the instrument console.

#### What You'll Cover:

- ▶ Basic FT-NMR theory
- ▶ Fundamentals of solution and solid state NMR experiments, equipment, and techniques
- ▶ Troubleshooting and repairs
- ▶ Spectral editing
- ▶ and more!

**For details on this important  
course, CALL COLLECT  
(202) 872-4508, extension 97.**

## C&EN INDEX Annual 1987

**All the information  
that appeared in C&EN  
last year is at your  
fingertips**

Whether you are interested in wide coverage of a general topic or just a brief letter to the editor—if C&EN published it last year, you will find it listed in this comprehensive index.

You'll find information on many subject fields—drugs, energy, health, mergers, nuclear power etc.—over 60 pages of listings!

Just published, this comprehensive, useful index is available paperbound or in microform.

**Save time and effort . . . CALL  
TOLL FREE 800-424-6747 or use  
the coupon below to order your  
C&EN INDEX now!**

**Distribution Office  
American Chemical Society  
1155 Sixteenth Street N.W.  
Washington D.C. 20036**

Please rush me C&EN INDEX at prices and quantities listed below.

**1986, 1987**  
\_\_\_\_\_ Paper \$50 \_\_\_\_\_ Microfiche \$50  
\_\_\_\_\_ Microfilm \$60

Back issues ea. specify year  
\_\_\_\_\_ Paper \$35 (1979-85)  
\_\_\_\_\_ Microfiche \$35 (1974-85)  
\_\_\_\_\_ Microfilm \$60 (1953-85)

☐ Payment enclosed  
(Payable to American Chemical Society)

☐ Purchase order PO No. \_\_\_\_\_

☐ VISA ☐ MasterCard  
☐ ACCESS ☐ Diners Club/Carte Blanche  
☐ Barclaycard ☐ American Express

Account No. \_\_\_\_\_

Expiration Date \_\_\_\_\_

Interbank No. \_\_\_\_\_  
(MasterCard and ACCESS) only

Signature \_\_\_\_\_

Name \_\_\_\_\_

Address \_\_\_\_\_  
\_\_\_\_\_  
\_\_\_\_\_

# INDEX TO ADVERTISERS IN THIS ISSUE

CIRCLE INQUIRY NO.	ADVERTISERS	PAGE NO.
22	Baird Corporation Design 2 Inc.	614A
20, 21	Beckman Instruments/Altex Division Cochrane, Chase, Livingston & Company	622A
16	Bio-Rad Chemical Division Pan & Associates	646A
18	Brinkmann Instruments, Inc. Lavey/Wolff/Swift, Inc.	608A
30	Chrompack International B.V.	640D
32	Dialog Information Services, Inc. Humpal, Leftwich & Sinn, Inc.	645A
40	Edwards High Vacuum, Inc. Innovac, Inc.	629A
50, 51	Finnigan MAT Corporation Lena Chow, Inc.	637A
54	Fluka Chemie AG Atelier Wenger	640E
64	Hewlett-Packard Company Pinné, Garvin, Herbers & Hock, Inc.	OBC
75	I-Chem Research, Inc. Lena Chow, Inc.	627A
73	Isotec, Inc. Kenyon Hoag Associates	628A
70	J-Y Optical Systems/Instruments SA, Inc. Kathy Wyatt & Associates	611A
84	Lachat Instruments	IFC
86, 87	Leeman Laboratories JRJ Communications	651A, 653A
90	Link Analytical Workhead Publicity, Ltd.	626A
102, 103	Mallinckrodt, Inc. RichardsonSmith, Inc.	643A
98	Matheson Gas Products Kenyon Hoag Associates	615A
104	McMillan Company Cooley & Shillinglaw Inc.	616A
94	Merck & Company Dugan/Farley Communications Associates	649A
100	Millipore Corporation Mintz & Hoke, Inc.	634A
120	Ohaus Scale Corporation Techmarketing, Inc.	613A
127, 128	Perkin-Elmer Corporation AC&R/DHB & BESS Advertising	631A, 633A
130	Philips Scientific/Analytical Division Connors Publicity, Ltd.	640B
125	Plenum Publishing Corporation Plenum/Da Capo Advertising	629A
158	Tekmar Company Kenyon Hoag Associates	620A
156	Thermo Jarrell Ash Corporation Noon, Inc.	607A
177, 178	Waters/Division of Millipore Millicomm, Inc.	617A, 618A-619A
175	Wheaton Instruments The Wheaton Agency	632A

CIRCLE INQUIRY NO.	ADVERTISERS	PAGE NO.
180	Wiley-Interscience Flamm Advertising, Inc.	638A

Classified advertising section, see page 652A.

Directory section, see page 652A.

\* See ad in ACS Laboratory Guide.

\*\* Company so marked has advertisement in Foreign Regional edition only.

Advertising Management for the American Chemical Society Publications

## CENTCOM, LTD

President

Thomas N. J. Koerwer

Executive Vice President Senior Vice President

James A. Byrne Benjamin W. Jones

Clay S. Holden, Vice President

Robert L. Voepel, Vice President

Joseph P. Stenza, Production Director

500 Post Road East

P.O. Box 231

Westport, Connecticut 06880

(Area Code 203) 226-7131

Telex No. 643310

## ADVERTISING SALES MANAGER

Bruce E. Poorman

## ADVERTISING PRODUCTION MANAGER

Jane F. Gatenby

## SALES REPRESENTATIVES

Philadelphia, PA... Patricia O'Donnell, Marybeth Stewart, CENTCOM, LTD., GSB Building, Suite 405, 1 Belmont Avenue, Bala Cynwyd, Pa. 19004. Telephone: 215-667-9666

New York, NY... CENTCOM, LTD., 60 East 42nd St., New York, N.Y. 10165. Telephone: 212-972-9660

Westport, CT... Edward M. Black, CENTCOM, LTD., 500 Post Road East, P.O. Box 231, Westport, Ct. 06880. Telephone: 203-226-7131, Telex 643310

Cleveland, OH... Bruce E. Poorman, John C. Guyot, CENTCOM, LTD., 325 Front St., Suite 2, Berea, Ohio 44017. Telephone: 216-234-1333

Chicago, IL... Michael J. Pak, CENTCOM, LTD., 540 Frontage Rd., Northfield, Ill. 60093. Telephone: 312-441-6383

Houston, TX... Michael J. Pak, CENTCOM, LTD., Telephone: 312-441-6383

San Francisco, CA... Paul M. Butts, CENTCOM, LTD., Suite 1070, 2672 Bayshore Frontage Road, Mountain View, CA 94043. Telephone: 415-969-4604

Los Angeles, CA... Clay S. Holden, CENTCOM, LTD., Newton Pacific Center, 3142 Pacific Coast Highway, Suite 200, Torrance, CA 90505. Telephone: 213-325-1903

Boston, MA... Edward M. Black, CENTCOM, LTD., Telephone: 203-226-7131

Atlanta, GA... Edward M. Black, CENTCOM, LTD., Telephone: 203-226-7131

Denver, CO... Paul M. Butts, CENTCOM, LTD., Telephone: 415-969-4604

## United Kingdom

Reading, England... Malcolm Thiele, Technomedia Ltd., Wood Cottage, Shurlock Row, Reading RG10 0QE, Berkshire, England. Telephone: 073-434-3302, Telex #848800

Lancashire, England... Technomedia Ltd., c/o Meconomics Ltd., Meconomics House, 31 Old Street, Ashton Under Lyne, Lancashire, England. Telephone: 061-308-3025

Continental Europe... Andre Jamar, International Communications, Inc., Rue Mallar 1, 4800 Verviers, Belgium. Telephone: (087) 22-53-85, Telex #49263

Tokyo, Japan... Sumio Oka, International Media Representatives Ltd., 2-29 Toranomon, 1-Chome Minato-ku Tokyo 105 Japan. Telephone: 502-0656, Telex #22633



# CA SELECTS®

## clears your path through current literature

Maybe you enjoy cutting your own trail—going to the library, reviewing hundreds of original articles, taking notes. But you might prefer sitting at your desk and reviewing CA SELECTS—concise English-language abstracts of current chemical literature, retrieved from CHEMICAL ABSTRACTS®.

CA SELECTS will help you quickly and easily discover what's new or what's already been tried in research for drugs, cosmetics, adhesives, materials, biotechnology, paints, environmental technology and other subjects. There are 198 topics to choose from. If your research touches on any of these topics, CA SELECTS will bring you abstracts of the relevant literature; 26 issues for as little as \$140.

For just \$5.38 an issue, less than 5 cents per abstract (on the average), CA SELECTS will clear your path through the jungle of chemical literature. CA SELECTS brings your subject specialty out in the open for your inspection.

To receive your copy of our CA SELECTS Catalog of descriptions of all 198 topics, simply complete this coupon and return it to the address indicated.

### CA SELECTS Catalog Coupon

YES! Please send me the descriptions of all 198 topics. This Catalog is FREE.

Name \_\_\_\_\_

Job Title \_\_\_\_\_

Organization \_\_\_\_\_

Address \_\_\_\_\_  
\_\_\_\_\_

City \_\_\_\_\_

State/Zip \_\_\_\_\_

Country \_\_\_\_\_

Phone Number \_\_\_\_\_

Mail coupon to:  
Chemical Abstracts Service  
Marketing, Dept. 31288  
2540 Olentangy River Road  
P.O. Box 3012  
Columbus, Ohio 43210, U.S.A.

Or call us at:  
(614) 421-3731; or  
1-800-848-6538  
(ask for Customer Service)

Chemical Abstracts Service is a division of the  
American Chemical Society.

EDITOR: GEORGE H. MORRISON

ASSOCIATE EDITORS: Klaus Blemann,  
Georges Guloichon, Robert A. Osteryoung,  
Edward S. Yeung

## Editorial Headquarters

1155 Sixteenth St., N.W.  
Washington, D.C. 20036  
Phone: 202-872-4570  
Teletype: 710-8220 151

Managing Editor: Sharon G. Boots

Associate Editors: Rani A. George,  
Louise Voress, Mary Warner

Assistant Editors: Ivan Amato, Keith B. Belton,  
Grace K. Lee

Director, Operational Support: C. Michael  
Phillippe

Production Manager: Leroy L. Corcoran

Art Director: Alan Kahan

Staff Artist: Amy Meyer Phifer

Production Editor: Elizabeth E. Wood

Circulation: Cynthia G. Smith

Editorial Assistant, LabGuide: Joanne Mullican

## Journals Dept., Columbus, Ohio

Associate Head: Marianne Brogan

Assistant Manager: Joseph E. Yurvati

Associate Editor: Rodney L. Temos

Advisory Board: Harry V. Drushel, Michael S.  
Epstein, Larry R. Faulkner, Peter R. Griffiths,  
Nobuhiko Ishibashi, Peter C. Jurs, Mary A. Kai-  
ser, David L. Nelson, Lawrence A. Pachla, Erno  
Pungor, Fred E. Regnier, Dennis Schuetzle,  
Ralph E. Sturgeon, Nicholas Wingrad, Mary J.  
Wirth, Andrew T. Zander Ex Officio: Roland  
F. Hirsch

Instrumentation Advisory Panel: Howard G.  
Barth, Richard F. Browner, James B. Callis,  
Bruce Chase, L. J. Cline Love, Joel M. Harris,  
Ronald E. Majors, Linda B. McGown, R. Mark  
Wightman

Published by the  
AMERICAN CHEMICAL SOCIETY

1155 16th Street, N.W.  
Washington, D.C. 20036

## Publications Division

Director: Robert H. Marks

Journals: Charles R. Bertsch

Research and Development: Lorrin R. Garson

Special Publications: Randall E. Wedin

Manuscript requirements are published in the  
January 1, 1988 issue, page 91. Manuscripts  
for publication (4 copies) should be submitted  
to ANALYTICAL CHEMISTRY at the ACS Washing-  
ton address.

The American Chemical Society and its editors  
assume no responsibility for the statements and  
opinions advanced by contributors. Views  
expressed in the editorials are those of the  
editors and do not necessarily represent the  
official position of the American Chemical  
Society.

Arnold, M. A., 1080

Bains-Sahota, S. K., 1084

Baumann, S. A., 1046

Beary, E. S., 971

Bhatnagar, A., 986

Blom, K. F., 966

Bond, A. M., 1023

Bourne, A. R., 1023

Boyle, J. R., 1033

Brumbaugh, W. G., 1051

Brumley, W. C., 975

Buck, R. P., 1018

Burkes, L. J., 962

Bushee, D. S., 971

Canas, B. J., 975

Corneliusson, P. E., 975

Cox, J. A., 986

Delaney, T. E., 962

Diamandis, E. P., 1069

Fong, K. L., 1074

Fujiwara, K., 1065

Galante, L. J., 995

Gamp, H., 1083

Ha, S. T. K., 1055

Hasan, M. N., 978

Hedges, J. I., 988

Hieftje, G. M., 995

Hollenkamp, A. F., 1023

Horvai, G., 1018

Huf, P. A., 1023

Iglehart, M. L., 1018

Jang, G.-W., 1003

Jardine, I., 1086

Jurs, P. C., 978

Karube, I., 1078

Koertyohann, S. R., 1051

Lazrus, A. L., 1074

Lee, R. W. K., 1055

Liberato, D. J., 1086

Lind, J. A., 1074

Maeder, M., 1083

Maltby, D. A., 962

Marshall, D., 982

McCrone, W. C., 1009

McGown, L. B., 1043

Millington, D. S., 962

Moody, J. R., 971

Mossoba, M. M., 975

Nithipatikorn, K., 1043

Opsal, R. B., 1060

Owens, G. D., 962

Palmer, R. A., 1027

Paulsen, P. J., 971

Perfetti, G. A., 975

Pinkston, J. D., 962

Pungor, E., 1018

Que Hee, S. S., 1033

Rajeshwar, K., 1003

Ramjeesingh, M., 1069

Reichstein, E., 1069

Reilly, J. P., 1060

Robbat, A., Jr., 982

Scanlan, G. F., 1086

Shami, Y., 1069

Simeonsson, J. B., 1065

Smith, B. W., 1065

Sphon, J. A., 975

Strathman, M. D., 1046

Suib, S. L., 1046

Suzuki, H., 1078

Tamiya, E., 1078

Thiemens, M. H., 1084

Thompson, M. M., 1027

Thompson, S. B., 1023

Tsarbopoulos, A., 1086

Walters, J. S., 988

Wangsa, J., 1080

Watson, T. G., 1023

Wilkins, C. L., 1055

Winefordner, J. D., 1065

Xyrafas, G., 982

Zuberbühler, A. D., 1083

# Capillary Supercritical Fluid Chromatography-Mass Spectrometry Using a "High Mass" Quadrupole and Splitless Injection

J. David Pinkston,\* Grover D. Owens, Leisa J. Burkes, and Thomas E. Delaney

The Procter & Gamble Co., Miami Valley Laboratories, P.O. Box 398707, Cincinnati, Ohio 45239-8707

David S. Millington and David A. Maltby

Duke University Medical Center, Division of Pediatric Genetics and Metabolism, Box 3028, Durham, North Carolina 27710

Most capillary supercritical fluid chromatography-mass spectrometry (SFC-MS) has been done on instruments of mass range of less than 1500 Da, though SFC is able to elute species of molecular masses in the thousands of daltons. In addition, splitting injection is usually employed in SFC, which hampers quantitation. This work addresses both these problems by using a 3000-Da mass range quadrupole in combination with splitless injection. A solution of poly(dimethylsiloxane) in carbon dioxide is introduced to the ion source by supercritical fluid injection for tuning purposes. Poly(dimethylsiloxanes) and derivatized oligosaccharides are transported intact through the SFC-MS interface. Simple ammonia chemical ionization spectra, dominated by the ammonium adduct ion, are seen to the mass limit of the instrument. A signal-to-noise ratio of approximately 4 is measured for the ammonium adduct ion of 0.8 ng of methyl arachidate.

Capillary supercritical fluid chromatography (SFC) is an important analytical separation method, complementary to both gas chromatography (GC) and high-performance liquid chromatography (HPLC). SFC separations may be performed at temperatures as low as 35 °C with CO<sub>2</sub> mobile phase, thus allowing the determination of thermally labile species (1). Mixtures containing solutes of molecular mass of several thousand daltons have been successfully analyzed by SFC with flame ionization detection (SFC-FID) (2).

Mass spectrometry (MS) has been shown to provide sensitive, universal, and specific detection for SFC (3-5). Consistent progress in understanding the SFC-MS interface and in applications of SFC-MS has been reported by Smith, Wright, and co-workers (6-12). Significant contributions have also been made by the groups guided by Henion (13, 14) and Voorhees (15, 16).

Most SFC-MS work has been done with quadrupole mass analyzers that have mass ranges of less than 1500 Da. However, many potential SFC-MS applications involve solutes of mass greater than 1500 Da. Progress has been made in performing SFC-MS on an extended-mass-range, double-focusing magnetic instrument (17). Early attempts were slowed by high-voltage breakdown in the ion source. SFC-MS using Fourier transform ion cyclotron resonance mass spectrometry (FTMS) has also been attempted (18). The high mass capabilities of FTMS were not demonstrated, however. This lack of success at high mass is probably due to difficulties in maintaining supercritical conditions throughout the long transfer line to the FTMS cell and to high pressure within the cell (18).

Here we describe SFC-MS using an extended mass range (3000 Da) quadrupole instrument. The low-voltage ion source of the quadrupole simplifies the interface design and facilitates the direct introduction of the chromatographic effluent. Since our purpose was the evaluation of the SFC-MS interface and of the mass spectrometer itself, test mixtures were chosen that are chromatographically well-behaved. In particular, instrumental performance was evaluated in terms of signal-to-noise ratio (S/N) near the limit of detection, mass range, and sensitivity as a function of mass resolution.

A successful interface for microbore and high-flow-rate capillary column SFC-MS has been reported using splitless injection (12). For high chromatographic efficiency using narrow (<100  $\mu$ m i.d.) capillary columns in SFC and SFC-MS, mobile phase linear velocities must be slower than those for which this interface is designed. Injection volumes must also be very small. Thus most work in capillary SFC and SFC-MS has been done using split injection techniques. The dependence of split ratios on temperature, pressure, and molecular weight can be a severe hindrance to quantitative analysis (19). This study demonstrates that splitless injection with conventional 50- $\mu$ m capillary hardware can be used in SFC-MS at linear velocities similar to those commonly used in capillary SFC while maintaining reasonable chromatographic resolution.

## EXPERIMENTAL SECTION

The instrument used in these experiments is similar in design to that described in previous publications (5). In overview, a microcomputer controls a high-pressure syringe pump modified for pressure control (20). The pump delivers the mobile phase (liquid carbon dioxide in these experiments) through an internal loop injection valve to a capillary SFC column. Eluent from the chromatographic column is introduced into the mass spectrometer ion source via a custom-built interface probe that fits the direct-insertion-probe vacuum lock.

The capillary SFC system has been described previously (20). One modification was made to the standard configuration: the split-injection "tee" and vent assembly were removed. Splitless injection was accomplished by directly coupling a 50 cm  $\times$  50  $\mu$ m i.d. retention gap to the electrically actuated injection valve (EC14W.06, Valco, Houston, TX) via an internal reducing union (IZR1.5, Valco). Care was taken to insert the retention gap only 1.3 cm into the reducing union, flush with the end of the ferrule, to avoid the formation of an unswept dead volume inside the reducing union. Low dead volume unions (ZU.5, Valco) were used to connect the column (DB-1, 10 m, 50  $\mu$ m i.d., 0.2- $\mu$ m film thickness, J&W Scientific, Inc., Folsom, CA) to the mass spectrometer interface.

Figure 1 shows the SFC-MS interface probe. The heart of the probe is an 80-cm length of uncoated 25  $\mu$ m i.d., fused-silica tubing (25VS-025ID, Scientific Glass Engineering, Inc., Austin, TX). The end of this tube has been tapered, sized, and cut to form a restrictor in the manner previously described (20). The tapered end narrows to an aperture of approximately 3.4-4  $\mu$ m diameter over a taper length of 2-4 cm. This restrictor is housed inside

\* To whom correspondence should be addressed.



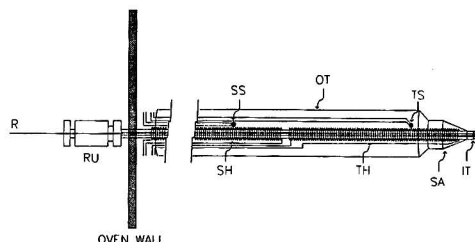


**Figure 1.** SFC-MS interface probe: R, flow restrictor; RU, reducing union; SH, stem heater; SS, stem sensor; OT, outer tube; TH, tip heater; TS, tip sensor; SA, source adaptor; IT, inner tube.

the "inner" tube, a 70 cm length of 0.25 mm i.d.  $\times$  1.59 mm o.d. stainless steel tubing (3005, Alltech Associates, Deerfield, IL).

The inner tube is divided into two heated regions. A 5 cm length at the tip of the probe has been wrapped with a layer of glass tape and a 60 cm length of 4  $\Omega$ /ft nichrome wire (Pelican Wire Co., Naples, FL) to form a tip heater. This heater is connected to a 22-W dc power supply (PAT 15-1.5, KEPCO, Flushing, NY) by 22-gauge, Teflon-insulated leads which have been silver soldered to the nichrome wire. The temperature of the tip heater is measured by an all-glass insulated, 30-gauge, iron-constantan thermocouple (Omega Engineering, Stamford, CT). This thermocouple and the entire tip heater are potted in a high-temperature ceramic adhesive (AREMCO Products, Inc., Ossining, NY). The remaining 65 cm of the inner tube is wrapped with glass tape and 1.6  $\Omega$ /ft nichrome wire (Pelican) to form a stem heater. The temperature of the stem heater is measured by a second, identical, iron-constantan thermocouple. This heater is powered by a variable ac powerstat (10B, Superior Electric Co., Bristol, CT). The entire stem heater is encased in braided ceramic sleeving (XC-14, Omega Engineering). The SFC-oven end of the inner tube is coupled to a reducing union (ZRU1.5, Valco). This union forms a vacuum seal between the restrictor and the inner tube.

The outer diameter of the interface probe and the shape of its tip are dictated by the mass spectrometer's direct insertion port and ion source inlet. The probe's outer tube is a 28-cm length of 7.9 mm o.d.  $\times$  6.5 mm i.d. stainless steel tubing (Microgroup Inc., Medway, MA). The tip of the probe, or source adaptor, was custom-machined from 316 stainless steel. It is 1.3 cm long and is silver soldered to both the inner tube and the outer tube to form a vacuum seal. The conical section at the probe tip was fabricated with a 25° angle, with respect to the inner tube, to mate with the mass spectrometer source.

The interface probe required between 8 and 12 man-hours to construct. Under normal use, probe lifetime is indefinite. The flow restrictor plugged after the initial supercritical fluid injection experiments. A second restrictor was used for all the SFC-MS work.

A VG 30-250 automated quadrupole mass spectrometer (VG Masslab, Altrincham, England) was used for this work. The VG 250-11J data system was used to control the instrument and collect the data.

The standard EI/CI ion source was operated in CI mode, using anhydrous grade ammonia (Union Carbide Corp., Linde Division, Danbury, CT) as the CI reagent gas. Source manifold pressure was monitored with an uncalibrated Bayert-Alpert ion gauge. The base pressure in the source housing was  $2 \times 10^{-7}$  Torr. The source manifold pressure with only ammonia CI reagent added was typically  $(5-6) \times 10^{-5}$  Torr. With the SFC-MS interface in place and the  $\text{CO}_2$  pressure in the chromatographic system at 200 atm, the source manifold pressure was  $(1-2) \times 10^{-4}$  Torr. During pressure-programmed chromatographic runs the analyzer manifold pressure reached  $(2-3) \times 10^{-6}$  Torr. The base pressure in the analyzer manifold region was approximately  $1 \times 10^{-7}$  Torr.

A 3% solution of poly(dimethylsiloxane) (DC200, Contour Chemical Co., North Reading, MA) in SFC Grade  $\text{CO}_2$  (Scott Specialty Gases, Plumsteadville, PA) was prepared for supercritical fluid injection as described elsewhere (21). This solution was introduced directly into the ion source through the heated in-

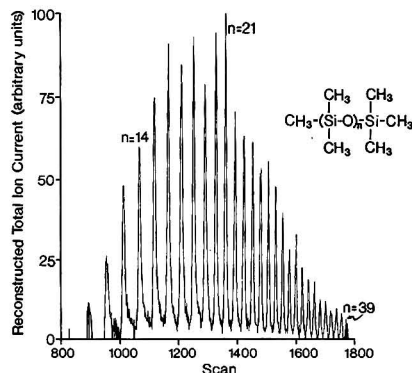


**Figure 2.** Reconstructed total-ion-current chromatogram of SFC-MS run of DC-200 poly(dimethylsiloxane).

terface probe. It supplied a steady ion current for tuning, calibration, and studying mass resolving power vs sensitivity throughout the instrument's mass range under ionization conditions similar to those encountered during SFC-MS (21).

Typical MS-tuning parameters for SFC-MS runs included: electron emission currents of 70–100  $\mu\text{A}$ , electron energy at 200 eV, ion repeller at 7–12 V, ion energy at 4–15 V, ion energy ramp of 10 mV/Da, ion extraction at 0 V, ion focus at 20–30 V, and a multiplier voltage of 1500–1700 V. The sensitivity of the mass spectrometer for high mass ions ( $>1500$  Da) was improved at least 10-fold by decreasing the instrument's mass resolving power. The resolving power was adjusted such that the valley between adjacent ions in the isotope multiplets above  $m/z$  1500 was roughly 90% the height of the peak corresponding to the less abundant ion. The scan rate was 2 s/scan over a range of  $m/z$  500–3000 except where indicated otherwise. The temperature of the CI source was held between 270 and 300 °C.

Chromatographic separations were typically performed by using linear pressure gradients of SFC grade  $\text{CO}_2$  (Scott Specialty Gases) from 100 to 300 atm. The SFC oven temperature was set between 80 and 100 °C, the stem heater on the SFC-MS interface was held at 90 °C, and the tip heater was maintained at 350 °C.

Solutions of poly(dimethylsiloxane) (DC200), tristearin (NU-CHEK-PREP, Inc., Elysian, NJ), sucrose octooleate (synthesized in-house), and methyl arachidate (Alltech Associates, Deerfield, IL) were prepared in methylene chloride (American Burdick and Jackson, Muskegon, MI) prior to chromatographic runs. Maltrin 100 (Grain Processing Corp., Muscatine, IA), a commercial corn syrup solid, was silylated prior to SFC-MS: approximately 10 mg of this material was added to 0.2 mL of 5/1 *N*-(trimethylsilyl)imidazole (TMSI) (Pierce Chemical Co., Rockford, IL) and *N,O*-bis(trimethylsilyl)trifluoroacetamide (BSTFA) (Pierce Chemical Co.) and heated at 80 °C for 1 h. After cooling, the resulting solution was diluted to 1 mL with dry methylene chloride (American Burdick and Jackson). All other solvents were ACS reagent grade (Fisher Scientific, Fair Lawn, NJ).

## RESULTS AND DISCUSSION

**SFC-MS of Poly(dimethylsiloxane).** Figure 2 is a plot of the reconstructed total ion current (RTIC) chromatogram obtained during an SFC-MS run of the DC 200 poly(dimethylsiloxane). Peaks from oligomer number ( $n$ ) 11 through 39, corresponding to ammonium adduct ions of  $m/z$  (most abundant isotope) 920 through 2998, are shown. Higher molecular weight oligomers were not detected since the instrument's mass range is limited to 3000 daltons.

During runs of high molecular weight oligomeric series such as the poly(dimethylsiloxanes), the resolving power of the instrument was purposely reduced as described in the Experimental Section and the peak detection parameters were adjusted such that the isotopic multiplets corresponding to the major ions of the tuning mixture merged into single, broad

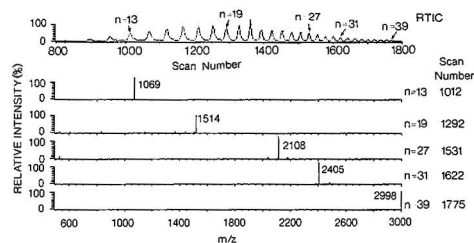


**Figure 3.** Reconstructed total-ion-current chromatogram (top) and selected ammonia CI spectra from SFC-MS run of poly(dimethylsiloxane).

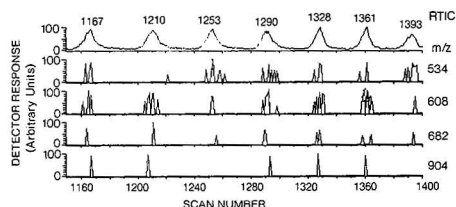


**Figure 4.** Reconstructed total-ion-current chromatogram (top) and selected mass chromatograms showing structurally related ions produced during  $\text{NH}_3$  CI SFC-MS run of poly(dimethylsiloxane).

**Table I.** Monoisotopic Masses and Most Abundant Isotopes of Selected Ammonium Adducts of Poly(dimethylsiloxane) Oligomers

degree of polymerization ( $n$ ) <sup>a</sup>	monoisotopic mass, Da	most abundant isotope mass, Da
9	772	772
13	1068	1069
19	1512	1514
23	1808	1811
27	2104	2108
29	2252	2256
31	2400	2405
33	2548	2553
39	2992	2998

<sup>a</sup> Refer to structure in Scheme I. <sup>b</sup> Rounded to nearest integral mass.

peaks. The instrument was mass calibrated such that the centroid of the broad peak was near the most abundant isotope ( $\pm 1$  Da) of the cluster. This dramatically improved the signal-to-noise ratio of the measurements. The reduction in resolving power increased the signal intensity by a factor of roughly 10 at  $m/z$  2000 as directly measured on the oscilloscope during the tuning process.

Figure 3 illustrates representative spectra collected during the SFC-MS run of the poly(dimethylsiloxanes), the TIC of which is shown in Figure 2. All of the oligomers show  $[M + 18]^+$  ammonium adduct ions. The centroid  $m/z$  values are within one unit of the expected most abundant isotope. As an aid to the reader, Table I lists the degree of polymerization ("n" value) associated with representative siloxane oligomers, the monoisotopic mass of the ammonium adduct, and the mass of the most abundant adduct isotope. Most spectra also show a weak signal corresponding to the protonated molecule. The largest chromatographic peaks in the series also show very weak ions at  $m/z$  534, 608, 682, 756, 830, and 904. This is illustrated in Figure 4. The ions are separated by intervals of 74 Da, corresponding to the oligomeric unit,  $\text{SiC}_2\text{H}_5\text{O}$ . It

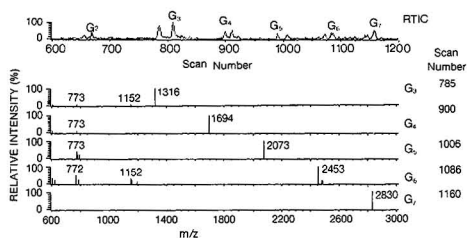


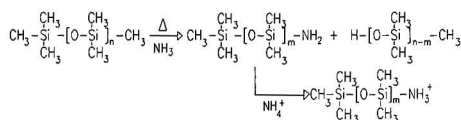
**Figure 5.** Reconstructed total-ion-current chromatogram (top) and selected spectra from  $\text{NH}_3$  CI SFC-MS run of derivatized Maltin 100.

**Table II.** Monoisotopic Masses and Most Abundant Isotopes of Selected Ammonium Adducts of Derivatized Oligosaccharides

no. of glucose units ("G" value)	monoisotopic mass, Da	most abundant isotope mass, Da
3	1314	1316
4	1692	1695
5	2070	2073
6	2448	2452
7	2826	2830

<sup>a</sup> Rounded to the nearest integral mass.

**Scheme I**



appears that a similar series has been previously observed in  $\text{NH}_3$  CI, though the spectrum is not shown and the  $m/z$  values are not listed (22). The structure of these ions cannot be determined unambiguously from our data. A possible scheme yielding ions corresponding to these  $m/z$  values is shown in Scheme I. These structures may thus be due to ammonolysis of the poly(dimethylsiloxanes), where neutral ammonia reacts with an oligomer to form a new chemical species which is subsequently ionized. This type of behavior has been previously observed in  $\text{NH}_3$  CI of oligomeric compounds (23, 24). The amine-containing fragment (1) would be preferentially ionized over the hydroxy species (2) by the ammonium ion due to the difference in their proton affinities. An experiment with nitrogen-labeled ammonia would confirm or refute this hypothesis.

**SFC-MS of Oligosaccharides.** The trimethylsilyl derivatives of oligosaccharides can be easily eluted with unmodified  $\text{CO}_2$  mobile phase in capillary SFC over a wide molecular weight range (2). The oligomeric series elutes as a series of irregularly spaced doublets. The corn syrup solid used, once derivatized, more than adequately covers the mass range of the VG instrument and is chromatographically well-behaved. Analyzing this mixture by SFC-MS not only allowed us to test our SFC-MS interface and the VG quadrupole but also allowed us to confirm the assignment of the doublets as anomeric forms of the reducing end of the oligosaccharide (25).

Figure 5 illustrates the TIC chromatogram for the oligosaccharides containing two through seven glucose units ( $G_2$ – $G_7$ ). The molecular weights of the oligosaccharides  $G_8$  and above were beyond the mass range of the mass spectrometer. Figure 5 also illustrates representative spectra collected during this  $\text{NH}_3$  CI run. The mass spectral peaks were centroided,

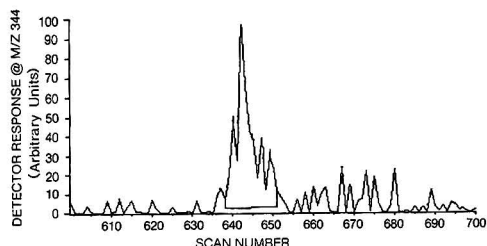


Figure 6. Mass chromatogram of  $m/z$  344, ammonium adduct ion of methyl arachidate, about elution time of 0.8 ng run by  $\text{NH}_3$  CI SFC-MS.

as described above. Each oligosaccharide displays a base peak within 1 mass unit of that expected for its ammonium adduct ion. Table II lists the glucose unit number, the monoisotopic mass, and the "centroided" mass of the ammonium adduct ions of selected oligosaccharides.

The more intense spectra usually displayed fragment ions at or near  $m/z$  773 and  $m/z$  1152 as shown in Figure 5. These fragment ions were sometimes sporadic and always of low relative abundance (<10%). The difference in mass between these two ions of 379 Da is near the mass of the repeating unit of the derivatized oligosaccharide (378 Da). These ions may thus be related to the structure of the oligosaccharide. Such fragments are not unexpected given previous studies of the  $\text{NH}_3$  CI of oligosaccharides (23, 24). The data collected are insufficient to unambiguously determine the structure of these ions.

**Evaluation of the Signal-to-Noise Ratio (S/N) Near the Detection Limit.** Evaluation of the S/N near the detection limit in capillary SFC-MS is complicated by the customary use of splitting injection, standard in SFC-FID. Split ratios vary with temperature, pressure, and molecular weight (19, 26). To avoid these problems, the retention gap was directly linked to a nominal 0.06- $\mu\text{L}$  injection valve without splitting. The lower mass scan limit was above any ions produced by the broad solvent front, which we expected from previous SFC-FID experience. The column flow rate was not directly measured, but the robot-pulled tapered flow restrictor was typical (4.0 cm taper length, 3  $\mu\text{m}$  aperture), and retention times of standards were near those expected. This mode of splitless injection in SFC-MS worked better than anticipated. The detection of early eluting peaks did not seem to be adversely affected by the solvent front. All the work discussed in this publication was performed in this mode of splitless injection, with adequate chromatographic resolution, as shown in the reconstructed TIC chromatograms. These separations were developed using a similar SFC instrument equipped with conventional split injection and flame ionization detection. A drop in chromatographic peak resolution was expected in moving from the split SFC-FID runs to the splitless SFC-MS runs, and such a drop was observed. For example, the seventh and eighth peaks in Figure 2, corresponding to oligomers with  $n = 16$  and 17, are separated with a resolution of 2.1 in the SFC-MS run while the same peak pair in an SFC-FID run was separated with a resolution of 4.2.

Three standards were used to evaluate the S/N of this SFC-MS combination near the detection limit. All three were well-behaved chromatographically. One was methyl arachidate, with a molecular weight of 326. It has often been used to evaluate S/N in GC-MS. The second was tristearin, molecular weight 890. The third was sucrose octaoctate, with a molecular weight of 2454. The instrument was tuned to "unit" resolution (10% valley definition) before the S/N measurements were made.

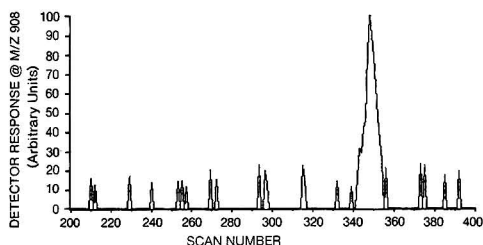


Figure 7. Mass chromatogram of  $m/z$  908, ammonium adduct ion of tristearin, about elution time of 12 ng run by  $\text{NH}_3$  CI SFC-MS.

Figure 6 is the mass chromatogram of  $m/z$  344,  $[\text{M} + \text{NH}_4]^+$  for methyl arachidate, produced upon injection of 0.8 ng of the ester in dichloromethane. The scan range was  $m/z$  100–500 with a 1-s scan cycle time. The S/N is approximately 4. The contribution to this particular run of methyl arachidate of carry-over from previous runs was negligible. Sensitivities at least an order-of-magnitude higher have been reported for substituted biphenyls in SFC-MS using  $\text{CH}_4$  CI (7). The authors have measured limits of detection (S/N of 3) in the tens of picograms for naphthalene using  $\text{CH}_4$  CI SFC-MS (scanning over a 100 dalton or greater mass range) (27). The S/N is affected by the method of ionization chosen, the nature and molecular weight of the species in question, the chromatographic peak width, and the transmission/detection efficiency of the mass spectrometer.

While the methyl arachidate runs were performed with a relatively clean ion source, the tristearin runs were performed after about 60 h of nearly continuous  $\text{NH}_3$  CI SFC-MS operation. Removal of the ion source after the tristearin runs revealed that the source was very dirty. This is the most probable cause of the lower signal levels and higher background noise levels for the oligosaccharides and tristearin runs. Figure 7 is a mass chromatogram of  $m/z$  908,  $[\text{M} + \text{NH}_4]^+$  for tristearin, collected after a splitless injection containing 12 ng of tristearin. The scan range was from  $m/z$  500 to 1000 with a scan cycle time of 1.1 s. The S/N is roughly 5.

This work was performed over a 3-day period and involved equipment from two distant sites. We were not able to repeat the tristearin S/N experiments under optimal conditions due to these logistical constraints. However, we feel that these preliminary data are useful in at least establishing a "worst case" S/N figure obtained with no real attempt at optimization. In previous SFC-MS work it was shown that a simple cryopumping attachment dramatically reduces the ion source manifold pressure (by a factor of 5 under typical operating conditions) and improves signal levels (by a factor of 2 to 3) in SFC-MS (26). The VG instrument used in these experiments had no such means of additional pumping.

The beneficial effects of additional pumping are especially important at high mobile phase pressure (pressures of 300–400 atm are often present at the end of a pressure-programmed run). This may explain the poor results obtained during runs of the relatively high-mass S/N standard, sucrose octaoctate. The elution pressure of this species is 370 atm under the SFC conditions chosen. The ion source manifold pressure was over  $3 \times 10^{-4}$  Torr at this elution pressure. We observed no ions related to sucrose octaoctate under the  $\text{NH}_3$  CI conditions used. This may also be due to nucleation and precipitation of the sucrose octaoctate in the tapered flow restrictor due to insufficient solubility in the unmodified  $\text{CO}_2$  mobile phase (10). However, if this were the case, one would expect to also see detector "spiking" when this species is analyzed by SFC-FID. Such spiking has not been observed.

This work demonstrates that species of molecular weights up to at least 3000 can be introduced intact to the ion source

as solutes in supercritical CO<sub>2</sub> through a simple interface probe and ionized by traditional CI mass spectrometry. Ammonium adduct ions of the poly(dimethylsiloxanes) were observed to the mass limit of the spectrometer by supercritical fluid injection. The only limit to mass range in this case appears to be the upper mass limit of the mass analyzer itself. Spectra were obtained which were indicative of both molecular weight and structure in the case of the poly(dimethylsiloxanes) and of the oligosaccharides.

The mode of splitless injection used in this work is a step toward making SFC-MS a quantitative, trace analysis technique. Injection technology being developed in a number of laboratories which will allow the splitless injection of solutes present in microliter volumes will strengthen the standing of SFC and SFC-MS in this area. Capillary supercritical fluid chromatography-mass spectrometry using an unmodified CO<sub>2</sub> mobile phase as presented here is limited to relatively nonpolar solutes. The use of modified and more polar mobile phases should extend the range of solute polarities which SFC-MS can handle (28). As the high-mass performance of quadrupole mass analyzers improves and as problems in interfacing SFC to mass spectrometer ion sources operating at high voltage are overcome (17) SFC-MS and SFI-MS will become even more powerful tools in characterizing mixtures containing high molecular weight, less volatile species.

#### ACKNOWLEDGMENT

The authors thank T. L. Chester, T. Keough, and R. J. Strife for guidance and useful discussions.

**Registry No.** Methyl arachidate, 1120-28-1; tristearin, 555-43-1.

#### LITERATURE CITED

- Markides, K. E.; Fields, S. M.; Lee, M. L. *J. Chromatogr. Sci.* **1986**, *24*, 254-257.
- Chester, T. L.; Innis, D. P. *HRC CC, J. High Resolut. Chromatogr. Commun.* **1986**, *9*, 209-212.
- Gouw, T. H.; Jentoft, R. E.; Gallegos, E. J. *J. High Pressure Sci. Technol. AIRAPT Conf. 6th* **1979**, 583-592.
- Randall, L. G.; Wahrhaftig, A. L. *Rev. Sci. Instrum.* **1981**, *52*, 1283-1295.
- Smith, R. D.; Felix, W. D.; Fjeldsted, J. C.; Lee, M. L. *Anal. Chem.* **1982**, *54*, 1883-1885.
- Smith, R. D.; Udseth, H. R. *Anal. Chem.* **1983**, *55*, 2266-2272.
- Smith, R. D.; Kalinoski, H. T.; Udseth, H. R.; Wright, B. W. *Anal. Chem.* **1984**, *56*, 2476-2480.
- Smith, R. D.; Udseth, H. R.; Kalinoski, H. T. *Anal. Chem.* **1984**, *56*, 2971-2973.
- Smith, R. D.; Udseth, H. R.; Wright, B. W. *J. Chromatogr. Sci.* **1985**, *23*, 192-199.
- Smith, R. D.; Fulton, J. L.; Peterson, R. C.; Kopriva, A. J.; Wright, B. W. *Anal. Chem.* **1986**, *58*, 2057-2064.
- Wright, B. W.; Kalinoski, H. T.; Udseth, H. R.; Smith, R. D. *HRC CC, J. High Resolut. Chromatogr. Commun.* **1986**, *9*, 145-153.
- Smith, R. D.; Udseth, H. R. *Anal. Chem.* **1987**, *59*, 13-22.
- Crowther, J. B.; Henion, J. D. *Anal. Chem.* **1985**, *57*, 2711-2716.
- Lee, E. D.; Henion, J. D. *HRC CC, J. High Resolut. Chromatogr. Commun.* **1986**, *9*, 172-174.
- Holzer, G.; Deluca, S.; Voorhees, K. J. *HRC CC, J. High Resolut. Chromatogr. Commun.* **1985**, *8*, 528-531.
- Zaug, S. D.; Deluca, S. J.; Holzer, G. U.; Voorhees, K. J. *HRC CC, J. High Resolut. Chromatogr. Commun.* **1987**, *10*, 100-101.
- Kalinoski, H. T.; Udseth, H. R.; Chess, E. K.; Smith, R. D. *J. Chromatogr.* **1987**, *394*, 3-14.
- Lee, E. D.; Henion, J. D.; Cody, R. B.; Kinsinger, J. A. *Anal. Chem.* **1987**, *59*, 1309-1312.
- Chester, T. L.; Burkes, L. J.; Delaney, T. E.; Innis, D. P.; Owens, G. D.; Pinkston, J. D. "Capillary Supercritical Fluid Chromatography with Applications in the Food Industry". Presented at the 193rd National Meeting of the American Chemical Society, Denver, CO, April 5-10, 1987.
- Chester, T. L.; Innis, D. P.; Owens, G. D. *Anal. Chem.* **1985**, *57*, 2243-2247.
- Pinkston, J. D.; Owens, G. D.; Millington, D. S.; Maltby, D. A.; Burkes, L. J.; Delaney, T. E. "Supercritical Fluid Chromatography-Mass Spectrometry Using a 'High Mass' Quadrupole Mass Spectrometer and Splitless Injection". Presented at the 35th ASMS Conference on Mass Spectrometry and Allied Topics, Denver, CO, May 24-29, 1987.
- Bertrand, M. J.; Maltby, L.; Evans, M. J. *Anal. Chem.* **1987**, *59*, 194-197.
- Westmore, J. B.; Alauddin, M. M. *Mass Spectrom. Rev.* **1986**, *5*, 381-465.
- Reinhold, V. N. *Methods of Enzymology*; Academic: New York, 1987; Vol. 138, Chapter 5.
- Chester, T. L.; Pinkston, J. D.; Owens, G. D., unpublished work, The Procter & Gamble Co., Miami Valley Laboratories, 1986.
- Burkes, L. J.; Owens, G. D.; Lacey, M. P.; Simms, J. R.; Keough, T.; Pinkston, J. D. "Design Considerations and Industrial Applications of a Supercritical Fluid Chromatography-Mass Spectrometer." Presented at the 1987 Pittsburgh Conference and Exposition on Analytical Chemistry and Applied Spectroscopy, Atlantic City, NJ, March 9-13, 1987.
- Owens, G. D.; Burkes, L. J., unpublished work, The Procter & Gamble Co., Miami Valley Laboratories, 1985.
- Kuel, J. C.; Markides, K. E.; Lee, M. L. *HRC CC, J. High Resolut. Chromatogr. Commun.* **1987**, *10*, 257-262.

RECEIVED for reviewed May 28, 1987. Accepted January 7, 1988.

## Average Mass Approach to the Isotopic Analyses of Compounds Exhibiting Significant Interfering Ions

Karl F. Blom

E. I. du Pont de Nemours & Company, Medical Products Department, Experimental Station, E336/29A, Wilmington, Delaware 19898

The recently proposed average mass approach to isotopic analysis is extended to the analyses of materials for which the molecular ion groups are distorted by the presence of one or more overlapping species. The method is simple and direct and could prove to be more general and accurate than conventional approaches to these problems.

Mass spectrometry is the method of choice for the quantification of stable isotope labels in organic and inorganic

materials (1) with only a few possible exceptions (2). The conventional approach to deducing the isotopic content of a sample from its mass spectral pattern is to construct a set of simultaneous equations which describe the molecular ion distribution in terms of the various isotopic forms comprising it. One then solves this set of simultaneous equations for the relative proportions of the labeled species in the sample. If the labeled material is comprised of elements that are predominantly monoisotopic in their natural forms (e.g., C, H, N, O, F, etc.) and gives rise to a "pure" molecular ion (i.e., there are no interfering fragment ions), then the set of simultaneous

equations is linear and relatively simple to solve. The isotopic analyses of these systems are thoroughly understood and well documented (1). However, if the labeled material contains polyisotopic elements (e.g., Cl, Mo, Sn, Os, Pt, etc.), then the set of simultaneous equations can be much more difficult to solve. And, if the labeled material gives rise to significant abundances of ions which interfere with the molecular ion distribution (such as  $(M - H)^+$ ), the set of simultaneous equations is much more complex and can be nonlinear. Although reasonably accurate solutions have been reported for the simplest situations involving interfering fragment ions (3), it is often impossible to solve the more complex systems exactly. There have been several reports of sophisticated numerical methods which can provide approximate solutions for some of the more complex situations (4-6). However, these approaches usually require one to make assumptions about the distributions of naturally occurring isotopes of the elements and/or the relative distributions of fragment ions for the labeled and the unlabeled materials; these approximations could lead to significant errors in some cases.

Recently, a new approach to isotopic analysis based on the mass spectrometrically determined average mass of the sample was proposed (7). The average mass method could be a viable alternative to conventional means of analysis in some situations. Since the solution to the average mass equation is direct and exact for compounds with complex naturally occurring isotopic distributions, this method may be ideally suited to the isotopic analyses of materials which contain polyisotopic elements (such as inorganic and organometallic compounds). Work in other laboratories has demonstrated that it is possible to measure the average mass of an isotopic cluster precisely even at high mass (8) and when the peaks in the cluster are not resolved (9-11). Consequently, the average mass approach could eventually prove useful in the isotopic analyses of high molecular weight samples and those which require the use of mass spectral methods which cannot provide unit mass resolution. The introductory report did not, however, address the difficult and commonly encountered problem of analyzing materials which give rise to molecular ion groups that are distorted by the presence of interfering ionic species (such as  $(M - H)^+$  fragment ions). The relationships presented were not directly applicable to these systems. The purpose of the present communication is to extend the average mass method to the analyses of those compounds whose molecular ion groups are complicated by interfering ionic species. The result will be a method which should be more exact and more widely applicable than the conventional methods for analyzing these systems.

## EXPERIMENTAL SECTION

The isotopic distributions were acquired with at least unit mass resolution and the masses of the peaks were measured with unit mass precision (i.e., only the integer masses of the peaks were determined). The data for the *p*-chloro-*N*-trifluoroacetylaniline were obtained with a Finnigan MAT 8230 mass spectrometer under methane chemical ionization,  $CI(CH_3)$ , conditions. The pressure of the  $CH_4$  reagent gas was not measured directly but was estimated to be approximately 1 Torr. The ionizing voltage was 250 eV and the ionizing current was 0.05 mA. The source block temperature was 220 °C. The samples were introduced with a heated direct insertion probe. The resolution was 1000 amu<sup>-1</sup>, the scan rate was 2 s/decade, and the mass range scanned was 75-800 amu. The <sup>15</sup>N-labeled material was estimated to be 100 atom % enriched (12).

The data for the benzhydrols were obtained with an HP 5982A quadrupole mass spectrometer operated in the EI mode. The ionizing voltage was 70 eV and the ionizing current was 0.2 mA. The source block temperature was 70 °C. The benzhydrols were introduced with an unheated direct insertion probe. The intensities of the peaks in the molecular ion group were sampled 1000 times per determination in a bidirectional, cyclic fashion

(e.g., a-b-c; c-b-a; a-b-c; etc.) to simulate simultaneous detection of the peaks. The <sup>2</sup>H-labeled benzhydrol was 99.0 ± 0.6 atom % enriched (3).

The average masses of the measured isotopic distributions for the molecular ion groups were calculated with

$$M_a = \frac{\sum_{i=1}^n m_i I_i}{\sum_{i=1}^n I_i} \quad (1)$$

where  $n$  is the number of peaks in the molecular ion group and  $m_i$  and  $I_i$  are the mass and intensity for peak  $i$ .

## THEORY

A material that has been partially enriched in the heavy isotopic form of one element will be a mixture of isotopic variants of the sample compound; where each isotopic variant contains a different number and/or distribution of the heavy isotope. Each of the isotopic variants will give rise to a unique mass spectral pattern which can be characterized by the average mass of its molecular ion group,  $M_i$ . The average mass of the molecular ion group for the mixture of variants comprising the enriched material,  $M_a$ , is the weighted sum of the average masses of the molecular ion groups for all of the isotopic variants

$$M_a = \frac{\sum_{i=1}^n S_i X_i M_i}{\sum_{i=1}^n S_i X_i} \quad (2)$$

where  $n$  is the number of isotopic variants present,  $S_i$  is the relative molar response factor or sensitivity for variant  $i$ , and  $X_i$  is the mole fractional abundance of variant  $i$  in the isotopically enriched material.

The average mass for a collection of elements (like a molecular ion) is just the sum of the average masses for the constituent elements

$$M_i = \sum_j N_j m_j \quad (3)$$

where  $N_j$  is the number of occurrences of element  $j$  and  $m_j$  is its average mass. Now, consider the material in which  $N$  occurrences of one element are enriched in the heavy isotopic form of the element; by a simple extension of eq 3, one can describe the average mass of the "pure" molecular ion for the isotopic variant which contains  $N_i$  occurrences of the heavy isotope as

$$M_i = \sum_j N_j m_j + N_i m_H + (N - N_i) m_L \quad (4)$$

where  $m_H$  and  $m_L$  are the nuclidic masses for the heavy and light isotopic forms of the labeled element and  $N_j$  and  $M_j$  now represent the number of occurrences and average masses for those elements in the sample compound other than the  $N$  occurrences of the labeled element.

In general, the physicochemical properties of isotopically labeled variants are very nearly the same. Consequently, the relative response factors,  $S_i$ , for the isotopic variants of a compound will be approximately equal (6). Substituting eq 4 into eq 2 for  $M_i$  and assuming that the relative response factors are the same for all isotopic variants give

$$M_a = \sum_i X_i [\sum_j N_j m_j + N_i m_H + (N - N_i) m_L] \quad (5)$$

Evaluating the summations in eq 5 and rearranging produces an expression which relates the average mass of the "pure" molecular ion group to the isotopic content of the material

$$M_a = M_0 + N(m_H - m_L) X_H \quad (6)$$

where  $X_H$  is the mole fractional abundance of the enriched element present as the heavy isotope averaged over the entire sample and  $M_0$  replaces the cumbersome collection of terms,  $\sum_j N_j m_j + N m_L$ . Equation 6 is identical with that which was reported previously (7); however, the derivation presented here is more rigorous and general in its approach. Let us now use



this same approach to see how the average mass method might be applied in more complicated situations.

In most cases it is either not convenient or not possible to produce a "pure" molecular ion for the material being analyzed. The molecular ion group is most often a mixture of the molecular ions and one or more interfering ionic species (usually fragment ions such as  $(M - H)^+$ ). For a "mixed" molecular ion group composed of the molecular species and  $n$  different interfering species, the average mass of the ionic distribution for isotopic variant  $i$  will be

$$M_i = X(m)_i M(m)_i + \sum_{k=1}^n X(f)_{ik} M(f)_{ik} \quad (7)$$

where  $M(m)_i$  and  $X(m)_i$  are the average mass and mole fractional abundance of the molecular species in the mixed cluster and  $M(f)_{ik}$  and  $X(f)_{ik}$  are the average mass and abundance of interfering species  $k$  for isotopic variant  $i$ . Rewriting the abundance of the molecular species as  $(1 - \sum_k X(f)_{ik})$  and rearranging give

$$M_i = M(m)_i - \sum_k X(f)_{ik} [M(m)_i - M(f)_{ik}] \quad (8)$$

The differences between the average masses of the molecular and interfering species,  $[M(m)_i - M(f)_{ik}]$ , are equal to the average masses of the neutral difference,  $M(n)_k$ . Making this substitution in eq 8 and replacing the average mass for the molecular species,  $M(m)_i$ , with eq 4 give

$$M_i = M_0 + N_i(m_H - m_L) - \sum_k X(f)_{ik} M(n)_k \quad (9)$$

where  $M_0$  again represents the quantity  $\sum_j N_j m_j + N m_L$ .

Equation 9 represents a general description for the average mass of a mixed molecular ion group for a single isotopic variant of the sample molecule. However, the relative abundances of the interfering ions in the cluster,  $X(f)_{ik}$ , will generally not be known and may depend on the isotopic labeling. Specifically, if an ionic decomposition producing an interfering fragment ion involves atoms which are isotopically enriched, then the fragment ion may be "split" into two or more isotopic variants. For example, the  $(M - H)^+$  fragment ion in the EI spectrum of  $\alpha$ -deuterio-labeled benzhydrol is split into an  $(M - H)^+$  fragment and an  $(M - D)^+$  fragment (3, 13).

If all of the enriched sites are chemically equivalent, then the "splitting ratio" for an isotopic variant will be proportional to the number of occurrences of the light and heavy isotopes. The simple case in which one fragment ion is split into two isotopic variants is described in eq 10a and 10b, where  $X(f)_L$

$$X(f)_L = \alpha(N - N_i) \quad (10a)$$

$$X(f)_H = \beta N_i \quad (10b)$$

is the mole fraction of the interfering fragment ion containing the light isotope (e.g.,  $(M - D)^+$ ) and  $X(f)_H$  is the abundance of the heavy isotopic variant of the fragment (e.g.,  $(M - H)^+$ ). The splitting coefficients,  $\alpha$  and  $\beta$ , are related to the relative rates of the ionic decompositions and are dependent upon the experimental conditions. If there is a kinetic isotope effect associated with the ionic fragmentation (as there usually is) then these coefficients will not be equal ( $\alpha \neq \beta$ ). Substituting eq 10a and 10b into eq 9 for the mole fractions of the isotope variants of the split fragment ion,  $X(f)_{ik}$ , and rearranging give the result

$$M_i = M_0 + N_i[(m_H - m_L) + \alpha M(n)_L - \beta M(n)_H] \quad (11)$$

where  $M(n)_L$  and  $M(n)_H$  represent the average masses for the neutral fragments eliminated in forming the light and heavy isotopic forms of the fragment ions. Note that since  $\alpha$  and  $\beta$  are constants for a given material under a given set of experimental conditions, the collection of terms within the braces is also a constant.

Equation 11 describes the average mass of the molecular ion group for an isotopic variant which produces a single interfering fragment ion which is split into two isotopic forms by the labeling. Expressions describing more complex situations in which the mixed molecular ion group contains many interfering species and/or the fragment ions are split into many isotopic variants can be exceedingly complex and cumbersome. However, so long as the enriched sites involved in the splitting are equivalent (i.e., so long as eq 10a and b are valid), the general form and behavior of the final expressions are identical with those described in eq 11. In general, the expression describing the relationship between the number of heavy isotope labels in a specific variant and the average mass of its mixed molecular ion group can be simplified to

$$M_i = M_0 + N_i \Delta M \quad (12)$$

where  $M_0$  represents the average mass of the molecular ion group for the isotopic variant which contains zero (0) occurrences of the heavy isotope label and  $\Delta M$  represents the increase in the average mass of the molecular ion group per heavy isotope substitution. As in eq 11, if the enriched sites in the sample compound are equivalent, then the coefficients  $M_0$  and  $\Delta M$  are fixed quantities for that material under a given set of experimental conditions. Thus, eq 12 has the general form of a linear equation in which  $M_0$  is the intercept and  $\Delta M$  is the slope. (It is not actually a linear equation, however, because it is not a continuous function.)

Now, inserting this expression for the average mass of the mixed molecular ion group of a single isotopic variant, eq 12, into eq 2 and evaluating the summations generate a simple expression relating the average mass of the mixed molecular ion group for the enriched material to the degree of labeling

$$M_a = M_0 + X_H N \Delta M \quad (13)$$

where  $X_H$  is again the mole fractional abundance of the heavy isotope in the enriched population averaged over the entire sample. Note that eq 13 is just a more general expression of eq 6; this relationship should be valid regardless of overlapping species. Finally, solving eq 13 for the mole fractional abundance of the heavy isotope label,  $X_H$ , gives

$$X_H = (M_a - M_0) / N \Delta M \quad (14)$$

This is the equation that is used to determine the total isotopic contents of isotopically enriched materials from the average masses of their molecular ion groups.

## RESULTS AND DISCUSSION

For cases in which the labeling sites in the sample compound are equivalent, eq 12 postulates that the average mass of the molecular ion group for an isotopic variant,  $M_i$ , is proportional to the number of heavy isotope labels the variant contains,  $N_i$ . This relationship is the foundation of the average mass approach to isotopic analysis outlined above. The validity of this relationship may be demonstrated with a simple example. The average masses of the mass spectral patterns for natural methane and the four deuterio-labeled methanes (representing the five possible deuterio-variants of methane) are given in Table I. The  $H^+$  and  $H_2^+$  fragment ions have been included in this analysis because they are also split by the isotopic labeling. The average masses were calculated from the data in ref 1 and 14. A least-squares linear regression of these data gave a slope ( $\Delta M$ ) of  $0.894 \pm 0.006$  amu, an intercept ( $M_0$ ) of  $14.812 \pm 0.014$  amu, and a correlation coefficient of 0.9999. These results indicate that the relationship between  $M_i$  and  $N_i$  is a "linear" one as postulated in eq 12 and affirms the validity of the average mass approach described above.

**Determining Coefficients.** In many cases it will not be possible to evaluate the coefficients in eq 14,  $M_0$  and  $\Delta M$ , a



Table I. Average Masses of the  $^2\text{H}$  Variants of Methane

no. of labels	ref	av mass <sup>a</sup>	$(M_i - M_0)/N_i^b$
0	1	14.804	
1	14, API-0458	15.716	0.912
2	14, API-0457	16.613	0.905
3	14, API-0456	17.468	0.888
4	14, API-0455	18.395	0.898

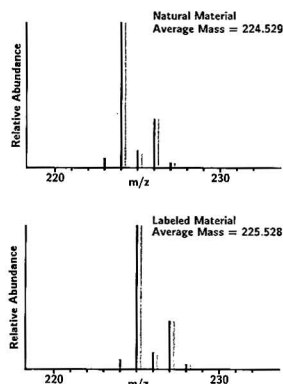
<sup>a</sup>In amu, includes all peaks from  $m/z$  2 through  $m/z$  21.<sup>b</sup>Change in average mass per heavy isotope substitution, in amu.

Figure 1.  $(M + H)^+$  ion groups in the  $\text{Cl}(\text{CH}_3)_3$  mass spectra of natural and  $^{15}\text{N}$ -labeled  $p$ -chloro- $N$ -trifluoroacetylaniline. The black peaks represent the measured patterns; the gray peaks represent the calculated isotope patterns for  $(M + H)^+$ .

priori. However, the values of these coefficients can be determined experimentally by using samples of known isotopic content. There are two cases we should consider. In the simpler of the two cases the processes producing the interfering ions do not involve the isotopic labels; consequently, the interfering ions are not isotopically split. For example, the elimination of H from an  $M^+$  ion will not be split or significantly affected in any way by the presence of  $^{13}\text{C}$  labels. In this case the change in the average mass of the molecular ion group per heavy isotope substitution,  $\Delta M$ , is simply equal to the difference in the masses of the light and heavy isotopic forms of the labeled element,  $(m_H - m_L)$ . After  $\Delta M$  is calculated, the value of  $M_0$  can then be ascertained from the measured average mass of the molecular ion group for one sample of known isotopic composition by using

$$M_0 = M_a - X_H N \Delta M \quad (15)$$

It will usually be convenient to use the unlabeled or natural sample for this purpose; in which case  $X_H$  will just be the naturally occurring abundance of the heavy isotope for the labeled element (e.g.,  $X_H = 0.0111$  for carbon).

This situation is illustrated in Figure 1 which shows the  $(M + H)^+$  ion groups in the  $\text{Cl}(\text{CH}_3)_3$  mass spectra of  $p$ -chloro- $N$ -trifluoroacetylaniline ( $\text{C}_8\text{H}_6\text{NOF}_3\text{Cl}$ ) and its mono- $^{15}\text{N}$ -labeled analogue. The measured distributions are in black; the gray peaks represent the calculated isotopic distributions for the  $(M + H)^+$  species. The measured distributions are dominated by the  $(M + H)^+$  species, but the patterns are distorted by the presence of small amounts of  $M^+$  (which have relative abundances of about 6% that of the  $(M + H)^+$  ions). The relative abundances of overlapping species should be unaffected by the  $^{15}\text{N}$  labeling. Thus,  $\Delta M$  for this system should just be equal to the difference in the nucleic masses of  $^{14}\text{N}$  and  $^{15}\text{N}$ ; i.e.,  $\Delta M = 1.000$  amu. (Note that all the mass calculations presented here will use the integer masses of the

Table II. Molecular Ion Distributions for Natural and  $\alpha$ -Deuterio-Labeled Benzhydrol

Natural Benzhydrol		
<i>m/z</i>	major species present	rel abundance <sup>a,b</sup>
183	(M - H) <sup>+</sup>	27.60
184	M <sup>++</sup> , <sup>13</sup> C(M - H) <sup>+</sup>	100.00
185	<sup>13</sup> C(M <sup>++</sup> ), <sup>13</sup> C <sub>2</sub> (M - H) <sup>+</sup>	14.54
186	<sup>13</sup> C <sub>2</sub> (M <sup>++</sup> )	1.19
Average Mass = 183.927 ± 0.002 amu		
α-D-Labeled Benzhydrol		
<i>m/z</i>	major species present	rel abundance <sup>a,b</sup>
183	(M - D) <sup>+</sup>	4.05
184	(M - H) <sup>+</sup> , <sup>13</sup> C(M - D) <sup>+</sup>	28.38
185	M <sup>++</sup> , <sup>13</sup> C(M - H) <sup>+</sup> , <sup>13</sup> C <sub>2</sub> (M - D) <sup>+</sup>	100.00
186	<sup>13</sup> C(M <sup>++</sup> ), <sup>13</sup> C <sub>2</sub> (M - H) <sup>+</sup>	15.12
187	<sup>13</sup> C <sub>2</sub> (M <sup>++</sup> )	1.96
Average Mass = 184.883 ± 0.002 amu		
Gravimetric Mixture		
<i>m/z</i>	rel abundance <sup>a,c</sup>	
183	25.98	
184	100.00	
185	57.84	
186	7.82	
187	0.87	
Average Mass = 184.260 ± 0.002 amu		

<sup>a</sup>Relative to base peak = 100%. <sup>b</sup>Average for 11 determinations. <sup>c</sup>Average for five determinations.

peaks or isotopic forms of interest. This point will be discussed in detail later.) It is a simple matter to test this hypothesis. The abundance of  $^{15}\text{N}$  in the natural aniline is 0.37% and the isotopic purity of the labeled aniline is estimated to be 100 atom %; these materials essentially represent the pure unlabeled and mono- $^{15}\text{N}$ -labeled variants of the aniline. Consequently, the difference in the average masses of their molecular ion groups is equivalent to  $\Delta M$ . The measured average masses for the natural and labeled materials are  $224.529 \pm 0.003$  and  $225.528 \pm 0.003$  amu (average for 20 scans  $\pm 1$  standard deviation), respectively. The difference in the average masses is  $0.999 \pm 0.004$  amu, in agreement with the calculated value for  $\Delta M$ .

The value of  $M_0$  is calculated directly with eq 15 by using the measured average mass for the natural material ( $M_a = 224.529$  amu), the calculated value for  $\Delta M$  ( $\Delta M = 1.000$  amu), and the natural occurring abundance of  $^{15}\text{N}$  ( $X_H = 0.0037$ ). Using these quantities, one calculates the value for  $M_0$  under these experimental conditions as  $224.525 \pm 0.004$  amu.

In the second case, decompositions forming interfering fragment ions involve the isotopic labels and the fragment ions may be split. The value of  $\Delta M$  cannot be calculated a priori in this case. However, the value of  $\Delta M$  can be evaluated from a simultaneous solution of eq 14 for two samples of different, but known, isotopic content

$$\Delta M = [M_a(1) - M_a(2)] / [X_H(1) - X_H(2)] \quad (16)$$

where (1) and (2) denote the quantities for the two samples of known composition and  $N$  is the number of labels. The value of  $\Delta M$  thusly determined can then be used with eq 15 to calculate  $M_0$ .

This situation is exemplified by the molecular ion groups in the EI mass spectra of natural and  $\alpha$ -deuterio-labeled benzhydrol which are given in Table II. The molecular ion groups consist of an  $M^+$  species and an  $(M - H)^+$  fragment

which is split into  $(M - H)^+$  and  $(M - D)^+$  by the  $\alpha$ -deuterio-labeling. The average masses of the distributions for the natural and labeled materials, as calculated with eq 1, are  $183.927 \pm 0.002$  amu and  $184.883 \pm 0.002$  amu (average for 11 determinations  $\pm 1$  standard deviation). The naturally occurring abundance of  $^2H$  in the unlabeled benzhydrol is 0.015% and the labeled material is  $99.0 \pm 0.6$  atom % enriched (3). Inserting these values into eq 16 and using  $N$  equal to one give the value of  $\Delta M$  as 0.966 amu. Note that the value of  $\Delta M$  will always be less than the difference in the nuclidic masses of the isotopes if the fragment ions are isotopically split. Now, inserting this value for  $\Delta M$  and the average mass for the unlabeled material into eq 15, one calculates a value for  $M_0$  of 183.927 amu.

Note that the second method is the more general of the two since it requires no direct knowledge about the origins of the interfering species or the effect of the labeling on the pattern of interfering species in the molecular ion groups. Thus, this method should be used if there is any doubt about splitting of the interfering species. However, the first procedure may be preferred in some cases because it does not require the use of an enriched sample of known isotopic content.

**Calculating Isotopic Content.** Once the coefficients,  $M_0$  and  $\Delta M$ , have been determined by one of the procedures described above, it is a relatively simple matter to calculate the isotopic content of "unknown" samples using eq 14. For demonstrative purposes, a mixture of the natural and  $\alpha$ -deuterio-labeled benzhydrols was prepared gravimetrically in which  $X_H$  was equal to  $0.3448 \pm 0.0020$ . (The value of  $X_H$  was corrected for the naturally occurring  $^2H$  in the unlabeled sample and the  $^1H$  impurity in the labeled material.) The molecular ion distribution for this mixture is listed in Table II. The average mass for the distribution is  $184.260 \pm 0.002$  amu. Inserting this quantity and the values calculated above for  $M_0$  and  $\Delta M$  into eq 16, one obtains a value of  $0.345 \pm 0.002$  for  $X_H$ . This result is in agreement with the gravimetric composition.

**Limitations of Approach.** The method of isotopic analysis outlined above may not be applicable if the isotopically labeled sites within the sample compound are chemically different. This is because the value of  $\Delta M$  could be different for ionic decompositions occurring from chemically different enrichment sites. As an example, the major peaks in the molecular ion groups of the EI mass spectra for natural toluene, (monodeuteriomethyl)benzene, 1-deuterio-4-methylbenzene, and 1-deuterio-2-methylbenzene are shown in Table III. These data are from ref 14. The  $^2H$  labeling splits the  $(M - H)^+$  ion into  $(M - H)^+$  and  $(M - D)^+$  fragments. The splitting ratio (the relative abundances of the  $(M - H)^+$  and  $(M - D)^+$ ) depends upon where the  $^2H$  label is located within the toluene. The value of  $\Delta M$  for a labeled toluene is equivalent to the difference between the average masses for the natural and the labeled materials. (The average masses of the molecular ion groups are given in Table III.) With these differences  $\Delta M$  is 0.8852 amu for the methyl-labeled toluene, 0.9710 amu for the 1-4-ring-labeled toluene, and 0.9702 amu for the 1-2-ring-labeled material. The values of  $\Delta M$  are essentially equal for the two ring-labeled toluenes because the labeling sites are essentially equivalent. However,  $\Delta M$  is smaller for the methyl-labeled material than for the ring-labeled materials because the extent of the isotopic splitting is greater, i.e., because there is more of the lighter fragment,  $(M - D)^+$ , formed by the methyl labeling.

To describe the molecular ion group for a toluene sample labeled on both the methyl group and the aromatic ring would require an additional parameter, i.e., the relative amounts of methyl- and ring-labeled species. It may be possible to derive this information from higher order moments of the ionic

Table III. Molecular Ion Groups for Natural and  $^2H$  Labeled Toluenes<sup>a</sup>

Natural Toluene		
<i>m/z</i>	major species present	rel abundance <sup>b</sup>
91	$(M - H)^+$	100.0
92	$M^{++}, ^{13}C(M - H)^+$	77.0
93	$^{13}C(M^{++})$	5.4
Average Mass = 91.2974 amu		
(Monodeuteriomethyl)benzene		
<i>m/z</i>	major species present	rel abundance <sup>b</sup>
91	$(M - D)^+$	25.9
92	$(M - H)^+, ^{13}C(M - D)^+$	100.0
93	$M^{++}, ^{13}C(M - H)^+$	82.1
94	$^{13}C(M^{++})$	6.2
Average Mass = 92.1826 amu		
1-Deuterio-4-methylbenzene		
<i>m/z</i>	major species present	rel abundance <sup>b</sup>
91	$(M - D)^+$	8.5
92	$(M - H)^+, ^{13}C(M - D)^+$	100.0
93	$M^{++}, ^{13}C(M - H)^+$	71.8
94	$^{13}C(M^{++})$	6.1
Average Mass = 92.2684 amu		
1-Deuterio-2-methylbenzene		
<i>m/z</i>	major species present	rel abundance <sup>b</sup>
91	$(M - D)^+$	8.9
92	$(M - H)^+, ^{13}C(M - D)^+$	100.0
93	$M^{++}, ^{13}C(M - H)^+$	72.4
94	$^{13}C(M^{++})$	6.1
Average Mass = 92.2676 amu		

<sup>a</sup>Data from ref 14. <sup>b</sup>Relative to base peak = 100%.

distribution (15); this approach will be investigated in later communications. However, the present equations cannot be used in these situations.

While this does (for now) represent a limitation to the average mass method of isotopic analysis, the limitation should not be a serious one. In practice, systems of this type are rarely encountered because one generally directs the isotopic enrichment toward a specific functionality or chemically specific site; e.g., one will generally enrich the methyl group of the toluene or the aromatic ring, but one would seldom do a partial enrichment of both simultaneously.

**Using Normal Masses.** The mathematical properties and physical significance of an average mass calculated from the nominal (or integer) masses of the components in a distribution are the same as those of an average mass arising from the "exact" masses. Consequently, the relationships presented here are equally correct whether one uses the "nominal" average mass (the average mass arising from the nominal masses of the distribution) or the "exact" average mass (the average mass calculated from the "exact" masses of the distribution). However, if one uses the nominal masses of the mass spectral peaks, then nominal masses must be used throughout; i.e.,  $m_L$  and  $m_H$  must be the nominal nuclidic masses of the isotopes. All of the calculations presented in this communication used the nominal masses of the peaks and/or isotopic forms.

No accuracy or precision is sacrificed by using nominal or integer masses. This point is easily demonstrated with an example. The calculated statistical isotopic distributions for natural dodecane and 25 atom %  $^{13}C$  enriched dodecane are shown in Table IV. The distributions were calculated for unit

Table IV. Calculated Molecular Ion Distributions for Natural and 25 atom %  $^{13}\text{C}$ -Enriched Dodecane<sup>a</sup>

integer mass	"exact" mass <sup>b</sup>	relative distributions <sup>c</sup>	
		natural	25 atom % enriched
170	170.2034	100.0000	12.2298
171	171.2068	13.8596	48.9667
172	172.2101	0.8848	89.8757
173	173.2135	0.0345	100.0000
174	174.2168		75.1267
175	175.2202		40.1522
176	176.2235		15.6571
177	177.2269		4.4896
178	178.2302		0.9401
179	179.2336		0.1403
"Integer" Average Mass (amu):		170.1371	173.0036
"Exact" Average Mass (amu):		170.3409	173.2171

<sup>a</sup> Simulated isotope patterns for natural and 25 atom %  $^{13}\text{C}$ -enriched dodecane,  $\text{C}_{12}\text{H}_{26}$ . <sup>b</sup> Mass of peak to a precision of 0.0001 amu. <sup>c</sup> Relative to base peak = 100%. Peaks with relative abundances less than 0.02% of the base peak are not included in listing.

mass resolution and the masses of the peaks are reported with integer precision and with a precision of 0.0001 amu. The average masses of the distributions calculated by using the integer masses and the "exact" masses of the peaks are given in Table IV. Since there are no interfering ions, the value of  $\Delta M$  will just be the difference between the masses of  $^{12}\text{C}$  and  $^{13}\text{C}$ ;  $\Delta M$  is equal to 1.000 00 amu for the nominal masses of the isotopes and 1.003 35 amu for the exact masses. Using these values for  $\Delta M$ ,  $N$  equal to 12, the average masses for the natural distribution, and eq 15, one calculates  $M_0$  as 170.0039 amu for the nominal mass data and 170.2073 amu for the "exact" mass data. Finally, by insertion of these values

for the coefficients and the average masses for the isotopically enriched distribution (Table IV) into eq 14, the degree of enrichment is calculated to be 0.249 98 with the integer mass data and 0.249 98 using the "exact" mass data. Both results are close to the actual value of 0.25; the small deviations are the result of round-off errors in the calculations. Clearly, the calculation of the isotopic content does not depend upon whether one uses the nominal or the exact masses of the mass spectral peaks.

## LITERATURE CITED

- (1) Blomann, K. *Mass Spectrometry: Organic Chemical Applications*; McGraw-Hill: New York, 1962; Chapter 5.
- (2) Irving, C. S.; Klein, P. D.; Navratil, P. R.; Boutton, T. W. *Anal. Chem.* **1986**, *58*, 2172-2178.
- (3) Blom, K.; Schuhardt, J.; Munson, B. *Anal. Chem.* **1985**, *57*, 1986-1988.
- (4) Sukharev, Y. N.; Nekrasov, Y. S. *Org. Mass Spectrom.* **1976**, *11*, 1239-1241.
- (5) Lee, W. N. P.; Whiting, J. S.; Fymat, A. L.; Boettger, H. G. *Biomed. Mass Spectrom.* **1983**, *10*, 641-645.
- (6) Benz, W. *Anal. Chem.* **1980**, *52*, 248-252.
- (7) Blom, K.; Dybowski, C.; Munson, B.; Gates, B.; Hasselbring, L. *Anal. Chem.* **1987**, *59*, 1372-1374.
- (8) Yergey, J.; Heller, D.; Hansen, G.; Cotter, R. J.; Fenselau, C. *Anal. Chem.* **1983**, *55*, 353-356.
- (9) Hakansson, P.; Kamenski, I.; Sundqvist, B.; Fohlman, J.; Petersen, P.; McNeal, C. J.; McFarlane, R. D. *J. Am. Chem. Soc.* **1982**, *104*, 2948-2949.
- (10) McNeal, C. J.; Ogilvie, K. K.; Theriault, N. Y.; Nemer, M. J. *J. Am. Chem. Soc.* **1982**, *104*, 976-980.
- (11) Ens, W.; Standing, K. G.; Westmore, J. B.; Ogilvie, K. K.; Nemer, M. J. *Anal. Chem.* **1982**, *54*, 960-966.
- (12) Shine, H. J., Texas Tech University, personal communication, 9 August 1984.
- (13) Blom, K. *Org. Mass Spectrom.* **1987**, *22*, 530-533.
- (14) *Atlas of Mass Spectral Data*; Stenhagen, E., Abrahamson, S., McLafferty, F. W., Eds.; Wiley: New York, 1969.
- (15) Blom, K. *Org. Mass Spectrom.*, in press.

RECEIVED for review August 3, 1987. Accepted January 12, 1988.

## Inductively Coupled Plasma Mass Spectrometric Analysis of Ultrapure Acids

Paul J. Paulsen, Ellyn S. Beary, Diane S. Bushee, and John R. Moody\*

Center for Analytical Chemistry, National Bureau of Standards, Gaithersburg, Maryland 20899

The inductively coupled plasma mass spectrometer (ICP-MS) and chemical procedures have been developed which enable the analysis of ultrapure acids and similar materials for trace elements at concentrations of a few picograms per gram ( $10^{-12}$  g/g) and less. Compared to previously reported methods for multielement analysis, the sensitivity has been improved for all elements, some by an order of magnitude and more. Sample throughput has been dramatically improved compared to the spark source mass spectrometer and methods have been developed to quantify simultaneously elements by either isotope dilution analysis or external standard calibration techniques.

The NBS Center for Analytical Chemistry has been producing and using ultrapure reagent acids since first reported

in 1972. Through the intervening years there has been substantial progress in the techniques of handling and distilling the reagents; however their analyses have been by the same spark source mass spectrometric (SSMS) isotope dilution procedure described originally (1). The last publication from this group detailed a new laboratory facility for the production of the acids and presented a summation of analytical data obtained up to that time (2). The purpose of this work was to provide an improved overall assessment of the quality of NBS ultrapure acids by means of the inductively coupled plasma mass spectrometer (ICP-MS).

Both the SSMS used previously and the ICP-MS used in this work provide wide element coverage and high absolute elemental sensitivity (subnanogram per gram). In the full mass scan mode, elements will be detected even if their presence is not anticipated. The ICP-MS was used in this work because liquid samples with low solids content ( $<0.01\%$ )

are well suited for analysis by ICP-MS, and sample throughput is significantly faster than is possible with the SSMS procedure which requires loading of samples as conducting solids (by mixing with 99.999% pure gold) (1).

Higher sensitivity (picograms per gram) is obtained by preconcentration of several hundred milliliters of acid by evaporation. ICP-MS results were obtained by two methods. Stable isotopic dilution analysis provides reliable results after equilibration of "spike" and analyte even if part of an analyte is lost during processing, because the concentration is based on a measured isotopic ratio and not the absolute signal level. Additional elements are determined by comparison to an external standard analyzed under identical ICP-MS operating conditions.

Improved methods of characterizing trace-element impurities in reagent acids are needed because instrumental and chemical improvements in trace analysis now permit much improved detection limits. To produce and monitor a high-purity product, the method of analysis becomes one of the most important factors. This paper does not present any claimed improvements in the quality of acid produced, but it does present a method of analysis which should enable us to measure any such future improvements.

### EXPERIMENTAL SECTION

**Sample Preparation.** All of the sampling and preconcentration procedures to be described were performed in a new clean laboratory similar to one previously described (2) except that the air quality in the new laboratory measures approximately Class 1 as extrapolated from Federal Standard 209b (3).

Prior to sampling, a set of sample beakers previously dedicated to the analysis of each high-purity acid was cleaned by sequential leaching for 1 week in reagent grade (1 + 1) HCl and then reagent grade (1 + 1) HNO<sub>3</sub>. The last steps of the cleaning process involved heating samples of the NBS ultrapure acid to be analyzed in the covered quartz or Teflon PFA beaker for about 3 h at temperatures just below the boiling point. When this "steaming" process was completed, the beakers were rinsed with NBS ultrapure water and heated in the same manner with about 50 mL of ultrapure water. Just prior to sampling, the beakers were again rinsed with the NBS ultrapure water.

Bottles of the reagents were taken from the inventory at random and brought to the clean laboratory where the outside surfaces of the bottles were rinsed down with distilled water before opening to sample the acid. A sample of 200–500 g was weighed into a cleaned, tared Teflon PFA beaker (quartz for H<sub>2</sub>SO<sub>4</sub>) using a top loading balance.

The samples were spiked with three solutions that contained separated isotopes of 25 elements. The nominal amount of separated isotopic spike used for each sample was 10 ng (10<sup>-8</sup> g) per element. The beakers were gently swirled to mix the spikes with the sample and then the samples were placed on hot plates inside a Class 1 fume hood for evaporation. All samples were carefully monitored to evaporate the samples completely and yet avoid baking the residue.

When dry, the sample residues were dissolved in a few drops of (1 + 1) NBS ultrapure HNO<sub>3</sub> and diluted with a few drops of distilled water. The contents were transferred to small, clean polyethylene centrifuge tubes with integral caps and diluted to a total volume of 1.5 mL. Under these conditions a preconcentration of >100 was achieved.

**Inductively Coupled Plasma Mass Spectrometry.** The ICP/MS used for this work was a VG PlasmaQuad (VG Isotopes, Ltd.). When this work was carried out, the diffusion pump on the quadrupole chamber had been replaced with a Balzer Model TPU 330 turbomolecular pump. The operating parameters for the ICP were an rf power of 1.3 kW and a coolant, auxiliary, and nebulizer argon flow of 13, 0.5, and 0.7 L/min, respectively. A peristaltic pump fitted with silicone tubing was used to introduce a constant sample flow of 0.15 mL/min. The spray chamber was cooled to 8 °C. The sampler and skimmer orifices in this study were both 0.7 mm in diameter. This resulted in pressures of 1.1 Torr (140 Pa) between the sampler and skimmer cones, 8 × 10<sup>-4</sup> Torr in the lens stack region, and 5 × 10<sup>-6</sup> Torr in the quadrupole

region. The mass range from 4 to 240 was scanned for 600 sweeps with a dwell time of 250 μs/channel. The data were summed in a 2048-channel multichannel analyzer for a data collection time of 5 min. Each solution was aspirated for about 30 s prior to data collection to equilibrate the system. The system was washed by nebulizing 1% HNO<sub>3</sub> for 5 min between samples. The computer processed the data to give integrated peak areas for each mass.

The ICP-MS ion lens voltages were optimized with a 100 ng/mL solution of Mg, In, and Pb. The lens voltages were varied to obtain a maximum signal for <sup>24</sup>Mg and <sup>115</sup>In while maintaining an adequate sensitivity for <sup>208</sup>Pb. In the scanning mode, peak areas are measured valley to valley. Requirements for sensitivity must be balanced with those of resolution. The mass resolution was adjusted to give a valley between adjacent Pb isotopes which was 1% of the maximum peak intensity. For our instrument this adjustment results in equal or better resolution for all lines below the mass of Pb. Higher resolution is obtainable but at a cost in sensitivity.

Improved sensitivity for the ICP-MS was obtained by two procedural changes. First, the sample flow rate was decreased from the usual 1–1.5 mL/min. Longerich et al. (4) have reported that sample flows to the nebulizer of 0.025 mL/min give a signal (counts per second) that is 40% of the signal obtained with a sample flow of 1 mL/min using the same sample solution. This is a 16-fold increase in instrument sensitivity (total counts per nanogram of element introduced) for the lower flow rate. We have observed similar improved sensitivity at low sample introduction rates and have selected 0.15 mL/min for most of our analyses. Changing the sample flow to the nebulizer requires reoptimization of the ion lens voltages at each flow rate in order to obtain maximum sensitivity. Thus, for our samples containing a fixed amount of material, improved sensitivity was obtained by preconcentration to 1.5 mL total sample and pumping to the nebulizer at 0.15 mL/min as compared to preconcentration to 10–15 mL that would be required for the 1–1.5 mL/min sample consumption rate normally reported.

Second, detectability was improved for elements determined by stable isotope dilution analysis by decreasing the amount of spike used. Normally, detection limits are controlled by instrumental sensitivity; however, with isotope dilution the lowest measurable concentration for each element is also controlled by the amount and isotopic purity of the spike added. As the measured isotopic ratio approaches the separated spike ratio, a measurement limit is reached and may be above the conventional detection limit of the instrument. Spikes at 10<sup>-7</sup> g of each element of interest have been used for survey analyses similar to this project [1]. However, we recognized that a lower concentration could be measured by isotope dilution ICP-MS with a 10<sup>-8</sup> g spike, since the impurity levels expected in the acids and water were at the picogram per gram level. The 10<sup>-8</sup> g spike resulted in the loss of Se measurements in these samples since the <sup>82</sup>Se spike could not be detected. Other poor sensitivity elements would also be lost if the amount of spike were reduced below 10<sup>-8</sup> g. While the 10<sup>-8</sup> g spike level consistently over spikes some elements in these acids, this amount of spike provides the broadest elemental coverage while maintaining an acceptably low detectability level.

Isotope dilution results were calculated from the integrated peak areas of the "spike" and "natural" isotope for each element by

$$C = \frac{WK(A_{sp} - B_{sp}R)}{M(BR - A)} \quad (1)$$

where  $C$  is the concentration in parts per billion (nanograms per gram),  $W$  is the weight of isotopically enriched material ("spike") added in nanograms,  $M$  is the weight of sample in grams,  $A$  and  $B$  are the natural abundances of the analyte isotopes  $a$  and  $b$ ,  $A_{sp}$  and  $B_{sp}$  are the abundances of isotopes  $a$  and  $b$  in spike,  $R$  is the measured altered ratio of isotope  $a$  to isotope  $b$ , and  $K$  is the ratio of the natural atomic weight to the atomic weight of the spike. Enriched isotopes purchased from the Oak Ridge National Laboratory included <sup>208</sup>Pb, <sup>203</sup>Tl, <sup>195</sup>Pt, <sup>183</sup>W, <sup>145</sup>Nd, <sup>142</sup>Ce, <sup>137</sup>Ba, <sup>125</sup>Te, <sup>123</sup>Sb, <sup>115</sup>In, <sup>111</sup>Cd, <sup>110</sup>Pd, <sup>97</sup>Mo, <sup>91</sup>Zr, <sup>87</sup>Rb, <sup>86</sup>Sr, <sup>73</sup>Ge, <sup>71</sup>Ga, <sup>67</sup>Zn, <sup>65</sup>Cu, <sup>62</sup>Ni, <sup>57</sup>Fe, <sup>53</sup>Cr, <sup>47</sup>Ti, and <sup>26</sup>Mg. Isotope dilution calculations were made by using the ratio of the intensities of spiked isotope to the major isotope of the element except where

**Table I. Elements Determined in NBS Distilled Water, pg/g ( $10^{-12}$  g/g)<sup>a</sup>**

By Isotope Dilution			
Pb	13	In (0.1)	Ga (0.9)
Tl	(0.1)	Cd (3)	Zn 91
Pt	(2)	Pd (0.1)	Cu 9
W	(11)	Mo (0.3)	Ni <sup>b</sup> 200
Ce	(0.2)	Zr (1.1)	Fe <sup>c</sup> (150)
Nd	(0.5)	Sr (1.1)	Cr (6)
Ba	19	Rb (0.3)	Ti (3)
Te	(4)	Ge (3)	Mg 76
Sb	(0.6)		
By External Standardization			
U	(<0.2)	Mn (2)	Na 200
Sn	(3)	V (4)	B (6)
As	(1)	Ca <sup>d</sup> (91)	Be (<2)
Co	(8)	Al 36	Li (1.5)

$\Sigma = <0.95$  ng/g  
(for 37 elements)

<sup>a</sup> All concentrations reported have one significant figure. All concentrations reported in parentheses are indistinguishable from the measurement limit. <sup>b</sup> See text. <sup>c</sup> ArO<sup>+</sup> interference. <sup>d</sup> Ar interference.

**Table II. Trace Elements Determined in NBS Nitric Acid, pg/g ( $10^{-12}$  g/g)<sup>a</sup>**

By Isotope Dilution			
Pb	(4)	In (0.2)	Ga (1.3)
Tl	(0.3)	Cd (5)	Zn 62
Pt	(8)	Pd (0.8)	Cu (3)
W	(7)	Mo (0.7)	Ni <sup>b</sup> 100
Ce	(0.3)	Zr (2)	Fe <sup>c</sup> (190)
Nd	(0.3)	Sr (0.5)	Cr 12
Ba	48	Rb (0.5)	Ti 95
Te	(8)	Ge (2)	Mg 29
Sb	(1)		
By External Standardization			
U	(0.2)	Mn (0.8)	Na (39)
Sn	(9)	V (8)	B (12)
As	(1)	Ca <sup>d</sup> (36)	Be (<5)
Co	(0.2)	Al 78	Li (<5)

$\Sigma = <0.79$  ng/g  
(for 37 elements)

<sup>a</sup> All concentrations reported have one significant figure of accuracy. All concentrations reported in parentheses are indistinguishable from the measurement limit. <sup>b</sup> See text. <sup>c</sup> ArO<sup>+</sup> interference. <sup>d</sup> Ar interference.

isobaric interferences occurred.

The external standard method was used to determine U, Sn, As, Co, Mn, V, Ca, Al, Na, B, Be, and Li. Calibration was done with a blank of NBS ultrapure 1% HNO<sub>3</sub> in ultrapure water and a standard containing 10 ng/mL of each of the elements to create a linear response curve. These two solutions were run along with the spiked samples in order to estimate concentrations.

## RESULTS AND DISCUSSION

**Purity of Ultrapure Acids.** By use of the two procedural changes previously described to enhance sensitivity, ICP-MS enabled us to lower the measurement limit and to demonstrate that the acids have total impurities at the picogram per gram to nanogram per gram level. A limitation in the analyses of high-purity solutions is that the reagent analysis cannot be isolated from the "system" blank. When an element is detected in an analysis of an acid at the picogram per gram range, it is sometimes difficult to determine whether the element is present in the acid or was leached from the container used for the processing or came from an external source. For example, if dilute HNO<sub>3</sub>, H<sub>2</sub>O, or HCl were used to determine a system blank for the HNO<sub>3</sub> analysis, the impurities found

**Table III. Trace Elements Determined in NBS Hydrochloric Acid, pg/g ( $10^{-12}$  g/g)<sup>a</sup>**

By Isotope Dilution			
Pb	(3)	In (0.4)	Ga (1.1)
Tl	(0.4)	Cd (7)	Zn (14)
Pt	78	Pd (0.9)	Cu (3)
W	(3)	Mo 8	Ni <sup>c</sup> 180
Ce	4	Zr (2)	Fe <sup>d</sup> (69)
Nd	(<4)	Sr (0.4)	Cr (2)
Ba	11	Rb (0.3)	Ti 14
Te	(9)	Ge <sup>b</sup> (18)	Mg 53
Sb	(0.5)		
By External Standardization			
U	(<0.2)	Mn (0.8)	Na (26)
Sn	72	V (<10)	B 280
As	20	Ca <sup>e</sup> (<53)	Be (<5)
Co	(8)	Al 97	Li (<1.5)

$\Sigma = <1.1$  ng/g  
(for 37 elements)

<sup>a</sup> All concentrations reported have one significant figure of accuracy. All concentrations reported in parentheses are indistinguishable from the measurement limit. <sup>b</sup> Volatile chloride. <sup>c</sup> See text. <sup>d</sup> ArO<sup>+</sup> interference. <sup>e</sup> Ar interference.

**Table IV. Trace Elements Determined in NBS Perchloric Acid, pg/g ( $10^{-12}$  g/g)<sup>a</sup>**

By Isotope Dilution			
Pb	13	In (0.4)	Ga <sup>b</sup> (6)
Tl	(0.3)	Cd (9)	Zn 90
Pt	(4)	Pd (1.2)	Cu 16
W	(7)	Mo (4)	Ni <sup>c</sup> (370)
Ce	(0.3)	Zr (0.8)	Fe <sup>d</sup> (280)
Nd	(<4)	Sr (0.6)	Cr <sup>e</sup> (110)
Ba	160	Rb (1.2)	Ti 21
Te	(18)	Ge (3)	Mg 37
Sb	(5)		
By External Standardization			
U	(<0.2)	Mn (2)	Na 110
Sn	36	V <sup>f</sup> (<140)	B 50
As <sup>g</sup>	(80)	Ca <sup>h</sup> (<10)	Be (<5)
Co	(0.3)	Al 27	Li (4)

$\Sigma = <1.6$  ng/g  
(for 37 elements)

<sup>a</sup> All concentrations reported have one significant figure of accuracy. All concentrations reported in parentheses are indistinguishable from the measurement limit. <sup>b</sup> Ba<sup>2+</sup> interference. <sup>c</sup> See text. <sup>d</sup> ArO<sup>+</sup> interference. <sup>e</sup> ClO<sup>+</sup> interference (compared to Mn external standard). <sup>f</sup> ArCl<sup>+</sup> interference. <sup>g</sup> ClO<sup>+</sup> interference. <sup>h</sup> Ar interference.

would not necessarily be representative of the impurities leached with concentrated HNO<sub>3</sub>. The decision of whether a detected element is reported as present in an acid is a subjective judgement based on the comparison of the results of all the reagents analyzed.

The results of these ICP-MS analyses are shown in Tables I-VI. All of the results are in picograms per gram ( $10^{-12}$  g/g). The results for the elements Pb-Mg (25 in all) have been determined by isotope dilution analysis. The remaining elements, U-Li (12 in all) have been determined by the external standard method. The confidence in the values obtained by using the external standard method is substantially less than for those determined by the isotope dilution method because they depend on complete recovery of the element. Many of the results given are in "parentheses". In these instances, either the element was not detected and the value reported is the instrument measurement limit or the element was detected but judged to be primarily due to the system blank. In either situation the value given in parentheses is considered an upper limit for the element in the particular acid sample.

**Table V. Trace Elements Determined in NBS Hydrofluoric Acid, pg/g ( $10^{-12}$  g/g)<sup>a</sup>**

By Isotope Dilution			
Pb 38	In (0.9)	Ga <sup>b</sup> (9)	
Tl (0.6)	Cd 30	Zn 1200	
Pt (3)	Pd (4)	Cu 35	
W (4)	Mo (1.4)	Ni <sup>c</sup> 530	
Ce (0.1)	Zr (1.5)	Fe 600	
Nd (0.3)	Sr (12)	Cr 86	
Ba 200	Rb (0.9)	Ti 140	
Te (9)	Ge (1)	Mg 640	
Sb (3)			

By External Standardization			
U (<0.2)	Mn 550	Na 1200	
Sn 240	V (<10)	B 2400	
As 61	Ca 4500	Be (<5)	
Co (1.2)	Al 320	Li (2)	

$\Sigma = <13$  ng/g  
(for 37 elements)

<sup>a</sup> All concentrations reported have one significant figure of accuracy. All concentrations reported in parentheses are indistinguishable from the measurement limit. <sup>b</sup> Ba<sup>+</sup> interference. <sup>c</sup> See text.

**Table VI. Trace Elements Determined in NBS Sulfuric Acid, pg/g ( $10^{-12}$  g/g)<sup>a</sup>**

By Isotope Dilution			
Pb 70	In (0.2)	Ga (8)	
Tl (4)	Cd 56	Zn 2700	
Pt 20	Pd (3)	Cu 270	
W (4)	Mo (1)	Ni <sup>b</sup> 1100	
Ce (1)	Zr (14)	Fe 1500	
Nd (0.5)	Sr (4)	Cr 78	
Ba 30	Rb (5)	Ti <sup>c</sup> <100	
Te (15)	Ge (3)	Mg 770	
Sb (3)			

By External Standardization			
U (0.6)	Mn 16	Na 2600	
Sn 40	V (<8)	B (<4)	
As (7)	Ca 1900	Be (<3)	
Co (5)	Al 1200	Li 36	

$\Sigma = <13$  ng/g  
(for 37 elements)

<sup>a</sup> All concentrations reported have one significant figure of accuracy. All concentrations reported in parentheses are indistinguishable from the measurement limit. <sup>b</sup> See text. <sup>c</sup> SO<sup>+</sup> interference.

All other reported values are real, detected quantities of impurities. When all values (upper limits and real values) are summed, an overall assessment of the maximum possible impurity in each acid is obtained. The summations are given along with individual values for each acid in Tables I-VI.

Table VII contains summation values for all reagents determined by ICP-MS (see Tables I-VI). For purposes of comparison, summation values previously obtained by SSMS isotope dilution for 19 elements are also listed in Table VII. These SSMS values have remained consistent for more than 10 years and therefore an average value was used. In this work we have examined 37 elements and actually found less total impurity than previously reported by SSMS for 19 elements. The summation of the impurities in each acid is primarily affected by a few elements such as Al, Na, K (not determined by ICP/MS), Ca, Mg, and sometimes Ni, Cr, Cu, and Zn. In Table VIII, the average SSMS analysis of HNO<sub>3</sub> is presented for comparison to Table II. One finds that an element by element comparison of the results obtained by ICP-MS and SSMS shows consistently lower values by ICP-MS. Table VII, however, gives the overall evaluation of reagent purity. With the improved sensitivity of the current ICP-MS procedure we

**Table VII. Total Concentration of Impurities Detected in NBS Ultrapure Reagents, ng/g ( $10^{-9}$  g/g)**

reagent	ICP-MS <sup>a</sup>	SSMS <sup>b</sup>
H <sub>2</sub> O	<0.95	<1.0
HCl	<1.1	<6.0
HNO <sub>3</sub>	<0.79	<2.7
HClO <sub>4</sub>	<1.6	<9.0
HF	<13	<14
H <sub>2</sub> SO <sub>4</sub>	<13	<21

<sup>a</sup> 36 elements, not including K. <sup>b</sup> 19 elements, including K.

**Table VIII. Elemental Concentrations in NBS Nitric Acid as Determined by SSMS, pg/g ( $10^{-12}$  g/g)<sup>a</sup>**

Pb 30	Cu 50
Tl 60	Ni 80
Ba 20	Fe 350
Te 30	Cr 60
Sn 20	Ca 110
Cd 20	K 170
Ag 60	Mg 90
Sr 20	Al 700
Se 60	Na 700
Zr 60	

$\Sigma = <2.7$  ng/g  
(for 19 elements)

<sup>a</sup> These results are the average values obtained by SSMS analysis of NBS HNO<sub>3</sub> over a 10-year period. No improvement in overall reagent quality was detected during this time period.

were able to prove that the reagents were of higher purity than we could show by using the SSMS procedure. The primary role of either the SSMS or the ICP-MS in pure reagent analysis is to give an overall profile of the reagent quality and to be able to compare reagents of differing quality. Compared to the SSMS procedure for acid analysis, the ICP-MS procedure has better sensitivity, a significant reduction in instrument analysis time, and an increase in the number of elements determined.

Iron, Ca, and Na are major contributors to the total impurities in the reagents analyzed. These elements may be introduced in substantial quantities from the sample-processing steps. Whether these impurities come from the acid containers (Teflon FEP) or from the evaporation beaker and environment is difficult to say. Since these detected impurities are much greater than the detection limit, they are real in the sense that they are detected. However, previous experience has shown that the same impurities are extracted from labware at approximately the nanogram level.

The element Ni is known to be biased high in these analyses because of the Ni sampler and skimmer cones on the ICP-MS instrument. The values of elements Zn, Cu, and Cr are all substantially lower than those previously reported by SSMS.

Many other elements such as Pb, Tl, and Sr are in the low picogram per gram range and these present values are an order of magnitude lower than those previously reported with the SSMS. This capability allows us to obtain a much more accurate representation of the low trace impurity concentrations in these reagents. For example, lead in nitric acid has been reported as an upper limit between 10 and 50 pg/g by the SSMS. With the ICP-MS the value for Pb is 4 pg/g. Previous measurements in this laboratory of Pb in HNO<sub>3</sub> by thermal ionization mass spectrometry gave concentrations <1 pg/g. Thus, in this case, the multielement ICP-MS is approaching the best sensitivity of this single element technique.

## SUMMARY

This ICP-MS procedure is capable of measuring impurities in solutions to a few picograms per gram. The high sensitivity



is obtained through a combination of solution preconcentration and optimization of sample introduction rate into the ICP nebulizer.

Quantification was achieved by a combination of stable isotope dilution analysis and comparison to an external standard. This combination allowed us to determine a total of 37 elements simultaneously. The use of isotope dilution gives more reliable results since partial loss after equilibration would not alter the concentration as calculated using the isotope dilution equation (eq 1). The added spike also serves as an internal monitor of recovery since complete loss due to sorption or volatility can be detected by the absence of the spike isotope.

The ICP-MS instrument was designed for high sample throughput of dilute solutions and was ideal for this application. Using the mass scan mode, we have essentially complete elemental coverage and it is possible to expand the number of elements determined by both isotope dilution and the use of external standards in future surveys.

**Registry No.** Pb, 7439-92-1; Tl, 7440-28-0; Pt, 7440-06-4; W, 7440-33-7; Ce, 7440-45-1; Nd, 7440-00-8; Ba, 7440-39-3; Te, 13494-80-9; Sb, 7440-36-0; In, 7440-74-6; Cd, 7440-43-9; Pd,

7440-05-3; Mo, 7439-98-7; Zr, 7440-67-7; Sr, 7440-24-6; Rb, 7440-17-7; Ge, 7440-56-4; Ga, 7440-55-3; Zn, 7440-66-6; Cu, 7440-50-8; Ni, 7440-02-0; Fe, 7439-89-6; Cr, 7440-47-3; Ti, 7440-32-6; Mg, 7439-95-4; U, 7440-61-1; Sn, 7440-31-5; As, 7440-38-2; Co, 7440-48-4; Mn, 7439-96-5; V, 7440-62-2; Ca, 7440-70-2; Al, 7429-90-5; Na, 7440-23-5; B, 7440-42-8; Be, 7440-41-7; Li, 7439-93-2; H<sub>2</sub>O, 7732-18-5; HCl, 7647-01-0; HNO<sub>3</sub>, 7697-37-2; HClO<sub>4</sub>, 7601-90-3; HF, 7664-39-3; H<sub>2</sub>SO<sub>4</sub>, 7664-93-9.

#### LITERATURE CITED

- (1) Kuehner, E. C.; Alvarez, R.; Paulsen, P. J.; Murphy, T. J. *Anal. Chem.* **1972**, *44*, 2050-2056.
- (2) Moody, J. R.; Beary, E. S. *Talanta* **1982**, *29*, 1003-1010.
- (3) Federal Standard 209b, Government Services Administration, Boston, MA, 1973.
- (4) Longrich, H. P.; Strong, D. F.; Kantipuly, C. J. *Can. J. Spectrosc.* **1986**, *37*, 111-121.

RECEIVED for review September 14, 1987. Accepted January 15, 1988. Certain commercial equipment, instruments, or materials are identified in this report to specify adequately the experimental procedure. Such identification does not imply recommendation or endorsement by the National Bureau of Standards, nor does it imply that the materials or equipment identified are necessarily the best for the purpose.

## Quantitation of Ethyl Carbamate in Whiskey, Sherry, Port, and Wine by Gas Chromatography/Tandem Mass Spectrometry Using a Triple Quadrupole Mass Spectrometer

William C. Brumley,\*<sup>1</sup> Benjamin J. Canas, Gracia A. Perfetti, Magdi M. Mossoba, James A. Sphon, and Paul E. Corneliusen

*Division of Contaminants Chemistry and Division of Food Chemistry and Technology, Food and Drug Administration, Washington, D.C. 20204*

A procedure was developed for the quantitation of ethyl carbamate (EC) in whiskey, sherry, port, and wine using gas chromatography/mass spectrometry/mass spectrometry (GC/MS/MS) on a triple quadrupole instrument. An extraction/isolation procedure yielded an ethyl acetate solution of EC, and an aliquot of this solution was injected onto a bonded Carbowax capillary GC column for separation. The MS technique used isobutane chemical ionization to produce an (M + H)<sup>+</sup> ion for EC and for the stable isotope-labeled EC internal standard. Quantitation was based on the daughter ions of *m/z* 62 of EC and *m/z* 64 of labeled EC. Levels of EC between 3 and 330 ppb were found in a number of extracts and results were compared to GC/matrix isolation Fourier transform infrared and GC/nitrogen/thermal energy analyzer quantitations as independent determinative techniques. Recoveries of EC averaged >90% with a limit of quantitation of 1 ppb.

Ethyl carbamate (EC) or urethane is a carcinogen (1, 2) that is of continuing interest in carcinogenicity studies (3, 4). Since EC can occur naturally in fermented foods and beverages (5,

6), its presence in alcoholic beverages is a public health problem. Recent reports from Health and Welfare Canada (7) indicated that levels found in some alcoholic beverages exceeded Canadian guidelines.

A rapid and reliable procedure for quantitating EC in various beverages is needed. A gas chromatographic (GC) determination of EC in wines was reported that used electron ionization (EI) mass spectrometry (MS) for confirmation of identity (8). However, the method was relatively time-consuming and required substantial cleanup prior to GC/MS confirmation of EC in the extracts. Lofroth and Gejvall (9) reported a radioisotopic dilution technique. Walker et al. (10) and Ough (5) based their quantitations on a Coulson electrolytic conductivity detector with confirmation by GC/MS. A recent report (11) described the use of two-dimensional capillary GC with a heart cut from the first column transferred to a second column and flame ionization detection.

While this paper was undergoing review, two additional papers concerned with determination of EC by mass spectrometry were published (12, 13). Cairns et al. (12) used GC/MS under methane CI conditions, with quantitations based on *m/z* 90 and 92 of an internal standard, which was, in fact, custom synthesized for the present authors. Cairns et al. (12) reported problems with accuracy, precision, and adequate sampling of the GC peak. The paper of Lau et al. (13) determined EC by high-resolution mass spectrometry on

<sup>1</sup> Present address: Environmental Protection Agency, P.O. Box 93478, Las Vegas, NV 89193.

the basis of  $m/z$  62 of EC. The isolation procedure was that adopted in this paper so that a direct comparison of MS procedures might be made.

This paper presents a method for quantitating EC in alcoholic beverages using a direct capillary GC/MS/MS introduction of extracts and a stable isotope-labeled internal standard (ECL). The quantitations are accurate in spite of the presence of coextractives, and the precision compares favorably with the usual GC/MS approaches and with other determinative procedures using GC. Levels of EC are reported for a number of extracts and compared to findings obtained by using GC/matrix isolation (MI) Fourier transform infrared (FT-IR) and GC/nitrogen/thermal energy analyzer (N/TEA) results as independent quantitative approaches.

## EXPERIMENTAL SECTION

**Chemicals.** All solvents were distilled in glass (Burdick & Jackson, Muskegon, MI). [ $^{13}\text{C}_1$ ,  $^{15}\text{N}$ ]-EC (>99+ atom % each) was custom synthesized by MSD Isotopes, Montreal, Canada, for the Food and Drug Administration's Division of Contaminants Chemistry, and today resides with that division. Chemical purity was checked by GC/MS.

**Isolation/Concentration.** The procedure of Conacher et al. (14) was followed: 50 g of beverage was extracted with methylene chloride, the extract was dried with sodium sulfate and concentrated to 5 mL in ethyl acetate. At the 100 ppb level, a concentration of 1 ng of EC/ $\mu\text{L}$  would result. At the 1 ppb level, the sample was concentrated to 300  $\mu\text{L}$ , resulting in a solution of 300 pg of EC/ $\mu\text{L}$ , of which 3  $\mu\text{L}$  was injected.

**GC/MS/MS.** A Finnigan MAT TSQ-46 instrument interfaced to an INCO 2300 data system with TSQ software (Revision C) was used. The collision activated decomposition was monitored under experimental control of the data system. The instrument was sequentially set to monitor  $m/z$  90, 62, and 44 when Q1 passed  $m/z$  90 of EC, and  $m/z$  92, 64, and 46 when Q1 passed  $m/z$  92 of ECL. Ion dwell times of 0.05 s per ion resulted in a total cycle time of about 0.38 s. After data acquisition, the original file was split into two files holding the decomposition of  $m/z$  90 (EC) and  $m/z$  92 (ECL), respectively. Quantitative results were based on the relative areas of  $m/z$  62 (EC) and 64 (ECL) and the spiking level. The response factor for  $m/z$  62 versus 64 was unity throughout the levels encountered in this work. Standard procedures suggest spiking samples at levels close to those expected for the measured quantity. The capillary column was 60-m SP-10 (bonded, Carbowax, Supelco, Bellefonte, PA), 0.25- $\mu\text{m}$  film thickness, 0.25 mm i.d. Temperature was programmed at 40–150 °C at 12.5 °C/min and then to 250 °C at 20 °C/min; 180 °C injector; 220 °C interface/transfer line; 38 cm/s helium at 40 °C. Chemical ionization (CI) isobutane pressure was 0.50 Torr: source temperature, 140 °C; 0.35 mA emission at 70 eV; 2 mTorr argon collision gas at -10 eV energy; pre-amp, multiplier, and conversion dynode at  $10^{-8}$  A/V, -1400 V, and -5 kV, respectively.

**GC/MI/FT-IR.** An MI/Cryolect/Sirius 100 Mattson FT-IR spectrometer was interfaced to a Model 5890 Hewlett-Packard gas chromatograph with a DBWAX-30W (J&W Scientific, Inc.) capillary column (30 m  $\times$  0.32 mm i.d., 0.25- $\mu\text{m}$  film). The carrier gas was helium containing 1.5% argon. The effluent was split, with 20% going to a flame ionization detector, while the remaining 80% was sprayed onto a slowly rotating collector disk placed in a vacuum chamber and held at 11 K. MI FT-IR measurements were carried out after EC and ECL were deposited on the collector disk. Assignments of characteristic frequencies of EC and ECL observed under MI/FT-IR were based in part on published work (15–18). Quantitation was based on observed peak heights with base-line correction and the fortification level of ECL. Peak heights were derived from the intense and sharp bands at 1325 and 1298  $\text{cm}^{-1}$  in EC and ECL that were assigned as the asymmetric C–O–C(O) stretching mode. Details of the GC/MI/FT-IR procedures will be published separately (19).

**GC/N/TEA.** A Hewlett-Packard Model 5710A gas chromatograph interfaced to an N/TEA with 610R nitrogen converter was used. The column was 9 ft (2.7 m)  $\times$  4 mm i.d. glass packed with 10% EGA on 100/120 mesh Chromosorb-WHP: 200 °C injector; 100–130 °C at 1 °C/min oven; GC interface, 225 °C; pyrolyzer furnace, 825 °C; vacuum, 1.3–1.4 Torr; carrier gas, argon

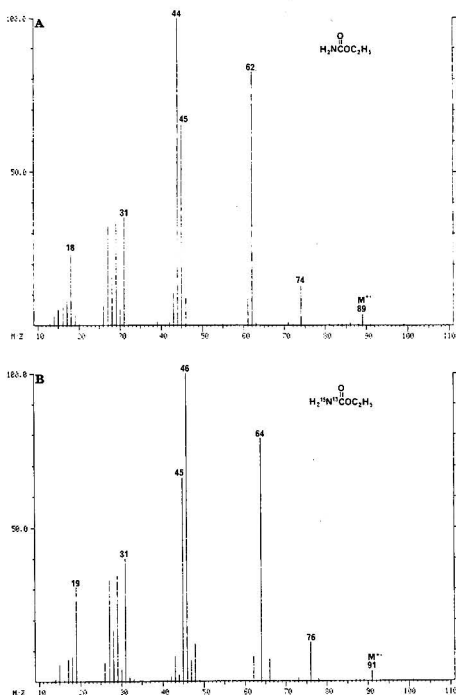


Figure 1. EI mass spectra, 70 eV, source 140 °C of (A) EC and (B) ECL.

at 40 mL/min; cold trap, liquid nitrogen/pentane slush (-130 °C).

## RESULTS AND DISCUSSION

**EI Mass Spectra.** The EI mass spectrum of EC (Figure 1A) consists of the molecular ion at  $m/z$  89 and principal fragment ions at  $m/z$  74 ( $\text{M} - \text{CH}_3$ ) $^+$ , 62 ( $\text{M} - \text{C}_2\text{H}_5$ ) $^+$ , 45 ( $\text{C}_2\text{H}_5\text{O}$ ) $^+$ , 44 ( $\text{NH}_2\text{CO}$ ) $^+$ , 31, 29, 27, and 18 ( $\text{NH}_4$ ) $^+$ . Suggestions, partly based on the mass spectrum of the ECL in Figure 1B, are made for structural assignments to certain of the fragment ions. The principal mass shifts observed between the spectra of EC and ECL are  $m/z$  89 to 91, 62 to 64, 44 to 46, and 18 to 19.

The loss of 27 u to produce  $m/z$  62 in the spectrum of EC is verified as  $\text{C}_2\text{H}_5$  $^+$  and must involve a double hydrogen rearrangement. The ion at  $m/z$  44 must consist primarily of  $\text{NH}_2\text{CO}$  $^+$  in view of the mass shift to  $m/z$  46 observed in the spectrum of ECL. The ion at  $m/z$  45 has the same relative abundance in both spectra and presumably represents ( $\text{C}_2\text{H}_5\text{O}$ ) $^+$ . The ion at  $m/z$  18 represents  $\text{NH}_4$  $^+$ , as verified by the shift to  $m/z$  19 ( $^{15}\text{N}$ ). These results are entirely consistent with the scheme proposed by Lau et al. (13) and serve to verify the chemical identity of ECL.

Collisional activation (CA) mass spectra of  $m/z$  89, 74, and 62 reveal the following relationships. The molecular ion at  $m/z$  89 fragments primarily to  $m/z$  62 and 45. The ion at  $m/z$  74 fragments to  $m/z$  44, presumably by loss of  $\text{CH}_2\text{O}$ , and  $m/z$  62 also leads to  $m/z$  44, presumably by loss of  $\text{H}_2\text{O}$ .

**MS/MS Quantitation.** To confirm the presence of and to quantitate EC in extracts of various beverages, some enhancement of the ion indicating molecular weight was deemed appropriate. The CI ( $\text{CH}_4$ ) mass spectrum of EC consists predominately of the ( $\text{M} + \text{H}$ ) $^+$  ion at  $m/z$  90 and  $m/z$  62.

**Table I. EC (ppb) in Whiskey, Sherry, Port, and Wine**

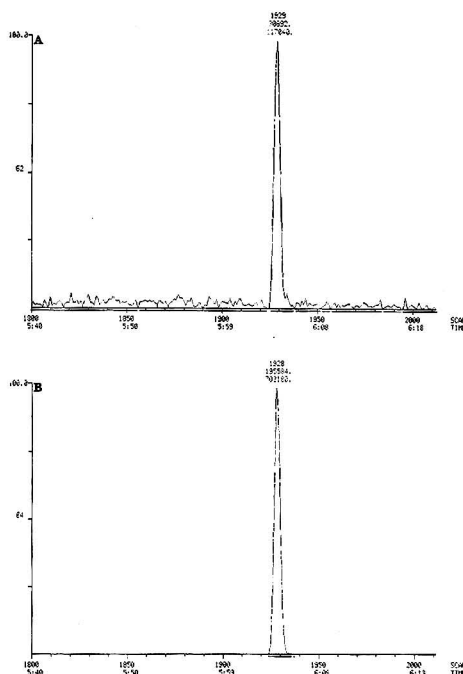
beverage	MS/MS	N/TEA	MI/FT-IR
whiskey			
1	116	123	117
2	108	139	126
3	60.0	83	68
4	330	323	389
5	166	163	183
sherry			
1	47.0	47	
2	38.7	32	
3	232	242	
4	39.6	50	
port			
1	31.0	33	
2	56.0	60	
3	22.9	22	
4	13.6	16	
wine			
1	8.3	9	
2	7.7	8	
3	3.1	3	
4	3.3	4	
5	4.4	9	
6	7.0	7	

Additional selectivity and specificity were necessary with the particular isolation procedure chosen, and two MS refinements were added. First, isobutane was used as the reagent gas to provide greater ionization selectivity for EC compared to matrix coextractives and to provide all of the ion current in the  $(M + H)^+$  ion. Second, the  $(M + H)^+$  ion of EC was subjected to CA with ions at  $m/z$  90, 62, and 44 monitored. ECL was added as an internal standard before analytical workup and a parallel CA experiment was followed ( $m/z$  92 yielding ions at 92, 64, and 46). Quantitation was based on the relative areas of  $m/z$  62 (EC) and 64 (ECL) based on the known fortification of ECL.

Specificity, accuracy, and precision, and applicability to a variety of matrices are of concern with this approach. Table I reports a number of quantitations by GC/MS/MS and provides comparisons of GC/MI/FT-IR and GC/N/TEA data. Both of these latter instrumental approaches have high specificity. Good agreement was reached among the different techniques. The accuracy of the GC/MS/MS quantitations was judged by both incurred EC residues and spiked beverages. The matrices consisted of whiskey, sherry, port, and wine, thereby providing evidence that the GC/MS/MS procedure is applicable to extracts from a variety of matrices. Generally, the GC/MS/MS value is the lowest in Table I, and this presumably results from its high specificity and lack of interferences.

The decomposition of  $m/z$  90  $\rightarrow$  62 (92  $\rightarrow$  64) appears to be absolutely specific for EC (ECL) in the beverages using the isolation procedure. Figure 2 is a chromatogram of wine quantitated at 8 ppb EC. The GC/MS/MS approach very likely could be applied to extracts from other matrices without modification.

The precision of repeat analysis of the same solution over the same day and over several days was determined. Whiskey, analyzed three times over several days, gave results of 38.5, 38.7, and 38.6 ppb EC. Four sherry solutions, analyzed two or three times per day, gave results of 47.0 and 47.6; 116 and 118; 108, 109, and 107; and 60.0 and 63.3 ppb. The technique is highly reproducible and comparable to usual GC/MS quantitations (20). The precision of determinations for replicate injections was  $\pm 1\%$ . Variability of the extraction/isolation procedure was estimated from four whiskey samples that were analyzed in duplicate by GC/N/TEA. An average variation of 2.9% was obtained with an individual high of 6%

**Figure 2.** Ion chromatograms for (A)  $m/z$  62 of EC and (B)  $m/z$  64 of ECL in wine quantitated at 8 ppb.**Table II. Recovery of EC in Whiskey, Sherry, Port, and Wine Based on GC/N/TEA Determination**

beverage	spike, ppb	EC + spike, ppb	recovery, <sup>a</sup> %
whiskey			
1	100	212	95
2	200	315	87
4	500	823	99
sherry			
1	77	121	97
2	154	167	85
3	154	428	121
4	77	132	104
port			
1	38.5	68	94
2	38.5	105	112
3	38.5	59	92
4	38.5	49	86
wine			
1	50	56	96
2	50	62	104
3	50	57	108
4	50	51	90
5	50	51	84
6	50	57	100

<sup>a</sup> Calculated using data in Table I.

for EC levels from 80 to 343 ppb.

Recoveries using the isolation procedure averaged 97% (Table II) and were verified in all four matrices by using GC/N/TEA determination. These data verify that the extraction quantitatively recovers EC from the beverage. Quantitations by MS/MS are automatically corrected for recoveries by beverage spiking with ECL before extraction. The only variability not corrected by the MS/MS procedure is that introduced by the spiking procedure. Reagent blanks

had no measurable EC (<1 ppb).

The present study is based entirely on tandem MS in comparison to TEA and GC/FT-IR techniques, whereas the study reported earlier by Cairns et al. (12) examined a limited number of samples by tandem MS. The precision of the data presented here is clearly superior to that reported earlier by tandem MS. We encountered no problems with sampling the GC peak that was about 3 s wide, and no column cleanup step was necessary. The choice of isobutane as reagent gas in the present study may have contributed to the improved results. Factors attributable to relative instrument stabilities could also account for some of the differences.

Our results may be compared directly to those of Lau et al. (13), who used the same cleanup. In the context of this problem, the tandem MS determination compares favorably with high-resolution MS with respect to precision, specificity, and limit of determination. Of particular interest is the absence of responses on  $m/z$  62 other than that of EC under tandem MS conditions. This may be compared with the  $m/z$  62 ion chromatogram under high-resolution EI conditions (13), in which one or two additional responses were noted before the elution of EC. Both the present study and the high-resolution study exhibited acceptable reproducibility and specificity.

Few quantitations based on MS/MS techniques have been reported. Thus, a general assessment of the performance of quantitative MS/MS analyses at parts-per-billion levels is not yet possible. This study demonstrates that the MS/MS approach is capable of providing routine quantitations at an acceptable level of accuracy and precision while maintaining unequivocal specificity with minimal sample cleanup.

Registry No. EC, 51-79-6.

## LITERATURE CITED

- (1) Nettleship, A.; Henshaw, P. S.; Meyer, H. L. *J. Natl. Cancer Inst.* **1943**, *4*, 309-319.
- (2) Mirvish, S. S. *Adv. Cancer Res.* **1968**, *11*, 1-42.
- (3) Malkinson, A. M.; Thaele, L. G. *Cancer Res.* **1986**, *46*, 1694-1697.
- (4) Malkinson, A. M.; Nesbitt, M. N.; Skamene, E. J. *Natl. Cancer Inst.* **1985**, *75*, 971-974.
- (5) Ough, C. S.; *J. Agric. Food Chem.* **1976**, *24*, 323-328.
- (6) Ough, C. S.; *J. Agric. Food Chem.* **1976**, *24*, 328-331.
- (7) Conacher, H. B. S.; Page, B. D. **1986 IUPAC EURO FOOD TOX II Meeting**, Zurich, Switzerland, 1986; pp 237-242.
- (8) Joe, F. L.; Kline, D. A.; Miletta, E. M.; Roach, J. A. G.; Roseboro, E. L.; Fazio, T. J. *Assoc. Off. Anal. Chem.* **1977**, *60*, 509-516.
- (9) Lofroth, G.; Gejvall, T. *Science* **1971**, *174*, 1248-1250.
- (10) Walker, G.; Winterlin, W.; Fouda, H.; Seiber, J. J. *J. Agric. Food Chem.* **1974**, *22*, 944-947.
- (11) van Ingen, R. H. M.; Nijssen, L. M.; van der Berg, F.; Maarse, H. *HRC CC, J. High Resolut. Chromatogr. Commun.* **1987**, *10*, 151-152.
- (12) Cairns, T.; Slegmund, E. G.; Luke, M. A.; Doose, G. M. *Anal. Chem.* **1987**, *59*, 2055-2059.
- (13) Lau, B. P.-Y.; Weber, D.; Page, B. D. *J. Chromatogr.* **1987**, *402*, 233-241.
- (14) Conacher, H. B. S.; Page, B. D.; Lau, B. P.-Y.; Lawrence, J. F.; Bailey, R.; Calway, P.; Hanchay, J.-P.; Mori, B. J. *Assoc. Off. Anal. Chem.* **1987**, *70*, 749-751.
- (15) Chen, J.-T.; Benson, W. R. *J. Assoc. Off. Anal. Chem.* **1966**, *49*, 412-452.
- (16) Bellamy, L. J.; Williams, R. L. *Spectrochim. Acta* **1957**, *9*, 341-345.
- (17) Cutmore, E. A.; Hollam, H. E. *Spectrochim. Acta, Part A* **1969**, *25A*, 1767-1784.
- (18) Carter, J. C.; Devia, J. E. *Spectrochim. Acta, Part A* **1973**, *29A*, 622-632.
- (19) Mossoba, M. M.; Chen, J. T.; Brumley, W. C.; Page, S. W. *Anal. Chem.* **1988**, *60*, 945-948.
- (20) Millard, B. J. *Quantitative Mass Spectrometry*; Heyden: London, 1979; p 89.

RECEIVED for review July 22, 1987. Accepted January 27, 1988.

# Computer-Assisted Prediction of Gas Chromatographic Retention Times of Polychlorinated Biphenyls

Mohamed Noor Hasan and Peter C. Jurs\*

Department of Chemistry, 152 Davey Laboratory, The Pennsylvania State University, University Park, Pennsylvania 16802

**The gas chromatographic retention times of polychlorinated biphenyls (PCBs) were predicted by using descriptors derived directly from the molecular structures. A five-variable regression equation with  $R^2$  of 0.997 and relative standard deviation of 1.7% was developed. Descriptors that represent degree of chlorination, substitution pattern, and geometry of the molecules were among the variables included in the equation. At least 40 compounds are needed in order to accurately predict the retention times of all 209 PCB congeners.**

Polychlorinated biphenyls (PCBs) are well-known for their persistence and widespread occurrence in the environment. Presently, capillary column gas chromatography coupled either with an electron capture detector or with a mass spectrometer is the most commonly used technique for analysis of PCBs in environmental samples. A great deal of research has been carried out in this area, and it has been summarized in several recent reviews (1, 2).

There are 209 possible PCB isomers and congeners. For many of these compounds, however, standards are not readily available. A common approach in peak identification is to compare the patterns produced by the sample with those obtained by running a mixture of commercial preparations such as Clophen or Aroclor (3-5). The PCB contents of the samples are often expressed in terms of these mixtures. Unfortunately, in some cases degradation and metabolism of selected compounds have caused dissimilarities and can lead to erroneous conclusions.

Many authors have described attempts to assign the structure of individual peaks produced by the commercial mixtures of environmental samples by comparison with standard compounds (6-9). The work by Mullin et al. (10) is considered the most extensive congener-specific GC analysis of PCBs reported in the literature. They have synthesized all of the 209 PCBs and carried out the separation on a single column. All but 11 pairs were completely separated.

In general the retention times of PCBs increase with the number of chlorines in the molecule. For isomeric PCBs (the same degree of chlorination), the retention times are highly

Table I. Dihedral Angle between the Two Phenyl Rings

substitution pattern	dihedral angle, deg	ref
non-ortho	44	21
ortho subs. on one ring	57	22
ortho subs. on both rings	74	23

Table II. List of Descriptors Used in the Regression Analysis

1. number of chlorines
2. number of chlorines squared
3. number of chlorines at ortho position
4. number of chlorines at meta position
5. number of adjacent chlorines
6. 2nd moment of inertia
7. 3rd moment of inertia
8. 1st/2nd moment of inertia
9. 1st/3rd moment of inertia
10. sigma charge separation

dependent on the substitution pattern. For example, chlorines at the meta and para positions increase the retention while chlorines at the ortho position decrease the retention. Other researchers observed similar retention behavior when the separation was performed on various types of stationary phases (11–13). A recent comparative study showed that elution order of PCBs on a liquid crystal phase is also dependent on the shape of the molecules (14).

An attempt to predict the GC retention of PCBs has been described by Sisson and Welti (15) and later was implemented by others (6, 16). In their method the retention index for each PCB compound is considered as a sum of retention indexes of two phenyl rings of similar substitution pattern. Deviations from experimental values are observed, however, when the difference in the number of chlorines between the two rings is greater than three or when the two rings are highly substituted.

In the present study, we investigated the possibility of predicting the GC retention of PCBs by using information obtained directly from their molecular structures. This approach to the computer-assisted prediction of chromatographic retention has been applied previously to polycyclic aromatic hydrocarbons (17, 18). Basically, a regression equation is developed by using measured retention times as the dependent variable and molecular structure descriptors as the predictors (independent variables). The ability to predict the retention times of PCBs before the actual separation process will certainly facilitate the analysis, especially when standard compounds are not readily available.

### EXPERIMENTAL SECTION

The procedure involved in this study consists of three stages: (a) entry and storage of molecular structures, (b) generation of molecular structure descriptors, and (c) regression analysis. All

computations were performed on the Chemistry Department's PRIME 750 computer using the ADAPT software system (19, 20).

**The Data Set.** The retention data for all 209 PCB congeners used in this study were taken from Mullin et al. (10) and are available as supplementary material. (See paragraph at end of paper regarding ordering information.) They were measured on a 50-m fused silica capillary column (0.2 mm i.d.) coated with SE-54. Retention times were expressed relative to octachloronaphthalene (RT = 124.9 min). Relative retention times (RRT) resulted.

**Structure Entry.** The molecular structures of all compounds in the data set were entered into the computer by sketching them on a graphics terminal. These were converted by ADAPT into connection tables for storage. Subsequently energy-minimized three-dimensional models of the structures were generated by using molecular mechanics calculations. The dihedral angles between the two phenyl rings were fixed according to literature values (Table I).

**Descriptor Generation.** The descriptors generated can be divided into four classes: (a) topological descriptors, (b) geometric descriptors, (c) electronic descriptors, and (d) calculated physical property descriptors. Topological descriptors include fragment descriptors, molecular connectivity indexes, substructure counts, and substructure environment descriptors. Geometric descriptors include principal moments of inertia, van der Waals volume and surface area, and shape parameters. Electronic descriptors include the total  $\sigma$  charge, distance between atoms with the most positive and negative  $\sigma$  charges, and electron density of the atom with the most negative  $\sigma$  charges. Calculated physical property descriptors include calculated log  $P$  and molecular polarizability. After they were generated, these descriptors were subjected to a screening procedure to prune descriptors that do not contain enough information and to eliminate serious intercorrelation among descriptors. Values of descriptors used are available as supplementary material.

**Regression Analysis.** Two variable selection procedures were used in this study—stepwise multiple linear regression (24) and leaps and bounds regression (25). Once an equation was developed it was subjected to a number of statistical tests in order to ascertain its validity and stability of the coefficients.

### RESULTS AND DISCUSSION

The structures of the compounds in the data set do not differ very much, so many of the descriptors generated were intercorrelated. For instance, van der Waals volume was highly correlated with the path-one molecular connectivity index, molecular weight, and number of chlorines. Therefore, some of the descriptors must be discarded prior to the model selection procedure. Given a choice, we tried to retain descriptors that are easy to generate and those that have direct physical interpretations. A final pool of 10 descriptors used as independent variables in the regression analysis are listed in Table II. The correlation matrix of the descriptors is shown in Table III.

Table III. Correlation Matrix of Descriptors Used in the Regression Analysis

desc <sup>a</sup>	1	2	3	4	5	6	7	8	9	10
1	1.000									
2	0.976	1.000								
3	0.636	0.621	1.000							
4	0.636	0.621	-0.015	1.000						
5	0.841	0.868	0.333	0.677	1.000					
6	0.828	0.815	0.170	0.644	0.779	1.000				
7	0.909	0.896	0.683	0.687	0.704	0.593	1.000			
8	-0.226	-0.233	-0.087	0.026	-0.126	-0.442	0.024	1.000		
9	-0.374	-0.330	-0.614	-0.249	-0.167	0.080	-0.594	-0.317	1.000	
10	0.000	-0.020	-0.348	0.211	0.041	0.229	-0.060	-0.006	0.364	1.000

<sup>a</sup> Descriptors are numbered as in Table II.

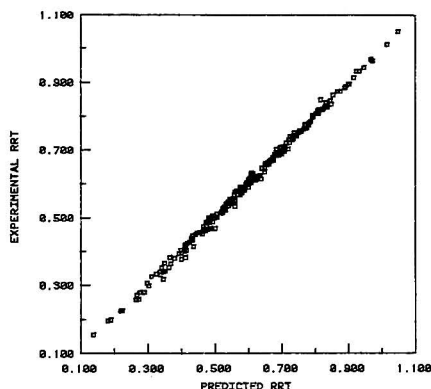


Figure 1. Experimental vs predicted RRT.

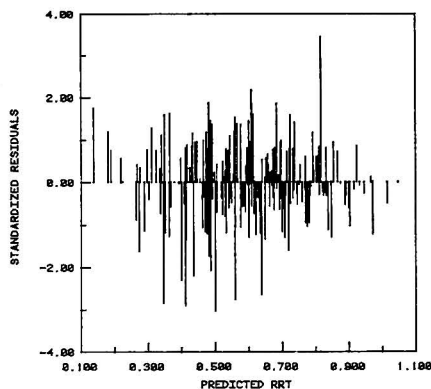


Figure 2. Standardized residuals vs predicted RRT.

Many good equations can be developed by using the descriptors available. Several criteria— $R^2$ , standard error,  $F$  value, and the Cp criterion—were used in order to select the best equation. One of the best equations is as follows:

$$\begin{aligned} \text{RRT} = & [0.1284 \pm 0.0047 \text{ (no. of Cl)}] - \\ & [0.0327 \pm 0.0033 \text{ (no. of ortho subs.)}] + [0.0254 \pm \\ & 0.0021 \text{ (no. of adjacent Cl)}] - \\ & [0.00482 \pm 0.00041 \text{ (no. of Cl squared)}] + [0.0000268 \\ & \pm 0.0000046 \text{ (second moment of inertia)}] + 0.0205 \quad (1) \end{aligned}$$

$$n = 209, \quad R^2 = 0.997, \quad F(5, 203) = 13177, \\ s = 0.0100$$

The variables are listed in the order they were chosen by the stepwise regression routine. These are also the best set of variables selected by the leaps and bounds regression. No significant improvement in  $R^2$  or standard deviation was observed when any additional variable was added to the equation. The 95% confidence intervals of the coefficients are as indicated. The standard deviation corresponds to about 1.7% of the mean RRT values. A scatter plot of the experimental vs predicted RRT is shown in Figure 1. The residual plot (Figure 2) indicates that the error variance is constant. Further examinations of residuals show that they are normally distributed and independent of any other variables.

A good fit alone does not guarantee that the equation will be useful for prediction purposes. Some kind of validation

Table IV. Stability of Coefficients

variable <sup>a</sup>	coefficient	s
1	0.1290	0.0021
2	-0.0330	0.0018
3	0.0254	0.0007
4	-0.00485	0.00020
5	0.0000265	0.0000022
const	0.0194	0.0079

<sup>a</sup> Variables are numbered in the order they appear in the equation.

is necessary to test how stable the equation is and how well it predicts. To perform the cross validation procedure, the data set was divided into two halves by using the DUPLEX data splitting algorithm (26). This is to ensure that the two subsets have similar statistical properties. The first half, the training set, was used to estimate the coefficients. The equation obtained was then used to predict the RRT of compounds in the second half (prediction set). The correlation coefficient between the observed and the predicted RRT was 0.998 and the prediction standard deviation was 0.0108. These clearly indicate that the equation is stable over the entire data set and has a very good predictive ability. The stability of the coefficients was further tested by fitting 10 equations with 10 different training sets. These training sets were randomly generated, and each contains 105 of the 209 compounds. The estimates of the coefficients were quite stable, and the mean values of the 10 equations (Table IV) did not differ greatly from the values obtained by fitting the full data set.

The types of descriptors included in the equation can be related to the retention mechanisms involved in the separation process. The number of chlorines is the most important variable in the equation. By itself, it accounts for about 90% of the total variance. Obviously, the dispersion forces that control the retention mechanism are proportional to the number of chlorine atoms in the molecule. Chlorines at the ortho position seem to decrease the RRT, and this is reflected by the minus sign of the second coefficient in the equation. This must have something to do with the planarity of the molecules. Ortho substituents impose steric restrictions which prevent free rotation around the inter-ring bond, causing the structure to be strictly nonplanar.

The role of the third variable (number of adjacent Cl) in the retention behavior of PCBs is unclear. However, molecules with two chlorine substituents side by side do have longer retention times than those isomers in which the chlorines are far apart. For example 2,3-dichlorobiphenyl has a longer retention time than the 2,4 or 2,5 isomers, although the last two compounds are supposed to be longer in shape. One possible explanation was given by McKinney and co-worker: adjacent Cl increases the C-Cl dipoles and therefore increases the net molecular polarizability (27).

The fourth variable (number of chlorines squared) was added at a later stage during the selection procedure after we found out that without it the residuals showed a curvilinear relation when plotted against number of chlorines. In order to determine the optimal value of the exponent we have fitted several nonlinear equations using a simplex optimization routine (28). The program essentially selects the best set of parameters, including the exponent, that produce the minimum error. We found the value of the exponent was very close to 2.

The final variable (the second principal moment of inertia) can be related to the width of the molecule. Coincidentally, this is the only variable that requires prior three-dimensional modeling of the structures, since the first four variables are topological descriptors which can be calculated directly from the connection table. Therefore a simpler equation with only



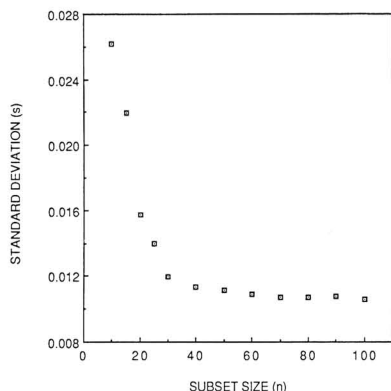


Figure 3. Prediction standard deviation vs subset size.

four variables can be obtained by dropping this variable from the equation. The four-variable equation is as follows:

$$\begin{aligned} \text{RRT} = & [0.1451 \pm 0.0048 \text{ (no. of Cl)}] - [0.0489 \pm 0.0024 \text{ (no. of} \\ & \text{ortho subs.)}] + [0.0215 \pm 0.0025 \text{ (no. of adjacent Cl)}] \\ & - [0.00424 \pm 0.00050 \text{ (no. of Cl squared)}] + 0.0446 \quad (2) \\ n = 209, \quad R^2 = 0.995, \quad F(4, 204) = 10052, \\ & s = 0.0128 \end{aligned}$$

This equation still has a high  $R^2$  and a very small standard deviation. Although it might be inferior to eq 1 in terms of predictive quality, it has the advantage that the variables can be easily calculated from the topology of the molecular structures without having to generate the three-dimensional models.

As mentioned earlier, not all of the PCB isomers are available in a form suitable to be used as chromatographic standards. For identification purposes one either has to synthesize them in advance or make comparisons with the patterns exhibited by commercial formulations. The results of this study suggested that an analyst can measure the retention times of only a few selected compounds, use the retention data to build an equation, and use the equation to predict the retention of other isomers. The question is, how many compounds are needed to generate the equation in order to get reasonably accurate predictions? To answer this question, we have performed the following experiment to determine the size of the subset required.

Fifty training sets were generated by randomly selecting  $n$  compounds from the 209 possible compounds in the full data set. For each training set an equation was developed by using the five variables of eq 1. The equations were then used to predict the RRT of the compounds not included in the training set, the remaining  $(209 - n)$ . Comparisons were made against the observed values, and the residual mean squares were calculated as a measure of precision. The procedure was repeated with  $n$  values between 10 and 100.

The results of this experiment can be best described by plotting the prediction standard deviation ( $s$ ) against the size of the subset (Figure 3). The  $s$  value decreases rapidly as  $n$  increases and stabilizes when  $n$  is about 40. Thus, a subset of  $40/209 = 19\%$  of the entire data set was sufficiently large to allow the generation of a predictive equation of high quality. In this particular experiment, the mean value of  $s$  for  $n = 40$  observations (0.01016) is almost the same as the standard error of fitting the whole data set. When this experiment was repeated using different training sets, and the standard deviation was plotted against  $n$ , a curve of similar shape was

obtained. Again the minimum size of the subset was 40. However, when only four variables were used, we found the minimum size of the subset was 50. This is not surprising because the predictive power of the equation will be reduced when less variables are involved.

The experiment described above was the first attempt to determine the minimum size of the subset required to get a high-quality predictive equation. Two things should be considered before applying the results to actual analyses. First, the experiment was performed by using the five variables of eq 1, and it has been shown that the results are dependent on the number of variables involved. A different set of variables may require a different size subset in order to get the same precision. Second, these results were obtained by averaging the prediction standard deviations of 50 randomly generated training sets. Some of the standard deviations are likely to be larger than the mean value. Therefore, one must be careful in selecting which compounds to be used to build the predictive equation. It is important that the training set has similar statistical properties with the whole data set, otherwise the equation developed would not be able to accurately predict the retention of compounds not included in the training set. The DUPLEX algorithm mentioned above is well suited for this purpose.

We have shown that the relative retention times of PCBs can be predicted by using descriptors derived from the molecular structures. The types of descriptors included in the equations are also consistent with previous reports on the retention behavior of PCBs. It should be noted, however, that the equations were developed by using retention data measured on a specific column. This appears to significantly limit the usefulness of the models. However, we feel that these equations can be applied to columns of similar polarity with only slight modifications in the values of the model coefficients. With the availability of retention data on other columns, we would be able to assess the effects of column polarity, column size, etc. on the parameters in the predictive equations.

**Supplementary Material Available:** Listings of retention data and values of the descriptors used in predicting retention for the 209 PCBs (12 pages). Photocopies of the supplementary material from this paper or microfiche (105 × 148 mm, 24× reduction, negatives) may be obtained from Microforms & Back Issues Office, American Chemical Society, 1155 16th Street, NW, Washington, DC 20036. Orders must state whether for photocopy or microfiche and give complete title of article, names of authors, journal issue date, and page numbers. Prepayment, check or money order for \$20.50 for photocopy (\$22.50 foreign) or \$10.00 for microfiche (\$11.00 foreign), is required and prices are subject to change.

## LITERATURE CITED

- (1) Erickson, M. D. *Analytical Chemistry of PCBs*; Butterworth: Stoneham, MA, 1986.
- (2) Pellizari, E. D.; Moseley, M. A.; Cooper, S. D. *J. Chromatogr.* **1985**, *334*, 277-314.
- (3) Webb, R. G.; McCall, A. C. *J. Chromatogr. Sci.* **1973**, *11*, 366-373.
- (4) Gordon, R. J.; Szita, J.; Feeder, E. J. *Anal. Chem.* **1982**, *54*, 478-481.
- (5) Newton, D. A.; Laski, R. R. *J. Chromatogr. Sci.* **1983**, *21*, 161-165.
- (6) Ballschmiter, K.; Zell, M. *Fresenius' Z. Anal. Chem.* **1980**, *302*, 20-31.
- (7) Albro, P. W.; Lorbett, J. T.; Schroeder, J. L. *J. Chromatogr.* **1981**, *205*, 103-111.
- (8) Bush, B.; Connor, S.; Snow, J. J. *Assoc. Off. Anal. Chem.* **1982**, *65*, 555-566.
- (9) Duinker, J. C.; Hillebrand, M. T. *J. Environ. Sci. Technol.* **1983**, *17*, 449-456.
- (10) Mullin, M. D.; Pochini, C. M.; McCrindle, S.; Romkes, M.; Safe, S. H.; Safe, L. M. *Environ. Sci. Technol.* **1984**, *18*, 468-476.
- (11) Bush, B.; Murphy, M. J.; Connor, S.; Snow, J.; Barnard, E. *J. Chromatogr. Sci.* **1985**, *23*, 509-515.
- (12) Onuska, F. I.; Terry, K. A. *HRC CC, J. High Resolut. Chromatogr. Chromatogr. Commun.* **1986**, *9*, 671-675.
- (13) Ballschmiter, K.; Schafer, W.; Buchert, H. *Fresenius' Z. Anal. Chem.* **1987**, *326*, 253-257.

- (14) Zielinski, W. L., Jr.; Miller, M. M.; Ulma, G.; Wasik, S. P. *Anal. Chem.* **1986**, *58*, 2692-2696.
- (15) Sisson, D.; Welti, D. J. *Chromatogr.* **1971**, *60*, 15-32.
- (16) Albro, P. W.; Haseman, J. K.; Clemmer, T. A.; Corbett, B. J. *J. Chromatogr.* **1977**, *136*, 147-153.
- (17) Hasan, M. N.; Jurs, P. C. *Anal. Chem.* **1983**, *55*, 263-269.
- (18) Rohrbaugh, R. H.; Jurs, P. C. *Anal. Chem.* **1986**, *58*, 1210-1212.
- (19) Stuper, A. J.; Brugger, W. E.; Jurs, P. C. *Computer Assisted Studies of Chemical Structure and Biological Function*; Wiley-Interscience: New York, 1979.
- (20) Jurs, P. C.; Chou, J. T.; Yuan, M. In *Computer-Assisted Drug Design*; Olson, E. C., Christoffersen, R. E. Eds.; American Chemical Society: Washington, DC, 1979; pp 103-129.
- (21) Almenningen, A.; Bastiansen, O.; Fernholt, L.; Cyvin, B. N.; Cyvin, S. J.; Samdal, S. J. *Mol. Struct.* **1985**, *128*, 59-76.
- (22) McKinney, J. D.; Gottschalk, K. E.; Pedersen, L. J. *Mol. Struct.* **1983**, *104*, 445-450.
- (23) Romming, C.; Selp, H. M.; Aanesen Oymo, I.-M. *Acta Chem. Scand., Ser. A* **1974**, *28*, 507-514.
- (24) Draper, N.; Smith, H. *Applied Regression Analysis*, 2nd ed.; Wiley-Interscience: New York, 1981; pp 307-312.
- (25) Furnival, G. M.; Wilson, R. W., Jr. *Technometrics* **1974**, *16*, 499-511.
- (26) Snee, R. D. *Technometrics* **1977**, *19*, 415-428.
- (27) McKinney, J. D.; Singh, P. *Chem.-Biol. Interact.* **1981**, *33*, 271-283.
- (28) Jurs, P. C. *Computer Software Applications in Chemistry*; Wiley-Interscience: New York, 1986; pp 133-140.

RECEIVED for review August 26, 1987. Accepted January 4, 1988. This work was supported by the National Science Foundation under Grant CHE8503542. The Prime 750 computer was purchased with partial financial support of the National Science Foundation. M.N.H. also acknowledges financial support from the Malaysian Government and University of Technology, Malaysia.

## Prediction of Gas Chromatographic Retention Characteristic of Polychlorinated Biphenyls

Albert Robbat, Jr.,\* George Xyrafas, and Durwood Marshall

Department of Chemistry, Tufts University, Medford, Massachusetts 02155

Two models have been developed that describe the relationship between the molecular structure of polychlorinated biphenyls (PCBs) and their gas chromatographic linear temperature programmed retention characteristics on a 50-m fused silica capillary column (0.2 mm I.d.) coated with SE-54 stationary phase. Model variables account for the number and position of chlorine atoms present, the relationships between chlorine atoms on each aromatic ring, the chlorine atom interactions between the two rings, and skeletal structure of each PCB isomer. Prediction of the relative retention times (RRT) for PCBs for this stationary phase was made based on linear models between RRT and molecular descriptors. Regression equations were derived for both models having a multiple correlation coefficient greater than 0.9985. The model based on molecular connectivity descriptors was used to predict the retention index of 108 PCBs on a DB-5 stationary phase.

The suspected toxicity of polychlorinated biphenyls (PCBs) is the primary reason for continued effort in developing analytical methods for their identification and quantitation.

PCBs have been widely used since 1929 in the United States in a variety of applications. Their wide use was related to the physical properties of PCBs which include high resistance to chemicals, resistance to redox systems, excellent insulating properties, stability, and nonflammability. Improper use and disposal of commercial PCB-containing material have resulted in contamination of the environment, in soil, water, as well as marine life. With the growing pressure from industry and federal and state governments to eliminate hazardous waste materials by incineration, concomitant with the growing body of knowledge that the full range of PCBs are produced during combustion, a need exists for identifying PCB isomers in particulate and gaseous emissions that are not commonly present in Aroclor mixtures.

In many cases the identification of a single isomeric PCB from the possible 209 PCB isomers is extremely difficult to accomplish experimentally. For example, Mullin and co-workers (1) have shown that many of the isomeric PCBs coelute under their most carefully considered gas chromatographic experimental conditions. In addition, only about 100 of the 209 PCBs are available for use as standards while 125-175 PCB isomers are often present in a single environmental sample.

In this publication, we report two multiple regression models for predicting linear temperature programmed gas chromatographic retention characteristics on a SE-54 stationary phase (1). Retention in chromatography is the result of competitive solubility of the solute between mobile and stationary phases. The partitioning of solute between these phases is determined by the molecular structure and electronic and chemical properties of the solute. Gas and liquid chromatographic retention characteristics have been predicted for many chemical classes by utilizing molecular-structure-based descriptors (2-13). The predictive models developed relate molecular structure of each PCB isomer to their experimental relative retention time. Different structural classifications are used in each model. In an effort to arrive at a regression model that could predict PCB relative retention time (RRT) and elution order satisfactorily, a backward stepwise modeling approach was employed relating RRT as a function of molecular connectivity and a chlorine substitution indicator.

Schwartz and co-workers (14, 15) have generated linear temperature programmed gas chromatographic retention indexes for 108 PCBs on DB-5 stationary phase. Molecular connectivity descriptors were used to model the retention index values. Based on the excellent agreement between experimental and predicted retention index, the remaining PCBs can be predicted. Moreover, the results described below and in our earlier work (on nitrated PAH (13)) suggest that one need only a subset of the complete set of PCB retention data for modeling on widely different stationary phases to generate predicted retention behavior for all PCBs. On the

basis of these values, the appropriate column can be chosen in order to identify PCBs that may coelute on any given stationary phase.

## EXPERIMENTAL SECTION

**Model 1.** Molecular connectivity descriptors as devised by Randic (16) and later expanded by Kier and Hall (17) have been correlated with solubility parameters, boiling points, densities, partition coefficients, and retention data. They are a topological description of molecular structure based on a count of skeletal atom groupings, weighted by the degree of branching. Molecular connectivities,  ${}^m\chi^i$ , are calculated by considering various fragments of the molecule. The superscript *m* denotes order while superscript *i* denotes fragment type, i.e., paths of one or more bonds, clusters (c) where three atoms are adjacent to a single common atom, and path clusters (pc), which are similar to a cluster with the addition of one or more atoms. A valence value equal to the valence of an atom minus the number of hydrogen atoms attached to that atom or a nonvalence value, the number of non-hydrogen atoms connected to the atom of interest, is assigned to each atom in a molecule excluding hydrogen atoms. Valence molecular connectivity indexes are calculated by using valence values which account for the nature of non-hydrogen atoms and the differences in bond orders. Nonvalence molecular connectivity indexes are calculated by using the nonvalence values where all non-hydrogen atoms and bonds between them are considered to be identical. The 24 molecular connectivities used in this study are listed in Table I. The calculations were made on a Digital Equipment Corp. Series 10 (DEC-10) computer. Examples of molecular connectivity calculations are shown in previous papers (13, 18, 19) and references listed therein.

**Model 2.** The position descriptors used in this paper are similar to those previously described by Hileman et al. (8) for modeling the linear temperature programmed gas chromatographic retention indexes of polychlorinated dibenzofurans. They are derived based on chlorine atom interactions in each ring as well as between rings (intra-ring and inter-ring interactions). The position descriptors (indicators) were chosen to account for a particular interaction. For example, indicator TWO represents the number of chlorine atoms present at the 2, 2', 6, and 6' PCB positions. Positions 6 and 6' are considered equivalent to positions 2 and 2', respectively. Since there are four such possible positions, indicator TWO takes on values from 0 to 4. In the same way indicators THREE and FOUR account for the number of chlorine atoms present at the 3,3', 5,5', and 4,4' positions in each ring, respectively. Again, positions 5 and 5' are considered equivalent to positions 3 and 3'. Indicator THREE takes on values from 0 to 4 while indicator FOUR is from 0 to 2.

To encode intra-ring interactions between chlorine atoms, the indicators ORTHO, META, and PARA are used. The ORTHO indicator accounts not only for the ortho relationships between the chlorine atoms attached to each ring, but also for the ortho relationships of chlorine atoms to the C-C bond of the biphenyl linkage. The ORTHO indicator may have values from 0 to 12 since there are six ortho relationships in each ring, 12 for both rings.

The META indicator accounts for all the possible meta relationships between chlorine atoms in the ring as well as between chlorine atoms and the biphenyl linkage. The META indicator is assigned the value zero when no meta relationship exists, the value 1 when one meta relationship is present with neither a chlorine atom nor the biphenyl linkage intervening, and the value 0.5 when one meta relationship is present with either a chlorine atom or the biphenyl linkage intervening. Indicator PARA has the value zero when no para relationships exist, the value 2/3 when one para relationship exists with either one chlorine atom or the biphenyl linkage intervening, and the value 1/3 when one para relationship is present with two intervening chlorine atoms or one chlorine and the biphenyl linkage intervening. In addition, it takes on the value 1 when there are neither chlorine atoms nor the biphenyl linkage intervening. The HBOND indicator was assigned the value zero when no hydrogen bonding occurred, the value 1 when one hydrogen and one chlorine atom were present at either 2,2' or 6,6' positions, and the value 2 when two hydrogen bond possibilities existed. For example, the indicator values for 2,3,5-trichlorobiphenyl are as follows: TWO, 1; THREE, 2; FOUR,

Table I. Molecular Connectivities,  ${}^m\chi^i$

${}^3\chi^c$	${}^3\chi^{vc}$	$1\chi$	$1\chi^v$
${}^5\chi^{ca}$	${}^5\chi^{vca}$	$2\chi$	$2\chi^v$
${}^4\chi^{pc}$	${}^4\chi^{vpc}$	$3\chi$	$3\chi^v$
${}^5\chi^{pc}$	${}^5\chi^{vpc}$	$4\chi^a$	$4\chi^v$
${}^6\chi^{pc}$	${}^6\chi^{vpc}$	$5\chi^a$	$5\chi^v$
$0\chi$	$0\chi^v$	$5\chi^c$	$5\chi^v$
		$5\chi^c$	$5\chi^v$

\* Indicates molecular connectivities that are moderately correlated with each other (Pearson correlation  $\leq 0.96$ ).

Table II. Regression Coefficients and Statistical Information for Model 1

Equation 2			
constant	-3.5066	<i>S</i>	0.0064
${}^4\chi^{pc}$	0.2455	<i>F</i> value	31057
$({}^2\chi^v)({}^5\chi)$	-0.0807	<i>DF</i>	(5,200)
$2\chi^v$	0.5189	<i>R</i> <sup>2</sup>	0.9987
${}^5\chi^{vc}$	-5.6936	<i>N</i>	206
${}^5\chi^v$	3.1571		

0; ORTHO, 2; META, 2.5; PARA, 1.3; and HBOND, 1. Indicators TWO, THREE, FOUR, ORTHO, and HBOND are evident. META is assigned the above value since there are three meta relationships with one having an intervening chlorine atom. The chlorine atoms at the 3 and 6 positions are para to each other and since the biphenyl linkage and chlorine atom at the 5 position intervene, PARA has the value  $2 \times 0.667 = 1.3$ .

The relative retention time and retention index for 209 and 108 PCB congeners have been experimentally measured by Mullin (1) and Schwartz (14, 15), respectively, and were used in this paper. Multiple regression analyses were computed on a Digital VAX 11/780 computer using the SAS statistical package.

## RESULTS AND DISCUSSION

**Model 1.** The best single variable regression between relative retention time (RRT) and  ${}^m\chi^i$  yielded the following equation (1):  $RRT = 5.131^6\chi^v - 1.610$ ,  $r^2 = 0.9250$  and  $s = 0.0487$ . The 24 descriptors evaluated are shown in Table I. The single-variable equation does not sufficiently predict either the PCB relative retention times or the elution sequence for use in environmental applications.

Backward stepwise multiple linear regression analyses performed on the 24 molecular connectivities resulted in a five-descriptor equation which better correlated RRT with  ${}^m\chi^i$ ,  $r^2 = 0.9973$ , and  $s = 0.0094$ . However, the plot of predicted RRT versus experimental RRT resulted in a nonlinear response while the plot of RESIDUAL versus experimental RRT revealed a pattern of over/under prediction of RRT. The latter plot is in direct contrast to what one would expect, viz., random noise about the zero value. Pearson correlation on the five indicators revealed that some of the variables were highly correlated ( $\geq 0.98$ ).

An attempt was made to remove the structure from the residual plots by evaluating  ${}^m\chi^i$  descriptors that were moderately correlated with each other (Pearson correlation  $\leq 0.96$ ). In addition  ${}^m\chi^i$  descriptors that produced steplike behavior with RRT were excluded. Stepwise regression on the set of descriptors identified in Table I was performed. The  ${}^m\chi^i$  descriptors (10) that appeared at least once in each of the three best five-descriptor equations and their products (45) formed a third data set. Because of the large number of all possible variable subsets and the demand on CPU time, multiple regression analyses were performed on random subsets of the total set of variables. It should be noted that the resulting equation was the best obtained and is representative of the results if one were to accomplish an exhaustive evaluation. Shown in Table II is the best five-descriptor relationship between RRT and variables. Plots of predicted RRT versus experimental RRT and RESIDUAL versus experimental RRT are shown in Figures 1 and 2, respectively. Evident from the

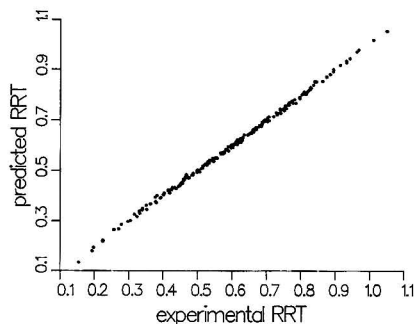


Figure 1. Plot of predicted RRT versus experimental RRT based on eq 2.

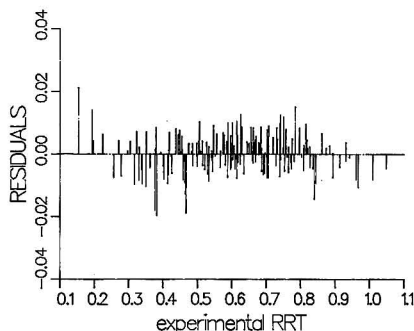


Figure 2. Plot of RESIDUAL versus experimental RRT based on eq 2.

figures are the linearity of the first plot and the random noise response about the zero value in the second plot. Equations based on six-descriptor combinations resulted in residuals slightly better than those of the five-descriptor case. Relationships based on less than five descriptors yielded results slightly better than those obtained for the single-descriptor case.

**Model 2.** A second approach was evaluated for predicting the PCB gas chromatographic relative retention times utilizing the molecular structure indicator terms described in the Experimental Section. Stepwise linear regression analysis between RRT and the seven-indicator variables yielded results strikingly similar to findings in model 1; specifically, plots of predicted versus experimental RRT were nonlinear and resulted in structured residual plots. Therefore, product terms for each of the seven indicators were calculated and exhaustive stepwise multiple regression analyses was performed on the new data set consisting of 28 variables (7 indicators and 21 product terms). The resulting equation is shown in Table III. In contrast to model 1, Pearson correlation on eq 3 variables revealed that the variables were not highly correlated (coefficient values were between 0.00 and 0.75, except two, moderately correlated at 0.90). Shown in Figures 3 and 4 are plots of predicted RRT versus experimental RRT and RESIDUAL versus experimental RRT. The plots indicate the relationship between gas chromatographic relative PCB retention time and molecular structure as modeled by the position descriptors. Equations based on less than seven indicators resulted in mean square error of regression greater than 0.015.

Multiple linear regression analyses based on a combination of the molecular structure descriptors in models 1 and 2 did

Table III. Regression Coefficients and Statistical Information for Model 2

Equation 3			
constant	0.0464	ORME <sup>b</sup>	-0.0020
FOUR	0.1678	S	0.0059
THREE	0.1605	F value	26504
TWO	0.0879	DF	(7,198)
META	-0.0217	R <sup>2</sup>	0.9989
PARA	-0.0102	N	206
TWOHB <sup>a</sup>	0.0022		

<sup>a</sup> TWOHB = (TWO)(HBOND). <sup>b</sup> ORME = (ORTHO)(META).

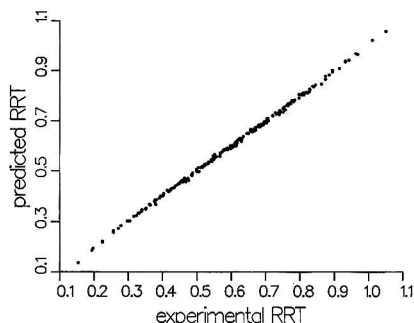


Figure 3. Plot of predicted RRT versus experimental RRT based on eq 3.

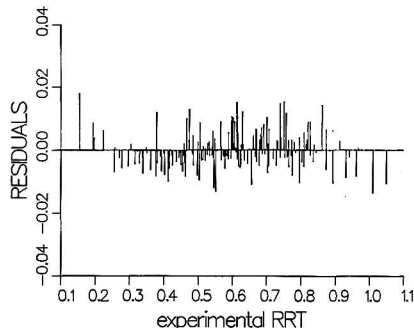


Figure 4. Plot of RESIDUAL versus experimental RRT based on eq 3.

not produce results statistically more significant than those obtained from eq 2 and 3. In the above work 206 of the 209 isomeric PCBs were used for developing the predictive equations that related RRT with molecular structure descriptors. Recall that the mean square error of regression for 2 and 3 was approximately 0.006. Inclusion of three octachlorobiphenyls, IUPAC numbers 199, 200, and 201, in the regression analyses resulted in mean square error of regression of about 0.009, an increase of 30%. No other compounds influenced the regression model in this manner. This result is surprising since RRT values as reported by Mullin and co-workers for these compounds differ appreciably.

The validity of eq 2 and 3 was tested by dividing the data set randomly into two equal subsets (103 data points). For each model, regression equations were refit to each of the two subsets. The remaining 103 compounds were predicted by using each model. The equations obtained correlated the predicted RRT with the experimental RRT values to 0.999, indicating an excellent fit of the data. In order to determine

**Table IV. Regression Coefficients and Statistical Information for Retention Index versus  $^m\chi^t$  Listed Below**

	eq 6	eq 7
constant	-6275.99	-6236.22
$4_{\text{PC}}$	321.61	320.96
$(^2\chi^v)(^6\chi)$	-154.38	-153.46
$2_{\text{PC}}^v$	882.09	886.41
$5_{\text{PC}}^{\text{vc}}$	-7152.33	-7156.92
$5_{\text{PC}}^{\text{v}}$	6529.49	6461.30
$S$	9.99	9.97
$F$ value	14826	16709
$DF$	(5,93)	(5,102)
$R^2$	0.9987	0.9988
$N$	100	108

the minimum number of data required to develop a reliable equation to predict PCB retention characteristics, data sets ranging between 10 and 100 compounds (with each subset incremented by five) were randomly constructed from the entire set of PCB data. Five random sets of each subset were refit by using eq 2 and 3. It was found that about 35 to 40 compounds were required to produce the same statistical significance as when the data was split into two equal subsets.

The molecular connectivity descriptors from eq 2 were used to regress PCB retention index ( $I$ ) values obtained from linear temperature programmed gas chromatography on a DB-5 stationary phase (14, 15). The results are shown in Table IV, eq 4. The mean square error of regression is 9.99 index units representing an approximate error of <1% over the retention index range. As the regression results indicate, the equation is an excellent fit of the data. Plots of predicted  $I$  versus experimental  $I$  and RESIDUAL versus experimental  $I$  showed no systematic structure in the data. The validity of eq 4 was tested by an analogous fashion as above. That is, the retention index values from 70 of the 100 PCB isomers were randomly selected and regressed against the  $^m\chi^t$  descriptors in eq 2. The remaining 30 PCB  $I$  values were predicted from the resulting regression equation and found to be highly correlated with their corresponding experimental  $I$  (Pearson correlation = 0.999).

During the preparation of this paper additional retention data was provided (14) and comparison between experimental and predicted  $I$  was made based on eq 4. The results are presented in Table V. Equation 5, Table IV, is the regression result inclusive of all PCBs currently available. These findings and a comparison of the statistical data generated from the complete set of PCB retention illustrate the point that given a reasonable number of retention data, one can predict the retention characteristics for those compounds in the original data set quite well.

### CONCLUSION

The above findings and results reported by Albro (20) suggest that the optimum approach for characterizing PCB isomers in complex samples is to perform GC experiments that use two or more dissimilar stationary phases (e.g., three stationary phases that have pairwise retention data correlation coefficients much less than 0.9 in absolute value). Retention data on 40 PCBs at each stationary phase is needed to develop reliable equations for predicting the retention characteristics of the remaining PCBs. Note, for each different set of retention data, one should begin model development with the

**Table V. Comparison of Experimental and Predicted Retention Index for Compounds Not in Equation 4**

IUPAC	exptl RI	pred RI	residual
30	997.2	1004.08	-6.87
27	1053.26	1032.23	21.03
110	1455.76	1452.59	3.17
114	1527.70	1521.23	6.47
13	1522.65	1521.64	1.01
180	1737.14	1749.84	-12.87
169	1774.33	1775.20	-0.87
195	1870.77	1868.39	2.38

complete set of structural descriptors to obtain the regression model which yields good statistical fit of data with no structure in the residuals. The choice of molecular connectivity descriptors (or position descriptors) is preferred over experimentally obtained physical/chemical descriptors (e.g., boiling points, dipole moments, etc.) because  $^m\chi^t$  values are generated without error. This avoids the need for predicting experimentally obtained  $x$  variables for PCBs that are not in the data set introducing additional error. The use of the predictive models should allow the analyst to better identify and quantitate PCB isomers most likely to be present in complex environmental samples than simply relying on GC/ECD response factors.

### ACKNOWLEDGMENT

The authors thank M. D. Hale, F. D. Hileman (Monsanto Co.), T. R. Schwartz, D. L. Stalling (U.S. Fish and Wildlife Service), and M. D. Mullin (U.S. EPA) for helpful discussions and Derek Kram for contributing to this work.

Registry No. DB-5, 26468-79-1.

### LITERATURE CITED

- Mullin, M. D.; Pochini, D. M.; McCrindle, S.; Romkes, M.; Safe, S. H.; Safe, L. M. *Environ. Sci. Technol.* **1984**, *18*, 468-476.
- Cohen, A. S.; Grushka, E. J. *Chromatogr.* **1985**, *318*, 221.
- Saura-Calixto, F.; Garcia-Raso, A.; Garcia-Raso, J. J. *Chromatogr.* **1985**, *322*, 35.
- Peetre, I.; Ellren, O.; Smith, B. E. F. J. *Chromatogr.* **1985**, *318*, 41.
- Jinno, K.; Kawasaki, K. J. *Chromatogr.* **1984**, *316*, 1.
- Sabljic, A. J. *Chromatogr.* **1985**, *319*, 1.
- Buydens, L.; Massart, D.; Geerlings, P. *Anal. Chem.* **1983**, *55*, 738.
- Hale, M. D.; Hileman, F. D.; Mazer, T.; Shell, T. L.; Noble, R. W.; Brooks, J. *Anal. Chem.* **1985**, *57*, 640-648.
- Whalen-Pedersen, E. K.; Jurs, P. C. *Anal. Chem.* **1981**, *53*, 2184.
- Rohrbaugh, R. H.; Jurs, P. C. *Anal. Chem.* **1985**, *57*, 2770.
- Dunn, W. J., III; Koehler, M.; Stalling, D. L.; Schwartz, T. R. *Anal. Chem.* **1986**, *58*, 1835.
- Wells, M. J. M.; Clark, C. R.; Patterson, R. M. *Anal. Chem.* **1986**, *58*, 1625.
- Robbat, A., Jr.; Corso, N. P.; Doherty, P. J.; Marshall, D. *Anal. Chem.* **1986**, *58*, 2072-2077.
- Schwartz, T. R., National Fisheries Contaminant Research Center, U. S. Fish and Wildlife Service, Columbia, MO, personal communication, July 1986.
- Schwartz, T. R.; Petty, J. D.; Kaiser, E. M. *Anal. Chem.* **1983**, *55*, 1839.
- Randic, M. J. *Am. Chem. Soc.* **1975**, *97*, 6604-6615.
- Kier, L. B.; Hall, L. H. *Molecular Connectivity in Chemistry and Drug Research*; Academic: New York, 1976.
- Doherty, P. J.; Hoes, R. M.; Robbat, A., Jr.; White, C. M. *Anal. Chem.* **1984**, *56*, 2697-2701.
- Robbat, A., Jr.; Corso, N. P.; Doherty, P. J.; Wolf, M. H. *Anal. Chem.* **1986**, *58*, 2078-2084.
- Albro, P. W.; Corbett, J. T.; Schroeder, J. L. J. *Chromatogr.* **1981**, *205*, 103-111.

RECEIVED for review August 19, 1987. Accepted February 1, 1988.

# Ligand-Accelerated Coupled Transport of Metals across a Liquid Membrane Containing a General Complexing Agent

James A. Cox\* and Atul Bhatnagar

Department of Chemistry, Miami University, Oxford, Ohio 45056

**Uphill transport of Zn(II) across a dithizone-containing liquid membrane that is composed of a mixture of carbon tetrachloride and kerosene in a microporous polypropylene support is reported. The rate of transport from a pH 4.7 buffer into 0.1 M HCl is slow unless the sample includes an auxiliary ligand such as thiosulfate or thiocyanate to displace water from otherwise unfilled coordination sites of the zinc(II)-dithizone complex. With a 200-mL sample that contains 10 mM thiosulfate and a 5-mL receiver, a 60-min experiment with a 11.3-cm<sup>2</sup> membrane yields an enrichment factor of 14.7. It is independent of concentration over the range  $1 \times 10^{-5}$  to  $2.5 \times 10^{-7}$  M Zn(II). When the sample also contains Cu(II), the transport rate of Zn(II) decreases; however, for a given concentration of Cu(II) in the sample, the enrichment factor is still independent of Zn(II) concentration.**

The determination of trace components of a sample must often be preceded by a preconcentration. Transport of species from a sample (source phase) across a membrane into a receiver (receiving phase) results in preconcentration if two conditions are met. The transport must be by a mode that permits it to continue against the net concentration gradient of the species of interest (uphill transport), and the volume of the receiver must be less than that of the sample.

Uphill transport can be accomplished by three general approaches. An external driving force such as current or potential can be used; however, relating the final concentration of the analyte in the receiver to its initial concentration in the sample is difficult unless the electroanalysis is exhaustive (1). A chemical reaction in the receiver can be employed to maintain the concentration gradient of the analyte across the membrane; for example, a redox or a complexation reaction in the receiver will allow passive diffusion to continue even when the analytical concentration (i.e., the sum of the molarities of species in various equilibrium and oxidation states) of the species of interest in the receiver exceeds that in the sample (2). The most common mode is coupled transport. In this case a species that is both readily transported across the membrane and has a much higher concentration in the receiver than in the sample provides the driving force. For example, in Donnan dialysis, where an ion-exchange membrane is the barrier, a relatively concentrated receiver electrolyte is used; passive diffusion into the sample of ions with a charge sign opposite to that of the fixed exchange sites of the membrane provides the driving force. Enrichment factors, the ratio of the final concentration of the analyte in the receiver to its initial concentration in the sample, of more than 50 in 15 min or less have been attained both by using microliter-scale receivers in conjunction with dialysis times that allow Donnan equilibrium to be reached (3) and by using the fixed-time kinetic mode and milliliter-scale receivers (4). The kinetic mode is more appropriate for analytical applications since it yields enrichment factors that are independent of the sample matrix over a wide range of conditions (5).

Another means of performing coupled transport is to use a liquid membrane that contains a mobile carrier which re-

versibly reacts with the analyte in a manner that is controlled by the composition of the sample and receiver solutions. For example, where the mobile carrier is a complexing agent that is the conjugate base of a weak acid and the analyte is a cation of a metal, a relatively low pH receiver causes coupled, uphill transport. Transport of the metal into the receiver is balanced by proton flux into the sample. The theory was described several years ago (6-9). The method is now considered an important emerging technology for the removal of metals from feed solutions. Most of the previous studies dealt with either copper or uranium. Exceptions include extractions of platinum (10), nitrate (11), europium (12), and zinc (13) and the separation of cobalt and nickel mixtures (14).

Recently the liquid membrane approach has been shown to be useful for quantitative preconcentrations. With Cu(II) as the analyte, a commercial mixture of oximes as the complexing agent, and kerosene as the host membrane, we demonstrated that the enrichment factor after a prescribed time was independent of the analyte concentration over the range 0.1 mM to 0.1  $\mu$ M Cu(II) (15). Enrichment factors of 13 were attained after a 60-min preconcentration even though a rather large receiver volume, 5.0 mL, was used. Using cells to promote uphill transport across liquid membranes, Uto et al. (2) found that the voltammetric current due to the reduction of various cations in the receiver at equilibrium is in direct proportion to the original concentration in the sample over a limited concentration range. For example, after 3.5 h the measured current was directly proportional to Cd(II) concentration in the range 0.5-2 ppm. Sakamoto et al. (16) used a liquid membrane of lipophilic crown nitrophenols for the separation and preconcentration of lithium by coupled transport. The flux of cation transport from 0 to 10 h was nearly proportional to the sample concentration over about an order of magnitude.

These reports indicate that the liquid membrane method may permit the design of practical analytical preconcentration procedures. The development of the technique would be aided if information in the liquid-liquid extraction literature can be directly applied. One question in this regard is the extent to which factors that influence the rate of partitioning of the analyte into the organic phase will affect fluxes across the liquid membrane. In this work the transport of Zn(II) across a membrane that contains diphenylthiocarbazone (dithizone) was selected as the test system since the rate of liquid-liquid extraction is known to be very slow unless an auxiliary ligand is present in the sample to occupy coordination sites that are otherwise filled by water (17). Because dithizone is a general complexing agent, this system allows also evaluation of the effect of competing cations on the transport of the analyte.

## EXPERIMENTAL SECTION

The complexing agent acting as the mobile carrier, diphenylthiocarbazone (dithizone), was obtained from Matheson Coleman & Bell. It was purified before use by recrystallization from carbon tetrachloride. A saturated solution of dithizone in a mixture of equal volumes of carbon tetrachloride (Fisher Chemical Co.) and kerosene (Standard Oil) was used as the liquid phase of the membrane. The mixed solvent was used because the solubility of dithizone in kerosene is too low to use that solvent



**Table I. Effect of Thiosulfate on the Coupled Transport of Zn(II) across a Dithizone-Containing Liquid Membrane**

thiosulfate, mM	EF <sup>a</sup>	thiosulfate, mM	EF <sup>a</sup>
0	1.2	8.0	9.5
2.0	5.9	10.0	14.6 <sup>b</sup>

<sup>a</sup> Concentration of Zn(II) in the 5-mL receiver after a 60-min preconcentration divided by the initial sample concentration,  $1.52 \times 10^{-5}$  M. <sup>b</sup> Relative standard deviation, 3.4% (four trials).

alone whereas the evaporation rate of pure carbon tetrachloride complicated its use as the supported liquid. The dithizone concentration was 0.04% (w/v) in the mixed solvent. The support was Celgard 2400 microporous polypropylene (Celanese Corp.) which has a 38% porosity, an effective pore size of 0.02  $\mu$ m, and a thickness of 0.025 mm.

The water was purified with a Sybron/Barnstead Nanopure II system. Pure hydrochloric acid stock solutions were prepared by collecting HCl vapors in distilled water; here, concentrated HCl and distilled water in Petri dishes were placed side-by-side in a desiccator for a few days. The resulting HCl solution was diluted and standardized. The pH 4.7 acetate buffer (0.1 M) was purified by passing it through a column of chelating ion-exchange resin. Other chemicals were of reagent grade and used without purification.

The apparatus used for the transport experiment was the same as that which was previously described except that a magnetic stirrer was not used on the membrane-receiver interface (18). The dialysis cells were made of Plexiglas cylinders; the Celgard membranes formed the bottom of the cells. The dithizone solution was pipetted on top of the dry membrane to form a shallow pool. After 5–10 min, it filled the pores. The excess was removed from the bottom of the membrane by brief contact with tissue paper. The receiver (stripping solution), 5 mL of 0.1 M HCl, was placed in the cell. The experiment was initiated when the cell containing the receiver was dipped into 200 mL of sample (feed solution). Convection was provided by a magnetic stirrer. The area of the supporting membrane was 11.3 cm<sup>2</sup>. Unless otherwise noted, the dialysis time was 60 min.

Quantification was by atomic absorption spectrometry with a Perkin-Elmer 2280 system. Generally the receiver was diluted to 25 mL prior to the measurement. Flame atomization was used unless the zinc concentration was below  $10^{-6}$  M, in which case a Perkin-Elmer HGA-300 graphite furnace was employed.

## RESULTS AND DISCUSSION

Initial experiments were performed with a 200-mL sample of  $1.52 \times 10^{-5}$  M Zn(II) in a 0.1 M acetate buffer at pH 4.7. The receiver was 0.1 M HCl. The enrichment factor after a 60-min preconcentration was 1.2.

For the purpose of comparison, the experiment was repeated by Donnan dialysis with an identical cell except that the membrane was an R-1010 (RAI Research Corp.) cation exchanger. The sample was adjusted to pH 4.7 with dilute HCl. The sample did not include a buffer since a high ionic strength will slow the dialysis. The stripping solution was a mixture containing 0.2 M MgSO<sub>4</sub> and 0.5 mM Al<sub>2</sub>(SO<sub>4</sub>)<sub>3</sub> (19). The enrichment factor was  $10.2 \pm 0.5$  (five trials). We have previously shown that under comparable conditions Donnan dialysis and chemically uncomplicated coupled transport across a liquid membrane yield similar enrichment factors (15). Hence, in the present study the lower enrichment factor when the liquid membrane method was used is caused by the chemistry of the extraction step. Because the zinc-dithizone complex is coordinatively unsaturated, the slow partitioning into the organic phase is expected (17, 20).

The liquid membrane experiment was repeated except that thiosulfate was included in the sample to displace water from the coordination sites of Zn(II). The results are reported in Table I. With 10 mM thiosulfate added to the sample, the enrichment factor exceeded that which was obtained by Donnan dialysis by about the same factor as previously re-

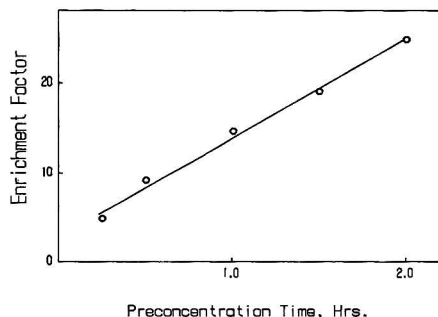


**Figure 1.** Influence of time on the quantity of Zn(II) transported into the receiver solution: sample, 200 mL of  $1.52 \times 10^{-5}$  M Zn(II) and 10 mM thiosulfate at pH 4.7; receiver, 5 mL of 0.1 M HCl.

ported for a study of Cu(II) with a commercial oxime mixture as the mobile carrier (15).

Thiocyanate is perhaps a more common reagent for accelerating the rate of extraction (17). It was, however, less effective than thiosulfate in the present case. For example, a repeat of the experiments in Table I but with  $6.5 \times 10^{-3}$  and  $1.3 \times 10^{-2}$  M SCN<sup>-</sup> in the sample rather than thiosulfate yielded enrichment factors of 7.7 and 8.2, respectively. These results on ligand-acceleration generally agree with those in a study on liquid surfactant membranes (21).

The enrichment factor is directly proportional to preconcentration time over the range 0.25–2.0 h (Figure 1). At longer times, the approach to equilibrium causes a negative deviation from linearity. For example, at 4.5 h the enrichment factor is 32.0. This corresponds to 80% removal of the Zn(II) from the sample solution. The efficiency of the system would certainly be improved by using more effective mixing and/or a more favorable cell geometry. This has been demonstrated by the use of tubular cation exchange membranes in conjunction with high mixing for Donnan dialysis (4) and with tubular microporous supports for liquid membranes (22).

The enrichment factor is independent of Zn(II) concentration over a wide range, so if the attendant analytical method yields a signal in direct proportion to concentration, the combination of coupled transport with that method will have a linear calibration curve. In the range  $1.0 \times 10^{-5}$  to  $2.5 \times 10^{-7}$  M Zn(II) (eight points), the enrichment factor was  $14.7 \pm 0.2$  (six trials) with a 60-min preconcentration from a 0.1 M acetate buffer at pH 4.7 when 10 mM thiosulfate was included in the sample. Lower concentrations were not studied because of residual Zn(II) in the purified buffer. At higher concentrations the enrichment factor decreased, presumably because of saturation of the active sites on the membrane surface. With a  $1.0 \times 10^{-4}$  M sample, the enrichment factor was 3.3.

The supported liquid membranes were very stable. Up to five trials (1.0 h dialyses) were performed with the same membrane. The long-term stability was limited by the light sensitivity of the dithizone.

A problem in the application of the method is that the presence of other metals in the sample can decrease the rate of transport of the analyte if they form strong complexes with dithizone. For example, with  $1.0 \times 10^{-5}$  M Zn(II) as the analyte, the addition of  $1.0 \times 10^{-6}$  M Cu(II) decreases the enrichment factor from 14.6 to 4.3. With  $1.0 \times 10^{-5}$  and  $1.0 \times 10^{-4}$  M Cu(II) added to the sample, the respective enrichment factors for zinc are 1.5 and 0.2. For a given concentration of Cu(II), the enrichment factor for the analyte is still independent of the Zn(II) concentration; the respective values for samples of  $5.0 \times 10^{-7}$ ,  $1.0 \times 10^{-6}$ ,  $5.0 \times 10^{-6}$ , and  $1.0 \times 10^{-5}$  M Zn(II) are 4.2, 4.3, 3.7, and 3.7 in the presence of  $1 \times 10^{-6}$

M Cu(II). Therefore, by use of the standard addition method, this coupled transport technique can be used if the objective of the experiment is a preconcentration prior to an analytical determination.

The influence of Cu(II) on Zn(II) transport suggests a limitation on applications where the objective is the efficient stripping of several metals from a feed solution by use of a general complexing agent. A very slow removal of certain metals of a set may occur until the interferent is almost quantitatively extracted, especially when the interferent complexes more strongly than the analyte. In the present case,  $\log \beta_2$  for the 1:2 zinc(II)-dithizonate complex is 15.1 at 25 °C vs 22.3 for the comparable Cu(II) complex. The use of selective ligands undoubtedly diminishes this problem for a given metal, and perhaps general complexing agents other than dithizone may not behave in this manner. However, at this time Donnan dialysis, which can be performed without interference from mixtures, may be advantageous for simultaneous removal of several metals from a feed solution as long as the sample ionic strength does not exceed about 0.01.

**Registry No.** Zn, 7440-66-6; Cu, 7440-50-8; dithione, 60-10-6; carbon tetrachloride, 56-23-5; polypropylene, 9003-07-0; thiosulfate, 14383-50-7; thiocyanate, 302-04-5.

#### LITERATURE CITED

- (1) Cox, J. A.; Carlson, R. H. *Anal. Chim. Acta* **1981**, *130*, 313-321.
- (2) Uto, M.; Yoshida, H.; Sugawara, M.; Umezawa, Y. *Anal. Chem.* **1986**, *58*, 1798-1803.
- (3) Blaedel, W. J.; Kissel, T. R. *Anal. Chem.* **1972**, *44*, 2109-2111.

- (4) Cox, J. A.; Litwinski, G. R. *Anal. Chem.* **1983**, *54*, 1640-1642.
- (5) Cox, J. A.; Twardowski, Z. *Anal. Chim. Acta* **1980**, *119*, 39-45.
- (6) Cussler, E. L. *AIChE J.* **1971**, *17*, 1300-1303.
- (7) Smith, K. A.; Meldon, J. H.; Colton, C. K. *AIChE J.* **1973**, *19*, 102-111.
- (8) Schultz, J. S.; Goddard, J. D.; Suchdeo, S. R. *AIChE J.* **1974**, *20*, 417-444.
- (9) Goddard, J. D.; Schultz, J. S.; Suchdeo, S. R. *AIChE J.* **1974**, *20*, 625-645.
- (10) Nishiki, T.; Bautista, R. G. *AIChE J.* **1985**, *31*, 2093-2095.
- (11) Kreevoy, M. M.; Nitsche, C. I. *Environ. Sci. Technol.* **1982**, *16*, 635-637.
- (12) Danesi, P. R.; Horwitz, E. P.; Rickert, P. G. *Sep. Sci. Technol.* **1982**, *17*, 1183-1192.
- (13) Fernandez, L.; Aparicio, J.; Muhammed, M. J. *Membr. Sci.* **1986**, *27*, 77-91.
- (14) Danesi, P. R.; Reichle, Yinger, L.; Cianetti, C.; Rickert, P. G. *Solvent Extr. Ion Exch.* **1984**, *2*, 781-814.
- (15) Cox, J. A.; Bhatnagar, A.; Francis, R. W. *Talanta* **1986**, *33*, 713-716.
- (16) Sakamoto, H.; Kimura, K.; Shono, T. *Anal. Chem.* **1987**, *59*, 1513-1517.
- (17) Subbaraman, P. R.; Cordes, Sr. M.; Freiser, H. *Anal. Chem.* **1969**, *41*, 1878-1880.
- (18) Cox, J. A.; Tanaka, N. *Anal. Chem.* **1985**, *57*, 385-387.
- (19) Cox, J. A.; Gray, T.; Yoon, K. S.; Kim, Y. T.; Twardowski, Z. *Analyst (London)* **1984**, *109*, 1603-1605.
- (20) Miniczewski, J.; Chwastowska, J.; Dybczynski, R. *Separation and Pre-concentration Methods in Inorganic Trace Analysis*; Ellis Harwood Ltd.: Chichester, England, 1982; Chapter 5.
- (21) Gu, Z. M.; Wasan, D. T.; Li, N. N. *J. Membr. Sci.* **1986**, *26*, 129-142.
- (22) Danesi, P. R.; Rickert, P. G. *Solvent Extr. Ion Exch.* **1986**, *4*, 149-164.

RECEIVED for review July 20, 1987. Accepted December 16, 1987. This work was performed in part at Southern Illinois University with support by the National Science Foundation under Grant CHE-8215371 to J.A.C.

## Simultaneous Determination of Uronic Acids and Aldoses in Plankton, Plant Tissues, and Sediment by Capillary Gas Chromatography of *N*-Hexylaldonamide and Alditol Acetates

Jeffrey S. Walters and John I. Hedges\*

School of Oceanography, WB-10, University of Washington, Seattle, Washington 98195

**A method for simultaneous extraction and quantification of aldoses and uronic acids from natural samples is described which combines a new hydrolysis technique employing trifluoroacetic acid at 135 °C with a reproducible derivatization producing *N*-alkylaldonamide and alditol acetates that are completely separated by capillary gas chromatography. Optimal hydrolysis conditions for rapid, maximum recoveries are presented. Quantification is based on tests of polymer hydrolysis and monomer derivatization recovery efficiencies.**

A uronic acid is an aldehydic acid that differs from an aldose by having a terminal carboxyl carbon opposite the C-1 carbonyl carbon. Reducing the carbonyl to an alcohol produces an aldonic acid while oxidizing it to an acid produces an aldaric acid. Uronic, aldonic, and aldaric acids are often collectively referred to as acidic sugars. Uronic acids appear to be many times more prevalent in nature than the other two acidic sugars (1). Uronic acids are widely distributed in animals, plants, and bacteria where they serve in both ion-regulatory and structural roles. Some commercially important plant structural polysaccharides, such as pectin and alginic acid are

almost entirely composed of glycosidically bound uronic acids (2). Bacteria contain a wide variety of uronic acids as major components of structural and extracellular polysaccharides. Many unique and possibly genus-specific *O*-alkyl-, amino-, and deoxyuronic acid derivatives have been identified in bacteria (3). Microbial extracellular polysaccharides have been associated with sediment stabilization (4) and microfouling (5).

Although commercially and environmentally important, quantitative analysis of uronic acids from natural samples is difficult because these acidic polymers are resistant to hydrolysis and the resulting monomers are difficult to isolate and derivatize. In part, these complications arise from the multiple functionality of uronic acids. Intramolecular condensations of carbonyl and carboxyl groups with hydroxyl groups allow uronic acids to exist in at least six different structural forms (one acyclic form, two anomeric forms for each pyranose and furanose ring, and at least one lactone form).

The complexity in quantifying the many different structural forms has been overcome with high-performance liquid chromatography (HPLC) using anion exchange resins, since each compound produces only one or two peaks. One recent analysis uses HPLC to simultaneously measure both neutral

and acidic sugars and reports numerous bacterial exopolysaccharide compositions in the form of molar ratios, but absolute recoveries of standards were not quantified and some acid peaks were not completely resolved (6). Other HPLC techniques using ion-exchange chromatography have employed reference standards to quantify recoveries, yet complete resolution is difficult and the commercially available resins are unstable and degrade rapidly (7, 8). One differential method using gas-liquid chromatography (GLC) involved reducing uronic acids to aldonic acids, thereby lowering the number of possible forms to one free acid and one lactone (9). However, standard recovery data were not reported and guluronic acid was not studied.

Even if obstacles to derivatizing uronic acids in monomeric form can be overcome, extracting them from natural samples such as plant tissues or sediment presents a problem. Polysaccharides containing uronic acid constituents are difficult to hydrolyze in good yields because the carboxyl group reportedly stabilizes glycosidic linkages (10). Most reported hydrolyses have used HCl or H<sub>2</sub>SO<sub>4</sub> at temperatures at or below 100 °C and hydrolysis times ranging up to 18 h (11, 6). Fazio et al. circumvent poor hydrolysis recoveries by reducing carboxyl groups of the uronic acids with sodium borodeuteride prior to hydrolysis (12), but their procedure requires routine gas-liquid chromatography-mass spectrometry (GLC-MS) analysis of the deuterated alditol peracetates.

This paper describes a relatively simple analytical method for the simultaneous determination of uronic acids and aldoses which combines a new hydrolysis technique with a derivatization scheme adapted from one presented by Lehrfeld for aldoses and aldonic acids (13). The method employs trifluoroacetic acid (TFA) at 135 °C to reproducibly hydrolyze polysaccharides containing uronic acid in less than 2 h with good yields. Environmental samples containing acidic polysaccharides are also hydrolyzed with good reproducibility. This method should prove useful to chemists wishing to obtain reliable neutral and acidic sugar data from a wide variety of samples with commonly available laboratory instrumentation.

## EXPERIMENTAL SECTION

**Materials.** Reagents, cation-exchange resin, and monomer and polymer standards are obtained from Sigma Chemical Co. All standards are greater than 95% pure.

**Hydrolytic Extraction of Aldoses and Uronic Acids.** Plankton, kelp, and sediment samples are freeze-dried and wood samples are oven-dried overnight at 60 °C. All samples are ground in a Wiley mill, or with a mortar and pestle, to pass a 0.351-mm sieve.

As many as 10 samples, each containing 5–15 mg of organic carbon (20 mg for most tissue samples to 300 mg for sediments) are weighed directly into 2-dram Pyrex vials that have screw-caps fitted with Teflon-lined silicone seals. A Teflon-coated magnetic stirring bar is added to each sample, followed by 3 mL of nitrogen-sparged 0.5 N trifluoroacetic acid. The vials are capped under a stream of N<sub>2</sub> before being stirred in a snug-fitting, 12-hole aluminum heating block. The block has an initial temperature of 140 °C but stabilizes at 135 °C after 15 min. After 2 h, the vials are removed and cooled in an ice slurry for 5 min.

After removal from the ice slurry, the samples are individually spiked with 100 µL of a 0.1 mg/mL aqueous solution of allose and ribonolactone, which are used as relative recovery standards. After the samples are mixed thoroughly and centrifuged for 10 min at 700g, the overlying clear supernatant is drawn off with a pasteur pipet and transferred to a Pyrex culture tube (16 × 150 mm). A 10-port Haake-Buchler vortexing evaporator with a water bath temperature of 50 °C is used to evaporate the acid solutions down to 0.5 mL, whereupon 1 mL of water is added and the solutions are further evaporated to a final volume of 0.1 mL. The samples are then thoroughly dried overnight over a bed of silica desiccant in an evacuated desiccator.

**Conversion of Aldoses and Uronic acids to Peracetylated Alditols and *N*-Hexylaldonamides.** To split any lactones

present, 0.5 mL of a 0.1 M sodium carbonate solution is added to the residue in each tube (sediment samples require an additional 0.5 mL of 0.5 M sodium carbonate solution to produce a sample pH > 7). If a precipitate forms in sediment samples at this point, it is removed via centrifugation for 5 min at 700g. The sample is then placed in a heating block at 30 °C for 1 h. The carbonyl carbons of aldoses and uronic acid salts are reduced when 0.5 mL of a 5% sodium borohydride solution is added and the solution is allowed to react at room temperature for 90 min. To decompose any excess sodium borohydride, a 25% acetic acid solution is added dropwise until bubbling stops.

Sodium and other cations are removed by passing the solution through 2 mL of cation-exchange resin (Dowex 50W-X8 200–400 mesh) in a 1 cm i.d. by 20 cm column and washing with 7 mL of distilled water. The combined eluates are evaporated to dryness by use of the vortex evaporator (50 °C water bath temperature). The resulting crusty borate residue is removed as the tetramethylborate/methanol azeotrope by twice evaporating 2 mL of methanol from each tube. While the sample tubes are still attached to the evaporator under vacuum, the water bath is heated to 85 °C for 2 h to convert aldonic acids to aldolactones. To produce the *N*-hexylaldonamides, the residue in each tube is dissolved in 0.3 mL of pyridine and 0.3 mL of *N*-hexylamine and the capped sample tubes are heated in the block at 55 °C for 30 min. After the tubes are removed and have cooled to below 45 °C, the caps are removed and the open tubes are placed back on the block at 55 °C where N<sub>2</sub> is blown over the solutions until dry residues remain. To make acetate derivatives, 0.3 mL of pyridine followed by 0.3 mL of acetic anhydride is added to each tube. The tubes are then capped and heated on the block at 95 °C for 1 h. Just prior to GLC analysis, each sample is spiked with 100 µL of a 1 mg/mL solution of perisitol peracetate, which is used as an absolute (GC internal) standard. Samples may be concentrated to a final volume of 100 µL by blowing N<sub>2</sub> over the solutions at room temperature. In the interest of safety, the entire procedure is done in a fume hood with a protective shield around the heating block during hydrolysis.

**GLC Analysis.** Gas chromatographic analysis was performed with a Hewlett-Packard Model 5710A GC equipped with a flame ionization detector. A split-type injector is used having a glass injection liner filled with silylated glass beads. The injection port and flame ionization detection (FID) temperatures are kept at 300 °C. Base-line separation of 19 peracetylated derivatives is achieved in 40 min on a DB-1701 capillary column (30 m × 0.25 mm i.d.) obtained from J&W Scientific, Inc. (Figure 1). The temperature program is from 220 to 270 °C at a rate of 1 °C/min with a helium flow rate of 1.2 mL/min at 220 °C. The split ratio is 1:50 and sample injection volumes are 1–5 µL. The signal from the FID is recorded and processed by a Hewlett-Packard 3390A integrator. The same column and operating parameters were used to obtain mass spectra with a Hewlett-Packard Model 5890 gas chromatograph equipped with a Hewlett-Packard Model 5970 series mass selective detector.

Since allitol, rhamnitrol, and fucitol are not commercially available, standard mixtures are prepared in a culture tube by simultaneously reducing allose, rhamnose, and fucose to their corresponding alditols, as described in the previous experimental section, to the point just after the first methanol addition. The remaining commercially available alditols and aldonic acids are added, followed by 2 mL of methanol. The resulting solution is then carried through the remainder of the derivatization procedure (dehydration at 85 °C for 2 h, *N*-hexylaldonamide formation followed by peracetylation). The final standard concentrations are typically about 1 mg/mL. Calibration runs are made for every set of 10 samples, but absolute response variation over several months is less than 5%.

## RESULTS AND DISCUSSION

This method combines a new hydrolysis method with an adaptation of a derivatization technique developed by Lehrfeld (13) for the simultaneous determination of aldonic acids and aldoses. In order to take advantage of his optimization studies, Lehrfeld's derivatization conditions (pH, temperatures, reaction durations, etc.) are not altered. One slight difference, is the use of smaller reagent volumes that are adjusted because

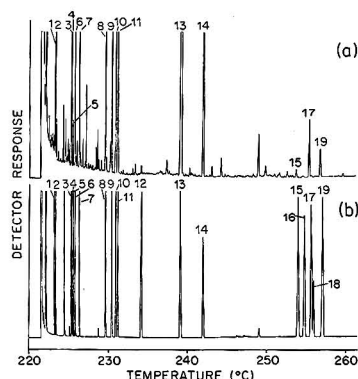


**Figure 1.** Gas chromatographic traces of (a) peracetate derivatives from a marine surface sediment from Saanich Inlet, BC (0–20 cm interval) and (b) a standard mixture. Peak identification numbers (in terms of original compounds) are as follows: 1, erythritol; 2, threitol; 3, rhamnose (Rha); 4, fucose (Fuc); 5, ribose (Rib); 6, arabinose (Ara); 7, xylose (Xyl); 8, allose (All) (relative recovery standard); 9, mannose (Man); 10, galactose (Gal); 11, glucose (Glu); 12, *epi*-inositol (absolute recovery standard); 13, perseitol (absolute recovery standard); 14, ribonolactone (relative recovery standard); 15, mannuronic acid (ManA); 16, guluronic acid (GulA); 17, glucuronic acid (GluA); 18, iduronic acid; 19, galacturonic acid (GalA). Chromatography conditions are described in the text.

of lower monomer concentrations in our samples. The major differences between this procedure and that of Lehrfeld are that internal recovery standards are employed and uronic acids are reduced in addition to aldoses.

A weak base solution added to the dry hydrolysate opens any lactones present by forming sodium uronates. The carbonyl carbons of aldoses and uronates are then quantitatively reduced with sodium borohydride yielding alditols and aldonates, respectively. Base-catalyzed epimerization is negligible as indicated by the absence of significant C-2 epimer byproducts when monomers are carried through the procedure individually. After sodium and boric acid are removed, aldonolactones are quantitatively produced via dehydration and converted to alkylamide derivatives. The amides and alditols (present during the amide formation) are then peracetylated to form volatile derivatives for GLC analysis. To further Lehrfeld's work, rigorous derivatization reproducibility and recovery studies have been done with the use of standard solutions. To allow the derivatization procedure to be used for the analysis of common tissue and environmental samples, a new, more rapid hydrolysis technique has been developed.

**Hydrolytic Extraction.** Time series hydrolyses of alginic acid, polygalacturonic acid, kelp, and a reducing marine surface sediment from Saanich Inlet (14) were done by using TFA concentrations ranging from 0.3 to 2.5 M at temperatures ranging from 100 to 140 °C. Although the time necessary to reach an optimal recovery varied, maximum recoveries were quite similar for hydrolyses with acid strengths between 0.5 and 1.5 M and temperatures between 120 and 140 °C. Monomeric forms of aldoses and uronic acids exposed to the same range of hydrolysis conditions exhibited little difference in recoveries. An acid strength of 0.5 M and a temperature of 135 °C were chosen for routine analysis because, with sediment, these conditions produced the best balance between fast hydrolysis time and high, stable uronic acid and aldose recoveries. Figure 2a shows that the peaks in uronic acid recoveries from sediment occur between 90 and 180 min and stabilize (or "plateau") after 120 min. Sediment aldose curves (Figure 2b) show little loss over time. Although not shown,

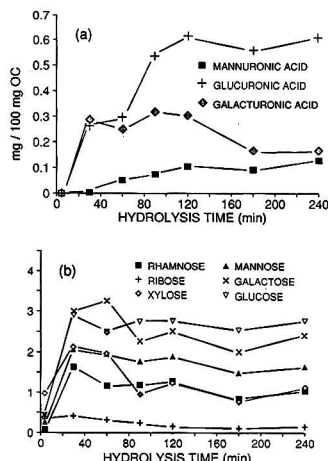


**Figure 2.** Recoveries as a function of hydrolysis time, expressed in mg of compound/100 mg of organic carbon (mg/100 mg OC), for (a) uronic acids (ribonolactone-based recoveries) and (b) selected aldoses (aldose-based recoveries) from a surface marine sediment from Saanich Inlet, BC (0–20 cm interval, 3.4% organic carbon). Hydrolysis conditions are described in the text.

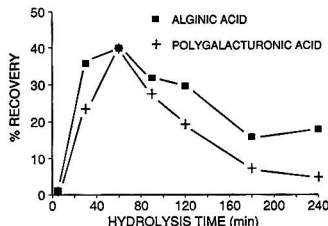


**Figure 3.** Recovery as a function of hydrolysis time for alginic acid and polygalacturonic acid, determined on a percent basis, from GalA recoveries for polygalacturonic acid and the sum of ManA plus GulA recoveries for alginic acid. Both yields are corrected for hydration of individual monomers by assuming mg of monomer(s) = 1.1 × mg of polymer.

curves for kelp also plateau after 120 min. Based on these results the optimal hydrolysis conditions were chosen to be 0.5 M TFA at 135 °C for 120 min.

Figure 3 shows that curves for polygalacturonic acid and alginic acid, hydrolyzed under these conditions, peak at earlier times than the curve for sediment and never reach a well-defined plateau. Hydrolysis curves having more stable plateaus at similar recoveries were obtained with lower temperatures (105–120 °C) at the same or greater acid strengths (0.5–2 N). This result points out that hydrolysis conditions ideal for one type of sample are not necessarily optimal for another. The curve shapes appear to be produced by two simultaneous processes with opposing effects: (1) monomer release from the original polymer and (2) monomer loss, possibly due to dehydration or condensation reactions (15). This second process is evidenced by browning of hydrolysis solutions as hydrolysis temperature, acid strength and time increase. The rates of these processes are probably affected by the same parameters (temperature, acid strength, substrate concentration, and reaction time), explaining why uronic acid recoveries under differing temperatures and acid strengths are remarkably similar, varying only in the time at which they are reached. Uronic acids are known to decarboxylate in acid

Table I. Absolute Recoveries and Reproducibilities<sup>a</sup>

	Rha	Fuc	Rib	Ara	Xyl	All	Man	Gal	Glu	RibA	ManA	GluA	GalA
Recoveries from Derivatization													
SMD	98.3	93.1	91.8	99.6	99.2	83.7	91.9	92.1	92.4	104	85.9	94.5	89.7
%SMD	5.98	4.91	5.28	2.45	2.7	7.90	2.02	2.75	3.21	2.05	4.09	3.73	5.70
%SMD	6.08	5.27	5.75	2.46	2.09	9.44	2.19	2.99	3.48	1.98	4.76	3.95	6.35
Recoveries from Hydrolysis													
SMD	45.1	46.2	35.9	48.4	44.1	72.4	67.9	62.7	74.7	92.5	55.7	53.9	27.5
%SMD	6.05	5.93	9.59	7.99	8.19	6.53	8.97	7.07	8.90	5.81	5.04	5.90	2.71
%SMD	13.4	12.8	26.7	16.5	18.5	9.02	13.2	11.3	11.9	6.29	9.06	11.0	9.86
% loss	54.1	50.4	60.9	51.4	55.6	13.5	26.2	32.0	19.1	10.7	35.2	43.0	69.4

<sup>a</sup> Absolute recoveries were calculated on a percent basis from peracetyl-based recoveries and initial amount of the given compounds. Reproducibilities are expressed as sample mean deviations and percent sample mean deviations (SMD and %SMD,  $n = 5$  for derivatization and  $n = 3$  for hydrolysis). Refer to Figure 1 for compound abbreviations. % loss = percent loss due to hydrolysis, calculated from the ratio of hydrolysis to derivatization recoveries.

media (16). However, since the pentoses that would result were not detected in hydrolysis mixtures from standard polymers (poly(galacturonic acid) and alginic acid), this type of loss is probably insignificant.

**GLC Standard Preparation, Sensitivity, and Reproducibility.** To test for losses due to exposure to base and/or incomplete reduction, relative GLC response factors were calculated from a standard made with aldonic acids and alditols exposed solely to the dehydration, amide formation, and peracetylation steps. These compounds were added to allitol, rhamnitol, and fucitol produced from their respective aldoses via the reduction step in the procedure. Mass spectra of alditol peracetates were essentially identical with library spectra of the same compounds. Response factors of aldoses, five-carbon alditols, six-carbon alditols, and aldonic acids were similar relative to peracetyl and decreased in the order listed from about 1.1 for aldoses to 0.8 for aldonic acids. Good relative response factor linearity ( $r^2$  values  $\geq 0.99$ ) and reproducibility (% mean deviations  $\leq 5\%$ ) were obtained with injection volumes between 0.5 and 5  $\mu$ L and standard concentrations between 0.001 and 10 mg/mL. Under normal integrator settings, the detection limit of the gas chromatograph for the peracetate derivatives is 0.1 ng. With a maximum injection amount of 5  $\mu$ L and a minimum sample volume of 100  $\mu$ L, the practical detection limit was on the order of 0.2  $\mu$ g for both aldoses and uronic acids in natural samples. Sample blanks, carried through the entire procedure with no added sample, contained less than 1.0  $\mu$ g of glucose, xylose, and galacturonic acid and less than 0.5  $\mu$ g of the remaining quantified compounds. Since these amounts are less than 3% of those recovered from the samples described here, no blank corrections were made.

**Aldose and Uronic Acid Monomer Recoveries and Reproducibilities.** Peracetyl (a seven-carbon alditol), peracetylated separately and added to samples via micropipet just prior to injection, was the absolute recovery standard in all analyses. Absolute recoveries and reproducibilities of aldoses and uronic acids taken through the derivatization alone (recoveries from derivatization) and the complete procedure including hydrolysis (recoveries from hydrolysis) are shown in Table I. Ribonolactone (the  $\gamma$ -lactone of ribonic acid) and allose (a six-carbon aldose) were chosen to serve as relative recovery standards. They were added to the cold hydrolysate for hydrolysis recoveries and along with all other compounds for the derivatization recoveries. Ribonolactone was expected to compensate for differences in uronic acid recoveries due to variability in amide formation. Allose was expected to compensate for differing recoveries of all compounds caused by reduction variability. Both standards were expected to compensate for physical losses. Allose has the lowest absolute derivatization recovery and therefore is the least efficiently

derivatized compound while ribonolactone is the most efficiently derivatized compound (Table I). For both derivatization and hydrolysis, the ratio of absolute allose recovery to absolute ribonolactone recovery is 0.8.

This result suggests that exposing the standards to the acid evaporation step of the hydrolysis does not affect their derivatization efficiency. Assuming that this is the case for all compounds, one can determine monomer losses caused by hydrolysis by comparing recoveries from derivatization to recoveries from hydrolysis. The hydrolysis-induced monomer losses (% LOSS) are shown at the bottom of Table I. Ribose, rhamnose, and galacturonic acid are especially susceptible to loss during hydrolysis (Table I). More steeply dropping hydrolysis recoveries over time also show that galacturonic acid is less stable than other uronic acids (Figures 2a and 3). Recoveries of aldoses and uronic acids relative to allose and ribonolactone (allose-based and ribonolactone-based recoveries), shown in Table II, were calculated by setting the recovery of the relative recovery standard at 100% and adjusting the other recoveries proportionately. Because allose is the least efficiently derivatized compound, allose-based derivatization recoveries are over 100% for all compounds. Allose-based allose reproducibilities are generally greater than those relative to ribonolactone, while ribonolactone-based uronic acid reproducibilities are greater than those relative to allose (Table II). This difference occurs because allose should behave in a manner representative of other aldoses, while ribonolactone, as an aldonic acid, should behave similarly to uronic acids once they have been reduced. While the allose-based uronic acid recoveries are not as precise as ribonolactone-based recoveries (because they cannot compensate for variability in amide formation), they are important to monitor, because uronic acids are reduced and ribonolactone is not. Consequently ribonolactone-based recoveries cannot compensate for reduction variability. The ideal uronic acid recovery standard would be a uronic acid not found in nature, but since such a compound is not yet readily available, allose was used to compensate for reduction variability and ribonolactone was used to compensate for amide formation variability.

**Hydrolysis Recoveries and Reproducibilities from Polymers and Natural Samples.** Average recoveries and reproducibilities of polysaccharides containing uronic acids hydrolyzed alone and spiked into sediment are shown in Table III. Because the recoveries are very similar, it appears that the sediment matrix does not significantly affect polymer hydrolysis efficiency. Notice that while ratios of allose-based recoveries to ribonolactone-based recoveries are similar for both polymers, they are much lower than those obtained for hydrolyzed monomers. Though not shown, this is also the case for relative recoveries from natural samples. For the most



Table II. Relative Recoveries and Reproducibilities<sup>a</sup>

Recoveries from Derivatization													
	Rha	Fuc	Rib	Ara	Xyl	All	Man	Gal	Glu	RibA	ManA	GluA	GalA
Ribonolactone-Based Recoveries													
SMD	95.2	90.1	88.9	96.4	95.9	81.1	89.0	89.1	89.4	100	82.8	91.1	86.3
%SMD	7.33	5.81	6.45	3.47	2.95	8.97	3.02	2.97	3.73	0.00	2.37	1.83	3.89
R/A	7.70	6.46	7.26	3.60	3.07	11.1	3.39	3.33	4.17	0.00	2.87	2.01	4.50
Allose-Based Recoveries													
SMD	121	115	113	126	126	100	116	116	116	133	111	122	117
%SMD	7.36	7.82	6.12	13.4	14.5	0.00	12.5	12.0	10.6	18.5	17.3	18.0	19.7
R/A	6.08	6.79	5.42	10.6	11.5	0.00	10.7	10.2	9.17	13.9	15.5	14.7	16.8
	0.79	0.78	0.79	0.77	0.76	0.81	0.76	0.77	0.77	0.75	0.74	0.75	0.74
Recoveries from Hydrolysis													
	Rha	Fuc	Rib	Ara	Xyl	All	Man	Gal	Glu	RibA	ManA	GluA	GalA
Ribonolactone-Based Recoveries													
SMD	49.3	50.4	39.3	52.9	48.2	78.8	74.0	68.3	81.5	100	60.2	58.1	29.6
%SMD	8.36	8.32	12.1	10.7	10.8	10.1	12.6	10.3	12.7	0.00	3.49	2.61	1.02
R/A	16.9	16.5	30.6	20.3	22.4	12.8	17.0	15.0	15.6	0.00	5.80	4.50	3.43
Allose-Based Recoveries													
SMD	62.2	63.7	48.7	66.5	60.3	100	93.4	86.4	103	129	78.3	75.5	38.3
%SMD	4.96	2.91	8.28	4.70	5.47	0.00	3.89	1.84	3.25	15.1	13.2	11.6	4.50
R/A	7.98	4.57	17.0	7.07	9.07	0.00	3.95	2.13	3.15	11.7	16.8	15.4	11.8
	0.79	0.79	0.81	0.80	0.80	0.79	0.79	0.79	0.79	0.77	0.77	0.77	0.77

<sup>a</sup>Relative recoveries were calculated on a percent basis by setting recovery of relative recovery standard at 100%. R/A = ratio of ribonolactone-based to allose-based recoveries. Refer to Figure 1 and Table I for other abbreviations.

Table III. Acidic Polysaccharide Recoveries<sup>a</sup>

	alginate acid		poly(galacturonic acid)	
	alone	spiked	alone	spiked
Ribonolactone-Based Recoveries				
SMD	20.0	17.0	18.1	23.6
%SMD	6.47	4.43	2.94	5.19
	32.4	26.0	16.3	22.0
Allose-Based Recoveries				
SMD	56.9	36.3	55.6	47.2
%SMD	4.66	8.59	13.9	12.3
R/A	8.19	23.7	25.0	26.1
	0.35	0.47	0.32	0.50

<sup>a</sup>Recoveries were determined on a percent basis from relative recoveries and initial polymer amounts. Alginate acid recoveries were calculated from combined ManA and GluA recoveries and poly(galacturonic acid) recoveries from GalA recoveries ( $n = 5$ ). Refer to Tables I and II for abbreviations.

part, this relationship is a result of a drop in absolute allose recovery, probably due to lower reduction efficiencies of all compounds caused by the presence of other material. Since there is no prior isolation step, any dissolved material resulting from hydrolysis, e.g. mineral salts or amino acids, could potentially interfere with reduction. However, since the ratios for all compounds drop equally, the drop in reduction efficiency is correctable by using allose as the relative recovery standard. Because allose-based recoveries can compensate for lowered reduction efficiencies, allose is used as a relative recovery standard for both aldoses and uronic acids from natural samples. While they do not compensate for lower reduction efficiencies, ribonolactone-based recoveries for uronic acids are important because they provide more precise results within this group and therefore should be used in computing uronic acid ratios that are discussed later.

When  $\alpha$ -cellulose was hydrolyzed under the previously described optimal conditions, recoveries (based on glucose) were 20% or less. Pretreatment with concentrated TFA did

not significantly increase the recoveries of any of the studied polymers. Total carbohydrate amounts from this method will therefore be lower than those obtained with methods employing concentrated  $H_2SO_4$  pretreatment, which does effectively hydrolyze  $\alpha$ -cellulose (17).

Table IV shows the recoveries from marine sediment, kelp, plankton, and wood. Though not unacceptable, variability for natural samples is higher than that obtained from standards, suggesting that matrix effects induce variability. Aldose results for plankton and wood agree well with  $\alpha$ -cellulose corrected results obtained with the method of Cowie and Hedges (17), varying by less than a factor of 1.5 for most compounds. The presence of alditol peracetates was confirmed by comparing mass spectra from natural samples to library spectra. The mass spectra of assigned uronic peaks from natural samples matched those from standards. The presence of 4-O-methylglucuronic acid in wood was confirmed by comparing the mass spectrum of the assigned peak from wood samples to that obtained from standard 4-O-methylglucuronoxylan. Recovery linearity was tested for sediment samples over a 2 order-of-magnitude range of sample weight. The  $r^2$  values calculated for samples within the organic carbon (OC) loading limits of 0.3 and 30 mg are shown in Table V. Higher  $r^2$  values were obtained for samples containing between 0.3 and 3.0 mg OC.

**Recovery Ratios.** In addition to the determination of sample uronic acid content, other useful applications of this method involve determinations of relative variation between individual compounds. The recoveries of aldoses and uronic acids relative to that of galactose (a major component in all samples) for various sample types are shown in Table VI. The ratios for aldoses agree well with those obtained with the Cowie and Hedges analysis (17), varying by less than a factor of 1.5. Reproducibilities are better for recovery ratios than for recoveries, indicating that recoveries vary partially due to factors affecting all compounds equally. Such universal factors could include variations in spiking of relative and absolute recovery standards.

**Additional Comments on Hydrolysis: TFA vs HCl.** Sulfuric acid was not considered for this method because it



Table IV. Recoveries from Natural Samples<sup>a</sup>

mg of compound/100 mg of organic carbon														
	Rha	Fuc	Rib	Ara	Xyl	Man	Gal	Glu	ManA	GulA	GluA	GalA	4OMGA	TCH <sub>2</sub> O
Sediment														
SMD	0.99	0.85	0.15	0.80	1.27	1.66	2.36	2.50	0.13	ND	0.80	0.40	ND	11.9
%SMD	0.13	0.13	0.02	0.14	0.35	0.22	0.32	0.37	0.05		0.26	0.12		2.08
%SMD	13.5	15.9	11.3	17.6	27.5	13.1	13.7	14.8	37.8		32.0	30.3		17.5
Kelp														
SMD	0.20	4.06	0.46	0.43	0.96	18.5	1.63	2.59	34.2	9.15	4.19	ND	ND	76.2
%SMD	0.02	0.36	0.23	0.13	0.26	1.12	0.16	0.08	7.44	0.61	1.04			8.58
%SMD	10.5	8.82	51.2	31.1	26.7	6.11	9.84	3.04	21.8	6.67	24.9			11.3
Plankton														
SMD	0.16	0.23	0.47	0.27	1.21	0.49	0.74	1.98	0.05	1.33	0.31	0.15	ND	7.37
%SMD	0.02	0.04	0.23	0.06	0.41	0.09	0.12	0.38	0.03	0.36	0.16	0.06		1.65
%SMD	14.6	17.5	48.6	23.7	34.3	17.5	16.5	19.1	50.2	26.9	50.4	39.5		22.4
Wood														
SMD	0.22	ND	0.06	1.67	5.96	25.2	4.54	15.1	0.10	0.09	0.16	1.37	1.13	54.5
%SMD	0.05		0.04	0.34	1.45	4.73	1.04	4.48	0.07	0.07	0.10	0.53	0.59	13.1
%SMD	25.0		59.1	20.6	24.4	18.8	23.0	29.7	68.4	73.5	61.6	38.7	51.9	24.4

<sup>a</sup>Sediment, 0–20 cm homogenized section from Saanich Inlet box core, 200 mg, 3.4% organic carbon,  $n = 5$ . Kelp, whole, homogenized *Laminaria longipes*, 20 mg, 38.4% organic carbon,  $n = 3$ . Plankton, 64–300  $\mu$ m mesh sieve fraction of plankton tow in Dabob Bay, 40 mg, 32.0% organic carbon,  $n = 5$ . Wood, Douglas Fir trunk wood, 20 mg, 46.8% organic carbon,  $n = 5$ . TCH<sub>2</sub>O = total carbohydrate. ND = not detected at quantifiable levels. Refer to Figure 1 and Table I for abbreviations.

Table V. Hydrolysis Recovery Linearity<sup>a</sup>

com- pound	corr ( $r^2$ )	% TCH <sub>2</sub> O	compound	corr ( $r^2$ )	% TCH <sub>2</sub> O
rhamnose	0.9797	8.32	galactose	0.9967	19.8
fucose	0.9979	7.14	glucose	0.9469	21.0
ribose	0.9883	1.26	Mann. UA	0.9971	1.09
arabinose	0.9962	6.72	Glu. UA	0.8426	6.72
xylose	0.9886	10.7	Gal. UA	0.9889	3.36
mannose	0.9895	14.0	TCH <sub>2</sub> O	0.9969	100

<sup>a</sup>Linearity of allose-based hydrolysis recoveries for Saanich Inlet sediment (10-, 50-, 200-, 500-, and 1000-mg samples, 3.4% OC). Correlation coefficients ( $r^2$ ) calculated by linear regression. TC-H<sub>2</sub>O : percent of total carbohydrate.

is not volatile. Hydrolyses employing it, therefore, require neutralization steps involving precipitates that complicate isolation and might provide a substrate for uronic acid adsorption and subsequent loss. TFA and HCl are both attractive alternatives because of their volatility. To compare the hydrolysis efficiencies of the two acids, a time-series hy-

drolysis of alginic acid and poly(galacturonic acid) was done in 2 N HCl at 100 °C. For both polymers, maximum reproducible recoveries with HCl of about 30% were obtained after 3 h. Curve shapes were characterized by a rise to a "peak", followed by a rather sharp subsequent decrease in recovery at later times. Although not drastically different, the recoveries with HCl are lower and the optimal times are longer than for the TFA hydrolysis. In addition, the HCl hydrolyses are more difficult to dry than those obtained with TFA. These results led to the choice of TFA over HCl as the routine acid for hydrolysis.

**Additional Considerations.** This method should be useful for several reasons. It is relatively simple and fast; with the capability of analyzing 3.3 samples/day (10 samples in three 8-h days). Completely derivatized samples and standards are stable for at least 6 months when stored in a freezer. The GC traces for natural samples show simple, well-separated suites of peaks that correspond to five-carbon deoxy aldoses, five-carbon aldoses, six-carbon aldoses, and uronic acids (Figure 1). There are time gaps between the five-carbon and six-carbon aldose suites and the six-carbon aldose and uronic acid

Table VI. Recovery Ratios<sup>a</sup>

	Rha	Fuc	Rib	Ara	Xyl	Man	Gal	Glu	ManA	GulA	GluA	GalA	4OMGA
Sediment													
SMD	0.42	0.36	0.07	0.34	0.53	0.68	1.00	1.06	0.05	ND	0.33	0.17	ND
%SMD	0.04	0.03	0.01	0.02	0.07	0.08	0.00	0.04	0.01		0.07	0.03	
%SMD	8.53	7.25	18.9	5.56	13.6	11.6	0.00	4.14	25.3		21.9	20.2	
Kelp													
SMD	0.12	2.49	0.28	0.26	0.59	11.2	1.00	1.58	32.7	8.91	3.99	ND	ND
%SMD	0.01	0.16	0.09	0.05	0.10	0.28	0.00	0.17	2.73	0.19	0.42		
%SMD	11.9	10.2	49.5	29.0	28.0	3.91	0.00	11.3	13.2	3.44	16.7		
Plankton													
SMD	0.21	0.31	0.65	0.36	1.57	0.67	1.00	2.66	0.07	1.77	0.40	0.19	ND
%SMD	0.00	0.00	0.18	0.02	0.54	0.01	0.00	0.22	0.00	0.47	0.06	0.01	
%SMD	0.84	0.81	27.8	5.05	34.5	0.98	0.00	8.19	2.61	26.6	15.5	5.34	
Wood													
SMD	0.05	ND	0.01	0.38	1.32	5.54	1.00	3.27	0.02	0.02	0.03	0.29	0.24
%SMD	0.00		0.00	0.03	0.23	2.74	0.00	0.86	0.00	0.00	0.00	0.02	0.00
%SMD	0.42		0.49	8.47	17.2	49.5	0.00	26.3	1.12	1.13	1.36	5.70	8.25

<sup>a</sup>Recovery ratios are allose-based and normalized to those of galactose. Uronic acid ratios were calculated from ribonolactone-based recoveries. Refer to Figure 1 and Tables I and IV for abbreviations.

suites where *O*-alkyl forms such as 6-*O*-methylglucose and 4-*O*-methylglucuronic acid can be resolved. Flexibility of uronic acid retention times is possible, if desired, through the substitution of other alkylamines such as *N*-propyl- and *N*-amylamines in the derivatization (13). Furthermore, the ability to analyze samples with GC-MS adds identification capabilities not readily available with HPLC methods.

Iduronic acid, an important uronic acid in some animal polysaccharides, is completely resolved with the described GC conditions. It was detected in amounts of less than 5  $\mu$ g in wood samples and less than 0.2  $\mu$ g in all other samples. Because it could serve as a very effective relative recovery standard for uronic acids, iduronic acid warrants further study. However, it appears to be only commercially available as the 1,2-isopropylidene derivative (Calbiochem) which must be hydrolyzed before it is derivatized.

*epi*-Inositol peracetate is another well-resolved compound that could serve as a recovery standard. Because an impurity in the perisitol standard coelutes with 4-*O*-methylglucuronic acid, *epi*-inositol should be used as an absolute recovery standard when quantification of this characteristic vascular plant-derived uronic acid is desired. By use of the described method, peracetate derivatives of threitol and erythritol (three-carbon alditols) are both detected as completely resolved peaks (Figure 1) and were recovered in total sample amounts between 0.2 and 10  $\mu$ g.

With the described experimental conditions, one is unable to distinguish aldonic acids that are present prior to reduction from those produced from uronic acids by reduction. However, since uronic acids appear to be much more prevalent in most natural samples (1), it is assumed that insignificant amounts of aldonic acids contribute to the reported uronic acid recoveries. Nevertheless, if sodium borodeuteride is used as the reducing agent, the two types of compounds should be distinguishable via GC-MS, because deuteriated aldonic acids would be produced from the reduced uronic acids.

Since there do not appear to be significant matrix-induced changes in polymer hydrolysis recoveries and since these recoveries are about 50%, the reported uronic acid recoveries from natural samples are probably half the actual uronic acid content. Assuming this, kelp is as much as 40% (w/w) mannuronic acid and reducing coastal marine sediment contains amounts of galacturonic and glucuronic acid comparable to those of the neutral sugars. Uronic acids are therefore potentially important components of natural samples that, due to their analytically elusive nature, may not have been

given adequate consideration. Furthermore, it appears that uronic acid compositional patterns (expressed in Table VI as ratios) could be distinct for different sample types and therefore could help to more comprehensively determine the relative contributions from different organic matter sources.

#### ACKNOWLEDGMENT

The authors thank Tim Bates for the use of the GC-MS, Karen Weliky and Miguel Goni for helpful reviews, and Gregory Cowie for advice and assistance.

**Registry No.** Rha, 3615-41-6; Fuc, 2438-80-4; Rib, 50-69-1; Ara, 147-81-9; Xyl, 58-86-6; Man, 3458-28-4; Gal, 59-23-4; Glu, 50-99-7; ManA, 1986-14-7; GulA, 21675-52-5; GluA, 6556-12-3; GalA, 685-73-4; 4OMGA, 4120-73-4.

#### LITERATURE CITED

- Theander, O. "Acids and Other Oxidation Products". In *The Carbohydrates*, 2nd ed.; Pigman, W., Horton, D., Eds.; Academic: New York, 1980.
- Stephen, A. "Other Plant Polysaccharides". In *The Polysaccharides*; Aspinall, G. O., Ed.; Academic: New York, 1983.
- Kenne, L.; Lindberg, B. "Bacterial Polysaccharides". In *The Polysaccharides*; Aspinall, G. O., Ed.; Academic: New York, 1983.
- Rhoads, D. C.; Yingst, J. Y.; Ullman, W. J. "Seafloor stability in central Long Island Sound: 1. Seasonal changes in erodibility of fine grained sediment". In *Estuarine Interactions*; Wiley, Ed.; Academic: New York, 1978; pp 221-244.
- Nickels, J. S.; Bobble, R. J.; Lott, D. F.; Martz, R. F.; Benson, P. H.; White, D. C. *Appl. Environ. Microbiol.* **1981**, *41*, 1442-1453.
- Kennedy, A. F. D.; Sutherland, I. W. *Biotechnol. Appl. Biochem.* **1987**, *9*, 12-19.
- Hicks, K. B.; Lim, P. C.; Hass, M. J. *J. Chromatogr.* **1985**, *319*, 159-171.
- Voragen, A. G. J.; Schols, H. A.; De Vries, J. A.; Plinik, W. J. *Chromatogr.* **1982**, *244*, 327-336.
- Lehrfeld, J. *Anal. Biochem.* **1981**, *115*, 410-418.
- Lindberg, B.; Lonngrén, J.; Svensson, S. *Adv. Carbohydr. Chem. Biochem.* **1975**, *31*, 185-239.
- Mopper, K. *Mar. Chem.* **1977**, *5*, 585-603.
- Fazio, S. A.; Uhlinger, D. J.; Parker, J. H.; White, D. C. *Appl. Environ. Microbiol.* **1982**, *43*, 1151-1159.
- Lehrfeld, J. *Anal. Biochem.* **1985**, *148*, 346-348.
- Hamilton, S.; Hedges, J. I. *Geochim. Cosmochim. Acta* **1988**, *52*, 129-142.
- Hodge, J. E. *J. Agric. Food Chem.* **1953**, *15*, 928-942.
- Tracey, M. V. *Biochem. J.* **1948**, *43*, 185.
- Cowie, G. L.; Hedges, J. I. *Geochim. Cosmochim. Acta* **1984**, *48*, 2075-2087.

RECEIVED for review August 20, 1987. Accepted January 12, 1988. This research was supported by NSF Grants OCE 82-19294 and OCE 84-21023. Funds for purchase of the vortexing evaporator were supplied by the University of Washington's School of Oceanography. This is contribution No. 1741 from The School of Oceanography, The University of Washington, Seattle, WA.

# Universal Detection of Ions by Replacement-Ion Chromatography Employing an Anion-Replacement Method and an Ultraviolet-Visible Spectrophotometric Detector

Leonard J. Galante and Gary M. Hieftje\*

Department of Chemistry, Indiana University, Bloomington, Indiana 47405

**A new ion-chromatographic (IC) detection method involving replacement-ion chromatography (RIC) and an anion-replacement arrangement is employed for cation and anion analysis. In the instrument, a conventional dual-column IC system is followed by a continuously regenerating anion-exchange (ionomeric) fiber, which serves as the replacement column. This third column converts all ionic solutes into their iodate or nitrate salts, which are detected sensitively at 215 nm by a UV-visible spectrophotometer. The detection method is especially useful for cation separations, for which the influence of various system parameters is discussed in detail. Good precision (<5% relative standard deviation), low detection limits (1–15 ng), and universal calibration were achieved for several monovalent cations. However, the method does not appear to be useful for anion determinations.**

At present, no completely satisfactory detector exists for quantitating anions and cations by ion chromatography (IC) (1–7). The conductivity detector is the most widely used because of its simplicity and generality. However, it is strongly influenced by temperature; most ionic solutions experience a 2% change in conductivity per degree Celsius. Thus, the sensitivity achievable by conductometric-detection methods depends on the ability to minimize background variation caused by temperature fluctuation. Of course, temperature control is more critical when background levels are high. Moreover, detector cells must be well insulated and some are equipped with temperature-compensation circuitry (5, 6). Columns and valves can also be environmentally isolated (8).

A number of alternative general detection methods have been investigated for IC. For example, spectroscopic or electrometric methods can be employed after separated ions are reacted with specific reagents. Such postcolumn derivatization methods have been reviewed (6). Unfortunately, a single postcolumn reagent cannot often be used for a wide variety of ions; as a result, these methods cannot be considered to be generally applicable.

In the last few years, indirect photometric chromatography has proven to be a competitively sensitive single-column detection method for IC (9–11). In this technique, light-absorbing eluent ions are displaced by nonabsorbing sample ions, which are then measured by a spectrophotometric detector as "trough" peaks in the base-line absorbance. This method has been most extensively employed in anion chromatography with eluents such as phthalate. Detection limits of 1 ng of sulfate (9) and 2 ng of chloride (10) have been reported. Alkali and alkaline-earth metals have been separated with  $\text{Cu}^{2+}$  (9, 11) or  $\text{Ce}^{3+}$  (11) as the eluent cation with detection limits in the range of 8–1200 ng and 0.08–4.0 ng (11), respectively.

A few years ago, a method called replacement-ion chromatography (RIC) was described that allows otherwise species-specific detectors to be used as general detectors for suppressed IC (12). In RIC, a third ion-exchange column called the replacement column is used to replace solute ions

(or their co-ions) with another ion (the replacement ion) that can be sensitively monitored by a suitable detector. In the first demonstration of RIC (12), ionic solutes eluting from the suppressor column were converted to their lithium salts by a replacement column containing a cation-exchange resin in the lithium form. Solutes were subsequently detected (indirectly) by monitoring their lithium atomic emission in a hydrogen-air flame.

There are several fundamental advantages to RIC. First, ion replacement allows other desirable detectors to be used as general detectors for IC. More importantly, detectors can be used that are less sensitive to temperature and possibly more sensitive than the conductivity detector. In addition, the integrated detector response of all solutes should be the same in RIC because each solute is stoichiometrically converted into a single detected form. Consequently, RIC is a universal-detection method, and a single calibration curve should apply to all species of the same charge.

In the present publication, we describe an alternative mode of RIC involving anion replacement. Iodate and nitrate were both explored as replacement ions because of their high molar absorptivities at 210 nm (13). Sensitive detection was accomplished with a UV-visible spectrophotometer. We employed a hollow ionomeric anion-exchange fiber (14, 15) as the replacement column because of its low contribution to band broadening and its ability to operate continuously (unlike packed-bed resin columns, which must be regenerated periodically).

In this study, theoretical and experimental guidelines for optimal operation of the fiber-replacement column are discussed. Figures of merit such as sensitivity, detection limits, precision, and dynamic range are evaluated for both cation and anion determinations. The possibility of universal calibration is assessed, and the limitations of the technique are critically evaluated.

## EXPERIMENTAL SECTION

Designing an RIC system requires appropriate selection of the replacement ion, replacement column, and detector. Solute must be exchanged conveniently and efficiently with a replacement ion that can be detected sensitively. Ideally, the detector should be simple and easily interfaced to an ion chromatograph. In the current study, a UV-visible spectrophotometer was chosen; it satisfies adequately these criteria and is also available in most LC laboratories. Furthermore, a number of anions absorb strongly in the UV region near 210 nm (13, 16–18), making them suitable replacement ions. The reported molar absorptivities of iodate and nitrate are 2632 and 9091  $\text{L mol}^{-1} \text{cm}^{-1}$ , respectively, at 210 nm (13). Iodate and nitrate ions also possess low and moderate resin affinities (7), respectively. Replacement ions that are weakly retained on the ion-exchange sites of the fiber favor efficient and stoichiometric ion exchange. A schematic diagram of the analytical system used for cation determinations is shown in Figure 1.

**Equipment.** Equipment included an LC pump (Model 396 MiniPump, Milton Roy Co., Riviera Beach, FL) and sample-injection valve with a 20- $\mu\text{L}$  sample loop (Model 7010, Rheodyne, Cotati, CA). All columns were Dionex products (Dionex Corp., Sunnyvale, CA). The cation separator column (either CS1, Model

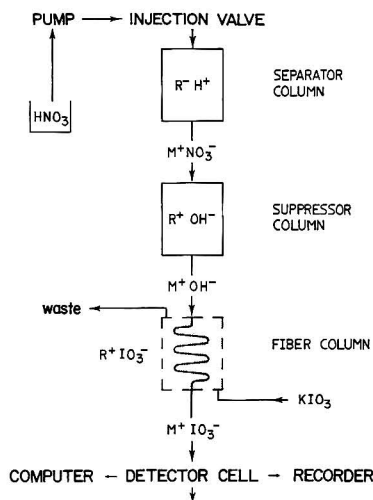


**Figure 1.** Schematic diagram of RIC system used for cation determinations using  $\text{IO}_3^-$  as the replacement ion. Here, the fixed charge (either  $\text{R}^+$  or  $\text{R}^-$ ) and the counter ion of each column are shown. The ions associated with the separated cations ( $\text{M}^+$ ) as they exit each column are shown also.

30831, or CS2, Model 35371) was followed by either a small (CSC-1, Model 30832) or large (CSC-2, Model 30834) packed-bed cation suppressor column. The anion separator column (AS3, Model 30985) was followed by a large packed-bed anion suppressor (ASC-2, Model 30828). The replacement column for both anion and cation determinations was a Dionex fiber-suppressor unit (Model 35352, including fiber, fiber-housing reservoir, and regenerant reservoir (14, 15)). The fiber is hollow, approximately 2.3 m long (dry length), and coiled around a support rod in the housing reservoir. The fiber material is proprietary. Columns were connected by 0.8 mm i.d.  $\times$  1.6 mm o.d. Teflon tubing with Omnifit (Atlantic Beach, NY) polypropylene tube-end bushings and grippers.

Column effluent was monitored at either 210 or 215 nm by a digital UV-visible spectrophotometer (Model GC-55, Perkin-Elmer Corp., Norwalk, CT) modified to perform as an LC detector. The instrument is equipped with a dynamic filter that provides a maximum time constant of 1 s. Chromatograms were simultaneously traced on a strip-chart recorder (Model SR-204, Heath Co., Benton Harbor, MI) and stored on a laboratory computer (MINC-11/23, Digital Equipment Corp., Marlboro, MA) for peak-height or peak-area measurement.

**Reagents.** Dilute acid solutions were prepared from analytical reagent grade concentrated nitric acid (Mallinckrodt, Inc., Paris, KY). Sodium hydroxide solutions were prepared by dilution of a 10.0 N volumetric solution (Mallinckrodt, Inc.). The solutions used to maintain the fiber in the  $\text{IO}_3^-$  or  $\text{NO}_3^-$  form (regenerant solutions) were prepared from analytical reagent grade  $\text{KIO}_3$  and  $\text{KNO}_3$ , respectively (Mallinckrodt, Inc.). All other solutions were prepared from analytical reagent grade (Mallinckrodt, Inc.) or ACS reagent grade salts (MCB, Cincinnati, OH, or Fisher Scientific Co., Fair Lawn, NJ). The water used in all experiments was distilled and deionized.

**Procedures.** Cation suppressors were regenerated with 0.3 N filtered  $\text{Ba}(\text{OH})_2$  or 0.1 N  $\text{NaOH}$ . The anion suppressor was regenerated with 0.35 N  $\text{HNO}_3$ . Regeneration involved pumping the appropriate solution through the column for at least 30 min at a flow rate of 2.0 mL/min. Columns were then rinsed copiously with water.

Regenerant solutions containing 40.0 mM tetramethylammonium hydroxide or potassium hydroxide are recommended for the fiber column when the device functions as an eluent suppressor in cation chromatography (15). Accordingly, solutions

containing 40.0 mM of the appropriate replacement ion were initially explored as regenerants for the fiber-replacement column. The fiber was converted into the desired ( $\text{IO}_3^-$ ,  $\text{NO}_3^-$ , or  $\text{Cl}^-$ ) form by copiously flushing the housing reservoir with a 40.0 mM solution of the respective salt. The fiber was left to soak in this solution for at least 24 h. During this time, the housing reservoir was periodically flushed with fresh solution to ensure complete conversion. When only the concentration of a regenerant was changed, the fiber was left to equilibrate with a new solution for at least 6 h. During operation, the regenerant flow rate through the fiber-housing reservoir was maintained between 2.5 and 3.5 mL/min countercurrent to column flow and regulated by gravity (15).

Background replacement-ion concentrations in the column effluent were calculated by comparing the background absorbance produced by column effluent to that of standard solutions at 210 or 215 nm.

Void volume and band broadening measurements were made by injecting 20- $\mu\text{L}$  aliquots of  $8.0 \times 10^{-4}$  M  $\text{KIO}_3$  both with and without the fiber inserted between the injector and detector cell. Water was used as the eluent at a flow rate of 2.0 mL/min.

## RESULTS AND DISCUSSION

**Background Replacement-Ion Concentrations in RIC.** A finite background replacement-ion concentration arises in RIC from a number of sources including regenerant penetration and contaminant ions. This background concentration causes a corresponding base-line signal upon which analyte peaks are observed. Such a background signal is particularly troublesome if multiplicative noise sources exist within the RIC detection system because they cause fluctuation in an otherwise stable background signal. In such a situation, detection limits are degraded in proportion to both the multiplicative noise and the magnitude of the background signal. Consequently, background levels and their dependence on operating conditions were assessed in the present system. This information can be used also to predict the attractiveness (e.g., detection limits) of alternative replacement-anion/detector combinations.

**Regenerant Penetration.** Ideally, the cations in the inner (chromatographic) and outer (regenerant) flow streams are selectively excluded from the fiber by the Donnan potential of the fiber pores, and only the anions can pass through the fiber wall during the exchange process. However, at high regenerant-ion concentrations, this potential is exceeded by the strong concentration gradient across the fiber. As a result, both anions and cations in the regenerant can penetrate the fiber and enter the inner flow system. The permeation rate depends principally on the size, charge, and concentration of the co-ion and upon fiber characteristics (15, 19–21). A regenerant salt and concentration should be chosen that provides adequate exchange but minimal background from regenerant penetration.

Figure 2 shows the background replacement-ion concentration that results from 40.0 mM  $\text{KIO}_3$  (\*, curve A) and  $\text{KNO}_3$  (○, curve B) regenerant solutions over a range of eluent (distilled water) flow rates. The unusually high background level and its strong dependence on pump rate indicate that background is caused principally by the penetration of regenerant ions through the fiber wall. Under this condition, background replacement-ion concentration is inversely proportional to pump rate (21). Linear-regression analysis of the data provides a good fit to the function  $y = B/X + A$ , where  $X$  is the pump rate and  $y$  is the observed background. For  $\text{KIO}_3$ ,  $B = (3.59 \pm 0.04) \times 10^{-9}$  mol/s,  $A = (3.04 \pm 0.26) \times 10^{-6}$  M, the square of the correlation coefficient ( $r^2$ ) = 0.999, and the standard error of estimate (SEE) =  $4.04 \times 10^{-6}$ . For  $\text{KNO}_3$ ,  $B = (3.17 \pm 0.02) \times 10^{-9}$  mol/s,  $A = (2.75 \pm 0.14) \times 10^{-5}$  M,  $r^2$  = 1.00, and the SEE =  $1.82 \times 10^{-6}$ . The coefficients,  $B$ , are the empirically derived permeation rates of  $\text{KIO}_3$  and  $\text{KNO}_3$  through the fiber at a regenerant concentration of 40 mM.

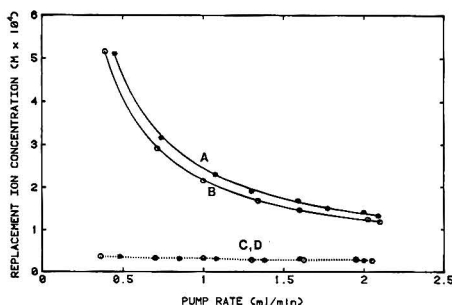


**Figure 2.** Variation of background replacement-ion concentration with pump rate using either  $\text{IO}_3^-$  (\*, curves A and C) or  $\text{NO}_3^-$  (O, curves B and D) as the replacement ion. Background levels obtained with a 40.0 mM regenerant solution (solid curves, A and B) and 4.0 mM regenerant solution (dotted curves, C and D) are shown. Eluent was distilled water.

The equations are displayed in Figure 2 as curves A and B, respectively.

Regenerant penetration is a relatively unimportant background source at high pump rates or lower regenerant concentrations. As shown in Figure 2 (dotted lines C and D), decreasing the regenerant concentration from 40.0 to 4.0 mM results in a dramatic drop in background concentration for both the  $\text{IO}_3^-$  and  $\text{NO}_3^-$  fibers. Moreover, the background concentration is then relatively insensitive to flow rate.

When the regenerant concentration is decreased further from 4.0 to 0.4 mM, background decreases by only another 15–20% over the flow rate range shown in Figure 2 and reaches an average value of about  $2.4 \times 10^{-6}$  M for both fibers. This background level persists even if the regenerant solution is replaced by distilled water, which suggests that a residual background component exists in the absence of significant regenerant penetration. This conclusion is supported also by the magnitude of the intercepts in the equations derived above for the 40.0 mM regenerant.

**Contaminant Sources.** This residual background component ( $\sim 2.0 \times 10^{-6}$  M) appears to be caused by a number of contaminant sources. Measurements by inductively coupled plasma emission spectrometry suggest that less than 10% of the background replacement-ion concentration could be caused by ionic impurities (mostly  $\text{Na}^+$ ,  $\text{Ca}^{2+}$ , and  $\text{Mg}^{2+}$ ) in our laboratory water. However, low levels of additional contaminant ions can be introduced by metallic chromatographic components that contact the flowing liquid. In addition, the pH of our laboratory water is typically between 5.5 and 6.0 because of dissolved  $\text{CO}_2$ . Dissolved  $\text{CO}_2$  introduces an additional ionic impurity,  $\text{HCO}_3^-$ .

To verify that the residual background absorbance is caused by the exchange of contaminant ions with the replacement ion and not by a light-absorbing contaminant (e.g., an organic absorber leaching from the fiber), a nonabsorbing replacement ion was employed. Chlorine ion was chosen because it absorbs negligibly at 215 or 210 nm compared to  $\text{NO}_3^-$  or  $\text{IO}_3^-$ . With the fiber in the  $\text{Cl}^-$  form, the relative background absorbance of the column effluent dropped to nearly zero, suggesting that the background signals measured previously with the  $\text{NO}_3^-$  or  $\text{IO}_3^-$  fiber were indeed caused by the exchange of contaminant ions with the corresponding replacement ion.

**Optimal Operating Conditions and Exchange Efficiency of the Fiber-Replacement Column.** The ion-exchange efficiency of a fiber column is affected by a number of parameters, including the influent ion concentration, regenerant concentration and flow rate, fiber length, and column-flow rate (21). The influence of these parameters on the

performance of the fiber-replacement column is discussed below.

**Effect of Regenerant Flow Rate and Concentration.** When the fiber column is employed as a suppressor column in conventional IC, it must continuously exchange millimolar concentrations of eluent ions. Accordingly, high regenerant flow rates and concentrations are often required. In contrast, the demands on the fiber are lower when it is used as a replacement column in RIC, because the fiber need exchange only solute ions, which elute discontinuously and experience considerable dilution during the separation. Consequently, regenerant flow rate and concentration have little effect on replacement-column performance and can be varied over a wide range. Flow rates in the range of 2.5–3.5 mL/min provide satisfactory performance.

The influence of regenerant strength on signal magnitude and reproducibility in RIC was investigated by injecting successive 20- $\mu\text{L}$  aliquots of 10.0 mM NaOH (a realistic upper-limit concentration encountered in IC) into the fiber-replacement column bathed with a 40.0, 4.0, and 0.4 mM  $\text{KIO}_3$  regenerant solution. NaOH was chosen because separated cations elute from the suppressor column and enter the fiber column as hydroxides in RIC (Figure 1). The peak heights and standard deviations obtained from these injections were compared with those produced by 10.0 mM  $\text{KIO}_3$  ( $\text{IO}_3^-$  does not require ion exchange). The eluent (distilled water) flow rate was 2.0 mL/min. The NaOH and  $\text{KIO}_3$  solutions produced an equivalent (0.5% relative standard deviation) peak-height response at all regenerant concentrations. These data suggest that the analyte response is independent of regenerant concentration and that the fiber quantitatively converts NaOH to  $\text{NaIO}_3$  within the accuracy of this measurement procedure.

On the basis of the foregoing discussion, the best signal-to-background ratios in RIC are obtained when the replacement column is bathed with regenerant solutions dilute enough to preclude ion penetration but sufficiently concentrated to prevent contaminant ions from concentrating on the fiber and competing with regenerant ions. A 4.0 mM regenerant concentration appears to be an acceptable compromise. With the UV-visible spectrophotometer, the base-line noise was similar when either a 4.0 or 40.0 mM regenerant concentration was employed, despite the much greater background produced by the latter. However, this insensitivity of base-line noise to background might not be observed for other detectors, particularly those more susceptible to multiplicative noise sources. In such cases, lower regenerant concentrations (e.g., 4.0 mM) would provide better signal-to-noise ratios (S/N). Alternatively, a regenerant co-ion less permeable to the fiber wall than potassium could be employed (15, 19).

**Fiber Length.** Long fibers are required to continuously exchange concentrated solutions because the mass transport of ions through the fiber wall limits the rate of ion exchange. In RIC, where the average influent ion concentration is low and noncontinuous, this process is unimportant because the ion-exchange sites of the fiber-replacement column are less likely to saturate and the inner wall acts like a perfect sink to ions requiring exchange. Under this condition, ion-exchange efficiency is limited by the transport of ions to the inner wall of the fiber and an exponential relationship exists between fiber length ( $L$ ) and the fraction of ions ( $f$ ) that are exchanged (21). For a linear, hollow fiber under laminar-flow conditions, the relationship is approximated by the Gormley-Kennedy equation (21)

$$1 - f = 0.8191e^{-3.857DL/F} + 0.0975e^{-22.3\pi DL/F} + 0.0325e^{-57\pi DL/F} \quad (1)$$

In eq 1,  $D$  is the diffusion coefficient of the ion being ex-

changed and  $F$  is the flow rate of the eluent.

Equation 1 can be used to predict the length of fiber required in the replacement column for the efficient exchange of solutes in cation analysis. Here, separated cations enter the replacement column as hydroxides (Figure 1), so the diffusion coefficient of  $\text{OH}^-$  ion,  $5.26 \times 10^{-9} \text{ m}^2/\text{s}$  at  $25^\circ\text{C}$  (22), is applicable. At 2.0 mL/min, 3.0- and 2.0-m fibers would be required for exchange efficiencies of 99.6% and 97.8%, respectively.

Actually, the length required for a particular exchange efficiency might be somewhat shorter than that predicted by eq 1 because of pump pulsations, turbulence caused by fiber-surface roughness, and other factors that enhance mass transport and increase exchange efficiency (21). Also, fibers are ordinarily coiled around a support rod and are sometimes packed with beads (23, 24) or filaments (21, 25-27). These modifications promote convective radial transport of ions to the walls and cause even greater departures from the simple theoretical model presented above for linear, hollow fiber devices.

In the current RIC system, a 2.3-m fiber was employed and provided adequate exchange efficiency for our application. Injections of NaOH into the  $\text{IO}_3^-$  fiber (previously discussed) had verified that  $\text{OH}^-$  is stoichiometrically replaced by  $\text{IO}_3^-$ . The quantitative replacement of  $\text{OH}^-$  by  $\text{NO}_3^-$  (with a 4.0 mM  $\text{KNO}_3$  regenerant) was also verified for a 0.4 mM NaOH solution that was pumped continuously through the fiber and detector cell at 2.0 mL/min; the absorbance of the column effluent was experimentally indistinguishable from that of 0.4 mM  $\text{KNO}_3$ . This result is consistent with eq 1; replacement efficiency depends upon the diffusion coefficient of the ion to be replaced ( $\text{OH}^-$ ) but not upon the identity of the replacement ion. However, one might expect that if the affinity of the fiber for the replacement ion were dramatically greater than its affinity for  $\text{OH}^-$ , the fiber would behave less like a perfect sink for  $\text{OH}^-$  ions. Consequently, ion-exchange efficiency would decrease and longer fibers would be required. In the extreme, ion-exchange efficiency would be minimal for a replacement ion that was irreversibly adsorbed onto the exchange sites.

**Detector Evaluation.** Peak-to-peak noise levels of  $1.5 \times 10^{-4}$  absorbance unit (AU) were measured at 215 nm with the detector cell filled with distilled water. The absolute detection limits ( $S/N = 3$ ) for  $\text{IO}_3^-$  and  $\text{NO}_3^-$  ion were calculated to be  $5.5 \times 10^{-7}$  and  $2.0 \times 10^{-7}$  M, respectively, based on the net absorbances produced above that of water by  $8.0 \times 10^{-5}$  M standard solutions of the ions. When detection at 210 nm was investigated, signal levels increased by a factor of 1.3 to 1.4, but noise levels increased proportionately. At 215 nm, the detector response became nonlinear at concentrations above  $2 \times 10^{-3}$  and  $8 \times 10^{-4}$  M for  $\text{IO}_3^-$  and  $\text{NO}_3^-$  ion, respectively, thereby defining the absolute upper limit of linearity. The linear dynamic range is therefore approximately  $10^4$  for both anions.

**Cation Determination by RIC.** *Working Curves and Dynamic Range.* The dynamic range was investigated for cations by injecting lithium concentrations between  $10^{-4}$  and  $10^{-1}$  M into the system shown in Figure 1. (Three injections were made at each concentration.) The portion of the peak-height calibration curve that provides the best linear fit extends from at least the lowest injected concentration,  $1.0 \times 10^{-4}$  M, to about  $5.0 \times 10^{-3}$  M. Linear regression analysis of the data points in this concentration range provides the equation  $y[\text{peak height}] = 77300C[\text{Li}^+ \text{ concentration (M)}] - 2.12$  ( $r^2 = 1.00$  and  $\text{SEE} = 1.01$ ). Peak heights at greater concentrations deviate negatively from those predicted by this equation because the column's sample capacity is exceeded. For example, the response at  $1.0 \times 10^{-2}$  M is low by 5-6%.

**Table I. Mean Peak-Height Response<sup>a</sup> Produced by Several  $\text{KNO}_3$  Solutions with and without the Fiber Column<sup>b</sup> Preceding the Detector Cell**

injected $\text{KNO}_3$ concn, mM	mean peak height, arbitrary units		signal recovery with fiber, <sup>c</sup> %
	without fiber	with fiber	
0.08	23.1	16.0	69.3
0.16	46.3	35.0	75.7
0.40	115	94.9	82.4
0.80	226	199	88.2

<sup>a</sup> Determined by six or more 20- $\mu\text{L}$  injections eluted with distilled water at 2.0 mL/min and detected at 215 nm. <sup>b</sup> Fiber bathed with a 4.0 mM  $\text{KNO}_3$  solution flowing at 3.4 mL/min. <sup>c</sup> Calculated as the ratio of the peak heights obtained with and without the fiber column (multiplied by 100).

The degree of deviation increases progressively at injected concentrations above  $10^{-2}$  M.

In contrast, the linear dynamic range extends well beyond  $1.0 \times 10^{-2}$  M when peak area is measured; up to  $10^{-2}$  M,  $y[\text{peak area}] = 1140C[\text{Li}^+ \text{ concentration (M)}] - 0.021$  ( $r^2 = 1.00$  and  $\text{SEE} = 0.0264$ ). At concentrations approaching 0.1 M, peak areas begin to deviate from this equation because the detector response no longer obeys Beer's law. However, the effect is usually minor because peak heights no longer increase proportionately at concentrations that exceed the column's sample capacity. For example, the area response at 0.1 M is low by only 1.7%.

Interestingly, both calibration equations presented above have small negative intercepts, a feature common to all RIC working curves generated in this study. We believe these negative intercepts occur because the relationship between RIC response and injected concentration is slightly nonlinear. On the basis of unweighted least-squares analysis of the accumulated data, the exponential function,  $y = AX^B$  (where  $B$  usually equals 1.02 or 1.03 and  $A$  is a constant), often provides a similar ( $R^2$  also equals 1.00) or slightly better fit (lower standard error of estimate) than a linear equation with a negative intercept.

The cause of this slightly nonlinear response is not certain but appears to be linked to the replacement column. The effect of the fiber column on signal recovery was evaluated by injecting  $\text{KNO}_3$  into the detector cell with or without the fiber column ( $\text{NO}_3^-$  form) inserted between the injector and detector. The results are shown in Table I. The peak heights obtained without the fiber (second column in Table I) are linear with respect to concentration. Least-squares analysis indicates that the data fit best a line passing through the origin or a line having a slightly positive intercept. In both cases  $r^2 = 1.00$ , but the latter provides a slightly lower standard error of estimate.

The peak heights obtained with the fiber in place (Table I, column 3) should be lower by a constant percentage than those measured without the fiber because of the fiber's void volume. Instead, the percent recovery of the signal (Table I, column 4) increased as the injected ion concentration increased. Least-squares analysis indicates that the best linear fit for the peak heights in column 3 of Table I produces a small negative intercept with  $r^2 = 1.00$ . Moreover, the function  $y = AX^B$  where  $B = 1.09$  provides a slightly better fit ( $r^2 = 1.00$  and lower standard error of estimate).

The reason for the observed influence of the fiber on analyte response is not clear. However, nonlinearity at low concentrations in IC is not a problem unique to RIC. Calibration curves in dual-column IC are also frequently nonlinear at the low-concentration end and do not typically intersect the conductance axis at the origin (7, 25). The nonlinear response has been attributed to interactions between the suppressor-



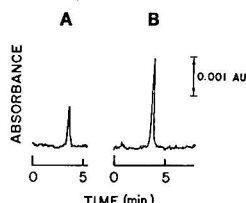


**Figure 3.** Chromatograms illustrating the signal-to-noise ratio for injections of 14 ng of  $\text{Li}^+$  with the fiber-replacement column conditioned in (A) the  $\text{IO}_3^-$  form and (B) the  $\text{NO}_3^-$  form, fiber bathed with 40.0 mM  $\text{KIO}_3$  and 40.0 mM  $\text{KNO}_3$ , respectively, flowing at 3.0 mL/min. Otherwise, both chromatograms were obtained under identical conditions. Conditions were as follows: columns, CS1 separator and CSC-2 suppressor; eluent, 7.0 mM  $\text{HNO}_3$ , pumped at 3.0 mL/min; sample,  $1.0 \times 10^{-4}$  M  $\text{Li}^+$ ; injection volume, 20  $\mu\text{L}$ ; detector wavelength, 215 nm.

column effluent and the eluted ion (7) or the inability of fiber suppressors to be 100% efficient (25). Even very efficient devices (>99.90% suppression) pass micromolar amounts of unsuppressed eluent ions that appear to interfere with the detection of sample ions at low injected concentrations (25).

**Reproducibility.** The relative standard deviation of peak-height measurements for lithium was 5% or better for injected concentrations  $\leq 2 \times 10^{-4}$  M and 1% or lower in the concentration range between  $5 \times 10^{-4}$  and  $10^{-3}$  M. The relative standard deviation of peak-area measurements for lithium varied between 0.3% and 0.4%.

**Detection Limits.** Five successive 20- $\mu\text{L}$  injections of  $1 \times 10^{-4}$  M (0.7 ppm)  $\text{Li}^+$  yielded a mean signal-to-background noise ratio of 40, with  $\text{IO}_3^-$  as the replacement ion. This injection, corresponding to an absolute mass of 14 ng of  $\text{Li}^+$ , produces an extrapolated detection limit ( $S/N = 3$ ) at a 99.9% confidence level (28) of 1.1 ng. The detection limits for  $\text{Na}^+$ ,  $\text{NH}_4^+$ , and  $\text{K}^+$  are 5.0, 6.0, and 15 ng, respectively.

The detection limits quoted above necessarily assume that the RIC working curve is linear at low analyte concentrations and passes through the origin. However, the data and discussion presented earlier revealed that the exponential function,  $y = AX^B$ , might be even more accurate, particularly at low analyte concentrations. Accordingly, the lithium detection limit was calculated also by converting the lithium peak heights to signal-to-noise ratios and extrapolating to  $S/N = 3$  using the best least-squares fit of the data to this function. This approach yields a detection limit for lithium of 1.2 ng, nearly the same as the value obtained by linear extrapolation (1.1 ng).

Sensitivity and detection limits should improve by employing a replacement ion of greater molar absorptivity. As illustrated in Figure 3, the signal-to-base-line noise ratio of a 14-ng  $\text{Li}^+$  injection increased by a factor of about 2.2 when  $\text{NO}_3^-$  was substituted for  $\text{IO}_3^-$  as the replacement ion under otherwise identical experimental conditions. The extrapolated detection limit for  $\text{Li}^+$  detected as  $\text{LiNO}_3$  is correspondingly lower (0.5 ng).

**Universal Calibration.** The universality of the method was evaluated for  $\text{Li}^+$ ,  $\text{Na}^+$ ,  $\text{NH}_4^+$ , and  $\text{K}^+$  by peak-area integration. Three to four injections were made of each ion at concentrations between  $8 \times 10^{-4}$  and  $8 \times 10^{-3}$  M. Each synthetic sample contained only two components, consisting of either  $\text{Li}^+$  and  $\text{NH}_4^+$  or  $\text{Na}^+$  and  $\text{K}^+$ , in order to eliminate the possibility of peak overlap or solute interaction and to simplify peak-area integration. The relative standard deviation of peak areas for the individual ions varied from less than 4% at lower concentrations to less than 2% at higher concentrations.

Table II summarizes the best least-squares linear fit of the data and verifies that the integrated detector response can be considered to be universal; the agreement among  $\text{Li}^+$ ,  $\text{Na}^+$ ,

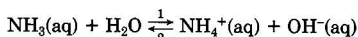
**Table II.** Least-Squares Linear Fit of Peak-Area Calibration Curves for Several Cations<sup>a</sup>

cation	least-squares slope	least-squares intercept ( $\times 10^3$ )	corr coeff	std error of estimate
$\text{Li}^+$	$1089 \pm 4$	$-4.87 \pm 1.62$	1.00	0.0230
$\text{Na}^+$	$1085 \pm 4$	$-4.03 \pm 1.65$	1.00	0.0234
$\text{NH}_4^+$	$1052 \pm 3$	$-2.61 \pm 1.27$	1.00	0.0181
$\text{K}^+$	$1078 \pm 6$	$-4.95 \pm 2.31$	1.00	0.0328

<sup>a</sup> Replacement ion,  $\text{IO}_3^-$ ; fiber-column regenerant, 40.0 mM  $\text{KIO}_3$ ; detection wavelength, 215 nm; eluent, 10.0 mM  $\text{HNO}_3$ ; flow rate, 2.2 mL/min; sample size, 20  $\mu\text{L}$ ; concentration range,  $8 \times 10^{-4}$  to  $8 \times 10^{-3}$  M.

and  $\text{K}^+$  is excellent. The slope of the  $\text{NH}_4^+$  working curve is slightly lower by about 2–3% than those of the other cations.

The slightly different response for  $\text{NH}_4^+$  is not at first surprising. In conventional dual-column IC, the working curve of  $\text{NH}_4^+$  is not linear but deviates negatively at high concentrations, which complicates the determination of this ion (6, 29). Nonlinearity occurs because the ion forms  $\text{NH}_3$  in the suppressor column, which is only partially ionized in the conductivity detector cell. For example, a 0.4 mM solution of  $\text{NH}_3$  in water is only 19% ionized, based on the base-dissociation constant,  $K_b$ , of  $\text{NH}_3$  at 25 °C (30). In contrast, the RIC working curve of  $\text{NH}_4^+$  (Table II) is linear. Moreover, the magnitude of the slope is much greater than would be predicted from the fractional ionization of  $\text{NH}_4\text{OH}$ . The enhanced ionization of  $\text{NH}_3$  can be explained by a dynamic equilibrium effect that occurs in the third (replacement) column (29). The pertinent equilibrium reaction is



As the  $\text{NH}_3$  passes through the replacement column and  $\text{OH}^-$  ion is exchanged (replaced) with  $\text{IO}_3^-$ , the above reaction is continually shifted toward the formation of  $\text{NH}_4^+$  from  $\text{NH}_3$  to replenish the depleted  $\text{OH}^-$  concentration.

The integrated response of  $\text{NH}_4^+$  did not appear to deviate more severely from those of the other cations at higher concentrations but varied consistently by 1.6–2.9%. The lower response might be caused by incomplete conversion of  $\text{NH}_3$  to  $\text{NH}_4\text{IO}_3$ . Alternatively, incomplete exclusion of the solute by the Donnan potential of the suppressor-column resin or of the fiber ionomer might be responsible. The partially neutral character of  $\text{NH}_4\text{OH}$  allows it to penetrate these materials more extensively than do the hydroxides of the other cations. Increased penetration could result in signal losses via several mechanisms including the adsorption of  $\text{NH}_3$  by the suppressor-column resin (5) or the diffusion of  $\text{NH}_3$  through the wall of the fiber.

Incomplete exclusion is known to be serious for  $\text{NH}_4^+$  ion when packed-bed suppressor columns are employed in conventional IC; retention times, peak heights, and, in some cases, peak areas are strongly influenced by the degree of exhaustion and by the type of the suppressor column (5, 29). Solute adsorption in the large packed-bed suppressor column used in the present RIC experiments might be primarily responsible for the lower integrated response of  $\text{NH}_4^+$ . The RIC response of  $\text{NH}_4^+$  would probably agree more closely to those of the other cations if the suppressor column were replaced with a fiber device.

Nevertheless, the results in Table II show that for many applications, only one calibration curve or standard is required in RIC. In addition, in applications where only the relative molar amounts of various cations are important, standard calibration is not even required. For example, parts A and B of Figure 4 each show a representative chromatogram of

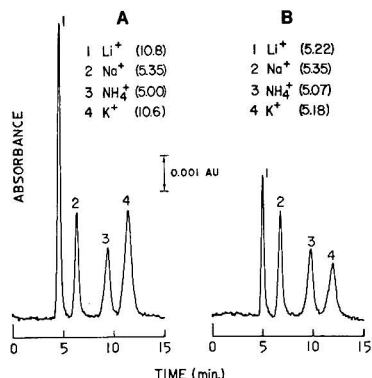


**Figure 4.** Chromatogram illustrating the response produced by a synthetic mixture containing (A)  $1.0 \times 10^{-3}$  M  $\text{Li}^+$ ,  $1.0 \times 10^{-3}$  M  $\text{K}^+$ ,  $5.0 \times 10^{-4}$  M  $\text{Na}^+$ , and  $5.0 \times 10^{-4}$  M  $\text{NH}_4^+$  and (B)  $5.0 \times 10^{-4}$  M of each cation. Integrated areas appear in parentheses. Columns utilized include a CS2 separator, CSC-2 suppressor, and fiber-replacement column. Fiber was bathed with 40.0 mM  $\text{KIO}_3$  at 3.2 mL/min. Conditions were as follows: eluent, 7.0 mM  $\text{HNO}_3$ , pumped at 2.2 mL/min; injection volume, 20  $\mu\text{L}$ ; detector wavelength, 215 nm.

a synthetic sample containing  $\text{Li}^+$ ,  $\text{Na}^+$ ,  $\text{NH}_4^+$ , and  $\text{K}^+$ . The mean peak-area response of each cation after six replicate injections appears in parentheses. The peak areas indicate that  $\text{Li}^+$  and  $\text{K}^+$  are present at twice the molar concentration ( $1.0 \times 10^{-3}$  M) of  $\text{Na}^+$  and  $\text{NH}_4^+$  ( $5.0 \times 10^{-4}$  M) in Figure 4A but that species are present at equal concentrations ( $5.0 \times 10^{-4}$  M) in Figure 4B.

These chromatograms demonstrate the ability of RIC to perform quantitative analysis without prior identification of sample ions. For example, in the chromatogram of Figure 4B, it is apparent that all the monovalent ions, regardless of identity, are present at a relative normal concentration of about 25% with respect to the total ion concentration of the sample. The relative normal concentration of an unknown ion could be determined in a similar fashion.

Two single-column IC methods possess this same capability. Wilson, Yeung, and Bobbitt have shown that solutes can be quantitated without prior identification with errors less than a few percent when either a conductivity or absorbance detector is employed (31, 32). This novel method, not applicable only to IC, requires measurement of the area response produced by the analyte when two different eluents are employed and requires solving several equations simultaneously. The procedure suffers from the disadvantage that two individual chromatograms are needed and that the analyte ion must produce a significantly different response when separated by the two eluents. Although the method is conceptually interesting, it could be difficult to implement in practice.

Indirect photometric chromatography also provides universal detection capability without identification. However, that technique possesses its own intrinsic disadvantages. Ion detection and separation are interrelated because both are accomplished via the eluent. Consequently, conditions that provide optimal sensitivity or chromatographic resolution might not be the same (9-11, 33). Furthermore, one must assume that only the eluent and not the analyte absorbs at the selected absorption wavelength. This information would not be available for an unknown ion.

In each of the universal calibration methods discussed above, the analyte's signal is proportional to charge. This is true also of RIC. For example, a divalent cation produces twice the signal of a monovalent cation because it coelutes with two replacement anions. The doubling of analyte signal

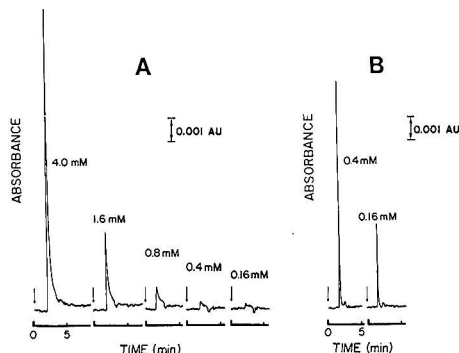


**Figure 5.** Representative chromatograms of  $\text{IO}_3^-$  at several injected concentrations by RIC (A) and dual-column IC (B). Columns utilized include ASS separator, ASC-2 suppressor, and fiber-replacement column (latter column used only for RIC injections). Fiber was bathed with 40.0 mM  $\text{KIO}_3$  at 2.8 mL/min. Conditions were as follows: eluent, 10.0 mM  $\text{NaOH}$ , pumped at 2.0 mL/min; injection volume, 20  $\mu\text{L}$ ; detector wavelength, 215 nm.

for doubly charged cations in RIC was verified here by injecting  $2.0 \times 10^{-4}$  M  $\text{KCl}$  and  $2.0 \times 10^{-4}$  M  $\text{BaCl}_2$  directly into the fiber-replacement column ( $\text{NO}_3^-$  form). As expected, the mean peak-height response for  $\text{BaCl}_2$  was twice that produced by  $\text{KCl}$  within 1.0%. Accordingly, the charge of an unidentified ion must be determined by varying the eluent concentration and measuring the ion's retention time (9, 32) before it can be quantitated.

**Anion Determinations.** The determination of anions was investigated by use of equipment analogous to that shown in Figure 1 but with the appropriate separator and suppressor columns. Unfortunately, unusually poor sensitivity, peak shape, and reproducibility were encountered for this RIC mode, in contrast to that obtained for the detection of cations. To further characterize the influence of the third column on the analyte signal, solutions of  $\text{KIO}_3$  between 0.16 and 4.0 mM were injected into the RIC instrument. Sample chromatograms appear in Figure 5A. Injections were made also in the absence of the replacement column under otherwise identical experimental conditions. Sample chromatograms resulting from the injection of 0.4 and 0.16 mM  $\text{KIO}_3$  appear in Figure 5B.

**Sensitivity.** When the dual-column system (no solute replacement) was employed, iodate ion was sensitively detected and peak heights were proportional to concentration (Figure 5B). However, the peak heights decreased dramatically when the replacement column was added (Figure 5A). Moreover, peak heights were not proportional to concentration. Instead, peak heights generally increased more than proportionately as concentration increased.

**Peak Shape.** The RIC peaks in Figure 5A are unusually asymmetrical and unlike those obtained without the replacement column in place (Figure 5B); the leading edge is sharp, and there is significant tailing before the peak returns to base line. This severe tailing obviously accounts at least partially for the abnormally low peak heights shown in Figure 5A. The peaks of  $\text{F}^-$ ,  $\text{Cl}^-$ , and  $\text{Br}^-$  were likewise poorly shaped when they were detected by RIC (with the replacement column in place). Peak asymmetry was most noticeable for  $\text{F}^-$  but less so for the later-eluting peaks ( $\text{Cl}^-$  and  $\text{Br}^-$ ). This severe peak tailing seriously degraded resolution when mixtures of these ions were injected.

**Reproducibility.** Peak-height reproducibility for anions was measurably worse by RIC than by dual-column IC. Relative

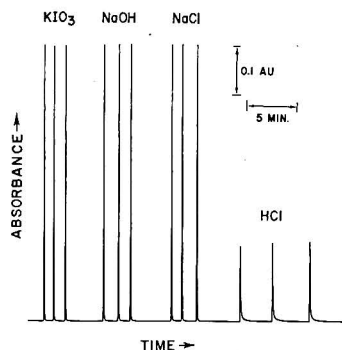


**Figure 6.** Response produced by  $\text{KIO}_3$ ,  $\text{NaOH}$ ,  $\text{NaCl}$ , and  $\text{HCl}$  (each 10.0 mM) injected directly into the fiber-replacement column ( $\text{IO}_3^-$  form). Fiber was bathed with 40.0 mM  $\text{KIO}_3$  at 3.0 mL/min. Conditions were as follows: eluent, distilled water, pumped at 2.0 mL/min; injection volume, 20  $\mu\text{L}$ ; detector wavelength, 210 nm.

standard deviations (RSDs) for two to three consecutive injections of  $\text{IO}_3^-$  at the higher concentrations shown in Figure 5A were about 2% with the tricolour system but about 0.5% with the dual-column system. The RSDs for 2.0 mM  $\text{F}^-$ , 2.0 mM  $\text{Cl}^-$ , and 2.0 mM  $\text{Br}^-$  injected as a synthetic mixture and detected by RIC were 5.6%, 0.3%, and 2.0%, respectively.

The long-term reproducibility of the tricolour system was particularly poor. For example, the mean peak-height response of a 1.6 mM  $\text{IO}_3^-$  injection increased by about 40% after the system was operated continuously for 1.5 h and after several anion species were injected at various concentrations. The width of the peak base decreased correspondingly. Day-to-day peak-height response varied considerably, sometimes by as much as 50%. The response changed dramatically also when different suppressor columns were employed. The reason for these variations is not yet clear.

**Universal Calibration.** Conceptually, a universal peak-area response should exist for all anions at the same concentration. However, a quantitative comparison was not pursued here because of the poor reproducibility and peak tailing that were encountered. The severe tailing made it difficult to accurately define peak base lines or to obtain adequate resolution for multicomponent samples. Consequently, even if a universal detector response exists for anions, it cannot be practically exploited in this anion-replacement RIC method.

**Interactions in the Replacement Column.** The low sensitivity, poor peak shape, and irreproducibility seem to arise because the separated anions enter the replacement column as their conjugate acids after passing through the anion suppressor column. The effect of the replacement column is illustrated in Figure 6, which compares the detector response produced by 0.01 M  $\text{KIO}_3$ ,  $\text{NaOH}$ ,  $\text{NaCl}$ , and  $\text{HCl}$  injected directly into the fiber-replacement column. Again, the fiber was in the  $\text{IO}_3^-$  form. An alkali hydroxide, in this case  $\text{NaOH}$ , represents the chemical form in which cations enter the replacement column during cation analysis. The strong acid,  $\text{HCl}$ , represents the chemical form in which anions enter the replacement column when anion analysis is performed. The neutral salt,  $\text{NaCl}$ , was introduced for comparison. The sodium salts of  $\text{OH}^-$  and  $\text{Cl}^-$  reproducibly generated a nearly identical response to that of  $\text{KIO}_3$ . In contrast,  $\text{HCl}$  yielded a far lower peak signal and also exhibited much greater tailing. In addition, the peak-height response was not as reproducible as those produced by the other solutions and usually increased slightly with each successive injection of  $\text{HCl}$ . Similar results were observed when  $\text{HNO}_3$  was injected into the fiber column (in its  $\text{NO}_3^-$  form).

We believe that acids (cf.  $\text{HCl}$  in Figure 6) are being partially absorbed by the fiber ionomer because they are incompletely excluded from the fiber pores. As discussed earlier, anions pass easily through the fiber pores and are ion-exchanged, whereas cations are comparatively excluded, especially those that are large and multicharged (19). Among cations, the proton should pass most easily through the fiber pores because of its small size and charge. Moreover, diffusion of protons through the fiber wall might be exacerbated because the fiber imbibes water. The diffusion of  $\text{HNO}_3$  through the fiber was compared to that of  $\text{KNO}_3$  by pumping distilled water through the fiber ( $\text{NO}_3^-$  form) and measuring the background  $\text{NO}_3^-$  concentration in column effluent. Both a 40.0 mM  $\text{HNO}_3$  and 40.0 mM  $\text{KNO}_3$  regenerant solution were tested. The background  $\text{NO}_3^-$  concentration produced by the 40.0 mM  $\text{HNO}_3$  regenerant solution was 4.6 times greater than that produced by the  $\text{KNO}_3$  solution at a flow rate of 2.0 mL/min. These data suggest that the diffusion rate of  $\text{H}^+$  (as  $\text{HNO}_3$ ) in the fiber material is 4.6 times greater than that of  $\text{K}^+$  (as  $\text{KNO}_3$ ).

Better success with anion determinations might be obtained if the fiber were fabricated from a different ionomer. Recently, Dasgupta (34) evaluated the performance of several types of anion-exchange membranes that permit the sensitive determination of anions by postsuppression ion exchange chromatography, identical in concept to the original RIC (12). Several detection modes were investigated by using anthranilate, a fluorescent and optically absorbing anion, as the replacement ion with no apparent problem from unusual peak tailing (34). Alternatively, anions can be detected by RIC utilizing a cation-replacement method (12, 34, 35).

**Limitations of RIC.** RIC possesses a number of inherent liabilities that cannot be eliminated. The addition of a third column clearly increases the complexity of IC instrumentation, although the use of a fiber-replacement column minimizes the disadvantage. Also, peak-area integration is necessary to exploit the universal calibration feature of RIC. Peak-area determinations require an integrator or computer and adequate chromatographic resolution. However, the third column also degrades chromatographic resolution and increases retention times. Fortunately, the fiber void volume is small, measured here to be only 218  $\mu\text{L}$ . Accordingly, peak retention times increase only 6–7 s at a flow rate of 2.0 mL/min.

The band broadening introduced into the IC system by the fiber column was studied by measuring peak widths at half height with and without the fiber inserted between the injector and detector. For simplicity, the peaks were assumed to be Gaussian in shape, and their base widths taken to be twice the width at half height, which corresponds to  $4.7\sigma$  ( $4.7\sigma$  includes 98% of the area of a Gaussian profile). The fiber's contribution to peak width,  $V_F$ , was then determined from eq 2 (36). In eq 2,  $V_{W0}$  is the width of the peak without the fiber and  $V_W$  is the width of the peak with the fiber. From this relation,  $V_F$  was calculated to be 75  $\mu\text{L}$  at 2.0 mL/min.

$$(V_W)^2 = (V_{W0})^2 + (V_F)^2 \quad (2)$$

The relative increase in peak width of an RIC system over that of a conventional dual-column system can be predicted from eq 2 rearranged into the following form (36):

$$\frac{V_W}{V_{W0}} = \left[ 1 + \left( \frac{V_F}{V_{W0}} \right)^2 \right]^{1/2} \quad (3)$$

In this case,  $V_{W0}$  is the peak width observed in dual-column IC.

It is evident from eq 3 that the relative increase in peak width will be worse for early-eluting peaks or peaks separated by very efficient columns (small  $V_{W0}$ ). Because peak widths

in IC are relatively large, there is relatively little influence of added void volume before the detector. For example, a peak eluting in dual-column IC with a base width of 0.5 mL and with  $V_F = 75 \mu\text{L}$  should broaden by only 1% when the fiber is added.

Importantly, the value of  $V_F$  stated above should be regarded as a conservative estimate of the band broadening introduced by the fiber, because only symmetrical band broadening has been considered; any tailing that might result from added dead volume has been ignored. Moreover, the determination of  $V_F$  has assumed that the eluting peaks are Gaussian. In fact, the peaks obtained by this flow-injection procedure were somewhat asymmetric. The long time constant, 1 s, of the spectrophotometric instrument might be partially responsible for the asymmetric peak profiles. A time constant of 0.3 s would have been more appropriate for these measurements, based on the standard deviation of the observed peaks (36).

### CONCLUSIONS

The detection method described is not only general but also universal and clearly applicable to the determination of alkali metals and  $\text{NH}_3$ . Detection limits (absolute mass) are similar to those reported earlier for dual-column IC with conductometric detection (7) but are more than an order of magnitude larger than those recently reported for cations detected by indirect photometric chromatography (11, 37). We are currently exploring alternative replacement-ion/detector arrangements that will potentially provide lower detection limits.

Although not demonstrated in the present paper, this RIC method should be applicable to the sensitive determination of alkylamines (29) with the potential advantage of providing linear working curves not offered by dual-column IC with conductometric detection. RIC should be useful also for the determination of alkaline-earth ions and  $\text{Ni}^{2+}$  (5). These cations were not chromatographically separated and detected by RIC in the present study because the recommended eluent contains millimolar amounts of *m*-phenylenediamine (*m*-PDA). *m*-PDA absorbs strongly at 210 and 215 nm, so the detector would not be able to sensitively discriminate between absorbing eluent and solute species. An alternative eluent or replacement-ion/detector scheme insensitive to *m*-PDA is required.

### ACKNOWLEDGMENT

We are grateful to Milos V. Novotny for the loan of the UV-visible spectrophotometer employed in this study and to Dionex Corp. for providing the chromatographic columns.

Registry No.  $\text{IO}_3^-$ , 15454-31-6;  $\text{NO}_3^-$ , 14797-55-8; Li, 7439-93-2; Na, 7440-23-5;  $\text{NH}_4^+$ , 14798-03-9; K, 7440-09-7.

### LITERATURE CITED

- (1) Small, H.; Stevens, T. S.; Bauman, W. C. *Anal. Chem.* **1975**, *47*, 1801-1809.
- (2) Gjerde, D. T.; Fritz, J. S.; Schmuckler, G. J. *Chromatogr.* **1979**, *186*, 509-519.
- (3) Gjerde, D. T.; Schmuckler, G.; Fritz, J. S. *J. Chromatogr.* **1980**, *187*, 35-45.
- (4) Fritz, J. S.; Gjerde, D. T.; Becker, R. M. *Anal. Chem.* **1980**, *52*, 1519-1522.
- (5) Pohl, C. A.; Johnson, E. L. *J. Chromatogr. Sci.* **1980**, *18*, 442-452.
- (6) Fritz, J. S.; Gjerde, D. T.; Pohlandt, C. *Ion Chromatography*; Dr. Alfred Hüthig Verlag: Heidelberg, West Germany, 1982.
- (7) Smith, F. C., Jr.; Chang, R. C. *The Practice of Ion Chromatography*; Wiley: New York, 1983.
- (8) Johnson, E. L. *Am. Lab. (Fairfield, Conn.)* **1982**, (Feb), 98-104.
- (9) Small, H.; Miller, T. E., Jr. *Anal. Chem.* **1982**, *54*, 462-469.
- (10) Naish, P. J. *Analyst (London)* **1984**, *109*, 809-812.
- (11) Sherman, J. H.; Danielson, N. D. *Anal. Chem.* **1987**, *59*, 490-493.
- (12) Downey, S. W.; Hietje, G. M. *Anal. Chim. Acta* **1983**, *153*, 1-13.
- (13) Buck, R. P.; Singhadeja, S.; Rogers, L. B. *Anal. Chem.* **1954**, *26*, 1240-1242.
- (14) Slingsby, R. W.; Rivello, J. M. *LC Mag.* **1983**, *1*(6), 354-356.
- (15) Dionex Product Document No. 032244.
- (16) Williams, R. J. *Anal. Chem.* **1983**, *55*, 851-854.
- (17) Reeve, R. N. *J. Chromatogr.* **1979**, *177*, 393-397.
- (18) Leuenberger, V.; Gauch, R.; Rieder, K.; Baumgartner, E. *J. Chromatogr.* **1980**, *202*, 461-468.
- (19) Dasgupta, P. K.; Bligh, R. Q.; Lee, J.; D'Agostino, V. *Anal. Chem.* **1985**, *57*, 253-257.
- (20) Hanaoka, Y.; Murayama, T.; Muramoto, S.; Matsuura, T.; Nanba, A. *J. Chromatogr.* **1982**, *239*, 537-548.
- (21) Dasgupta, P. K. *Anal. Chem.* **1984**, *56*, 96-103.
- (22) Atkins, P. W. *Physical Chemistry*; W. H. Freeman: San Francisco, CA, 1978; Chapter 25.
- (23) Stevens, T. S.; Jewett, G. L.; Bredeweg, R. A. *Anal. Chem.* **1982**, *54*, 1206-1208.
- (24) Stevens, T. S. *Ind. Res. Dev.* **1983**, (Sept), 96-99.
- (25) Dasgupta, P. K. *Anal. Chem.* **1984**, *56*, 103-105.
- (26) Dasgupta, P. K. *Anal. Chem.* **1984**, *56*, 769-772.
- (27) Dasgupta, P. K.; Bligh, R. Q.; Mercurio, M. A. *Anal. Chem.* **1985**, *57*, 484-489.
- (28) St. John, P. A.; McCarthy, W. J.; Winefordner, J. D. *Anal. Chem.* **1987**, *59*, 1495-1497.
- (29) Bouyoucos, S. A. *Anal. Chem.* **1977**, *49*, 401-403.
- (30) Brown, T. L.; LeMay, H. E., Jr. *Chemistry: The Central Science*; Prentice-Hall: Englewood Cliffs, NJ, 1977; p 467.
- (31) Wilson, S. A.; Yeung, E. S. *Anal. Chim. Acta* **1984**, *157*, 53-63.
- (32) Wilson, S. A.; Yeung, E. S.; Bobbitt, D. R. *Anal. Chem.* **1984**, *56*, 1457-1460.
- (33) Jenke, D. R. *Anal. Chem.* **1984**, *56*, 2468-2470.
- (34) Dasgupta, P. K.; Shintani, H. *Anal. Chem.* **1987**, *59*, 1963-1969.
- (35) Galante, L. G.; Hietje, G. M. *Anal. Chem.* **1987**, *59*, 2293-2302.
- (36) Snyder, L. R.; Kirkland, J. J. *Introduction to Modern Liquid Chromatography*, 2nd ed.; Wiley: New York, 1979; pp 31-33, 130.
- (37) Sherman, J. H.; Danielson, N. D. *Anal. Chem.* **1987**, *59*, 1483-1485.

RECEIVED for review June 23, 1987. Resubmitted December 22, 1987. Accepted December 22, 1987. Supported by the National Science Foundation through Grant CHE 83-20053, by the Office of Naval Research, by American Cyanamid, and by Monsanto.

# Computer Simulation of Differential Scanning Calorimetry: Influence of Thermal Resistance Factors and Simplex Optimization of Peak Resolution

Guang-Way Jang and Krishnan Rajeshwar\*

Department of Chemistry, The University of Texas at Arlington, Arlington, Texas 76019

Computer simulations of differential scanning calorimetry (DSC) are presented based on an electrical equivalent-circuit model. The influence of variables including heating rate, sample mass, and thermal resistance factors on the DSC peak shape, and associated peak parameters, was simulated. Melting was chosen as a test thermal transition for this purpose. The application of simplex optimization to the peak resolution problem in DSC is described for the first time. This methodology is illustrated for two test cases involving the melting of a two-component mixture.

Computer simulation offers a powerful route to testing the influence of parametric variables which are not easily amenable to experimental control by the analytical chemist. A case in point concerns thermal resistances in a differential scanning calorimetry (DSC) cell. The thermal resistances of the major heat-flow paths in a DSC cell are recognized to be crucial to the performance of this analytical technique (1); however, a systematic evaluation of their influence on DSC peak shapes presents many experimental problems. In a previous paper, an equivalent-circuit model was presented for a DSC cell of the heat-flux type (2). This model was subsequently utilized to guide the development of a DSC peak resolution-enhancement methodology based on the use of He as a purge gas (3). This paper details further refinement of this model, and its application to computer simulations of a DSC scan. In particular, the model and simulations were used to probe the influence of thermal resistances on peak area, amplitude, onset temperature, and resolution.

A second objective of this study was to explore the applicability of the simplex optimization technique (4) to DSC. The simplex technique is applied, we believe, for the first time, to the optimization problem involving the resolution of overlapping DSC peaks. Overlapping DSC peaks are usually resolved by decreasing either the sample mass, the heating rate, or both. Obviously, selection of an optimal combination of these two operational parameters will be critical to maintaining an acceptable level of analytical sensitivity and analysis time (and costs).

## MODEL AND SIMULATION PROTOCOL

The manner in which thermal resistances manifest themselves in the morphology of a DSC thermogram perhaps is best treated in terms of electrical equivalent circuits (2, 5-9). Figure 1 illustrates the equivalent circuit that was used by us earlier (2) for a DSC cell of the heat-flux type. In Figure 1,  $T_S$  is the sample temperature,  $T_R$  is the reference temperature,  $T_P$  is the heater (source) temperature,  $T_{SH}$  is the sample platform temperature,  $T_{RH}$  is the reference platform temperature,  $R_D$  is the thermal resistance between heater and sample (or reference) platforms,  $R_S$  is the thermal resistance between temperature sensor and sample,  $R_R$  is the thermal resistance between temperature sensor and reference,  $R_D'$  is

the thermal resistance of the disk between sample and reference platforms,  $R_G$  is the gas thermal resistance between heater and sample (or reference), and  $R_G'$  is the gas thermal resistance between sample and reference. The heat flow rates in the sample and reference channels are given by  $dq_S/dt$  and  $dq_R/dt$ , respectively. Implicit in the circuit representation in Figure 1 is the reasonable assumption that the cell design is such that the sample and reference channels are precisely matched in terms of their resistances to heat flow (i.e.,  $R_D$  and  $R_G$  are the same in both channels).

In the computer simulations to be discussed below, each of the component resistances in Figure 1 was varied systematically, and corresponding DSC "scans" were synthesized, via the use of our model and appropriate software. In this manner, the relative importance of the various resistances could be readily assessed. In this respect, the experimental bottleneck is that none of the resistances in Figure 1 can be varied individually without perturbing the rest of the system! For example, substitution of Ar (or  $N_2$ ) by a more conductive purge gas, such as He, influences not only  $R_G$  but also  $R_G'$ ,  $R_S$ , and  $R_R$ .

Melting of a metal (e.g. In) was initially chosen as a test thermal transition for the DSC simulations. As shown in Figure 2, such a transition can be decomposed into three successive stages. Previous authors (6, 10, 11) have treated appropriate mathematical models to describe the pretransition, transition ( $0 < t < t_{max}$ ), and posttransition ( $t > t_{max}$ ) regimes of the thermogram. These models yield eq 1-3 for the net heat flow,  $dq/dt$ , in the three regimes respectively.

$$\frac{dq}{dt} = (C_S - C_R) \frac{dT_P}{dt} \quad (1)$$

$$\frac{dq}{dt} = (C_S - C_R) \frac{dT_P}{dt} + S \frac{dT_{SH}}{dt} t \quad (2)$$

$$\frac{dq}{dt} = (C_S - C_R) \frac{dT_P}{dt} + H \exp\left(-\frac{t - t_{max}}{R_T C_S}\right) \quad (3)$$

$C_S$  and  $C_R$  are the mass-specific heats of the sample and reference, respectively (including the Al pan material, cf. ref 12),  $dT_P/dt$  is the (programmed) heating rate,  $dT_{SH}/dt$  is the heating rate of the sample holder,  $S$  is the slope of the leading edge of the melting endotherm,  $H$  is the DSC peak amplitude, and  $R_T = R_D + R_S$ . The derivation of eq 1-3 in the previous models are based on the assumptions that (a) the specific heats, thermal resistances, and the heating rate are temperature independent, (b) the instrumental time constant (cf. ref 13) is zero, and (c) heat losses from convection or radiation are negligible.

Table I contains the thermogram parameters that are required to carry out the DSC simulation. The parameters that are available in the earlier models are also identified in this compilation. There are at least three difficulties in the exclusive use of these models for a computer simulation. First, the thermogram equations (eq 1-3) were all expressed in terms

Table I. Required Parameters for Computer Simulation of DSC and Parameters Available in Earlier Models

model	before transition	during transition	after transition
parameter	$dT_{SH}/dt$	$S$	$dT_{SH}/dt$
ref 8	$dT_P/dt$	$g/(D + R_D r)/(R_D/R_T) + (1/KR_D) + (1/KR_G)$	$dT_{SH}/dt$
ref 10	$dT_P/dt$	$1/R_T$	$dT_P/dt$
ref 2 and present study	$dT_P/dt$	$(1/R_S) - (1/R_D) + (1/KR_D) + (1/KR_G)$	$dT_P/dt$

<sup>a</sup>  $D = 1 + R_S/R_D + 2R_S/R_D'$ ;  $r = 1/[1/R_G + 1/(R_D + R_S)]$ , cf. ref 8. <sup>b</sup> NA = not available. <sup>c</sup>  $R_T = R_S + R_D$ . <sup>d</sup>  $T_m$  = melting temperature of the sample.

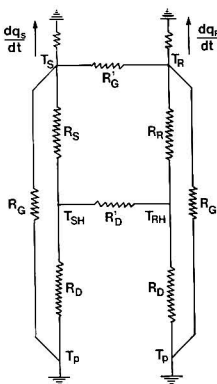


Figure 1. Equivalent circuit of a heat-flux DSC system. Refer to the text for definition of symbols.

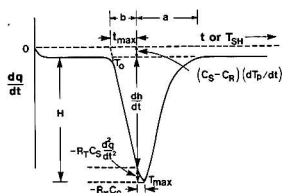


Figure 2. Characteristic parameters of a hypothetical DSC thermogram.

of heat flow vs time rather than heat flow vs temperature. The lack of availability of the parameter,  $dT_{SH}/dt$  for  $t > 0$  (Table I) introduces difficulties into the time  $\rightarrow$  temperature translation of the thermogram profiles. Second, heat leakage through the purge gas and the disk material (the importance of which has been established in other studies; cf. ref 2 and 8) was neglected in the Gray model (10). Finally, computation of the endotherm slope,  $S$ , requires the troublesome need for the knowledge of a "g" parameter in the Claudy treatment (8); i.e.  $dq/dt = g(T_{RH} - T_{SH})$ . Because of the above difficulties, we have chosen to use largely our earlier model (2) to generate the required simulation parameters.

Derivations of appropriate expressions for  $t_{max}$  and  $dT_{SH}/dt$  for  $t > t_{max}$  are contained in Appendix A. The derived expression for  $t_{max}$  (eq A8) is similar in form to the Gray equation (Table I) with the important difference that the heat leakage effect is explicitly taken into account in our expression. The posttransition DSC curve shape is described by eq A13. The important points to be noted in this equation are the following: (a) the heat flow rate decreases exponentially with increasing time,  $t$ ; (b) this rate increases with decreasing magnitude of

Table II. Summary of Input Data, Variables, and Output Format Along with Relevant Units in Parentheses in the Computer Simulations

input data	variable	output
sample mol wt (g/mol)	sample mass (mg)	$dq/dt$ (mW)
heat capacity (cal/(deg·mol))	heating rate ( $^{\circ}\text{C}/\text{min}$ )	$T_{SH}$ ( $^{\circ}\text{C}$ )
enthalpy (J/g)	$R^a$ ( $^{\circ}\text{C}/\text{mW}$ )	time, (min)
melting point ( $^{\circ}\text{C}$ )		

<sup>a</sup>  $R$  = thermal resistance factor; cf. Figure 1 and text.

the  $R_S/R_T$  ratio; and (c) the endotherm tailing is affected by how fast  $T_{SH}$  catches up with  $T_P$  after the transition. This, in turn, is controlled by the magnitude of  $R_D$  (vide infra). Note that the Gray treatment assumes instantaneous approach of the sample platform to the programmed temperature ramp,  $dT_P/dt$  (Table I).

The sample platform heating rate,  $dT_{SH}/dt$ , during the transition ( $0 < t < t_{max}$ ) is available from our model (2) as

$$\frac{dT_{SH}}{dt} = K \frac{dT_P}{dt} \quad (4)$$

$K$  is a phenomenological lag parameter which contains key contributions from  $R_S$ ,  $R_D$ , and  $R_D'$

$$K = \left( \frac{R_S}{R_D} + \frac{R_S}{R_D'} \right) / \left( 1 + \frac{R_S}{R_D} + \frac{R_S}{R_D'} \right) \quad (5)$$

Expressions for the endotherm slope,  $S$ , as well as the endotherm amplitude,  $H$ , are also available from our model (2) as follows:

$$S = \frac{1}{R_S} - \frac{1}{R_D'} + \frac{1}{KR_D'} + \frac{1}{KR_G} + \frac{2}{KR_G'} \quad (6)$$

$$H = \frac{T_{max} - T_m}{R_S} \quad (7)$$

$T_m$  is the sample melting point.

Computer simulations thus were facilitated by use of the parameters contained in the third row of Table I. These simulations were performed in segments, viz., pretransition, transition ( $0 < t < t_{max}$  or, equivalently,  $T_0 < T < T_{max}$ ) and posttransition ( $t > t_{max}$  or  $T > T_{max}$ ). The boundaries for these three segments were defined by the endotherm onset temperature (time),  $T_0$  ( $t = 0$ ), and the temperature (time) corresponding to the endotherm peak,  $T_{max}$  ( $t = t_{max}$ ). Figure 3 is a flow chart of the simulation procedure. Table II summarizes the requisite input data, the parametric variables, and the output format along with a compilation of the relevant units and unit conversions. Multiple DSC transitions were individually simulated prior to summation to yield the composite DSC thermogram. A computer program for these



Table III. Simulated Influence of Seven Variables on Selected DSC Peak Parameters for a Melting Transition

	$dT_p/dt$ 10 °C/min <sup>b</sup>			$m^a$ 10 mg <sup>b</sup>		$R_s$ 0.10 °C/mW <sup>b</sup>		$R_D$ 0.11 <sup>b</sup>	$R_D'$ 0.21 <sup>b</sup>	$R_G$ 100 <sup>b</sup>	$R_G'$ 100 <sup>b</sup>
	10	30	50	3	5	0.5	0.01	0.33	100	1	1
$K$	0.58	0.58	0.58	0.58	0.58	0.87	0.12	0.44	0.48	0.58	0.58
$S$	13.49	13.49	13.49	13.49	13.49	2.72	134.62	16.18	10.07	15.19	16.90
$H$	26.34	40.10	47.48	12.75	17.52	12.58	40.26	26.70	17.49	27.81	30.93
$H/W$	1.54	1.13	1.08	1.08	1.24	0.40	3.31	0.74	1.18	1.54	1.57
$I$	3.68	5.63	5.68	5.43	4.98	2.69	22.25	11.04	3.71	4.31	5.00
$T_0$	157.28	157.64	157.82	156.93	157.05	158.27	156.70	157.62	156.61	157.55	157.86
$T_{max}$	159.23	160.61	161.35	157.88	158.35	162.89	157.00	159.27	158.35	159.38	159.69
$t_{max}$	0.34	0.17	0.12	0.16	0.22	0.53	0.25	0.38	0.36	0.32	0.32

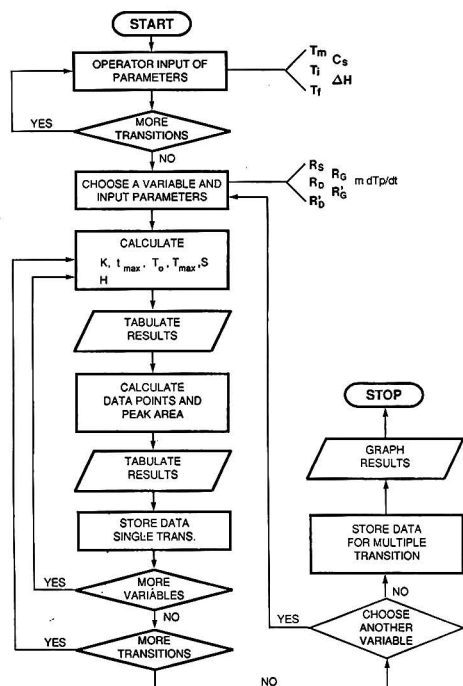
<sup>a</sup> Sample mass. <sup>b</sup> Standard value.

Figure 3. Flow chart for computer simulation of a DSC thermogram.

simulations was written in BASIC; copies of the program are available from the authors upon request. Computer graphics utilized the GRAPHER (Golden Software Inc.) subroutine. All simulations were performed on an IBM PC/XT.

## RESULTS AND DISCUSSION

**Simulation of Thermal Resistance Effects on DSC Peak Shape.** It is established that an increase of either the heating rate or the sample mass brings about a corresponding increase in the DSC peak temperature, peak amplitude, and peak area (14). The sample simulations in Figure 4 faithfully reproduce this trend for three arbitrarily chosen values of the two variables. With the establishment of the efficacy of our simulation procedure, the influence of thermal resistances on the DSC endotherm morphology and associated peak parameters was next probed. Figure 5 contains representative simulated thermograms wherein  $R_s$ ,  $R_D$ ,  $R_D'$ ,  $R_G$ , and  $R_G'$  were sequentially perturbed while maintaining the other resistances and parameters (Table II) constant. Of all the component

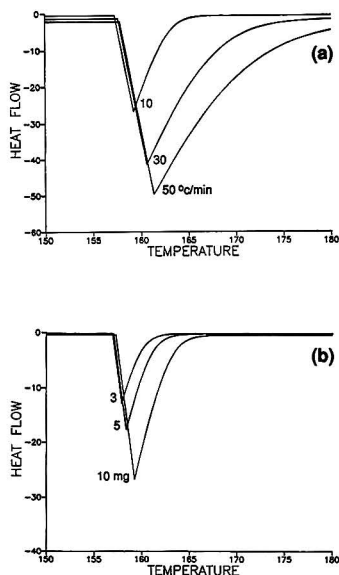
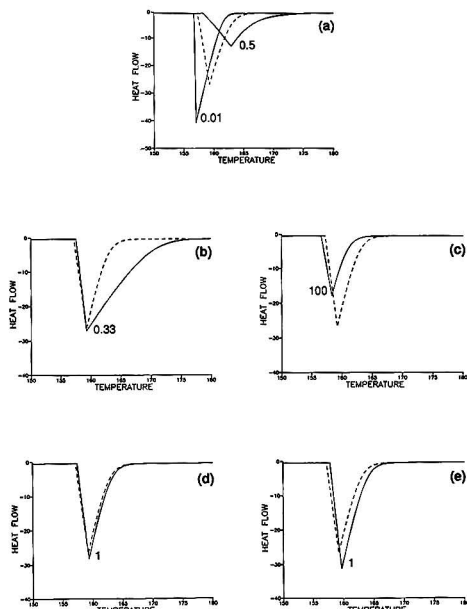


Figure 4. Simulated DSC thermograms showing the influence of variable heating rate (a) and sample mass (b). Heating rates are in degrees Celsius per minute, and the sample mass is expressed in milligrams (cf. Table III).

resistances in Figure 1,  $R_s$  clearly has the most influence on the endotherm morphology.

More detailed analyses are afforded by the simulation results contained in Table III. The input variable was perturbed around a "standard" value which is shown in the second row of Table III. These perturbations are identified in row 3 of Table III. Since, unlike the heating rate and the sample mass, test values for the thermal resistances are not a priori known, recourse to them was made via the combination of eq 5-7. DSC thermograms are usually acquired in a thermally resistive inert gas such as Ar or N<sub>2</sub>. If the initial and reasonable assumption is then made that  $R_G = R_G' = \infty$ , we have three unknowns, namely,  $R_s$ ,  $R_D$ , and  $R_D'$ , and three equations, eq 5-7. Standard values for  $R_s$ ,  $R_D$ , and  $R_D'$  (Table III, second row) were thus generated from the use of these equations, coupled with experimental knowledge of  $S$ ,  $H$ ,  $K$ , and  $T_{max}$ . A standard value of 100 was arbitrarily assigned to  $R_G$  and  $R_G'$ . The second column in Table III shows the DSC output parameters calculated by the computer simulation program for these standard input variables. These provide a reference framework within which the influence of parametric pertur-



**Figure 5.** Simulated DSC thermograms illustrating the influence of variable thermal resistance factors: (a)  $R_S$ , (b)  $R_D$ , (c)  $R_G$ , (d)  $R_{D'}$ , (e)  $R_{G'}$ . The value of each variable is shown in degrees Celsius per milliwatt (cf. Table III). The dashed curves in each case correspond to the "standard"  $R$  value listed in the second row of Table III.

bations (Table III, third row) may be assessed.

The analytical sensitivity in a heat-flow DSC system depends on the temperature difference that develops between the sample and reference platforms

$$T_{RH} - T_{SH} = t \left( \frac{dT_{RH}}{dt} - \frac{dT_{SH}}{dt} \right) = t \frac{dT_P}{dt} (1 - K) \quad (8)$$

Equation 8 clearly shows that the lower the lag factor,  $K$ , the higher is the measurement sensitivity. The simulation results in Table III illustrate the influence of  $R_S$  on  $K$ ;  $K$  decreases from the reference level of 0.58 to 0.12 when  $R_S$  is decreased by an order of magnitude. Concomitantly, the endotherm amplitude,  $H$ , increases. The other factor governing analytical sensitivity is the endotherm slope,  $S$ . A reduction in  $R_S$  leads to a hefty increase in  $S$ , and thus in the measurement sensitivity. Note that neither the heating rate nor the sample mass influences  $S$  (10). This is also apparent from an examination of Figure 4. An increase of  $R_S$  from the "standard" level of 0.10 °C/mW brings about the opposite trends in  $K$  and  $S$ ; i.e., the analytical sensitivity is impaired. These simulations clearly underscore the overriding influence of the thermal resistance factor,  $R_S$ , on the performance of a heat-flux system. The simulated thermograms in Figure 5a illustrate this fact.

A less dramatic influence is exerted by the heater-sample thermal resistance,  $R_D$ , as the simulation results in Figure 5b and Table III illustrate. By the same token, however, this parameter exerts a significant influence on the DSC peak resolution (vide infra). An increase in  $R_{D'}$  also brings about a deterioration in the analytical sensitivity of the DSC system (Figure 5c and Table III). An order-of-magnitude decrease in  $R_G$  and  $R_{G'}$  has a positive effect on the sensitivity as Figure 5d and Table III illustrate.

**Table IV.** Simulated Influence of Thermal Resistance Factors on the DSC Cell Calibration Constant

	$R_S$			$R_D$		$R_{D'}$	
	0.5 <sup>a</sup>	0.1 <sup>a</sup>	0.01 <sup>a</sup>	0.11 <sup>a</sup>	0.33 <sup>a</sup>	0.21 <sup>a</sup>	1.00 <sup>a</sup>
$A_{std}/A^b$	1.22	1.00	0.87	1.00	0.45	1.00	1.82

<sup>a</sup> Expressed in units of °C/mW. <sup>b</sup> Peak area ratio.  $A_{std}$  is the endotherm area corresponding to the "standard" values for  $R_S$ ,  $R_D$ , and  $R_{D'}$  in Table III of 0.1, 0.11, and 0.21 °C/mW, respectively.  $A$  is the peak area corresponding to the variable value.

The peak amplitude/width ratio,  $H/W$ , is a useful figure-of-merit for the performance of the DSC system. This parameter is tabulated in Table III as a function of the seven variables. A reduction of  $R_G$  and  $R_{G'}$  enhances this ratio, whereas an increase of  $R_D$ ,  $R_{D'}$ , or  $R_S$  causes a diminution of it. It should be noted that an increase of  $W$  can be caused not only by a reduction in the slope but also by an enhanced tailing of the decay portion of the peak. Because of its rather weak influence on the slope and peak amplitude, Table III,  $R_D$  exerts its influence mainly via its effect on the decay portion. The two effects can be deconvoluted by means of the shape index,  $I$ , as defined by previous authors (14). This index is defined as

$$I = a/b \quad (9)$$

The terms  $a$  and  $b$  in eq 9 have been defined in Figure 2 (14). As shown in Table III, a reduction in  $I$  is effected by a decrease in the heating rate,  $R_D$  or  $R_{D'}$ . On the other hand,  $I$  is increased by a diminution in the sample mass,  $R_S$ ,  $R_G$ , or  $R_{G'}$ . The slope, however, is much more sensitive to a perturbation in  $R_S$  than the endotherm tailing portion.

**Application of the Simulation Procedure to Experimental DSC Thermograms.** While the two parameters, namely the heating rate and sample mass, are amenable to control by the experimenter, the thermal resistance factors are usually intrinsic to the DSC cell. Yet, rather large variations in these parameters are indirectly introduced, for example, when the inert gas is switched from Ar (or  $N_2$ ) to He, when samples that are much less conductive than metals are employed, or on prolonged use of the instrument over a time period in which the thermal characteristics of the sample platform gradually change. Under these circumstances, it is useful to be able to match the observed experimental DSC thermogram with a simulated counterpart generated by the procedure outlined in the preceding section. Fitting of the two sets of DSC curves is accomplished by using the five resistance factors as variables. Rounding of the experimental DSC thermograms induced by a finite time constant (13) has not been explicitly considered herein; this additional capability is easily incorporated within the framework of our simulation protocol.

A second realm of application of computer simulations in DSC involves assessment of measurement errors. Variations in the disk thermal resistance factors ( $R_D$ ,  $R_{D'}$ ) or in  $R_S$  can induce significant error in the cell calibration constant, as illustrated by a set of representative simulations in Table IV. The cell calibration constant connects the measured endotherm area with the transition enthalpy. How this constant is affected by perturbations in the thermal resistance factors is expressed in terms of a peak area ratio in Table IV. The peak area ratio is seen to increase with a corresponding increase of  $R_S$ . Interestingly enough, these simulations also reveal that when a thermally conductive metal (e.g., In) is used as a calibration standard in the enthalpy determination of a transition involving a poorly conductive material (e.g., an organic compound), there will be a negative error in the estimated enthalpy value. An increase of  $R_D$  and  $R_{D'}$  is seen

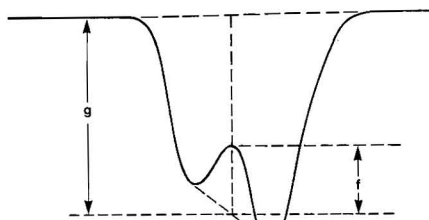


**Figure 6.** Definition of the peak separation parameter,  $P$  (cf. ref 16 and eq 10 in the text).

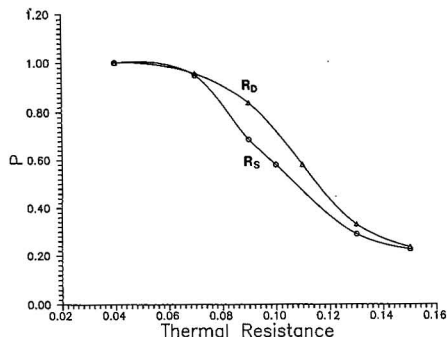


**Figure 7.** Simulated dependence of the peak separation parameter,  $P$  (cf. ref 16) on  $R_D$  and  $R_S$ . A mixture of adipic acid (3 mg) and In (5 mg) was chosen as the test system. The melting transitions occur at 152.0 °C and 156.6 °C and have associated enthalpies of 253 and 28.4 J/g, respectively.

to bring about opposite effects on the calibration constant, Table IV. The influence of heating rate and sample mass on the cell calibration constant has been addressed via experiments in a recent study (15).

### Peak Resolution and Simplex Optimization in DSC.

The peak separation parameter introduced by previous authors for chromatographic applications (16) is useful for assessing the influence of thermal resistance factors in the DSC case. This parameter,  $P$ , is defined in eq 10

$$P = f/g \quad (10)$$

The terms  $f$  and  $g$  are further defined in Figure 6. The key factor in DSC peak resolution is the degree of endotherm tailing. Equation A13 in the Appendix reveals that the lower the  $R_S/R_T$  ratio, the smaller is the endotherm tailing, and consequently the better is the peak resolution. This point is further illustrated in Figure 7, which shows the simulated dependence of  $P$  on  $R_S$  and  $R_D$ . The extent of peak resolution is seen to be more sensitive to  $R_D$  than to  $R_S$ . This is explained by the fact that  $R_D$  serves as the heat flow path for thermal equilibration of  $T_{CH}$  with  $T_D$  after the transition event.

The computer simulation protocol may be coupled with simplex optimization methodology to arrive at an optimal combination of experimental parameters for a DSC scan involving multiple, closely spaced thermal transitions. This latter situation could arise from either a single sample undergoing sequential thermal transitions or a mixture of two components each having a single transition. Two test cases are considered herein: (a) a large peak followed by a small endotherm (cf. Figure 8a) and (b) an initial weak endotherm followed by a large peak (cf. Figure 8b).

The experimental variables which control DSC peak resolution are inert gas composition, sample mass, and heating

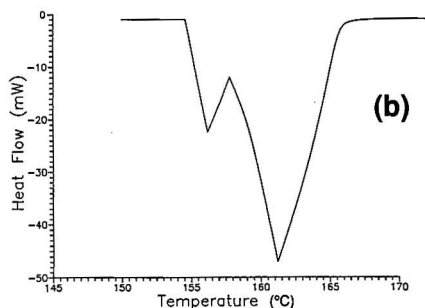
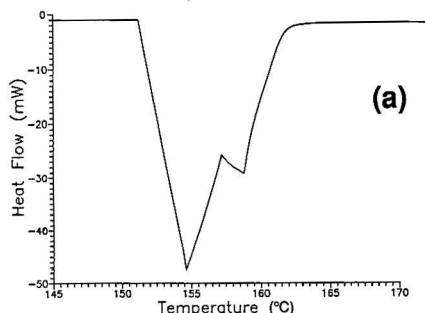


**Figure 8.** Simulated DSC thermograms of a two-component mixture. The transition temperatures were assumed to be 154.0 and 156.6 °C, respectively. The thermograms in parts a and b pertain to case a and case b in the text.

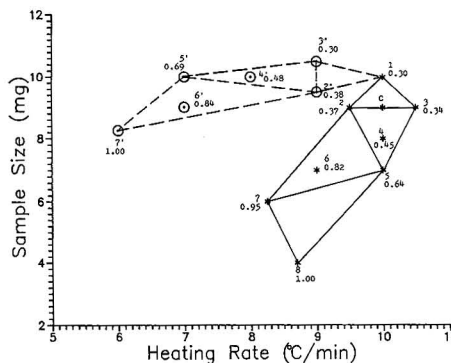


**Figure 9.** A representative simplex scheme for determining an optimal combination of sample mass and heating rate which brings about base-line DSC peak resolution ( $P = 1$ ). Two different initial simplexes are shown. Refer to the text for vertex notation and other details. This scheme pertains to case a in the text.

rate. The inert gas composition controls indirectly the magnitude of the thermal resistance factors (3). Suppose that an appropriate inert gas is selected first. This leaves sample mass and heating rate as the two remaining variables, and thus 2 + 1 initial simplex vertices will be needed (4). The initial values of sample mass and heating rate which yield overlapping DSC peaks may be chosen as one of these vertices. The other two vertices can be generated by perturbing each or both

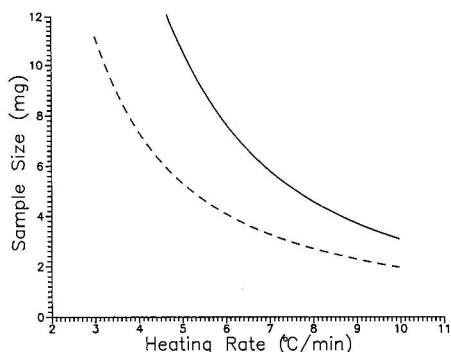


**Figure 10.** Contour plots connecting points such as 8 and 7' in Figure 9. The solid line refers to case a (cf. text), and the dashed line pertains to case b. The latter was obtained from simplex searches such as those illustrated in Figure 9. All combinations of sample mass and heating rate which lie below each of the two plots yield complete resolution of the two DSC peaks.

of these parameters by a certain amount.

The simplex algorithm for case a above is illustrated in Figure 9. Two different initial simplexes are shown; the objective function in this exercise is the peak resolution parameter,  $P$ , which was defined earlier. The vertex numbers in Figure 9 indicate the sequence of evolution of the search. The corresponding  $P$  values generated in each case are also shown. For example, vertex 2 was generated by -10% and -5% perturbations in the sample mass and heating rate, respectively, from the initial vertex 1. Similarly, vertex 3 was generated by decreasing the initial sample mass by 10% and increasing the heating rate by 5%. The corresponding  $P$  values for vertices 1, 2, and 3 are 0.30, 0.37, and 0.34, respectively. Since vertex 1 obviously yields the worst response within the initial simplex, vertex 4 was generated by rejecting vertex 1 and reflecting through the center,  $C$ , of the plane bisecting vertices 2 and 3. Vertex 4 yields a response,  $P = 0.45$ . This response being better than the previous best value of 0.37 justifies simplex expansion. Vertices 2, 3, and 5 constitute the new simplex and the search is continued. Finally, the search is terminated at vertex 8 with the objective function attaining the optimum value of 1. An alternative route involving the initial simplex 1, 2', 3', leads to 7'.

Optimization of  $P$  can be done with the further constraint that the DSC analysis must be completed within a preset time (heating rate) and level of sample utilization. Any vertex that attempts to go beyond these limits is then treated as a boundary violation. Analysis time and sensitivity, therefore, will fall within an acceptable range. Contraction of the termination step may be a viable approach in selected instances.

If an entire family of simplex searches with different starting simplexes is generated and vertices such as 8 and 7' in Figure 9 are connected, plots such as those in Figure 10 are obtained. The solid line in Figure 10 refers to case a and the dashed line pertains to case b. All combinations of the two parameters which fall below these two plots will yield completely resolved ( $P = 1$ ) DSC peaks. Of the two variables, however, a reduction in heating rate is generally favored over a reduction in sample mass. This is because the peak tailing (which controls resolution, vide supra) is more sensitive to heating rate than to sample mass. (This is seen from an examination of the shape index in Table III as a function of the two variables.)

Figure 10 also illustrates how the relative size of the two peaks influences the sensitivity of  $P$  to heating rate and sample mass. The influence of heating rate on the extent of peak separation becomes milder when the first endotherm reduces

in size. A wide latitude in the heating rates that can be tolerated is thus offered by case a relative to case b. In practical terms, this favorable situation may be induced in the analysis of mixtures, since the relative amounts of the two components are often amenable to control by the experimenter.

In summary, this study has attempted to explore several realms of applicability of computer simulations to DSC methodology. Further refinements of the simulation protocol as well as extension to other thermal analysis techniques such as thermogravimetry are currently under investigation in this laboratory.

## GLOSSARY

$A$	area of the DSC endotherm for a given value of the variable thermal resistance factor
$C_R$	mass specific heat of the reference including the pan material
$C_S$	mass specific heat of the sample including the pan material
$H$	DSC peak amplitude
$I$	DSC peak shape index
$K$	thermal lag factor between sample temperature and the programmed heating rate
$m$	sample mass
$P$	peak resolution parameter
$R_D$	thermal resistance between heater and sample (or reference) platform
$R_D'$	thermal resistance of the disk between sample and reference platforms
$R_G$	gas thermal resistance between heater and sample (or reference)
$R_G'$	gas thermal resistance between sample and reference
$R_R$	thermal resistance between temperature sensor and reference
$R_S$	thermal resistance between temperature sensor and sample (including thermal resistance of the sample itself)
$R_T$	total thermal resistance between heater and sample (i.e., $R_T = R_S + R_D$ )
$S$	slope of the leading edge of the DSC endotherm
$T_f$	final simulation temperature
$T_i$	initial simulation temperature
$T_m$	melting temperature of the sample
$T_0$	endotherm onset temperature
$T_P$	temperature of the source (heater)
$T_R$	temperature of the reference
$T_{RH}$	temperature of reference platform
$T_S$	temperature of sample
$T_{SH}$	temperature of sample platform
$T_{max}$	temperature corresponding to DSC peak maximum
$t$	time
$t_{max}$	time to peak maximum

## ACKNOWLEDGMENT

The authors thank the Du Pont Co. for generous instrumental support during the course of this work.

## APPENDIX A

An expression for  $t_{max}$ , the time to peak maximum in a DSC thermogram, is derived as follows. The heat flow into the sample during the transition is given by

$$\frac{dq_S}{dt} = \frac{T_{SH} - T_S}{R_S} + \frac{T_P - T_S}{R_G} + \frac{T_R - T_S}{R_G'} \quad (A1)$$

Since all the temperatures except  $T_S$  in eq A1 are time dependent during the transition, the rate of heat flow into the sample is given by

$$\frac{d^2 q_S}{dt^2} = \left( \frac{K}{R_S} + \frac{1}{R_G} + \frac{1}{R_G'} \right) \frac{dT_P}{dt} = \frac{1}{R_x} \frac{dT_P}{dt} \quad (A2)$$

The thermal resistance factor,  $R_x$ , is defined as

$$\frac{1}{R_x} = \frac{K}{R_S} + \frac{1}{R_G} + \frac{1}{R_G'} \quad (A3)$$

Integration of eq A2 with the boundary condition, eq A4, yields a general equation (eq A5) for the sample response during a melting transition

$$\left. \frac{dq_S}{dt} \right|_{t=0} = C_S \frac{dT_P}{dt} \quad (A4)$$

$$\frac{ds}{dt} = \frac{1}{R_x} \frac{dT_P}{dt} t + C_S \frac{dT_P}{dt} \quad (A5)$$

Use of the energy conservation law (10) in conjunction with the condition  $dT_S/dt = 0$  yields eq A6 for the rate of enthalpy change,  $dh/dt$ , during melting

$$\frac{dh}{dt} = \frac{1}{R_x} \frac{dT_P}{dt} t + C_S \frac{dT_P}{dt} \quad (A6)$$

Integration of eq A6 between the limits  $t$  and 0 and  $t_{\max}$  gives the total enthalpy of fusion,  $\Delta H$ , of the sample

$$\Delta H = \int_0^{t_{\max}} \frac{dh}{dt} dt = \frac{1}{2R_x} \frac{dT_P}{dt} t_{\max}^2 + C_S \frac{dT_P}{dt} t_{\max} \quad (A7)$$

Equation A7 may be solved for  $t_{\max}$

$$t_{\max} = R_x C_S \left\{ \left( 1 + \frac{2\Delta H}{R_x C_S^2 (dT_P/dt)} \right)^{1/2} - 1 \right\} \quad (A8)$$

Note that the above expression is similar to that derived by Gray (10) with the important difference that the heat leakage effect is explicitly included herein.

Another parameter, namely the time derivative of the sample holder temperature at  $t > t_{\max}$ , i.e.  $dT_{SH}/dt|_{t>t_{\max}}$ , is required to simulate the posttransition DSC curve-shape. This is derived from our model as follows.

According to Newton's law, at  $t > t_{\max}$

$$H \exp \left\{ -\frac{t - t_{\max}}{R_T C_S} \right\} = \frac{T_P - T_S}{R_T} \quad (A9)$$

$$H \exp \left\{ -\frac{t - t_{\max}}{R_T C_S} \right\} = \frac{T_{SH} - T_S}{R_S} \quad (A10)$$

In eq A9 and A10,  $R_T = R_S + R_D$ . The time derivative of eq A9 yields the rate of catch up of  $T_S$

$$\left. \frac{dT_S}{dt} \right|_{t>t_{\max}} = \frac{dT_P}{dt} + \frac{H}{C_S} \exp \left\{ -\frac{t - t_{\max}}{R_T C_S} \right\} \quad (A11)$$

The rate of catch up of the sample platform temperature,  $T_{SH}$ , is given by the time derivative of eq A10

$$\left. \frac{dT_{SH}}{dt} \right|_{t>t_{\max}} = \left. \frac{dT_S}{dt} \right|_{t>t_{\max}} - \frac{R_S H}{C_S R_T} \exp \left\{ -\frac{t - t_{\max}}{R_T C_S} \right\} \quad (A12)$$

Substitution of eq A11 in eq A12 yields the required expression

$$\left. \frac{dT_{SH}}{dt} \right|_{t>t_{\max}} = \frac{dT_P}{dt} + \frac{H}{C_S} \left( 1 - \frac{R_S}{R_T} \right) \exp \left\{ -\frac{t - t_{\max}}{R_T C_S} \right\} \quad (A13)$$

The rate expressed by eq A13 decreases exponentially with increasing  $t$  and will equal the programmed rate at  $t \gg t_{\max}$ .

## LITERATURE CITED

- (1) Brennan, W. P.; Miller, B.; Whitwell, J. C. In *Analytical Calorimetry*; Porter, R. S., Ed.; Plenum: New York, 1976; Vol. 2, p 441.
- (2) Jang, G.-W.; Rajeshwar, K. *Anal. Chem.* 1986, 58, 416-421.
- (3) Jang, G.-W.; Segal, R.; Rajeshwar, K. *Anal. Chem.* 1987, 59, 684-687.
- (4) Nelder, J. A.; Mead, R. *Computer J.* 1965, 7, 308-313.
- (5) O'Neill, M. J. *Anal. Chem.* 1964, 36, 1238-1245.
- (6) Baxter, R. A. In *Thermal Analysis*; Schwenker, R. F., Jr., Garn, P. D., Eds.; Academic: New York, 1969; Vol. 1, p 65.
- (7) O'Neill, M. J. *Anal. Chem.* 1975, 47, 630-637.
- (8) Claudy, P.; Commercon, J. C.; Letoffe, J. M. *Thermochim. Acta* 1983, 68, 305-316.
- (9) Schönborn, K. H. *Thermochim. Acta* 1983, 69, 103-114.
- (10) Gray, A. P. In *Analytical Calorimetry*; Porter, R. S., Johnson, J. F., Eds.; Plenum: New York, 1972; Vol. 3, p 17.
- (11) Brennan, W. P. Ph.D. Thesis, Princeton University, 1971.
- (12) O'Neill, M. J. *Anal. Chem.* 1966, 38, 1331-1336.
- (13) Flynn, J. H. *NBS Spec. Publ. (U.S.)* 1970, No. 338, 119-136.
- (14) Van Dooren, A. A.; Müller, B. W. *Thermochim. Acta* 1981, 49, 151-161.
- (15) Van Humbeeck, J.; Bijlvet, M. *Thermochim. Acta* 1987, 120, 55-61.
- (16) Morgan, S. L.; Deming, S. N. J. *Chromatogr.* 1975, 112, 267-285.

RECEIVED for review June 23, 1987. Resubmitted November 18, 1987. Accepted January 14, 1988.

## The Vinland Map

Walter C. McCrone

McCrone Research Institute, 2820 South Michigan Avenue, Chicago, Illinois 60616

A recent paper in this journal presents analytical data that caused those authors to differ with our conclusion published in 1974 that the Vinland Map is a modern forgery. A summary of our data pertaining to authenticity is included here to support our conclusion.

The Vinland Map (VM) was first revealed to the world in 1965 with the appearance of a book, *The Vinland Map and the Tartar Relation*, by Skelton, Marston, and Painter (1). The map, an unassuming pen and ink rendering, is a world

map on 27.8 × 40 cm parchment folded in two leaves. It is, however, remarkable for its purported date of 1440 in depicting lands to the west of Greenland, their shape, size, and position resembling the Northeastern extensions of North America (i.e., Vinland).

The lack of a convincing provenance for the VM and "grave doubts" by some scholars and scientists led Yale University, the owners, to discuss with McCrone Associates (MA) an investigation of the map in an effort to evaluate its authenticity.

In February 1972, Ken Nesheim of the Yale Beinecke Library brought to Chicago the Vinland Map (VM) which had

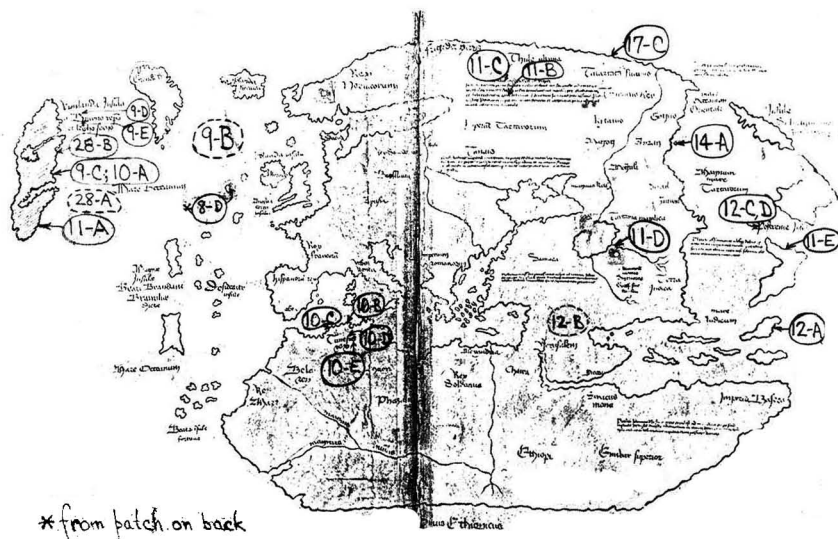


Figure 1. Vinland Map, sampling locations are designated by number-letter pairs; Vinland has been hatched.

been bound with two manuscripts: the "Tartar Relation" (TR) and the "Speculum Historiale" (SH). These two manuscripts, accepted as authentic 15th and 13th century documents, respectively, had been bound together with the VM as indicated by contiguous worm holes. The two manuscripts and the VM were examined by MA personnel and sampled by Anna Teetsov, MA microscopist. A total of 54 nanogram-to-microgram samples were taken: 29 from VM, 7 from TR, and 18 from SH. The sites for the 29 VM samples are indicated on the map (Figure 1) and described in Table I. These were subsequently examined by polarized light microscopy (PLM), X-ray (XRD) and electron diffraction (SAED), and scanning (SEM) and transmission (TEM) electron microscopy and with electron (EMA) and ion (IMA) microprobes in the McCrone Associates laboratory.

The McCrone Associates report covering their investigation was submitted to Yale University in January 1974. A brief paper (2) was presented at a symposium on the map in London in February 1974. In 1976, a further general paper on the map was published in *Analytical Chemistry* (3). Until now, however, no complete description of the 1972-1974 work at McCrone Associates has appeared.

#### EXPERIMENTAL DATA

**Preliminary Examination, Stereo Microscope.** Initial examination of the Vinland Map (VM) by stereo microscope disclosed what appeared to be a normal hand-drawn map. The black ink line was bordered along its length by a yellowish discoloration which was at first assumed to be the stain normally resulting from discoloration by ink components having migrated into the fibers over time. During sampling, however, this yellow discoloration was observed to have body, unlike a stain. It could be removed as tiny fragments with a fine-tipped tungsten needle while viewing the map with a stereo microscope at 20-60 $\times$ . The black pigment itself existed as a thin shiny black layer easily flaked from the yellow line; indeed much of the black line layer had already flaked away in all parts of the map.

Examination of the map lines showed that the black line had been carefully drawn over and, more or less, down the middle of a previously drawn yellow line. There was evidence of some

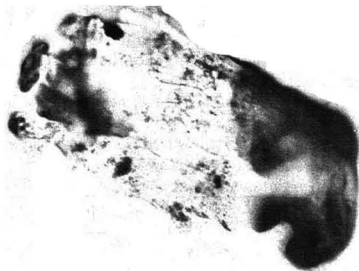


Figure 2. Parchment fragment, about 100  $\times$  200  $\mu$ m, coated with black (right one-third) and yellow ink (left two-thirds), transmitted light micrograph. The bar represents 20  $\mu$ m.

wobble in placement of the black line relative to the yellow line and in, at least, one area (West Coast of England) the second (black) line applied over the yellow line had "cut corners" and missed its registration with the yellow line.

**Polarized Light Microscopy (PLM).** Figures 2 and 3 show a portion of the same parchment fiber with adherent black and yellow ink (taken from the East coast of Vinland itself, sample 10-A). Careful examination of this fiber at higher magnifications (1000-2500 $\times$ ) showed further details of the small white (birefringent) spots and smaller dark (pseudo-opaque) particles visible in the center portion of the fiber. A polarized light microscopist, especially one trained in pigment identification, would note the high birefringence ( $\Delta n = 0.161$ ) and low refractive indexes ( $n = 1.658$ ,  $n = 1.487$ ) of the white particles and assume they are calcite (limestone). Similarly, he would note that the dark particles are submicrometer with a very high refractive index (or indices). If such very tiny pigment particles appear dark by transmitted light and white by reflected light, as these do, they are most likely titanium white (TiO<sub>2</sub>). The absence of polarization colors then indicates low birefringence and therefore anatase ( $\Delta n = 0.06$ ) rather than rutile ( $\Delta n = 0.28$ ). A similar examination of 19 of



**Table I. Vinland Map Samples**

sample	location on map
8-A	inscription on back, yellow ink <sup>a</sup>
8-B	inscription on back, yellow ink plus parchment
8-D	fibers from patch over wormhole, west of British Isles
8-E	parchment fiber from back (hair side) of map
9-A	from map crease, loose black particles plus parchment
9-B	from background North Atlantic, black particles
9-C	from Vinland coast, black ink particle with yellow ink
9-D	from top of "B" of "Byarno" in legend 66: "Vinlanda Insula...", yellow ink
9-E	from bottom of "B" "Byarno" in legend 66: yellow ink
10-A	from Vinland coast, ink stain
10-B	from N. African coast, South of Sardinia, black ink plus yellow ink
10-C	from Coastline West of 10-B, yellow ink
10-D	from first "S" in "Tunesis" (Legend 20), black ink plus yellow ink
10-E	from second "S" in "Tunesis" (legend 20), yellow ink
11-A	from Vinland coast, yellow ink
11-B	from SE edge of wormhole in legend 39 below "Thule Ultima", black ink particles with adhering yellow ink
11-C	from "s" in "Montes" (legend 39), black ink plus yellow ink
11-D	from river above "Kemmodi" (legend 37), black particles plus yellow ink
11-E	from coast of island below "Postreme Insula" (legend 58), black ink plus yellow ink
12-A	from coast of next island south of 11-E, yellow-brown ink
12-B	from background, Iraq, black particles with yellow ink
12-C	from "P" of "Postreme" (legend 58), black ink plus yellow ink
12-D	from yellow ink from same letter (12-C)
12-E	from ocean SE of Africa, fibers
14-A	from just off coast marked Ayram, orange lining of wormhole
28-A	from just off Vinland coast, parchment
28-B	from East coastline of Vinland, black ink

<sup>a</sup> The yellow ink along both sides of the black ink line appears yellow, orange, or brown depending on thickness and relative percentages of calcite and anatase.



**Figure 3.** Same parchment fragment in Figure 2 shown here with slightly uncrossed polars. The small white particles are calcite (limestone); the smaller dark particles are anatase. This is a transmitted light micrograph with slightly uncrossed polars. The bar represents 20  $\mu$ m.

the samples that showed at least some portions of yellow ink disclosed that, at least, 16 showed the same two kinds of particles. The high birefringent (limestone?) particles are also associated with other low refractive index particles, probably associated minerals like quartz, clays, feldspars, etc.

The black ink areas also showed (by PLM) very tiny, but truly opaque particles, possibly carbon black (soot?) or an iron tannate; they were not magnetic (i.e., not  $\text{Fe}_3\text{O}_4$ , magnetite). Another important PLM observation was the fact that the samples varied

considerably in the relative amounts of yellow and black ink as well as in the distribution of pigments in the yellow ink. This illustrates the difficulty of mixing very fine particles in a suspension to achieve a uniform dispersion. It also explains why different portions of the same sample analyzed by different techniques sometimes show different compositions. It was not difficult to find small areas, a few square micrometers, of pure components. Two such areas of pure anatase are shown later (Figures 8 and 9) by transmission electron microscope (TEM).

A final PLM observation has to do with shapes of the calcite and anatase particles, since this has a strong bearing on the origin of these particles. A regular uniform shape and micrometer particle size of calcite would indicate a man-made precipitated product available commercially only in the 19th century and later. The ground mineral limestone, however, has been used for hundreds of years. The calcite in the VM is ground limestone and therefore not helpful in dating this map; most calcite in modern paintings, etc., is the precipitated mineral. The anatase, on the other hand, is of uniformly small diameter particles averaging about 0.15  $\mu$ m. The larger anatase particles can be resolved by PLM as rounded crystalline shapes typical of commercial titanium white (4). This product has been produced only since 1917. For a few years after 1917, the color of this anatase ( $\text{TiO}_2$ ) pigment was yellow due to traces of iron. The observed color of the yellow ink line may be due to early yellow  $\text{TiO}_2$ . In any case we observed no other yellow particles.

Examination of successive VM yellow ink flakes by PLM consistently confirmed the above results (Table II). At this point, after finding submicrometer anatase in samples 9-C, 9-D, 10-D, 10-E, 11-A, 12-A, and 12-C by PLM, we were convinced the VM was of recent origin. In fact, the sampling steps showing the presence of an applied yellow ink line simulating the natural staining of ink line boundaries would be sufficient to label the Vinland Map as a forgery. We proceeded, however, to obtain as much confirmation as possible through the use of other ultramicroanalytical instrumentation. Most of these data are summarized in Table II. The different area samples are denoted by a figure and a letter (e.g., 10-A); an added third digit signifies a small portion of that sample. These portions often yield different results due to heterogeneity of the nanometer samples.

**X-Ray Diffraction (XRD).** We used a special micro X-ray diffraction camera capable of excellent powder diffraction patterns on subnanogram samples to X-ray a portion (about 7  $\mu$ m in average diameter) of yellow ink (sample 9-C) which had been assumed (by PLM) to contain anatase and calcite. The resulting powder diffraction pattern (Table III) shows about equal amounts of anatase and calcite with a small quantity of quartz thus confirming the PLM identification. Quartz particles are ubiquitous and accompany most quarried or mined materials, e.g., limestone. Titanium is also reasonably ubiquitous, being ninth in order of abundance of the chemical elements. Titanium dioxide as anatase, however, is not so common and in the modern pigment form it has been available only since about 1920. Similar XRD patterns were obtained on other portions of 9-C and 11-A (Table III).

**Scanning Electron Microscopy (SEM).** As a next step, we examined a small portion of VM yellow ink sample 9-D by using the scanning electron microscope (SEM) with its energy dispersive detection system (EDS). Figures 4 and 5 show typical yellow ink particles at 11000X. The surface asperities are likely due to the small anatase and calcite particles observed by PLM and XRD. This is further indicated by the corresponding energy dispersive X-ray spectra (Figures 6 and 7). The 9-D-3 yellow ink particle shows (Figure 6) titanium as its strongest EDS peak, presumably corresponding to anatase; a black ink particle (Figure 7, 9-C-2), shows equally strong iron and chromium peaks. Even though it is difficult to be sure each of the two ink samples is not, at least slightly, cross-contaminated, the two are shown to be very different.

**Transmission Electron Microscopy (TEM).** Because of the unique character (size and shape) of modern anatase pigment particles, the size and shape of the observed VM anatase particles then became crucially important. We turned next, then, to transmission electron microscopy (TEM). Jagged irregular particles with widely varying particle sizes would signify ground mineral anatase; well-formed, although rounded, regular crystal shapes and a narrow submicrometer size range would indicate

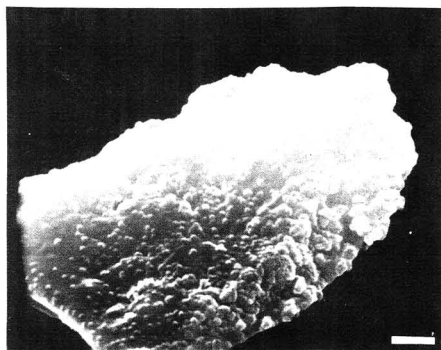


**Figure 4.** VM yellow ink flake (9-D-2) about 10  $\mu\text{m}$  in maximum dimension. The tiny rounded protuberances may be the pigment particles anatase and calcite. This is an SEM micrograph taken at 11000X. The bar represents 1  $\mu\text{m}$ .

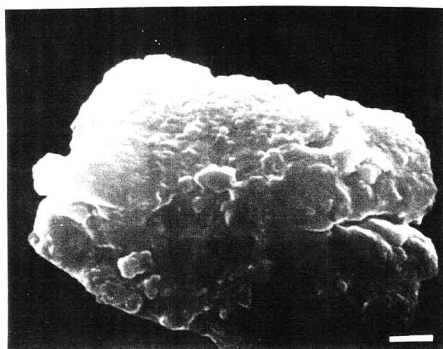


**Figure 5.** Flake of VM yellow ink (9-D-3) under the same conditions as given in Figure 4. The energy dispersive X-ray pattern for this sample is shown in Figure 6.

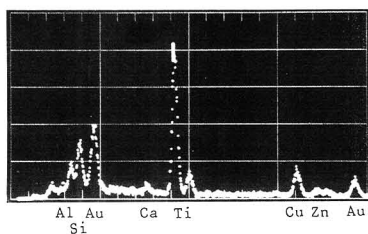


**Figure 6.** Energy-dispersive X-ray pattern for VM yellow ink sample 9-D-3 (full scale is 10 keV). The cursor is set on the titanium peak at 4.51 keV; the peaks, left to right, are magnesium, aluminum, silicon, gold, calcium, titanium (two peaks), copper, zinc, copper, and gold.

a precipitated man-made product. The TEM easily resolves these submicrometer particles, thus making possible size and shape determination, and its selected area electron diffraction (SAED) capability identifies the crystallographic phase and, thereby, the chemical composition.

The smallest possible subnanogram portion taken from VM sample 11-A (Vinland, S.E. coast) was crushed between two clean glass surfaces and the flattened residue (amounting to only a few picograms) was mounted on a TEM grid. Figure 8 confirms the size and shape characteristics of the VM anatase (i.e., rounded single crystals less than about 0.5  $\mu\text{m}$  in diameter). Figure 9 shows

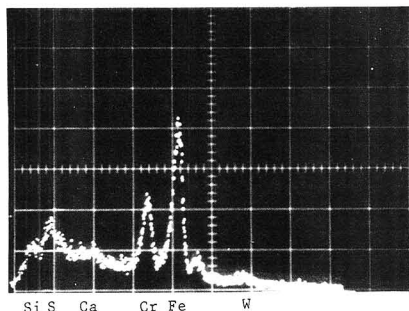


**Figure 7.** Energy dispersive X-ray pattern for VM black ink samples 9-C-2 showing an expanded portion of the pattern from silicon (1.74 keV) to tungsten (8.40 keV; from our tungsten needle). The two tallest peaks are chromium (5.41 keV) and iron (6.40 keV) (full scale is 15.31 keV).

modern commercial anatase pigment samples from NL Industries (Titanium Pigments Division). Finally, Figure 10 shows the typical shapes of ground mineral anatase. Figures 8 and 10 were taken at 25000X, Figure 9(left) at 50000X, and Figure 9(right) at 20000X. Good SAED data for anatase obtained on VM samples 9-D, 11-A, and 12-A are tabulated in Table IV. The observed diffraction patterns show spotty rings as expected with small samples, but the ring diameters are in good agreement with the lattice parameters previously observed by XRD for anatase.

The shapes of the VM anatase particles (Figure 8) show them to be characteristic of the commercial pigment, i.e., rounded, reasonably uniformly sized, single, post-1917 crystals (Figure 9). It is impossible for ground mineral anatase (Figure 10) to show the particle shape and size distribution of the commercial product.

**Particle Size Measurements.** One of the additional means chosen at this point to further characterize the anatase found in the VM was a particle size distribution measured from the TEM images such as those illustrated in Figures 8 and 9. The distribution of sizes based on more than 300 particles for the two commercial samples is shown graphically in Figure 11. The similarity between the particle size distribution curves for VM sample 11-A and NL Industries (Titanium Pigments Division) anatase pigment is obvious as is the size distribution difference between these two precipitated pigments and the ground mineral anatase in Figure 10. A ground material always shows increasing numbers of smaller and smaller particles with a wide size range and (usually) irregular jagged particles. It is extremely difficult even today to grind any sample to yield *all* submicrometer particles.

**Electron Microprobe Analyzer (EMA).** This instrument is capable of elemental analyses on samples ranging down to femtogram levels ( $10^{-15}$  g) with a 1- $\mu\text{m}$  beam diameter. Its analysis, however, is produced from about a 100  $\mu\text{m}^3$  volume of the sample. It detects and identifies all elements except the four lightest (H, He, Li, and Be). The EMA analyses of 16 yellow VM inks (Table V) show significant amounts of titanium; the single black ink sample (9-C-2) and the parchment sample (28-A) analyzed by electron microprobe show little or no titanium (Table V).

**Ion Microprobe Analyzer (IMA).** The ARL ion microprobe, newly acquired at McCrone Associates in 1971, was also used to analyze several VM ink samples (Table VI). At that early date, the sensitivity of the IMA for different elements was not well understood—hence accurate quantitation was impossible. It is, however, extremely sensitive for many elements and in subatogram ( $10^{-18}$  g) quantities. For most elements, it is strictly a qualitative surface analyzer covering areas as small as 5  $\mu\text{m}^2$  and a few atom layers deep. Depth profiles at nanometer levels are also possible with IMA.

The ink samples analyzed by IMA ranged in size from 4  $\mu\text{m}$  to slightly more than 10  $\mu\text{m}$  in average diameter. The small size accounts, no doubt, for some variations in EMA and IMA data (Table II) but the sensitivity for different elements also varies greatly from EMA to IMA. There is good agreement for most

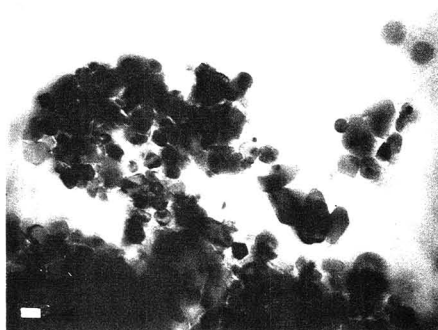
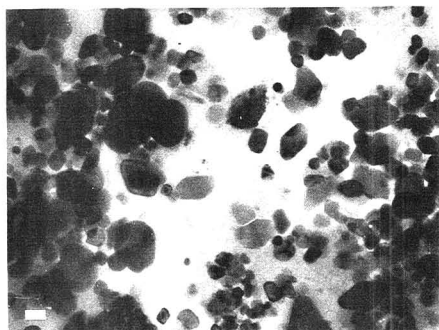


Figure 8. Particles of anatase from the Vinland Map (particle 11-A-5, left; particle 9-D-1, right) viewed at 25000X, TEM. The bars represent 0.15  $\mu\text{m}$ .

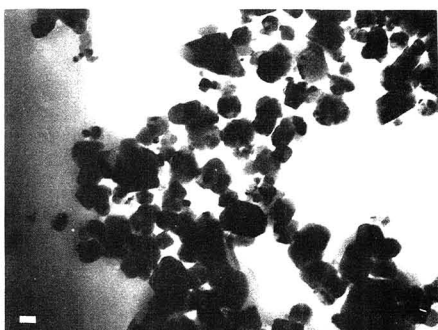
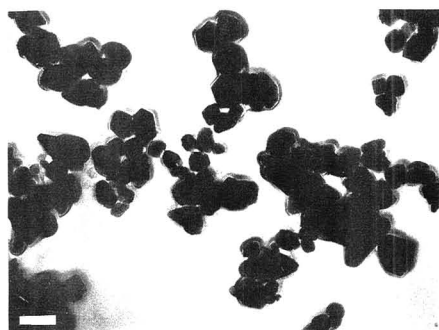


Figure 9. Precipitated  $\text{TiO}_2$  (anatase), samples from National Lead Industries (Titanium Pigments Division), viewed at 50000X (left) and 20000X (right) TEM. The bars represent 0.15  $\mu\text{m}$ .

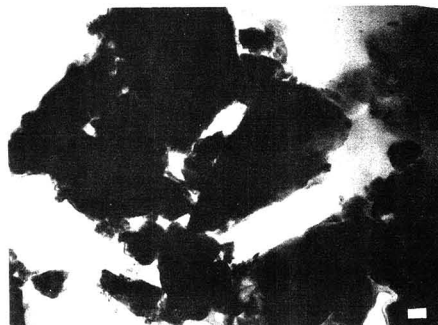


Figure 10. Ground mineral anatase, sample from the Smithsonian Institution, fine (left) and coarse (right) fractions, viewed at 25000X, TEM.

replicate samples by EMA: 8-A-1 and -2, 8-B-1 and -2, 11-A-1, -2, -3, and -4, as well as 12-A-1, -3, and -4 (Table V). Table VI shows IMA data for 23 different VM samples, including all those that showed any indication of yellow ink. The absence of data for trace elements for samples 8-11 does not mean absence of trace elements. We were looking only for major and minor elements at the time they were analyzed.

The IMA is very sensitive for alkali and alkaline-earth elements but much less sensitive for transition elements and especially insensitive for the noble metals. Barium was reported as "major" based on our then understanding of the highly sensitive IMA (subattogram,  $10^{-18}$  g) whereas the EMA, a more quantitative but less sensitive (subfemtogram,  $10^{-15}$  g) instrument, found only about 1% barium. Titanium is one of the elements for which the IMA is relatively sensitive; hence "major" may be reported for low

percentages (e.g., 8-B-1). The inhomogeneity of ultramicrosamples can cause apparent discrepancies, but these are usually explained by microscopical examination of the sample(s). Sample 12-A, for example, shows variable composition depending on the portion analyzed. Table V shows data for four different portions of this sample. Three agree quite well (12-A-1, -3, and -4) but 12-A-2 is very different. It was very small (average diameter, 4  $\mu\text{m}$ ) and apparently was a tiny patch of anatase similar to those selected for the TEM pictures shown in Figure 8. This illustrates the necessity of understanding the capabilities and limitations of each microanalytical tool.

Table II summarizes the extent to which each of the ultramicroanalytical instruments was used on the VM ink samples.

**Comparison of VM, TR, and SH Ink Samples.** The ion microprobe was also used to compare samples from the "Tartar

Table II. Summary of Major Microanalytical Results<sup>a</sup>

sample <sup>b</sup>	type <sup>c</sup>	PLM	XRD	TEM		SEM micrograph	EMA			IMA		
				micro- graph	SAED		% Ca	% Fe	% Ti	major	minor	trace
8-A-1	ink, Y						15	0.5	8	Ti, Ba, Ca		
8-A-2	ink, Y						15	1.5	9			
8-B-1	ink, Y						8	0.8	4	Ti, Ba		
8-B-2	ink, Y						15	1.5	8	Ca (8-C)	Ba (8-C)	
8-D	fiber									organic		
8-E	fiber									organic		Ca
9-C-1	ink, Y, B	anatase	anatase				4	0.8	28-35	Ti		
9-C-2	ink, B					Fe, Cr, S	1-2	high <sup>d</sup>	0			
9-D-1	ink, Y	anatase		anatase	anatase		3-5		15-20	Ti, Ba		
9-D-2	ink, Y					anatase						
9-D-3	ink, Y	anatase		anatase	anatase		3-5		15-20			
9-D-4	ink, Y	anatase				anatase	3-5		15-20			
9-E	ink, Y									Ti, Ba		
10-A	ink, Y									Ti, Ba, Ca		
10-B	ink, Y, B	anatase?								Ti, Ca, Ba		
10-C	ink, Y											
10-D	ink, Y, B	anatase								Ti, Ca		
10-E	ink, Y	anatase								Ti		
11-A-1	ink, Y	anatase		anatase			7-9		15-22	Ca, Ti, Ba		
11-A-2	ink, Y	anatase	anatase	anatase	anatase		4-6		12-16			
11-A-3	ink, Y	anatase					4-5		10-15			
11-A-4	ink, Y	anatase					4-8	1-2	5-7			
11-A-5	ink, Y			anatase	anatase							
11-B	ink, Y, B									Ca, Ti, Ba		
11-C	ink, Y	anatase?								Ti, Ca, Ba		
11-D	ink, Y	anatase?								Ca, Ti		
11-E	ink, Y, B									Ti		
12-A-1	ink, Y, B	anatase					7-9		20-28			
12-A-2	ink, Y	anatase		anatase	anatase				40-45	Fe, Ca, Si, K		Na, Mg, Al, Ti, Cr
12-A-3	ink, Y	anatase					7-9		15-20			
12-A-4	ink, Y	anatase					7-9		12-15			
12-A-5	ink, Y	anatase										
12-B	ink, Y, B									Ca, Ti, Fe		Na, Mg, Al, Si, Cr
12-C	ink, Y, B	anatase								Ti, Ca, Ba		Na, Mg, Al, Si, K
12-D	ink, Y	anatase								Ca, Fe, Ti		Na, Mg, Al, Si
12-E	fiber	anatase								org, N	S	Ca, K, Na, Mg, Al, Si
28-A	fiber								<0.1			
28-B	ink, B								<0.1			

<sup>a</sup> PLM, polarized light microscope; XRD, X-ray diffraction; TEM, transmission electron microscope; SAED, selected area electron diffraction; SEM, scanning electron microscope; EMA, electron microprobe analyzer; IMA, ion microprobe analyzer. <sup>b</sup> The different area samples have a number-letter designation; a third digit indicates another subnanogram portion of that sample. <sup>c</sup> Y, yellow ink; B, black ink. <sup>d</sup> 9-C-2 showed 10-15% Cr, 20-30% Fe by EMA.

Relation" (TR) and the "Speculum Historiale" (SH) documents "originally bound" with the Vinland Map. Representative data appear in Table VII. The IMA analyses showed that the TR and SH inks contained at least 2 orders of magnitude less titanium than the VM inks. The titanium content of the TR and SH inks was estimated to be a maximum of about 200 ppm and averaging about 100 ppm. These estimates are based on comparisons of the peak heights for Ti in the respective samples. The general pattern of the TR and SH inks resembles aged iron gallotannate inks when compared with British Museum samples. The VM inks do not match any known inks by IMA.

### CONCLUSIONS

The presence of a double ink line is a strong indication that the Vinland Map was intended to appear ancient. The black upper line was drawn, and generally well-centered, over a broader yellow line. The latter simulates the natural diffusion and yellowing of an ink medium into the parchment which takes place normally over hundreds of years. The VM yellow line, far from being simply a discolored ink medium, is a suspension of tiny pigment particles in a dried ink medium. One of the pigments dispersed within this yellow ink and under the black ink line is the modern anatase "titanium

white" pigment. The pigment is identical in composition, crystal structure, size and shape with commercial titanium white available only since 1917. The materials needed and the processing steps required for its preparation are a convincing argument against its availability before 1917. During the first few years after 1917, before the manufacturers were able to effectively remove all of the iron, titanium white was yellow.

The identity of the titanium white as anatase was determined by its optical properties using the polarized light microscope, by elemental analysis using the scanning electron microscope and both electron and ion microprobes, and by its crystal diffraction pattern using both X-ray and electron diffraction.

The titanium white was shown to be the modern anatase pigment by particle size and shape using the transmission electron microscope.

### DISCUSSION

Before an object is proclaimed to be a forgery, it is necessary to find an anachronistic or other mistake the forger has made. For the Vinland Map this includes stylistic errors: having a

**Table III. X-ray Powder Diffraction (XRD) Data for VM Inks**

VM 11-A-2 <sup>a</sup>			anatase ASTM 4-0477			calcite ASTM 5-0586			quartz ASTM 5-0490		
<i>d</i>	<i>I</i> / <i>I</i> <sub>0</sub>		<i>d</i>	<i>I</i> / <i>I</i> <sub>0</sub>		<i>d</i>	<i>I</i> / <i>I</i> <sub>0</sub>		<i>d</i>	<i>I</i> / <i>I</i> <sub>0</sub>	
		4.23	<5						4.26	35	
		3.89	10			3.86	10				
3.53	100	3.52	100	3.51	100				3.34	100	
3.36	10	3.36	<5								
3.05	100	3.04	75			3.04	100				
2.49	25	2.49	<5			2.50	14				
		2.435	<1	2.435	9				2.46	12	
		2.38	5	2.379	22						
		2.33	<5	2.336	9						
		2.28	<5			2.29	18	2.28	12		
2.22	50	2.24	<1								
2.10	40	2.09	10			2.10	18				
1.91	40	1.90	25	1.891	33	1.91	17				
1.70	10	1.69	10	1.699	21						
1.67	10	1.66	10	1.665	19						
1.47	<5	1.48	5	1.48	13						
1.26	5	1.264	10	1.264	10						

<sup>a</sup> 12–16 h exposures with unfiltered Cu X-rays; 42 kV and 34 mA with a 28.65-mm camera.

too-accurate North coast of Greenland and showing it as an island; also for using a name for Spain (Hispanorum) possible only 35 years later than 1440; chemical composition errors (a yellow ink rather than a yellow stain); a form of a constituent substance not known in 1440 (a post-1917 anatase pigment); and, where datable, the date must agree with 1440. On three of these four criteria the VM fails and must be judged a forgery. We might well discuss each of these in somewhat more detail.

**Stylistic Errors.** One can not be certain the North coast of Greenland was not better known or even that the name for Spain could not have been anticipated. These two arguments against authenticity were made, however, by one of the foremost ancient map scholars: Helen Wallis, until recently, head of the Map Department at the British Museum (5).

**A Yellow Ink Not a Yellow Stain.** The forger apparently knew that the medium in an old ink line diffuses very slowly over a few hundred years to cause a yellow border along its length. Not having time to wait, he decided to paint such a line by first outlining the entire map with a faint but broad yellow line. He then carefully inked a finer black line down the center of the yellow line. A tour de force, but in at least one area (coast of England) he was careless and missed the yellow line.

**Table IV. Selected Area Electron Diffraction Data (TEM/SAED) for VM Inks<sup>a</sup>**

VM 12-A-2		VM 11-A-2		VM 11-A-5		VM 9-D-1		standard patterns			
<i>d</i>	<i>I</i> / <i>I</i> <sub>0</sub>	<i>d</i>	<i>I</i> / <i>I</i> <sub>0</sub>	<i>d</i>	<i>I</i> / <i>I</i> <sub>0</sub>	<i>d</i>	<i>I</i> / <i>I</i> <sub>0</sub>	anatase		calcite	
								<i>d</i>	<i>I</i> / <i>I</i> <sub>0</sub>	<i>d</i>	<i>I</i> / <i>I</i> <sub>0</sub>
3.51	100	3.51	s	3.51	s	3.51	s	3.51	s		
						3.05	m			3.04	vs
		2.48	w	2.48	ms	2.47	w	2.48	w		
2.43	s							2.435	m		
		2.38	m	2.38	m	2.39	m	2.38	w		
2.33	m	2.34	m	2.34	m			2.34	w		
		2.09	w	2.095	w					2.10	s
1.89	m	1.90	m	1.904	w	1.89	m	1.89	m		
1.78	m	1.77	m	1.77	m	1.77	m	1.78	m		
1.69	s	1.68	m	1.665	m	1.68	m	1.66	m		
1.64	vw										
1.49	m	1.486	m	1.480	m	1.49	m	1.49	m		
1.37	m	1.38	mw	1.367	mw	1.36	w	1.367	w		
1.27	w	1.27	mw	1.266	mw	1.26	w	1.263	w		
		1.16	mw	1.161	w	1.16	w	1.161	w		

<sup>a</sup> A fair SAED pattern was also obtained for VM 9-D-3.

**Table V. Electron Microprobe (EMA) Analysis of the VM Inks**

sample	elements, wt %										
	Al	Ca	Cl	K	P	S	Ba	Si	Ti	C	other
8-A-1	0.5	12–18	1–2	0.5		1–2	<1	0.5–1	7–10	15–20	0.5 Fe
8-A-2	0.5	12–18	3–4	3–4		5–8	<1	1–2	8–10	10–20	1–2 Fe, 3 Na
8-B-1		5–10	1–2	1–2		2–3	<0.5	0.5–1	3–4	20–40	0.8 Fe, 1–2 Na
8-B-2	1–2	12–18	3–4	3–4		5–8	<0.8	1–2	5–10	10–20	1–2 Fe, 1–2 Na
9-C-1		2–5				1–2		0.8–1	28–35	10–20	0.5–1 Fe
9-C-2 <sup>a</sup>	0.2–0.8	1–2				3–4		1–2	0	5–10	10–15 Cr, 20–30 Fe
9-D-1	3–5	3–5					<1	4–7	15–20	high	3–4 Zn
9-D-3	3–5	3–5					<1	4–7	15–20	high	3–4 Zn
9-D-4	3–5	3–5					<1	4–7	15–20	high	3–4 Zn
11-A-1	1–2	7–9	2–3	3–4	1–2	4–5	<2	1–2	15–22	20–30	6–10 Na
11-A-2	3–4	4–6					<1	4–7	12–16	maj	3–5 Zn
11-A-3	3–4	4–5					<1	4–7	10–15	maj	3–4 Zn
11-A-4	1–2	4–8		2–3		3–4		2–3	5–7	15–20	1–2 Fe, 2–5 Zn
12-A-1	1–2	7–9	2–3	3–4	1–2	4–5	<3	1–2	20–28	15–20	6–10 Na
12-A-2							<4	10–12	40–45		
12-A-3	1–3	7–9	2–3	3–4	1–2	4–5	<2	1–2	15–20	15–20	6–10 Na
12-A-4	1–2	7–9	2–3	3–4	1–2	4–5	<2	1–2	12–15	15–20	6–10 Na
28-A									<0.1		
28-B									<0.1		

<sup>a</sup> Sample 9-C-2 is a black ink particle with little or no adhering yellow ink.

Table VI. Ion Microprobe (IMA) Data on VM Inks

sample	major	minor	trace
8-A-1	Ti, Ba, Ca		
8-B-1	Ti, Ba		
8-C	Ca, Ba		
8-D <sup>1</sup>	only organic		
8-E <sup>1</sup>	only organic	Ca	
9-C-1	Ti		
9-D-1	Ti, Ba		
9-E	Ti, Ba		
10-A	Ti, Ba, Ca		
10-B	Ti, Ca, Ba		
10-C <sup>a</sup>	organic		
10-D	Ti, Ca		
10-E	Ti		
11-A	Ca, Ti, Ba		
11-B	Ca, Ti, Ba		
11-C	Ca, Ba, Ti		
11-D	Ca, Ti		
11-E	Ti		
12-A-1	Fe, Ca, Si, K <sup>b</sup>	Na, Mg, Al, Ti, Cr, Mn	
12-B	Ca, Ti, Fe	Na, Mg, Al, Si, K, Cr, Mn	
12-C	Ti, Ca, Ba	Fe, Na, Mg, Al, Si, K, Cr, Mn	
12-D	Ca, Fe, Ti	Na, Mg, Al, Si	
12-E <sup>a</sup>	organic, N	S, Ca, K, Na, Mg, Al, Si, P, Fe	

<sup>a</sup> Parchment fibers alone, no ink. <sup>b</sup> These and the following data are later IMA results when more experience enabled us to make some corrections for ionizability of the various elements and to differentiate additional elements from many molecular fragments.

The forger compounded this error by using an ink with dispersed particles in an ink medium. (The EDS analyses in Figures 6 and 7 show a small organic background.) If he had used a stain (diluted wine, tea, or urine have been used as ancient ink media), we might not have been able to detect forgery of the VM.

**Form of the Components.** In one last major mistake the forger used a modern pigment in his yellow ink line. This pigment, TiO<sub>2</sub> as anatase, was unavailable in the form he used (uniform diameter, very fine, precipitated and calcined anatase) before about 1920. At that time, this product was slightly yellow and he may have chosen it for that reason.

As a result of these errors, I feel fully justified in concluding the Vinland Map is a post-1920 forgery.

**Views of Others.** It has been proposed (6) that the mineral ilmenite (an iron titanate), if reacted with sulfuric acid, would in 1440 have yielded TiO<sub>2</sub> and iron sulfate; the latter could then have been washed away leaving crystalline anatase. Such an experiment has, indeed, been carried out

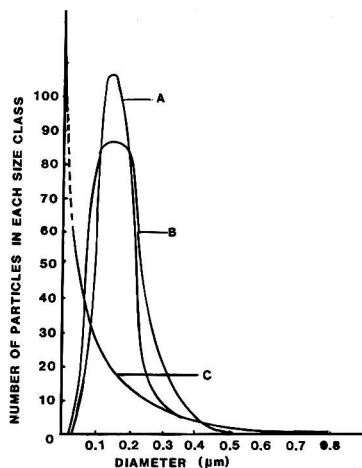


Figure 11. Size distribution of anatase: curve A, VM sample 11-A; curve B, commercial anatase from NL Industries, Titanium Pigments Division; curve C, a ground mineral sample from the Smithsonian Institution.

successfully but the product consisted of extremely finely divided, almost amorphous, anatase—unresolved by PLM and giving very broad powder diffraction lines by XRD. To convert this product to a VM-type anatase requires a calcining step at very high temperatures (800–1000 °C). This is inconceivable as a 15th century process.

It is important to realize that concentrated sulfuric acid is also required to produce anatase from ilmenite. To obtain the proper size and shape of the anatase pigment as found on the VM also requires the 800–1000 °C calcining step to produce the commercial product. Why anyone in the 15th century would choose to go through such a complex process starting with a black substance to produce a yellow pigment when there were at least six good yellow pigments (yellow ochre, gamboge, raw sienna, raw umber, lead-tin yellow, and orpiment) readily available in the Middle Ages is also difficult to understand.

There is substantial disagreement between McCrone Associates and the University of California, Davis (7). They report much less titanium in their samples than we find in

Table VII. Comparative Ion Probe (IMA) Analyses of VM, TR, and SH Ink Samples<sup>a</sup>

element	TR			SH				VM			
	13B	13C	13E	14C	14E	14D	15B	12B	12C	12D	12E
Na	t	m	t	t	t	m	m	t	t	t	t
Mg	t		t			t		t	t	t	t
Al								t	t	t	t
Si	t		t		t			t	t	t	t
P		t		t	m	M	m				t
S	M	m	M	m	m	m	m				m
Cl			t								
K	m	m	t	M	m	m	m	t	t		t
Ca	M	M	M	M	M	M	M	M	M	M	t
Ti	t	t	t	t	t	t	t	M	M	M	
Fe	m	m	m	m	m	m	m	M		M	
Ba									M		
Cr								t	t		
Mn								t	t		
N											M
S											m

<sup>a</sup> M, >5%; m, 1–5%; t = <1%.



**Table VIII. Electron Microprobe (EMA) Analyses of VM Yellow & Black Ink Lines from VM Ink Sample 9-C**

element	amount, wt %	
	yellow line	black line
Al		0.2-0.8
Ca	2-5	1-2
Cr		10-15
C	10-20	5-10
Fe	0.5	20-30
K		
S	1-2	3-4
Si	0.8-1	1-2
Ti	28-35	

the ink itself. They do, however, show more titanium in 26 of 33 ink lines as compared with adjacent parchment.

I believe the difference between our two conclusions is due to the different instruments best used for trace analysis as compared with ultramicroanalysis. Trace analysis is the detection or measurement of trace substances in large samples. Ultramicroanalysis, on the other hand, involves very tiny but quite pure samples. The instrument Cahill et al. used (particle-induced X-ray emission, PIXE) is an excellent trace analysis tool but it is not the instrument of choice for the detection and study of subnanogram samples and subpicogram particles.

If Cahill et al. were correct in asserting that "titanium and other medium and heavy elements are present in only trace amounts in the inks, with titanium reaching a maximum value of 10 ng/cm<sup>2</sup>, or about 0.0062% by weight", we could never have obtained good XRD and TEM/SAED patterns for anatase TiO<sub>2</sub> as well as the SEM/EDS, EMA/EDS, and WDS and IMA results showing major percentages of Ti. XRD requires 0.1-ng amounts of reasonably pure crystalline substance or several nanogram samples containing at least 5% of a given crystalline substance to give readable diffraction patterns. SEM/EDS, EMA/EDS, and EMA/WDS all showed percentages ranging from about 10% to 40% on subnanogram samples of the yellow inks. IMA showed major amounts of Ti in the yellow ink. If there were only 0.0062% titanium in the ink as measured by Cahill, we would probably not have detected Ti or, much less likely, have identified TiO<sub>2</sub> by diffraction on subnanogram samples.

We do not doubt that Cahill obtained the number 0.0062%, but that number is a measure of the percentage in the total PIXE sample of much greater sample volume than we used. It is not a measure of the concentration of Ti in the yellow ink. That is the important number and it is what we measured, using the appropriate ultramicroparticle analysis techniques available to us. If Cahill's 10 ng/cm<sup>2</sup> is concentrated in an ink line, it corresponds to nearly 4 million anatase particles in a 1 cm length of ink line.

Few analytical chemists appreciate the difference between trace analysis techniques (e.g., atomic absorption spectroscopy, neutron activation analysis, and PIXE) and ultramicroanalytical techniques (e.g., microscopical techniques). Some instruments are able to do trace analyses on ultramicrosamples (e.g., ion microprobe). There is also the general attitude that large, expensive instruments are superior to less costly simpler instruments. For example, electron microscopists generally assume that if magnifications of 10<sup>5</sup>-10<sup>6</sup>× are routine with SEM and TEM, no one should bother to use a light microscope limited to 1000×-2000×. This attitude has almost eliminated all academic courses that teach chemical microscopy. Very few analytical chemists today have any idea of the potential of that ancient symbol of research, the polarized light microscope. We all use and trust the methods and instruments we were trained to use. The conclusions drawn

by anyone who uses PLM are highly suspect by most analytical chemists who lack all training in that field. Confidence in analytical data derived from PIXE and other particle-beam instruments is not necessarily based on understanding but an attitude that Hi-Tech instruments are more likely to be correct.

Yet, in trained hands, PLM can solve many of today's complex chemical problems. Ideally, all such problems would begin with a light microscope and, if unsolved there or if confirmation is desired, other microscopical instrumentation should be used. This includes any tool or technique able to characterize single micrometer particles or areas. McCrone Associates has been very successful during more than 30 years in following what they term the "particle approach". Besides light microscopes they use a variety of electron and ion microscopes, electron and ion microprobes as well as Auger, ESCA, microFTIR, microXRD, laser raman microprobe, and microradiography. Nearly all of the samples examined with any of these instruments are first prepared and characterized by light microscopists. Many samples are analyzed solely by light microscopists who, incidentally, outnumber particle-beam microscopists at McCrone Associates.

The reason for this style of problem-solving is simply its past success. The light microscope yields more analytical characterization data in a shorter time than any other instrument. These include particle size, shape and surface character, color and pleochroism, light absorption characteristics, refractive indices, birefringence, extinction angles, optic sign, sign of elongation, optic axial angle, etc. These characteristics quickly identify many substances, suggest purity, and detect polymorphism, solvation, and surface reactions. All of these relate directly to process and material problems in industry. They enable a forensic microscopist to characterize and compare trace evidence, an industrial hygienist to differentiate asbestos fibers from innumerable harmless fibers, and an environmentalist to identify individual particles of air or water pollution.

All of these microscopical tools and techniques were used on the Vinland Map to look for any mistakes a forger might have made. We found two such mistakes: a yellow ink line almost undoubtedly present in order to simulate an ancient ink stain, and, whether or not that was its purpose, an integral part of that yellow ink consists of significant amounts of a pigment that became available only during the 20th century.

That 20th century pigment is a "trace component" of any large VM parchment area (e.g., 500 μm by 1000 μm as examined by PIXE). But, it is not a trace component of the ink itself as analyzed by ultramicroanalytical techniques like PLM, XRD, SEM/EDS, TEM/SAED, EMA, and IMA. These latter instruments are the ones to choose for problems like authenticity of the VM.

#### ACKNOWLEDGMENT

Don Brooks, Anna Teetsov, John Gavrilovic, and Tim Vanderwood of McCrone Associates and Lucy McCrone and John Dely of the McCrone Research Institute greatly assisted in reviewing and reevaluating our own work and that of the University of California (Davis). The original work was performed by Anna Teetsov (sampling and PLM), Ralph Hinch (XRD), John Brown (SEM), Gene Grieger (TEM and SAED), John Gavrilovic (EMA), Mike Bayard (IMA), and Lucy and Walter McCrone (PLM). We were also greatly helped by a number of outsiders: A. D. Baynes-Cope and Helen Wallis (both now retired from the British Museum), Norbert Baer (New York University), Ken Towe (Smithsonian), and Kurt Heinrich (National Bureau of Standards).

**Registry No.** Na, 7440-23-5; Mg, 7439-95-4; Al, 7429-90-5; Si, 7440-21-3; P, 7723-14-0; S, 7704-34-9; Cl, 7782-50-5; K, 7440-09-7; Ca, 7440-70-2; Ti, 7440-32-6; Fe, 7439-89-6; Ba, 7440-39-3; Cr,

7440-47-3; Mn, 7439-96-5; N<sub>2</sub>, 7727-37-9; C, 7440-44-0; Zn, 7440-66-6; anatase, 1317-70-0.

### LITERATURE CITED

- (1) Skelton, R. A.; Marston, R. E.; Painter, G. D. *The Vinland Map and the Tartar Relation*; Yale University Press: New Haven and London, 1965.
- (2) McCrone, W. C.; McCrone, L. B. *Geol. J.* 1974, 140, 212-214 Part II.
- (3) McCrone, W. C. *Anal. Chem.* 1978, 48, 676A-679A.

- (4) *Pigment Handbook*; Patton, Temple C., Ed.; Wiley: New York, 1973; Vol. I, p 7.
- (5) Wallis, Helen, private communication.
- (6) Olin, Jacqueline S., Private communications.
- (7) Cahill, T. A.; Schwab, R. N.; Kusko, B. H.; Eldred, R. A.; Möller, G.; Dutschke, D.; Wick, D. L.; Pooley, A. S. *Anal. Chem.* 1987, 59, 829-833.

RECEIVED for review August 13, 1987. Accepted February 1, 1988.

## Plasticized Poly(vinyl chloride) Properties and Characteristics of Valinomycin Electrodes. Current-Time Responses to Voltage Steps

Michael L. Iglehart and Richard P. Buck\*

Department of Chemistry, University of North Carolina, Chapel Hill, North Carolina 27514

György Horvai and Ernő Pungor

Technical University of Budapest, Gellért tér 4, 1111 Budapest XI, Hungary

**Approximate analysis of current-time transients in the Kval<sup>+</sup> ion-carrier system can be done for short- and long-time responses. The whole transport problem is nonlinear, but good approximations are possible for fixed-site membranes. A unique value of  $D_{val}$ , calculated from short- and from long-time data, agrees with the steady-state value already reported. There is no evidence for K<sup>+</sup> hopping; motion of Kval<sup>+</sup> from fixed site-to-site with back diffusion of free valinomycin is sufficient to explain transient and steady-state responses.**

Current-time curves of electrochemical systems are determined in the course of defining and understanding normal behavior. Current-time curves of metal electrode/electrolyte interfaces show up two of the characteristic phenomena in conventional electrochemistry: mass transport controlled fluxes at reversible interfaces and surface kinetic control of fluxes at electrochemically irreversible interfaces. Although transient analysis is not as common for membrane systems, theoretical treatment (1) and an experimental example of detailed current-time curve analysis of a fully dissociated mobile site membrane system exist (2). Digital simulation methods can be used for a variety of transient response analyses (3, 4). Transients have also been analyzed for simple, fixed-site systems as well (5-7). Kinetic parameters of neutral carriers have been measured from current-time transients of lipid bilayers (siteless membranes) bathed in aqueous solutions (8, 9).

More complicated kinetic situations can often be diagnosed from deviations of  $I-t$  curves from expected behavior of simpler systems. One of these is the case of a reversible interfacial process combined with a high-resistance electrolyte treated by Chapman and Newman (10). The results reported in this paper bear a formal resemblance to their system, even though we are dealing with an ionic conductor (the PVC membrane) bathed on two sides by low-resistance electrolytes. The fixed site, neutral carrier PVC membrane behaves as a resistance

at short times after application of a voltage step. Subsequently, concentration polarization of the neutral carrier, valinomycin, confers diffusion control and a limiting current that is generally less, but can approach, the short-time ohmic current value. Mathematically, the two physical systems are coupled in similar ways and give similar  $I-t$  curves, although the details of interfacial potentials are quite different.

In the five preceding papers of this series (11-15), the presence of membrane-trapped, anionic, fixed impurity sites in commercial poly(vinyl chloride) (PVC) has been demonstrated by a number of techniques and analysis of resulting electrochemical effects. Ordinarily, the conclusion to be drawn is that the membranes are simply fixed, low-site density ion exchangers. In the absence of Donnan exclusion failure conditions, current-voltage curves would be entirely ohmic at all sensible applied voltages, and current-time curves would be uninteresting constant values for all times after the interfacial double layer charging. The experimental  $I-V$  results (14) are quite different and resemble mobile-site ion exchanger curves with limiting currents at applied voltages above the ohmic region (16-18). These results have been interpreted by the steady-state carrier mechanism, Morf's "closed loop" process (19), with an amended ion budget, in which current at high applied voltages is controlled by consumption and release of neutral carrier at the two membrane-electrolyte interfaces and the consequent linear concentration polarization profile of carrier throughout the membrane.

This paper continues the observations on neutral carrier behavior in low site density, fixed-site membranes. The basic reversible interfacial potential equations and IR terms are now viewed in the transient state. The flux equation for neutral carrier is developed and the two terms are analyzed, but not solved, to suggest the expected form of the  $I-t$  response at applied voltages in the ohmic, transition, and limiting current regions as defined and illustrated in part IV (14). Unfortunately, this transport problem is nonlinear and defies analytical solution. However, the form of the  $I-t$  response at short, and separately at long times, can be determined. De-

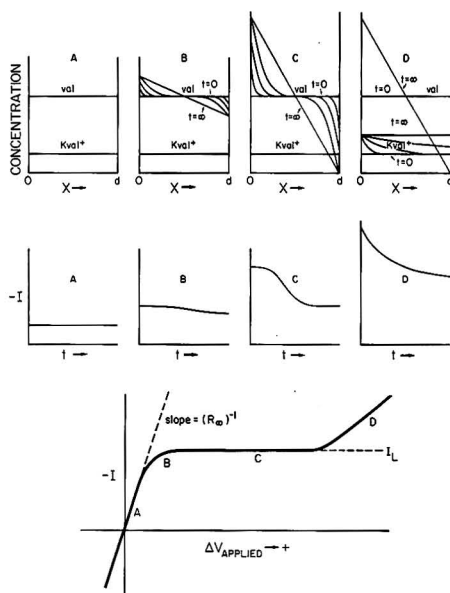


Figure 1. Composite view of carrier concentration profiles,  $I$ - $t$  curves and steady-state  $I$ - $V$  curve: upper panels A-D, concentration-distance plots; middle panels A-D, current-time curves; lower, current-voltage.

pendence of the current on carrier loading and on applied voltage define the controlling processes and the principal terms in the response function.

### MODEL

Normal PVC membranes contain fixed negative sites at low concentrations,  $\approx 0.05$ – $0.5$  mM (15), typically  $0.1$  mM in our system. The normal valinomycin loading is  $\approx 10$  mM, and the concentration of  $\text{Kval}^+$  is the same as the negative sites, while free  $\text{K}^+$  is negligibly small. The  $I$ - $V$  curve is easily divided into three or four typical parts and there are corresponding  $I$ - $t$  curves expected for each  $I$ - $V$  segment. The different  $I$ - $t$  curves arise from the corresponding free valinomycin concentration profiles and their changes with time. The model is summarized in Figure 1 where the concentration-distance-time profiles of carrier, corresponding  $I$ - $t$  curves, and steady-state  $I$ - $V$  curves are illustrated schematically.

At low applied voltages, A, the  $I$ - $t$  curve is a constant (in time) and depends only on applied voltage because current is carried by  $\text{Kval}^+$ , while back diffusion of valinomycin is sufficiently rapid that only small interfacial potential changes result from the profile tipping. There must be some concentration polarization of carrier for all finite currents, but it is not until the surface concentration on the depletion side interface is nearly zero that a significant portion of applied voltage appears at the depletion interface, rather than across the membrane bulk. The length of region A, on the applied voltage axis, depends on the size of the valinomycin diffusion coefficient.

In regions B and C, the initial current is the appropriate ohmic value determined by applied voltage and resistance of  $\text{Kval}^+$  motion. At each succeeding period of time, the carrier concentration rises at  $x = 0$  and decreases at  $x = d$  for negative currents (positive applied voltages  $V_{\text{applied}} = \phi_1 - \phi_2$ ). The  $\phi$ 's are inner potentials of the solutions on either side of the membrane.  $V_{\text{applied}}$  appears as these solution potentials when

the voltage is applied to two identical junction-type reference electrodes, junction potentials are equal, and  $IR$  drops in the bathing electrolytes are small and negligible. Note that the constancy of current implies that carrier concentration profiles remain parallel to each other, e.g. have equal slopes at  $x = 0$  and  $x = d$  at each instant of time. At some later time, the surface carrier concentrations reach steady values. Redistribution of carrier occurs until the steady-state profile is reached which is linear across the membrane and has a higher value than  $\bar{V}$  at  $x = 0$  and a lower value at  $x = d$ .  $\bar{V}$  is the average carrier concentration. The midcell value remains at  $\bar{V}$ . In B, the surface concentrations of carriers have not reached the extreme values that correspond to the limiting current. In the limiting current region C, ohmic current at  $t = 0$  is maintained until the surface concentration of carrier has risen at  $x = 0$  to  $2\bar{V}$  and reached zero at  $x = d$ . Current falls while the carrier becomes distributed in a linear way across the membrane. These statements are illustrated schematically, but not precisely, in Figure 2.

These deductions are based on the forms of the equations and on the experimental results. It is not clear what happens at high applied voltages in region D. The current starts at the ohmic value, but there is an almost immediate decrease that does not compare with backward running "flattened S" curves for regions A-C. It is likely that anions from the electrolytes are no longer excluded, and the total salt, as  $\text{Kval}^+\text{Cl}^-$ , rises in the membrane especially on the side with excess carrier. This result, in panel D, shows the  $\text{Kval}^+$  concentration line moving from the low value set by site concentration, to a higher value at each new applied voltage, corresponding to the observed higher steady-state currents above the limiting value.

### MODEL MATHEMATICS

Originally by Morf, Wuhmann, and Simon (19), and again in part III (13), it was shown that the total voltage across the membrane can be expressed as three terms:  $IR_m$  and two interfacial potential differences (pds). From the time domain, this equation transformed is

$$V_{\text{applied}}/s = -I(s)R_m + \mathcal{L}(RT/F) \ln (C_v(x=0)/C_v(x=d)) \quad (1)$$

$V_{\text{applied}}$  or  $V_{\text{applied}}$  is the applied voltage,  $s$  is the Laplace transform variable,  $I$  is the current and a function of time,  $I(s)$  is the transformed current,  $R_m$  is the high-frequency resistance,  $R$  is the gas constant,  $T$  is temperature, and  $F$  is the Faraday. Valinomycin concentrations are in parentheses (val) or  $C_v$ , with  $x$  the spacial membrane coordinate. The concentration of valinomycin  $C_v$  is subject to two constraints: the total carrier concentration remains constant, and the fluxes at the boundaries are equal and proportional to the current. Thus the boundary concentration transforms have a familiar form

$$C_v(s) = \bar{V} \pm [I(s)/FA(D_{\text{val}}s)^{1/2}] \tanh [(s/d)^{1/2}(d/2)] \quad (2)$$

where the plus applies to  $x = d$  and minus to  $x = 0$ . The concentration profile, in the steady state is

$$C_v(x) = C_v(x=0) + (2\bar{V} - C_v(x=0))x/d \quad (3)$$

and the limiting current,  $I_L$ , in the plateau region is

$$I_L = 2FA\bar{V}D_{\text{val}}/d \quad (4)$$

This result is found from eq 2 by passing to the limit of  $sI(s)$  as  $s \rightarrow 0$ . A linear concentration profile of lesser slope can be found at other lower voltages, as well. The transformed  $I$ - $V$  curve is found by substituting eq 2 into eq 1. The  $I$ - $V$  curve in the time domain cannot be obtained by inversion because

Table I. Transition Times for DNA Membranes<sup>a</sup>

$\bar{V}/I$ , mol/(cm <sup>3</sup> A)	$\tau^{1/2}$ , s <sup>1/2</sup>	$\bar{V}/I$ , mol/(cm <sup>3</sup> A)	$\tau^{1/2}$ , s <sup>1/2</sup>
0.222	1.82	2.13	15.4
0.433	3.31	2.16	15.9
0.498	3.99	2.40	18.4
0.499	4.05	2.45	20.9
0.512	4.22	2.63	19.5
0.676	5.15	2.82	20.7
2.08	15.6	2.84	22.2

<sup>a</sup> Slope,  $7.57 \pm 0.2$ ;  $Y$  int,  $0.1 \pm 0.4$ ; correlation coefficient, 0.995;  $D_{\text{val}}$ ,  $(1.27 \pm 0.04) \times 10^{-6}$  cm<sup>2</sup>/s.

of the great nonlinearity. However the general expression can be formally written

$$V_{\text{applied}}(\text{right-left}) = -IR_{\infty} - \frac{\bar{V} + \mathcal{L}^{-1} \frac{I(s)}{FA(D_{\text{val}}s)^{1/2}} \tanh [(S/d)^{1/2}(d/2)]}{(RT/F) \ln \frac{\bar{V} - \mathcal{L}^{-1} \frac{I(s)}{FA(D_{\text{val}}s)^{1/2}} \tanh [(s/d)^{1/2}(d/2)]}{\bar{V}}} \quad (5)$$

Equation 5 shows that the applied voltage is distributed over two terms. In the ohmic region, eq 5 is dominated by the  $IR$  term because the (val) profile changes only slightly from the initial constant value across the membrane for each applied voltage. In region A, any changes in the surface (val) are not sufficiently large to cause the second term in eq 5 to dominate the first, ohmic term. The transition region occurs when the first term dominates initially, but both terms are comparable in the steady state. This means that the surface concentrations of valinomycin are significantly perturbed by the higher currents. In the plateau region, the first term dominates at short times, but the second term controls in the steady state because the valinomycin concentration at one interface approaches zero.

Relatively more complete analysis of the  $I$ - $t$  curves can be done for applied voltages in the plateau region C. It happens that the initially ohmic current drives the surface concentrations of carrier to the steady-state conditions before the concentration profiles of carrier become sufficiently perturbed in the membrane interior to affect the slopes of valinomycin concentrations at the interfaces. One can then treat the current-driven buildup at one interface and depletion at the other without worry about interactions because we can assume that some of the membrane interior maintains a constant carrier concentration. During this initial time period  $I$  remains constant at the ohmic value. Of course, this is a gross simplification because  $I$  does not remain constant over a significant fraction of the transition time. However, at the surfaces, concentrations obey approximately

$$C_v = \bar{V} \pm 2V_{\text{applied}} t^{1/2} / FAR_{\infty} (D_{\text{val}} \pi)^{1/2} \quad (6)$$

Defining  $\tau$  in the usual way

$$\tau^{1/2} = FA \bar{V} (D_{\text{val}} \pi)^{1/2} / 2(V_{\text{applied}} / R_{\infty}) \quad (7)$$

the initial period of nearly constant current should persist to about time  $\tau/4$  to  $\tau/2$  according to

$$I(t) = I(t = 0) - (RT/FR_{\infty}) \ln \{ [1 + (t/\tau)^{1/2}] / [1 - (t/\tau)^{1/2}] \} \quad (8)$$

This approximation is not expected to hold at all times prior to  $t = \tau$  because it predicts the current drops to zero. Experimentally, the initial approximation must merge smoothly into the long-term response.

These initial current regions, behaving like induction periods, are more abrupt at each increasing applied voltage along

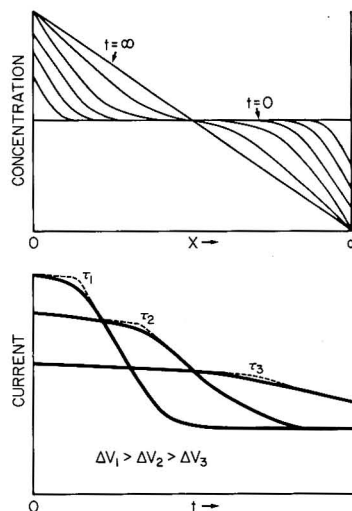


Figure 2. Schematic version of time-dependent carrier-distance profiles, carrier surface concentrations vs time, and current-time plots for different applied voltages along the plateau (limiting) current.

Table II. Transition Times for DOS Membranes

$\bar{V}/I$ , mol/(cm <sup>3</sup> A)	$\tau^{1/2}$ , s <sup>1/2</sup>	$\bar{V}/I$ , mol/(cm <sup>3</sup> A)	$\tau^{1/2}$ , s <sup>1/2</sup>
0.30	2.17	1.25	9.49
0.32	2.33	1.91	14.4
0.35	2.96	1.98	16.2
0.36	2.79	2.02	15.7
0.39	2.88	2.08	16.2
0.53	4.24	2.20	16.6
0.69	5.48	2.22	17.8
0.70	5.74	2.30	19.1
0.76	5.57	2.40	18.7
0.77	6.09	2.80	21.2
1.05	7.35		

<sup>a</sup> Slope,  $7.84 \pm 0.12$ ;  $Y$  int,  $-0.08 \pm 0.2$ ; correlation coefficient, 0.998;  $D_{\text{val}}$ ,  $(1.36 \pm 0.02) \times 10^{-6}$  cm<sup>2</sup>/s.

the plateau, limiting current region, as shown schematically in Figure 2. Experimentally, the shortening of the induction period is very clear for a series of applied voltages. To demonstrate the effect, Table I gives the initial ohmic current values against the apparent  $\tau^{1/2}$  values for dinonyl adipate (DNA) plasticized membranes. Table II displays similar data for dioctyl sebacate (DOS) plasticized membranes. The relationship is linear for membranes with different carrier loadings,  $\bar{V}$ . The  $\tau$  values are measured by extrapolating  $I$  to the intersection with the best straight line through the breaking region. Not only do the data obey the prediction of eq 7, but calculated valinomycin diffusion coefficients agree with steady-state values.

After the initial nearly constant current region of the  $I$ - $t$  plot, current falls abruptly and eventually approaches, asymptotically, the steady-state limiting current  $I_L$ . This behavior has been treated before (20) and is a standard form in diffusion theory for finite systems. The basic solution follows from inversion of eq 2 for fixed concentrations at the boundaries. The solution, for long times arises from the exact  $\theta$  function solution

$$I(\text{long times}) = I_L [1 + 2 \exp(-4\pi^2 D_{\text{val}} t / d^2) \dots] \quad (9)$$

The interesting observation from our experimental data is that

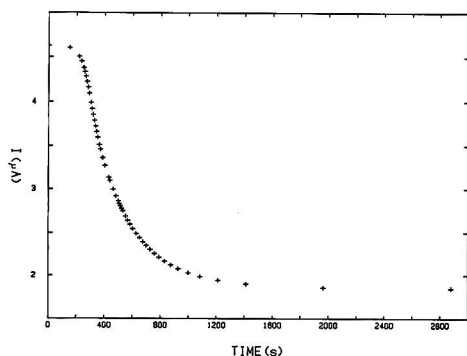


Figure 3. Current-time transient of 1.04% valinomycin membrane  $-V_{\text{appl}} = 15$  V; bathing electrolytes, 0.001 M KCl.

Table III. Correlation between Initial dc Resistance and ac Resistance

% val	plas	$I$ , $\mu\text{A}$	$V_{\text{appl}}$	$R_{\text{DC}}$ , M $\Omega$	$R_{\text{ac}}$ , M $\Omega$
0.25	DNA	10.2	55.26	5.42	5.66
0.25	DNA	12.6	55.26	5.38	4.60
0.26	DNA	1.12	4.648	4.15	4.25
0.26	DNA	1.13	4.240	3.75	3.85
1.01	DNA	20.0	54.22	2.71	2.77
1.01	DNA	17.2	55.24	3.21	3.32
1.00	DNA	14.2	55.23	3.89	3.95
1.00	DNA	4.02	17.14	4.26	4.29
1.02	DOS	18.9	55.23	2.92	2.81
1.02	DOS	4.02	10.87	2.70	2.60

the exponential form applies over a very long time period, almost from the transition time  $\tau$ .

### EXPERIMENTAL SECTION

The chemicals, apparatus, electrodes and cells, and the procedure were described in part IV (14).

### RESULTS AND DISCUSSION

The principal results of this study are the  $I$ - $t$  curves for normal membranes at applied voltages in the plateau or limiting current range. An example is shown in Figure 3. There is an initial current that declines slowly for about 250 s. The current then breaks into a sharp monotonic decrease until the steady state is reached. The initial current is exactly given by the applied voltage divided by the high-frequency resistance. Comparison of  $R_{\infty}$  calculated from  $I(t=0)$  with the width of the impedance plane semicircle is given in Table III. The width of the initial constant current region, reported as  $\tau$ , is inversely proportional to the square of the initial average current. This observation is critical to establishment of the model and is illustrated by the data in Tables I and II. The sharpness of the break-over depends on the precision of surface concentration change dependence on root  $t$ . For longer  $\tau$ 's, and therefore lower currents, concentration profile interactions across the membrane may cause some lowering of carrier slopes at the interfaces and corresponding rounding of the  $I$ - $t$  curves.

There is an inflection in the  $I$ - $t$  curves, but no center of symmetry as one sees for reversible polarographic waves. From the inflection point time, to the steady state, a plot of  $\log(I - I_L)$  vs time is linear. The slope is accurately  $-4\pi^2 D_{\text{val}}/d^2$  because the values of  $D_{\text{val}}$ , which can be independently determined, agree with other values from  $\tau$  and from  $I_L$  itself. A log plot of Figure 3 is shown in Figure 4 where recurrent positive deviations are apparent in the vicinity of  $t = \tau$ . Extrapolation of the log plot to  $t = 0$  gives the value  $3I_L$ .

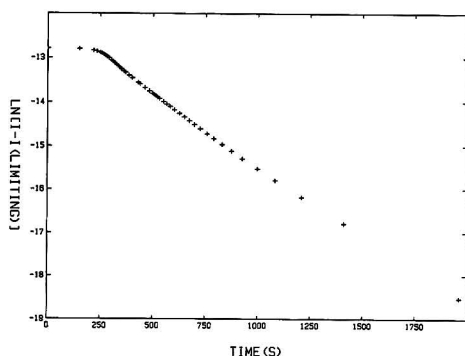


Figure 4. In plot of  $[I - I_L]$  for times from Figure 3: slope,  $-0.003418$ ; Y intercept,  $-12.13$ ; correlation coefficient,  $0.99978$ ;  $D_{\text{val}}$  from slope,  $1.40 \times 10^{-8}$  cm<sup>2</sup>/s;  $D_{\text{val}}$  from Y intercept,  $2.26 \times 10^{-8}$  cm<sup>2</sup>/s.

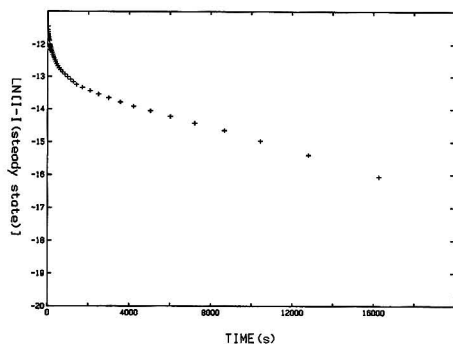


Figure 5. In plot of  $[I - I_{\text{steady state}}]$  for time transient from Donnan failure region,  $-V_{\text{appl}} = 55$  V.

Table IV. Diffusion Coefficients from Current Decay ( $\ln[I - I_L]$  vs  $t$ ) of DNA Plasticized Membranes

% val	slope	intercept	corr coef	$D_{\text{val}}$
0.24	-0.00357	-14.0	0.9952	1.70
0.26	-0.00427	-13.3	0.9991	1.83
1.00	-0.00292	-12.7	0.9990	1.25
1.00	-0.00363	-12.0	0.9950	1.56
1.03	-0.00337	-11.9	0.9970	1.44
1.47	-0.00282	-12.1	0.9998	1.24
1.47	-0.00260	-11.9	0.9976	1.26
0.99*	-0.00492	-11.0	0.9927	2.10
0.99*	-0.00454	-11.4	0.9977	1.94
1.00*	-0.00420	-11.8	0.9994	1.80

\*DOS plasticized membranes.

However, the intercept does not give an accurate indication of  $D_{\text{val}}$  because eq 9 does not apply at short times. Calculating  $D_{\text{val}}$  at the transition time as the intercept time (when diffusion control dominates) gives a value that is close to, but not in complete agreement, with other diffusion coefficients from limiting currents (14). Table IV gives an analysis of the monotonic decay of currents for membranes with 0.25–1.5% valinomycin. The average diffusion coefficient of valinomycin computed from the slope of these plots is  $1.5 \times 10^{-8}$  cm<sup>2</sup>/s while steady-state measurements give also  $1.5 \times 10^{-8}$  cm<sup>2</sup>/s. This result agrees with  $D_{\text{val}}$  measured by Thoma (21) for a similar system. Linear plots of  $\ln(I - I_{\text{steady state}})$  vs time, after

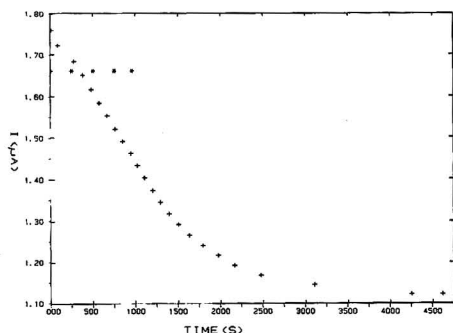


Figure 6. Low voltage current-time traces: (\*) normal membrane,  $-V_{\text{appl}} = 5.33$  V; (+) mobile site membrane,  $-V_{\text{appl}} = 0.759$  V.

the initial induction-type period, are limited to applied voltages on the plateau; at high voltages, such that Donnan exclusion fails, they become nonlinear. The induction period is nearly lost and there is no significant current range giving a linear semilog plot. This result is illustrated in Figure 5.

The low-voltage region A response is illustrated in Figure 6. The current is constant with time at low  $V_{\text{applied}}$  for normal membranes. Pure ohmic behavior is characteristic of fixed-site membranes when current is carried by a single species  $\text{Kval}^+$  and no constraints are imposed by valinomycin back diffusion. When 1.30 mM KTp-C1PB mobile sites are added to a membrane containing the same amount of carrier, current decays with time from the origin. We have not succeeded in demonstrating Cottrell behavior, but analysis of the decay reveals two time constants that vary with the membrane used, applied voltage, and previous history of a membrane. These time constants cannot be interpreted by our present theory. The low dielectric constant of these membranes prevents complete dissociation and diffusion of ion pairs complicates the interpretation.

### CONCLUSIONS

Current-time curves show an ohmic behavior at  $t = 0$  with declining values in a backward "flattened S" shaped function

of time, to the steady state. This characteristic is routinely found over a 20-V range for plateau, limiting current in the corresponding steady  $I-V_{\text{applied}}$  curves. Analysis of the  $I-t$  curves by the constant current theory for short-time behavior, and total membrane carrier polarization theory at long times, predict four different methods for determining  $D_{\text{val}}$ . Computed values by all methods must be the same if the model, with its mathematical approximations, is correct. Close agreement is found.

Registry No. PVC, 9002-86-2; DNA, 151-32-6; DOS, 2432-87-3;  $\text{Kval}^+$ , 27073-68-3; K, 7440-09-7; valinomycin, 2001-95-8.

### LITERATURE CITED

- (1) Buck, R. P. *J. Electroanal. Chem.* **1986**, *210*, 1-20.
- (2) Sandblom, J.; Walker, J. L., Jr.; Eisenman, G. *Biophys. J.* **1972**, *12*, 587-596.
- (3) Brumleve, T. R.; Buck, R. P. *J. Electroanal. Chem.* **1978**, *90*, 1-31.
- (4) Stover, F. S.; Brumleve, T. R.; Buck, R. P. *Anal. Chim. Acta* **1979**, *109*, 259-273.
- (5) Buck, R. P.; Krull, I. J. *Electroanal. Chem.* **1968**, *18*, 387-399.
- (6) Saito, T.; Yamane, R.; Mizutani, Y. *Bull. Chem. Soc. Jpn.* **1969**, *42*, 279-284.
- (7) Wikby, A.; Johansson, G. *J. Electroanal. Chem.* **1969**, *23*, 23-40.
- (8) Stark, G.; Ketterer, B.; Benz, R.; Lauger, P. *Biophys. J.* **1971**, *11*, 981-994.
- (9) Laprade, R.; Ciani, S.; Eisenman, G.; Szabo, G. *Membranes*; Eisenman, G., Ed.; Marcel Dekker: New York, 1975; Vol. 3, Chapter 3.
- (10) Chapman, T. W.; Newman, J. J. *Phys. Chem.* **1967**, *71*, 241-245.
- (11) Horvai, G.; Graf, E.; Toth, K.; Pungor, E.; Buck, R. P. *Anal. Chem.* **1986**, *58*, 2735-2740.
- (12) Toth, K.; Graf, E.; Horvai, G.; Pungor, E.; Buck, R. P. *Anal. Chem.* **1986**, *58*, 2741-2744.
- (13) Buck, R. P.; Toth, K.; Graf, E.; Horvai, G.; Pungor, E. *J. Electroanal. Chem.* **1987**, *223*, 51-66.
- (14) Iglehart, M. L.; Buck, R. P.; Pungor, E. *Anal. Chem.* **1988**, *60*, 290-295.
- (15) Lindner, E.; Graf, E.; Niegels, Z.; Toth, K.; Pungor, E.; Buck, R. P. *Anal. Chem.* **1988**, *60*, 295-301.
- (16) Conti, F.; Eisenman, G. *Biophys. J.* **1966**, *6*, 227-246.
- (17) Walker, J. L., Jr.; Eisenman, G. *Biophys. J.* **1966**, *6*, 513-533.
- (18) Sandblom, J.; Eisenman, G.; Walker, J. L., Jr. *J. Phys. Chem.* **1967**, *71*, 3871-3878.
- (19) Mori, W. E.; Wuhrmann, P.; Simon, W. *Anal. Chem.* **1976**, *48*, 1031-1040.
- (20) Mori, W. E.; Simon, W. *Helv. Chim. Acta* **1986**, *69*, 1120-1131.
- (21) Thoma, A. P. Dissertation, Swiss Federal Institute of Technology, Zurich, 1977.

RECEIVED for review September 25, 1987. Accepted December 29, 1987. Support from NSF (under Grants CHE8406976 and INST-8403331) and the Hungarian Academy of Sciences is gratefully acknowledged.



# Analytical and Mechanistic Aspects of the Electrochemical Oxidation of Keto Steroids Derivatized with Phenylhydrazine, (4-Nitrophenyl)hydrazine, and (2,4-Dinitrophenyl)hydrazine

Alan M. Bond,\* Anthony F. Hollenkamp, and Stephen B. Thompson

*Division of Chemical and Physical Sciences, Deakin University, Waurn Ponds, Victoria 3217, Australia*

Anthony R. Bourne, Peter A. Huf, and Thomas G. Watson\*

*Division of Biological and Health Sciences, Deakin University, Waurn Ponds, Victoria 3217, Australia*

The electrochemical oxidation of biologically important 3- and 17-keto steroids derivatized with phenylhydrazines has been investigated at platinum and glassy carbon electrodes in aqueous methanol. The oxidation process has been used in the amperometric detection of keto steroids in nonmammalian biological fluids after separation by reverse-phase liquid chromatography. The derivatization was shown to be quantitative, and the response linear with the detection limit of 1–5 ng for injection volumes of 20  $\mu$ L. Voltammetric studies on various nitro derivatives of phenylhydrazine and their corresponding phenylhydrazones show that the oxidation process occurs at the hydrazine moiety and not the nitro group. Coulometric data indicate the occurrence of a two-electron transfer and mass spectroscopic evidence indicates that the immediate product is a diazene which reacts with methanol. Chemical oxidation and polymerization of the products occur if the electrochemically oxidized solution is left exposed to the atmosphere. The mechanism proposed for the underivatized phenylhydrazines is then  $RNHNH_2 \rightarrow RN=NH + 2H^+ + 2e^- \rightarrow$  further products, with a related mechanism applying for oxidation of steroid hydrazones.

Voltammetric (polarographic) methods for the determination of keto steroids have usually been based on reduction of the ketone group (1–4) which occurs at relatively negative potentials. The use of these reduction processes requires the removal of oxygen which is notoriously difficult if separation procedures, such as high-performance liquid chromatography (HPLC), are coupled with electrochemical detection in a flow-through configuration (5, 6). Additional problems with electrode stability and less favorable detection limits have weighed against the use of reductive detection modes (6). The advantage of using oxidation rather than reduction processes at mercury electrodes has recently been described for some acetylenic steroids (7, 8). Analytical methods based on direct oxidation have also been developed for phenolic (9) and other non-carbonyl-containing steroids (10).

If the advantages of using electrochemical oxidation processes for keto steroids rather than reduction processes are to be exploited in a general sense at solid electrodes, then derivatization is necessary. Recently some 17-keto steroids and their sulfates have been detected in urine by electrochemical oxidation after separation by reverse-phase HPLC with precolumn derivatization using (4-nitrophenyl)hydrazine which is commonly known as (p-nitrophenyl)hydrazine (pNPH) (11, 12). The derivatization can also be undertaken with phenylhydrazine (PH) and (2,4-dinitrophenyl)hydrazine (DNPH). The mono- and dinitrohydrazones can be detected in either an oxidative or reductive mode, but the detection limits for reduction are less favorable (13, 14). Colorimetric

methods for detection of the nitrophenyl derivatives of keto steroids are relatively insensitive (15–19).

The presence of keto steroids in vertebrates and invertebrates has been well documented (20). As well as the 17-keto steroids that have been examined previously (11), a need exists for detecting 3- and 11-keto steroids, which are also biologically significant. For example epitestosterone and testosterone have been identified in lizards (21, 22) and 11-keto testosterone in fish (23, 24).

In the present paper the general applicability of the derivatization method with oxidative electrochemical detection to a wide range of keto steroids will be demonstrated. The methodology has been applied to plasma obtained from the lizard *Tiliqua rugosa* (25). A survey of the literature has shown that mechanistic aspects of keto steroid oxidation have not been investigated although polarographic reduction studies have been reported (26). Based on data obtained from cyclic voltammetry, rotating disk electrode (RDE) voltammetry, and controlled-potential electrolysis (CPE), a mechanism is proposed for the electrochemical oxidation of derivatized 3- and 17-keto steroids.

## EXPERIMENTAL SECTION

**Chemicals.** Steroids and phenylhydrazines were obtained from Sigma Chemicals (St. Louis, MO). In all experiments in aqueous media, potassium dihydrogen phosphate (analytical reagent (AR) grade, BDH) was used at a buffer strength of 0.5% in deionized water, the pH being adjusted with orthophosphoric acid (AR grade, BDH) to pH 3.0 unless otherwise stated. Methanol (AR grade, BDH) was distilled before use. The solvents used for electrochemical studies were methanol–buffer mixtures (8:2). For HPLC with electrochemical detection the addition of tetrahydrofuran (THF, AR grade, BDH) or acetonitrile (HPLC grade, Mallinckrodt) at 10% by volume to the mobile phase was required. Prior to HPLC, the mobile phase was passed through a 0.45- $\mu$ m filter (Millipore Corp.).

**Instrumentation.** Voltammetric measurements were made at 20 °C with a Princeton Applied Research (PAR) Model 174A polarographic analyzer. Electrode potentials were measured against an aqueous Ag/AgCl (3 M KCl) reference electrode. The counter electrode was a platinum wire and working electrodes were either platinum or glassy carbon disks polished with alumina. The electrodes were either used in the stationary mode (cyclic voltammetry) or rotated with a Metrohm Model 628-10 drive unit in conjunction with a Metrohm Model 628-50 electrode assembly. CPE and coulometric studies were undertaken with a PAR Model 173 potentiostat/galvanostat in conjunction with a PAR Model 179 digital coulometer. The reference electrode was the same as that used for voltammetry. The counter electrode was isolated from the test solution by a salt bridge. The working electrode was either a platinum gauze or a glassy carbon rod assembly. Electron impact mass spectrometric studies on the products of CPE experiments were carried out with a Finnigan 3200 system.

The instrumentation was periodically calibrated in the methanol–buffer solvent using the reversible oxidation of  $10^{-3}$  M ferrocene. This process possessed a reversible half-wave potential

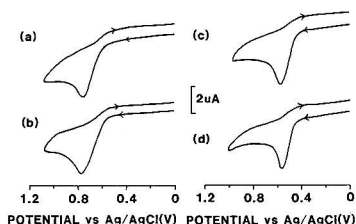


**Figure 1.** Cyclic voltammograms at a glassy carbon electrode for the oxidation of  $3 \times 10^{-4}$  M steroid (*p*-nitrophenyl)hydrazones in methanol-buffer: (a) DHA, (b) A, (c) T, and (d) DHT. Scan rate =  $100 \text{ mV s}^{-1}$ .  $T = 20^\circ \text{C}$ .

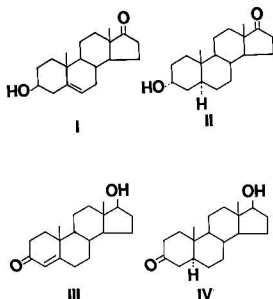
( $E_{1/2}$ ) of  $0.40 \text{ V}$  vs Ag/AgCl under these conditions. Coulometric monitoring of the oxidative electrolysis of ferrocene in the same solvent showed the expected one-electron transfer.

The HPLC system used consisted of a Waters M-45 solvent delivery pump, Rheodyne injector, Model 7125 (sample loop of  $20 \mu\text{L}$ ), and  $\text{C}_{18}$  reverse-phase columns (Extach: length,  $25 \text{ cm}$ ; width,  $4.6 \text{ mm}$ ; particle size,  $5 \mu\text{m}$ ). Waters:  $300 \times 2.9 \text{ mm}$ ; particle size,  $10 \mu\text{m}$ ). Electrochemical detection was achieved with a Bioanalytical Systems Model LC-3A amperometric detector using a Model TL-5A glassy carbon working electrode, platinum counter electrode, and an aqueous Ag/AgCl ( $3 \text{ M KCl}$ ) reference electrode. A Milton Roy Model C1-10 digital integrator and recorder was used to quantify the chromatograms.

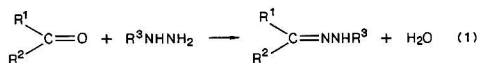
**Procedures.** Acetylation of steroids was undertaken in pyridine-acetic anhydride (1:1) by heating at  $50^\circ \text{C}$  for 2 h and then removing the solvent under vacuum. Steroids were derivatized with phenylhydrazines in the analytical work by heating in benzene/acetic acid (10:1) at  $80^\circ \text{C}$  for 10 min. The solvent was then evaporated and the residue reconstituted in the appropriate solvent.

## RESULTS AND DISCUSSION

Structural representations of the steroids studied in this work are given below (structures I–IV). The derivatization



of these compounds takes place according to eq 1. The cyclic



steroid + hydrazone  $\rightarrow$  steroid hydrazone +  $\text{H}_2\text{O}$

$\text{R}^3 = \text{C}_6\text{H}_5-$ ,  $4-(\text{NO}_2)\text{C}_6\text{H}_4-$ ,  $2,4-(\text{NO}_2)_2\text{C}_6\text{H}_3-$

voltammograms of the four steroids derivatized with *p*NPH give well-defined oxidation waves as shown in Figure 1. The derivatives of the 17-keto steroids (dehydroepiandrosterone (DHA, I) and androsterone (A, II)) both exhibit chemically irreversible oxidation responses in methanol-buffer which have peak potentials ( $E_p^{\text{ox}}$ ) of  $0.74$  and  $0.76 \text{ V}$  vs Ag/AgCl, respectively (scan rate ( $\nu$ ) =  $200 \text{ mV s}^{-1}$ ). The 3-keto steroid

**Table I.** Cyclic Voltammetric Data<sup>a</sup> for the Oxidation of Some Steroid (*p*-Nitrophenyl)hydrazones in Methanol-Buffer (80:20) at  $20^\circ \text{C}$

steroid <sup>c</sup>	peak potential, <sup>b</sup> V
androsterone (A)	0.76
dehydroepiandrosterone (DHA)	0.74
testosterone (T)	0.57
5 $\alpha$ -dehydrotestosterone (DHT)	0.58

<sup>a</sup> Glassy carbon electrode, scan rate =  $200 \text{ mV s}^{-1}$ . <sup>b</sup> V vs Ag/AgCl.  $E_{1/2}[(\text{C}_5\text{H}_5)_2\text{Fe}^+ / (\text{C}_5\text{H}_5)_2\text{Fe}] = 0.400 \text{ V}$  vs Ag/AgCl. <sup>c</sup> Steroid concentration =  $3 \times 10^{-4} \text{ M}$ .

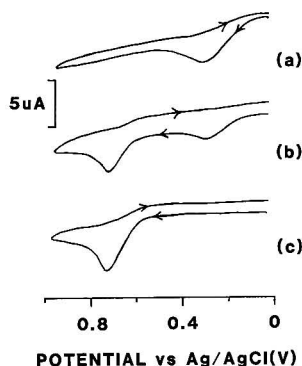


**Figure 2.** Cyclic voltammograms at glassy carbon for the oxidation of  $3 \times 10^{-4} \text{ M}$  (a) *p*NPH, (b) DHA-*p*NPH hydrazone with excess *p*NPH present, and (c) DHA-*p*NPH hydrazone, in methanol-buffer. Scan rate =  $100 \text{ mV s}^{-1}$ .  $T = 20^\circ \text{C}$ .

derivatives (dihydrotestosterone (DHT, IV) and testosterone (T, III)) also exhibit an irreversible oxidation process, but at less positive potentials. The medium chosen for the electrochemical study was similar to that used in chromatography, and the electrochemical data are summarized in Table I. The compound *p*NPH is oxidized at  $0.45 \text{ V}$  vs Ag/AgCl which is at a considerably less positive potential than the derivatized steroid species.

Figure 2 shows cyclic voltammograms for *p*NPH with increasing concentration of the steroid (DHA). In the absence of any 3-keto steroid (Figure 2a) a single chemically irreversible process is observed at  $0.45 \text{ V}$  vs Ag/AgCl. In the presence of steroid and when the concentration ratio of DHA:*p*NPH is less than 1:1, the cyclic voltammogram (Figure 2b) shows two peaks, one due to the steroid hydrazone ( $E_p = 0.74 \text{ V}$  vs Ag/AgCl) and one due to unreacted *p*NPH. The latter is not present when the ratio reaches or exceeds 1:1 (Figure 2c). Data obtained from these experiments confirm that the derivatization reaction is quantitative.

The peak height, wave shape, and position of the oxidation process for the steroid hydrazones were almost independent of pH over the range  $2.0$ – $4.6$  in the methanol-buffer mixture. That is the peak height is constant at the  $\pm 5\%$  level and peak position at the  $\pm 10 \text{ mV}$  level. (The pH was altered by changing the concentration of phosphoric acid and the figure refers to the pH of the buffer solution prior to the addition of methanol (80% (v/v)).) Data for solutions of the phenylhydrazines also show behavior that is almost independent of pH. These results suggest that the rate-determining part of the electrochemical oxidation process does not include acid-base terms over the pH range of investigation.

Cyclic and rotating disk voltammograms at a glassy carbon electrode were carried out on the phenylhydrazines and their respective steroid (DHA) phenylhydrazones. The data are

**Table II. Voltammetric Data<sup>a</sup> for the Oxidation of PH, *p*NPH, and 2,4-dNPH and Their Respective DHA-Hydrazones in Methanol-Buffer (80:20) at 20 °C**

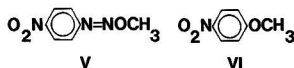
	cyclic voltammetry <sup>b</sup>	rotating disk voltammetry <sup>c</sup>	
	$E_p^{ox}$ , e V	$E_{1/2}$ , e V	$i_l/c$ , e mA M <sup>-1</sup>
A. Hydrazine			
PH	0.41	0.36	124
<i>p</i> NPH	0.45	0.39	137
2,4-dNPH	0.58	0.54	189
B. DHA/-Hydrazone			
DHA-PH	0.52	0.46	95
DHA- <i>p</i> NPH	0.74	0.70	150
DHA-2,4-dNPH	1.06	1.00	203

<sup>a</sup> Glassy carbon electrode. <sup>b</sup> Scan rate = 200 mV s<sup>-1</sup>. <sup>c</sup> Rotation rate = 2000 rpm. <sup>d</sup> Limiting current per unit concentration. <sup>e</sup> V vs Ag/AgCl.  $E_{1/2}[(C_6H_5)_2Fe^+/(C_6H_5)_2Fe] = 0.400$  V vs Ag/AgCl. /DHA, dehydroepiandrosterone.

summarized in Table II. The important aspects of these data are that the oxidation potential is a function of the degree of nitro substitution for both the hydrazines and the steroid hydrazones. Interestingly the current per unit concentration, at a rotating disk electrode, also increases with increasing nitro substitution but remains constant for a given hydrazine-hydrazone pair. From these data the conclusion is reached that the oxidation process for the derivatized steroid is based on the hydrazine moiety and not the nitro groups.

Exhaustive controlled-potential electrolysis (CPE) of derivatized (*p*NPH) DHA at 1.0 V vs Ag/AgCl at a glassy carbon electrode resulted in the transfer of  $1.8 \pm 0.1$  faraday mol<sup>-1</sup>. Cyclic voltammetry confirmed that the reaction had proceeded to completion at this stage. Electrode fouling during the course of the CPE experiments caused difficulties in completing the electrolysis and the working electrode needed periodic cleaning throughout the experiment. CPE of *p*NPH at a platinum or glassy carbon electrode at 0.50 V vs Ag/AgCl in methanol-buffer resulted in the passage of  $2.0 \pm 0.1$  faraday mol<sup>-1</sup> of charge. Since the hydrazines are easier to oxidize than the steroid hydrazones, their oxidation behavior may be studied at both platinum and glassy carbon electrodes. The superior positive potential range of glassy carbon facilitates studies of the oxidation processes for the derivatized keto steroids at this electrode surface. However, the mechanism shows no indication of changing with electrode material.

Examination of the products from CPE of *p*NPH was undertaken by extracting the CPE solution into dichloromethane and examining the residue obtained after evaporation by mass spectrometry (MS). The two principal products identified are shown below (structures V and VI). These compounds



were identified by their *m/e* values and fragmentation patterns. The presence of structure V was indicated by a response with *m/e* 181 (M<sup>+</sup>) and *m/e* 135 ([M - NO<sub>2</sub>]<sup>+</sup>), while for structure VI, *m/e* 153 (M<sup>+</sup>), *m/e* 138 ([M - CH<sub>3</sub>]<sup>+</sup>), and *m/e* 107 ([M - NO<sub>2</sub>]<sup>+</sup>). Also evidence for the protonated diazene intermediate (see eq 2) was given by the response with *m/e* 152. Other unidentified products were also formed. On standing, the electrolysis solution yielded a greater complexity of species with MS now showing a number of high molecular weight compounds. MS of the residue from solutions of steroid hydrazones after CPE showed species V without species VI, although other unidentified products also are formed.

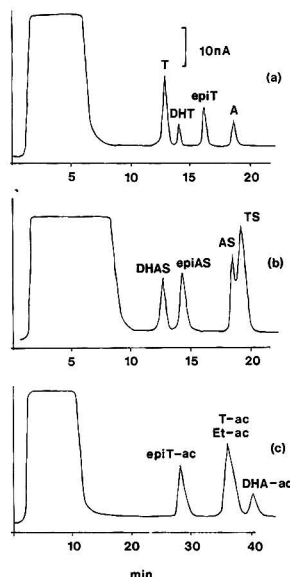
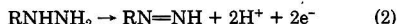
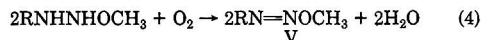
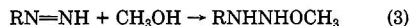


**Figure 3.** Chromatograms for typical separations of steroid standards derivatized with *p*NPH: (a) Free steroids, 5-μm reverse-phase column; solvent, methanol:buffer:THF, 7:2:1; T, testosterone; DHT, 5α-dihydrotestosterone; epiT, epitestosterone; A, androsterone. (b) Steroid sulfates, 10-μm reverse-phase column; solvent, methanol:buffer 7:2; DHAS, dehydroepiandrosterone sulfate; epiAS, epiandrosterone sulfate; AS, androsterone sulfate; TS, testosterone sulfate. (c) Steroid acetates, 5-μm reverse-phase column; solvent, methanol:buffer:acetonitrile, 4:1:1; epiT-ac, epitestosterone acetate; Et-ac, etiocholanolone acetate; DHA-ac, dehydroepiandrosterone acetate; T-ac, testosterone acetate. Concentrations are 30 ng per 20 μL injection volume. Large initial peak corresponds to excess *p*NPH.

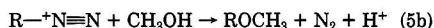
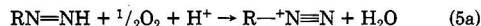
Electrochemical oxidation of hydrazines is generally agreed to involve initially the formation of diazenes (also known as diimides) as in eq 2 (27–32). The final product is determined



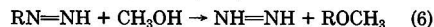
by the solvent, pH, and the presence of any acids or bases. The diazenes are very reactive and the identification of species V indicates that nucleophilic addition of methanol, followed by oxidation by oxygen, occurs as shown in eq 3 and 4. The



formation of the anisole (VI) may occur via several possible mechanisms: (a) oxidation of the diazene intermediate to 4-nitrobenzenediazonium, followed by nucleophilic substitution by methanol, with dinitrogen as the leaving group, giving the overall reaction



(b) protonation of nitrogen (adjacent to the aromatic ring), followed by nucleophilic substitution by methanol, with hydrazine as the leaving group giving an overall reaction



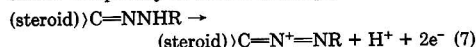
Methanolysis reactions with other diazenes have been reported previously (32, 34).

Table III. Chromatographic Data for Steroid Hydrazones<sup>a</sup>

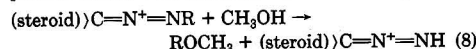
steroid	hydrazine <sup>c</sup>	capacity factor <sup>b</sup>			
		1 <sup>d</sup>	2 <sup>e</sup>	3 <sup>f</sup>	4 <sup>e</sup>
testosterone	pNPH	6.6		11.8	
	PH				6.9
epiandrosterone	pNPH	7.6			
	PH				8.2
dehydroepiandrosterone	pNPH	8.5	7.6		
	PH				6.6
etiocholanolone	pNPH	9.1		10.6	
	PH				7.5
androsterone	pNPH	9.5			
	PH				8.4
5 $\beta$ -androstenedione	PH				>16.4
epitestosterone	pNPH	8.3		10.6	
	PH				6.7
androstenedione	PH				>16.4
5 $\alpha$ -dihydrotestosterone	pNPH	7.3			
	PH				>16.4
5 $\alpha$ -epidihydrotestosterone	pNPH			11.8	
5 $\beta$ -epidihydrotestosterone	pNPH			13.7	
epitestosterone acetate	pNPH			18.5	
testosterone acetate	pNPH			24.2	
etiocholanolone acetate	pNPH			24.2	
DHA acetate	pNPH			26.9	
testosterone sulfate	pNPH		10.4		
DHA sulfate	pNPH		6.5		
etiocholanolone sulfate	pNPH		8.8		
androsterone sulfate	pNPH		10.0		
epiandrosterone sulfate	pNPH		7.0		
estrone sulfate	pNPH		4.3		
DHA glucuronide	pNPH		5.8		

<sup>a</sup> Detected at a glassy carbon electrode at 0.80 V vs Ag/AgCl.  $E_{1/2}[(C_6H_5)_2Fe^+/[(C_6H_5)_2Fe]] = 0.400$  V vs Ag/AgCl. <sup>b</sup> Capacity factor =  $(R_v - R_0)/R_0$ ,  $R_v$  = retention volume (mL),  $R_0$  = dead volume (mL). <sup>c</sup> PH = phenylhydrazine, pNPH = (p-nitrophenyl)-hydrazine. <sup>d</sup> 5- $\mu$ m reverse-phase column; solvent, methanol:buffer:THF 7:2:1. <sup>e</sup> 10- $\mu$ m reverse-phase column; solvent, methanol:buffer 7:2:1. <sup>f</sup> 5- $\mu$ m reverse-phase column; solvent, methanol:buffer:acetonitrile 4:1:1. <sup>g</sup> As for c but with ratio of solvent constituents, 5:2:3.

In the case of the steroid derivatives, a reaction that is similar to eq 2 may be written as in eq 7.



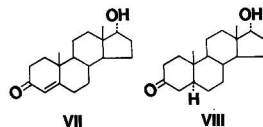
The reactive species generated will be susceptible to attack by nucleophiles present in solution and results suggest that, as in the case of the hydrazines, methanolysis of the initial product occurs. This scheme is represented in eq 8.



Mass spectral evidence has been obtained for the products of eq 8. Interestingly species VI is not detected, suggesting that retention of the nitrogen group by the steroid moiety yields a species of greater relative stability than is the case without derivatization. However, since other products are formed in addition to those identified by mass spectrometry, a complete description of the mechanism is not available.

The above electrochemical study suggests that all the keto steroids, in addition to the 17-keto steroids proposed by Shimada et al. (11, 12), should be amenable to oxidative electrochemical detection in methanol-buffer with HPLC separation. For chromatographic reasons, 10% of either THF or acetonitrile was added to the mobile phase to lower the retention times of samples. Figure 3 shows a HPLC profile for some standard steroid samples. The range of steroids detectable by this method includes the four compounds discussed above as well as the 3-keto steroids epitestosterone (VII) and dihydroepitestosterone (VIII). In addition steroid

acetates and sulfates have also been detected (refer to Table III). Detection limits obtained with this method were typically in the range 1–5 ng in an injection volume of 20  $\mu$ L. Colorimetric detection of keto steroids derivatized in a similar fashion has proven to be a much less sensitive technique (15–19).



Extensive investigations of plasma from the lizard *T. rugosa* using electrochemical detection have confirmed the presence of significant levels of the 3-keto steroids, epitestosterone and testosterone (21, 22). In addition testosterone sulfate has been identified (25). This present study employing electrochemical detection has revealed a number of new responses which have tentatively been assigned to steroids which were not previously detected with UV-based detection methods (21, 22). New steroid species detected electrochemically are undergoing further characterization in these laboratories.

**Registry No.** I, 53-43-0; I-pNPH, 113036-12-7; I-sulfate-pNPH, 113036-16-1; I-acetate-pNPH, 113036-21-8; I-hydrazone, 63015-10-1; I-pH, 113036-24-1; I-2,4-DNPH, 2497-74-7; I-acetate, 853-23-6; I-sulfate, 651-48-9; I-glucuronide, 5716-14-3; II, 53-41-8; II-pNPH, 113036-13-8; II-epi-sulfate-pNPH, 113036-17-2; II-sulfate-pNPH, 113036-18-3; II-pH, 113036-29-6; III, 58-22-0; epi-III, 481-30-1; III-pNPH, 113036-14-9; III-epi-pNPH, 113036-15-0; III-sulfate-pNPH, 113036-19-4; III-epiacetate-pNPH, 113036-20-7; III-acetate-pNPH, 113036-23-0; III-pH, 113055-93-9; III-epi-pH, 113055-94-0; III-acetate, 1045-69-8; III-epiacetate, 1425-09-8; III-sulfate, 651-45-6; IV, 521-18-6; IV-pNPH, 113055-72-4; IV-pH, 113036-30-9; V, 21857-39-6; VI, 100-17-4; pH, 100-63-0; pNPH, 100-16-3; 2,4-DNPH, 119-26-6; Et-ac-pNPH, 113036-22-9; epiandrosterone, 481-29-8; epiandrosterone-pNPH, 113036-25-2; epiandrosterone-pH, 113036-26-3; etiocholanolone, 53-42-9; etiocholanolone-pNPH, 113036-27-4; etiocholanolone-pH, 113036-28-5; 5 $\beta$ -androstenedione, 1229-12-5; androstenedione, 63-05-8; 5 $\alpha$ -epidihydrotestosterone, 571-24-4; 5 $\alpha$ -epidihydrotestosterone-pNPH, 113249-27-7; 5 $\beta$ -epidihydrotestosterone, 5692-03-5; 5 $\beta$ -epidihydrotestosterone p-nitrophenylhydrazine, 113036-31-0; etiocholanolone acetate, 1482-78-6; etiocholanolone sulfate, 977-36-6; etiocholanolone sulfate-pNPH, 113036-32-1; androsterone sulfate, 2479-86-9; epiandrosterone sulfate, 977-35-5; estrone sulfate, 481-97-0; estrone sulfate-pNPH, 113036-33-2; dehydroepiandrosterone glucuronide-pNPH, 113055-73-5.

## LITERATURE CITED

- Brezina, M.; Zuman, P. *Polarography in Medicine, Biochemistry and Pharmacology*; Interscience: New York, 1981.
- Chowdhry, B. Z. In *Polarography of Molecules of Biological Significance*; Smyth, W. F., Ed.; Academic: London, 1979.
- Kutner, W.; Debowalski, J.; Kemula, W. *J. Chromatogr.* **1980**, *191*, 47.
- Topics in Organic Polarography*; Zuman, P., Ed.; Plenum: London, 1970.
- Johnson, D. C.; Weber, S. G.; Bond, A. M.; Wightman, R. M.; Shoup, R. E.; Krull, I. *Anal. Chim. Acta* **1986**, *180*, 187.
- Laboratory Techniques in Electroanalytical Chemistry*; Kissinger, P. J.; Heineman, W. R., Eds.; Marcel Dekker: New York, 1984; Chapter 22.
- Bond, A. M.; Heritage, I. D.; Briggs, M. H. *Anal. Chim. Acta* **1982**, *138*, 35.
- Bond, A. M.; Heritage, I. D.; Briggs, M. H. *Langmuir* **1985**, *1*, 110.
- Watanabe, K.; Yoshizawa, H. *J. Chromatogr.* **1985**, *337*(A), 114.
- Samuel, A. J.; Webster, T. J. N. In *Electrochemical Detectors. Fundamental Aspects and Analytical Applications*; Ryan, T. H., Ed.; Plenum: New York, 1984; p 43.
- Shimada, K.; Tanaka, M.; Nambara, T. *Anal. Lett.* **1980**, *B13*, 1129.
- Shimada, K.; Tanaka, M.; Nambara, T. *J. Chromatogr.* **1984**, *307*, 23.
- Jacobs, W. A.; Kissinger, P. T. *J. Liq. Chromatogr.* **1982**, *5*, 881.
- Jacobs, W. A. *Curr. Sep.* **1982**, *4*, 72.
- Nishina, T.; Sakai, Y.; Kimura, M. *Steroids* **1984**, *4*, 255.
- Kimura, M.; Nishina, T. *Chem. Pharm. Bull.* **1987**, *15*, 1239.
- Kimura, M.; Nishina, T. *Chem. Pharm. Bull.* **1987**, *15*, 1242.
- Kimura, M.; Nishina, T. *Chem. Pharm. Bull.* **1987**, *15*, 1315.
- Kimura, M.; Nishina, T.; Sakamoto, T. *Chem. Pharm. Bull.* **1987**, *15*, 454.
- Sandhor, T.; Mehdi, A. Z. In *Hormones and Evolution*; Barrington, E. J. W., Ed.; Academic: New York, 1979; Chapter 1.

- (21) Bourne, A. R.; Taylor, J. L.; Watson, T. G. *Gen. Comp. Endocrinol.* **1985**, *58*, 394.
- (22) Bourne, A. R.; Taylor, J. L.; Watson, T. G. *Gen. Comp. Endocrinol.* **1986**, *61*, 278.
- (23) Kime, D. E. In *Steroids and Their Mechanism of Action in Nonmammalian Vertebrates*; Delno, G., Brachet, J., Eds.; Raven: New York, 1980; p 17.
- (24) Ozon, R. In *Steroids in Nonmammalian Vertebrates*; Academic: New York, 1972; Chapter 6.
- (25) Huf, P. A.; Bourne, A. R.; Watson, T. G. *Gen. Comp. Endocrinol.* **1987**, *66*, 364.
- (26) Brázina, M.; Volková, V.; Volke, J. *Collect. Czech. Chem. Commun.* **1954**, *19*, 894.
- (27) Cauquis, G.; Genies, M. *Tetrahedron Lett.* **1968**, *32*, 3537.
- (28) Cauquis, G.; Genies, M. *Tetrahedron Lett.* **1970**, *33*, 2903.
- (29) Eisner, U.; Zemer, Y. *J. Electroanal. Chem.* **1972**, *38*, 381.
- (30) Eisner, U.; Gileadi, E. *J. Electroanal. Chem.* **1970**, *28*, 81.
- (31) Eisner, U.; Zommer, N. *J. Electroanal. Chem.* **1971**, *30*, 433.
- (32) Glicksman, R. *J. Electrochem. Soc.* **1961**, *108*, 922.
- (33) Cohen, S. G.; Nicholson, J. *J. Am. Chem. Soc.* **1964**, *86*, 3892.
- (34) Nicholson, J.; Cohen, S. G. *J. Am. Chem. Soc.* **1966**, *88*, 2247.

RECEIVED for review June 29, 1987. Accepted December 14, 1987.

## Design, Characterization, and Applications of a Photoacoustic Cell for Temperature and Atmosphere Control

Meg M. Thompson<sup>1</sup> and Richard A. Palmer\*

P. M. Gross Chemical Laboratory, Duke University, Durham, North Carolina 27706

A photoacoustic cell designed for controlled temperature operation up to 500 °C with a flowing coupling gas is described. The compact design and the easy access to the cell windows permit use of the cell interchangeably between ultraviolet-visible-near-infrared and mid-infrared spectrometers. The separation of the sample and microphone compartments of the cell, which is necessary to protect the microphone from high temperatures, creates a Helmholtz resonator configuration for which the resonance is in the region of useful photothermal modulation frequencies. The performance characteristics of the cell, including the effects of the resonance, are illustrated, and its application to the study of thermal decomposition reactions, phase transitions, and solid-gas reactions is demonstrated.

The ability of photoacoustic spectroscopy (PAS) to provide absorption data for condensed media has led to the application of this technique to a wide range of investigations in physics, chemistry, and biology (1). The reasons for the rapid development and attention that this technique has experienced are self-evident: (1) PAS requires little to no sample preparation, (2) PAS involves direct detection of the radiation absorbed by the sample and as a result facilitates the detection of weakly absorbing species in the presence of strongly absorbing species, (3) PAS measurements are relatively insensitive to scattering and particle size effects, and (4) PAS may be used to probe the subsurface of the sample or to obtain "depth profile" information. Although most previous condensed phase photoacoustic investigations have involved examinations of samples at ambient temperatures, several laboratories have extended the conditions of the photoacoustic experiment to temperatures above and below ambient (2-17). However, of these studies, only two investigators have reported measurements above 200 °C (7, 14-17). There is also increasing interest in using photoacoustic detection for the study of solid-gas reactions in situ. In this application the cell must be compatible with a reactive coupling gas and should also provide for gas flow during spectral measurements.

This paper describes an elevated temperature photoacoustic cell with atmosphere control, which has been developed in our laboratory for use in monitoring solid-gas reactions. Results using carbon black as a broad wavelength, strong absorber illustrate the performance characteristics of the cell with respect to modulation frequency and sample temperature in both dispersive and interferometric instrumentation. In addition, the use of the cell to examine samples at elevated temperatures, as well as samples in a flowing gas stream, is demonstrated with ultraviolet-visible (UV-vis) spectral studies of the thermal decomposition of  $\text{CoCl}_2 \cdot 6\text{H}_2\text{O}$  and of the melting of indium, and a Fourier transform infrared (FTIR) spectral investigation of  $\text{Na}_2\text{CO}_3$  reacting with  $\text{SO}_2$ .

### EXPERIMENTAL SECTION

**Cell Construction.** The high-temperature photoacoustic (HT-PA) cell consists of four main parts: (1) window holder; (2) cell body; (3) microphone holder; and (4) cooling system. Figure 1 presents cross-sectional views of the cell. The stainless steel window holder ( $1\frac{1}{2}$  in. high,  $1\frac{1}{8}$  in. o.d.) is designed to hold two windows (32 mm diameter  $\times$  2 mm thick, 25 mm diameter  $\times$  2 mm thick). The windows are easily changed and may be selected for the spectral region of interest. They are held in place  $\sim$ 1 in. apart by threaded retainer rings and sealed with Teflon gaskets. The volume between the windows may be evacuated in order to provide added insulation (7) and temperature stability. The entire window holder screws into the stainless steel body of the cell such that the bottom window is 0.08 in. from the top of the sample. For operation at temperatures  $<400$  °C all seals are made with Teflon gaskets. For temperatures above 400 °C, copper is substituted for the Teflon.

The cell body houses the sample chamber, gas and microphone channels, and heater. A removable sample holder with a copper plug at its base ( $\frac{1}{2}$  in. diameter  $\times$   $\frac{1}{4}$  in. thick) fits closely into the sample chamber and rests on another copper plug at the center of the cell body. These copper plugs ( $\frac{1}{4}$  in. diameter  $\times$   $\frac{1}{8}$  in. thick) enhance the transfer of heat from the heater coil located directly below the sample chamber to the sample. In addition, the base of the sample holder is made with slanted sides (7) to prevent jamming of the holder in place due to expansion from heating. Four  $\frac{1}{8}$  in. square grooves at 90° intervals around the sides of the sample holder correspond to the positions of the gas inlet, gas outlet, and microphone channels and a positioning pin.

The gas inlet and outlet channels are made from  $\frac{1}{8}$  in. o.d. stainless steel tubing. The tubing is press fitted into holes in the cell body which are open to the sample chamber. At  $\frac{1}{16}$  in. from the sample chamber, the holes in the cell body reduce to  $\frac{1}{16}$  in.

<sup>1</sup> Current address: Lorillard Research Center, 420 North English St., Greensboro, NC 27405.

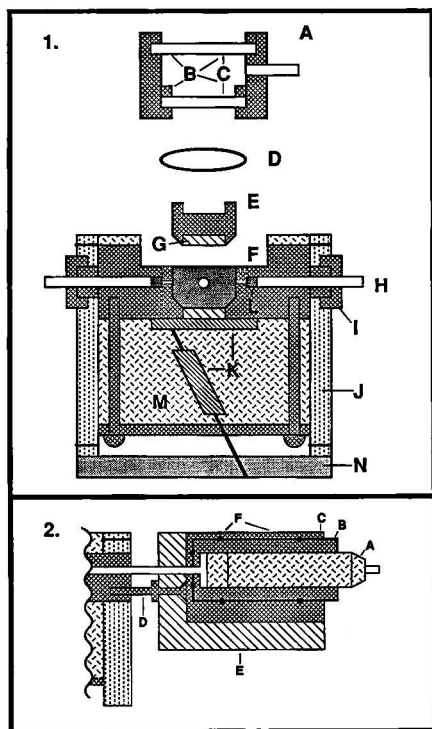


**Figure 1.** Cross-sectional view of the HT-PA: (1) front, (A) window holder, (B) stainless steel rings, (C) window, (D) gasket, (E) sample holder, (F) stainless steel cell body, (G) copper plug, (H) gas channels, (I) Swagelok fitting, (J) water-cooling jacket, (K) coil heater with insulated wire adaptor, (L) stainless steel frit, (M) insulation, (N) foam; (2) side, (A) microphone, (B) cylindrical microphone holder, (C) microphone encasing, (D) stainless steel bolt, (E) Mylar insulation, (F) O-ring.

diameter. The sample ends of the gas channel tubing are fitted with 2- $\mu$ m stainless steel frits (Alltech) and seat against this  $1/16$  in. shoulder. As demonstrated by Royce et al. (14–16) although the frits allow the gas to flow through the sample chamber, they do not significantly reduce the acoustic integrity of the cell. The tubing of the gas channels is further secured in place with stainless steel Swagelok fittings threaded into the body of the cell. The microphone channel, or acoustic coupling tube (2.1 in. long), is made of thin-walled  $1/16$  in. stainless steel tubing (1 mm i.d.). The thin-walled tubing limits the conduction of heat from the sample region to the microphone chamber.

The microphone (Bruel and Kjaer 4165) is threaded into a stainless steel cylinder  $3/4$  in. o.d. which in turn is sealed with two O-rings into the cylindrical cavity of the aluminum microphone chamber, with the microphone cylinder flush against the end of the cavity, at the end of the acoustic coupling tube. The weight of the microphone chamber is borne by two stainless steel bolts which also connect it to the cell body. The side of the microphone chamber exposed to the cell body is faced with  $1/4$  in. thick Mylar insulation.

The sample is heated by a 400-W bendable cartridge heater (0.062 in. o.d.; 31 in. long; ARI Industries, Inc.) coiled into a 2 in. diameter spiral. This heater is held firmly against the bottom of the sample chamber (0.08 in. below the sample) by a 1 in. thick block of machinable mineral fiber insulation (Moldatherm II, Lindberg). A  $1/2$  in. thick layer of this insulation is also placed around the cell body. Furthermore, a cylindrical ring of insulation ( $1/4$  in. thick) is placed around the window holder and over the

remaining stainless steel areas of the cell. The temperature of the sample is regulated with a PID temperature controller (Rika Kogyo Co.) and a type-J (iron-constantan) thermocouple (0.010 in. diameter; Cole Parmer) which is positioned  $1/8$  in. from the sample holder.

Although insulation at least  $1/4$  in. thick surrounds all stainless steel areas of the cell body, with the exception of the area directly over the sample, a cooling system is required to prevent the eventual heating of the spectrometer. For this purpose, a cylindrical aluminum water jacket surrounds the body of the HT-PA cell. Before water flows through the water jacket it passes through  $1/8$  in. copper tubing wrapped around the sample-microphone acoustic coupling tube and the two support bolts to reduce the conductive heat transferred to the microphone. Consequently, the incoming water cools the sample-microphone acoustic coupling tube first before removing heat from the outside of the cell insulation.

**Ultraviolet-Visible-Near-Infrared Spectral Measurements.** UV-vis spectral measurements were made with a Princeton Applied Research ultraviolet-visible-near-infrared (UV-vis-near-IR) spectrometer (PAR 6001) (18). This is a ( $f/4.2$ ) dispersive instrument equipped with an electronically modulated 1000-W Xe arc lamp and a pyroelectric detector for source compensation. Sample spectra were divided by the 25 °C spectrum of Norit-A carbon black (MCB) to yield (S/R) plots vs energy ( $\text{cm}^{-1}$ ); otherwise plots of single beam intensity (S) are presented to illustrate temperature effects. The optics of the PAR 6001 direct the tightly focused output of the monochromator downward to the sample position, and thus no additional transfer optics are necessary for use of the HT-PA cell. However, a separate amplifier (PAR 6005) is applied to the microphone signal before it is fed to the standard PAR 6001 electronics. When pertinent, spectra recorded with the HT-PA cell were compared to those obtained with the PAR 6003 standard sample-gas-microphone nonresonant photoacoustic cell. Samples of Norit-A carbon black and  $\text{H}_2\text{O}_2\text{O}_3$  (Alfa) were examined to evaluate the performance of the cell. PA spectra of carbon black were collected as a function of sample temperature and modulation frequency. The PA spectra of  $\text{H}_2\text{O}_2\text{O}_3$  were recorded as a function of modulation frequency from 200 to 750 nm at a scan rate of 100 nm/min and slit width of 2 mm. Elevated temperature spectra of  $\text{CoCl}_2 \cdot 6\text{H}_2\text{O}$  were recorded as four coadded scans from 275 to 750 nm at a scan rate of 100 nm/min and slit width of 4 mm. Spectra were measured only after the sample had been held at constant temperature for at least 60 min and was at apparent equilibrium. The melting of indium was observed by monitoring the signal at 1000 nm from carbon black dispersed in the metal sample, since indium itself is reflective to near-IR radiation and thus gives a very weak PA response. (2).

**FTIR Spectral Measurements.** All IR measurements were made with the IBM/FTIR-95 spectrometer (19). Because the converging beam from the interferometer enters the sample chamber horizontally, transfer optics (Spectra-Tech) are used with the cell to direct and more tightly focus the beam downward to a 4 mm diameter spot size on the sample. These optics consist of two flat and one off-axis ellipsoidal mirrors which are mounted to an optical plate supported  $5 1/2$  in. above the base of the sample chamber.

The output of the HT-PA cell is amplified with the PAR 6005 preamplifier before being fed into the signal input of the FTIR spectrometer. Spectra were normally acquired using 8  $\text{cm}^{-1}$  resolution and a mirror velocity of 0.059 cm/s (optical velocity, 0.236 cm/s), yielding Fourier frequencies of 141–944 Hz over the spectral range of 600–4000  $\text{cm}^{-1}$ . For modulation frequency experiments, the mirror velocity was incrementally increased from 0.059 to 0.236 cm/s (optical velocity, 0.944 cm/s) yielding Fourier frequencies of 566–3776 Hz over the same spectral range at the highest velocity. Standard measurements were made with 512 to 2048 coadded interferograms transformed using standard instrument software. When appropriate, FTIR HT-PA spectra were compared to spectra recorded using the IBM Instruments nonresonant PA cell (Model A6120890). PA spectra of carbon black were collected as a function of sample temperature and modulation frequency (mirror velocity). Spectra of  $\text{Na}_2\text{CO}_3$  exposed to  $\text{SO}_2$  at elevated temperatures were normalized to the 25 °C spectrum of Norit-A carbon black.



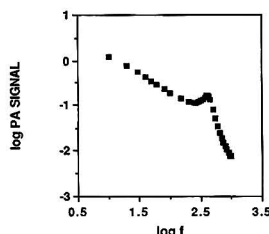


Figure 2. Carbon black photoacoustic amplitude at 1000 nm versus modulation frequency,  $f$ , using the HT-PA cell.

## RESULTS AND DISCUSSION

**Determination of the Helmholtz Resonance Frequency.** As in other PA cells designed for nonambient temperatures, the HT-PA cell described here is constructed in the form of a Helmholtz resonator (14). This design enables the microphone to be maintained at room temperature regardless of sample temperature, while still keeping the gas volume of the cell small ( $<1 \text{ cm}^3$ ). In addition, the microphone membrane is protected from direct illumination. Although the Helmholtz resonance can cause signal distortion, it can also be used to enhance selected signals. The Helmholtz resonance frequency,  $f_R$ , is given by

$$f_R = (cd/4\pi)[(V_{MC} + V_{SC})/(V_{MC}V_{SC}(l + 0.85d))]^{1/2} \quad (1)$$

where  $c$  is the speed of sound in the coupling gas,  $V_{SC}$  and  $V_{MC}$  are the volumes of the sample chamber and microphone chamber, respectively, and  $d$  is the diameter of the sample/microphone acoustic coupling tube of length,  $l$ , connecting  $V_{SC}$  and  $V_{MC}$  (20).

As in the cell described here, the Helmholtz resonance may occur in the range of commonly used photoacoustic modulation frequencies. According to theory, the magnitude of the photoacoustic signal depends inversely on the modulation frequency, that dependence being specifically  $f^{-1}$  for photothermally saturated signals and  $f^{-3/2}$  below saturation (21). Near a cell resonance the cell response will be much stronger than this prediction. For the HT-PA cell this effect is illustrated in Figure 2, where the 25 °C carbon black PA signal monitored at 1000 nm is plotted as a function of  $f$ . The resonant enhancement on top of the ca.  $f^{-1}$  dependence is seen to be centered at  $430 \pm 5 \text{ Hz}$ .

The effect of the cell resonance on PA measurements made with rapid-scanning FTIR instrumentation is distinctly different than for those made at a fixed wavelength or with a dispersive spectrometer utilizing single-frequency modulation. This is because the photoacoustic modulation in rapid scanning FTIR is generated interferometrically. As a result, each wavelength is intensity modulated at its own frequency ( $f(\text{Hz}) = 4V_m/\lambda$ , where  $V_m$  is the velocity of the moving mirror and 4 is the factor appropriate for the Genzel interferometer of the IR/95 (2 being the factor for a Michelson interferometer). Thus, with a resonant cell, the transform of the FTIR-PA interferogram will show greatest intensity enhancement at the wavelength for which the Fourier frequency equals the cell resonance frequency (provided, of course, that this frequency is in the observed range of the experiment for the mirror velocity used). As seen in Figure 3, the comparison of the FTIR-PA spectrum of carbon black powder measured with the nonresonant IBM-A6120890 cell (A), and with the resonant HT-PA cell (B), to the open beam spectrum of the instrument acquired with the DTGS detector (C), shows clearly the resonance enhancement of the PA response of the HT-PA cell in the region of  $1850 \text{ cm}^{-1}$ . As expected from the fixed wavelength measurements (Figure 2), this corresponds to a

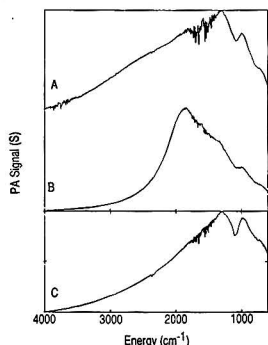


Figure 3. FTIR-PA spectrum of carbon black acquired by using (A) the HT-PA resonant cell, (B) IBM A6120890 nonresonant cell, and (C) DTGS spectrum of the FTIR source.

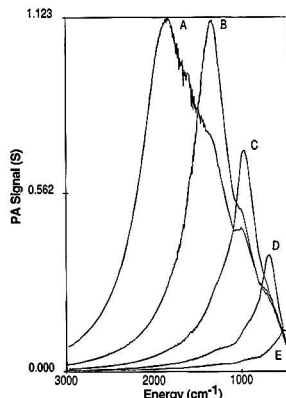
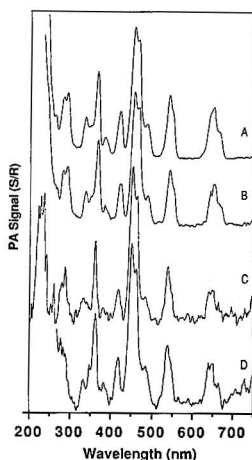


Figure 4. Single-beam FTIR-PA spectra of carbon black (25 °C) acquired by using the HT-PA cell at scanning mirror velocities ( $\text{cm s}^{-1}$ ) as follows: (A) 0.059; (B) 0.083; (C) 0.118; (D) 0.166; and (E) 0.236.

Fourier frequency of  $\sim 430 \text{ Hz}$ , for the particular mirror velocity used ( $V_m = 0.059 \text{ cm s}^{-1}$ ). The dependence of the enhancement (as well as the overall signal strength) on mirror velocity in the FTIR experiment is further illustrated in Figure 4.

In many instances the Helmholtz resonance frequency is regarded as undesirable. However, the enhancement of the PA signal can be particularly useful in certain instances. For example, Figure 5 compares spectra of  $\text{H}_2\text{O}_2$  measured with the PAR 6003 nonresonant cell and with our resonant HT-PA cell under identical conditions (100 nm/min, 2-mm slits) at 20 and 430 Hz, the particular Helmholtz resonance frequency for the HT-PA cell. The comparison of spectra accumulated at 20 Hz shows similar results in terms of spectral definition and signal-to-noise ratio. However, when the modulation frequency is increased to 430 Hz, the resonant cell exhibits superior base-line signal-to-noise (S/N) and spectral definition. This is especially apparent for bands between 300 and 500 nm in which the resonant cell spectrum exhibits realistic band ratios and superior S/N as compared to the nonresonant cell spectrum.

Although the PA signal, either for fixed frequency modulation or for rapid scanning FTIR, is commonly normalized by division by a reference spectrum (usually of carbon black), a relative increase in S/N should be expected: for the whole spectrum when the fixed modulation frequency of a dispersive



**Figure 5.** UV-vis PA spectra of  $\text{H}_2\text{O}_2$  acquired by using the nonresonant PAR 6003 cell at (A) 20 and (C) 430 Hz and resonant HT-PA cell at (B) 20 and (D) 430 Hz.

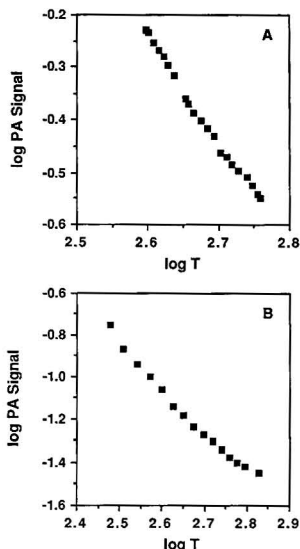


**Figure 6.** PA signal for carbon black as a function of temperature: (A) near-IR measurements (1000 nm); (B) FTIR measurements (902  $\text{cm}^{-1}$ ).

PA experiment is in the vicinity of the cell resonance, or for the region of the spectrum with Fourier frequencies close to the cell resonance in a rapid scanning FTIR-PA measurement.

**Effect of Temperature upon the PA Signal.** The temperature characteristics of the PA signal were evaluated by using PA measurements of carbon black powder. After temperature equilibrium was established at a given temperature, the PA amplitude was measured. Figure 6 depicts the PA signals measured for a carbon black sample in the temperature range 298–673 K. The near-IR signal was measured at 1000 nm at a modulation frequency of 100 Hz, while the FTIR signal is reported for 902  $\text{cm}^{-1}$  at a (Fourier) modulation frequency of 213 Hz (mirror velocity 0.059  $\text{cm s}^{-1}$ ).

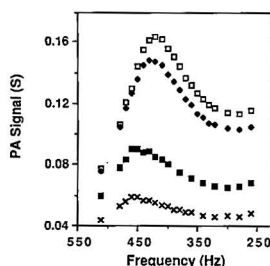


**Figure 7.** Plot of PA signal (1000 nm) versus modulation frequency as a function of temperature: ( $\square$ ) 25; ( $\blacklozenge$ ) 50; ( $\blacksquare$ ) 104; ( $\times$ ) 152  $^{\circ}\text{C}$ .

As predicted by the Rosencwaig-Gersho (R-G) theory, the photoacoustic amplitude decreases as temperature increases (21). In the simplest analysis, the R-G theory examines only the PA signal dependence on the sample temperature and predicts a  $T^{-1}$  relationship. However, the data in Figure 6 show a  $T^{-1.9}$  dependence for both near-IR and FTIR measurements. Similar deviations from the R-G theory have been observed by Coufal et al. (20) ( $T^{-2.9}$ ) and by Bechtold (7, 22) ( $T^{-1.7}$ ). The greater than  $T^{-1}$  dependence of the PA signal may be due to other factors of signal generation affected by temperature, such as the thermal conductivity of the sample and coupling gas, the density of the coupling gas, and/or the temperature gradient along the sample-microphone connecting tube.

For high-temperature FTIR-PAS measurements, McGovern et al. (17) have pointed out that an additional temperature dependence is expected due to the modulation of the black body radiation from the sample by the interferometer itself acting effectively as a chopping mirror. The interferometrically modulated emission, returned to the sample, can create an "antiinterferogram", i.e., a signal 180° out of phase with the absorption interferogram. This will progressively diminish the net signal as the temperature increases, independently of other temperature effects. The fact that the data in Figure 6 show the same  $T^{-1.9}$  dependence for both the near-IR dispersive and the mid-IR interferometric measurements suggests that emission is not a significant factor in the spectra reported here. In fact, efforts to detect the emission signal, as described by McGovern et al., by turning off the spectrometer source while maintaining the sample at high temperature, were not successful.

**Effect of Temperature upon the Helmholtz Resonance Frequency.** As illustrated in Figure 7, when the temperature of the sample and coupling gas increases, so too does the resonance frequency. According to eq 1 the resonance frequency is dependent upon the speed of sound,  $c$ , in the coupling gas. Since the velocity of sound in a gas increases with temperature (23), the resonance frequency also increases. Temperature also affects the range of signal enhancement via the resonance frequency. As shown in Figure 7 the enhancement of the PA signal is spread over a greater range of frequencies, although the maximum relative enhancement for each temperature remains approximately constant.

The effects of temperature upon the resonance frequency are also observed in the FTIR-PA spectra of carbon black (Figure 8). As the temperature is increased from 25 to 400  $^{\circ}\text{C}$ , the resonance enhancement of the PA signal shifts from 1800 to 2000  $\text{cm}^{-1}$ . In addition, the prominence of the signal enhancement feature in the spectra decreases as the temperature increases due to the broadening of the enhancement effect, which is also seen in the fixed wavelength data of Figure 7.

The shift in the enhancement maximum is not sufficient to cause a significant distortion of the qualitative spectra

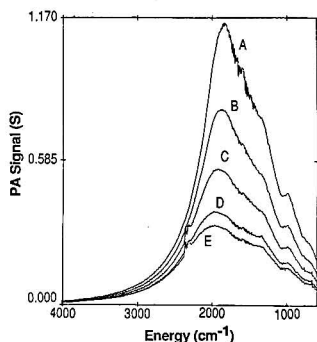


Figure 8. FTIR-PA spectra of carbon black at (A) 27, (B) 75, (C) 125, (D) 175, and (E) 200 °C.

reported here, even though the reference spectrum used for all spectra was that of carbon black obtained at 25 °C. Use of a reference spectrum taken at the same temperature would be required for quantitative use of the data. However, the reduced S/N at higher temperatures for the reference as well as the sample magnifies the noise problem for such measurements. Division by a smoothed high-temperature reference spectrum is a possible solution to this problem.

**Applications. Thermal Decomposition Study.** Figure 9 depicts the HT-PA UV-vis spectra of  $\text{CoCl}_2 \cdot 6\text{H}_2\text{O}$  measured at 25, 65, 100, and 200 °C. At 25 °C, (A) the spectrum of  $\text{CoCl}_2 \cdot 6\text{H}_2\text{O}$  exhibits three maxima at 455, 500, and 540 nm. When the sample is heated to 65 °C (B), new maxima appear at 530, 620, 665, and 690 nm. The spectrum observed at 100 °C (C) shows only two peaks at 520 and 615 nm. Finally at 200 °C, a single broad maximum at 600 nm is observed.

The changes in the PA spectra reflect the stepwise loss of  $\text{H}_2\text{O}$  from the hydrate. The bands in spectrum A at 455, 500, and 540 nm are characteristic of octahedral  $\text{CoCl}_2 \cdot 6\text{H}_2\text{O}$ , in which two waters are external to the  $\text{Co}(\text{H}_2\text{O})_4\text{Cl}_2$  inner coordination sphere and are hydrogen bonded to  $\text{Cl}^-$  ions in adjacent  $\text{CoCl}_2(\text{H}_2\text{O})_4$  complexes (24).

The appearance of bands in the 65 °C spectrum (B) at 620, 665, and 690 nm indicates that a tetrahedral intermediate species is present. This is consistent with earlier literature reports of the existence of a  $\text{Co}(\text{H}_2\text{O})_4 \cdots \text{CoCl}_4$  ( $T_d$ ) complex (25, 26). However, the relative intensities of the octahedral and tetrahedral bands suggest that only a small fraction of the cobalt(II) ions are in a tetrahedral environment, since the molar absorptivity of tetrahedral  $\text{Co(II)}$  at 650 nm is ca.  $10\times$  that of octahedral  $\text{Co(II)}$  at 530 nm. The presence of  $T_d$  species has been observed in a previous high-temperature diffuse reflectance investigation (27); however, a separate DRS study in which the sample was heated and then cooled to room temperature before recording the sample spectrum showed no presence of the tetrahedral complex (24, 28). This suggests that the sample cooling process results in the transformation of the intermediate species to a more stable form reported as  $\text{CoCl}_2(\text{H}_2\text{O})_4$ . The appearance of bands in the 100 °C spectrum (C) at 520 and 615 nm indicates the loss of two more water molecules resulting in the formation of  $\text{CoCl}_2 \cdot 2\text{H}_2\text{O}$ . The spectrum of the sample at 200 °C (D) shows a single broad maximum at 600 nm indicative of  $\text{CoCl}_2$ , in which each  $\text{Co(II)}$  ion is centered in an octahedron of  $\text{Cl}^-$  ions (24, 28).

UV-vis-near-IR decomposition and deaquation spectra are often difficult to obtain by using conventional transmittance and reflection techniques because of scattering due to the powdered sample as well as the changing effective particle size or physical nature of the sample. It is significant that for this experiment, spectral data were obtained without disturbing

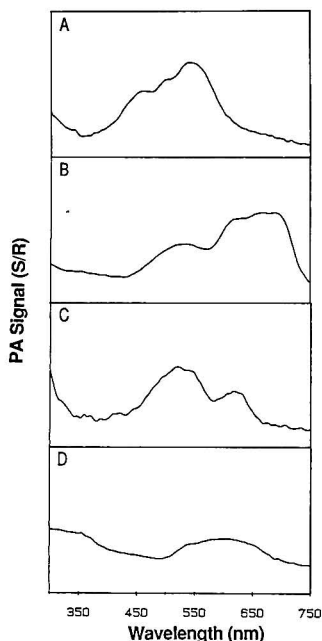


Figure 9. UV-vis PA spectra of  $\text{CoCl}_2 \cdot 6\text{H}_2\text{O}$  recorded at (A) 25, (B) 65, (C) 100, and (D) 200 °C.

the sample. In addition, although during the heating process the originally finely powdered sample ( $50 < x < 100 \mu\text{m}$  particle diameter) contracted into a small pellet, spectral definition of the data was retained. The ability to obtain in situ PA spectra at elevated temperatures was essential for the identification of intermediate decomposition species.

**Phase Transition Study.** The application of photoacoustic spectroscopy to phase transition studies has been well illustrated (2-4, 8, 9, 11-13, 15, 29-35). The use of our HT-PA cell for such measurements is illustrated in Figure 10, where the melting and subsequent freezing of indium are monitored by using the PA signal at 1000 nm of a carbon black dispersion in the metal. Similar measurements have been reported by Korpun (30). In the experiment recorded in Figure 10, the sample was first heated slowly through the melting transition and then more rapidly cooled through the freezing transition.

The behavior of the PA signal is easily interpreted in terms of the R-G (21) and Korpun-Tilgner (K-T) (30) theories. Below the melting point there is a slight decrease in the PA signal as predicted by the R-G theory. As the sample melts, the signal drops precipitously to a minimum at 156.8 °C ( $m_p$ , 156.61 °C). According to the K-T theory the decrease in PA signal is due to the transfer of thermal energy generated by the deexcitation of absorbed incident light to energy involved in the solid-to-liquid transition, or heat of fusion. Once this transition is complete, the heat generated by the absorption of incident radiation in the now liquid sample again generates a PA signal as described by the R-G theory. The PA signal at 159 °C is greater in magnitude than that of the sample at 150 °C before melting since the liquid sample occupies a greater volume than the solid and thereby reduces the effective PA cell gas volume. As the sample is cooled after being held briefly at 159 °C, the phase transition is reversed (with some supercooling), as indicated by the slight dip in the PA signal at ca. 147 °C. The subtleties of the interaction of the photothermal effect with the heat of fusion during the freezing

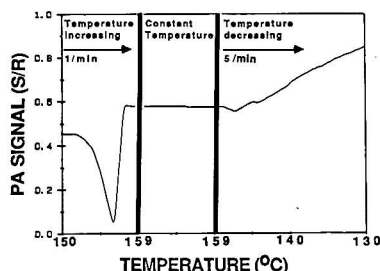


Figure 10. PA signal (1000 nm) for the indium/carbon black mixture while being heated and then cooled in the temperature region of the solid-liquid phase transition.

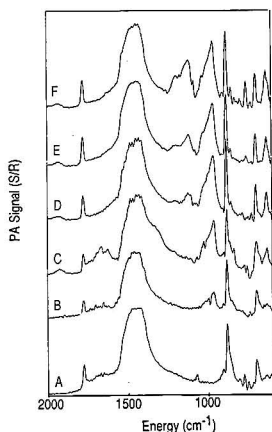


Figure 11. FTIR-PA spectra of (A)  $\text{Na}_2\text{CO}_3$  and  $\text{Na}_2\text{CO}_3$  exposed to  $\text{SO}_2$  as a function of temperature: (B) 25; (C) 75; (D) 100; (E) 200; (F) 300 °C.

process have been discussed by Korpiun and Tilgner (30).

**Solid-Gas Reaction Study.** As a third application of the HT-PA cell, *in situ* spectral measurements acquired during the reaction of 40 mg of  $\text{Na}_2\text{CO}_3$  and 1.5%  $\text{SO}_2$  in  $\text{N}_2$  at a flow rate of 2 mL/min from 25 to 300 °C are reported. A typical ambient temperature spectrum of  $\text{Na}_2\text{CO}_3$  (36) is shown in trace A of Figure 11. After initial exposure of the sample to  $\text{SO}_2$  at 25 °C, the presence of a band centered at ca. 960  $\text{cm}^{-1}$  is observed (trace B). Continued exposure of the sample to  $\text{SO}_2$  at 25 °C results in increased intensity of the 960- $\text{cm}^{-1}$  band and the appearance of bands at 1650, 1330, 840, and 629  $\text{cm}^{-1}$  (trace C). The bands at 960 and 629  $\text{cm}^{-1}$  are characteristic of those reported for  $\text{Na}_2\text{SO}_3$  (37) and are assigned to the  $\nu_1 + \nu_3$  symmetric and asymmetric S-O stretching modes and the  $\nu_2$  symmetric bending mode of the sulfite ion, respectively (37). The 1650-, 1330-, and 840- $\text{cm}^{-1}$  bands, which appear after extensive exposure of the  $\text{Na}_2\text{CO}_3$  sample to  $\text{SO}_2$  under mild temperature conditions, are similar to bands observed for  $\text{NaHCO}_3$  in a previous study of alkali and alkaline-earth carbonates (38). These peaks are no longer present in the spectrum acquired at 100 °C due to the decomposition of the  $\text{NaHCO}_3$  to  $\text{Na}_2\text{CO}_3$ ,  $\text{H}_2\text{O}$ , and  $\text{CO}_2$  (trace C). On the other hand, when the sample is exposed to increasing amounts of  $\text{SO}_2$  at elevated temperatures, the absorption bands centered at 960 and 629  $\text{cm}^{-1}$  continue to increase in intensity (traces D, E, and F). Bands at 1140 and 617  $\text{cm}^{-1}$ , which first appear in the 100 °C spectrum (trace D) and increase with increasing

temperature and exposure of the sample to  $\text{SO}_2$  (traces E and F) are indicative of  $\text{Na}_2\text{SO}_4$  (39). Finally, the presence of other bands at 1080, 1030, and 752  $\text{cm}^{-1}$  in the spectrum recorded at 300 °C are indicative of the formation of other  $\text{S}_2\text{O}_y^{n-}$  species on the surface of the  $\text{Na}_2\text{CO}_3$  particles.

The results presented here demonstrate the ability of FTIR-PAS to detect reaction intermediates and reaction products when measurements are recorded with a cell which permits sample heating and gas flow. The ease of sample preparation and the ability to examine samples unsuitable for transmission or diffuse reflectance spectroscopy, affords PAS an advantage for studying solid-gas reactions.

#### LITERATURE CITED

- Ganguly, P.; Rao, C. N. R. *Proc. Indian Acad. Sci.* **1981**, *90*, 153-214.
- Florian, R.; Pelz, J.; Rosenberg, M.; Vargas, H.; Wenhardt, R. *Phys. Status Solidi A* **1978**, *48*, K35-K38.
- Korpiun, P.; Baumann, J.; Luscher, E.; Papamokos, E.; Tilgner, R. *Phys. Status Solidi A* **1980**, *58*, K13-K16.
- Siqueria, M. A. A.; Ghizone, C. C.; Vargas, J. I.; Menezes, E. A.; Vargas, H.; Miranda, L. C. M. *J. Appl. Phys.* **1980**, *51*, 1403-1406.
- Bechtold, P. S.; Campagna, M.; Schober, T. *Solid State Commun.* **1980**, *36*, 225-231.
- Bechtold, P. S.; Campagna, M. *Opt. Commun.* **1981**, *36*, 373-377.
- Bechtold, P. S. *J. Photoacoust.* **1982**, *1*, 87-102.
- Fernandez, J.; Exebarria, J.; Tello, M. J.; Echarr, A. L. *J. Phys. D* **1983**, *16*, 269-274.
- Korpiun, P.; Tilgner, R.; Schmidt, D. *J. Phys. Colloq. C6* **1983**, *44*, 43-53.
- Kinney, J. B.; Staley, R. H. *Anal. Chem.* **1983**, *55*, 343-348.
- Exebarria, J.; Fernandez, J.; Arriandaga, M. A.; Tello, M. J. *J. Phys. C* **1985**, *18*, L13-L17.
- Louis, G.; Peretti, P.; Mangeot, B.; Billard, J. *Mol. Cryst. Liq. Cryst.* **1985**, *122*, 261-267.
- Somasundaram, T.; Ganguly, P.; Rao, C. N. R. *J. Phys. C* **1986**, *19*, 2137-2151.
- McGovern, S. J.; Royce, B. S. H.; Benziger, J. B. *Appl. Surf. Sci.* **1984**, *18*, 401-413.
- Royce, B. S. H.; McGovern, S.; Benziger, J. B. *Am. Lab. (Fairfield, Conn.)* **1985**, *17*(3), 16-26.
- Benziger, J. B.; McGovern, S. J.; Royce, B. S. H. *ACS Symp. Ser.* **1985**, No. 288, 449-463.
- McGovern, S.; Royce, B. S. H.; Benziger, J. *Appl. Opt.* **1985**, *24*, 1512-1514.
- Röhl, R.; Childers, J. W.; Palmer, R. A. *Anal. Chem.* **1982**, *54*, 1235-1238.
- Martin, M. A.; Childers, J. W.; Palmer, R. A. *Appl. Spectrosc.* **1987**, *41*, 120-126.
- Coufal, H.; Möller, U.; Schneider, S. *Int. Conf. Photoacoustic Effect* **1981**, 420-430.
- Rosenkwaig, A.; Gersho, A. *J. Appl. Phys.* **1976**, *47*, 64-69.
- Bechtold, P. S. *Int. Conf. Photoacoustic Effect* **1981**, 375-411.
- Beranek, L. *Acoustics*; McGraw-Hill: New York, 1954.
- Ribas, J.; Escuer, A.; Serra, M.; Vicente, R. *Thermochim. Acta* **1986**, *102*, 125-135.
- Katzin, L. I.; Gebert, E. *J. Am. Chem. Soc.* **1953**, *75*, 2830-2832.
- Bassett, H.; Croucher, H. *J. Chem. Soc.* **1930**, 1784-1819.
- Wendlandt, W. *Modern Aspects of Reflectance Spectroscopy*; Wendlandt, W., Ed.; Plenum: New York, 1968; p 53.
- Grindstaff, W. K.; Fogel, N. *J. Chem. Soc., Dalton Trans.* **1972**, *14*, 1476-1481.
- Korpiun, P.; Tilgner, R. *J. Appl. Phys.* **1980**, *51*, 6115-6119.
- Korpiun, P. *Int. Conf. Photoacoustic Effect* **1981**, 211-241.
- Korpiun, P.; Tilgner, R. *Phys. Status Solidi A* **1981**, *67*, 201-204.
- Bibi, I.; Jenkins, T. E. *J. Phys. C* **1983**, *16*, L57-L60.
- Louis, G.; Peretti, P.; Billard, J. *C. R. Acad. Sci., Ser. II* **1984**, *298*, 435-438.
- Junge, K.; Bein, B.; Pelz, J. *J. Phys. Colloq. C6* **1983**, *44*, 55-60.
- Pichon, C.; Liboux, M.; Fournier, D.; Boccaro, A. *C. Appl. Phys. Lett.* **1979**, *35*, 435-437.
- Nakamoto, K. *Infrared Spectra of Inorganic and Coordination Compounds*; Wiley-Interscience: New York, 1963.
- Evans, J. C.; Bernstein, H. J. *Can. J. Chem.* **1955**, *33*, 1270-1272.
- Miller, F. A.; Wilkins, C. H. *Anal. Chem.* **1952**, *24*, 1253-1294.
- Steger, E.; Schmidt, W. *Ber. Bunsen-Ges. Phys. Chem.* **1964**, *68*, 102-109.

RECEIVED for review November 3, 1987. Accepted January 5, 1988. Support by Cooperative Agreement CR-813023 (Project Officer, N. Dean Smith) from the Environmental Protection Agency is acknowledged. Although this research was funded by the U.S. EPA, it has not been subjected to full Agency review and therefore does not necessarily reflect the views of the Agency; thus, no official endorsement should be inferred. Provision of special transfer optics by Spectra-Tech, Inc., is also gratefully acknowledged.

# Simultaneous Multielemental Analysis of Some Environmental and Biological Samples by Inductively Coupled Plasma Atomic Emission Spectrometry

Shane S. Que Hee\* and James R. Boyle

Department of Environmental Health, University of Cincinnati Medical Center,  
3223 Eden Avenue, Cincinnati, Ohio 45267-0056

The Parr bomb technique is found to be the preferred acid digestion method for multielemental analysis by simultaneous inductively coupled plasma atomic emission spectroscopy (ICP-AES) when compared with microwave and hot plate methods for many environmental and biological specimens, but especially for the latter. One digestion alone often did not produce quantitative results compared with a sequential digestion scheme. The digestions were then refined to be as similar as possible for the various substrates studied. The interference of carbon on As and Se had to be corrected at  $\geq 3000 \mu\text{g of C/mL}$  in the analysis solution, and thus the C content had to be monitored to assess the efficiency of the digestions and to determine if interelemental correction for C presence was required. The C correction was adequate in the range 3000–10000  $\mu\text{g of C/mL}$ . The use of modified  $k$  values was demonstrated to provide accuracy and had to be used for ICP-AES spectrometers where background corrections were performed first for fixed channels. The results on Cincinnati soils and feces of Cincinnati children showed that Si and Ti were possible tracer elements for soil ingestion by the children.

Simultaneous multielemental analysis of environmental and biological samples potentially can minimize the large systematic errors inherent in analyses using different digestion techniques as often encountered for such single-element methods as atomic absorption spectrophotometry (AAS); the type of wet or dry ashing process utilized often varies from element to element in the same tissue for AAS (1). Most investigators are concerned with the adequacy of their methodology for a single element rather than its applicability to other elements. Furthermore, the need to store samples for a long period when many single-element determinations are required enhances the likelihood of contamination and nonrepresentative results as compared with "fresh" samples, in addition to lengthy analysis times.

Simultaneous inductively coupled plasma atomic emission spectroscopy (ICP-AES) is a multielemental complement to AAS since much of the same methodology in collection, storage, and digestion of tissues is applicable. Though some ICP-AES methods exist for environmental (2–8) and biological (1, 8–12) samples, few guidelines for accuracy exist apart from the need to obtain values close to those of the available certified NBS reference materials (13, 14).

Wet ashing of samples has become more efficient with the advent of microwave techniques (3, 5, 15–19). Though certainly faster than conventional hot plate methods, digesting in microwave ovens still may entail losses through partial or complete volatilization of some or all elements. Though Parr bomb methodology can resolve if volatilization is occurring (3, 11) and in addition allow fast, efficient digestions with the use of small amounts of acids, there are some disadvantages: prior treatment of tissues is sometimes required; the Teflon vessels become deformed with use; the metallic parts of the bomb can still contaminate; often a final evaporation is

necessary; and only a limited amount of substrate can often be digested.

The present investigation sought to optimize the methodology for simultaneous ICP-AES analysis of selected environmental and biological samples.

## EXPERIMENTAL SECTION

**Reagents.** Concentrated nitric ( $\text{HNO}_3$ ) and concentrated perchloric ( $\text{HClO}_4$ ) acids were Ultrax distilled in Vycor (G. F. Smith); concentrated hydrofluoric (HF), concentrated hydrochloric (HCl), and boric acids were Fisher Scientific A-147, A-144C, and A73500, respectively; all aqueous ICP-AES metal standards were at least 99.999% pure (Spex Industries (20)); Milli-Q Type I deionized water (20) was used for all dilutions (resistance  $\geq 15 \text{ M}\Omega$ ). The liquid argon for the ICP-AES plasma was of 99.999% purity.

**Standards.** The NBS standards utilized were water (NBS 1643a), bovine liver (NBS 1577a), lead paint (NBS 1579), phosphate rock (NBS 120b and 694), citrus leaves (NBS 1572), and human serum (NBS-909).

**Samples.** The samples selected were six soils representative of the Cincinnati area uncontaminated by anthropogenic activity (21) (they were dried and then pulverized by mortar and pestle until all of the material passed through a 1-mm sieve (21)); a sample of volcanic magma from the United States; a leaded paint powder sample (21) (obtained by mechanically stripping the paint from the exterior of an old house and then slicing the dry paint flakes); human blood, urine, and serum samples from several humans; feces from three children by direct collection in acid-washed plastic containers (stored at  $-70^\circ\text{C}$  before analysis); testes, urine, liver, spleen, and kidney samples obtained from Sprague Dawley rats fed the American Institute of Nutrition diet (AIN-76) and stored for analysis as described elsewhere (22). The soils, paint, blood, serum, urine, and fecal samples were part of an on-going study to study the effects of lead and other elements on children and adults in the Cincinnati area (21).

**Apparatus.** All glassware was decontaminated from trace-element impurities by physical cleaning with an appropriate test tube brush and a neutral detergent, rinsing with hot water to remove all detergent, washing with type II water and soaking in 10%  $\text{HNO}_3$  at least for 16 h, rinsing with type II water at least 5 times before drying in a dustless oven, and storing in a plastic bag closed with a paper-wire necktie in a closed cupboard.

All required filtrations were performed in a metal-free, all-Pyrex vacuum filter holder system (Millipore XX 15047000) that included a 0.50- $\mu\text{m}$  poly(tetrafluoroethylene) filter 47 mm in diameter (Millipore, FHUP 04700).

**Microwave Oven.** The CEM Corp. microwave drying/digestion system MDS-81 equipped with a Teflon-coated cavity and rotating turntable was utilized. The power system can be varied from 0 to 600 W in 1% increments with time ranges up to 99 h, 99 min, or 99 s. The 0.0231- $\text{m}^3$  cavity is evenly heated, and fumes were exhausted with a variable-speed exhaust fan into a perchloric acid fume hood.

**Parr Bomb.** The Parr bomb (Parr 4745; Fisher Scientific 01-023-2) consisted of a sealable bomb lined with Teflon which contained a 25-mL Teflon cup with cover. The bomb can operate up to  $150^\circ\text{C}$  and pressures up to 8.3 MPa without corrosion or loss of volatile elements.

**Jarrell-Ash/Allied Chemical ICAP-9000.** The vacuum spectrometer equipped with 40 fixed channels, variable-wavelength N+1 scanner, spectrum shifter, peristaltic pump, and argon pu-



rification train has been described elsewhere together with the analytical wavelengths (20).

The fixed channel elements were Ag, Al, As, Au, B, Ba, Be, Ca (two channels), Cd, Co, Cr, Cu, Fe, Hg, I, In, K, Li, Mg (two channels), Mn, Mo, Na (two channels), Ni, P, Pb, Pt, S, Sb, Se, Si, Sn, Sr (two channels), Ti, Tl, V, and Zn (20). The ( $N + 1$ ) channel at carbon I 247.8573 nm was chosen to assess the adequacy of the digestion procedures. The reference carbon compound was galactose (J. T. Baker M675) at 500 mg/L in water since it was not volatile, did not contain elements other than C, O, and H, and was also soluble in water without changing the surface tension of the water. In certain samples with high chlorine content, the ( $N + 1$ ) channel was set at the Cl I 725.53-nm analytical wavelength. The reference compound for Cl was 10% HCl.

**ICAP-9000 Analysis.** The procedures for quality control/assurance, standardization, and optimization of the ICAP-9000 including the dark current, white light, and integrator card tests; mercury arc calibration; optimization of the signal-noise ratio by using 10  $\mu\text{g/mL}$  cadmium chloride; scandium visualization; and the silicon signal/noise ratio have been described elsewhere (20).

A homogeneous digested sample was examined by spectrum shifter scanning to ascertain the major elements and which background corrections were necessary. When background correction was necessary (20) in the presence of spectral interference consisting of a broad band plus a peak, modified  $k$  factors of spectral interference were obtained for 100  $\mu\text{g/mL}$  of the interfering element (20) run with the appropriate background correction. These modified  $k$  factors produced more accurate and precise results than actual  $k$  factors (20) because the backgrounds and spectral interferences of real samples varied greatly. Most of the interferences consisted of a broad band plus a peak interference. The modified  $k$  factor corrects only for the peak interference after the broad band interference is accounted for by the initial background correction. If actual  $k$  factors are used in instances where the spectral interference consists of a broad band plus a peak and there is also an additional background component, overcorrection occurs leading sometimes even to negative values. The only instances where this procedure did not work were when the backgrounds were not flat (one-point correction) or oblique (two-point correction) or if the scanning monochromator channel was involved. In such cases, an unmodified  $k$  factor had to be used. The samples had to be digested so that the carbon content was less than 10000  $\mu\text{g/mL}$  since otherwise the peak from an interfering element could be eradicated by the broad band interference caused by C, an effect for which the use of modified  $k$  factors does partially account. No modified  $k$  factors were required at  $\leq 3000 \mu\text{g}$  of C/mL.

The appropriate background corrections and modified and actual  $k$  factors were added to the analytical control table (ACT). The instrument was then standardized with nine separate mixtures of elements in 11.6% HCl/2.8%  $\text{HNO}_3$  (20). The results were further confirmed by spectrum shifter scanning of a simulated sample containing the ICP-AES measured concentrations to assess if all the spectral and background interferences had been accounted for.

**Digestions.** The approach was to use the available NBS standards to validate the results for all samples. Where there were no NBS standards, three wet digestion methods (hot plate, closed container microwave, and Parr bomb) were compared for biological materials, and the Parr and open and closed container microwave digestion methods were investigated for environmental substrates. The Parr bomb method was established as the control technique since volatilization of elements is minimized.

Wet digestions not containing HF were chosen to extract the bioavailable (on the outside of the aluminosilicate matrix) component of the environmental samples independent of particle size. The most variable and difficult environmental matrix investigated in this study was paint. Thus, various concentrated mixtures (15 mL) were first evaluated for 100 mg (the maximum mass usable in the Parr bomb) or 50 mg dry weight of paint samples: 1:1:1 HF/ $\text{HNO}_3$ / $\text{HClO}_4$ ; 1:2 HF/ $\text{HNO}_3$ ; 1:1  $\text{HNO}_3$ / $\text{HClO}_4$ ; 5:4  $\text{HNO}_3$ / $\text{HClO}_4$ ; 3:2  $\text{HNO}_3$ / $\text{HClO}_4$ ; 9:1  $\text{HNO}_3$ / $\text{HClO}_4$ ; 1:3  $\text{HNO}_3$ / $\text{HClO}_4$ ; 1:3  $\text{HNO}_3$ /HCl; 6:2:5 HCl/ $\text{HNO}_3$ / $\text{HClO}_4$ ;  $\text{HNO}_3$ ; and HCl. All but the 1:2 HF/ $\text{HNO}_3$ ; 9:1  $\text{HNO}_3$ / $\text{HClO}_4$ ; and 5:4  $\text{HNO}_3$ / $\text{HClO}_4$  were used only for hot plate digestion investigations. In addition, two media for dissolving any residue left after

evaporation of a digest were investigated: 10%  $\text{HNO}_3$  (v/v) and 11.6% HCl/2.8%  $\text{HNO}_3$  (v/v). The latter keeps most elements in solution and 10%  $\text{HNO}_3$  is inferior as described elsewhere (20). After the optimum acid mixture not containing HF using the hot plate technique and also the optimum residue recovery method were chosen, these were then utilized in open and closed vessel microwave digestions, and the results then compared with those given by the Parr bomb method.

The dissolved residues (and such aqueous samples as water, urine, and water-diluted serum) were then tested for the presence of salt effects by progressive dilution (1/1, 1/2, 1/5, 1/7, 1/10, 1/20, and 1/30) with the appropriate aqueous medium. The test for absence of salt effects was the establishment of consensus data independent of dilution factor after correction for blank. The salt effect produces low answers relative to the actual concentration. The dilution which allowed sensitivity and linearity (described in ref 20) and minimized memory problems was then chosen.

Solutions containing HF attack the quartz torch and the Pyrex spray chamber of the ICAP; 0.8 g of boric acid ( $\text{H}_3\text{BO}_3$ )/mL of HF was initially added to these solutions, and the amount of added  $\text{H}_3\text{BO}_3$  was further optimized so that the original Si signal/noise ratio during optimization on HF-containing blank solutions was obtained with the minimum added amount of  $\text{H}_3\text{BO}_3$ .

Amounts 0.1x, 0.5x, and 2x, where x is the original mass of substrate digested were then evaluated to ensure that the elements were released quantitatively from their matrix. If an NBS standard were available, it was spiked at a level of 0.5x, and the observed elemental masses (obtained by difference) were compared with those expected, to ascertain recovery for each element. The same procedure was performed on aqueous samples, but spiking was performed with a simulated sample containing the ICP-AES measured concentration at a level of 0.5x.

All simulated samples were progressively diluted to define the lowest quantifiable level or LQL (the lowest concentration where each element in its particular matrix still agreed with its expected concentration to within 10% (20)). One solution providing acceptable data near the LQL and another at the most frequently observed concentrations from a given set of environmental samples were used for quality control/assurance after every 10 samples were analyzed.

All digestions/sample treatments were performed in triplicate. The following procedures detail the optimized digestion methods.

#### Materials of the Earth's Crust, Paint Powder, and Feces.

**Procedure 1.** Paint powder, materials of the Earth's crust (NBS rocks SRM 120b and 694, Cincinnati soils, and volcanic magma), and feces (recovered by scraping from the plastic containers after thawing) were dried to constant weight at 110  $^\circ\text{C}$  (usually for 2 days for the drier materials) and were ground in a metal-free mortar and pestle until each sample passed entirely through a 100-mesh (149  $\mu\text{m}$ ) sieve. Each sieved sample was tumble-shaken overnight (16 h) before a known weight (approximately 50 mg) was taken for digestion. Feces did not require sieving. For Parr bomb analysis, the sample was weighed in the Teflon cup; 2.8 mL of concentrated  $\text{HNO}_3$  was added and the sample allowed to stand for approximately 15 min to decompose carbonates and to allow oxidation of any surface organics. Concentrated HF (3.0 mL) was added, the cap was placed on the cup, and the bomb was assembled. The samples were heated at 140  $^\circ\text{C}$  in an oven for 1–4 h or until no precipitate remained. All samples except phosphate rocks required only 1 h, though the phosphate rock samples required 4 h. They were then removed and cooled to room temperature.  $\text{H}_3\text{BO}_3$  (2.5 g) was weighed into empty 125-mL narrow-mouth polypropylene bottles precalibrated for 100 mL. The cooled samples were transferred quantitatively into the bottle with three rinses of water (three 5-mL portions). The solutions were mixed by swirling to dissolve the sample residue and  $\text{H}_3\text{BO}_3$ . Concentrated HCl (11.6 mL) and concentrated  $\text{HClO}_4$  (0.1 mL) were added to each bottle and mixed. Finally, the samples were diluted to 100 mL with  $\text{H}_2\text{O}$  and shaken well. There must be no particulates present at this stage. The 11.6% HCl/2.8%  $\text{HNO}_3$  facilitates the dissolution of the iron oxide/manganese oxide fraction of the residue and its associated elements. The  $\text{HClO}_4$  was added to be uniform with the biological sample digestions. Its presence is not essential. One-milliliter of the 100-mL sample was diluted to 10 and 20 mL by using 11.6% HCl/2.8%  $\text{HNO}_3$ .



The original and diluted digests were analyzed by ICP-AES as described above. The final results were expressed both in terms of micrograms element/milligrams of soil and micrograms of oxides/milligrams of soil. The latter unit allows an assessment of mass balance.

**Procedure 2.** The concentrated HF/HNO<sub>3</sub> digestion in the Parr bomb above was compared with the microwave method. Soil (100 mg) was placed in a metal-free 125-mL narrow-mouth, polypropylene bottle, 2.8 mL of concentrated HNO<sub>3</sub> was added, and the mixture was allowed to stand for approximately 15 min. Concentrated HF (3 mL) was added and the bottles were capped and placed in the microwave oven at 10% power for 2 min (four times), 15% power for 1 min (six times), and 10% power for 1 min (nine times), and then cooled. The procedure was repeated until no precipitate remained or excess pressure produced on cooling. Generally, only one digestion was necessary. The homogeneous solution was then treated with boric acid as in procedure 1.

**Procedure 3.** For microwave and hot plate open-container digestions, the optimum acid digestion medium not containing HF was 5:4 concentrated HNO<sub>3</sub>/HClO<sub>4</sub> or 1:1 concentrated HNO<sub>3</sub>/HClO<sub>4</sub> (see results section). The 50-mg sample was weighed into a metal-free 100-mL Pyrex beaker, and 5:4 concentrated HNO<sub>3</sub>/HClO<sub>4</sub> (10 mL) was added. The sample was covered with a watchglass and allowed to stand for 15 min before being placed in the microwave oven at 10 min 25% power, 10 min 75% power, and then 15 min 0% power, the optimum conditions necessary to dissolve the sample. The supernatant was carefully transferred to a 50-mL beaker by Pasteur pipet. The digestion was repeated twice and the supernatants were combined and evaporated just to dryness at 200 °C on a hot plate. After cooling, 11.6% HCl/2.8% HNO<sub>3</sub> (3 mL) or, for NBS materials, 10% HNO<sub>3</sub> (3 mL) was added, and heated at 100 °C for 5 min. The supernatant was transferred quantitatively by Pasteur pipet to 17 × 100 mm polypropylene tubes (Fisher 14-956-1H) precleaned to 10 mL by weighing water aliquots. This cycle was repeated twice, the supernatants were combined in the tubes, and the volume was adjusted to 10 mL. Three- and twenty-fold dilutions were then analyzed. The addition of 10% HNO<sub>3</sub> for NBS materials was followed by one leaching with 11.6% HCl/2.8% HNO<sub>3</sub>.

Hot-plate digestions were performed as for the microwave oven procedure except that the hot plate was maintained at 90 °C with the watchglass on the beaker until no more brown fumes were observed (usually 1 h). The supernatant was transferred as above, the cycle was repeated twice with the supernatants being combined in a 50-mL beaker, and the combined supernatants were evaporated and resublimized with 11.6% HCl/2.8% HNO<sub>3</sub> or 10% HNO<sub>3</sub> as above.

**Water, Rat and Human Urine, and Blood Serum.** **Procedure 4.** Surface waters (also NBS SRM 1643a) without particulate matter were examined with and without dilution with 11.6% HCl/2.8% HNO<sub>3</sub>. Samples with turbidity greater than that of type I water reference at a nonabsorbing wavelength (e.g. 400 nm) in the visible spectrum were filtered through a 0.50-μm Teflon filter, and the filtrate was analyzed as above. No dilution was necessary in general. The residue on the filter was then treated (along with a blank filter) as for the sieved rock sample described earlier.

**Procedure 5.** Urine samples could not be analyzed directly even after acidification (for preservation) and filtration because the high salt content caused clogging of the ICP nebulizer and also large memory effects. Sequential dilution with 11.6% HCl/2.8% HNO<sub>3</sub> along with subsequent spiking of a simulated sample of known elemental content (0.5 times the appropriate concentrations in the sample) to estimate element recovery was then performed. Generally, a 1/10 dilution was adequate.

**Procedure 6.** Rat urines developed a white precipitate on acidification. Hence, 1 mL of rat urine was diluted with 600 μL of concentrated HNO<sub>3</sub> followed by 2.5 mL of concentrated HCl, and type I water was added to a final volume of 20 mL. If still turbid, the sample was centrifuged and more concentrated HNO<sub>3</sub> was added in 10-μL aliquots if a white precipitate was observed. If there was no white precipitate but only particulate matter, the samples were treated as in the case of the turbid water sample above to yield a filtrate and a filter residue. Generally, filtration was not necessary once the white precipitate was solubilized.

**Procedure 7.** The NBS serum SRM-909 received in the form of a freeze-dried powder was reconstituted according to the NBS certificate of analysis. Blood sera could not be analyzed directly because the high organic content caused an interfering deposit of carbon on the torch tip which changed standardization slope and intercept values. Acidification caused precipitation. Since dilution in type I water caused no precipitation, sequential dilution with type I water was performed. A 1/2 dilution was adequate to negate salt effects and to achieve adequate sensitivity. NBS human serum at 0.50x (where x was the approximate concentration of the most abundant element in the test serum) was also spiked to evaluate recoveries at each dilution.

**Organs and Whole Blood.** **Procedure 8.** Organs were diced into 6 mm squares of known wet weight. If dry weights were desired, the organ was dried to constant weight at 110 °C in a Teflon beaker. NBS SRM 1577a liver was also used. For the hot plate and microwave methods, procedure 3 was used except for the following: 9:1 concentrated HNO<sub>3</sub>/HClO<sub>4</sub> mixture; overnight standing period; and use of a final volume of 11.6% HCl/2.8% HNO<sub>3</sub> (10 mL) directly for analysis (that is, no further dilution).

**Procedure 9** For Parr bomb digestions, concentrated HNO<sub>3</sub> (2.75 mL) was added to the sample (100 mg of dry weight/400 mg of wet weight) in a Teflon beaker and heated to 50 °C for 15 min (Teflon cover on) and allowed to stand overnight (16 h). The sample was placed in the Parr bomb, left in an oven at 140 °C for 2 h (the overnight standing period can be avoided, but the oven digestion time should be 4 h), and cooled, 100 μL of concentrated HClO<sub>4</sub> was added, and the solution was evaporated at 80 °C to approximately 50 μL. A 2-mL aliquot of 11.6% HCl/2.8% HNO<sub>3</sub> was added, the beaker heated at 90 °C for 5 min (cover on), and the solution transferred. This procedure was repeated two more times, and the volume of the combined transferred solutions was adjusted to 7 mL.

**Procedure 10.** For microwave digestions, narrow-mouthed 500-mL Teflon bottles were used; 3 mL of concentrated HNO<sub>3</sub> was added to 100 mg dry weight or approximately 400 mg wet weight of organ/tissue. The microwave program was as follows: 1 min at 15% power and then cool 1 min repeated five times until no precipitate was evident; 100 μL of concentrated HClO<sub>4</sub> was added, and the digest evaporated at 90 °C to approximately 50 μL, and as before, consecutive recovery with 11.6% HCl/2.8% HNO<sub>3</sub> (2 mL) was performed.

## RESULTS AND DISCUSSION

The lowest quantifiable levels (LQLs) for the elements in the ICAP-9000 array are (in μg/mL): 1–5 for C; 0.1–1 for I, In, Sn; 0.05–0.1 for As, B, K, Ti; 0.01–0.05 for Ag, Hg, Na, P, Pb, S, Se, Zn; 0.005–0.01 for Au, Ba, Cr, Fe, Ni, Sb, Si; 0.001–0.005 for Al, Ca, Cd, Co, Cu, Mg, Mn, Mo, Pt; <0.001 for Be, Li, Sr, Ti, V. The optimum conditions used for all determinations were as follows: rf power, 1.16 kW; torch height, 12 mm; Ar pressure, 30 psi; pump flow rate, 1.6 mL/min; coolant flow, 19 L/min. They are identical with the LQLs for single elements because the *k* factor and background corrections render the determinations independent of matrix.

The *k* factors relevant to carbon revealed interferences on As, Se, S, Hg, and Ni. The respective *k* factors (pg/mL affected channel per μg/mL affecting element) were 154, 30.3, 17.7, 3.95, and 0.925. The modified *k* factors (background corrected) for As and Se were 14.0 and 4.10, respectively. The most important correction was on As (LQL between 0.05 and 0.10 μg/mL) and Se (LQL between 0.01 and 0.05 μg/mL) and this interference had to be accounted for at C concentrations >3000 μg/mL. Thus, an inefficient digestion or a technique utilizing dilution, e.g. for urine and serum, produced inaccurate concentrations for these elements because of the high C concentrations. This interference has not been reported before. The response to C was linear at least up to 10000 μg/mL. The carbon concentration is a very useful indicator of the efficiency of the digestion process.

The only *k* factor for Cl was on B at 250 pg/mL affected element per μg/mL affecting element. Since most of the determinations occurred in 11.6% HCl/2.8% HNO<sub>3</sub>, the B

Table I. Some Modified  $k$  Values for Samples Containing Priority Pollutant Metals

affecting element	modified $k$ value for affected element <sup>a</sup>	affecting element	modified $k$ value for affected element <sup>a</sup>	affecting element	modified $k$ value for affected element <sup>a</sup>
Al	As, 9950 Pb, 1820 Pt, 2840 Sb, 1640 Se, 2570	Mg	As, 1600 C, 144000 <sup>b</sup> Ni, 2500 Sn, 82700 <sup>b</sup>	Ti	Hg, 110 I, 269000 Mg II, 1600 Pb, 600 Si, 13600 Tl, 55100
As	Cd, 41600	Mn	As, 1400 Se, 1690		
C	As, 14.0 Se, 4.10	Mo	As, 2260 Cr, 1170 Pb, 1900		
Ca	Al, 1300	Ni	Cd, 522 Cr, 786 Pb, 2380 Sb, 706 Tl, 58600		
Co	As, 2600				
Cr	Ag, 9800 As, 2000 Au, 5000 P, 13000 Pt, 5300 Sb, 1900 Sn, 90700 <sup>b</sup>	S	I, 1850 P, 1920		
Cu	Pb, 1670	Si	Hg, 970		
Fe	As, 1010 C, 2150000 <sup>b</sup> Ni, 594 Pt, 10200 Se, 2540	Ti	Ag, 17000 Al, 853 C, 82000 Ca II, 3500 Co, 1700 Fe, 220		

<sup>a</sup>  $\mu\text{g/mL}$  affected element per  $\mu\text{g/mL}$  affecting element. <sup>b</sup> Not modified.Table II. Comparison of Digestions (Closed Vessel Parr, Closed Vessel Microwave (Micro) and Open Vessel Microwave 5:4 Concentrated  $\text{HNO}_3/\text{HClO}_4$  (Extraction)) of NBS Phosphate Rocks Using 10%  $\text{HNO}_3$  Acid for Recovery<sup>d</sup>

oxide	NBS SRM 694				NBS SRM 120b			
	certified wt, %	% recovery relative to NBS			certified wt, %	% recovery relative to NBS		
		Parr	micro	extraction		Parr	micro	extraction
Al <sub>2</sub> O <sub>3</sub>	1.8 ± 0.05	96 ± 5 <sup>a</sup>	98 ± 4 <sup>a</sup>	57 ± 3 <sup>a</sup>	1.07 ± 0.02	99 ± 5 <sup>a</sup>	97 ± 6 <sup>a</sup>	89 ± 2 <sup>a</sup>
BaO	NR	0.01 <sup>b</sup>	0.01 <sup>b</sup>	0.01 <sup>b</sup>	NR	0.01 <sup>b</sup>	0.01 <sup>b</sup>	0.006 <sup>b</sup>
CaO	43.6 ± 0.2	102 ± 1 <sup>a</sup>	105 ± 2 <sup>a</sup>	94 ± 3 <sup>a</sup>	49.4 ± 0.06	103 ± 2 <sup>a</sup>	104 ± 1 <sup>a</sup>	95 ± 2 <sup>a</sup>
CdO	0.015 ± 0.002	93	93	100 ± 7	0.0023 ± 0.005	<0.02 <sup>b</sup>	<0.02 <sup>b</sup>	<0.02 <sup>b</sup>
Cr <sub>2</sub> O <sub>3</sub>	(0.10)	110	100	93 ± 4 <sup>a</sup>	NR	<0.03 <sup>b</sup>	<0.03 <sup>b</sup>	<0.03 <sup>b</sup>
Fe <sub>2</sub> O <sub>3</sub>	0.79 ± 0.03	94 ± 11 <sup>a</sup>	92 ± 3 <sup>a</sup>	77 ± 3 <sup>a</sup>	1.10 ± 0.03	93 ± 3 <sup>a</sup>	96 ± 2 <sup>a</sup>	74 ± 4 <sup>a</sup>
K <sub>2</sub> O	0.51 ± 0.01	88 ± 2	89 ± 2	57 ± 4	0.090 ± 0.006	97 ± 7	89	70 ± 7
Li <sub>2</sub> O	NR	<0.004 <sup>b</sup>	<0.004 <sup>b</sup>	0.002 <sup>b</sup>	NR	<0.004 <sup>b</sup>	<0.004 <sup>b</sup>	<0.001 <sup>b</sup>
MgO	0.33 ± 0.01	109 ± 6 <sup>a</sup>	109 ± 3 <sup>a</sup>	88 ± 3 <sup>a</sup>	0.28 ± 0.02	107 ± 4 <sup>a</sup>	107 <sup>a</sup>	96 ± 4 <sup>a</sup>
MnO	0.0116 ± 0.0010	86	86	95 ± 9	0.032 ± 0.001	94	94	91 ± 3
Na <sub>2</sub> O	0.86 ± 0.02	115 ± 1	109 ± 1	124 ± 5	0.35 ± 0.01	111 ± 3	100	120 ± 6
P <sub>2</sub> O <sub>5</sub>	30.2 ± 0.1	104 ± 1	93 ± 1	116 ± 7	34.57 ± 0.08	95 ± 2	89 ± 1	113 ± 1
S	NR	1.00 ± 0.04 <sup>b</sup>	0.91 ± 0.06 <sup>b</sup>	0.99 ± 0.06 <sup>b</sup>	NR	0.21 ± 0.01 <sup>b</sup>	0.80 ± 0.002 <sup>b</sup>	0.26
SiO <sub>2</sub>	11.2 ± 0.02	89 ± 1	83 ± 11	12 ± 1	4.68 ± 0.04	89 ± 3	87 ± 6	1.0 ± 0.3
SrO	NR	0.11 <sup>b</sup>	0.11 <sup>b</sup>	0.117 ± 0.003 <sup>b</sup>	NR	0.083 ± 0.006 <sup>b</sup>	0.80 <sup>b</sup> ± 0.02 <sup>b</sup>	0.26
TiO <sub>2</sub>	(0.11)	100 <sup>c</sup>	91 ± 9 <sup>a</sup>	<0.07	0.15	100 ± 13 <sup>a</sup>	100 ± 7	6.7
V <sub>2</sub> O <sub>5</sub>	0.31 ± 0.04	97 ± 3 <sup>a</sup>	106 ± 3 <sup>a</sup>	90 ± 3 <sup>a</sup>	NR	0.013 ± 0.006 <sup>b</sup>	0.013 ± 0.006 <sup>b</sup>	0.016 ± 0.001 <sup>b</sup>
ZnO	(0.19)	89	63 ± 5	97 ± 3	NR	0.01 <sup>b</sup>	0.03 ± 0.01 <sup>b</sup>	0.01 <sup>b</sup>
balance <sup>c</sup>	89.6	92.3	88.3	81.2	91.7 ± 0.2	90.8	89.1	88.7

<sup>a</sup> 1/20 dilution. <sup>b</sup> % by weight (no dilution). <sup>c</sup> NBS Certified element mass balance as the oxide. <sup>d</sup> NR means none recorded; values in parentheses in the certified column are uncertified. NOTE: A further recovery with 11.6%  $\text{HCl}/2.8\%$   $\text{HNO}_3$  did not leach appreciably more elements (<2% (w/w)).

interference was dwarfed by the contribution of the blank and was only important for serum diluted with water and for surface waters where no  $\text{HClO}_4$  was added. The Cl response was linear at least up to 10 000  $\mu\text{g/mL}$ .

Table I shows a typical set of modified  $k$  values for the determination of the Priority Pollutant Elements in a salt matrix. Comparison with the  $k$  values in ref 20 shows that these modified  $k$  values are much smaller and indicates that

a background correction nullifies many small  $k$  factors. Because background corrections are made in the ICAP-9000 before the interelemental corrections, the use of modified  $k$  factors prevents overcorrection when there is also a sample background. In cases where there are unexpected matrix effects leading to high backgrounds, this approach allows variations between individual samples to be accounted for. When there are interferences allowing no background value

Table III. Elemental Content of Pristine Soils of the Cincinnati Region (units are in  $\mu\text{g}$  of element/mg of soil)<sup>a</sup>

element	soil 1			soil 2			soil 3		
	Parr	micro	extraction	Parr	micro	extraction	Parr	micro	extraction
Al	43.6	49.2	20.9	49.2	54.5	16.9	63.6	67.9	31.9
Ba	0.336	0.340	0.108	0.392	0.378	0.102	0.406	0.418	0.158
Ca	115	111	72.9	52.1	62.1	36.7	57.0	68.0	41.2
Co	<0.2	<0.2	<0.006	<0.2	<0.2	0.0113	<0.2	<0.2	0.0097
Cu	<0.1	<0.1	0.0459	<0.1	<0.1	0.0157	<0.1	<0.1	0.0188
Fe	30.3	34.6	25.6	33.1	37.0	27.3	40.0	42.8	34.1
K	17.1	18.1	6.02	15.9	16.6	3.59	22.5	22.0	9.24
Li	0.0220	0.0280 <sup>b</sup>	0.0256	0.032	0.030	0.0250	0.0400	0.0380	0.0427
Mg	32.3	37.3	25.6	21.2	24.4	15.1	24.6	27.2	17.8
Mn	0.574	0.652	0.494	0.466	0.516	0.392	0.528	0.524	0.440
Na	7.13	8.13	0.392	6.81	6.96	0.266	5.52	6.00	0.674
P	7.16	<2 <sup>b</sup>	1.25	<2	<2	0.489	4.29	<2 <sup>b</sup>	0.485
S	3.96	4.72	3.36	<0.2	<0.2	0.0727	3.55	4.10	2.83
Si	200	226	4.38	264	277	13.0	289	227	32.3
Sr	0.178	0.194	0.133	<0.1	0.0960	0.0537	0.108	0.110	0.075
Ti	2.51	3.19 <sup>b</sup>	0.448	3.64	5.61 <sup>b</sup>	0.484	4.09	4.62	1.09
V	<0.2	<0.2	0.0407	<0.2	<0.2	0.0349	<0.2	<0.2	0.0648
Zn	<1	<1	0.0595	<1	<1	0.0627	<1	<1	0.0771

element	soil 4			soil 5			soil 6		
	Parr	micro	extraction	Parr	micro	extraction	Parr	micro	extraction
Al	67.0	74.4	25.4	80.2	85.3	24.1	38.9	41.9	12.0
Ba	0.438	0.458	0.149	0.402	0.408	0.0660	0.442	0.458	0.0738
Ca	9.90	10.1	8.49	30.9	28.7	24.9	2.21	2.48	0.961
Co	<0.2	<0.2	0.0100	<0.2	<0.2	0.0160	<0.2	<0.2	0.0065
Cu	<0.1	<0.1	0.0158	<0.1	<0.1	0.0168	<0.1	<0.1	<0.003
Fe	49.2	55.2	41.8	54.4	57.7	43.7	18.4	19.6	13.5
K	26.0	27.9	5.68	35.8	36.3	6.12	14.7	14.7	1.35
Li	0.0320	0.0420	0.0252	0.0600	0.0520	0.0503	<0.02	<0.02	0.0100
Mg	9.35	10.6	4.56	19.6	21.0	10.8	3.29	3.46	1.54
Mn	2.00	2.10	1.79	0.566	0.562	0.459	0.538	0.566	0.430
Na	4.74	5.25	0.224	6.43	6.57	0.566	9.84	9.32	<0.03
P	5.16	2.73 <sup>b</sup>	3.23	<2	<2	0.930	<2	<2	0.283
S	<0.2	<0.2	0.132	8.62	7.14	6.36	<0.2	<0.2	0.0914
Si	266	282	12.6	250	256	12.1	353	383	2.46
Sr	0.0680	0.0720	0.035	0.116	0.116	0.0821	0.0700	0.0700	0.0119
Ti	4.81	4.78	0.506	4.84	5.32	0.485	6.75	4.56*	0.431
V	<0.2	<0.2	0.418	<0.2	<0.2	0.427	<0.2	<0.2	0.0262
Zn	<1	<1	0.0577	<1	<1	0.0703	<1	<1	0.0350

<sup>a</sup> Soil: 1, unweathered Illinoian glacial till; 2, weathered Illinoian glacial till; 3, Illinoian lake bed clay; 4, fractured Kope formation shale soil; 5, Kope formation shale; 6, Fairview formation limestone soil. <sup>b</sup> Indicates the microwave closed-container value disagrees by more than 20% with the oven Parr bomb digestion. Parr, micro, and extraction are the results from digestions using the oven Parr bomb technique, the microwave closed container technique, and the 5:4 concentrated  $\text{HNO}_3/\text{HClO}_4$  microwave open container technique, respectively.

to be chosen because the base line is not flat or oblique, the unmodified  $k$  value must be used, e.g. at high concentrations of Al for the As channel.

In all the data that follow, the reported values are reproducible and precise (relative standard deviation) to within 10% since this was the actual daily variation of the signal/noise ratio of the ICAP spectrometer (20). Thus, the maximum number of significant figures used in all the data is three. Because a comparison between two averages of 10% tolerance is occurring, values within 80% of a true or reference value were adjudged to be acceptable.

**Crustal Materials.** The results of analyzing NBS phosphate rocks (SRM 694 and 120b) by the Parr (concentrated  $\text{HF}/\text{HNO}_3$ ), microwave closed-container (concentrated  $\text{HF}/\text{HNO}_3$ ), and the microwave open-container digestion methods (5:4 concentrated  $\text{HNO}_3/\text{HClO}_4$ ) are provided in Table II. As long as ICAP determinations were performed in the linear range and salt effects were nullified, both Parr and microwave methods gave results within 20% (and generally within 10%) of the certified values. The only exception was Zn. The elements in the refractory aluminosilicate fraction included Al, Fe, K, Si, and Ti (more than 85% of the Si and Ti). The rest of the elements, extracted in the open container 5:4 concentrated  $\text{HNO}_3/\text{HClO}_4$  digestion are more

available chemically than the elements in the aluminosilicate core. Use of 11.6%  $\text{HCl}/2.8\%$   $\text{HNO}_3$  after the 10%  $\text{HNO}_3$  acid recovery for the 5:4 concentrated  $\text{HNO}_3/\text{HClO}_4$  digestion only extracted small amounts (<2% by weight) of Al, Si, and Ti, since the digestions were optimized in  $\text{HNO}_3$ .

The corresponding results for the pristine soils of the Cincinnati region are given in Table III. The relative standard deviations were all within 10% except for the elements near the LQL. The microwave method consistently produced lower results (more than 20%) for P than for the Parr bomb digestions, and higher values (more than 20%) for Ti though more variable. When an oxide mass balance was computed in Table III, the Parr bomb mass balance was as follows: soil 1, 83%; soil 2, 85%; soil 3, 86%; soil 4, 86%; soil 5, 92%; and soil 6, 89%. The respective mass balances for the closed container microwave technique were 88%, 90%, 88%, 92%, 100%, and 91%. Some of the elemental imbalance can be attributed to B which could not be estimated by this technique.

The 5:4 concentrated  $\text{HNO}_3/\text{HClO}_4$  microwave digestion in open containers followed by 11.6%  $\text{HCl}/2.8\%$   $\text{HNO}_3$  recovery showed that all elements could be detected in the non-aluminosilicate matrix (Tables II and III). The elements in Cincinnati soils (Table III) which were present at greater

Table IV. Analysis of Volcanic Magma and Feces

element	volcanic magma, <sup>a</sup> mg/g	feces ( $\mu\text{g}$ of element/g of dry weight)					
		child 1		child 2		child 3	
		total <sup>a</sup>	extraction <sup>b</sup>	total <sup>a</sup>	extraction <sup>b</sup>	total <sup>a</sup>	extraction <sup>b</sup>
Ag	0.119	<0.1	<0.1	<0.1	<0.1	<0.1	<0.1
Al	61.5	522	501	332	287	731	698
Ba	0.0778	23.0	22.7	24.2	23.4	42.6	42.0
Be	1.01	<0.01	<0.01	<0.01	<0.01	<0.01	<0.01
Ca	65.8	17408	17389	32414	32382	16010	15984
Co	0.0800	1.39	1.39	1.04	0.920	0.890	0.778
Cr	0.468	0.482	0.482	1.40	1.40	1.42	1.42
Cu	0.100	66.2	66.1	45.1	45.1	49.9	49.8
Fe	85.4	462	453	1800	1795	599	593
K	2.20	7556	7540	9760	9001	11360	11334
Li	3.95	0.133	0.111	0.0634	0.0552	0.176	0.165
Mg	67.6	3055	2812	5065	5041	4900	4839
Mn	1.18	41.0	41.0	116	116	185	185
Na	20.0	3445	3435	1542	1531	7460	7439
Ni	0.0176	<0.01	<0.01	<0.01	<0.01	<0.01	<0.01
P	<0.1	13418	13404	23772	23749	27580	27542
Pb	<0.05	4.09	4.09	1.62	1.62	2.69	2.69
S	<0.01	5446	5444	5891	5887	8703	8693
Si	252	994	110 <sup>c</sup>	1255	23.7 <sup>c</sup>	2306	193 <sup>c</sup>
Sr	0.261	61.4	61.3	65.4	65.2	65.6	65.4
Ti	11.6	21.3	7.62 <sup>c</sup>	138	16.1 <sup>c</sup>	25.3	11.7 <sup>c</sup>
V	0.229	<0.05	<0.05	0.368	0.368	0.665	0.665
Zn	0.229	292	292	1367	1366	384	383
d	103	na	na	na	na	na	na

<sup>a</sup> Parr bomb closed container. <sup>b</sup> 5:4 concentrated  $\text{HNO}_3/\text{HClO}_4$  hot plate open container method. <sup>c</sup> Differs from the Parr bomb method concentration by more than 20%; na, not applicable. <sup>d</sup> Oxide mass balance (%).

Table V. Comparison of Digestion Methods for NBS Leaded Paint SRM-1579 (in mg/g)

element	certified value	digestions		extraction	
		Parr <sup>a</sup>	microwave <sup>a</sup>	10% $\text{HNO}_3$ <sup>b</sup>	additional 11.6% $\text{HCl}/2.8\% \text{HNO}_3$ <sup>c</sup>
Ag		0.17 $\pm$ 0.01	0.127 $\pm$ 0.003 <sup>d</sup>	<0.01 <sup>d</sup>	<0.01 <sup>d</sup>
Al		2.8 $\pm$ 0.3	2.6 $\pm$ 0.5	0.95 $\pm$ 0.09 <sup>d</sup>	<0.01 <sup>d</sup>
Ba		67.1 $\pm$ 0.2	69.8 $\pm$ 0.8	7.5 $\pm$ 0.5 <sup>d</sup>	10.8 $\pm$ 0.3 <sup>d</sup>
Ca		52.74 $\pm$ 0.02	54.0 $\pm$ 0.8	54 $\pm$ 4	<0.01
Cd		0.024 $\pm$ 0.003	0.0224 $\pm$ 0.0004	0.024 $\pm$ 0.001	<0.002 <sup>d</sup>
Co		0.069 $\pm$ 0.007	0.073 $\pm$ 0.007	0.074 $\pm$ 0.004	<0.002 <sup>d</sup>
Cr		0.187 $\pm$ 0.003	0.169 $\pm$ 0.002	0.162 $\pm$ 0.005	<0.01 <sup>d</sup>
Cu		0.70 $\pm$ 0.02	0.72 $\pm$ 0.02	0.69 $\pm$ 0.01	<0.001 <sup>d</sup>
Fe		6.05 $\pm$ 0.02	6.34 $\pm$ 0.04	2.7 $\pm$ 0.5 <sup>d</sup>	<0.001 <sup>d</sup>
K		<0.2	<0.2	0.201 $\pm$ 0.008	<0.02 <sup>d</sup>
Li		0.005 $\pm$ 0.001	0.006 $\pm$ 0.001	0.0029 $\pm$ 0.0004 <sup>d</sup>	<0.0002 <sup>d</sup>
Mg		5.19 $\pm$ 0.03	5.13 $\pm$ 0.04	2.1 $\pm$ 0.2 <sup>d</sup>	<0.002 <sup>d</sup>
Mn		0.20 $\pm$ 0.01	0.185 $\pm$ 0.002	0.18 $\pm$ 0.01	<0.002 <sup>d</sup>
Na		0.76 $\pm$ 0.03	0.85	0.69 $\pm$ 0.02	<0.01 <sup>d</sup>
P		<0.2	<0.4	<0.2	<0.02 <sup>d</sup>
Pb	118.7 $\pm$ 0.4	112 $\pm$ 1	114 $\pm$ 1	102 $\pm$ 10	3.8 $\pm$ 0.4 <sup>d</sup>
S		46 $\pm$ 1	47.3 $\pm$ 0.6	32 $\pm$ 2 <sup>d</sup>	4.0 $\pm$ 0.2 <sup>d</sup>
Sb		0.16 $\pm$ 0.04	0.30 $\pm$ 0.02 <sup>c</sup>	0.05 $\pm$ 0.01 <sup>d</sup>	<0.01 <sup>d</sup>
Si		17.2 $\pm$ 0.5	18 $\pm$ 1	<0.1 <sup>d</sup>	<0.02 <sup>d</sup>
Sr		1.06 $\pm$ 0.03	1.09 $\pm$ 0.02	0.66 $\pm$ 0.07	0.0038 $\pm$ 0.0003 <sup>d</sup>
Ti		55.4 $\pm$ 0.4	58.1 $\pm$ 0.7	0.51 $\pm$ 0.08	0.031 $\pm$ 0.018 <sup>d</sup>
Zn		60 $\pm$ 2	58.4 $\pm$ 0.4	51 $\pm$ 1	<0.01 <sup>d</sup>
	11.9 <sup>c</sup>	42.8 <sup>c</sup>	43.7 <sup>c</sup>	25.5 <sup>c</sup>	1.87 $\pm$ 0.09 <sup>c</sup>

<sup>a</sup> Closed container. <sup>b</sup> Recovery acid (five recoveries) after open container 5:4 concentrated  $\text{HNO}_3/\text{HClO}_4$  hot plate digestion (extraction). <sup>c</sup> One recovery only after five 10%  $\text{HNO}_3$  recoveries. <sup>d</sup> Differs from the Parr value by more than 20%. <sup>e</sup> Mass balance (wt %).

than 50% abundance in the aluminosilicate fraction were as follows (mean  $\pm$  standard deviation in %): Si, 95  $\pm$  5; Na, 95  $\pm$  4; Ti, 87  $\pm$  6; K, 76  $\pm$  12; Ba, 73  $\pm$  9; and Al, 65  $\pm$  8. These comparatively unavailable elements may be considered as potential tracers of the presence of soils in the feces of animals and of children who ingest soil.

Table IV provides the results for volcanic magma and feces. The oxide mass balance for the volcanic magma is around 100%. The feces samples consisted of a fraction analyzable by 5:4 concentrated  $\text{HNO}_3/\text{HClO}_4$  digestion and a remaining

fraction soluble only in HF. In the three samples of children's feces, only total Si (93  $\pm$  5%) and Ti (69  $\pm$  17%) mimicked the proportion soluble in HF in area soils. These two elements could be tracers of soil ingestion in children. The rest of the elements are mostly easily digestible, indicating their dietary origin.

Table V contains the comparison of the digestion techniques for NBS leaded paint SRM-1579. The paint had only one certified element (Pb). Apart from those elements near their LQLS, 1/20 dilution results had to be used for accuracy. If

Table VI. Comparison of Different Digestion Concentrated Acid Mixtures on the Digestion of Elements from One Paint (50 mg) by the Hot Plate Technique<sup>a</sup>

element	concentration ( $\mu\text{g}$ of element/g of paint) in digestion acid						
	1	2	3	4	5	6	7
Al	33.5	4.40	3.59	12.8	4.80	17.2	10.8
Ba	1.39	0.976	0.814	0.944	0.900	1.32	1.26
Cr	0.0425	0.044	<0.03	0.036	0.032	0.060	0.056
Cu	0.0626	0.0480	0.032	0.036	0.024	0.040	0.048
Fe	13.2	11.1	10.2	13.6	10.2	12.2	11.4
Mg	2.40	0.920	1.02	1.68	1.13	2.20	1.40
Mn	0.0526	0.0400	<0.02	<0.02	<0.02	<0.02	0.048
Pb	12.3	13.2	11.6	12.4	11.2	16.0	13.6
Sr	0.0626	0.0320	<0.01	<0.01	<0.01	<0.01	0.0320
Ti	9.48	0.600	0.343	0.376	0.208	0.400	0.281
Zn	0.265	0.252	0.295	0.310	0.244	0.300	0.253

<sup>a</sup> Acid: 1, 1:1:1 HNO<sub>3</sub>/HClO<sub>4</sub>/HF (25 mL); 2, 1:1 HNO<sub>3</sub>/HClO<sub>4</sub> (10 mL); 3, 1:1 HNO<sub>3</sub>/HClO<sub>4</sub> (20 mL); 4, 3:1 HCl/HNO<sub>3</sub> (8 mL); 5, 3:1 HCl/HNO<sub>3</sub> (12 mL); 6, 6:2:5 HCl/HNO<sub>3</sub>/HClO<sub>4</sub> (13 mL); 7, 6:2:5 HCl/HNO<sub>3</sub>/HClO<sub>4</sub> (19.5 mL). Each sample was digested five times with a fresh volume of acid, the supernatants combined, and then evaporated just to dryness, and 10% HNO<sub>3</sub> (10 mL then 5 mL  $\times$  2) used to solubilize the residue. The fifth digestion contained elements below their LQL concentrations signifying complete recovery for each acid medium.

Table VII. Concentrations of Elements in Red Blood Cells and Serum Fractions in One Human Sample and in NBS Serum

element	red blood cells ( $\mu\text{g}$ of element/g)			human serum, <sup>d</sup> ( $\mu\text{g}$ of element/g)	NBS serum value in $\mu\text{g/g}$ (recovery (%) rel to NBS 909 human serum <sup>d</sup> )
	hot plate <sup>a</sup>	microwave <sup>b</sup>	Parr bomb <sup>c</sup>		
Ba	0.124 <sup>i</sup>	0.236	0.234	<0.038	
Ca	22.8	23.3	23.0	109	121 (100 $\pm$ 8)
Cd	<0.038	<0.038	<0.038	<0.038	0.00124 (113 $\pm$ 13 <sup>h</sup> )
Cr	0.451	0.468	0.478	<0.013	0.0913 (66 $\pm$ 10)
Cu	0.913	0.991	0.992	1.06	1.10 (88 $\pm$ 5)
Fe	800	893	799	<0.63	1.98 (83 $\pm$ 3)
K	2445	2659	2363	166	138 (84 $\pm$ 6)
Li	<0.013	<0.013	<0.013	<0.013	11.5 (91 $\pm$ 6)
Mg	41.4	42.1	38.4	22.5	29.4 (97 $\pm$ 5)
Mn	0.0139 <sup>i</sup>	0.0141 <sup>i</sup>	0.0417	<0.038	
Mo	0.0923 <sup>i</sup>	0.0956 <sup>i</sup>	0.145	0.0754	
Na	1049	1100	1080	4300	3083 (116 $\pm$ 8)
P	570	610	605	186	
Pb	0.267	0.310	0.329	0.0763	0.020 (85 <sup>h</sup> )
S	1391 <sup>i</sup>	1984	1956	1522	
Sr	0.0101 <sup>i</sup>	0.0167	0.0150	0.0373	
Zn	12.4	13.4	12.0	<0.63	

<sup>a</sup> 10-mL sample (0.7916 g dry weight). <sup>b</sup> 10-mL sample (0.7916 g dry weight); closed container digestion. <sup>c</sup> 5-mL sample (0.2996 g dry weight); closed container digestion. <sup>d</sup> 1.15 mL (specific gravity 1.027) and diluted to 10 mL with type I water. <sup>e</sup> Prepared according to instruction using 845.3 mg of freeze-dried standard and then diluted 1/2, 1/3, 1/5, 1/7.5, and 1/15; the mean  $\pm$  standard deviation is reported for all these dilutions. <sup>f</sup> The NBS values for V (0.0027  $\mu\text{g/mL}$ ) were below the LQL (<0.01  $\mu\text{g/mL}$ ). <sup>g</sup> Mean  $\pm$  standard deviation for 1/2 and 1/3 dilutions only; the rest of the dilutions caused concentrations less than the LQL of 0.038  $\mu\text{g/g}$ . <sup>h</sup> At 1/2 dilution only; the rest of the dilutions caused concentrations less than the LQL of 0.095  $\mu\text{g/g}$ . <sup>i</sup> Signifies disagreement with Parr bomb results by more than 20%.

the Parr digestion is taken as reference, the microwave digestion disagreed by more than 20% for Ag and Sb, both near their LQLS. For the 5:4 concentrated HNO<sub>3</sub>/HClO<sub>4</sub> extraction (data not shown) followed by 10% HNO<sub>3</sub> recovery, the only elements extracted quantitatively (better than 80% of the Parr value) were Ca, Cd, Co, Cr, Cu, Mn, Na, Pb, and Zn. Additional treatment with 11.6% HCl/2.8% HNO<sub>3</sub> extracted more Ba (16% of Parr value), Pb (3.2%), S (8.7%), Sr (0.4%), and Ti (0.06%). In fact, the extra recovery extracted more Ba than did the three 10% HNO<sub>3</sub> acid recoveries.

Table VI shows how the hot plate analysis of different elements apart from Pb in a different leaded paint powder depends on the digestion acid mixture used. The amounts of Al, Mg, and Ti tend to vary irreproducibly apart for 1:1 concentrated HNO<sub>3</sub>/HClO<sub>4</sub> for Al and Mg, but Ba, Cr, and Zn tended to be more consistent for the same acid. The elements that are poorly digestible are thus part of an aluminosilicate-type matrix (silicon was confirmed) while those such as Ba, Cr, Fe, Pb, and Zn are much more chemically

available. Thus while the 6:2:5 concentrated HCl/HNO<sub>3</sub>/HClO<sub>4</sub> digestions are the most severe relative to the HF digestion in terms of Al dissolved, the next most severe digestion was 3:1 concentrated HCl/HNO<sub>3</sub>, with the most consistent being 1:1 concentrated HNO<sub>3</sub>/HClO<sub>4</sub>. The greater efficiency of 3:1 concentrated HCl/HNO<sub>3</sub> is associated with the solubilization of Al and Mg compounds. Five sequential digestions of the same paint powder caused concentrations below LQL levels to be attained in each acid mixture by the fifth digestion. This result showed the recovery of each element for that acid medium was complete. Commonly only one digestion and one recovery are performed and this practice could cause imprecise results.

**Water, Rat and Human Urine, and Rat Blood Cells/Serum.** Water samples did not require matrix matching, and the elemental content could be determined directly as long as samples with particulate were filtered. The observed values for the NBS-SRM 1643a standard agreed within 10% for As, Au, Ba, Be, Ca, Cd, Cr, Cu, Fe, Mg, Mn, Mo, Sr, V, and Zn;

Ag, Hg, and Se levels were below the LQLs (<20, <4, and <40 µg/mL, respectively). The levels for Co, K, Ni, and Pb agreed to within ±20%.

The analysis of elements in human urines showed that the values for Ca, Li, Mg, Na, and P were acceptable at a dilution of 1/4; Ba, Ca, Fe, K, and Si estimations were also acceptable (>80% recovery) at a dilution of 1/10. "Spike" studies revealed that Be, Co, Cr, Cu, Mn, Mo, Pt, Sr, Ti, Tl, and V were acceptable at 1/10 dilution (but not 1/4) even though these elements were below their LQLs in the original urine. Elements showing 70–80% recovery at 1/10 dilution but >80% at 1/20 dilution were Al, Cd, Pb, S, and Sb. Elements which gave results that were not acceptable were Ag and Hg (10% HNO<sub>3</sub> dilution was necessary), As, I, Ni, Se, Sn, and Zn. As, Hg, Se, and Sn, however, could all be analyzed through multielemental hydride generation as discussed elsewhere for foods (23), biological tissues (24–27), and aqueous samples (28–30).

Rat urine results were accurate for total element content if no white precipitate was present. Human urine showed no such precipitate, probably because it is much more dilute than rat urine. ICP-AES analysis of the white precipitate obtained after addition of HCl revealed that Mg, Cl, P, K, and C predominated (>126 µg/mL urine), Na, Ca, and S were minor elements (6–20 µg/mL urine), and Fe, Cu, and Zn were present in trace amounts (<60 ng/mL urine). It is possible that the mineral component of the precipitate is a complex phosphoroxometal halide compound since the content of Mg, K, and C varied markedly from one urine to another but not the P levels.

The elemental content of red blood cells and serum for the same human sample and also NBS SRM 909 serum are shown in Table VII. The values shown have relative standard deviations within 10%. For the red blood cells, the hot plate digestion caused significant losses of Ba (47%), Mn (67%), Mo (36%), S (29%), and Sr (33%) relative to the Parr bomb digestion. The elements also showing significant loss for the microwave digestion relative to the Parr bomb were Mn (66%) and Mo (34%) which must be very volatile since the rest of elements which were lost for the hot plate digestion were not in the microwave technique. The preferred method to analyze red blood cells is the Parr bomb method.

For the serum, a 1:2 dilution with water was sufficient to attain values within 20% of the NBS certified values except for Cr. Dilution of the serum is quicker, convenient, and more efficient than digestion.

**Other Biological Samples.** Table VIII contains the results for the Parr, microwave, and hot plate digestion for NBS citrus leaves (SRM 1572). All three techniques generally gave results within 20% of the certified value except the hot plate technique for Al (loss of 30%) and Fe (loss of 40%), and the Parr and microwave techniques for Pb where the values were only within 75% of the certified value.

Table IX compares the Parr bomb and hot plate methods for the various rat organs. All relative standard deviations are ≤10%. In addition, the Parr, microwave, and hot plate techniques are compared for NBS bovine liver SRM-1577a and the testes of a male Sprague-Dawley rat. The Parr bomb values agreed with the NBS certified values within 20% except for Al which were uncertified. Both microwave and hot plate techniques using 100 mg showed losses for Al, Cd, and Zn with losses for the hot plate method being demonstrated also for Co; both techniques led to overestimates for As. Even when a 1-g sample was used in the hot plate analysis (Table IX) to enhance sensitivity, values for Al, Cd, and Zn were low, confirming loss of these elements. For the testes samples, all the elements agreed well except for Fe, which was partially lost by the microwave and hot plate methods, as was probably

Table VIII. Comparison of Digestion Techniques for NBS Citrus Leaves SRM 1572 (Concentrations are in mg/g)<sup>a</sup>

element	certified value <sup>b</sup>	digestion technique		
		Parr <sup>c</sup>	microwave <sup>c</sup>	hot plate
Ag	NR	<0.005	<0.005	<0.005
Al	0.092 ± 0.015	0.087 ± 0.012	<0.1	0.064 ± 0.018 <sup>d</sup>
Ba	0.021 ± 0.003	0.0189 ± 0.0001	0.0195 ± 0.0006	0.0193 ± 0.0005
Ca	31.5 ± 1.0	31.5 ± 0.2	31.3 ± 1.4	32 ± 1
Cd	(0.00003)	<0.001	<0.0012	<0.001
Co	NR	<0.001	<0.001	<0.001
Cr	(0.0008)	<0.005	<0.005	<0.005
Cu	0.0165 ± 0.0010	0.017 ± 0.002	0.019 ± 0.002	0.016 ± 0.001
Fe	0.090 ± 0.010	0.081 ± 0.003	0.074 ± 0.006	0.054 ± 0.018 <sup>d</sup>
K	18.2 ± 0.6	16.8 ± 0.1	17.2 ± 0.4	17.6 ± 0.4
Li	NR	<0.0002	0.00015	0.00016
Mg	5.8 ± 0.3	5.48 ± 0.08	5.86 ± 0.17	5.59 ± 0.08
Mn	0.023 ± 0.002	0.021	0.025 ± 0.001	0.0215 ± 0.0007
Na	0.160 ± 0.020	0.177 ± 0.006	0.164 ± 0.003	0.183 ± 0.002
P	1.3 ± 0.2	1.48 ± 0.01	1.33 ± 0.03	1.4 ± 0.3
Pb	0.0133 ± 0.0024	0.010 ± 0.001 <sup>c</sup>	0.010 ± 0.001 <sup>d</sup>	0.011 ± 0.001
S	4.07 ± 0.09	4.40 ± 0.05	4.56 ± 0.06	4.42 ± 0.07
Sb	NR	<0.005	<0.005	<0.005
Si	NR	<0.04	<0.04	<0.04
Sr	0.100 ± 0.002	0.098 ± 0.001	0.101 ± 0.002	0.102 ± 0.002
Ti	NR	<0.001	<0.001	<0.001
Zn	0.029 ± 0.002	0.029 ± 0.002	0.0324 ± 0.0005	0.0268 ± 0.0004
b	6.14	6.02	6.07	6.15

<sup>a</sup>Other uncertified elements were as follows (in mg/g): As, 0.0031 ± 0.0003; Mo, 0.00017 ± 0.00009; Ni, 0.00006 ± 0.0003; Rb, 0.160 ± 0.020; N, 28.6; Cl, 0.414. <sup>b</sup>Certified elements mass balance (weight %). NR means not recorded; values in parentheses in the certified column are uncertified. <sup>c</sup>Closed container. <sup>d</sup>Signifies greater than 20% disagreement from the certified value.

Al. Sr was partially lost in the spleen, kidney, and testes for the hot plate technique. Li and P values by the hot plate technique for the spleen were significantly greater (29% and 22%, respectively). It is clear that the Parr bomb method remains the method of choice for animal organs and citrus leaves.

## CONCLUSIONS

There are no trends for the elements which did not show quantitative recovery (at <80%) relative to NBS certified values for the Parr bomb, microwave, and hot plate techniques. For example, for NBS phosphate rocks, Zn is the sole element not analyzable by the closed container microwave technique, and only in SRM 694. This confirms the results of Nadkarni (3) who showed that the microwave closed-container method compared well with the Parr bomb technique for many environmental sample types. The biological matrices can also be accurately analyzed except for Cr by dilution in serum SRM 909, Al and Fe (hot plate) and Pb (Parr and microwave) for citrus leaves (SRM 1572), and As, Cd, and Zn using both microwave and hot plate methods and also Co using the microwave method for liver (SRM 1577a). It is clear that the Parr bomb technique is the reference method. Each matrix has its specific volatile elements, there being no common trends. The same trend occurs for the comparisons with the Parr bomb technique where a suitable NBS reference was not available. The Cincinnati soil results indicate problems relative to closed-container microwave digestions for Li, P,



Table IX. Comparison of Digestion Techniques for Various Animal Organs

NBS Bovine Liver <sup>a</sup> SRM 1577a (μg/g of dry weight)									
element	certified value	Parr <sup>c</sup>	microwave <sup>e</sup>	hot plate <sup>c</sup>	hot plate (1 g)				
Ag	0.04	<4	<4	<4	<0.4				
Al	(2)	2.7 ± 0.4 <sup>f</sup>	1.5 ± 1.5 <sup>f</sup>	<3	0.66 ± 0.27 <sup>g</sup>				
As	0.047 ± 0.006	0.042 ± 0.005	0.059 ± 0.004 <sup>g</sup>	0.067 ± 0.005 <sup>g</sup>	0.036 ± 0.001				
Ba	NR	0.04 ± 0.03	0.08 ± 0.02	<0.1	0.21 ± 0.02				
Ca	120 ± 7	127 ± 3	115 ± 3	122 ± 26	109 ± 5				
Cd	0.44 ± 0.06	0.45 ± 0.24	0.29 ± 0.01 <sup>g</sup>	0.31 ± 0.02 <sup>g</sup>	0.24 ± 0.07				
Co	0.21 ± 0.05	0.24 ± 0.04	0.12 <sup>g</sup>	0.18 ± 0.16	0.22 ± 0.01				
Cr	NR	0.15 ± 0.06	<0.2	<0.2	<0.02				
Cu	158 ± 7	153 ± 1	145 ± 2	148 ± 1	131 ± 8				
Fe	194 ± 20	195 ± 17	159 ± 2	167 ± 7	144 ± 12 <sup>g</sup>				
Hg	0.004 ± 0.002	<1	<1	<1	<0.1				
K	9960 ± 70	8910 ± 180	8410 ± 96	8280 ± 110	6540 ± 570 <sup>g</sup>				
Li	NR	0.20 ± 0.04	0.22 ± 0.07	0.24 ± 0.03	0.17 ± 0.01				
Mg	600 ± 15	580 ± 9	527 ± 13	544 ± 18	443 ± 46 <sup>g</sup>				
Mn	9.9 ± 0.8	10.0 ± 0.6	8.3 ± 0.1	8.9 ± 0.3	7.3 ± 0.7 <sup>g</sup>				
Mo	3.5 ± 0.5	3.65 ± 0.05	3.30 ± 0.04	3.5 ± 0.2	2.9 ± 0.2				
Na	2430 ± 130	2900 ± 30	2930 ± 20	2948 ± 5	2390 ± 170				
P	11100 ± 400	11470 ± 630	12110 ± 80	12920 ± 430	11470 ± 1080				
Pb	0.135 ± 0.015	0.16	<0.2	<0.2	<0.02 <sup>g</sup>				
S	7800 ± 100	8620 ± 170	6820 ± 200	6600 ± 160	4670 ± 350 <sup>g</sup>				
Sb	(0.003)	<0.7	<0.7	<0.7	<0.07				
Se	0.71 ± 0.07	<2	<2	<2	<0.2				
Si	NR	12 ± 1	11 ± 2	4 ± 1	<0.2				
Sr	0.138 ± 0.003	0.14 ± 0.01	0.14 ± 0.03	0.16 ± 0.01	0.14 ± 0.01				
Ti	NR	<0.4	<0.4	<0.4	<0.04				
Tl	(0.003)	<8	<8	<8	<0.8				
V	NR	<0.4	<0.4	<0.4	<0.04				
Zn	123 ± 8	116 ± 2	89 ± 3 <sup>g</sup>	96 ± 3 <sup>g</sup>	67 ± 9 <sup>g</sup>				
e	3.25	3.31	3.13	3.18	2.60				
Sprague-Dawley Male Rat <sup>b</sup> (μg/g wet weight)									
	liver <sup>d</sup>		spleen <sup>d</sup>		kidney <sup>d</sup>		testes <sup>d</sup>		
	Parr	hot plate	Parr	hot plate	Parr	hot plate	Parr	hot plate	microwave
Ag	<4	<4	<4	<4	<4	<4	<4	<4	<4
Al	<4	<4	<4	<4	<4	<4	0.61	<1	<1
As	<4	<4	<4	<4	<4	<4	<4	<4	<4
Ba	<0.08	<0.08	<0.08	<0.08	<0.08	<0.08	<0.08	<0.08	<0.08
Ca	41	39	119	114	111	97	36	30	34
Cd	<0.8	<0.8	<0.8	<0.8	<0.8	<0.8	<0.8	<0.8	<0.8
Co	<0.8	<0.8	<0.8	<0.8	<0.8	<0.8	0.8	0.8	0.8
Cr	<4	<4	<4	<4	<4	<4	<4	<4	<4
Cu	4.5	4.4	3.2	3.7	13	12	1.6	1.6	1.3
Fe	84	78	1960	2070	108	97	18	11 <sup>g</sup>	14 <sup>g</sup>
Hg	<0.8	<0.8	<0.8	<0.8	<0.8	<0.8	<0.8	<0.8	<0.8
K	3170	3020	6030	6830	2640	2550	2210	1950	2015
Li	<0.08	<0.08	0.085	0.110 <sup>g</sup>	<0.08	<0.08	0.0075	0.0070	0.0071
Mg	228	225	474	540	330	310	130	104	109
Mn	2.4	2.3	<0.8	<0.8	1.7	1.6	0.25	0.20	0.22
Mo	<40	<40	<40	<40	<40	<40	0.105	0.100	0.100
Na	924	900	5630	5630	4380	3960	1540	1360	1410
P	3520	3670	9200	11200 <sup>g</sup>	5250	5240	1920	1720	1830
Pb	<4	<4	<4	<4	<4	<4	<2	<2	<2
S	2920	2770	6200	6710	4140	3850	1200	1010	1010
Sb	<4	<4	<4	<4	<4	<4	<4	<4	<4
Se	<4	<4	<4	<4	<4	<4	<2	<2	<2
Si	<8	<8	<8	<8	<8	<8	11	10	10
Sr	<0.08	<0.08	0.70	0.51 <sup>g</sup>	0.32	0.23 <sup>g</sup>	0.084	0.063 <sup>g</sup>	0.070 <sup>g</sup>
Ti	<0.8	<0.8	<0.8	<0.8	<0.8	<0.8	<0.8	<0.8	<0.8
Tl	<4	<4	<4	<4	<4	<4	<4	<4	<4
V	<0.8	<0.8	<0.8	<0.8	<0.8	<0.8	<0.8	<0.8	<0.8
Zn	22	22	45	52	35	33	24	22	22
f	1.09	1.07	2.97	3.32	1.70	1.62	0.709	0.622	0.646

<sup>a</sup> Other elements ( $\mu\text{g/g}$ ): Cl, 2800  $\pm$  100; Br, 9; N, (107000). <sup>b</sup> 132 days old with last 52 days exposed to AIN-76 diet. <sup>c</sup> 100 mg dry weight used; Parr and microwave digestions were closed container. <sup>d</sup> 240 mg homogenate used. <sup>e</sup> Certified elements mass balance (wt %). <sup>f</sup> Elemental mass balance (wt %). <sup>g</sup> Differs from the Parr bomb value by more than 20%.

and Ti and for Ag and Sb levels in the NBS leaded paint (SRM 1579). While the microwave technique is generally acceptable for most elements in environmental media, there

are problems for Al, Mn, Mo, and Fe in biological media. The hot plate technique definitely causes loss of Sr from biological samples and is significantly worse relative to the number of

elements (Ba, Fe, Li, Mn, Mo, P, S, Sr) giving results which may not agree within 20% of the Parr bomb values. Hence, the Parr bomb method must also be regarded as the reference technique in the absence of a NBS standard.

This work has shown that it is possible to obtain precise but inaccurate results if salt effects are not taken into account in ICP-AES analyses, e.g. the hot plate digestion of 1 g of NBS liver. The availabilities of digested elements for soils and paints to various acid mixtures differ with the optimum acid used for recovery in paint or Cincinnati soil analysis being 11.6% HCl/2.8% HNO<sub>3</sub> using sequential extractions; however, 10% HNO<sub>3</sub> is adequate for analysis of NBS phosphate rocks. The more digestible elements are more available to exert their toxic/desirable effects than those which are less available. In certain cases, therefore, the total elemental content of a sample may not be an indicator of the potential adverse effects expected from the sample, the more available toxic elements being the better indicators. The less available elements are potential tracers of soil or paint ingestion to be monitored in the feces. The only promising tracer elements in Cincinnati soils and feces from Cincinnati children were Si and Ti.

This work has also led to methodological advances; the carbon content of digestions is a good parameter of the effectiveness of the digestion technique used, and the magnitude of the carbon interference on As and Se signifies that the carbon content of the analyte has to be  $\leq 3000 \mu\text{g/mL}$  or else a modified  $k$  factor correction must be used, a correction adequate to  $10000 \mu\text{g of C/mL}$ . These results have not been reported before by previous investigators. Sequential digestion and sequential recovery, not just one digestion and one recovery, are necessary to obtain quantitative results. This conclusion also has not been reported by previous investigators except for a single-element determination for lead (21).

The use of modified  $k$  factors allows the variability of spectral interferences and sample background to be corrected for and shortens the setting up of analytical control tables (ACTs). This procedure is also applicable to the new Thermo Jarrell-Ash ICAP-61 spectrometer where background correction is more flexible (31) and is performed first.

Toward the end of this investigation, the Parr 4781 microwave bomb (32) became available and is still under investigation in our laboratory. This may combine the qualities of the Parr bomb in retaining volatiles and having a short time of heating characteristic of the microwave technique.

#### ACKNOWLEDGMENT

We thank Tim Macdonald for his assistance in the early part of this work, the Cincinnati Lead Program Project for a supply of environmental media and feces, and Diane Gorman for excellent typing.

**Registry No.** Ag, 7440-22-4; Al, 7429-90-5; As, 7440-38-2; Ba, 7440-39-3; Ca, 7440-70-2; Cd, 7440-43-9; Co, 7440-48-4; Cr, 7440-47-3; Cu, 7440-50-8; Fe, 7439-89-6; Hg, 7439-97-6; K, 7440-09-7; Li, 7439-93-2; Mg, 7439-95-4; Mn, 7439-96-5; Mo, 7439-98-7; Na, 7440-23-5; P, 7723-14-0; Pb, 7439-92-1; S, 7704-34-9; Sb,

7440-36-0; Se, 7782-49-2; Si, 7440-21-3; Sr, 7440-24-6; Ti, 7440-32-6; Tl, 7440-28-0; V, 7440-62-2; Zn, 7440-66-6; Ni, 7440-02-0; C, 7440-44-0.

#### LITERATURE CITED

- (1) Katz, S. A. *Am. Lab. (Fairfield, Conn.)* **1984**, *16*(12), 24-30.
- (2) Viets, J. G.; O'Leary, R. M.; Clark, J. R. *Analyst (London)* **1984**, *109*, 1589-1592.
- (3) Nadkarni, R. A. *Anal. Chem.* **1984**, *56*, 2233-2237.
- (4) Brenner, I. B.; Ehrlich, S. *Appl. Spectrosc.* **1984**, *38*, 887-890.
- (5) Matthes, S. A.; Farrell, R. F.; Mackie, A. J. *Tech. Prog. Rep.—U.S., Bur. Mines* **1983**, No. 120.
- (6) Hull, R. D.; Millson, M. NIOSH Method 7300; *NIOSH Manual of Analytical Methods*, 3rd ed.; Eller, P. M., Ed.; DHHS (NIOSH) Publication No. 84-100, Department of Health and Human Services, 1984.
- (7) Church, S. E. In *Developments in Atomic Plasma Spectrochemical Analysis*; Barnes, R. M., Ed.; Heyden: Philadelphia, PA, 1981; pp 410-434.
- (8) Munter, R. C.; Grande, R. A. In *Developments in Atomic Plasma Spectrochemical Analysis*; Barnes, R. M., Ed.; Heyden: Philadelphia, PA, 1981; pp 653-672.
- (9) Hull, R. D. NIOSH Method 8310; *NIOSH Manual of Analytical Methods*, 3rd ed.; Eller, P. M., Ed.; DHHS (NIOSH) Publication No. 84-100, Department of Health and Human Services, 1984.
- (10) Zhuang, M.; Barnes, R. M. *Appl. Spectrosc.* **1984**, *38*, 635-644.
- (11) Okamoto, K.; Fuwa, K. *Anal. Chem.* **1984**, *56*, 1758-1760.
- (12) Thompson, M.; Walsh, J. N. A *Handbook of Inductively Coupled Plasma Spectrometry*; Chapman and Hall: New York, 1983; pp 223-227.
- (13) U.S. Department of Commerce National Bureau of Standards *NBS Standard Reference Materials Catalog 1986-87*; NBS Special Publication 260; Seward, R. W., Ed.; National Bureau of Standards: Washington, DC, 1986.
- (14) Date, A. R. *Analyst (London)* **1982**, *107*, 7-12.
- (15) Abu-Samra, A.; Morris, J. S.; Koltrich, S. R. *Anal. Chem.* **1975**, *47*, 1475-1477.
- (16) Barrett, P.; Davidowski, L. J.; Penaro, K. W.; Copeland, T. R. *Anal. Chem.* **1978**, *50*, 1021-1023.
- (17) Mahan, K. I.; Federato, T. A.; Garza, T. L.; Martinez, R. M.; Maroney, G. A.; Trivisonno, M. R.; Willging, E. M. *Anal. Chem.* **1987**, *59*, 938-945.
- (18) Lamothe, P. J.; Fries, T. L.; Consul, J. J. *Anal. Chem.* **1986**, *58*, 1881-1886.
- (19) Kingston, H. M.; Jassie, L. B. *Anal. Chem.* **1986**, *58*, 2534-2541.
- (20) Que Hee, S. S.; Macdonald, T. J.; Boyle, J. R. *Anal. Chem.* **1985**, *57*, 1242-1252.
- (21) Que Hee, S. S.; Pearce, B.; Clark, C. S.; Boyle, J. R.; Bornschein, R. L.; Hammond, P. B. *Environ. Res.* **1985**, *38*, 77-95.
- (22) Igwe, O. J.; Que Hee, S. S.; Wagner, W. D. *Fundam. Appl. Toxicol.* **1986**, *6*, 733-746.
- (23) Hahn, M. H.; Wolnik, K. A.; Fricke, F. L.; Caruso, J. A. *Anal. Chem.* **1982**, *54*, 1048-1052.
- (24) Pruszkowska, E.; Thompson, M.; Thorne, L. *Analyst (London)* **1981**, *106*, 467-471.
- (25) Pruszkowska, E.; Parrett, P.; Ediger, R.; Wallace, G. *At. Spectrosc.* **1983**, *4*, 94-98.
- (26) Robbins, W. B.; Caruso, J. A. *J. Chromatogr. Sci.* **1979**, *17*, 360-367.
- (27) Subramanian, K. S.; Meranger, J. C. *Analyst (London)* **1982**, *107*, 157-162.
- (28) Nygaard, D. D.; Lowry, J. H. *Anal. Chem.* **1982**, *54*, 803-807.
- (29) Thompson, M.; Pahlavanpour, B.; Walton, S. J.; Kirkbright, G. F. *Analyst (London)* **1978**, *103*, 568-579.
- (30) Thompson, M.; Pahlavanpour, B.; Walton, S. J.; Kirkbright, G. F. *Analyst (London)* **1978**, *103*, 705-713.
- (31) Nygaard, D. D.; Luciano, V. J.; Sotera, J. J. *Am. Lab. (Fairfield, Conn.)* **1987**, *19*(8), 92-95.
- (32) Parr Instrument Company *Microwave Acid Digestion Bombs*; Bulletin 4780 2/87, 1987.

RECEIVED for review September 4, 1987. Accepted January 4, 1988. This work was supported by U.S. PHS Grant ES-00159.

# Effects of Metal Cations on the Fluorescence Intensity of Polycyclic Aromatic Hydrocarbons in Sodium Taurocholate Micellar Solutions

Kasem Nithipatikom and Linda B. McGown\*

Department of Chemistry, P. M. Gross Chemical Laboratory, Duke University, Durham, North Carolina 27706

The effects of  $Tb^{3+}$ ,  $Eu^{3+}$ , and  $Al^{3+}$  on the fluorescence intensity of polycyclic aromatic hydrocarbon (PAH) compounds in sodium taurocholate (NaTC) micellar solutions were determined. Aqueous solubility of the PAH appears to play an important role in the effects of the cations, which ranged from fluorescence quenching of relatively soluble PAHs to as much as 18-fold enhancement for the more hydrophobic PAHs. Sensitivities and detection limits were determined for five PAHs in sodium dodecyl sulfate (SDS) micelles, NaTC micelles, and NaTC micelles with  $Tb^{3+}$ . Although poorest results were obtained with NaTC micelles, the addition of  $Tb^{3+}$  increased sensitivities and decreased detection limits in most cases to levels at least as good as those obtained with SDS. Detection limits for benzo[k]fluoranthene were an order of magnitude lower in NaTC- $Tb^{3+}$  than in SDS.

Sodium taurocholate (2-[[[(3 $\alpha$ ,5 $\beta$ ,7 $\alpha$ ,12 $\alpha$ )-3,7,12-trihydroxy-24-oxocholan-24-yl]amino]ethanesulfonate sodium salt), NaTC, is a micelle-forming bile salt. The three hydroxy groups on the cholic acid part of the molecule play an important role in the micellar characteristics of NaTC and, along with the taurine group, serve to solubilize NaTC in aqueous solutions (1). The most commonly observed micellar form has an aggregation number of four and can bind other molecules in the relatively hydrophobic interior, usually with a 1:1 stoichiometry (2). The formation of secondary micelles has not been observed. Insoluble biological lipids can be solubilized by comicellization with NaTC (3) and NaTC can also form mixed micelles with detergent molecules (2).

The micellar properties of NaTC are relatively insensitive to experimental conditions. The aggregation number and critical micelle concentration (cmc) show very little dependence on pH in the range of 1.6-10 (1), on counterion concentration, and on temperature in the range of 10-60 °C (3). A cmc of 3 mM was found from the shift in the absorption wavelength maximum of Rhodamine 6G (3). In a recent study, fluorescent probes were used to study the properties of the NaTC micellar binding site (4).

We describe here the effects of the trivalent metal cations  $Tb^{3+}$ ,  $Eu^{3+}$ , and  $Al^{3+}$  on the fluorescence intensities of polycyclic aromatic hydrocarbons (PAHs) in NaTC micellar solutions. Sensitivities and detection limits for five PAHs were determined in NaTC micelles alone and in the presence of each of the metals, and in sodium dodecyl sulfate (SDS) micelles.

## EXPERIMENTAL SECTION

The NaTC (Mallinkrodt), SDS (Fluka), carbazole and perylene (Aldrich), phenanthrene, benzo[b]fluoranthene (BbF), benzo[k]fluoranthene (BkF), benzo[ghi]perylene (BgP), 9-methylanthracene (9MA), phenanthrene, and fluoranthene (Foxboro), and 9,10-dichloroanthracene (DCA, from Alfa) were all used without further purification. Pyrene, anthracene, benzo[a]pyrene (BaP), benzo[e]pyrene (BeP), 9,10-dimethylanthracene (DMA),

Table I. Effects of Metal Cations on PAH Intensity in NaTC Micellar Solutions<sup>a</sup>

compounds	solubility, <sup>b</sup> $\mu$ M	intensity ratio <sup>c</sup>		
		Tb	Eu	Al
phenanthrene	7.2	0.61	0.49	0.67
anthracene	4.1	1.3	1.2	1.2
9-methylanthracene	1.4	2.2	1.7	
fluoranthene	1.3	0.76	0.99	
pyrene	0.67	2.0	0.61	
9,10-dimethylanthracene	0.27	3.9	3.3	
2-methylanthracene	0.20	3.8	3.4	
benzo[a]pyrene	0.015	5.7	4.8	
perylene	0.0016	10.3	6.2	12.7
benzo[ghi]perylene	0.00094	7.8	6.5	
benzo[e]pyrene		1.1	1.0	
9-phenylanthracene		4.6	4.2	
benzo[b]fluoranthene		3.0	3.0	
benzo[k]fluoranthene		17.9	17.8	11.4
9,10-dichloroanthracene		3.6	3.7	
carbazole		0.65	0.45	

<sup>a</sup> PAHs 2.0  $\mu$ M, NaTC 10 mM, metal cations 10 mM, measurements made 1 h after mixing, 25 °C. <sup>b</sup> Solubilities from ref 6. <sup>c</sup> Ratio of PAH intensity in NaTC-metal to intensity in NaTC alone.

2-methylanthracene (2MA), and 9-phenylanthracene (9PA) were obtained from Aldrich and recrystallized from ethanol. The metal solutions were prepared from the nitrate salts (>99.99% purity) of the metals. Distilled demineralized water was used for solution preparations.

Stock solutions of the PAHs were prepared in ethanol. Aqueous stock solutions of the micelles were prepared fresh daily to avoid errors due to aging (5). Micellar solutions of the PAHs were prepared by gently evaporating the ethanol from the appropriate volume of the PAH stock solution, followed by dilution with the NaTC micelle stock solution in a volumetric flask and sonication for at least 1 h. None of the solutions was deoxygenated.

All fluorescence measurements were made with an SLM 4800S spectrofluorometer (SLM Instruments, Inc., Urbana, IL) with a 450-W xenon arc lamp source, excitation and emission monochromators for wavelength selection, and photomultiplier tube detectors. The sample chamber was maintained at  $25.0 \pm 0.1$  °C with a Haake A81 temperature controller. Fluorescence intensities were measured in triplicate in the "100-average" mode, in which each measurement is the average of 100 samplings over a 30-s period, performed internally by the spectrofluorometer electronics. The monochromator entrance and exit slits were set at 4 nm. Absorption spectra were collected on a Perkin-Elmer Lambda Array spectrophotometer.

## RESULTS AND DISCUSSION

### Effects of Metal Cations on Fluorescence Intensity.

The effects of  $Eu^{3+}$ ,  $Tb^{3+}$ , and  $Al^{3+}$  on the fluorescence intensities of PAHs in aqueous NaTC solutions are shown in Table I. The intensity ratios are expressed as the ratio of the intensity in the presence of the metal to the intensity in the absence of the metal, measured at the emission and excitation wavelength maxima of the PAH in NaTC without the

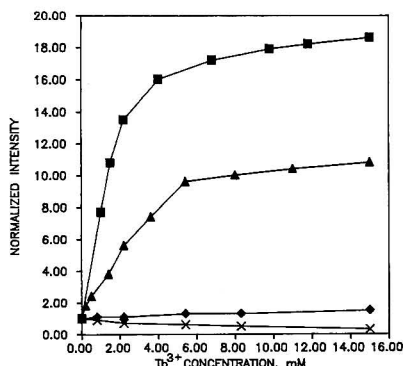


Figure 1. Fluorescence intensity of PAHs (2  $\mu$ M) in NaTC (10 mM) as a function of  $Tb^{3+}$  concentration: (■) BkF; (▲) perylene; (◆) anthracene; (X) carbazole.

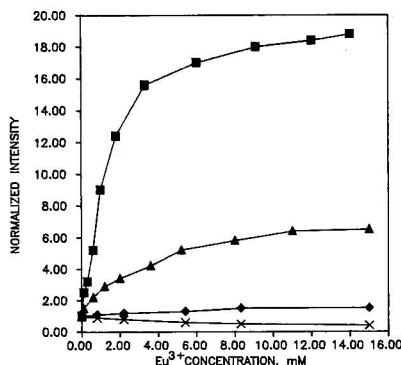


Figure 2. Fluorescence intensity of PAHs (2  $\mu$ M) in NaTC (10 mM) as a function of  $Eu^{3+}$  concentration, legend as in Figure 1.

metal. For most of the PAHs,  $Eu^{3+}$  and  $Tb^{3+}$  had very similar effects. One exception to this was pyrene fluorescence, which was enhanced by  $Tb^{3+}$  but quenched by  $Eu^{3+}$ . This may be due to different effects of the cations on the vibronic structure of pyrene, which is very sensitive to its microenvironment. Precipitation occurred in most of the NaTC-PAH solutions upon the addition of  $Al^{3+}$ , and intensity ratios were obtained for only four of the PAHs. These results agreed roughly with those obtained for the two heavy metals.

Aqueous solubilities have been reported in the literature for some of the PAHs (6) and are shown in Table I. There is a definite trend toward increased enhancement as the aqueous solubility of the PAH decreases. For all of the metals, BkF showed the most enhancement, followed by perylene and BgP which are the least soluble of those PAHs for which solubilities were reported. Carbazole, fluoranthene, and phenanthrene, all of which are relatively soluble, exhibited quenching in the presence of the metals.

Fluorescence intensity of four of the PAHs as a function of metal ion concentration is shown for  $Tb^{3+}$  in Figure 1 and for  $Eu^{3+}$  in Figure 2. The curves for each PAH are very similar for both metals, except for perylene which is more strongly enhanced by  $Tb^{3+}$ . Absorption spectra were collected from NaTC solutions of DMA and BkF in the presence and absence of  $Tb^{3+}$  and for DMA and phenanthrene in the presence and absence of  $Eu^{3+}$ . Absorption bands at 300 nm were identical with those observed in the absorption spectra

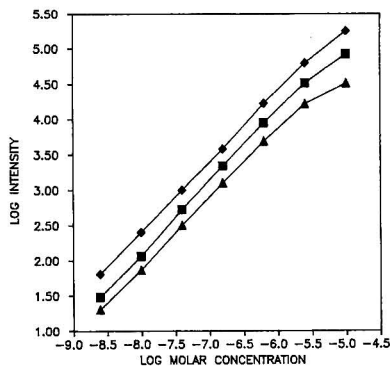


Figure 3. log plots of calibration curves for pyrene: (■) SDS, 10 mM; (▲) NaTC, 10 mM; (◆) NaTC, 10 mM with 10 mM  $Tb^{3+}$ .

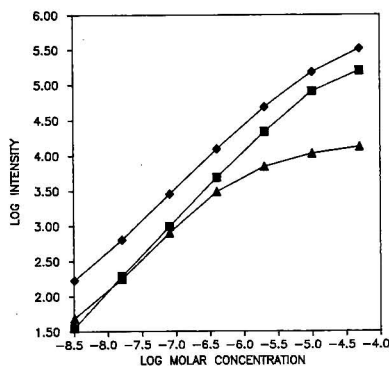


Figure 4. log plots of calibration curves for BgP, legend as in Figure 3.

of the metals in NaTC, and the bands were eliminated from the PAH-metal spectra upon subtraction of the metal spectra. No other absorption bands were observed in any of the spectra in the 250–400 nm range (the absorption bands of the PAHs were too weak to be observed), and the solutions of the metals in NaTC did not have any fluorescence emission in the region of the PAH fluorescence. Therefore, it appears that the fluorescence enhancements were due primarily to increased quantum efficiency rather than increased molar absorptivity.

Further studies are needed to determine, first, the mechanisms of the quenching and enhancement caused by the metal cations and, second, their relative contributions to the observed intensity changes and their dependence on PAH structure and solubility. Collisional quenching of the excited state of pyrene in NaTC by  $Cu^{2+}$  has been reported (7), and similar collisional quenching mechanisms may be involved in the systems discussed here. It is also possible that energy transfer from the PAH to the metal contributes to the quenching, although we did not observe any emission from the metals. Enhancements may result from increased structural rigidity of the NaTC-bound PAH in the presence of the metal cations, as well as from reduced access of the aqueous solution to the PAH molecule. These and other possible explanations for the observed intensity effects are currently under investigation.

**Sensitivity and Detection Limits.** Calibration curves of log intensity vs log PAH concentration are shown for pyrene in Figure 3 and for BgP in Figure 4, for SDS micellar solutions,

Table II. Detection Limits for PAH Compounds, in nM

	NaTC	NaTC-Tb <sup>3+</sup>	SDS
anthracene	4.4	0.68	0.46
BgP	4.4	0.69	2.0
pyrene	0.76	0.090	0.15
BkF	0.49	0.021	0.20
perylene	0.36	0.059	0.12

NaTC micellar solutions, and NaTC with Tb<sup>3+</sup>. For both PAHs, highest sensitivity was obtained with NaTC-Tb<sup>3+</sup>. It is also interesting that the linear range extends to higher concentrations for SDS and NaTC-Tb<sup>3+</sup> than for NaTC alone, especially in the case of BgP. This may be due to poorer solubilization of the PAHs in the NaTC solution, which would indicate that the addition of the metal to the NaTC solution increases either the binding equilibrium or the stoichiometry of the PAH-NaTC association.

Detection limits were found for five PAHs, including anthracene, BgP, pyrene, BkF, and perylene, in SDS, NaTC, and NaTC-Tb<sup>3+</sup> solutions. The results are shown in Table II. The detection limit was calculated as the concentration of PAH, found from a linear calibration curve of five points run in triplicate, required to produce a signal equal to the blank signal (averaged for 15 measurements) plus three times the standard deviation of the blank signal. For all five of the PAHs, highest detection limits were found for NaTC. For all but anthracene, detection limits were significantly lower for NaTC-Tb<sup>3+</sup> than for SDS, most notably for BkF for which the detection limits differed by an order of magnitude.

### CONCLUSIONS

Several conclusions may be drawn from the intensity ratio experiments. The effects of the heavy metals Eu<sup>3+</sup> and Tb<sup>3+</sup> are similar to each other and to the effects of Al<sup>3+</sup>, indicating that the ionic charge is probably more important than ionic size in determining the extent of enhancement. Ionic size is probably more critical to precipitate formation which occurred for most of the PAHs with NaTC-Al<sup>3+</sup> but not with the heavy metal ions in NaTC. It is likely that the metal cation is coordinated to the negatively charged taurine groups of the NaTC micelle. The resulting increase in structural rigidity and decrease in accessibility of the interior of the micelle (including the hydrophobic binding site) to the surrounding aqueous solution should serve to decrease nonradiative deexcitation pathways of the bound PAH, thereby increasing the fluorescence quantum yield. Such an effect has been

previously reported for Mg<sup>2+</sup> in NaTC micelles (2). It is also possible that the metal ion changes the properties of the NaTC micelle in terms of aggregation number, binding stoichiometry, and cmc. The role of PAH solubility may simply be to determine whether the PAH is located in the hydrophobic binding site, on an exterior portion of the micelle, or in the aqueous solution. Other properties of the PAHs may also need to be considered in order to explain the effects of the metal cations. These areas are currently under investigation.

Studies of NaTC micelles are clearly applicable to the analytical chemistry of PAHs. Micelles are often used to solubilize PAHs in aqueous solution and, although the intensities of PAHs in NaTC micelles are generally not as high as in detergent micelles, the work described here demonstrates that the addition of metal cations to the NaTC solutions can be used to increase the PAH intensities to levels at least as high as those observed in detergents. Aside from intensity considerations, NaTC micelles are in many ways preferable to detergent micelles. They are much easier to work with because they exhibit less sudsing and much lower light scattering levels. They are more versatile in terms of their tolerances of pH, ionic strength, temperature, and counterion concentrations and are less likely to precipitate. Therefore, the use of NaTC with metal enhancement may simplify experimental procedures without sacrificing sensitivity and detection limits, and in some cases can even improve detection limits by as much as an order of magnitude.

Registry No. NaTC, 145-42-6; SDS, 151-21-3; BbF, 205-99-2; BkF, 207-08-9; BgP, 191-24-2; 9MA, 779-02-2; DCA, 605-48-1; BaP, 50-32-8; BeP, 192-97-2; DMA, 781-43-1; 2MA, 613-12-7; 9PA, 602-55-1; Tb, 7440-27-9; Eu, 7440-53-1; Al, 7429-90-5; phenanthrene, 85-01-8; anthracene, 120-12-7; fluoranthene, 206-44-0; pyrene, 129-00-0; perylene, 198-55-0; carbazole, 86-74-8.

### LITERATURE CITED

- (1) Small, D. M. In *Molecular Association in Biological and Related Systems*; Advances in Chemistry Series No. 84; Gould, R. F., Ed.; American Chemical Society: Washington, DC, 1968; pp 31-52.
- (2) Chen, M.; Gratzel, M.; Thomas, J. K. *J. Am. Chem. Soc.* **1975**, *97*, 2052.
- (3) Carey, M. C.; Small, D. M. *J. Colloid Interface Sci.* **1969**, *31*, 382.
- (4) Nithipattikom, K.; McGown, L. B. *Photochem. Photobiol.*, in press.
- (5) Gratzel, M.; Thomas, J. K. *J. Am. Chem. Soc.* **1973**, *95*, 6885.
- (6) McKay, D.; Shiu, W. Y. *J. Chem. Eng. Data* **1977**, *22*, 399.
- (7) Hashimoto, S.; Thomas, J. K. *J. Colloid Interface Sci.* **1984**, *102*, 152.

RECEIVED for review October 14, 1987. Accepted January 26, 1988. This work was supported by the United States Army Research Office.

# Nondestructive Depth Profiling of Rare-Earth and Actinide Zeolites via Rutherford Backscattering Methods

Scott A. Baumann and Michael D. Strathman

Charles Evans and Associates, Redwood City, California 94063

Steven L. Suib\*

Departments of Chemistry, Chemical Engineering, and Institute of Materials Science, University of Connecticut, Storrs, Connecticut 06268

**Rutherford backscattering (RBS) methods have been used to study rare-earth and actinide-ion-exchanged small pore (A) and large pore (Y) zeolites. A theoretical discussion of the RBS method and a novel method of data treatment are given. Experimental data for zeolites have been simulated and theoretical depth profiles have been determined. Both experimental and theoretical data suggest that uranyl-exchanged A zeolite has a large uranium to oxygen surface ratio while the corresponding Y zeolite has a large uranium to oxygen bulk ratio. Relative atomic fractions of all zeolite elements are also given.**

Most surface science studies of zeolites have focused on the use of X-ray photoelectron spectroscopy (XPS) to study the elements of the zeolite framework, in particular Si and Al (1, 2). Recent XPS studies of zeolites have shown that surface aluminum impurities like  $\text{Na}_2\text{Al}_2\text{O}_4$  and  $\text{Al}_2\text{O}_3$  exist on moronite and ZSM-5 (3). These surface impurity phases may be responsible for some of the catalytic activity of the zeolites.

Several recent surface studies have addressed the effects of dealumination of zeolites (4-7). Valence-band XPS data have been used to track the dealumination of zeolites.

Chemical-state plots for Si and Al for zeolites have also been used to track the effects of dehydration of zeolites and aluminophosphate molecular sieves (8). X-ray excited Auger transitions have been correlated with the polarizability of oxygen ions surrounding  $\text{Si}^{4+}$  and  $\text{Al}^{3+}$  ions in zeolites (8) and in clays (9, 10).

The majority of surface science XPS studies of zeolites has dealt with the determination of oxidation states of metal and transition-metal species in zeolites (11-13). Studies of exchanged cations, sublimed neutral organometallic molecules, and coordination complexes have received a great deal of attention.

A problem in molecular sieve research that continually appears involves how to determine whether metal species are on the external surface of the sieve, in the pores, or in both places. We have recently shown that Rutherford backscattering (RBS) methods can provide this information since the mass of an element, a quantitative analysis of the element, and a depth profile of the concentration of the element can be determined (14).

Since our original communication (14) we have been modeling RBS data for zeolite catalysts. In this paper we review the RBS method, discuss data treatment procedures, and interpret RBS data collected on several zeolite catalysts.

## EXPERIMENTAL SECTION

(a) **Synthesis.** Zeolites Linde NaA and NaY were purchased from Alfa Ventron Corp. of Danvers, MA. All europium and uranyl salts were also purchased from Alfa Ventron. For ion exchange approximately 100 mL of 0.1 M aqueous solutions of

$\text{UO}_2(\text{CH}_3\text{COO})_2 \cdot 2\text{H}_2\text{O}$  and  $\text{Eu}(\text{NO}_3)_3 \cdot 6\text{H}_2\text{O}$  were added to 1 g of NaA or NaY zeolite and stirred in a round-bottom flask for 12 h. The exchanged samples were then filtered and washed with 5-10 mL of distilled deionized water and dried in a vacuum line at  $1 \times 10^{-3}$  Torr.

(b) **Microanalysis.** Samples were analyzed after ion exchange by atomic absorption, energy dispersive X-ray analysis, and thermogravimetric analysis. A Varian Techtron atomic absorption spectrometer was used to determine the amount of chromium present in exchanged clays; the flame was air/acetylene, the samples were dissolved in dilute hydrofluoric acid, and the method of standard additions was used.

Thermal gravimetric analyses were done with a System 113X instrument from Cahn Instruments, Cerritos, CA, equipped with a Cahn 2000 electrobalance. This instrument came equipped with a Micron process control system, Model 82300, from Research, Inc., Minneapolis, MN, for temperature programming. A vacuum bottle assembly (6754) with two 75/50 ball joints was used, with an end-cap in place. The access port containing the tare pan was closed with a Pyrex cap (2481). The access port containing the sample pan was fitted with a 140-mm Pyrex joint that also had a gas inlet port. To this joint was clamped a 300-mm quartz hangdown tube equipped with both a gas outlet port and a port for thermocouple assembly (type K: chromel/alumel). Inside this glassware was a quartz baffle (to minimize air currents) and a Nichrome suspension wire (10399) holding a Model 3056 9-mm platinum stirrup sample pan of semimicro size. A GowMac Model 70-750 X/Y recorder was calibrated with a Keithley 179 TRMS digital multimeter. For most experiments, the heating rate was  $10^\circ\text{C}/\text{min}$  and the recorder range was 1 mg (15).

(c) **X-ray Powder Diffraction.** Crystallinity of materials was studied by X-ray diffraction (XRD) using a DIANO-XRD 8000 X-ray powder diffractometer equipped with a Philips electronic source. Copper K $\alpha$  radiation was used and sample scans were done at  $2^\circ/2\theta/\text{min}$ . All solid samples were mounted on glass slides lightly coated with Vaseline. Basal spacings were determined either by a small-angle X-ray camera or via powder techniques using a Norelco instrument also equipped with a Philips Electronic source. Diffraction patterns were calibrated with either NaCl or a silicon powder disk.

(d) **Rutherford Backscattering.** A General Ionex Tandemtron Rutherford backscattering instrument at Charles Evans and Associates was used for all Rutherford backscattering (RBS) experiments (16). This instrument generates an ion beam of 2.2-MeV  $\text{He}^{2+}$  ions which "backscatter" from atoms in a target material. These backscattered He ions are detected by using two separate silicon surface barrier detectors. These detectors are located so that they intercept particles which exit the sample either (1) normal or (2) nearly perpendicular to the surface of the sample. The normal angle detector is used to obtain superior mass resolution while the grazing angle detector is used to obtain excellent depth resolution. The energy distributions of the backscattered He ions are then collected in a Nuclear Data ND62 multichannel analyzer. Data reduction and storage are performed with an IBM-PC computer using software developed at Charles Evans and Associates.

Samples for RBS studies were prepared by uniformly spreading a thin layer on 1-in. carbon disks. There will be some effects of surface roughness with this type of sample preparation but these will be minimal if the particle sizes of the samples are larger than



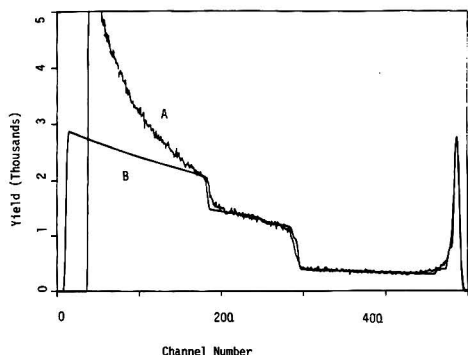


Figure 1. Rutherford backscattering data for (A)  $\text{UO}_2\text{A}$  zeolite, experimental data, and (B)  $\text{UO}_2\text{A}$  zeolite, theoretical fit.

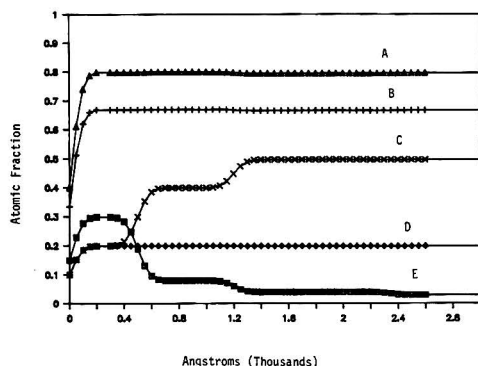


Figure 2. Theoretical depth profile for  $\text{UO}_2\text{A}$ : (A) Al, 10X; (B) O, 10X; (C) Na, 10X; (D) Si, 10X; (E) U, 10X.

1  $\mu\text{m}$ . All samples studied here have particle sizes greater than 1  $\mu\text{m}$ .

The theoretical depth profiles were generated by using the Rutherford backscattering cross sections, kinematic factors, and Bragg's rule to calculate stopping cross sections (17-21).

To calibrate the system, a standard consisting of a thin gold layer on a glass substrate has been used. The elements Si, Al, and Au were used to obtain a linear calibration curve to determine the keV/channel and the channel positions of other elements like O and U.

## RESULTS

(a) **Microanalyses.** Microanalyses of the ion-exchanged zeolites lead to approximate compositions of  $\text{Eu}_{3.5}\text{Na}_{1.5}\text{Al}_{12}\text{Si}_{12}\text{O}_{48}\cdot 27\text{H}_2\text{O}$  for europium(III) exchanged A zeolite, to  $\text{Eu}_{1.4}\text{Na}_{1.4}\text{Al}_{16}\text{Si}_{136}\text{O}_{384}\cdot 256\text{H}_2\text{O}$  for europium(III) Y zeolite, to  $(\text{UO}_2)_{2.5}\text{Na}_7\text{Al}_{12}\text{Si}_{12}\cdot 27\text{H}_2\text{O}$  for uranyl-exchanged A zeolite, and to  $(\text{UO}_2)_6\text{Na}_{44}\text{Al}_{56}\text{Si}_{126}\text{O}_{384}\cdot 256\text{H}_2\text{O}$  for uranyl-exchanged Y zeolite.

(b) **X-ray Diffraction.** All of the zeolites show X-ray powder diffraction patterns that indicate these materials are crystalline. No extra diffraction lines are observed.

(c) **Rutherford Backscattering.** A Rutherford backscattering spectrum for  $\text{UO}_2\text{A}$  is given in Figure 1 (A) along with a theoretical fit of the data (B). Figure 1 shows a pronounced yield for uranium at approximately channel 438. A theoretical depth profile of the  $\text{UO}_2\text{A}$  zeolite is given in Figure 2. While all elements show a rapid increase in atomic fraction close to the surface, it is observed that the uranium signal peaks and then continually decreases below all other elements. Also note that the decline in atomic fraction of U parallels

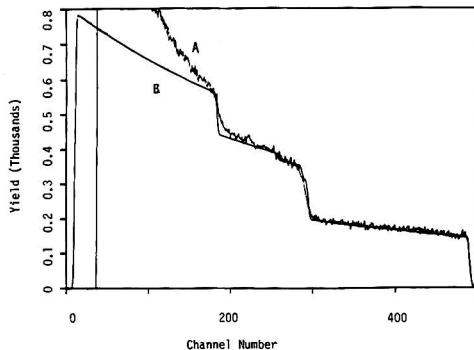


Figure 3. Rutherford backscattering data for (A)  $\text{UO}_2\text{Y}$  zeolite, experimental data, and (B)  $\text{UO}_2\text{Y}$  zeolite, theoretical fit.

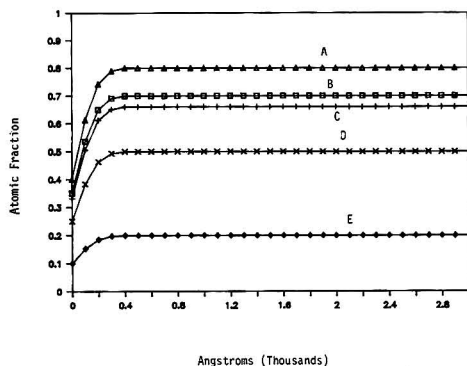


Figure 4. Theoretical depth profile for  $\text{UO}_2\text{Y}$ : (A) Al, 10X; (B) U, 100X; (C) O, 10X; (D) Na, 10X; (E) Si.

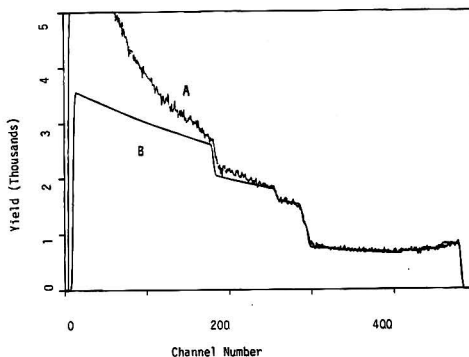


Figure 5. Rutherford backscattering data for (A) EuA zeolite, experimental data, and (B) EuA zeolite, theoretical fit.

an increase in the atomic fraction of Na.

For the  $\text{UO}_2\text{Y}$  sample the experimental RBS spectrum shows similar transitions as observed in Figure 3. The corresponding theoretical depth profile of Figure 4 shows that all elements gradually increase from the surface to the bulk where the relative atomic fractions are relatively constant.

The experimental RBS spectrum and theoretical fit of the raw data for Eu A zeolite are shown in Figure 5. Figure 6 is the theoretical depth profile for EuA. The relative atomic fractions of Eu, Si, Al, and Na are all lower than the O atomic

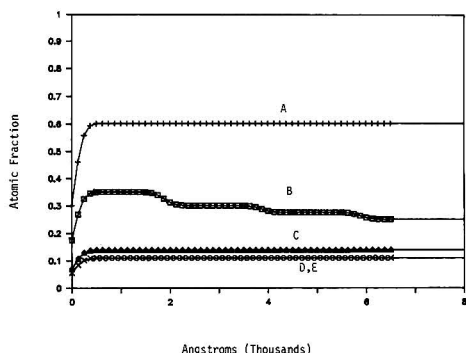


Figure 6. Theoretical depth profile for EuA: (A) O; (B) Eu, 25X; (C) Al; (D) Si; (E) Na.

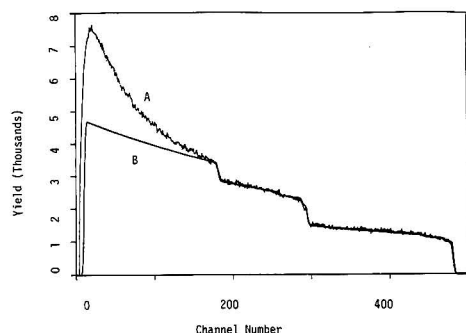


Figure 7. Rutherford backscattering data for (A) EuY, experimental data, and (B) EuY, theoretical fit.

fraction. Corresponding raw data and theoretical fits for EuY and the theoretical depth profiles for EuY are shown in Figures 7 and 8, respectively.

## DISCUSSION

**A. Theory of RBS.** Rutherford backscattering is one of several megaelectronvolt ion-beam techniques currently often used in the analysis of thin film systems. Backscattering is characterized by a projectile atom with mass  $M_1$ , charge  $Z_1$ , and energy  $E$  striking a target atom with mass  $M_2$  and charge  $Z_2$  at rest in the laboratory frame of reference. By measurement of the recoil energy of the projectile at a given angle, many physical parameters of the target can be measured, including the mass, quantity, and depth distribution of the elements which make up the target (22).

The first basic concept of RBS to be discussed is that of cross section. The differential cross section is a measure of the probability that a projectile and target atom will interact and send the projectile into a given solid angle. This scattering takes place because of the mutual repulsion of the two atoms due to the positive nuclear charge on each atom. In the case of a 1–2-MeV helium projectile, the energy of the helium atom is well below the level necessary to bring the nuclei close enough together so that quantum effects and nuclear reactions can have an effect on scattering probability. Therefore, it is possible to compute the Rutherford scattering cross section using classical physics according to (11)

$$N_s = N_i N \sigma_T t a \quad (1)$$

where  $N_s$  is the number of scattered particles,  $N_i$  is the number of incident particles,  $N$  is the number of target atoms/unit

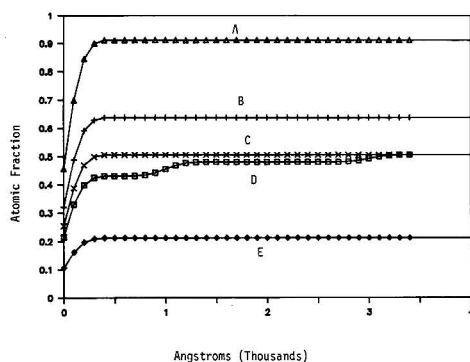


Figure 8. Theoretical depth profile for EuY: (A) Al, 10X; (B) O; (C) Na, 10X; (D) Eu, 25X; (E) Si.

volume,  $\sigma_T$  is the total cross section,  $a$  is the area intercepted by the beam, and  $t$  is the thickness of film.

At this point an example may help to illustrate this physical concept. Imagine a dark cave in which you want to find an exit. One method of finding an opening would be to throw a rock in a given direction and see if the projectile hits anything. If there is no opening, all of the projectiles will scatter off the solid wall (i.e.  $\sigma_T = 1$ ); likewise, if there is a hole, some of the projectiles will not scatter but will pass through the opening ( $\sigma_T < 1$ ). By repetition of this process many times, a measurement of the size of the hole can be obtained.

This example demonstrates the principles of RBS. In the case of nuclear scattering we are looking for a scattering center rather than a hole in a wall, but the same principles apply. That is, the bigger the scattering center (target atom), the more scattering events. As mentioned before, the scattering process is governed by the charge on the nucleus. Therefore, an atom like oxygen with  $Z = 8$  is effectively much smaller than nickel with  $Z = 28$ . The differential cross section, that is, the amount of scattering (18) into a given solid angle from a given target atom, is governed by the equation

$$\frac{d\sigma}{d\Omega} = \left( \frac{Z_1 Z_2 e^2}{4E} \right)^2 \frac{4}{\sin^4 \theta} \frac{[1 - R^2 \sin^2 \theta]^{1/2} + \cos \theta}{[1 - R^2 \sin^2 \theta]^{1/2}} \quad (2)$$

where  $R = M_1/M_2$ ,  $e$  is the electronic charge,  $\theta$  is the lab angle measured from the forward direction, and  $Z$ ,  $\sigma$ ,  $M_1$ , and  $E$  are as defined previously.

The difference in cross section between two elements is approximately equal to the ratio of the charge on the two nuclei squared. Thus in the above case the scattering cross section for nickel is  $(28/8)^2$  or 12.25 times greater than the cross section for oxygen.

The second important physical parameter in RBS is the kinematic factor (19). The kinematic factor,  $K_M$  is the ratio of the incident energy of the projectile to the energy of the projectile after the scattering event. Thus, as shown in eq 3

$$K_{M_2} = E_{\text{scattered}}/E_{\text{incident}} \quad (3)$$

An easy way to conceptualize this process is to use a cue ball as the projectile. When the cue ball is directed at a ball of similar mass, then both balls recoil from the collision site with a velocity lower than the velocity of the original projectile. If the target is replaced by a bowling ball, the cue ball will now retain most of its original velocity and only a small velocity will be imparted to the bowling ball. Rutherford backscattering is very similar to the above case and the process can be observed in Figure 9. When the target atom has a mass

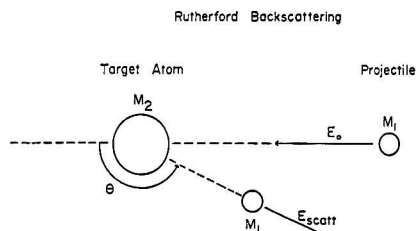


Figure 9. Schematic representation of an elastic collision:  $M_1$ , mass of projectile;  $E_0$ , energy of projectile;  $M_2$ , target mass;  $E_{scatt}$ , energy after collision;  $\theta$ , positive lab angle.

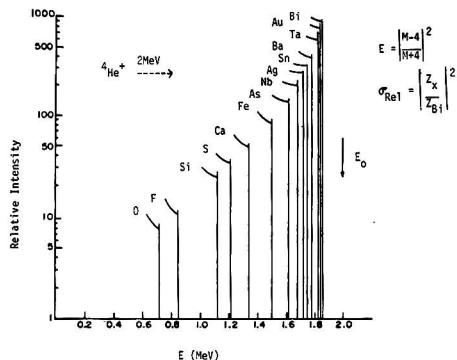


Figure 10. Relative intensities of various target atoms versus the scattered ion energies.

close to that of the projectile, the probing ion loses a significant amount of energy during the backscattering event and exists the sample with a low energy; conversely, when the target atom is heavy, the scattered energy of the probing ion is much closer to the incident energy. An equation for this process is given below

$$K_{M_2} = \frac{[1 - R^2 \sin^2 \theta]^{1/2} + R \cos \theta}{1 + R} \quad (4)$$

By use of the two physical parameters of cross section and kinematic factor, a graph can be plotted showing the relative intensities and the scattered energy from a number of different target atoms. This relationship is shown in Figure 10.

The last physical process to be covered is that of the interaction of the probing He ion with the electron cloud of the sample and the resulting energy loss (20) which can be used to determine a "depth scale". Electrons have a much lower mass ( $\sim 4$  orders of magnitude) than the projectile He ion, thus the effect of these multiple ion electron cloud interactions does not backscatter the incident ion but it does slow the helium ion and causes statistical variations in the ion energy at any given depth. Therefore, the deeper into a material the projectile penetrates before encountering a nuclear scattering event, the more energy,  $E_L$ , it will lose to nonscattering mechanisms. When the projectile does scatter from an atom within the bulk of the material, the impact energy of the particle is computed in the same fashion,  $E_{scatt} = EK_{M_2}$ , but now the actual energy of the projectile just prior to scattering must be substituted into the equation,  $E_{scatt}(E - E_L)K_{M_2}$ . The projectile will also lose energy traversing the sample on its way back to the surface of the target, thus the actual measured energy of the particle will be the following:

$$E_{measured} = (E - E_{L_{in}})K_{M_2} - E_{L_{out}} \quad (5)$$

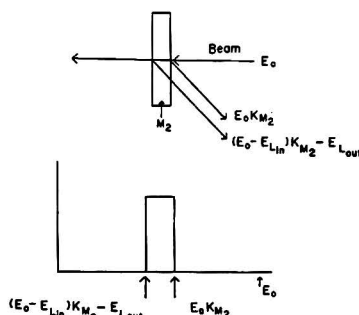


Figure 11. Diagram distinguishing surface and bulk scattering processes.

The phenomenon gives a breadth to the backscattered peak as illustrated in Figure 11. In summary, the three physical processes of cross section, kinematic factor, and energy loss allow the use of a megaelectronvolt ion beam to be used as an analysis tool for measuring quantitatively the (1) amount of an element present, (2) mass of that element, and (3) depth profile of the concentration of a given element.

Due to the rate at which spectra can be taken, Rutherford backscattering can be used as a survey tool to scan a large matrix of samples. It can also be used as a quantitative analysis tool due to the classical nature of the three physical processes involved.

**B. Data Treatment.** As mentioned earlier, scattering cross sections are proportional to the square of the target atom's atomic number and can be computed by using classical physics for all elements. Therefore, quantitative analysis can be performed without the use of standards.

An RBS spectrum includes data pertaining to both depth and concentration, but in a convoluted form. The data can be interpreted by hand, that is, one can measure the height and width of each peak then use the appropriate scattering cross section and energy loss parameters along with other known factors to calculate the sample composition at various depths. An alternative method involves using a computer program to generate a theoretical RBS spectrum for a given set of input parameters, such as film thickness and elemental composition. The values of these parameters can then be changed in an iterative fashion to achieve a close approximation of the experimental spectra. The computer program used for this particular work allows the analyst to specify up to nine different layers of differing thickness of elemental composition to describe each sample. As a result, samples can be described in a tabular form, listing the specific thickness and composition of each layer used to generate the theoretical spectrum which matches the experimental data. The thickness of each layer is given in angstroms followed by the average atomic fraction of each element in that layer. The first layer describes the surface of the sample with subsequent layers describing greater depths. To calculate the thicknesses used in the theoretical spectra, one must assume a density for the sample. Separate densities are calculated for each layer, but these may still differ from the actual sample density; therefore, error bars of  $\pm 20\%$  must be placed upon all thickness measurements. The densities used in this computer program are taken from Table I in ref 21.

Energy spectra are simultaneously obtained from each sample at both normal ( $160^\circ$ ) and grazing ( $105^\circ$ ) backscattering angles. In general, the  $160^\circ$  backscattering spectra provide useful data pertaining to the outer 1–2  $\mu\text{m}$  of the sample surface with depth resolution of approximately 300 Å. The  $105^\circ$  backscattering spectra provide accurate infor-

Table I. Atomic Concentrations for Europium Zeolites

sample	depth <sup>a</sup>	atomic concentrations				
		O	Na	Al	Si	Eu
Eu A	0-2000	60	11	13	15	1.4
	2000-4000	60	11	13	15	1.2
	4000-6000	60	11	13	15	1.1
	bulk	60	11	13	15	1.0
Eu Y	0-1000	63	5	13	17	1.7
	1000-3000	63	5	13	17	1.9
	bulk	63	5	13	17	2.0

<sup>a</sup>In angstroms.

material for only the upper 1000 Å but with much better depth resolution (approximately 50 Å). As the backscattering angle approaches 90°, depth resolution improves; therefore, in special cases angles less than 105° may be employed. The use of two detectors also allows the analyst to eliminate certain assumptions that must be made if only one detector is used. For example, both manganese (55 amu) on the surface and copper (64 amu) buried at a depth of 1000 Å in a silicon wafer will generate backscattering ions with the same energy at a 160° detection angle. However, when grazing angle detection is used, the ions which are backscattered from the buried copper must travel a greater distance and therefore, suffer a greater energy loss in order to leave the sample than those backscattered from the manganese on the surface of the sample. The result is that ions backscattered from the buried copper will have considerably less energy when detected at 105°, thereby allowing the analyst to separate the two cases. Careful scrutiny of both 160° and 105° spectra will usually remove any doubt as to the identity and depth of an element in the upper 1000 Å of a sample.

Some comments on the quantitation of light elements in high mass substrates is also appropriate. The relative sensitivity of RBS to an element is dependent on that element's backscattering cross section and quantitative accuracy upon the number of backscattering events measured. Thus, heavier elements such as iron can be more accurately measured than carbon or oxygen for a given incident He dose. In some cases, such as those involving gold, tantalum, tungsten, or any other high mass element, the number of counts obtained from the heavy elements in the matrix is so great that the counts from light elements such as carbon, nitrogen, or oxygen cannot be detected above the background created by the heavier elements. A second issue is that as the mass increases, the amount of energy loss between similar masses decreases, therefore reducing the ability to resolve adjacent elements of higher masses. For high mass elements, uncertainties of between 5 and 10 amu are typical.

The theoretical spectra in this paper do not include the effects of straggling. An actual grazing angle spectrum will normally not achieve the resolution shown for the buried layers. The normal angle spectrum demonstrates the capability to easily resolve 1000-Å layers in structures up to 2 μm in thickness.

**C. Zeolite Data.** The microanalytical and X-ray diffraction data suggest that there are no gross structural changes as a result of the ion exchange. Thermogravimetric analysis data were used to determine the water content of all samples.

We have previously communicated RBS data for UO<sub>2</sub>A and UO<sub>2</sub>Y zeolites (14) that show that UO<sub>2</sub>A has a U/O ratio on the surface that is 10 times greater than the U/O ratio of the bulk. On the other hand, data for UO<sub>2</sub>Y show a surface U/O ratio that is 9 times less than the U/O bulk ratio. These data were analyzed by hand.

In this paper we have theoretically fit the experimental data for these UO<sub>2</sub><sup>2+</sup> zeolite samples and have generated theoretical

depth profiles for the uranium zeolites. The depth profile provides much more useful information than can easily be determined by hand. Figure 2 clearly shows a surface enhancement of uranium for UO<sub>2</sub>A that decreases at about 400 Å into the material. The uranium atomic fraction falls off dramatically as the sodium concentration increases. The excellent theoretical fit to the experimental data in Figure 1 should also be noted.

An excellent match of theoretical and experimental data for UO<sub>2</sub>Y and all europium samples (Figures 3, 5, and 7) should also be noticed. A major point is that the U atomic fraction for UO<sub>2</sub>Y closely parallels the rise of all other elements of the zeolite (O, Si, Al, Na) observed by RBS. These data are consistent with ISS-SIMS data (23) and suggest that the majority of uranyl ions are exchanged into interior sites of the Y zeolite.

The EuA sample shows a depth profile in Figure 6 that indicates the Eu atomic fraction decreases slightly with depth. A pronounced change in atomic fraction for Eu of the Eu A sample as a function of depth is not observed here in contrast to the uranyl system. These data suggest that some europium(III) resides in the pores of zeolite A.

The EuY zeolite sample does show a small increase of the Eu atomic fraction in Figure 8 as a function of depth into the zeolite. Table I gives the atomic concentrations for the europium samples. Therefore, europium ions are in interior sites of zeolite Y. These conclusions for europium systems are consistent with Mössbauer (24), EXAFS (25), and fluorescence studies (26).

Due to the overlap of Al, Si, and Eu signals the detection limit for Na is about 2%, so there is some uncertainty in the Na concentrations. In addition, it is difficult to resolve Si from Al so these numbers also have a high degree of uncertainty. The sum of the Al and Si concentrations, however, are quite accurate. While the Si/Al ratio for EuY is greater than that of EuA (as expected), the absolute ratios do not agree well with bulk values (2.4 vs 1.0) from bulk microanalytical methods.

## CONCLUSION

We have described the general principles of RBS in this article. A discussion of computer simulation of RBS data is also given. Finally, RBS data have been collected for zeolite catalysts and theoretically fitted. Nondestructive depth profiling of zeolites can be carried out with RBS. These data are consistent with other surface studies of similar zeolite catalysts. RBS can potentially be useful in the study of other porous catalyst materials to distinguish surface and bulk metal concentrations. RBS has been shown to be a rapid, inexpensive, and reliable method for the nondestructive determination of depth profiles in zeolites.

**Registry No.** O<sub>2</sub>, 7782-44-7; Na, 7440-23-5; Al, 7429-90-5; Si, 7440-21-3; Eu, 7440-53-1; U, 7440-61-1.

## LITERATURE CITED

- (1) Barr, T. L. In *Practical Surface Analysis*; Briggs, D., Seah, M. P., Eds.; Wiley: New York, 1983; Chapter 8, pp 282-358.
- (2) Madey, T. E.; Wagner, C. D.; Joshi, A. J. *Electron Spectrosc. Relat. Phenom.* **1985**, *281*, 757.
- (3) Barr, T. L.; Lishka, M. A. *J. Am. Chem. Soc.* **1985**, *108*, 3178-3186.
- (4) Corma, A.; Fornes, V.; Pallota, O.; Cruz, J. M.; Ayerbe, A. J. *Chem. Soc., Chem. Commun.* **1986**, 333-334.
- (5) Ward, M. B.; Lunford, J. H. *J. Catal.* **1984**, *524*, 527.
- (6) Meyers, B. L.; Fleisch, T. M.; Marshall, C. L.; Hall, J. B. *Proceedings of the North American Catalyst Society Meeting*, Houston, TX, 1985; B15.
- (7) Andera, V.; Kubelkova, L.; Novakova, J.; Wichterlova, B.; Bednarova, S. *Zeolites* **1985**, *5*, 67-69.
- (8) Sulb, S. L.; Winiecki, A. M.; Kostapapas, A. *Langmuir* **1987**, *3*, 483-488.
- (9) West, R. M.; Castle, J. E. *SIA, Surf. Interface Anal.* **1982**, *4*, 68-75.
- (10) Castle, J. E.; Hazell, L. B.; West, R. M. *J. Electron Spectrosc. Relat. Phenom.* **1979**, *16*, 97-106.
- (11) Barr, T. L. *Am. Lab. (Fairfield, Conn.)* **1978** (Nov), 65-76.
- (12) Barr, T. L. *Appl. Surf. Sci.* **1983**, *15*, 1-35.

- (13) Turner, N. H.; Dunlap, B. I.; Colton, R. J. *Anal. Chem.* **1984**, *56*, 373R-416R.
- (14) Baumann, S.; Strathman, M. D.; Sulb, S. L. *J. Chem. Soc., Chem. Commun.* **1986**, 308-309.
- (15) Carrado, K. A.; Sulb, S. L.; Skoularikis, N. D.; Coughlin, R. W. *Inorg. Chem.* **1986**, *25*, 4217-4221.
- (16) Evans, C. A., Jr.; Blattner, R. J. *Annu. Rev. Mater. Sci.* **1978**, *8*, 181, and references therein.
- (17) Chu, W. K.; Mayer, J. W.; Nicolet, M. A. *Backscattering Spectrometry*; Academic: New York, 1978; pp 26-30.
- (18) Reference 17, pp 30-32.
- (19) Reference 17, pp 22-26.
- (20) Reference 17, pp 22-26.
- (21) Reference 17, pp 344-348.
- (22) Evans, C. A.; Strathman, M. D. *Ind. Res. Dev.* **1983**, *25*, (Dec) 99-101.
- (23) Sulb, S. L.; Coughlin, D. F.; Otter, F. A.; Conopask, L. F. *J. Catal.* **1983**, *84*, 410-422.
- (24) Sulb, S. L.; Zenger, R. P.; Stucky, G. D.; Emberson, R. M.; Debrunner, P. G.; Iton, L. E. *Inorg. Chem.* **1980**, *19*, 1858, 1962.
- (25) Sulb, S. L.; Zenger, R. P.; Stucky, G. D.; Morrison, T. I.; Shenoy, G. R. *J. Chem. Phys.* **1984**, *80*, 2203-2207.
- (26) Stucky, G. D.; Iton, L. E.; Morrison, T. I.; Shenoy, G. R.; Sulb, S. L.; Zenger, R. P. *J. Mol. Catal.* **1984**, *27*, 71-80.

RECEIVED for review August 26, 1987. Accepted January 15, 1988. We thank the U.S. Department of Energy, Office of Basic Energy Sciences Division of Chemical Science, for support of this research.

## Effects of Surface on the Atomization of Lead by Graphite Furnace

William G. Brumbaugh\*

National Fisheries Contaminant Research Center, U.S. Fish and Wildlife Service, Route 1, Columbia, Missouri 65201

Samuel R. Koirtyohann

Department of Chemistry, University of Missouri, Columbia, Missouri 65211

The effects of the surface of a graphite furnace on the atomization of lead in a magnesium chloride matrix were studied in an effort to explain the mechanism causing response differences related to such surfaces. We used various concentrations of magnesium chloride and compared lead charring profiles, atomic absorption peaks, and molecular background spectra of magnesium chloride with both uncoated and pyrolytically coated graphite platform surfaces. Although condensed-phase decomposition of magnesium chloride was seemingly enhanced on the uncoated surface, this effect was not sufficient to explain tube wall atomization differences.

Matrix interferences in graphite furnace atomic absorption (GFAA) have been widely studied since this method became popular in the early 1970s. Studies of interference mechanisms have contributed greatly to recent improvements in the technique (1). One of the more widely studied analyte-matrix systems in GFAA is lead in a chloride salt. It is generally accepted that chlorides cause interferences on volatile or semivolatile analytes, due to premature charring losses of molecular chloride analyte forms and to incomplete molecular dissociation and recombination during atomization. The effects of magnesium chloride on lead fit this general mechanism. However, effects of magnesium chloride are unusual because the atomization surface can affect the degree of the interference.

Fuller (2), who first showed that magnesium chloride effects on lead atomization decreased with increasing age of graphite tubes, reported severe suppression of peak heights by either a new tube or a used tube recoated with pyrolytic graphite. He concluded that surface reduction of lead by powdered graphite decreased the interference in the vapor phase. Manning and Slavin (3), who tested integrated response for lead in a magnesium chloride matrix for various tube treatments, found that uncoated and pyrolytically coated tubes

behaved similarly when treated with molybdenum. Like Fuller, they reported slightly decreased interference with well-used uncoated tubes compared with interferences with unused uncoated tubes. They also observed much greater interferences with pyrolytically coated tubes than with unused uncoated tubes. In two related investigations of lead peak shapes and ashing behavior in the presence of magnesium chloride, Erspamer and Niemczyk (4, 5) concluded that the matrix was more effectively removed from an uncoated surface than from a pyrolytically coated surface during ashing because of increased carbon reactivity toward the matrix. L'vov et al. (6) hypothesized that the physical difference in porosity reduced the interference by magnesium chloride on lead in uncoated tubes. They postulated that the effective atomization temperature of lead is increased when the metal is vaporized from a "pore", resulting in greater molecular chloride dissociation and more thorough atomization. Kantor and Bezur (7) concluded that the hydrolysis rate of magnesium chloride is increased on uncoated graphite over that on pyrolytically coated graphite. They hypothesized that adsorption hydrolysis on the more reactive uncoated graphite was responsible for the differences observed.

We compared the effects of magnesium chloride on lead volatilization with modified L'vov platforms made of either uncoated (porous) electrographite or pyrolytically coated graphite. Various concentrations of magnesium chloride were used to compare lead-charring profiles, molecular background spectra, and shapes of lead atomic absorption peaks for each surface. By changing only platform surfaces, we characterized each surface with respect to matrix-analyte interactions in the liquid and solid phases.

### EXPERIMENTAL SECTION

**Apparatus.** Absorption was measured with a Perkin-Elmer Model 5000 atomic absorption spectrophotometer equipped with a Model HGA-500 graphite furnace and a Model AS-1 autosampler. A Perkin-Elmer Model 3600 data station with "high speed graphics" software was used to plot absorbance against time. A

Table I. Operating Parameters for HGA-500 Furnace

step	temp, °C	ramp, s	hold, s	internal flow, mL/min
1 (dry)	230	5	25	300
2 (char)	350	2	45	300
3 (atomize)	1900	0	6	0
4 (burnout)	2700	1	5	300
5 (cool)	20	1	15	300

**BASIC** program was written to control wavelength slewing of the spectrophotometer between sample injections, and thus automate the measurement of molecular absorption spectra for the magnesium chloride. The two types of graphite tubes used were pyrolytically coated (P-E 290-1766) and standard uncoated (P-E 290-1633). Modified L'vov platforms were made similar to that of Kaiser et al. (8) by cutting four 5- by 7-mm sections from the grooved end sections of each type of graphite tube. The graphite tube containing the platform was always pyrolytically coated. The lead source lamp was a Perkin-Elmer electrodeless discharge lamp operated at 10 W. Molecular absorption from magnesium chloride was monitored with deuterium arc (below 300 nm) and tungsten filament (above 300 nm) lamps.

**Reagents.** A working stock solution of 3 µg/mL lead in 0.12 M hydrochloric acid was prepared from a commercially available (Fisher Scientific) 1000 ppm atomic absorption reference solution. Working stock solutions of 10 and 50 µg/mL magnesium were prepared from reagent grade (Mallinckrodt) magnesium chloride hexahydrate. High-purity water (specific resistance greater than 15 MΩ cm) was used in all test solutions. Hydrochloric acid, used in the dilution of some test solutions, was prepared by subboiling distillation of reagent grade acid (Baker) in a quartz evaporator. Prepurified argon (Linde) was used as the external and internal purge gas.

All experimental test solutions were prepared daily from working stocks with variable volume micropipets. The accuracy of micropipets was verified daily by gravimetric check to nearest 0.1 mg. Disposable pipet tips and autosampler vials were rinsed just before use with a mixture of dilute nitric and hydrochloric acid. Test solutions were prepared in sample vials in a total volume of 1.0 mL and with an effective acid matrix of 0.024 M hydrochloric acid. For most experiments, a 60 ng/mL lead solution was analyzed (10 µL of solution was injected giving 0.6 ng of lead). Magnesium chloride solutions studied ranged from 10 to 2000 µg/mL magnesium (0.1–20 µg injected).

**Operating Parameters.** The 283.3-nm line was used for all measurements with a spectral band-pass of 0.7 nm (low slit). Peak areas were measured with a 4-s integration and background correction enabled. The furnace operating parameters are given in Table I. Molecular background spectra were performed in the "BG" mode, with both deuterium arc and tungsten filament continuum lamps. Base line offset correction was used for all measurements to eliminate small errors caused by electronic drift. Char temperatures were based on the work of Manning and Slavin (1), who showed that lead could be lost at temperatures as low as 350 °C when vaporized from a platform in the presence of high concentrations of magnesium chloride. For experiments run on tube walls, test solutions were dried at 110 °C, charred at 250 °C, and atomized at 2300 °C (1 s ramp).

**Procedures.** We used only new platforms and replaced them after 50 firings to minimize changes in heating rate and surface reactivity caused by the aging of graphite. New surfaces were dry-fired 3 or 4 times before use to remove impurities and to condition the surface. We used pyrolytically coated tubes to heat both platform types and replaced them after 200 firings. Platforms were replaced by removing the right furnace window and, without removing the tube, installing the new platform with a positioning rod in very nearly the same spatial relationship as that of the previous one. Initially, we compared solid pyrolytic graphite platforms with uncoated platforms of the design of Kaiser et al. (8); however, the heating characteristics were different from those of the Kaiser design, probably due to differences in mass and geometry. The Kaiser design was subsequently used for all platforms (coated and uncoated).

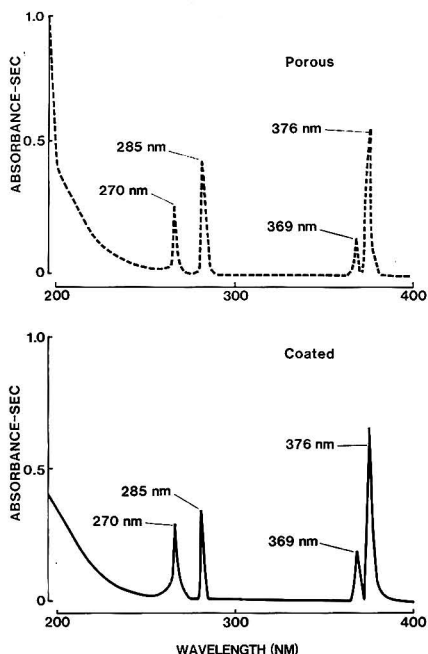


Figure 1. Background absorption as a function of wavelength for 20 µg of Mg as MgCl<sub>2</sub> obtained by platform atomization.

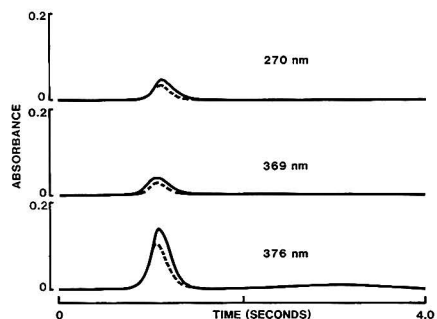


Figure 2. Background absorption as a function of time for 1 µg of Mg as MgCl<sub>2</sub> obtained by platform atomization: (---) porous; (—) coated.

Measurements of molecular absorption spectra for magnesium chloride were based on separate firings made at wavelengths of 200 to 400 nm, in 5-nm increments. Additional measurements were run at 1-nm intervals in the vicinity of observed peaks.

## RESULTS AND DISCUSSION

**(a) Molecular Absorption of Magnesium Chloride Matrix.** Differences in magnesium chloride background spectra were minor for the two platform surfaces (Figure 1). Peaks were observed from each surface at four wavelengths (nm): 285, 270, 369, and 376. The peak at 285 nm was probably due to the broadened magnesium atomic absorption line. The other three peaks behaved similarly in several respects, each showing the following features: similar absorbance vs time characteristics, a large increase in peak area with increasing atomization temperature, and a slightly stronger signal when a pyrolytically coated platform was used.



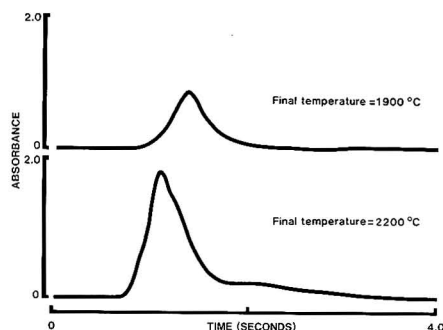


Figure 3. Background absorption at 376 nm for 20  $\mu\text{g}$  of Mg as  $\text{MgCl}_2$  obtained by a pyrolytically coated platform.

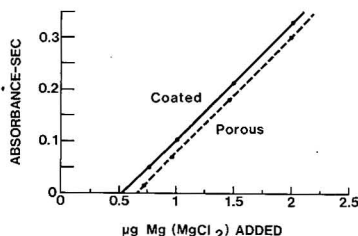


Figure 4.  $\text{MgCl}$  background absorption at 376 nm obtained by platform atomization as a function of  $\text{MgCl}_2$  concentration.

in place of an uncoated porous one (Figures 2 and 3). Incidentally, we detected no molecular absorption with similar magnesium chloride concentrations for tube wall sampling, probably because of the lower effective gas-phase temperature. We believe these three absorption peaks were from the  $\text{MgCl}$  molecule that resulted from the vaporization and dissociation of unhydrolyzed magnesium chloride. We measured no signal at any of these wavelengths when equivalent concentrations of either magnesium or chloride from other salts were vaporized. The direct relation between absorption and temperature suggests that the absorbing species was a simple diatomic molecule resulting from dissociation, such as  $\text{MgCl}$ , rather than some other  $\text{MgCl}_x$  species. Supportive evidence for  $\text{MgCl}$  as the absorbing species is shown in molecular spectra tables (9). Although we found no molecular spectra listings of simple magnesium species at 270 nm, there are listings for  $\text{MgCl}$  having bands headed at 378 and 371 nm and degrading to shorter wavelengths with relative intensities of 10 and 4, respectively. These listings, which are based on the work of Morgan (10), agree reasonably well with the peaks that we observed at 376 and 369 nm.

These observations imply that, under our experimental conditions, a significant fraction of the magnesium chloride matrix remained unhydrolyzed after charring and decomposed to  $\text{MgCl(g)}$ ,  $\text{Mg(g)}$ , and  $\text{Cl(g)}$  during atomization. This decomposition may have occurred in either the condensed or the gas phase. Furthermore, a slightly greater amount of magnesium chloride seemingly survived the charring step when the pyrolytically coated surface was used, rather than the uncoated surface; evidence and quantitation of this larger amount were supplied by observation of the molecular absorption at 376 nm of various concentrations of magnesium chloride with each platform surface. These data (Figure 4) suggest that decomposition of magnesium chloride was more thorough on the porous than on the coated surface by an amount equivalent to about 0.1  $\mu\text{g}$  of magnesium ( $x$  intercept,

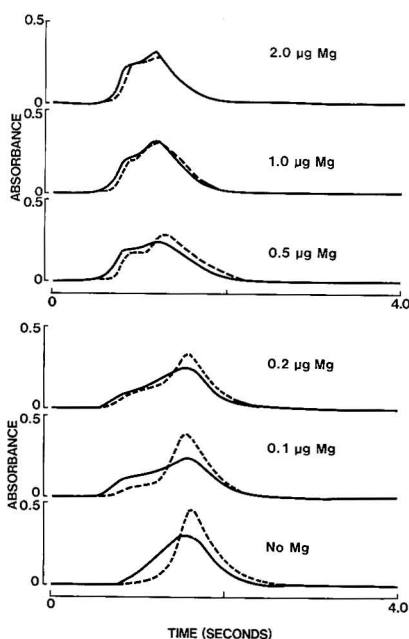
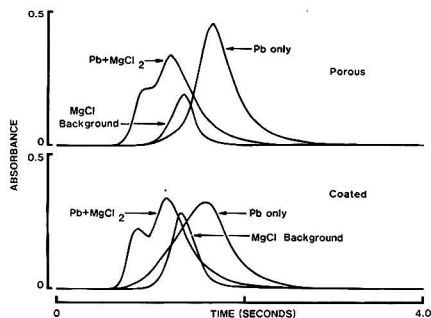


Figure 5. Pb atomic absorption (0.6 ng) obtained by platform atomization in the presence of  $\text{MgCl}_2$ : (---) porous; (—) coated.

0.65 vs 0.55  $\mu\text{g}$  of magnesium). The positive  $x$  intercept for either surface indicates that a surface reaction, dependent on the platform type and independent of the magnesium chloride concentration, was partly involved in the magnesium chloride decomposition. Others have made similar conclusions from related experiments (7); however, inconsistencies between our platform work and earlier tube wall studies (4) are apparent, especially with respect to molecular absorption spectra. This may be in part because we compared only relatively new surfaces, that are presumably less reactive than aged graphite. Differences for graphite tube heating rates and interactions between vapor and tube wall surfaces (probably not factors in our work because platform surface was the only variable) may also partly account for these apparent discrepancies.

**(b) Atomization of Lead in the Magnesium Chloride Matrix.** We observed significant differences in lead response between uncoated and pyrolytically coated tubes during atomization from the tube wall in the presence of magnesium chloride. In the presence of 0.2  $\mu\text{g}$  of magnesium, suppression of the integrated signal was about 50% for pyrolytically coated tubes but only 25% for uncoated tubes. Platform atomization produced less than 5% suppression for either surface with up to 5  $\mu\text{g}$  of magnesium. In tube wall atomization, the lead that vaporized as the chloride may not have dissociated completely due to the low gas-phase temperature (6). With the platform, the furnace atmosphere was sufficiently hot during vaporization to cause nearly complete dissociation of gaseous  $\text{PbCl}_2$  at much higher magnesium chloride concentrations. At low magnesium concentrations, however, the shapes of lead peaks differed between platform surface types.

Plots of lead atomized from each platform with 0.1  $\mu\text{g}$  of magnesium indicated that some of the lead was atomized earlier when the pyrolytically coated platform was used (Figure 5). At higher concentrations of magnesium chloride (0.5–2.0  $\mu\text{g}$  of magnesium), lead atomic absorption profiles were practically superimposable. Actually, the shapes of lead peaks



**Figure 6.** Relation of Pb atomic absorption (0.6 ng) obtained by platform atomization with and without the presence of  $\text{MgCl}_2$  ( $1.0 \mu\text{g}$  of Mg) and background absorption at 376 nm ( $1.0 \mu\text{g}$  of Mg as  $\text{MgCl}_2$ ).

for each surface type differed only at magnesium levels below  $0.2 \mu\text{g}$ —an observation consistent with our earlier finding that more magnesium chloride (about  $0.1 \mu\text{g}$  of magnesium) was decomposed when the porous platform was used.

From these plots, it appears that magnesium chloride caused two different atomization pathways for lead, each resulting in earlier lead vaporization. Atomization of lead in the absence of magnesium chloride is presumed to occur by hydrolysis of  $\text{PbCl}_2$  and reduction of  $\text{PbO}$  (11, 12) as the 0.024 M hydrochloric acid had no effect on peak shape. We suggest the following mechanism: Incomplete hydrolysis of magnesium chloride during drying and charring contributed to the formation of  $\text{PbCl}_2(\text{s})$ ; at higher magnesium chloride concentrations, some of the lead was occluded in  $\text{MgCl}_2$  crystals; upon heating, free or loosely adsorbed  $\text{PbCl}_2$  molecules vaporized, giving rise to the first lead peak, then melting and/or vaporization of  $\text{MgCl}_2$  released occluded  $\text{PbCl}_2$  causing the second lead peak. Consistent with this mechanism is the fact that the boiling point of lead chloride ( $950^\circ\text{C}$ ) is lower than that of anhydrous magnesium chloride ( $1412^\circ\text{C}$ ). Also, at low magnesium chloride concentrations (Figure 5), only the earliest lead peak is observed, and the second peak becomes prominent only at intermediate concentrations of magnesium chloride. Finally, the appearance of  $\text{MgCl}$  absorption coincides roughly with the appearance of the second lead peak (Figure 6). These effects probably depend on the degree of magnesium chloride hydrolysis, which in turn depends on the charring temperature, heating rate, and surface type. For example, charring at  $500^\circ\text{C}$  with  $2 \mu\text{g}$  of magnesium eliminated the  $\text{MgCl}$  absorption peak and gave a lead peak profile similar to that without magnesium chloride. However, some of the lead was lost during charring, presumably as  $\text{PbCl}_2$ , and the integrated signal was considerably lower. As judged by our platform studies, the ability of porous graphite to eliminate effects due to magnesium chloride strictly by condensed-phase surface interaction is apparently limited to fairly low levels of interferent. The degree of this surface interaction may increase with the age of the graphite surface; however, this effect would be difficult to control and evaluate.

**(c) Charring Plots for Lead in the Presence of Magnesium Chloride.** The optimum charring temperature for lead in the presence of magnesium chloride is reported to be about  $125^\circ\text{C}$  higher when tube wall atomization is used with porous rather than with pyrolytically coated graphite (5). We observed similar results with tube wall atomization (Figure 7) but detected no differences when platforms were used (Figure 8). Charring plots were similar for both platform surfaces with a given amount of magnesium chloride, though the plot shapes changed as the magnesium chloride concentration was increased. Our results suggest that differences

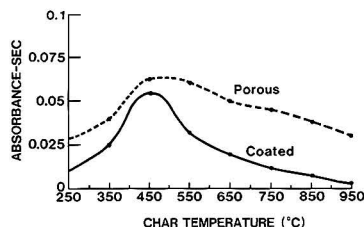


**Figure 7.** Pb atomic absorption (0.6 ng) as a function of char temperature obtained by tube wall atomization in the presence of  $2.0 \mu\text{g}$  of Mg (as  $\text{MgCl}_2$ ).

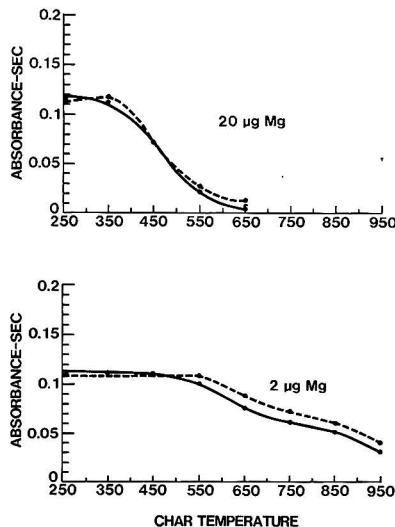


**Figure 8.** Pb atomic absorption (0.6 ng) as a function of char temperature obtained by platform atomization in the presence of  $\text{MgCl}_2$ : (---) porous; (—) coated.

in tube wall charring plots between surfaces were due to the degree of interference during atomization and not to differing losses of lead in charring. Otherwise, one might also expect differences in charring plots for platform atomization.

Two possible explanations for the tube wall differences are (a) the matrix is more efficiently decomposed at a given charring temperature on the porous surface, thereby reducing the amount of chloride during lead vaporization, and (b) the vapor-phase interference is reduced when the porous tube is used due to interactions between the vapor and the tube walls during atomization. Our results with different platform surfaces support this second mechanism because lead atomization peak shapes were nearly identical at the  $2.0\text{-}\mu\text{g}$  magnesium level (the level that resulted in considerably different charring plots for the tube wall atomization). This similarity in patterns of lead volatilization from the two platform surfaces with  $2 \mu\text{g}$  of Mg suggests that any differences in the relative amounts of the various chloride species surviving charring were small. However, the resistive heating rates can differ for porous and pyrolytically coated graphite (13), and this difference may in turn cause differences in magnesium chloride hydrolysis rates (7) and contribute to the differences observed for tube wall charring plots. This effect—an altered rate of magnesium chloride hydrolysis due solely to tube heating rate differences—should not be observed in platform

studies because heating is by radiational transfer.

### CONCLUSIONS

The ability of porous graphite to eliminate the effects of magnesium chloride on lead atomization by interaction in the condensed phase is apparently limited to relatively low levels of interferent. With a given set of heating conditions, slightly less MgCl molecular absorption was measured with a porous graphite surface than with a pyrolytically coated surface, suggesting that the decomposition of magnesium chloride is enhanced by a porous surface. This effect was not sufficient to explain the differences observed for tube wall atomization and we hypothesize that interactions between the vapor and porous graphite tube walls also play a role in reducing the interference. Such interactions would be less important when atomizing from the platform because the increased gas temperature realized eliminates the interference. Further experiments are needed to substantiate this hypothesis.

Most current graphite furnace atomic absorption methods for lead report the use of the pyrolytic graphite platform and our work suggests that an uncoated platform will provide little improvement with a magnesium chloride matrix. However, there may be situations where uncoated tubes and platforms are beneficial, especially if matrix modification is not used.

Further work in this area is in progress.

### ACKNOWLEDGMENT

We thank James G. Wiener, National Fisheries Contaminant Research Center, for helpful review comments.

Registry No. Pb, 7439-92-1; MgCl<sub>2</sub>, 7786-30-3.

### LITERATURE CITED

- (1) Manning, D. C.; Slavin, W. *Appl. Spectrosc.* **1983**, *37*, 1.
- (2) Fuller, C. W. *At. Absorpt. Newsl.* **1977**, *16*, 106.
- (3) Manning, D. C.; Slavin, W. *Anal. Chem.* **1978**, *50*, 1234.
- (4) Erspamer, J. P.; Niemczyk, T. M. *Anal. Chem.* **1982**, *54*, 538.
- (5) Erspamer, J. P.; Niemczyk, T. M. *Anal. Chem.* **1982**, *54*, 2150.
- (6) L'vov, B. V.; Bayunov, P. A.; Ryabchuk, G. N. *Spectrochim. Acta, Part B* **1981**, *36B*, 397.
- (7) Kantor, T.; Bezur, L. J. *Anal. At. Spectrosc.* **1986**, *1*, 9.
- (8) Kaiser, M. L.; Koptyyohann, S. R.; Hinderberger, E. J. *Spectrochim. Acta, Part B* **1981**, *36B*, 773.
- (9) Pearce, R. W. B.; Gaydon, A. G. *Identification of Molecular Spectra*; Whitefriars: London, 1963.
- (10) Morgan, F. *Phys. Rev.* **1936**, *50*, 603.
- (11) Sturgeon, R. E.; Mitchell, D. F.; Berman, S. S. *Anal. Chem.* **1983**, *55*, 1059.
- (12) Bass, D. A.; Holcombe, J. A. *Anal. Chem.* **1987**, *59*, 974.
- (13) Sturgeon, R. E.; Chakrabarti, C. L. *Anal. Chem.* **1977**, *49*, 90.

RECEIVED for review October 28, 1987. Accepted February 2, 1988.

## Direct Mixture Analysis Using Carbon-Proton *J*-Resolved Nuclear Magnetic Resonance

Charles L. Wilkins,\* Steven T. K. Ha, and Robert W. K. Lee

Department of Chemistry, University of California, Riverside, California 92521

One-dimensional long-range *J*-resolved (LRJR) nuclear magnetic resonance spectrometry is used to determine carbon connectivities for mixture components. This information, combined with reverse searches of a <sup>13</sup>C nuclear magnetic resonance (<sup>13</sup>C NMR) spectral library, permits qualitative mixture analysis without separation. Analyses of three- and five-component mixtures demonstrate use of the method. Use of the chemical shift reagent europium chloride to simplify application of the LRJR method to mixture analysis is demonstrated.

On-line spectroscopic analysis of mixture components, following their chromatographic separation, is one of the principal analytical methods in use today. Such "hyphenated" techniques have much to recommend them, including reasonable sensitivity, good specificity, and efficiency (1, 2). However, mismatches between chromatographic and spectroscopic requirements complicate use of such approaches and occasionally limit their utility. Because of the extensive chemical structure information available from nuclear magnetic resonance (NMR) spectroscopy, it is a particularly desirable on-line adjunct to HPLC chromatographic separations for mixture analysis. Unfortunately, due to sensitivity limitations, for practical purposes that application is presently restricted to <sup>1</sup>H NMR (3-8) of mixture components available in quantities in excess of 5 μg (5). In that application, as well

as for the present one, improved NMR sensitivity is an important long-term goal. Even so, methodologies such as that presented here represent useful analytical mixture analysis tools.

In recent publications (9-11), alternative interpretation schemes for mixture analysis based upon use of <sup>13</sup>C NMR were proposed and their applications to qualitative analysis of petroleum distillates (9), qualitative and quantitative analysis of organic wastes (10), and interpretation of gas chromatography-mass spectrometry data (11) described. All relied on interpretation of NMR data obtained from unseparated mixtures, where the wide <sup>13</sup>C NMR spectral bandwidth (typically, over 15 000 Hz for a 7.0-T spectrometer) relative to the spectral line width (well under 1 Hz) minimizes overlap of resonances. In previous work, quantitative <sup>13</sup>C NMR measurements were required when it was necessary to divide mixture carbon resonances into subsets corresponding to individual components, prior to reverse library searches for identification (9, 10). A relaxation reagent, chromium triacetylacetonate, was used to shorten relaxation times and level nuclear Overhauser effects.

Here, alternative means of dividing mixture <sup>13</sup>C NMR spectra into subsets corresponding to the spectra of individual components are investigated. Specifically, the one-dimensional version of the two-dimensional (2D) long-range *J*-resolved method (LRJR) introduced by Bax and Freeman (12-14) is used to infer carbon connectivity by carrying out a series of measurements which result in modulation of <sup>13</sup>C mixture

resonances by coupled hydrogens. Because the technique involves selective excitation of particular  $^1\text{H}$  resonances to achieve the observed modulation, only carbon resonances within the compound containing the chosen  $^1\text{H}$  resonance can be modulated. Thus, a series of measurements, followed by analysis of the modulation behavior, permits proper grouping of mixture carbon resonances into subsets. Occasionally, the LRJR experiment does not reveal modulation due to directly bonded C-H couplings. In those cases (i.e. where carbon resonance modulation is not observed in the LRJR measurements), another 2D technique, broad band homonuclear decoupled heteronuclear shift correlation spectroscopy (15), can be used to produce a heteronuclear chemical shift correlation map (CSCM) which can complement the LRJR data. Subsequently, a reverse library search of the NIH/EPA CNMR spectral library, containing 11 640 spectra, is carried out to match the chemical shifts of the spectral subsets for qualitative identification.

### EXPERIMENTAL SECTION

A Nicolet NMC 300 NMR spectrometer operating at 75.497 MHz for  $^{13}\text{C}$  nuclei and 300.0678 MHz for  $^1\text{H}$  nuclei was used for all measurements. A 5-mm fixed-frequency  $^{13}\text{C}$  probe was used. Processing of spectral data was performed by use of a Nicolet 1280 computer with Nicolet software. Library searches were carried out with a Digital Equipment Corp. MicroVAX II and Fortran programs written for that purpose.

**NMR.** Typical  $^{13}\text{C}$  data acquisition parameters were as follows:  $180^\circ$  pulse width, 44  $\mu\text{s}$ ;  $180^\circ$  proton selective pulse width, either 7.5 or 15 ms. For LRJR measurements, evolution times ( $\tau$ ) of 160, 230, 300, and 370 ms (chosen to ensure that modulations of  $\text{CH}$ ,  $\text{CH}_2$ , and  $\text{CH}_3$  carbons, due to coupling with the selected proton, would be observed) were used. Heteronuclear shift correlation spectra were obtained by using the following parameters:  $^{13}\text{C}$   $180^\circ$  pulse width, 44  $\mu\text{s}$ ;  $^1\text{H}$   $180^\circ$  pulse width, 38  $\mu\text{s}$ , delay  $\Delta_1 = 3.70$  ms and delay  $\Delta_2 = 2.00$  ms (see pulse sequence); 2048 data points were collected over a spectral width of 4520 Hz ( $F_2$ ); a variable evolution period was incremented in 256 steps to a maximum of 163.84 ms, yielding a spectral width ( $F_1$ ) of 1562.5 Hz; 32 spectra were coadded for each value of evolution time, recycle time was 1.5 s, with a total data acquisition time of 4 h. Spectra were plotted in magnitude mode.

Chemical shift assignments for LRJR experiments with amino acids used dioxane as internal reference (67.4 ppm relative to tetramethylsilane), which was added at the completion of the LRJR measurements.

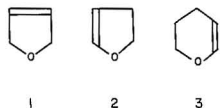
**Pulse Sequences.** For long-range  $J$ -resolved measurements, pulse sequence A (below) was used, and for heteronuclear shift correlation experiments, sequence B was used, with phases  $\phi$  and  $\psi$  cycled as described in ref 14.

A  $90^\circ_x(^{13}\text{C}) - \tau/2 - 90^\circ_x(^1\text{H}_{\text{sel}})$ ,  $180^\circ_x(^{13}\text{C})$ ,  $90^\circ_x(^1\text{H}_{\text{sel}}) - \tau/2 - t_2$

B

$90^\circ_x(^1\text{H}) - t_1/2 - 90^\circ_x(^1\text{H}) - 1/(2J) - 180^\circ_x(^1\text{H})$ ,  $180^\circ_x(^{13}\text{C}) - 1/(2J) - 90^\circ_x(^1\text{H}) - t_1/2 - \Delta_1 - 90^\circ_\phi(^1\text{H})$ ,  $90^\circ_\psi(^{13}\text{C}) - \Delta_2 - t_2$

**Samples.** Chemicals were purchased from either Aldrich or Sigma Chemical Co. and were used as received without further purification. A three-component mixture of 2,5-dihydrofuran (0.30 M), 1,2,3-dihydrofuran (0.40 M), 2, and 2,3-dihydrofuran (0.50 M), 3, in deuteriochloroform was prepared for the first analysis.



A second mixture was prepared by dissolving 30 mg each of L-valine, 4, L-threonine, 5, L-alanine, 6, and L-glycine, 7, and 60 mg of L-histidine, 8, in 0.75 mL of 99.5%  $\text{CD}_3\text{OD}$ . All samples were degassed in an ultrasonic bath for 10 min prior to NMR measurements. For shift reagent experiments, solutions containing

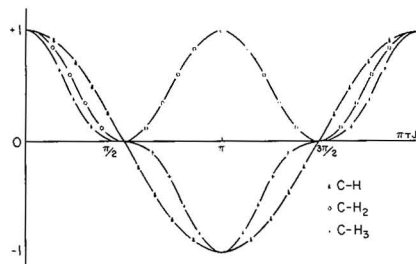
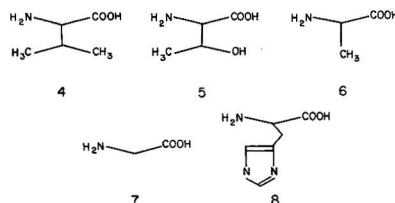


**Figure 1.**  $\tau$  dependence of  $^nJ(^{13}\text{C},^1\text{H})$ -modulated  $^{13}\text{C}$  magnetization intensities for methine, methylene, and methyl resonances. When  $\tau = 1/J$ , then both methine and methyl resonances are inverted. The regions  $\pi/2 \pm 20\%$  and  $3\pi/2 \pm 20\%$  are used to provide an identification of a methylene resonance, on the basis of its low relative intensity.

**Table I.** Coupling Constants between Carbon and Proton(s) at Various Regions of the Modulated Pattern as Shown in Figure 1, at Several Evolution Times,  $\tau$

$\tau$ , ms	$^nJ_{\text{C-H}}$ , Hz		
	$\pi/2$	$\pi$	$3\pi/2$
160	3.125	6.250	9.375
230	2.174	4.348	6.522
300	1.667	3.333	5.000
370	1.351	2.702	4.054

10 mg of L-valine, 15 mg of L-glycine, and either 4.5 or 9.0 mg of europium chloride in 1 mL of deuterium oxide were prepared.



### RESULTS AND DISCUSSION

For a heteronuclear coupled spin system (such as one which contains  $^{13}\text{C}$  and  $^1\text{H}$  nuclei), with long-range coupling (indicated by the notation C- $\text{H}_n$ ), the LRJR pulse sequence has the effect of introducing a phase dependence upon evolution period, rather than chemical shift. The functional dependence of carbon resonance intensity upon evolution time, shown in Figure 1, allows choice of values which can result in inversion of methyl and methine carbon resonances coupled to the selected proton (15). Because  $^nJ(\text{C,H})$  couplings are normally in the range of 0–60 Hz and  $^3J(\text{C,H})$  couplings in the 0–10 Hz range, evolution times between 160 and 370 ms should ensure inversion or diminution of most long-range coupled carbon resonances. As is seen from Table I, which summarizes the evolution times used, optimal modulation will occur for nuclei coupled with  $J$  between 1.351 and 9.375 Hz.

**Mixture Analysis.** For mixture analysis, a simple algorithm is used. LRJR NMR measurements for the selected evolution times and chosen proton resonances are first acquired. Following that, the carbon spectra are examined for selective modulation caused by irradiation in selected regions of the proton NMR spectrum. Modulated carbon resonances are then grouped into subspectra which are compared with library spectra for identification. Formation of subspectra is straightforward; e.g. if carbon nuclei A, B, and C show

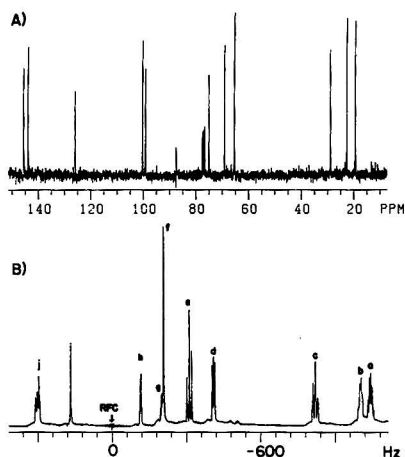


**Figure 2.** Spectra of furan/pyran mixture. (A) Broad band decoupled  $^{13}\text{C}$  spectrum, frequency 75.457 697 MHz, spectral width 11 000 Hz, 16 transients. Chemical shifts are relative to  $\text{CDCl}_3$  (77.0 ppm). (B)  $^1\text{H}$  spectrum spectral frequency 300.067 800 MHz, marked as RfC.

modulation when a particular proton is irradiated, and another set of nuclei, A, D, and E, are modulated via coupling with a second proton, then it can be inferred that the entire set A–E belong to the same mixture component and should be treated as a subset. As mentioned above, occasionally a 2D heteronuclear shift correlation measurement may be required to locate directly bonded couplings. Once every carbon has been assigned to a subset by these simple procedures, then library searches can be performed for component identification. In the present applications, library spectra which did not match all resonances of the “unknowns” within 1 ppm were rejected as not matching.

For clarity, and to demonstrate the use of the algorithm described above, a three-component model mixture (which has a well-resolved  $^1\text{H}$  spectrum) containing two dihydrofurans (2,3- and 2,5-) and 2,3-dihydropyran in deuteriochloroform was analyzed. Figure 2A shows the  $^{13}\text{C}$  spectrum of the mixture, which contains 11 resonances (in addition to a triplet arising from deuteriochloroform). Figure 2B is the  $^1\text{H}$  spectrum with the spectrometer carrier frequency (RfC) at 300.067 800 MHz indicated. Several proton resonances (b, c, g, and h) were used with four evolution times each to obtain 16 LRJR spectra which were sufficient to identify spectral subsets. Each spectrum is the result of coadding 40 spectra in the time domain (4 min per averaged spectrum, total measurement time of 64 min). Figure 3 contains the original unmodulated CNMR spectrum of the mixture, Figure 3A, along with five representative modulated spectra. Examination of these clearly provides the requisite information (e.g. Figure 3B shows that carbons 6 and 9 belong in the same subset, etc.). Table II summarizes the information obtained from these LRJR spectra. When library spectra were compared with the subsets, the three compounds all were identified unambiguously.

As a further test of this mixture analysis method, a mixture containing 30 mg each of L-valine, L-glycine, L-threonine, and L-alanine, in addition to 60 mg of L-histidine in 0.75 mL of 99.5%  $\text{CD}_3\text{OD}$  was analyzed. Figure 4A contains the  $^{13}\text{C}$  NMR spectrum of this mixture and Figure 4B the proton NMR spectrum. Examination of the proton NMR spectrum shows that most of the protons are well-separated from one another, with the exception of the pairs designated a and b and g and h. Thus, for initial LRJR experiments, all protons except

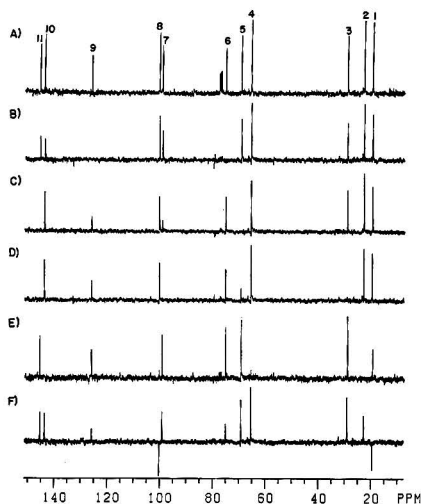


**Figure 3.** (A)  $^{13}\text{C}$  spectrum, same as Figure 2A. LRJR spectra of furan/pyran mixture with 40 transients coadded for each file. Total acquisition time per file is approximately 4 min.  $180^\circ$  proton selective pulse, at (B) h,  $\tau = 230$  ms, (C) c,  $\tau = 230$  ms, (D) c,  $\tau = 160$  ms, (E) b,  $\tau = 160$  ms, and (F) g,  $\tau = 300$  ms.

**Table II. Furan/Pyran Mixture Subspectra Collected Based upon LRJR  $^{13}\text{C}$  NMR Data**

peak	chemical shift, <sup>a</sup> ppm	LRJR experiments <sup>b</sup> of proton(s) selective			subspectra formed
		h	c	g	
1	19.27				1, 2, 4, 8, 10 <sup>c</sup>
2	25.50				—
3	28.80				3, 5, 7, 11 <sup>d</sup>
4	65.33				
5	69.08				
6	74.98				6, 9 <sup>e</sup>
7	99.02				
8	100.17				
9	125.86				
10	143.77				
11	145.44				

<sup>a</sup>Chemical shift assignments relative to  $\text{CDCl}_3$  (77.0 ppm). <sup>b</sup>0 stands for a null peak or one <10% of the magnitude of the unmodulated magnetization (explained in text). <sup>c</sup>—1 stands for an inverted resonance. See Figure 3. <sup>d</sup>Peaks 1, 2, 4, 8, and 10 correspond to 2,3-dihydropyran. <sup>e</sup>Peaks 3, 5, 7, and 11 correspond to 2,3-dihydrofuran. <sup>f</sup>Peaks 6 and 9 correspond to 2,5-dihydrofuran.

those were chosen for selective irradiation. As a result, all carbon resonances except number 1 and number 20 showed modulation. In a further LRJR experiment, a proton-selective pulse was applied 18 Hz to the high field side of proton g, which resulted in modulation of these two remaining resonances. Thus, the data compiled in Table III allowed grouping the carbon resonances into five subsets for spectral library searches. Figure 5 contains representative LRJR spectra and Figure 6 the CSCM for the mixture, which was measured to verify the validity of the LRJR assignments. As shown in Table III, each of the five subsets was correctly identified by the spectral library search.

**Chemical Shift Reagent Experiment.** One potential difficulty in using the LRJR methodology for mixture analysis is the requirement that the proton resonance chosen for se-

Table III. Amino Acid Mixture Subspectra Based upon LRJR  $^{13}\text{C}$  NMR and CSCM Data

peak	chemical shift, <sup>a</sup> ppm	CSCM <sup>b</sup>	LRJR experiments of proton(s)							subspectra formed
			i	k	e	g'	l	f	c	
1	17.05	1-d	-1							1, 8, 20 <sup>c</sup>
2	17.59	2-a			-1					2, 3, 6, 10, 19 <sup>d</sup>
3	18.87	3-b			-1					
4	20.37	4-c		-1						
5	29.03	5-f			0			0		
6	29.94	6-e			0					
7	42.29	7-g				7-g				7, 16 <sup>e</sup>
8	51.31	8-i	8-i							
9	55.59	9-j						0		
10	61.11	10-h			0					
11	61.18	11-h							-1	4, 11, 12, 17 <sup>f</sup>
12	66.85	12-k		-1				0		
13	11.75							0		
14	132.89						0			5, 9, 13, 14, 15, 18 <sup>g</sup>
15	137.12						-1			
16	173.26					0				
17	173.80			-1						
18	174.81									
19	175.13									
20	176.63		0					0		

<sup>a</sup> Chemical shift assignments relative to dioxane (67.4 ppm with respect to TMS). <sup>b</sup> One bond couplings between  $^{13}\text{C}$  and  $^1\text{H}$  in CSCM experiment. <sup>c</sup> Peaks 1, 8, and 20 correspond to alanine. <sup>d</sup> Peaks 2, 3, 6, 10, and 19 correspond to valine. <sup>e</sup> Peaks 7 and 16 correspond to glycine. <sup>f</sup> Peaks 4, 11, 12, and 17 correspond to threonine. <sup>g</sup> Peaks 5, 9, 13, 14, 15, and 18 correspond to histidine.

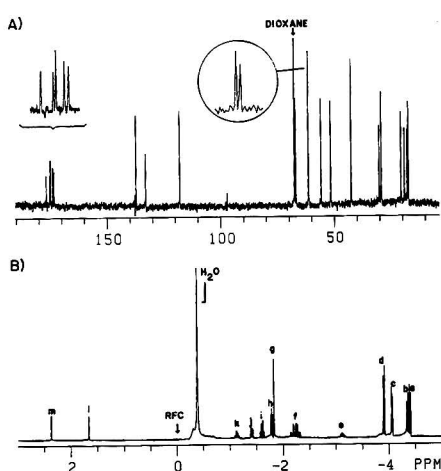


Figure 4. Spectra of amino acid mixture. (A) Broad band decoupled  $^{13}\text{C}$  spectrum, frequency 75.458 976 MHz, spectral width 14 000 Hz, 80 transients. Chemical shifts are relative to dioxane (67.4 ppm), a reference added after all LRJR experiments have been done. (B)  $^1\text{H}$  spectrum, spectral frequency 300.067 800 MHz, marked as RFC as indicated (no dioxane).

lective irradiation be well-separated from other resonances. In some cases, the enhanced dispersion afforded by use of a higher field NMR spectrometer can solve overlap problems. Alternatively, off-resonance LRJR experiments can be performed, as illustrated here for the amino acid mixture analysis. Another method investigated is use of a paramagnetic shift reagent. This technique has two potential advantages. First, it can reduce spin-lattice relaxation time for carbon nuclei (with concurrent reduction in CNMR measurement time) and second, proton resonances may be shifted to more convenient locations.

As a demonstration use of a shift reagent for LRJR applications, a mixture of 10 mg of valine and 15 mg of glycine

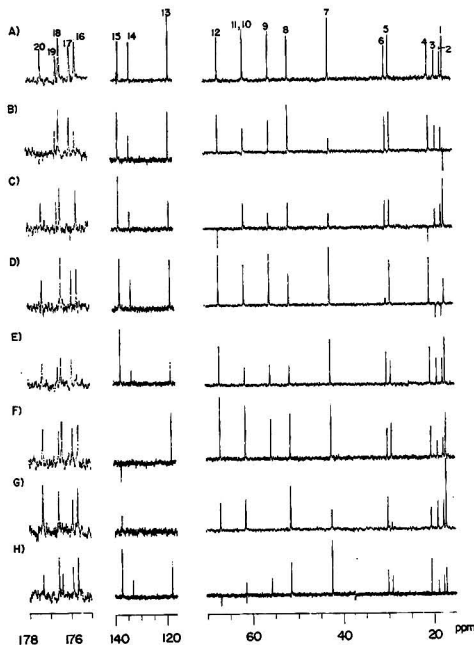
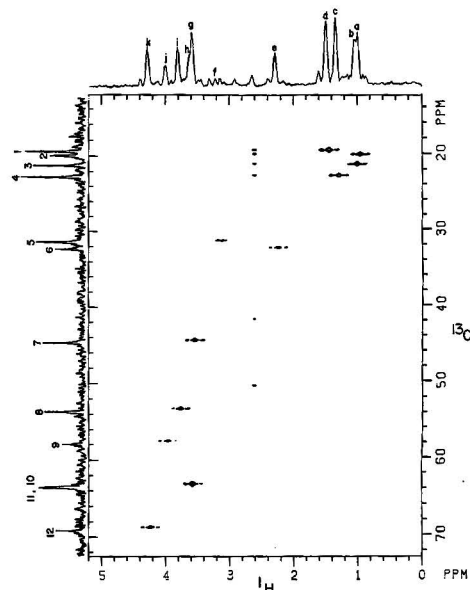


Figure 5. (A)  $^{13}\text{C}$  spectrum of amino acid mixture (no dioxane). LRJR spectra 500 coadded transients each. Acquisition time for each spectrum is approximately 20 min.  $180^\circ$  proton selective pulse, at (B) i,  $\tau = 170$  ms, (C) k,  $\tau = 170$  ms, (D) e,  $\tau = 170$  ms, (E) g',  $\tau = 170$  ms (an "off-resonance" irradiation, -18 Hz from proton g, explained in text), (F) l,  $\tau = 230$  ms, (G) h,  $\tau = 170$  ms ( $180^\circ$   $^1\text{H}$  selective pulse width 7.50 ms with 20-dB attenuation), (H) c,  $\tau = 170$  ms.

in 1 mL of 99.5% deuterium oxide was prepared. The separation of  $\alpha$ -proton resonances for that mixture is 13.8 Hz (marginal for LRJR measurements selecting one or the other





**Figure 6.** Contour plot of 2D  $^{13}\text{C}$ ,  $^1\text{H}$  homonuclear broad band decoupled magnitude-mode heteronuclear shift correlation spectrum of the aliphatic resonances of the amino acid mixture. The abscissa shows the  $\delta(^1\text{H})$  and the ordinate the  $\delta(^{13}\text{C})$ . Parameters:  $^{13}\text{C}$  frequency 75,454 685 MHz;  $^1\text{H}$  frequency at 300.066 999 MHz; dimension of matrix  $256 \times 2\text{K}$ ; 32 coadded transients for  $t_1$  value; acquisition time ca. 4 h; spectral width 4520 Hz.

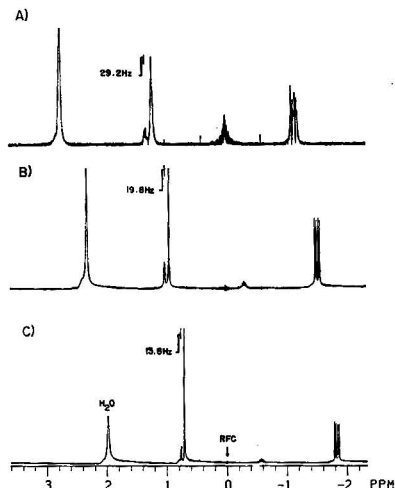


**Figure 7.**  $^1\text{H}$  spectra of valine and glycine mixture: (A) spectrum of the mixture with 9 mg of  $\text{EuCl}_3$ ; (B) with 4.5 mg of  $\text{EuCl}_3$ , and (C) with no shift reagent. Spectrometer frequency is 300.067 109 MHz.

of those resonances). Addition of 4.5 mg of europium chloride increased the separation to 19.8 Hz, and increasing the quantity of europium chloride to total 9.0 mg increased the separation to almost 30 Hz (sufficient for LRJR measurements). Figure 7 contains these three  $^1\text{H}$  NMR spectra, Figure

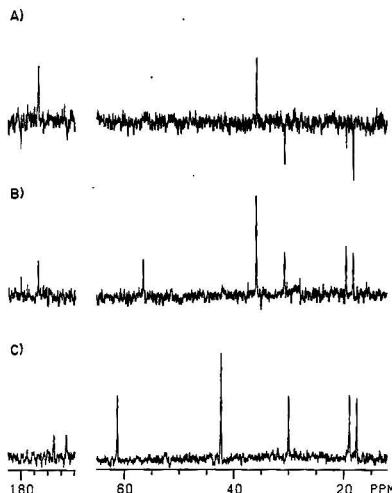


**Figure 8.** Shift-reagent experiment. (A) LRJR spectrum of valine and glycine mixture with 9 mg of  $\text{EuCl}_3$ .  $180^\circ$  proton selective pulse irradiation of  $\alpha$  protons of valine at  $\tau = 180^\circ$  ms. All carbon resonances of valine are inverted or diminished. (B)  $^{13}\text{C}$  spectrum of this mixture and (C)  $^{13}\text{C}$  spectrum of the same mixture without shift reagent. A change of chemical shift is observed after adding shift reagent.

8A the LRJR spectrum, and parts B and C of Figure 8 the carbon spectrum of the mixture with and without shift reagent, respectively. In this LRJR experiment, the valine carbon resonances were selectively modulated, while those of glycine were unaffected.

In summary, the present study establishes the feasibility of using LRJR experiments, systematically performed, in concert with a CNMR spectral library search for qualitative identification of simple mixture components without need for either separation or detailed spectral analysis. This can provide a useful alternative or complement to methods requiring quantitative carbon NMR analysis for the same purpose.

#### LITERATURE CITED

- (1) Wilkins, C. L. *Science* **1983**, *222*, 291-296.
- (2) Hirschfeld, T. *Anal. Chem.* **1980**, *52*, 297A-303A.
- (3) Laude, D. A., Jr.; Lee, R. W. K.; Wilkins, C. L. *Anal. Chem.* **1985**, *57*, 1464-1469.
- (4) Laude, D. A., Jr.; Wilkins, C. L. *Anal. Chem.* **1987**, *59*, 546-551.
- (5) Laude, D. A., Jr.; Wilkins, C. L. *TrAC, Trends Anal. Chem. (Pers. Ed.)* **1986**, *5*, 230-235.
- (6) Haw, J. F.; Glass, T. E.; Dorn, H. C. *Anal. Chem.* **1981**, *53*, 2332-2336.
- (7) Haw, J. F.; Glass, T. E.; Dorn, H. C. *Anal. Chem.* **1983**, *55*, 22-29.
- (8) Bayer, E.; Albert, K.; Nieder, M.; Grom, E.; Wolf, G.; Rindlisbacher, M. *Anal. Chem.* **1982**, *54*, 1747-1750.
- (9) Laude, D. A., Jr.; Wilkins, C. L. *Anal. Chem.* **1986**, *58*, 2820-2824.
- (10) Laude, D. A., Jr.; Wilkins, C. L. *Anal. Chem.* **1987**, *59*, 576-581.
- (11) Laude, D. A., Jr.; Cooper, J. R.; Wilkins, C. L. *Anal. Chem.* **1986**, *58*, 1213-1217.
- (12) Bax, A.; Freeman, R. J. *Am. Chem. Soc.* **1982**, *104*, 1099-1100.
- (13) Bax, A. In *Magnetic Resonance. Introduction, Advanced Topics and Applications to Fossil Energy*; Petrakis, L., Fraissard, J. P., Eds.; D. Reidel: Dordrecht, Holland, 1983; pp 137-145.
- (14) Bax, A. J. *Magn. Reson.* **1983**, *53*, 517-520.
- (15) Benn, R.; Gunther, H. *Angew. Chem., Int. Ed. Engl.* **1983**, *22*, 350-380.

RECEIVED for review September 14, 1987. Accepted January 4, 1988. Support from the National Science Foundation under Grant CHE-85-19087 and a Department Research Instrument Grant CHE-82-03497 is gratefully acknowledged.

# Ionization of Alkylbenzenes Studied by Gas Chromatography/Laser Ionization Mass Spectrometry

Richard B. Opsal<sup>1</sup> and James P. Reilly\*

Department of Chemistry, Indiana University, Bloomington, Indiana 47405

**Intensity-dependent relative laser ionization efficiencies and time-of-flight mass spectra are recorded for a variety of *n*-alkyl and multialkylbenzenes. With KrF excimer laser radiation the former ionize more efficiently than the latter. With ArF laser radiation the opposite is true. It is again demonstrated that by varying the incident light intensity, the laser ionization method can be either "soft" or "hard".**

During the past decade, laser ionization of polyatomic molecules has become a well established technique in molecular spectroscopy (1-4). One of its advantages relative to other laser-based methods is that easily detected charged particles, electrons and ions, are produced. This leads to a particularly sensitive technique when presently available high-power pulsed lasers are used in experiments. In addition, ions can be mass analyzed, enabling isotopically selective spectroscopy of parent compounds and neutral fragments to be undertaken (5-7). Time-of-flight mass spectrometry is a particularly versatile system for studying multiphoton ionization (MPI) since all ions generated during each laser pulse are detected (8-12). This is the key to its high sensitivity.

Even for the relatively simple process of two-step molecular ionization through a resonant intermediate state, ionization yields vary considerably from one molecule to the next and can be somewhat unpredictable (13-15). Quantitative experimental measurements of ionization efficiencies are non-trivial to perform since most methods of introducing samples are affected by their volatility and this can vary considerably over a series of compounds. One method that eliminates this problem is laser ionization gas chromatography/mass spectrometry (13-16). In this approach, accurately measured samples are introduced into a capillary column gas chromatograph that is interfaced to a mass spectrometer. The gas chromatograph (GC) not only provides a convenient method for quantitative sample introduction but also temporally separates the sample components from impurities. Compounds eluting from the column are reproducibly ionized leading to precise relative ionization yields. Ion yields and mass spectra of a large number of compounds can then be collected over a short period of time under virtually identical experimental conditions. This approach is employed in the present work to examine the ionization efficiencies of one particular class of compounds, the alkylbenzenes.

Although some aspects of the mass spectrometry of alkylbenzenes continue to draw the attention of researchers, the primary work in this field was performed 3 decades ago by Grubb and Meyerson with electron impact ionization (17). One of the main points of the present work is to compare mass spectral fragmentation patterns obtained by laser ionization with their electron impact counterparts and examine whether the trends observed by Grubb and Meyerson are also seen with laser ionization.

## EXPERIMENTAL SECTION

The GC/MS apparatus used in these studies is shown schematically in Figure 1. It consists of a Varian 3700 capillary column

**Table I. *n*-Alkylbenzene Mixture Components in Elution Order**

(0) benzene	(6) <i>n</i> -hexylbenzene
(1) toluene	(7) <i>n</i> -heptylbenzene
(2) ethylbenzene	(8) <i>n</i> -octylbenzene
(3) <i>n</i> -propylbenzene	(9) <i>n</i> -nonylbenzene
(4) <i>n</i> -butylbenzene	(10) <i>n</i> -decylbenzene
(5) <i>n</i> -pentylbenzene	(12) <i>n</i> -dodecylbenzene

**Table II. Alkylbenzene Mixture Components in Elution Order**

(1) toluene (methylbenzene)
(2) ethylbenzene
(3) isopropylbenzene (cumene)
(4) <i>n</i> -propylbenzene
(5) 1,3,5-trimethylbenzene (mesitylene)
(6) <i>tert</i> -butylbenzene
(7) <i>p</i> -isopropyltoluene ( <i>p</i> -cumene)
(8) <i>n</i> -butylbenzene
(9) 1,2,3,4-tetramethylbenzene (prehnitene)
(10) <i>n</i> -pentylbenzene
(11) naphthalene
(12) pentamethylbenzene
(13) hexamethylbenzene
(14) hexaethylbenzene
(15) <i>n</i> -dodecylbenzene

gas chromatograph equipped with an on-column injector and a reflectron time of flight mass spectrometer (18). The ionizing light source is a Lumonics TE-861 rare gas excimer laser operating with either KrF ( $\lambda = 249$  nm) or ArF ( $\lambda = 193$  nm) as gain medium. The capillary column (J&W Scientific, DB-1, 0.25  $\mu$ m film, 15 m length, 0.25 mm i.d.) extends from the GC oven through a direct heated interface into the ionization region of the mass spectrometer. Average laser power illuminating this region is measured with a Scientech Model 362 power meter and Model 36-0001 disk calorimeter. Before entering the spectrometer, the 10 ns duration light pulses are weakly focused by a 5 cm diameter, 500 mm focal length, Suprasil spherical lens. In the ionization region the beam profile is rectangular and its cross sectional area is approximately 8 mm<sup>2</sup>. Ions are detected at the end of the drift region by a tandem pair of microchannel plates. The anode current is directed to a Transiac 2001 waveform digitizer with Model 4100 averaging memory. Subsequently, the data are stored by an IBM 5150 computer both as an ion chromatogram and as TOF mass spectra associated with each chromatogram peak. Twenty mass spectra are summed every second to yield the total ion yield chromatograms displayed in this work. For comparison with laser ionization results, experiments were also performed with the gas chromatograph utilizing the same capillary column, but with a conventional flame ionization detector.

Two sets of reagent grade alkylbenzene solutions were utilized in this study. Mixture I was composed of a series of *n*-alkylbenzenes while mixture II contained an assortment of alkylbenzenes. Both were dissolved in methylene chloride. Their compositions are summarized in Tables I and II. Although not an alkylbenzene, naphthalene was included in mixture II as a reference since we have previously investigated its ionizing characteristics with this apparatus (13, 14). All experiments were performed by injecting 5 ng of each component into the gas chromatograph.

<sup>1</sup>Present address: Vestec Corp., Houston, TX 77054.

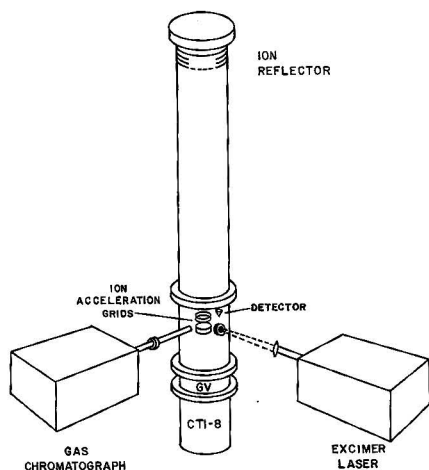


Figure 1. Diagram of the laser ionization gas chromatograph/reflectron TOFMS: GV, gate valve; CTI-8, vacuum cryopump.

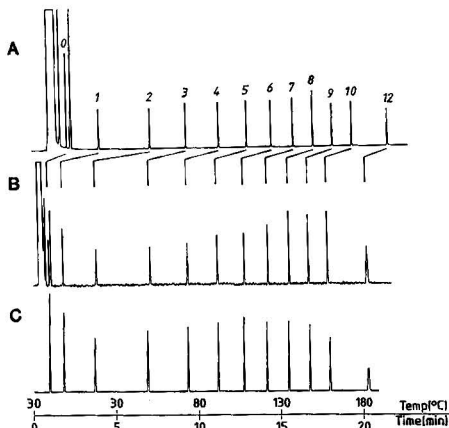


Figure 2. Chromatograms of *n*-alkylbenzene mixture detected by (A) flame ionization, (B) ArF laser ionization, 6.0 mJ/pulse, and (C) KrF laser ionization, 7.5 mJ/pulse. Numbers above peaks indicate the length of the *n*-alkyl chain. "0" is benzene. 5 ng of each component. In parts B and C, ions are summed from  $m/z$  10 to 590.

## RESULTS AND DISCUSSION

***n*-Alkylbenzene Studies.** Figure 2A displays a conventional gas chromatogram with flame ionization detection (FID) of the *n*-alkylbenzene sample, mixture I. The rough equivalence of peak areas reflects the reproducibility of injected component masses and the lack of chromatographic column discrimination against any of the compounds investigated. It underlines the fact that flame ionization is a mass- rather than a concentration-sensitive detection method. The congested collection of peaks at the beginning of the chromatogram arises predominantly from ionization of the methylene chloride solvent. Imbedded within this congestion is a peak corresponding to the 5-ng benzene component. The problem of overlapping solvent and analyte ionization is not eliminated when the sample is detected by ArF laser induced ionization (Figure 2B). However with KrF laser radiation, (Figure 2C) the solvent signal is strikingly absent. These results are easily explained. Methylene chloride's ionization potential of 11.35

eV cannot be reached by a pair of 5.0-eV KrF photons but is exceeded by two 6.4-eV ArF photons. Also noteworthy about the ArF results is that integrated ion yields appear to be constant or slightly increasing as the *n*-alkyl chain length increases. This trend is exactly opposite of what would be expected if each molecule leads to just a single ion and suggests that fragment ionization, in addition to parent molecule ionization, takes place. Fragment ionization has been confirmed in recent studies on aromatic molecules (8, 19–21). Chromatograms equivalent to that displayed in Figure 2C were recorded at three different laser intensities. The areas of all peaks were measured and in Figure 3A are plotted as a function of alkyl chain length. Curves I, II, and III correspond to KrF laser pulse energies of 2.1, 8.1, and 17.5 mJ, respectively. The solid curve was obtained with the flame ionization detector. At the lowest light intensity (curve I) ion yield monotonically decreases as the alkyl chain length grows. Probably under these conditions no more than a single ion per molecule is generated. As displayed in Figure 3B the number of molecules in a 5-ng sample decreases with increasing chain length at approximately the same rate as the observed low-intensity ion yield (Figure 3A, I). The particularly large difference between benzene and toluene evident in Figure 3A reflects their substantially different 249-nm extinction coefficients, which are displayed in Figure 3C. With increased light intensity (Figure 3A, curves II and III) the relative ion yields for the different *n*-alkylbenzenes become more equivalent indicating that detection response is proportional to component mass. This suggests that, as in the ArF case, both parent compounds and neutral fragments are being ionized at high KrF laser intensities.

It is well-known that 70-eV electron impact mass spectra of *n*-alkylbenzenes exhibit considerable ion fragmentation (17, 22–24). The largest peaks in these mass spectra are at  $m/z$  91 or 92. In contrast, Figure 4 displays mass spectra of these compounds ionized with relatively low-intensity KrF light (0.8 mJ/pulse). Nearly 100% of the ions are generated as parent ions. There are two reasons why such a small amount of fragmentation is induced. First, the absorption of two 5.0-eV photons only exceeds the 8–9 eV ionization potentials of these molecules by 1–2 eV. Second, photoelectron measurements indicate that most of this excess is carried off by the ejected electron (25). The latter is a direct consequence of the Franck-Condon principle; the structural similarity of electronically excited and ionized alkylbenzene molecules leads to little ion vibrational excitation.

Several studies on the ionization of alkylbenzenes have shown that the appearance potentials of  $C_7H_7^+$  and  $C_7H_8^+$  fragment ions are between 10 and 12 eV (26, 27). However in more recent work appearance potentials slightly below 10.0 eV have been measured for certain alkylbenzenes (28, 29). In the latter cases, the fragment ion yields were very low near the energetic thresholds for their observation. This may explain the appearance of small  $m/z$  91 and 92 peaks in the spectra of Figure 4.

Figure 5, which presents mass spectra recorded under high-intensity KrF irradiation conditions (17.5 mJ/pulse), stands in stark contrast with Figure 4. Fragmentation is pronounced; to generate some of the smaller ion fragments five or six photons must be absorbed (30, 31). Detailed inspection of this series of mass spectra reveals several fascinating trends. First of all, the entire region between masses 25 and 92 looks remarkably similar for all of these compounds. While the relative intensities of the  $C_3H_3^+$  ( $n = 0–5$ )  $C_4H_4^+$  ( $n = 0–4$ ),  $C_5H_5^+$ , and  $C_7H_7^+$  fragments are remarkably consistent over the entire range of compounds, certain species like  $C_2H_3^+$  and  $C_3H_5^+$  increase smoothly with alkyl chain length, while  $C_5H_6^+$ , which is a known daughter of the tro-

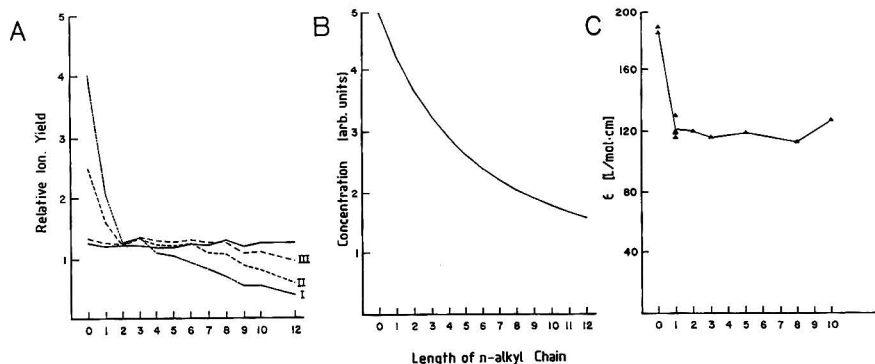


**Figure 3.** (A) Dependence of *n*-alkyl chain length on KrF laser-induced ion yield for three different light intensities: (I) 2.1 mJ/pulse, (II) 8.1 mJ/pulse, (III) 17.5 mJ/pulse. Solid curve is the variation in component response with flame ionization detection. (B) Variation in the relative number of molecules present in a 5-ng sample of an alkylbenzene as a function of *n*-alkyl chain length. (C) The molar extinction coefficients at 249 nm for various *n*-alkylbenzenes.

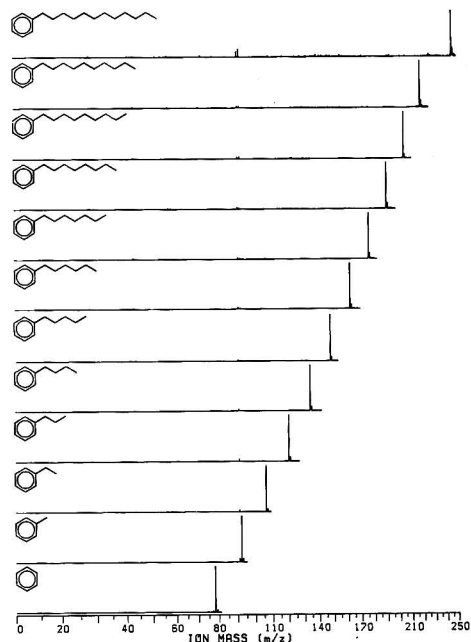


**Figure 4.** Mass spectra of *n*-alkylbenzenes ionized by relatively low intensity radiation (0.8 mJ/pulse).

pylium ion, decreases monotonically.  $C_2H_5^+$ ,  $C_3H_7^+$ , and  $C_4H_9^+$  exhibit more complicated behaviors. They grow in suddenly and inexplicably when the alkyl chain length reaches five, six, and eight carbons, respectively, and are among the few alkyl-derived ions present in the spectrum.

Perhaps the most interesting trend observed in Figure 5 involves the dependence of chain length on the 92/91 ion ratio. The  $m/z$  91 ion can be produced by a simple cleavage (although, of course, rearrangement of the resulting  $C_6H_5CH_2^+$  ion to the tropylium ion is possible). For molecules larger than toluene, mass 92 ions are rearrangement products. Previous mass spectral experiments have demonstrated that a  $\beta$  bond is weaker than the adjacent  $\alpha$  bond that connects an alkyl side

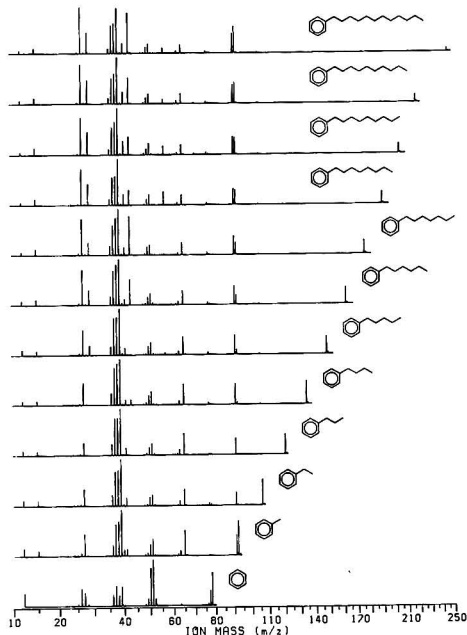


**Figure 5.** Mass spectra of *n*-alkylbenzenes ionized by relatively high intensity KrF radiation (17.5 mJ/pulse). These were recorded simultaneously with the chromatogram of Figure 2C.

chain to an aromatic ring. This is why mass 91  $C_7H_7^+$  ions predominate in both electron impact and laser ionization *n*-alkylbenzene mass spectra. There must be at least one hydrogen on the  $\gamma$  carbon of the alkyl chain to facilitate the rearrangement that produces  $m/z$  92 ions (17). This is why there are essentially no  $m/z$  92 ions in our ethylbenzene mass spectrum in Figure 5. Figure 6 graphically summarizes the trend observed at several laser pulse energies. Toluene is the first set of points in the figure and since toluene's molecular ion is at  $m/z$  92, the 92/91 ion ratio is quite high. Starting near zero at ethylbenzene the ratio grows smoothly with increasing length of the alkyl chain. This general trend has also

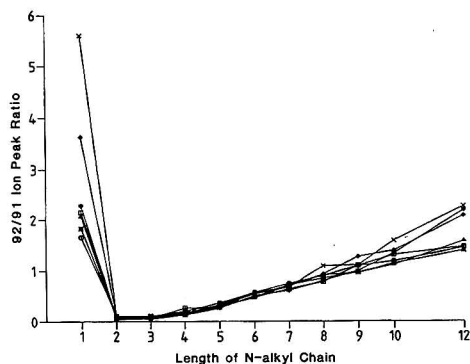


**Figure 6.** Dependence of the 92/91 ion ratio on *n*-alkyl chain length with KrF laser ionization: X, 1.8 mJ/pulse; ◇, 2.8 mJ/pulse; ☆, 8.0 mJ/pulse; △, 10. mJ/pulse; □, 15. mJ/pulse; \*, 17.5 mJ/pulse; ○, 21.0 mJ/pulse.

been observed with 70-eV electron impact ionization (24). Simply stated, the fraction of rearrangement ions increases with the length of the alkyl chain. Longer alkyl chains probably help to carry off excess vibrational excitation, stabilizing the mass 92 rearrangement ions relative to the mass 91 species.

As evident from Figure 6, the 92/91 ratio does not depend strongly on KrF laser pulse energy. Figures 4 and 5 illustrate the extremes of ion fragmentation. It is noteworthy that the 92/91 ratio is quite invariant to pulse energy. We believe that essentially all of our  $C_7H_7^+$  and  $C_7H_8^+$  ions are produced by a three-photon process and hypothesize that absorption of an additional photon (either by the parent molecule or by the fragments themselves) destroys them both. Therefore if the only mass 91 and 92 ions that we see have been produced by a three-photon process, their ratio must be independent of light intensity.

Competing cleavage and rearrangement processes provide insight into energy flow and disposal in polyatomic molecules (32). One of the more frequently studied system involves the relative production of  $C_7H_8^+$  and  $C_7H_7^+$ . The energy dependence of this fragmentation has been studied by a variety of techniques (33–37). The cleavage is known to require a higher activation energy (having a loose transition state) than the rearrangement (a tight transition state).  $C_7H_8^+$  is the dominant ion at low internal energies with a switch to  $C_7H_7^+$  production at higher internal energies. Harrison and Lin (33) and Chen, Hays, and Dunbar (34) studied the energy dependence of the fragmentation of *n*-butylbenzene molecular ions by using other methods. The 92/91 ion ratio was measured as a function of molecular ion internal energy. These two very different experiments yielded 92/91 fragment ion ratios at various molecular ion internal energies that were in good agreement.

The 92/91 ion ratio for *n*-butylbenzene in our KrF ionization study was found to be 1 to 6.1. According to Dunbar and co-workers (34) this corresponds to an ion internal energy of approximately 6.2 eV. This number agrees well with the energy of three KrF photons (15.0 eV) minus the ionization potential of *n*-butylbenzene (IP = 8.68 eV). Because ArF (6.8 eV) photons are significantly more energetic and tend to yield considerably more ion fragmentation than does KrF radiation, we did not attempt to record low-intensity ArF laser ionization mass spectra comparable to Figure 5. Nevertheless using 0.2–1.5 μJ 1920-Å light pulses obtained by Raman shifting the frequency doubled output from a Nd:YAG laser, we have recorded low-intensity laser ionization mass spectra of bu-

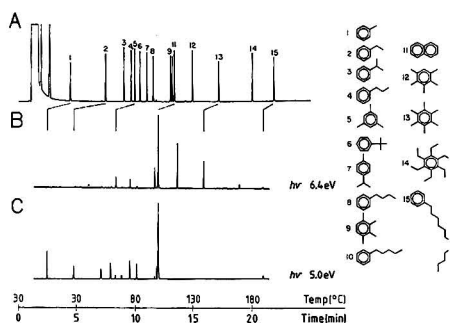


**Figure 7.** Chromatograms of alkylbenzene mixture (5 ng of each component): (A) flame ionization detection; (B) ArF laser ionization (2.1–2.7 mJ/pulse); (C) KrF laser ionization (6.4–7.1 mJ/pulse). In parts B and C, ions are summed from  $m/z$  28 to 260.

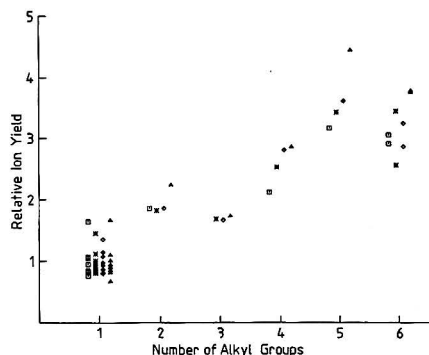


**Figure 8.** Dependence of the ArF laser-induced ion yield on the number of alkyl substituents on the benzene ring. Symbols correspond to different runs. Ion yield is normalized to unity for monosubstituted alkylbenzenes.

tylbenzene at this wavelength. With these laser fluences, the lowest at which ionization could be observed, we found that less than 1.8% of the ions were parent ions. Most were  $m/z$  91 and 92 ions. The 92/91 ratio was found to be  $0.4 \pm 0.05$  in all cases. According to Dunbar and co-workers (34) this corresponds to an ion internal energy of approximately 3.5 eV. The energy of two 1920-Å photons minus the ionization potential is 4.1 eV, in fairly good agreement.

**Other Alkylbenzene Studies.** Figure 7A is a reference FID chromatogram of mixture II whose components are identified in Table II. Parts B and C of Figure 7 show ion yield chromatograms obtained with ArF and KrF laser ionization, respectively. Ionization efficiency and specificity differ markedly among various alkylbenzenes at the two wavelengths. As displayed in Figure 8, with ArF radiation ion yields appear to increase monotonically with the number of alkyl substituents. However, with KrF radiation, molecules with just a single alkyl group are preferentially ionized. The causes of these propensities are not clear. The ionization potentials of multisubstituted alkyl aromatics tend to be 0.3–0.5 eV lower than their singly substituted isomeric counterparts (26, 27), presumably because of enhanced ion stabilization by electron-releasing alkyl substituents. Nevertheless, they are all within the range of 7.9–8.8 eV which is well below the energy of two excimer laser photons, so it is not obvious why this would be relevant. The difference in their wavelengths causes the two lasers to excite different electronic states. While the quantitative yields of fluorescence for the first excited singlet

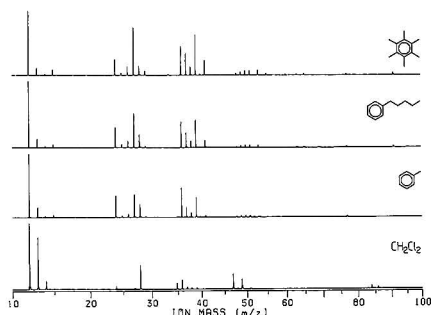


Figure 9. Representative ArF laser ionization mass spectra obtained under relatively high intensity conditions (5.2 mJ/pulse).

states of most of these molecules are substantial, those of second excited singlet states are invariably small (38). This implies that the nonradiative relaxation properties of the two electronic states differ substantially. Detailed relaxation paths have not been mapped out for either excited state and the relative contributions of internal conversion and intersystem crossing are generally unknown. One would expect that the plethora of C-H stretches that can be excited in hexamethyl- or hexaethylbenzene would act to accelerate any relaxation process that involves conversion of electronic to vibrational excitation, but once again the details of the process are presently indeterminate. Naturally, these ionization efficiency differences could result from variations in either the absorption cross sections or in the excited-state nonradiative relaxation properties of these alkylbenzenes. Reiser and Leyshon (39), Quina and Carroll (40), Murrell (41), and Petruska (42) have considered the effect of substituent symmetry on the electronic transition probability for a series of alkylbenzenes. Variations of no more than a factor of 2 are predicted or observed, so it is unlikely that this is the cause of the profound variations in ionization efficiency that we observe. On the other hand, several groups have studied nonradiative relaxation of excited alkylbenzene molecules (39, 40, 43-53). Most experiments have been performed in the liquid phase where it is found that branched substituents, like *tert*-butyl, tend to accelerate excited-state nonradiative relaxation and multiple (especially five or six) substituents lead to extremely fast nonradiative relaxation. Unfortunately, at least two gas-phase studies have yielded fundamentally different results. Breuer and Lee (52) and Prochorow, Hopewell, and El-Sayed (53) found relatively long (40-80 ns) fluorescence lifetimes for polymethylbenzenes and *tert*-butylbenzene. Excited-state relaxation on time scales this long should not substantially affect our ionization yields. However the wavelengths employed in the gas-phase studies were substantially longer than the excimer laser wavelengths used in the present work. Since nonradiative relaxation in aromatic molecules can dramatically depend on the degree of molecular vibronic excitation, the previously reported lifetimes may not be relevant to our situation. The ArF laser excites the second excited singlet states in these aromatic molecules, and the nonradiative relaxation characteristics of these states are particularly difficult to envision by extrapolation from the earlier gas-phase measurements. Fluorescence lifetime measurements at the KrF and ArF laser wavelengths would be helpful for interpreting the present data. The trend exhibited in Figure 8 could be a consequence of multisubstituted alkylbenzenes producing more ions per molecule or simply ionizing more efficiently. In principle this should be testable by conducting experiments under extremely low light intensity conditions, but this has not yet been done. Mass spectra of

a few of these compounds were obtained while recording a chromatogram with high intensity (5.2 mJ/pulse) ArF laser radiation and are displayed in Figure 9. The remarkable similarity of the three aromatic mass spectra in Figure 9 suggests that the fragment ions are formed from common precursors. The lack of evidence that considerable alkyl radical ionization is taking place implies that multisubstituted alkylbenzenes are ionizing more efficiently. The dramatic contrast between the high intensity aromatic mass spectra and the methylene chloride mass spectrum, also displayed in Figure 9, underlines the ability of laser mass spectrometry to distinguish different types of molecules. (Note that the  $m/z$  28 ion in Figure 9 is due to three-photon ionization of the nitrogen carrier gas and does not derive from methylene chloride.) It thus has potential impact in the field of computerized mass spectral pattern recognition.

## CONCLUSIONS

Laser ionization GC/MS allows further study of the multiphoton ionization process. The ion yield chromatograms presented in this paper facilitate the comparison of ionization efficiencies for different molecules. This would be difficult by other methods. These comparisons are possible because of the quantitative reproducibility of gas chromatography.

Relative ionization efficiencies must be taken from the integrated peak areas in the chromatograms as in other GC detection methods since components elute over a finite period of time in GC.

For studies involving examination of mass spectra, the laser ionization GC/MS system allows a large number of mass spectra to be generated relatively quickly. These mass spectra and ion yield chromatograms are obtained with virtually the same ionization conditions. Molecules eluting from the GC are at the same temperature i.e., that of the direct interface. Components elute at a constant carrier gas flow rate; i.e., the GC is equipped with a constant flow controller. Laser output is fairly constant during the time it takes to acquire an ion yield chromatogram. The *n*-alkylbenzene studies illustrate this point. Typically, in a period of 20 min an ion yield chromatogram and 12 mass spectra could be recorded. This is limited only by the resolving power of the capillary column and the data acquisition system.

Parent alkylbenzene molecular ions, which are not produced in large abundance by electron impact, can easily be generated with low-intensity excimer laser radiation. Fragmentation is extensive at higher light intensities. The relative yields of mass 91 and 92 ions under the latter conditions are similar to those previously measured by quite different methods. Multisubstituted alkylbenzenes and singly substituted *n*-alkylbenzenes ionize with quite different efficiencies. The reason for this is not understood but must be related to the different excited-state relaxation characteristics of the two types of compounds.

While the laser GC/MS method is proving to be a valuable probe for study of the multiphoton ionization process, additional versatility can be incorporated with the addition of tunable dye lasers, short pulse duration lasers, and multicolor experiments for more detailed spectroscopic studies.

## ACKNOWLEDGMENT

We wish to thank M. Yang and E. Sekreta for recording the low-intensity 1920-Å laser mass spectrum of *n*-butylbenzene.

**Registry No.** Benzene, 71-43-2; toluene, 108-88-3; ethylbenzene, 100-41-4; *n*-propylbenzene, 103-65-1; *n*-butylbenzene, 104-51-8; *n*-pentylbenzene, 538-68-1; *n*-hexylbenzene, 1077-16-3; *n*-heptylbenzene, 1078-71-3; *n*-octylbenzene, 2189-60-8; *n*-nonylbenzene, 1081-77-2; *n*-decylbenzene, 104-72-3; *n*-dodecylbenzene, 123-01-3; isopropylbenzene, 98-82-8; 1,3,5-trimethylbenzene, 108-67-8; *tert*-butylbenzene, 98-06-6; *p*-isopropyltoluene,



99-87-6; 1,2,3,4-tetramethylbenzene, 488-23-3; naphthalene, 91-20-3; pentamethylbenzene, 700-12-9; hexamethylbenzene, 87-85-4; hexaethylbenzene, 604-88-6.

## LITERATURE CITED

- (1) Lin, S. H.; Fujimura, Y.; Neusser, H. J.; Schlag, E. W. *Multiphoton Spectroscopy of Molecules*; Academic: Orlando, FL, 1984.
- (2) Johnson, P. *Acc. Chem. Res.* **1980**, *13*, 20.
- (3) Reiser, H.; Wittig, C. *Adv. Chem. Phys.* **1985**, *60*, 1.
- (4) Parker, D. H. *Ultraviolet Laser Spectroscopy*; Klier, D. S., Ed.; Academic: New York, 1983.
- (5) Boesl, U.; Neusser, H. J.; Schlag, E. W. *J. Am. Chem. Soc.* **1981**, *103*, 5058.
- (6) Whetten, R. L.; Fu, K. J.; Tapper, R. S.; Grant, E. R. *J. Phys. Chem.* **1983**, *87*, 1484.
- (7) Owens, K. G.; Reilly, J. P. *J. Opt. Soc. Am. B: Opt. Phys.* **1985**, *2*, 1589.
- (8) Zandee, L.; Bernstein, R. B. *J. Chem. Phys.* **1979**, *70*, 2574.
- (9) Lichtin, D. A.; Datta-Ghosh, S.; Newton, K. R.; Bernstein, R. B. *Chem. Phys. Lett.* **1980**, *75*, 214.
- (10) Rockwood, S.; Reilly, J. P.; Hohl, K.; Kompa, K. L. *Opt. Commun.* **1979**, *28*, 175.
- (11) Reilly, J. P.; Kompa, K. L. *J. Chem. Phys.* **1980**, *73*, 5468.
- (12) Boesl, U.; Neusser, H. J.; Schlag, E. W. *J. Chem. Phys.* **1980**, *72*, 4327.
- (13) Rhodes, G.; Opsal, R. B.; Meek, J. T.; Reilly, J. P. *Anal. Chem.* **1983**, *55*, 230.
- (14) Opsal, R. B.; Reilly, J. P. *Opt. News* **1986**, *12*, 18.
- (15) Opsal, R. B.; Reilly, J. P. *Anal. Chem.* **1986**, *58*, 2919.
- (16) Sack, T. M.; McCreary, D. A.; Gross, M. L. *Anal. Chem.* **1985**, *57*, 1291.
- (17) Grubb, H. M.; Meyerson, *Mass Spectrometry of Organic Ions*; McLafferty, F., Ed.; Academic: New York, 1963; p 453.
- (18) Mamyrin, B. A.; Karatev, V. I.; Shmikk, D. V.; Zagulin, V. A. *Sov. Phys.—JETP (Engl. Transl.)* **1973**, *37*, 45.
- (19) Hering, P.; Maaswinkel, A. G. M.; Kompa, K. L. *Chem. Phys. Lett.* **1981**, *83*, 22.
- (20) Sekreta, E.; Owens, K. G.; Reilly, J. P. *Chem. Phys. Lett.* **1986**, *132*, 450.
- (21) Chen, P.; Pallix, J. B.; Chupka, W. A.; Colson, S. D. *J. Chem. Phys.* **1986**, *84*, 527.
- (22) *Atlas of Mass Spectral Data*; Stenhagen, E.; Abrahamsson, S., McLafferty, F. W., Eds.; Wiley-Interscience: New York, 1969.
- (23) *Eight Peak Index of Mass Spectra*; The Mass Spectrometry Data Centre, Royal Society of Chemistry: Nottingham, United Kingdom, 1983.
- (24) King, A. B. *J. Chem. Phys.* **1965**, *42*, 3526.
- (25) Meek, J. T.; Long, S. R.; Reilly, J. P. *J. Phys. Chem.* **1982**, *86*, 2809.
- (26) Rosenstock, H. M.; Draxl, K.; Steiner, B. W.; Herron, J. T. *J. Phys. Chem. Ref. Data, Suppl.* **1977**, *6* (No. 1).
- (27) Levin, R. D.; Lias, S. G. "Ionization Potential and Appearance Potential Measurements 1971-1986", NSRDS-NBS 71; U.S. Government Printing Office: Washington, D.C., 1982.
- (28) McLoughlin, R. G.; Morrison, J. D.; Traeger, J. C. *Org. Mass Spectrom.* **1978**, *13*, 483.
- (29) McLoughlin, R. G.; Morrison, J. D.; Traeger, J. C. *Org. Mass Spectrom.* **1979**, *14*, 104.
- (30) Jonsson, B. O.; Lindholm, E. *Ark. Fysk.* **1969**, *39*, 65.
- (31) Hustrulid, A.; Kusch, P.; Tate, J. T. *Phys. Rev.* **1938**, *54*, 1037.
- (32) Brown, P. *Org. Mass Spectrom.* **1970**, *3*, 1175.
- (33) Harrison, A. G.; Lin, M. S. *Int. J. Mass Spectrom. Ion Phys.* **1983**, *51*, 353.
- (34) Chen, J. H.; Hays, J. D.; Dunbar, R. C. *J. Phys. Chem.* **1984**, *88*, 4759.
- (35) Dawson, P. H.; Sun, W.-F. *Int. J. Mass Spectrom. Ion Phys.* **1982**, *44*, 51.
- (36) McLuckey, S. A.; Sallans, L.; Cody, R. B.; Burnier, R. C.; Verma, S.; Freiser, B. S.; Cooks, R. G. *Int. J. Mass Spectrom. Ion Phys.* **1982**, *44*, 215.
- (37) Mukhtar, E. S.; Griffiths, F. M.; Harris, F. M.; Beynon, J. H. *Int. J. Mass Spectrom. Ion Phys.* **1981**, *37*, 159.
- (38) Gregory, T. A.; Hirayama, F.; Lipsky, S. J. *Chem. Phys.* **1973**, *58*, 4696 and 4697.
- (39) Reiser, A.; Leyshon, L. J. *J. Chem. Phys.* **1972**, *56*, 1011.
- (40) Quina, F. H.; Carroll, F. A. *J. Am. Chem. Soc.* **1976**, *98*, 6.
- (41) Murrell, J. N. *The Theory of the Electronic Spectra of Organic Molecules*; Wiley: New York, 1963; p 199.
- (42) Petruska, J. J. *Chem. Phys.* **1961**, *34*, 1111 and 1120.
- (43) Berendse, V. M.; Krongauz, V. A. *Theor. Exp. Chem. (Engl. Transl.)* **1967**, *3*, 63.
- (44) Rabalais, J. W.; Maria, H. J.; McGlynn, S. P. *J. Chem. Phys.* **1969**, *51*, 2259.
- (45) Cundall, R. B.; Tippett, W. *Trans. Faraday Soc.* **1970**, *66*, 350.
- (46) Lawson, C. W.; Hirayama, F.; Lipsky, S. J. *Chem. Phys.* **1969**, *51*, 1590.
- (47) Cundall, R. B.; Pereira, L. C. *Chem. Phys. Lett.* **1973**, *18*, 371.
- (48) Haaland, D. M.; Nieman, G. C. *J. Chem. Phys.* **1973**, *59*, 1013.
- (49) Froehlich, P. M.; Morrison, H. A. *J. Phys. Chem.* **1972**, *76*, 3566.
- (50) Schloman, W. W.; Morrison, H. J. *Am. Chem. Soc.* **1977**, *99*, 3342.
- (51) Cundall, R. B.; Robinson, D. A.; Voss, A. J. R. *J. Photochem.* **1973**, *74*, 2, 231.
- (52) Breuer, G. M.; Lee, E. K. C. *Chem. Phys. Lett.* **1972**, *14*, 404.
- (53) Prochorow, J.; Hopewell, W.; El-Sayed, M. A. *Chem. Phys. Lett.* **1979**, *65*, 410.

RECEIVED for review August 13, 1987. Accepted December 14, 1987. This work has been supported by the Environmental Protection Agency and by the National Science Foundation. J.P.R. is a Camille and Henry Dreyfus Teacher-Scholar.

## Waveguide Capillary Flow Cell for Fluorometry

Kitao Fujiwara,<sup>1</sup> J. B. Simeonsson, B. W. Smith, and J. D. Winefordner\*

Department of Chemistry, University of Florida, Gainesville, Florida 32611

A new technique of fluorescence detection involving the use of liquid core fibers has been developed and discussed. The analyte dissolved in a solvent of high refractive index was pumped through the hollow fiber (length up to 12 m), which was excited at one end by a dye laser, and the fluorescence was observed at the other end, in a unique 180° source-measurement geometry. The detection limits of perylene in carbon disulfide solution are 25, 7, and 0.4 pg/mL for 0.61-, 1.50-, and 12.0-m lengths of fiber, respectively. The experimental and theoretical behavior of the hollow fiber as a fluorescence cell is also given.

The detection power in fluorometry is a function of the path length as well as the absorption coefficients of the analyte,

the solvent, and any concomitants (*I*). The relationship between the fluorescence flux for the analyte,  $\Phi_F^A$ , and the path length, *l*, is given by

$$\Phi_F^A = C[1 - \exp(-[k(A) + k(B)]l)] \quad (1)$$

where the *k*(*A*) and *k*(*B*) are wavelength-dependent linear absorption coefficients for the analyte, *A*, and concomitants, *B*, *l* is the absorption path length, and *C* is a constant which includes the emission transition probability, the wavelength of fluorescence, the emission spectrometric characteristics, the entrance optics between the source and the sample and between the sample and the spectrometer-detector, and all optical losses due to transmission/reflection losses. If *l* → ∞, then the fluorescence flux reaches a maximum. In our work, we have developed a unique means of increasing the path length *l* by means of a long path length waveguide capillary cell where total internal reflections increase *l* over the geometric path length. The fluorescence is collected from the opposite end of the hollow fiber and sample solutions are pumped through the fiber by an high-performance liquid

\* Author to whom all correspondence should be addressed.

<sup>1</sup> Present address: Department of Chemistry, Faculty of Sciences, The University of Tokyo, Bunkyo-ku, Tokyo 113, Japan.

0003-2700/88/0360-1065\$01.50/0

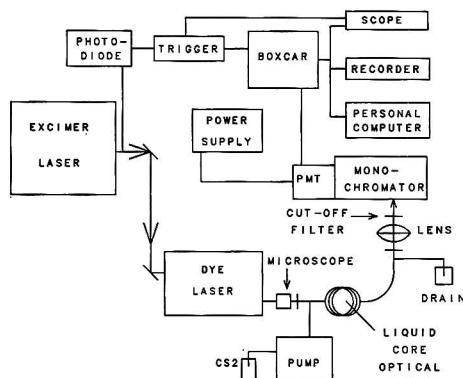


Figure 1. Block diagram for waveguide capillary flow cell with liquid core fiber for fluorescence spectrometry.

chromatographic pump. Solutions can be changed in a matter of minutes with no memory effects. Although the laser exciting radiation propagates through the waveguide, the fluorescence of the analyte (and the background) radiates in all directions. The angle over which fluorescence is detected is determined by

$$n_1/n_2 = \sin(90^\circ - \theta) \quad (2)$$

where  $n_2$  and  $n_1$  are the refractive indexes of the liquid sample in the hollow fiber and of the hollow fiber material, respectively, and  $\theta$  is the linear angle to the fiber surface over which total reflection within the fiber is collected and transmitted from the fiber. For quartz ( $n_1 = 1.472$ ) and the solvent carbon disulfide ( $n_2 = 1.627$ ),  $\theta$  is  $25.1^\circ$ . Therefore, about 10% of the fluorescence is collected and transmitted to the end of the fiber, assuming no other losses occur such as those due to wall roughness, turbulence at the wall surface, etc.

Liquid-filled optical fibers are finding considerable use in spectroscopy, especially in the areas of multiphoton absorption and nonlinear Raman spectrometry (2-6). The major use of liquid filled, waveguide capillary cells in analytical chemistry has so far been in colorimetry (7,8). However, up to now, there have been no applications of such cells in fluorescence spectrometry. In this paper, we describe a novel waveguide, capillary flow cell for fluorimetry and have evaluated its analytical as well as its response characteristics.

## EXPERIMENTAL SECTION

**Apparatus.** A block diagram of the experimental system is shown in Figure 1. The light source is a XeCl excimer laser (Lumonics, Model TE-861-S operated at 20 Hz) pumped dye laser (Molelectron, Model DL (II) with a flowing dye system (dye, Stilbene 420 at the concentration of  $1.4 \times 10^{-3}$  mol/L, Exciton Chemical Co.). The dye laser is tuned to 423 nm with an output energy of 0.5-1 mJ per pulse, which is sent to the fiber via a microscope objective. The output radiation from the fiber optic is passed through a cutoff filter (Schott Glass Co., type GG10; or Corion Corp., type LG450, or LG475) to minimize measurement of source light at the excitation wavelength. The fluorescence flux is detected by a photomultiplier (Hamamatsu Photonics, types R928 or R1414) after dispersion by a monochromator. Two monochromators are used in this experiment; a monochromator of 30-cm focal length (Heath, Model EU-700) is employed for observing the fluorescence spectrum of perylene and one of 10-cm focal length (American ISA, Inc., Model H-10V) for the quantitative measurement of perylene. A high-voltage power supply (John Fluor Manufacturing Co., Model 412A) is used for the photomultiplier, the output of which is preamplified (Evans Associates, Model 4163) and processed by a gated integrator/

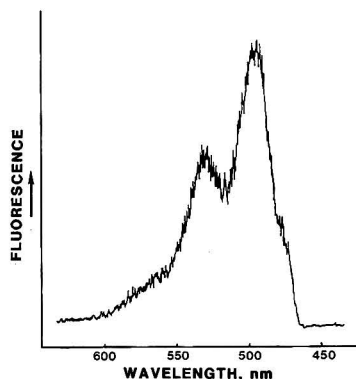


Figure 2. Fluorescence spectrum of perylene in the fiber. Emission spectrum was observed with 15-m fiber at an excitation wavelength of 423 nm. The concentration of perylene used in the fiber was 95 ng/mL.

boxcar averager (Stanford Research System, Model SR 250) and recorded by a strip-chart recorder (Fisher Recordal, Model 5000) or acquired by a personal computer (IBM-PC) for statistical calculations. More details about the present system are given in ref 9.

A pump for HPLC (Altex, Model 10 A) is used to pump solutions through the hollow fiber. Hollow fibers are (Gasukro Kogyo, Japan) made of fused quartz and coated with polyimide resin.

A commercial fluorescence spectrophotometer (Spex Fluorolog, Model DM3000-F) is used to obtain fluorescence spectra of the samples and a UV-vis spectrophotometer (Hewlett-Packard, Model 8450A) is used to obtain absorption spectra of the solvent and analyte.

**Chemicals.** Perylene (purchased from Fluka AG) is dissolved in carbon disulfide and used for fluorescence measurements. Carbon disulfide is purchased from Aldrich Chemical Co., Inc. (Spectrophotometric grade); this  $CS_2$  has a significant absorption below 410 nm. However, the absorption of carbon disulfide is not serious at the source light wavelength (lower than 0.01 absorbance at 423 nm) and so was used without further purification.

**Procedure.** Introduction of the sample solution and laser radiation into the hollow fiber was carried out with a stainless T-junction as discussed previously (7). The input aperture for the source light was made from a quartz rod fixed to the T-junction. The solution flowed at a rate of 1.5 mL/min in most experiments. The fibers employed here had internal diameters of 100, 250, and 530  $\mu$ m. In the case of the 100- $\mu$ m fiber, it was impossible to retain the quartz rod window due to the high back pressure even under the low sample flow rate. Fibers of 250 and 530  $\mu$ m i.d. were therefore used. It was also confirmed here that nonlinear effects such as stimulated Raman scattering were not observed in the present system.

## RESULTS AND DISCUSSION

Figure 2 shows the fluorescence emission spectrum of perylene through the fiber optic (15 m length, 530  $\mu$ m i.d.) at the excitation wavelength of 423 nm. Perylene exhibits fluorescence peaks at 460 and 490 nm and a shoulder at 530 nm in the Spex DM3000-F fluorescence spectrophotometer. However, the fluorescence peak at 460 nm does not appear in the figure because the cutoff filter significantly reduced the measured emission below 480 nm. Excitation at a wavelength of around 420 nm produced the maximum fluorescence intensity in the 490-nm region. An excitation wavelength of 423 nm (the maximum output of the stilbene 420 dye laser) with an emission wavelength of 490 nm was therefore chosen for all other experiments. A cutoff filter was necessary to minimize the background stray light ascribed to the source light at the excitation wavelength in this unique  $180^\circ$  angle source excitation-fluorescence detection scheme. The background signal and associated noise limited the detection power

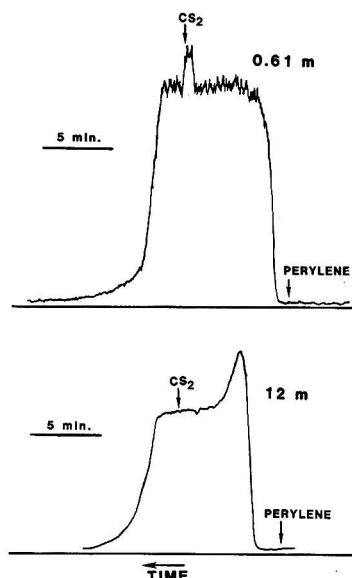


Figure 3. Temporal responses for appearance and disappearance of perylene fluorescence in the fiber. Flow rate of solution was 1.5 mL/min except when changing the solution. The arrow in the figures shows the time of changing the solution. The concentrations of perylene were 23 and 4 ng/mL for 0.61- and 12.0-m fibers, respectively.

(signal to noise ratio) of the present experimental system. A 0° angle (front surface) excitation-fluorescence scheme would be even more difficult to implement because of source scatter noise.

In this work, fibers of three different lengths (0.61, 1.50, and 12.0 m) were compared with respect to the fluorescence of perylene; the internal diameter of these fibers was 530  $\mu\text{m}$ . The transmission efficiency of this fiber filled with carbon disulfide is about 85% per 1 m at the wavelength of 423 nm and is attributable primarily to the small absorption of carbon disulfide at this wavelength region. As a result, the intensity of source light at the end of the 12-m fiber is 19% of that of a 1-m fiber.

Figure 3 shows the temporal behavior of appearance and disappearance of perylene fluorescence in the fibers of 0.61-m and 12-m lengths resulting from alternate application of solvent and perylene solution to the fibers. Because of the dead space between the entrance of the fiber sample reservoir (including the pump), it takes 3 to 5 min for the signal to recover for a change in the solution.

The most intense perylene signals result for the 0.61-m fiber for any given perylene concentration and experimental conditions. An increase in the fluorescence signal always resulted when the flow was terminated in order to change solution. In the case of the 12-m fiber, the dependence of signal level on the flow rate of solution is less critical compared to the shorter fibers. However, as can be seen in the lower figure, the fluorescence increased with the introduction of perylene into the fiber and then decreased to a constant level. This behavior can be explained by considering the progress of perylene solution into the fiber; the highest fluorescence signal occurred when the perylene solution reached an optimal distance from the entrance, and for greater lengths of perylene solution, the fluorescence is attenuated by self-absorption.

Figure 4 shows the dependence of the background fluorescence signal on the solvent flow rate for fibers of 0.61- and 1.50-m length. The fluorescence signal is related to the inverse of flow rate; i.e., higher flow rates give lower fluorescence signals. Higher flow rates appeared to cause turbulence which reduced the transmission of the fibers. In the case of the 12-m fiber, the background fluorescence signal decreased only above a flow rate of 3 mL/min. These results suggest the importance of maintaining a constant

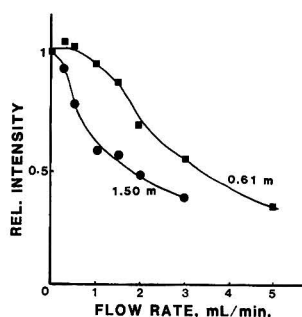


Figure 4. Dependence of background fluorescence emission on the flow rate of carbon disulfide.

Table I. Signal Output from the Boxcar Integrator<sup>a</sup>

fiber length, m	vol of cell, mL	applied solution	output, mV	S/B
0.61	0.54	CS <sub>2</sub>	8.04	5.5
		perylene (2 ng/mL)	44.2	
1.50	1.32	CS <sub>2</sub>	1.20	7.8
		perylene (2 ng/mL)	9.40	
12.0	10.6	CS <sub>2</sub>	0.22	13.3
		perylene (2 ng/mL)	2.66	

<sup>a</sup> S, perylene fluorescence; B, background emission from the solvent (carbon disulfide).

flow rate, especially for the fibers of shorter length.

In Table I, the cell volume, the signal-to-background ratios, and the signal outputs from the boxcar when using fibers of different lengths are given. The fluorescence signals of perylene and the background fluorescence (given by the solvent) decreased in the longer fiber. However, the background fluorescence signal decreased more rapidly with increased length of fiber than the perylene fluorescence signal. As a result, the longer fiber gave a higher signal to background ratio than the shorter ones; however, the shortest fiber (61 cm length) gave the largest fluorescence signal for perylene.

To explain the experimental results involving fluorescence signals as a function of fiber length, an expression for the fluorescence flux  $\Phi_F^A$  for a hypothetical analyte A in the presence of a hypothetical interferent(s) is necessary and is given below

$$\Phi_F^A = \Omega_F A_{sp} T_{sp} Y(A) F(\lambda_{em}, \Delta\lambda_{em}) G A_{so} E_o T_{so} f_{pref} f_{self} f_{post} [1 - \exp(-\{k(A) + k(B)\}l)] \quad (3)$$

where  $\Omega_F$  is the solid angle of luminescence collected by the spectrophotometer,  $A_{sp}$  is the area of luminescence measured,  $T_{sp}$  is the transmittance of the spectrophotometer system,  $Y(A)$  is the luminescence flux efficiency for analyte (perylene),  $f(\lambda_{em}, \Delta\lambda_{em})$  is the fraction of the luminescence band measured at  $\lambda_{em}$  by the emission spectrophotometer with band-pass  $\Delta\lambda_{em}$ ,  $G$  is the geometric factor accounting for isotropic emission,  $A_{so}$  is the source area,  $T_{so}$  is the transmission loss of source radiation due to optical components,  $f_{pref}$  is the prefilter effect,  $f_{self}$  is the self-absorption factor, and  $f_{post}$  is the postfilter effect. In the present case, the excitation paths of the sample solutions are identical ( $l = L$ , where  $l$  is the absorption path length and  $L$  is the emission path length). Therefore, the terms concerning the prefilter and postfilter effects can be excluded from the above equation. Equation 3 can be simplified as

$$\Phi_F^A = \Omega_F A_{sp} T_{sp} Y(A) F(\lambda_{em}, \Delta\lambda_{em}) G A_{so} E_o \{k(A)/[k(A) + k(B)]\} [1 - \exp(-\{k(A) + k(B)\}l)] / \{1/[k(A) + k(B)]\} [1 - \exp(-\{k(A) + k(B)\}l)] \quad (4)$$

where  $k(A)$  and  $k(A)$  are the linear absorption coefficients of the analyte at 423 nm (excitation) and at 490 nm (emission), respectively, and  $k(B)$  and  $k(B)$  are the linear absorption coefficients of solvent (blank) at 423 and 490 nm, respectively. Equation 4

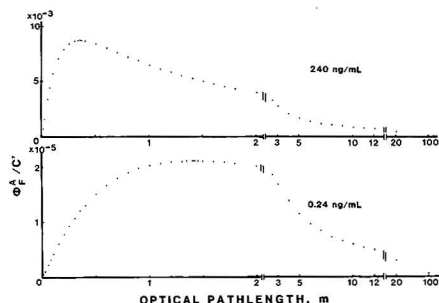


**Figure 5.** Theoretical dependence of fluorescence flux on the optical path length of the fiber. The equation and definitions of  $\Phi_F^A$  and  $C'$  are shown in the text.

for  $\Phi_F^A$  can be further simplified by retaining only those terms containing the cell length,  $l$ , and so

$$\Phi_F^A = \frac{C'(1/l)[1 - \exp(-k(A) + k(B))l][1 - \exp(-k'(A) + k'(B))l]}{(5)}$$

where  $C'$  contains all the factors constant with respect to  $l$ ,  $k$ , and  $k'$ . From absorption measurements, the following values were estimated for calculations by eq 5:  $k(A) = 0.0591 \text{ cm}^{-1}$ ,  $k'(A) = 0.0063 \text{ cm}^{-1}$  for 236 ng/mL perylene solution;  $k(B) = 0.0100 \text{ cm}^{-1}$ ,  $k'(B) = 0.0078 \text{ cm}^{-1}$ . For a 0.24 ng/mL perylene solution,  $k(A)$  and  $k'(A)$  were estimated to be  $10^{-3}x$  those of the 236 ng/mL perylene solution.

Figure 5 shows the theoretical dependence of the perylene fluorescence signal as a function of the optical pathlength ( $l$ ), calculated based on eq 5. For the 236 ng/mL perylene solution, the fluorescence signal reached a maximum for an optical path (cell length) of  $\approx 36 \text{ cm}$ . On the other hand, for the 0.24-ng perylene solution, the maximum fluorescence signal was reached for an optical path (cell length) of 142 cm. For carbon disulfide, the optimal length of the fiber cell does not exceed 150 cm for all solutions studied in the present case. Of course, the optical path length ( $l$ ) inside the capillary is several times the length of the cell (7, 10). Therefore, even the shortest cell used in the present experiment (cell length = 61 cm) probably exceeds considerably the optimal length of  $\approx 36 \text{ cm}$  predicted by the theory. These predictions agree with the results shown in Table I, where the shortest fiber produced the greatest fluorescence signals. The temporal behavior of the fluorescence signal appearance (lower figure of Figure 3) in the 12-m fiber agrees with the above discussion and the predictions based upon eq 5.

However, eq 5 does not account for the attenuation of light caused by the quality of fiber including such factors as surface roughness or light absorption by the inner wall of the fiber. Such factors could be included in the solvent linear absorption coefficients ( $k(B)$  and  $k'(B)$ ); of course, an increase in  $k(B)$  and  $k'(B)$  would result in a smaller  $l$  to achieve maximal fluorescence. This theoretical treatment suggests that short fibers (less than 0.5 m) are favorable for fluorescence detection. However, it should be noted that this discussion does not consider the background fluorescence, which is one of the major factors in determining the signal-to-noise ratio in the present system, which is largest in the longest fiber of 12 m.

Figure 6 shows the calibration curve of perylene fluorescence obtained with the 0.61-, 1.50-, and 12.0-m fibers; the linear dynamic

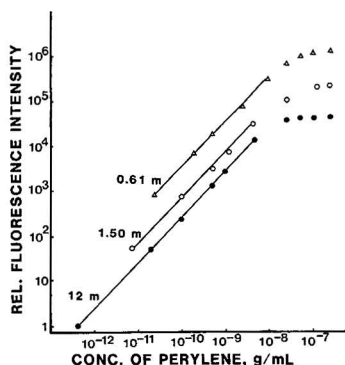


**Figure 6.** Calibration curves of perylene fluorescence for fibers of 0.61, 1.50, and 12.0 m. The lower left point of each calibration curve is the detection limit.

range is  $10^3$ – $10^6x$  and the detection limits (twice the standard deviation of the fluorescence background obtained with solvent in the fiber) are 0.4, 7, and 26 ppt for the fibers of 12.0, 1.5, and 0.61 m, respectively. The best previously reported detection limit of perylene is 1 ppt (11); a commercial fluorescence spectrophotometer (Spex, Model DM3000-F) in our laboratory gave a detection limit of 2 ppt. Therefore, the waveguide, capillary cell, with one dimensional fluorescence detection, resulted in excellent detection power for perylene and presumably for other polycyclic aromatic compounds. One-dimensional fluorescence can be applicable to other substances; excitation at shorter wavelengths would be possible with tetrachloroethylene ( $n = 1.506$ ) which is more transparent in the UV region than carbon disulfide. Therefore, even better analytical results would be expected with tetrachloroethylene.

The parent cell design could be readily adapted to use a detector in flow injection analysis and in high-performance liquid chromatography.

#### ACKNOWLEDGMENT

The authors thank Mario E. Tremblay for his assistance and helpful discussions.

Registry No.  $\text{CS}_2$ , 75-15-0; perylene, 198-55-0.

#### LITERATURE CITED

- (1) Van Geel, F.; Voigtman, E.; Winefordner, J. D. *Appl. Spectrosc.* **1984**, *38*, 228–234.
- (2) Walrafen, G. E.; Stone, J. *Appl. Spectrosc.* **1972**, *26*, 585–589.
- (3) Stone, J. *J. Chem. Phys.* **1978**, *69*, 4349–4356.
- (4) Schaefer, J.; Chabay, I. *Opt. Lett.* **1979**, *4*, 227–229.
- (5) Majumdar, A. K.; Hinkley, E. D.; Menzies, R. T. *IEEE J. Quantum Electron.* **1979**, *QF-15*, 408–410.
- (6) Ross, H. B.; McClain, W. M. *Appl. Spectrosc.* **1981**, *35*, 439–442.
- (7) Fuwa, F.; Wei, L.; Fujiwara, K. *Anal. Chem.* **1984**, *56*, 1640–1644.
- (8) Fujiwara, K.; Fuwa, K. *Anal. Chem.* **1985**, *57*, 1012–1016.
- (9) Tremblay, M. E.; Simeonsson, J. B.; Smith, B. W.; Winefordner, J. D. *Appl. Spectrosc.*, in press.
- (10) Dasgupta, P. K. *Anal. Chem.* **1984**, *56*, 1401–1403.
- (11) Jurgensen, A.; Inman, E. L., Jr.; Winefordner, J. D. *Anal. Chim. Acta* **1981**, *131*, 187–194.

RECEIVED for review September 23, 1987. Accepted January 26, 1988. Research supported by NIH-GM11373-25.

# Laser-Excited Time-Resolved Solid-Phase Fluoroimmunoassays with the New Europium Chelate 4,7-Bis(chlorosulfonyl)-1,10-phenanthroline-2,9-dicarboxylic Acid as Label

Esther Reichstein, Yehezkel Shami,<sup>1</sup> Mohabir Ramjeesingh,<sup>1</sup> and Eleftherios P. Diamandis<sup>2\*</sup>

CyberFluor, Inc., 179 John Street, Toronto, Ontario M5T 1X4, Canada

We have prepared biologically active highly fluorescent monoclonal and polyclonal antibodies suitable for time-resolved immunoassays. We have first labeled bovine serum albumin (BSA) with the new europium chelate 4,7-bis(chlorosulfonyl)-1,10-phenanthroline-2,9-dicarboxylic acid (BCPDA). We have incorporated maleimide groups on the antibody molecules by using the heterobifunctional reagent sulfo-succinimidyl 4-(*N*-maleimidomethyl)cyclohexane-1-carboxylate. We then reduced the labeled BSA with dithiothreitol and conjugated the labeled BSA with the derivatized antibody. We have tested the labeled antibodies on a model heterogenous competition fluorimmunoassay for serum cortisol and obtained satisfactory results. The amount of the bound antibody, which was inversely related to the amount of cortisol in the sample, was quantitated by measuring, in a time-resolved mode, the fluorescence of the complex antibody-BSA-BCPDA-Eu<sup>3+</sup> bound to cortisol immobilized on the solid phase after excitation with a nitrogen laser beam and monitoring delayed fluorescence at 615 nm.

Radioimmunoassays (RIA) and immunoradiometric assays (IRMA) are among the most sensitive and specific analytical techniques available today (1). Their exceptional performance characteristics arise from the use of antibodies as analytical reagents (specificity) and radioactive labels as the detection system (sensitivity). Immunoassay in general, is a universal analytical technique and has been used successfully for the assay of polypeptide, steroid, and thyroid hormones, drugs, metabolites, tumor markers, antigens, and antibodies of infectious agents, etc. The detection system used to monitor the immunological reaction need not be restricted to radioactive labeling. Despite their advantages which facilitated their establishment during the last 25 years (very high sensitivity of detection, invulnerability to environmental interference, accuracy and precision in measurement of signal, no background signal) radioactive labels have a number of serious disadvantages (potential health hazard, special licensing for their use, special disposal, unstable reagents, difficulty in automation) which prompted research for their replacement. During the last few years, in the field of clinical chemistry, a number of alternative labels have been explored. The most successful alternative labels currently used in both research and commercial applications are enzymes (2, 3), luminescent labels (4, 5), and fluorescent labels (6, 7).

Fluorescein, the most widely used conventional fluorescent label was very successful in applications where extreme sen-

sitivity is not required, i.e. in therapeutic drug monitoring assays. For highly sensitive immunoassays, fluorescein is not suitable because of the following limitations. It has only ~28 nm Stokes shift, the emission spectrum overlaps extensively with the emission spectrum of serum autofluorescence, and the molecule quenches the fluorescence of adjacent fluorescein molecules so that highly labeled reagents are not very useful. Recently, there is increasing interest in the use of rare earth metal complexes in devising new immunoassay systems (8). The fluorescence of Eu<sup>3+</sup> complexes with certain organic ligands has some interesting properties: (a) there is a very large Stokes shift of the order of ~290 nm. This is due to the fact that the excitation radiation is absorbed by the organic ligand and the energy is then transferred to the rare earth metal ion which emits its characteristic radiation at a very long wavelength (~615 nm for Eu<sup>3+</sup>) (9). (b) The emission spectrum is very narrow (~10 nm for Eu<sup>3+</sup> at 50% emission bandwidth). These two characteristics allow for very easy and specific isolation of the emitted light by using an interference filter at ~615 nm. Additionally, the fluorescent lifetime of these complexes is very long (between 10 and 1000  $\mu$ s) as compared to that of conventional fluorescent molecules (e.g. 49.5 ns for fluorescein). This property allows for fluorescence to be measured with a "time-resolved" technique as follows: After the molecule is excited with a short pulse of light, the emitted fluorescence is measured in a properly selected time window. Measurement starts after an initial delay time during which any short-lived fluorescence has decayed. When all the features of the fluorescence of europium complexes are taken into account (large Stokes shift, narrow emission band, long-lived fluorescence) in devising the instrument and chemical system for an immunoassay, it is possible to exclude practically all sources of background fluorescence and thus achieve very high sensitivity of specific signal detection. The only limiting background fluorescence measured, will be due to nonspecific binding of the labeled reagents used.

There are two general approaches in devising analytical immunoassay techniques with europium complexes as the detection system. The first approach is to introduce Eu<sup>3+</sup> into the immunoreactants to create the label and then excess chelate to form the fluorescent complex (10). This approach has been used successfully but suffers from some limitations; the most important being the vulnerability to Eu<sup>3+</sup> contamination. The second approach is to introduce the chelator into the immunoreactants and use excess Eu<sup>3+</sup> to form the fluorescent complex (11, 12). This approach, although tried in the past (13), was not successful because of the lack of appropriate Eu<sup>3+</sup> chelators. Such chelators should combine the following characteristics: a suitable reactive group for incorporation into proteins; a Eu<sup>3+</sup> chelating site with a high stability constant for the complex; a suitable excitation wavelength with high extinction coefficient; and an effective energy transfer mechanism to Eu<sup>3+</sup>. A molecule which fulfills these criteria has been synthesized recently (11). Its appli-

<sup>1</sup>Permanent address: Hybrisens, Ltd., York University Campus, 4700 Keele St., Farquharson Bldg., Room 104, Toronto, ON M3J 1P3, Canada.

<sup>2</sup>Also affiliated with Department of Clinical Biochemistry, University of Toronto, 100 College St., Toronto, ON M5G 1L5, Canada.



cability for immunoassays is discussed in detail elsewhere and practical examples are given (14).

In this report, we describe a method for labeling antibodies with this novel  $\text{Eu}^{3+}$  chelator. We have concentrated on two major considerations; how to introduce amplification to the system (high molar ratio of chelator/antibody) yet keep the antibody modification as low as possible so as to preserve the biological activity. We have selected to first exhaustively label a carrier protein, bovine serum albumin (BSA), with the chelator and then cross-link the labeled protein to the antibody molecule with a bifunctional reagent. We have demonstrated that high yields of active labeled antibodies can be achieved by using polyclonal and monoclonal anti-cortisol antibodies as a model system. These antibodies have been used successfully for devising a heterogeneous competition assay for serum cortisol, with ovalbumin-cortisol conjugate immobilized in microtiteration wells as the solid phase.

## EXPERIMENTAL SECTION

**Materials.** Bovine serum albumin (BSA, RIA grade), ovalbumin, hydrocortisone 21-hemisuccinate, and hydrocortisone 21-hemisuccinate BSA conjugate (cortisol-21-BSA) were purchased from Sigma Chemical Co., St. Louis, MO. Tri-*n*-butylamine was purchased from Aldrich Chemical Co., Milwaukee, WI, isobutyl chloroformate was from Chemical Dynamics Corp., South Plainfield, NJ, sulfosuccinimidyl 4-(*N*-maleimidomethyl)cyclohexane-1-carboxylate (sulfo-SMCC) was from Pierce Chemical Co., Rockford, IL, *N*-ethyl maleimide was from Eastman Kodak Co., Rochester, NY, and 2,2'-azobis[3-ethylbenzthiazoline-sulfonate] (66) (AETS) was from Boehringer Mannheim (Canada), Dorval, PQ. Gelatin (EIA purity) was obtained from Bio-Rad Laboratories (Canada), Ltd., Mississauga ON, and Sephadex G25 medium mesh from Pharmacia (Canada), Ltd. A radioimmunoassay (RIA) kit for cortisol, Coat-A-Count, was purchased from Diagnostic Products Corp., Los Angeles, CA. Europium chloride was purchased from Aldrich and a stock solution of 1 mM was prepared in 0.01 M HCl. 4,7-Bis(chlorosulfonylphenyl)-1,10-phenanthroline-2,9-dicarboxylic acid (Eurofluor S, BCPDA) was synthesized according to the procedure of Evangelista et al. (11). All other chemicals were reagent grade. Monoclonal antibody to cortisol was purchased from Medix Biotech, Inc., Foster City, CA, and polyclonal rabbit anti-cortisol (against cortisol-21-BSA) was purchased from Western Chemical Research Corp., Ft. Collins, CO. Protein concentration was carried out by centrifugation using Centricon 30 microconcentrators from Amicon Canada, Ltd., Oakville ON. The anti-rabbit IgG and anti-mouse IgG coupled to horseradish peroxidase were purchased from Tago Immunologics, Burlingame, CA.

Enzyme immunoassay (EIA) microtiteration plates were obtained from Flow Laboratories, Inc., McLean, VA, and read on a EL309 microplate reader, Bio-Tek Instruments, Inc., Winooski, VT. Fluoroimmunoassay (FIA) microtiteration plates, Microfluor W, white opaque 96-well plates were purchased from Dynatech Laboratories, Inc., Alexandria, VA, and read on the CyberFluor 615 fluorometer.

High-performance liquid chromatography (HPLC) was carried out with a BioSil TSK 400 size exclusion column from Bio-Rad Laboratories on a Model 600 gradient system equipped with a 490 variable wavelength detector (Waters, a division of Millipore (Canada), Ltd., Mississauga, ON).

**Instrumentation.** A specially designed instrument has been used for solid-phase time-resolved fluorescence measurements (CyberFluor Model 615 Immunoanalyzer). The instrument is essentially a gated fluorometer and consists of a nitrogen laser as the exciting source, a novel optical system, and a direct current technique for the quantitation of fluorescent light intensity. Measurements can be carried out in microtiteration plates or strips with a measuring time of 1 s per well. Specially designed software allows for automated data reduction by spline smoothing techniques. A brief description of the instrument is given in ref 14.

**Methods. Preparation of Cortisol-Ovalbumin Conjugate.** Cortisol ovalbumin was prepared by the mixed anhydride method (15). Fifty milligrams (0.1 mmol) of hydrocortisone 21-hemisuccinate was dissolved in 10 mL of dioxane and 0.1 mL of tri-

*n*-butylamine added. The solution was cooled to 10 °C, 0.02 mL of isobutyl chloroformate added, and the mixture stirred for 30 min. Then, 500 mg of ovalbumin (0.01 mmol) dissolved in 10 mL of water adjusted to pH 9 with NaOH was added to the reaction mixture and the solution was stirred 24 h at 4 °C. After the reaction was completed, a precipitate was present. The mixture was dialyzed for 36 h against water and the precipitate was removed by centrifugation. Urea was added to the supernatant to achieve a concentration of 6 M and this solution was again dialyzed exhaustively against water. The protein concentration was determined by the Bio-Rad protein assay.

**Conjugation of BCPDA to BSA.** Two milliliters of 0.5 M sodium carbonate buffer of pH 9.1 was added to 250 mg of BSA dissolved in 2 mL of water. One hundred milligrams of BCPDA (50 × molar excess) dissolved in 400  $\mu\text{L}$  of dimethylformamide (DMF) was added in five portions over a 5-min period. Unreacted BCPDA was removed by exhaustive dialysis against 0.1 M  $\text{NaHCO}_3$  and the labeled BSA (BSA-BCPDA) stored at 4 °C.

**Reduction of BSA-BCPDA.** Reduction was carried out just prior to conjugation with antibody. To BSA-BCPDA (30 mg/mL in 0.1 M  $\text{NaHCO}_3$ ) solid urea, dithiothreitol (DTT), and Tris base were added to achieve a concentrations of 6 M, 50 mM, and 0.1 M, respectively. The pH measured was 9. The mixture was incubated for 1 h at 37 °C.

**Conjugation of Antibody and Reduced BSA-BCPDA.** Conjugation with sulfo-SMCC was carried out by a modification of the method of Yoshitake et al. (16). 0.5 mL of anti-cortisol antibody solution (0.5 mL, 1 mg/mL) was dialyzed overnight against 0.1 M sodium phosphate buffer at pH 7.0. A 14.5- $\mu\text{L}$  portion of a 5 mg/mL solution of sulfo-SMCC dissolved in the same buffer was added and the solution shaken for 1 h at room temperature. Unreacted sulfo-SMCC was removed by desalting on a 25-mL column of Sephadex G 25 using 0.1 M sodium phosphate of pH 6.2 containing 5 mM ethylenediaminetetraacetate (EDTA) as the elution buffer. The fractions containing protein were combined and concentrated to 0.1–0.2 mL by centrifugation in a Centricon 30 device. A 0.35-mL sample of reduced BSA-BCPDA containing 9 mg of protein was also desalted to remove excess reducing reagent on a 25-mL Sephadex G25 column in the same phosphate buffer of pH 6.2, containing 5 mM EDTA, to retard disulfide formation (17). The protein containing fractions were combined and concentrated by centrifugation in a Centricon 30 device, to 0.6–0.8 mL. It is important to complete the reactions and the separation and concentration steps as quickly as possible to prevent hydrolysis of the maleimide group in the antibody and re-formation of the disulfide bonds in the reduced BSA. The derivatized antibody and reduced BSA were combined and incubated 20 h at 4 °C (BSA to IgG ratio is 30–40-fold). Prior to purification of the IgG-BSA conjugate, excess SH groups on the reduced BSA molecule (36 SH groups exist per reduced BSA molecule (17) were blocked by addition of a 2-fold excess of *N*-ethylmaleimide in DMF and incubation for 1 h at room temperature.

**Isolation of BSA-Conjugated Antibody.** The conjugated and unconjugated antibody and unconjugated labeled BSA were separated by size exclusion HPLC on a BioSil TSK 400 column (300 × 7.5 mm) eluted at 1 mL/min with 50 mM  $\text{Na}_2\text{SO}_4$  and 20 mM sodium phosphate pH 6.8 and fractions of 0.5 mL were collected automatically. Three or four injections of 250  $\mu\text{L}$  each were required per preparation to complete the isolation. Fractions were analyzed for total fluorescence, fluorescent antibody, and total antibody concentration, as described below.

Total fluorescence was measured by addition of 200  $\mu\text{L}$  of  $10^{-5}$  M  $\text{Eu}^{3+}$  solution in 50 mM Tris buffered saline pH 7.8 (TBS) to 5  $\mu\text{L}$  of each fraction and determining the fluorescence of the solution after 5 min, on an ARCUS gated fluorometer (LKB Wallac, Turku, Finland).

To measure the BSA-conjugated antibody concentration, 100- $\mu\text{L}$  portions of fractions diluted 1/20 and 1/200 in 1% BSA in TBS were added to the wells of coated Microfluor W plates. Coating was done overnight at 4 °C with 100  $\mu\text{L}$  per well of a 5  $\mu\text{g}/\text{mL}$  solution of cortisol-BSA conjugate in 0.1 M sodium bicarbonate and afterward the plates were blocked for 1 h at room temperature with 1% BSA in the same buffer. The plates were incubated for 1 h at 37 °C and then washed three to four times with water. One hundred microliters of  $1 \times 10^{-5}$  M  $\text{Eu}^{3+}$  solution



in TBS was then added. After 5 min, the plates were washed once with water and dried in a stream of cool air. Surface fluorescence of the antibody-BSA-BCPDA-Eu<sup>3+</sup> conjugate which was bound to the immobilized cortisol-BSA was measured in a CyberFluor 615 fluorometer.

The total antibody activity (conjugated to BSA and unconjugated) was measured by using a second antibody (anti-rabbit IgG or anti-mouse IgG for polyclonal or monoclonal anti-cortisol, respectively) coupled to horseradish peroxidase (HRP) in an enzyme-linked immunosorbent assay (ELISA). EIA plates were coated with cortisol-BSA conjugate and blocked as above. HPLC fractions were diluted, added to the EIA plate, and incubated at 37 °C as above. After the plates were washed with water, 100  $\mu$ L of horseradish peroxidase labeled goat anti-rabbit or anti-mouse IgG diluted 1/500 with 50 mM sodium phosphate pH 8.5 containing 1% NaCl and 1% BSA was added and the plates were incubated a further hour. The plates were washed with water and the enzymic activity of the bound anti-IgG-HRP bound to antibody which in turn was bound to immobilized cortisol-BSA was measured by adding 100  $\mu$ L of substrate (1 mg/mL of ABTS in 50 mM Na<sub>2</sub>HPO<sub>4</sub>, 25 mM citric acid, 0.03% H<sub>2</sub>O<sub>2</sub>). The optical density was determined on a microplate reader after 5–10 min.

**Cortisol Assays.** We used a solid-phase competition assay with immobilized antigen to measure cortisol. Microfluor W plates were coated overnight at 4 °C with 100  $\mu$ L of 2  $\mu$ g/mL cortisol-ovalbumin conjugate in 0.1 M NaHCO<sub>3</sub>. The plates were rinsed once with water and blocked for 1 h at room temperature with 0.1% gelatin, 0.1% Tween 20, and 50 mM phosphate buffer of pH 7.4 and stored in the same solution at 4 °C.

Before the assay, a plate was washed twice with 0.05% Tween 20 in saline (Tween/NaCl) and twice with water. Antibody was diluted to 1/400 with respect to the starting material (1 mg/mL) in TBS containing 0.3 M trichloroacetate (TCA), 1% BSA, and 150  $\mu$ g/mL BSA-BCPDA to prevent fluor-serum interactions. Ten microliters of serum was pipetted into the wells and 100  $\mu$ L of antibody solution added. The plate was briefly shaken and incubated 1 h at 37 °C. The plate was washed three times with Tween/NaCl and twice with water, then 100  $\mu$ L of  $1 \times 10^{-5}$  M Eu<sup>3+</sup> in TBS was added. After 5 min, the plate was rinsed once with deionized water and dried with a stream of cool air and surface fluorescence was determined on a CyberFluor 615 fluorometer.

## RESULTS AND DISCUSSION

**Conjugation of Antibodies.** The coupling scheme which we used to conjugate BSA-BCPDA to antibody is illustrated in Figure 1. The antibody, which has no free sulfhydryl groups, is reacted with a bifunctional coupling reagent containing an amino reactive *N*-hydroxysuccinimide moiety at one end and a sulfhydryl reactive maleimide group at the other end. The sulfonic acid group renders the reagent water soluble. The reagent is reacted first with the antibody to introduce maleimide groups (step 1). The BSA which has been exhaustively reacted with BCPDA (step 2) is reduced with DTT to create free sulfhydryl groups from intramolecular disulfide bonds in the native molecule (step 3). The exposed SH groups are then free to react with the maleimides introduced into the antibody (step 4).

Since it is possible to get inactivation of antibody at high concentrations of coupling reagent, we studied the effect of the concentration of coupling reagent in step 1 on the activity of the derivatized antibody preparation using both a polyclonal and a monoclonal anti-cortisol antibody. Antibodies were reacted for 1 h at varying molar excess of sulfo-SMCC in step 1. The titer of the modified antibody was measured by ELISA, using an HRP conjugated anti-IgG, in microtiter plates, as described in Methods (isolation of conjugated antibody). As shown in Figure 2 the monoclonal antibody preparation was highly active even after derivatizing with 500-fold excess of sulfo-SMCC; the polyclonal antibody inactivation was evident even at 25-fold molar excess of sulfo-SMCC (Figure 2B). The monoclonal was therefore treated with a 50-fold molar excess of sulfo-SMCC while the polyclonal

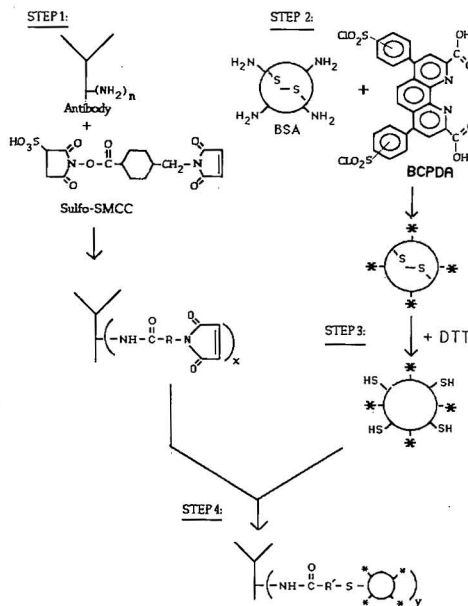


**Figure 1.** Procedure for the preparation of antibody-bovine serum albumin (BSA)-4,7-bis(chlorosulfonyl)-1,10 phenanthroline-2,9 di-carboxylic acid (BCPDA) conjugates. In step 1 antibody is reacted with sulfo-succinimidyl 4-(*N*-maleimidomethyl)cyclohexane-1-carboxylate (sulfo-SMCC) to introduce maleimide groups. In step 2 BSA is coupled to BCPDA. In step 3 labeled BSA is reduced by dithiothreitol (DTT) to create free SH groups. In step 4 the derivatized antibody is coupled to reduced BSA. Numbers *n*, *x*, and *y* represent the number of total amino groups, derivatized amino groups, and conjugated amino groups, respectively.

was treated with a 20-fold excess, in step 1. Because of the possibility of cross-linking networks in step 4 due to the reaction of one BSA molecule bearing many SH groups with multiple molecules of derivatized antibody and also, of one derivatized antibody molecule with multiple molecules of reduced BSA, the reduced BSA/derivatized antibody molar ratio was selected to be very high (>25-fold) so as to promote formation of IgG(BSA)<sub>n</sub>, rather than BSA(IgG)<sub>x</sub>.

After conjugation, the conjugated and unconjugated antibody were separated by gel filtration on HPLC. The fractions were monitored for optical density, total fluorescence, fluorescent antibody binding to cortisol-BSA coated plate, and total antibody binding to cortisol-BSA coated plates, using a second peroxidase conjugated anti-IgG antibody in an ELISA assay as described in Methods. The results of a typical monoclonal preparation are shown in Figure 3. There is a continuous spectrum of fluorescent antibodies present with different molecular weights, with a large fraction in the void volume. There are three peaks of total antibody activity as measured by the ELISA technique (Figure 3B), the void volume (peak A), an included peak also corresponding to coupled antibody (peak B), and an included peak corresponding to uncoupled antibody (peak C). Only peak A and the first fractions of peak B were combined for use in the assays so as to ensure that essentially all uncoupled antibody is excluded. Assuming that the binding of the second antibody HRP-conjugated anti-IgG is similar for all the fractions of anti-cortisol, irrespective of the degree of conjugation to BSA, 30–50% of the antibody is recovered in the conjugated antibody fractions combined and used for the immunoassay.

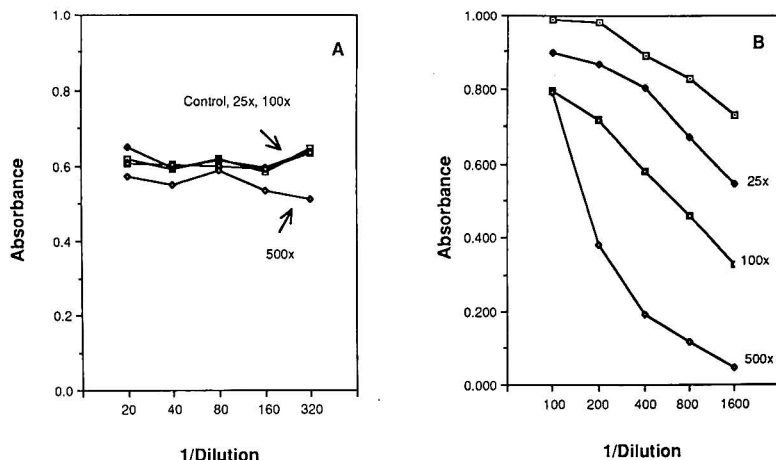


**Figure 2.** Titer of monoclonal (left) and polyclonal (right) antibodies after modification with sulfo-SMCC. Antibodies were modified with various molar excess of sulfo-SMCC as described under procedures. The antibody titer was then determined by ELISA as discussed under isolation of conjugated antibody.

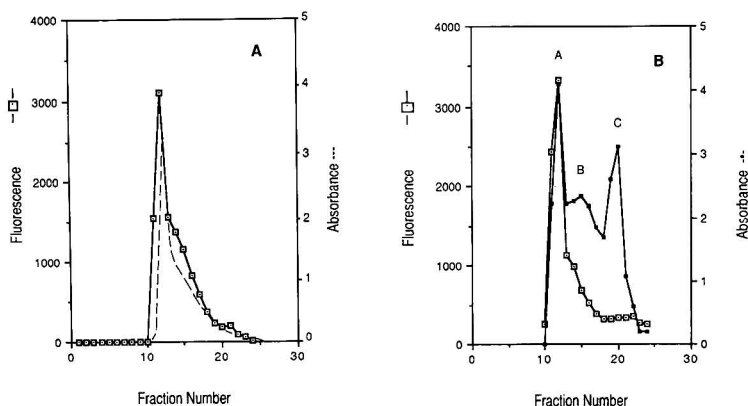


**Figure 3.** Separation of antibody-BSA-BCPDA conjugate on size exclusion HPLC: (A) (---) absorbance, (□) total fluorescence of fractions measured by diluting 5  $\mu$ L of each fraction in 200  $\mu$ L of  $10^{-9}$  M  $\text{Eu}^{3+}$  in TBS; (B) (●) total (conjugated and unconjugated) antibody concentration as measured by HRP-conjugated anti-mouse IgG in an ELISA assay, (□) conjugated fluorescent antibody binding to plates coated with ovalbumin-cortisol. For more details see text.

**Assay Optimization.** An outline of the cortisol competition assay is shown in Figure 4. The calibration curves for the cortisol assays were plotted in one of two ways: (a) the fluorescent readings for the standards were plotted vs the log of the cortisol concentration or (b) the ratios of the fluorescence of the standards, B, to the fluorescence of the zero standard,  $B_0$ , expressed as a percentage ( $B/B_0 \times 100\%$ ) were plotted vs the log of the cortisol concentration.

Variation in the amount of coating in the microtitration wells from 50 to 500 ng of cortisol-ovalbumin conjugate had little effect on the overall shape of the calibration curve when this is plotted as ( $B/B_0$ ), but the total antibody bound to the plate (proportional to  $B_0$ ) reached its maximum at a coating of 200 ng/well. We found that calibration curves with the conjugated polyclonal antibody became flat with no further change in ( $B/B_0 \times 100$ ) when this value reached 30%, regardless of increasing cortisol concentration, whereas the curves with conjugated monoclonal continued to drop until

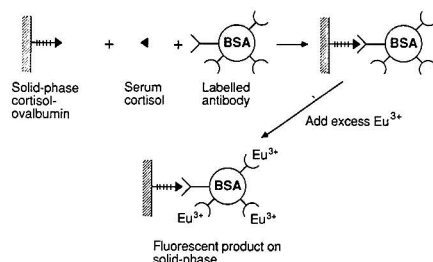


**Figure 4.** Principle of the competition assay of serum cortisol. Washing steps are not shown; more details are given under procedures. The figure has no quantitative meaning. The bond between BCPDA and BSA is covalent. Fluorescence is measured directly on the solid phase. BCPDA is represented schematically (□-). BSA represents bovine serum albumin.

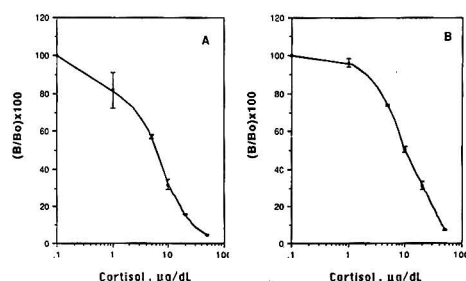


Figure 5. Standard curves for the cortisol assay in serum. Each point is the mean ( $\pm$  standard deviation) of three determinations: (A) 20- $\mu$ L sample volume; (B) 10- $\mu$ L sample volume.

Table I. Within-Run Precision of the Cortisol Assay

sample	no. of determinations	mean value, $\mu$ g/dL	std dev, $\mu$ g/dL	% CV <sup>a</sup>
1	9	5.6	0.6	10.2
2	10	14.8	1.0	7.0
3	10	24.8	1.3	5.3
4	9	53.8	0.7	1.4

<sup>a</sup> Percent coefficient of variation.

a value of  $(B/B_0 \times 100)$  close to zero was obtained. We thus continued experimentation exclusively with the monoclonal antibody.

Since >80% of the cortisol in serum is bound to transport proteins (18), a suitable dissociation reagent is required to release the cortisol before measurement by immunoassay. By use of the monoclonal antibody, two reagents were investigated: 8-anilino-1-naphthalenesulfonic acid, ANS, at a concentration of 5% in the final assay mixture and trichloroacetate, TCA (19), at a concentration of 0.3 M. TCA gave better results than ANS and thus it was preferred in the final assay design.

We tested the volume of serum required in order to obtain sensitive calibration curves. This parameter affected the shape of the calibration curve dramatically. The normal range of cortisol in human serum is 5–30  $\mu$ g/dL (19). Using 20  $\mu$ L of serum, we found that the curves were too shallow at concentrations greater than 20  $\mu$ g/dL. A better calibration curve is obtained with 10  $\mu$ L of sample volume. With 10  $\mu$ L of serum (Figure 5B), good sensitivity was achieved in the whole range of clinically important values (1–50  $\mu$ g/dL).

**Assay Performance.** A typical calibration curve is shown in Figure 5B. The steepest part of the curve is in the normal range where maximum accuracy and precision are usually needed.

The within-run precision for four patient samples is shown in Table I. This kind of precision (coefficient of variation of 2–10%) is typical of well-established cortisol assays currently available.

To test the linearity of the method, we have diluted four patient samples with the zero standard and reassayed them. We found a linear relationship between the measured concentration and the dilution, indicating that our assay is free from any serum matrix effects.

The recovery of added cortisol was measured in five different samples. The recovery of cortisol is shown in Table II and varied from 91% to 115%, with a mean of 102%.

We measured 27 patient samples by a commercial RIA kit (Diagnostic Products Corp.) as well as with the present method with conjugated fluorescent monoclonal antibody. The samples were selected to cover the whole range of the assay from

Table II. Recovery of Added Cortisol in Serum

sample	cortisol, $\mu$ g/dL			% recovery
	initially present	added	found	
1	1.3	3.0	3.5	115
1	1.3	11.0	12.2	111
2	6.6	9.3	8.4	91
2	6.6	15.3	14.9	97
3	10.9	12.7	12.0	95
3	10.9	18.7	18.8	101
4	15.2	22.2	22.9	103
5	18.2	24.5	26.5	108
6	35.0	38.0	36.9	97

1 to 50  $\mu$ g/dL and included clear, cloudy, lipemic, and haemolytic specimens. The correlation between the two assays was found to be good. The coefficient of correlation is 0.98 with a slope of 1.007 and an intercept of 0.51  $\mu$ g/dL.

Time-resolved fluoroimmunoassays perform better than conventional fluoroimmunoassays in biological fluids because of effective background rejection. Currently, the most appropriate fluorescent probes for time-resolved immunoassays appear to be the  $\text{Eu}^{3+}$  complexes. In addition to their long fluorescence lifetimes, these complexes have the advantages of large Stokes shifts and sharp emission bands. When  $\text{Eu}^{3+}$  is introduced into the immunoreactants as label, the assays are vulnerable to  $\text{Eu}^{3+}$  contamination from the skin, dust, etc. Therefore, during the performance of such assays, great care is needed in order to exclude the contamination sources. With the synthetic  $\text{Eu}^{3+}$  chelates as labels, excess  $\text{Eu}^{3+}$  is used and contamination problems are virtually eliminated.

The new  $\text{Eu}^{3+}$  chelate 4,7-bis(chlorosulfonyl)-1,10-phenanthroline-2,9-dicarboxylic acid, BCPDA, can be introduced covalently into the immunoreactants, by means of reaction of the sulfonyl chloride group, primarily with available amino groups of the antibody or antigen used. This reagent has two available  $\text{SO}_2\text{Cl}$  groups; thus, there is a possibility of polymer formation because proteins have also more than one amino group available. We have investigated this possibility by carrying out labeling experiments with BSA and separating the products by using HPLC with size exclusion columns (data not shown). We found that working with BCPDA in excess over BSA, the major product was an adduct of the form  $\text{BSA}(\text{BCPDA})_n$ . The value for  $n$  is between 1 and 40 depending on the molar excess used. It was assessed by measuring the absorbance of BCPDA at 325  $\mu\text{m}$ ;  $\epsilon = 1.52 \times 10^4 \text{ M}^{-1} \text{ cm}^{-1}$ . Protein-protein linkage, as assessed by the size of the peak at the void volume, was minimal.

Antibodies are highly reactive biological molecules. Upon extensive derivatization, they may lose their ability to bind to their respective antigens. For that reason, it is preferable to label antibodies with the minimum amount of the label used. On the other hand, extensive labeling is desirable because of the increased sensitivity in detection. Our approach for labeling antibodies combines the low degree of antibody modification with the high degree of labeling, by using BSA as a label carrier. The carrier protein is exhaustively labeled in one step and then cross-linked under mild conditions with the polyclonal or monoclonal antibody by using a bifunctional reagent.

The bifunctional reagent used, sulfo-SMCC, is now considered one of the state-of-the-art heterobifunctional cross-linkers. It is superior to the classical carbodiimides and glutaraldehyde reagents which have been used for creating protein-protein conjugates. Because it is heterobifunctional, antibody-antibody conjugates during the first step of the reaction (Figure 1) are not formed. However, it is still very likely to obtain a heterogeneous population of conjugates as the final product since one antibody molecule, carrying many

maleimide groups, can react with one or more reduced labeled BSA molecules. It is also possible to obtain, for the same reason, conjugates consisting of one labeled BSA molecule and many antibody molecules. The latter possibility is minimized by adding the reduced labeled BSA reagent in great excess over the derivatized antibody, during the final conjugation step (Figure 1, step 4).

The labeled monoclonal antibodies performed better than the labeled polyclonal antibodies in the model cortisol immunoassay. This was expected because the polyclonal antibody preparation contains, in addition to the specific cortisol antibodies, antibodies to the carrier protein and the hemisuccinate bridge of the immunogen, and other irrelevant antibodies as well. During the labeling procedure, the whole population of antibodies is labeled and this leads to increased nonspecific binding during the immunoassay. Additionally, there is binding of the carrier protein antibodies and of the bridge antibodies to the solid-phase which cannot be prevented by cortisol. This leads to calibration curves which appear flat (no change in the value of  $(B/B_0) \times 100$  upon increasing the cortisol concentration of the standards) after a certain cortisol concentration. These effects were minimal with the labeled monoclonal antibody preparations.

We have used an ELISA technique to monitor the distribution of both labeled and unlabeled antibody molecules during the HPLC gel filtration separation step. A solid-phase fluorescence technique was also used to monitor the distribution of only the labeled antibody population. Both techniques showed that the labeled antibody preparation is heterogeneous, with most of the activity eluted in the void volume. This heterogeneity is not a problem however, and a successful assay could be devised by mixing the void volume fraction and a limited number of the following fractions which are free from any unlabeled antibody molecules. The final mixture of labeled antibodies could be used in a dilution of about 1:400 (with respect to the initial starting material) which is typical for nonisotopic immunoassays.

The labeling procedure we have presented is general. Antibodies labeled with this method can be used for competitive and "sandwich" type immunoassays of any antigen, provided

that specific antibodies are available and the sensitivity is adequate. The performance of the competition cortisol assay, presented here as a model, is satisfactory.

In conclusion, we have reported a new detection system for devising time-resolved fluoroimmunoassays, with the novel  $\text{Eu}^{3+}$  chelate BCPDA as label. A number of different applications with the same detection system will be published in the near future.

Registry No. Cortisol, 50-23-7.

## LITERATURE CITED

- (1) Ekins, R. P. In *Alternative Immunoassays*; Collins, W. P., Ed.; Wiley: New York, 1985; pp 219-237.
- (2) Schuur, A. H. W. M.; Van Weemen, B. K. *Clin. Chim. Acta* **1977**, *81*, 1-40.
- (3) Monroe, D. *Anal. Chem.* **1984**, *56*, 920A-931A.
- (4) *Analytical Applications of Bioluminescence and Chemiluminescence*; Kricka, L. D., Stanley, P. E., Thrope, G. H. G., Whitehead, T. P., Eds.; Academic: London, 1984.
- (5) Campell, A. K.; Roberts, A.; Patel, A. In *Alternative Immunoassays*; Collins, W. P., Ed.; Wiley: New York, 1985; pp 153-184.
- (6) Soini, E.; Hemmila, I. *Clin. Chem. (Winston-Salem, N.C.)* **1979**, *25*, 353-361.
- (7) Hemmila, I. *Clin. Chem. (Winston-Salem, N.C.)* **1985**, *31*, 359-370.
- (8) Hemmila, I.; Dakubu, S.; Mukkala, V. M.; Siltari, H.; Lovgren, T. *Anal. Biochem.* **1984**, *137*, 335-343.
- (9) Sinha, A. P. B. *Spectrosc. Inorg. Chem.* **1971**, *2*, 255-288.
- (10) Lovgren, T.; Hemmila, I.; Pettersson, K.; Halonen, P. In *Alternative Immunoassays*; Collins, W. P., Ed.; Wiley: New York, 1985; pp 203-217.
- (11) Evangelista, R. A.; Pollak, A.; Alore, B.; Templeton, E. F.; Morton, R. C.; Diamandis, E. P. *Clin. Biochem.*, in press.
- (12) Shami, Y.; Reichstein, E.; Ramjessingh, M.; Van Gulck, K.; Zyulko, M. *Clin. Chem. (Winston-Salem, N.C.)* **1986**, *32*, 1072 [Abstract].
- (13) Wieder, I. In *Immunofluorescence and Related Staining Techniques*; Knapp, W., Holubar, K., Wick, G., Eds.; Elsevier: New York, 1978; pp 67-80.
- (14) Diamandis, E. P. *Clin. Biochem.*, in press.
- (15) Erlanger, B. F.; Borek, F.; Beiser, S. M.; Lieberman, S. J. *Biol. Chem.* **1957**, *228*, 713-727.
- (16) Yoshitake, S.; Yamada, Y.; Ishikawa, E.; Masseyeff, R. *Eur. J. Biochem.* **1979**, *101*, 395-399.
- (17) Anderson, L. O. *Arch. Biochem. Biophys.* **1969**, *133*, 277-285.
- (18) Chatteraj, S. C.; Watts, N. B. In *Fundamentals of Clinical Chemistry*; Tietz, N. W., Ed.; Saunders: Philadelphia, 1987; pp 559-569.
- (19) Eskola, J. U.; Nanto, V.; Meurling, L.; Lovgren, T. N. E. *Clin. Chem. (Winston-Salem, N.C.)* **1985**, *31*, 1731-1734.

RECEIVED for review May 18, 1987. Resubmitted August 5, 1987. Accepted February 1, 1988.

# Automated Fluorometric Determination of Formaldehyde in Air

Allan L. Lazrus,\* Karen L. Fong,<sup>1</sup> and John A. Lind

National Center for Atmospheric Research, Boulder, Colorado 80307

A completely automated system is described which initially strips formaldehyde vapor ( $\text{HCHO}$ ) from air into water at pH 2.0 by means of a glass coil through which air and water flow concurrently. The aqueous  $\text{HCHO}$  is then oxidized by nicotinamide adenine dinucleotide ( $\text{NAD}^+$ ) to produce the reduced form of the coenzyme ( $\text{NADH}$ ), which is measured fluorometrically. This reaction occurs in the presence of the enzyme formaldehyde dehydrogenase. The detection limit is 120 parts per trillion by volume. The calibration curve is linear to approximately 100 parts per billion by volume (ppbv). The coefficient of variation is 2.0% at 20 ppbv  $\text{HCHO}$ . The rise time of the signal from 10% to 90% is 80 s.

There is a strong need for rapid and sensitive techniques for measuring formaldehyde in both polluted and relatively pristine air. Formaldehyde vapor is an important intermediate which serves to carry the free radical chain reactions in atmospheric photooxidation. It is formed in air by oxidation of hydrocarbons and is in turn photolyzed to generate the odd hydrogen radical species responsible for further hydrocarbon oxidation. These chemical processes have recently been reviewed (1). In view of the reported increasing global secular trends in methane concentrations (2-4), there is great interest in exploring the oxidative efficiency of the atmosphere in regions which are remote from industrial sources of pollution. Average concentrations of shipboard measurements in remote regions of the ocean are approximately 200 parts per trillion by volume (pptv) (5). An appropriate  $\text{HCHO}$  vapor technique should therefore have a detection limit in the part per trillion

<sup>1</sup>Present address: 10306 N.E. Wygant, Apt. 19, Portland, OR 97220.

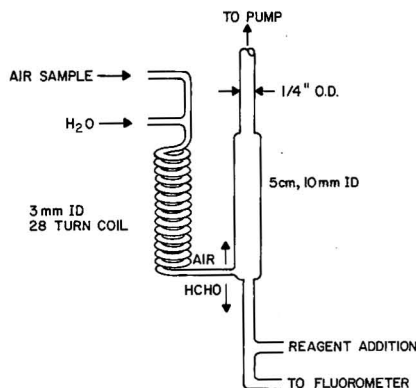


Figure 1. Pyrex glass stripping coil and separator. Typical flow rates are 1.0 L/min air and 0.42 mL/min scrubbing water.

by volume concentration range. The time resolution of an *in situ* analytical method should also be consistent with use on a rapidly moving aircraft in order to assay the levels of HCHO throughout the troposphere.

The analytical methods for HCHO vapor in general use have also been reviewed recently (1). Most of the *in situ* techniques rely on stripping HCHO from air by reacting it with a solution of 2,4-dinitrophenylhydrazine to form the hydrazone adduct. Several tens of minutes to several hours are required to collect a sufficient sample, depending on the ambient HCHO concentration. The samples are analyzed at a later time by using high-performance liquid chromatography or gas chromatography with electron capture detection (6-16).

Earlier colorimetric techniques based on the reaction of chromotropic acid with HCHO (17, 18) have recently been intercompared with the 2,4-dinitrophenylhydrazine method and have been found to give comparable results in urban air (19). A colorimetric method recently applied to analysis of atmospheric condensates utilizes Nash reagent (20). Several studies have been reported that use Fourier transform infrared spectroscopy (21, 22). Diffusion of atmospheric HCHO vapor to an enzyme-coated piezoelectric crystal detector has also been reported (23). The method described below uses similar enzyme-catalyzed chemistry but depends upon fluorometry for detection. The unique advantage of enzyme catalysis for atmospheric measurements is the ability of many enzymes to react selectively with a single species within a complex mixture of compounds. The automated instrument is comprised of a device for a continuous rapid transfer of HCHO vapor from the sample air to water, a peristaltic Technicon AutoAnalyzer pump, and a fluorometer fitted with a flow cell to analyze the aqueous HCHO.

The dissolved HCHO reacts reversibly with H<sub>2</sub>O to form the adduct dihydroxymethane CH<sub>2</sub>(OH)<sub>2</sub> which is the dominant form in solution. The CH<sub>2</sub>(OH)<sub>2</sub> reduces nicotinamide adenine dinucleotide (NAD<sup>+</sup>) to its fluorescent form (NADH), a reaction which is catalyzed by formaldehyde dehydrogenase (FDH). The suggested overall reaction mechanism is (24)



The automated technique is free of interferences from common atmospheric constituents, sensitive, and relatively fast.

## EXPERIMENTAL SECTION

Formaldehyde vapor is stripped from the atmosphere by means of concurrently pulling the air sample and scrubbing water through a 28-turn 3-mm-i.d. Technicon AutoAnalyzer mixing coil (Figure

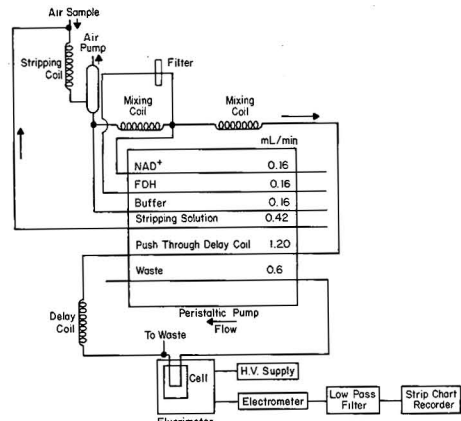


Figure 2. Diagram of the AutoAnalyzer pump manifold and other components.

1) (25). The scrubbing water is adjusted to pH 2.0 with hydrochloric acid and nominally flows at 0.42 mL/min through the coil. Air is typically sampled at 1.0 standard liter per min (L/min) giving a residence time of about 0.3 s. The scrubbing water, which is impelled by the air as it flows through the vertical coil, forms a thin film on the glass surface, providing a large surface for gas exchange. For maximum accuracy, the delivery rate of the pump tube introducing water into the scrubbing coil should be calibrated.

The aqueous HCHO is isolated from the scrubbing air in a vertical separator column by gravity. It is then mixed with buffer (0.2 M Na<sub>2</sub>HPO<sub>4</sub> adjusted to pH 8 with HCl) and led into a five-turn mixing coil. The FDH and NAD<sup>+</sup> are then added to the reaction stream, followed by a second five-turn mixing coil. The reaction mixture is then pumped through a reaction time delay coil (13.2-min delay) to allow production of NADH to come to completion (Figure 2). A filter is placed in the enzyme line downstream of the pump, to remove particles occasionally seen in this reagent. This polycarbonate filter, 8.0-μm pore size and 13-mm diameter, is contained in an in-line polycarbonate filter holder (both from Nuclepore Corp.).

The flow stream is segmented by air bubbles which help to maintain sharp concentration gradients along the stream. The delivery rate of the pump tube to the time delay coil is approximately 0.30 mL/min greater than the delivery rates of scrubbing water and reagents. This flow difference is made up by air drawn from the bottom of the separator column and forms the air bubbles in the flow stream. The bubbles are removed from the flow stream by a Technicon debubbler placed immediately upstream of the fluorometer flow cell. The excitation and emission wavelengths of NADH are 340 and 460 nm, respectively. A laboratory-built fluorometer (with phosphor-coated mercury lamp, 100-μL flow cell, appropriate interference filters, and side-on photomultiplier tube) and a McPherson Instruments HPLC fluorometer (Model FL748) were used in the course of these experiments.

Stock standard solutions are made by dissolving 0.30 g of paraformaldehyde in H<sub>2</sub>O (1 L), yielding a nominal concentration of 0.01 M HCHO. To dissolve the paraformaldehyde, it is necessary to alternately heat and stir the solution for 1 to 2 days. Typically we heat the solution to approximately 50 °C for 10 min and then stir for 10 min. The stock solutions are gravimetrically standardized by the methone method, in which HCHO is reacted with 5,5-dimethylcyclohexane-1,3-dione to form insoluble methylene bis(methone) (26). Standards of HCHO vapor are generated by equilibrating air with aqueous HCHO standards (27). Equilibrium concentrations as a function of temperature are described by eq 3. The standard generator apparatus (Figure 3) consists of a tube lined with glass-fiber filter paper. A liquid HCHO standard runs down the filter while air supplied by an AADCO Model 737 pure air generator runs in a counter current flow. The tube is thermostated (usually at 18 °C). Dilution of this air to yield the desired concentration of HCHO occurs in the

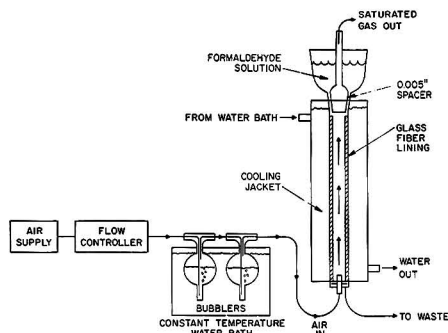


Figure 3. Vapor phase standard generator. Typical flow rate is  $<1$  L/min air.

test manifold. The coefficient of variation for the difference between calculated and observed HCHO in vapor-phase standards ranging between 1.8 and 4.4 ppbv is 10.3% ( $n = 11$ ) resulting principally from errors in gas flow control and dilution. No wall losses were detected when using an inlet of PFA tubing, 0.64 cm i.d. and 3 m in length. To set the instrument at zero, HCHO was initially removed from incoming air by passing it through a molecular sieve trap which is 25.4 mm i.d. and 152.4 mm long. The molecular sieve (Alfa Products) is 13X,  $1/8$  in. pellets. The apparent efficiency of the molecular sieve trap appears to decline too quickly for it to be useful as a zeroing device in this application. To irreversibly bind HCHO, a trap constructed of PFA Teflon (4 cm i.d., 6 cm long) was filled with silica gel coated with 2,4-dinitrophenylhydrazine (28). The collection efficiency, at 1.0 L/min, is 97% at 7.0 ppbv HCHO. When clean air is sampled (0.1–2.0 ppbv HCHO), two additional techniques can be used for establishing the instrumental zero. The first is simply to use "zero" air free of HCHO (e.g. from an AADC Model 737 pure air generator). The second is to use the reagent blank as the zero signal. The reagent blank is obtained by allowing the scrubbing solution to bypass the air scrubbing coil. The use of "zero" air and the reagent blank yield identical signals and are believed to be the most reliable means of zeroing the instrument at very low concentrations of HCHO.

To prepare the FDH reagent, formaldehyde dehydrogenase from *Pseudomonas putida* in the form of lyophilized powder (Sigma Chemical Co.) is dissolved in  $H_2O$  (16 enzyme units/100 mL (one enzyme unit will oxidize 1.0  $\mu$ mol of HCHO to formic acid per minute at pH 7 and 30 °C). This reagent is buffered at pH 8 with 0.01 M  $Na_2HPO_4$  (Fisher Scientific Co.). The concentration of enzyme may be adjusted to reduce the instrument lag time as described in the discussion section. The  $NAD^+$  reagent contains 35 mg/100 mL (approximately  $5 \times 10^{-4}$  M) of grade III-C, 99+ % crystalline  $\beta$ -nicotinamide adenine dinucleotide (Sigma Chemical Co.), adjusted to pH 4–5 with HCl for stabilization.

Potential interferences were tested with a manifold comprised of 1.27 cm o.d. PFA Teflon, PFA–Teflon fittings, Tylan mass flow controllers, an AADC Model 737 pure air generator, and a pump. Flow rates of diluting air, HCHO vapor standards, and potential interferences were controlled by Tylan mass flow controllers.

Interference tests with diluted mixtures of C-1 to C-4 hydrocarbons provided by Scott Specialty Gases contained methane (147 ppbv), ethane (122), ethylene (151), acetylene (113), propane (121), propylene (107), *n*-butane (118), isobutane (124), 1-butene (122), isobutylene (118), *cis*-2-butene (114), *trans*-2-butene (111), ethylacetylene (175) and 1,3-butadiene (106). Ozone for interference tests was generated by irradiating oxygen (Linde, extra dry grade) with a low-pressure Hg lamp. The ozone generator also produced small quantities of HCHO, which were removed by passing the ozone through a bubbler containing scrubbing water. The  $O_3$  concentration was monitored by a Thermoelectron  $O_3$  analyzer. Sulfur dioxide dilutions were made with a permeation tube and an AID Model 360 standard generator. The permeation tube was calibrated by using a modified West–Gaeke technique (29). The methylhydroperoxide was synthesized by the method

of Rieche and Hitz (30) and measured by a fluorometric technique (31). Nitric oxide interference was tested with dilutions of a 10 ppmv certified standard of NO in nitrogen (Scott Specialty Gases). Acetaldehyde gas mixtures for interference testing were generated by equilibrating air with aqueous solutions of acetaldehyde (Kodak Laboratory Chemicals). The apparatus was identical with that used for HCHO standards (Figure 3). Henry's law constant relating the aqueous concentration to the gas phase concentration was 15 M atm $^{-1}$  (32).

## DISCUSSION

The FDH enzyme is somewhat expensive and a longer reaction time provides a means of reducing the consumption of enzyme. The test is operated to yield approximately 99% conversion of the collected HCHO. The percent conversion is determined by comparing the signal from an HCHO standard with the equivalent NADH standard. The extent of conversion of formaldehyde is most easily controlled by both the enzyme concentration and the size of the reaction time delay coil. With coils which provide delay times of 3.6, 6.6, and 13.2 minutes, at least 99% reaction is attained with FDH concentrations of 0.60, 0.28, and 0.16 enzyme units mL $^{-1}$ , respectively. Only in the case of the 13.2-min delay coil was it found desirable to recycle the sample stream through the pump before entering the decoil, as shown in Figure 2. The reaction rate is not significantly increased by increasing the concentration of  $NAD^+$  above the suggested level, 35 mg/100 mL.

The rise time from a 10% to 90% signal is 80 s and is insensitive to the lag time. The rise time is determined primarily by the process in which HCHO is stripped from the air sample.

The reaction rate is independent of pH in the range pH 7–9, showing a gradual decrease at higher pH values. The test is buffered with  $Na_2HPO_4$ ,  $pK_A = 7.2$ . The stream leaving the fluorometric cell is at pH 7.5.

The collection efficiency of HCHO vapor in the scrubbing coil is a function of (1) the equilibrium partitioning of HCHO between the sample air and the scrubbing solution and (2) the rate at which this equilibrium is reached. HCHO is very soluble in water because it is rapidly hydrated to form the gem-diol, which is the dominant form in solution.

The equilibrium constant for the hydration reaction at 298 K is  $1.82 \times 10^6$  (33). Henry's law expression which relates the aqueous concentration of formaldehyde (molarity) to the equilibrium gas phase concentration (atmospheres) (34) is given by

$$[HCHO_{aq}] = 10^{[(4538/T) - 11.34]} [HCHO_g]^{(252.2/T) + 0.2088} \quad (3)$$

The length of the scrubbing coil is selected to optimize attainment of thermodynamic equilibrium concentrations of HCHO in the scrubbing solution. The rate at which equilibrium is attained is accelerated by general base or acid catalysis (33). We have therefore explored the use of both basic and acidic scrubbing solutions to speed up attainment of equilibrium. With the use of 0.40 mL/min of scrubbing solution at neutral pH, equilibrium is not attained at air sampling flow rates higher than 0.75 L/min. By operation with the scrubbing solution at pH 11.2 or pH 2.0, equilibrium can be established at air sampling rates up to 1.25 and 1.0 L/min, respectively.

The agreement between the observed collection efficiency and that predicted by eq 3 has been tested by flowing HCHO vapor standards (approximately 11 ppbv) through two scrubbing coils operating in series, each with its scrubbing solution at 0.38 mL/min, pH 2.0, and 20 °C. If  $\epsilon$  is the collection efficiency and  $X_T$  is the total HCHO concentration, then the concentration collected in the first coil is  $\epsilon X_T$ . The aqueous concentration in the second coil is  $\epsilon X_T(1 - \epsilon)$ , so that the ratio of the second to first concentration is  $1 - \epsilon$ . The



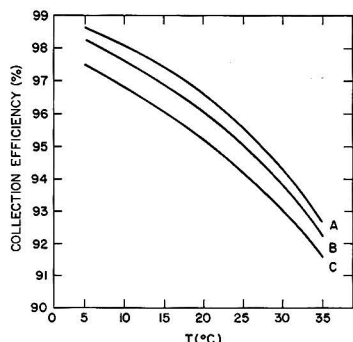


Figure 4. HCHO collection efficiency as a function of temperature ( $^{\circ}\text{C}$ ) and initial HCHO concentrations: 29.6 ppbv (A), 2.55 ppbv (B), and 0.10 ppbv (C).

observed value of  $\epsilon$  is 0.951, compared to an efficiency of 0.965 predicted from eq 3. The worst case error in applying eq 3 to equilibrium HCHO concentrations of  $10^{-9}$  atm is 10% (34). These experiments have confirmed eq 3 and also demonstrated that equilibrium is attained in the scrubbing coil. In typical application of this analytical method, it is not necessary to know the collection efficiency since calibration standards are introduced periodically. This is especially important when the equilibrium in the scrubbing coil is altered by significant temperature fluctuations. The dependence of the collection efficiency of HCHO on temperature over the range 5–35  $^{\circ}\text{C}$  is shown in Figure 4. These curves are calculated from eq 3 and assume a sample rate of 1.0 L/min and 0.4 mL/min scrubbing water. Figure 4 also illustrates the dependence of collection efficiency on HCHO concentration, as suggested by eq 3. Three plots are shown for initial HCHO concentrations of 29.6, 2.55, and 0.10 ppbv. These curves reveal that the collection efficiency varies only about 1% in changing from 0.10 ppbv HCHO to 29.6 ppbv HCHO in the sample air at a given temperature. Furthermore, over the typical operating range of 15–30  $^{\circ}\text{C}$ , only a 4.5% change in collection efficiency occurs. Such changes are completely compensated by calibrating with standards in the appropriate concentration range at the operating temperature.

Another relatively minor potential error is caused by evaporation of the scrubbing water in the coil. However, even if the relative humidity of air at 20  $^{\circ}\text{C}$  is 0.0%, less than a 4% loss in scrubbing water volume occurs. The use of periodic standards for calibration will completely compensate for changes in humidity.

The instrument may be calibrated by substituting aqueous HCHO standard solutions (pH 2.0) for the scrubbing water. The equilibrium partitioning of the HCHO between scrubbing water and air in the coil is identical for either an aqueous phase standard or an equivalent vapor phase standard. The equation relating the concentration of aqueous standard to the concentration of the vapor standard is

$$(\text{HCHO})_{\text{air}} = 22.4[\text{HCHO}]_{\text{aq}}F_A/F_V \quad (4)$$

where  $(\text{HCHO})_{\text{air}}$  represents the standard liters of HCHO/standard liters of air,  $[\text{HCHO}]_{\text{aq}}$  is the molarity of aqueous standard,  $F_A$  is liters per minute of stripping solution, and  $F_V$  is standard liters per minute of air sample. The observed difference between aqueous standards and vapor standards is governed primarily by the relatively large uncertainty ( $\sim 10\%$ ) in the vapor-phase standard.

The effects of potentially interfering gases were observed by adding known amounts to an HCHO standard in order to facilitate detection of negative as well as positive interferences.

These experiments were performed over a range of concentrations of potential interferents, HCHO standards, and pH values of scrubbing water.

No effects were observed for ozone alone at either pH 2 or pH 11. There was no interference by mixtures of hydrocarbons alone containing one-, two-, three-, and four-carbon alkanes, alkenes, and alkynes and 1,3-butadiene (see Experimental Section). Production of artifact formaldehyde was anticipated by reactions in a mixture of hydrocarbons and ozone. However, mixtures of hydrocarbons and ozone failed to generate a positive signal. The maximum estimated residence time of the gas mixture before entering the scrubbing coil was about 1 s, possibly accounting for the absence of reactions producing HCHO as an artifact.

At the low pH range (2.2) no interference was observed from either NO (75 ppbv) or NO (75 ppbv) +  $\text{O}_3$  (75 ppbv). Under the conditions of the latter experiment, only 4% of the NO is calculated to have been converted to  $\text{NO}_2$  by the reaction  $\text{NO} + \text{O}_3 \rightarrow \text{NO}_2 + \text{O}_2$ . However the method has been subsequently exposed to 125 ppbv  $\text{NO}_2$  with no apparent interference (35).

Neither methylhydroperoxide nor hydrogen peroxide (10 ppm) interfere in the test.  $\text{SO}_2$  is found to interfere over the entire pH range, presumably by reacting with HCHO to form hydroxymethanesulfonic acid. The solubility of  $\text{SO}_2$  is very sensitive to pH, since it exists either as  $\text{HSO}_3^-$  or  $\text{SO}_3^{2-}$  at higher pH values. This dependency explains why the negative interference caused by  $\text{SO}_2$  (75 ppbv) is larger at higher pH ( $-11\%$  at pH 11 compared to  $-4.1\%$  at pH 2.0). Ozone rapidly oxidizes dissolved  $\text{SO}_2$  at high pH, and its presence in the sample reduces the error at pH 11.0 (e.g.,  $-4.3\%$  at 60 ppbv  $\text{SO}_2$  and 27 ppbv  $\text{O}_3$ ). Though the oxidation of  $\text{SO}_2$  by  $\text{O}_3$  is slow below pH 4.0 (36), oxidation by  $\text{H}_2\text{O}_2$  is rapid. When the scrubbing water is at pH 2.0, the interference of  $\text{SO}_2$  is not only reduced because of lowered solubility but can be entirely eliminated by adding 10 ppm  $\text{H}_2\text{O}_2$  to the scrubbing water. This yielded 0% interference at 70 ppbv  $\text{SO}_2$  and 4.1 ppbv HCHO.  $\text{H}_2\text{O}_2$  oxidizes dissolved  $\text{SO}_2$  very slowly at high pH (37) and is therefore ineffective in removing the interference at pH 11.0.  $\text{H}_2\text{O}_2$  should be added if the  $\text{SO}_2$  is above 35 ppbv, which otherwise would cause about a  $-2\%$  error.

Though acetaldehyde vapor ( $\text{CH}_3\text{CHO}$ ) gives a very slight positive signal, the test is  $2.6 \times 10^3$  more sensitive to HCHO than to  $\text{CH}_3\text{CHO}$ .

The coefficients of variation using vapor phase standards 8, 20, and 82 ppbv are 3.3% ( $N = 4$ ), 2.0% ( $N = 3$ ), and 1.9% ( $N = 3$ ), respectively. The coefficient of variation with an aqueous standard equivalent to 4 ppbv is 1.5% ( $N = 4$ ). Given the convenience of using aqueous standards, the relative ease of preparing them, and their inherent greater accuracy compared to vapor standards, the instrument has been calibrated most frequently with the aqueous standards. The detection limit (3 times standard deviation of the base line) is 120 pptv. The rise time from a 10% to 90% signal is 80 s. The signal varies linearly with the concentration of aqueous standards to at least  $20 \times 10^{-6}$  M HCHO, equivalent to 160 ppbv HCHO. The instrument has operated in an unattended mode for periods up to 48 h.

Registry No.  $\text{CH}_2\text{O}$ , 50-00-0; NAD, 53-84-9.

#### LITERATURE CITED

- (1) Carlier, P.; Hannachi, H.; Mouvier, G. *Atmos. Environ.* **1986**, *20*, 2079–2099.
- (2) Fraser, P. J.; Hyson, P.; Rasmussen, R. A.; Crawford, A. J.; Khalil, M. A. K. *J. Atmos. Chem.* **1986**, *4*, 3–42.
- (3) Khalil, M. A. K.; Rasmussen, R. A. *Science (Washington, D.C.)* **1984**, *224*, 54–56.
- (4) Blake, P. R.; Mayer, E. W.; Tyler, S. C.; Makide, Y.; Montague, D. C.; Rowland, F. S. *Geophys. Res. Lett.* **1982**, *9*, 477–480.
- (5) Lowe, D. C.; Schmidt, U. *J. Geophys. Res.* **1983**, *88*, 10844–10858.
- (6) Cleveland, W.; Graedel, T.; Kleimer, B. *Atmos. Environ.* **1977**, *11*, 357–360.

- (7) Kuwata, K.; Uebori, M.; Yamasaki, Y. *J. Chromatogr. Sci.* **1979**, *17*, 264-268.
- (8) Kuntz, R.; Lonneman, W.; Namie, G.; Hull, L. A. *Anal. Lett.* **1980**, *13*, 1409-1415.
- (9) Fung, K.; Grosjean, D. *Anal. Chem.* **1981**, *53*, 168-171.
- (10) Neltzart, V.; Seiler, W. *Geophys. Res. Lett.* **1981**, *8*, 79-82.
- (11) Grosjean, D. *Environ. Sci. Technol.* **1982**, *16*, 254-262.
- (12) Kuwata, K.; Uebori, M.; Yamasaki, H.; Kuge, Y. *Anal. Chem.* **1983**, *55*, 2013-2016.
- (13) Tanner, R. L.; Meng, Z. *Environ. Sci. Technol.* **1984**, *18*, 723-726.
- (14) Cofer, W. R., III; Edahl, R. A. *Jr. Atmos. Environ.* **1986**, *20*, 979-984.
- (15) Levin, J.; Andersson, K.; Lindahl, R.; Nilsson, C. *Anal. Chem.* **1985**, *57*, 1032-1035.
- (16) Shulam, P.; Newbold, R.; Hull, L. A. *Atmos. Environ.* **1985**, *19*, 623-626.
- (17) Althuler, A. P.; McPherson, S. P. *J. Air Pollut. Control Assoc.* **1983**, *13*, 109-111.
- (18) Fushimi, K.; Miyake, Y. *J. Geophys. Res.* **1980**, *85*, 7533-7536.
- (19) Salas, L. J.; Singh, H. B. *Atmos. Environ.* **1986**, *20*, 1301-1304.
- (20) Snider, J. R.; Dawson, G. A. *J. Geophys. Res.* **1985**, *90*, 3797-3805.
- (21) Platt, U.; Perner, D.; Patz, H. W. *J. Geophys. Res.* **1979**, *84*, 6329-6335.
- (22) Tuazon, E. C.; et al. *Atmos. Environ.* **1978**, *12*, 865-875.
- (23) Guilbault, G. *Anal. Chem.* **1983**, *55*, 1682-1684.
- (24) Ando, M.; Yoshimoto, T.; Ogushi, S.; Rikitate, K.; Shibata, S.; Tsuru, D. *J. Biochem.* **1979**, *85*, 1165.
- (25) Zenner, H.; Belew, W. *Advances In Automated Analyses, Technicon International Congress; Futura*: Mt. Kisco, NY, 1970: Vol. II.
- (26) Yoe, J. H.; Reid, L. C. *Ind. Eng. Chem., Anal. Ed.* **1941**, *13*, 238-240.
- (27) Lind, J. A.; Kok, G. L. *J. Geophys. Res.* **1986**, *91*, 7884-7895.
- (28) Beasley, R. K.; Hoffman, C. E.; Rueppel, M. L.; Worley, J. W. *Anal. Chem.* **1980**, *52*, 1110-1114.
- (29) Kok, G. L.; Gittlin, S. N.; Gandrud, B. W.; Lazrus, A. L. *Anal. Chem.* **1984**, *56*, 1993.
- (30) Rieche, A.; Hiltz, F. *Ber. Dtsch. Chem. Ges.* **1920**, *62*, 2458.
- (31) Lazrus, A. L.; Kok, G. L.; Lind, J. A.; Gittlin, S. N.; Helkes, B. G.; Shetter, R. E. *Anal. Chem.* **1986**, *58*, 594-597.
- (32) Gaffney, J. S.; Strell, G. E.; Spall, W. D.; Hall, J. H. *Environ. Sci. Technol.* **1987**, *21*, 519-524.
- (33) Bell, R. P. *Adv. Phys. Org. Chem.* **1966**, *4*, 1-29.
- (34) Dong, S.; Dasgupta, P. K. *Environ. Sci. Technol.* **1986**, *20*, 637-640.
- (35) Kleindienst, T. E. *Atmos. Environ.*, in press.
- (36) Penkett, S. A.; Jones, B. M. R.; Brice, K. A.; Eggleton, A. E. *Atmos. Environ.* **1979**, *13*, 123-137.
- (37) Kunen, S. M.; Lazrus, A. L.; Kok, G. L.; Helkes, B. G. *J. Geophys. Res.* **1983**, *88*, 3671-3674.

RECEIVED for review April 27, 1987. Resubmitted February 3, 1988. Accepted February 3, 1988. The National Center for Atmospheric Research is funded by the National Science Foundation.

## CORRESPONDENCE

### Fabrication of an Oxygen Electrode Using Semiconductor Technology

*Sir:* Clark-type oxygen-sensing electrodes have been applied to various biosensors by immobilizing either enzymes or microorganisms which catalyze the oxidation of biochemical organic compounds (1, 2). Recently, demand has been increasing for miniaturized and integrated biosensors for use in clinical analysis. Therefore, several oxygen electrodes, based on conventional semiconductor technology, have been fabricated by several groups (3-7), but they have not yet reached the production line. One reason for this is that they contain a liquid electrolyte solution, making adhesion of the gas-permeable membrane to the substrate difficult, even if epoxy resin is used. Therefore, mass production of such a device is impossible. The objectives of this study were to develop a disposable oxygen electrode based on conventional semiconductor fabrication technology and to use the electrode in a biosensor. The key improvements were (1) to use a porous material (agarose gel) to support the electrolyte solution and (2) to use a hydrophobic polymer (negative photoresist) as the gas-permeable membrane and directly cast it over the porous material.

#### EXPERIMENTAL SECTION

**Materials and Reagents.** P-type silicon (100) oriented wafers were used to make the U-shaped structure. They were 2 in. in diameter and 350  $\mu$ m thick. All chemicals were reagent grade and needed no further purification. Solutions were prepared with distilled water. A 10 mM phosphate buffer solution (pH 7.0) was prepared. The agarose gel was adjusted by mixing 1 g of agarose in a 0.1 M potassium chloride solution. Distilled water was prepared for the experiment to check the function of the gas-permeable membrane. Glucose oxidase (type II, from *Aspergillus niger*; activity, 15000-25000 units per gram solid) was purchased from Sigma.

**Apparatus and Procedure.** Thermal oxidation of the silicon wafers was performed with a UP-5300-2 oxidation furnace (Yamato Semic Co., Tokyo, Japan). The photoresist was applied to the silicon substrate by using a spinner (1H-D2, Mikasa Co.,

Tokyo, Japan). The resist patterns were projected with an MA-10 mask aligner (Mikasa Co.), and the gold electrodes were deposited by use of an ULVAC EBH-6 vacuum chamber. The terminal voltage between the two gold electrodes was maintained at a constant level with a potentiostat (Hokuto Denko, HA-501) and the current output of the oxygen electrode was recorded with an electronic polyrecorder (Toa Electronics, Ltd., Model EPR-200A). The temperature of the buffer solution and distilled water was maintained at 27 °C for the oxygen electrode. For the glucose sensor, the temperature was held at 30 °C. Although enzyme activity itself increases at higher temperatures, the enzyme is easily degraded, affecting the sensor stability. Considering both the enzyme activity and its denaturation, the measuring temperature was set at 30 °C. The oxygen concentration in the buffer solution was adjusted either by bubbling nitrogen gas, by adding sodium sulfite, or by controlling the stirring speed. The output from the oxygen electrode was correlated with that of a dissolved oxygen meter (Toa Electronics, Ltd., Model DO-1B).

The characteristics of the oxygen electrode were evaluated mainly in the phosphate buffer solution by dipping its sensitive part into the solution and measuring. Experiments with the glucose sensor were performed by using a similar procedure.

**Oxygen Electrode Structure.** The structure of the oxygen electrode is illustrated in Figure 1. The electrode has a U-shaped groove, 300  $\mu$ m deep, and two gold electrodes over the SiO<sub>2</sub> layer that electrically insulates them. Each gold electrode covers about half of the oxygen electrode, that is, the bottom and side walls of the groove and the upper part. Our preliminary study (7) confirmed that oxygen electrodes with only two gold electrodes inside the gas-permeable membrane can respond to the oxygen concentration. Agarose gel containing a 0.1 M potassium chloride aqueous solution was poured into the groove, after which it was covered by the gas-permeable membrane. Several hydrophobic polymers were tested as the gas-permeable membrane, and a negative photoresist was found to be effective. In this oxygen electrode, a negative photoresist (Tokyo Oka Co., OMR-83; viscosity, 40 cP) was used as the gas-permeable membrane, because the resulting membrane can be selectively formed, its adhesive properties are adequate, it is tolerant of chemical agents, and it

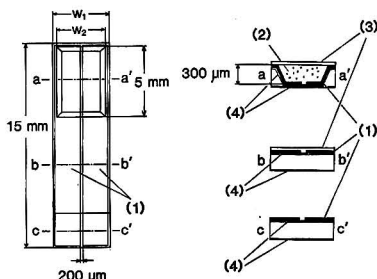


**Figure 1.** Structure of the oxygen electrode. The cross sections on the right side correspond to a-a', b-b', and c-c': (1) gold electrodes, (2) agarose gel, (3) gas-permeable membrane, (4) SiO<sub>2</sub> layer. W<sub>1</sub> is 2, 3, or 4 mm. W<sub>2</sub> is 1.4, 2.2, or 3 mm in each case.

is hard to break. The agarose layer was approximately 300  $\mu$ m thick, and the gas-permeable membrane was 2  $\mu$ m thick when applied at 1500 rpm. Only the pad areas of the two gold electrodes were left exposed, while the other parts were covered with the same hydrophobic polymer used for the gas-permeable membrane. This insulates each electrode when used in an aqueous solution. The cathode and the anode were the same size. Both gold electrodes were 200  $\mu$ m apart in each case.

**Fabrication of a Glucose Sensor.** The glucose sensor was fabricated by immobilizing glucose oxidase (GOD) on a sensitive part of the oxygen electrode by cross-linking with bovine serum albumin (BSA) and glutaraldehyde (GA). The enzyme-immobilized membrane was formed by dipping the sensitive part into a mixture containing 2 mg of glucose oxidase, 20  $\mu$ L of 10% BSA solution, and 10  $\mu$ L of 25% GA solution.

**Fabrication Process.** The oxygen electrode was fabricated by the following process. The basic procedure was similar to a conventional semiconductor fabrication process except for filling the U-shaped groove with agarose gel and not removing the photoresist in the final stage of the process.

(1) The silicon wafers (thickness 350  $\mu$ m, diameter 2 inches) were washed in a boiled, mixed solution, containing hydrogen peroxide, ammonium solution, and water. The solution was prepared by mixing 1 part of ammonium solution, 1 part of hydrogen peroxide solution, and 4 parts of distilled water.

(2) The wafer was submitted to thermal oxidation. The oxidation temperature was 1000  $^{\circ}$ C. The thickness of the SiO<sub>2</sub> layer was 1  $\mu$ m.

(3) The groove pattern was formed with negative photoresist (Tokyo Oka, OMR-83), after which the other side was coated with the same photoresist. About 50–60 s of exposure was suitable when the MA-10 mask aligner was used.

(4) The SiO<sub>2</sub> layer was etched with a mixed solution consisting of 1 part 50% hydrogen fluoride and 6 parts of 50% ammonium fluoride. The remaining SiO<sub>2</sub> layer became the mask for the nonisotropic silicon etching.

(5) The resist was removed in a 2/1 hydrogen sulfide/hydrogen peroxide solution at room temperature.

(6) The silicon was submitted to nonisotropic etching in a 35% potassium hydroxide solution. The temperature was maintained at 80  $^{\circ}$ C.

(7) The SiO<sub>2</sub> layer was removed with the same solution as was used in (4).

(8) The silicon wafers were washed with the same solution as was used in (1).

(9) The wafers were submitted to thermal oxidation. The oxidation temperature was 1000  $^{\circ}$ C. The SiO<sub>2</sub> layer was 500 nm thick.

(10) The resist pattern was formed for the gold electrodes by using the same photoresist as was used in (3).

(11) A 50-nm layer of chromium was deposited, followed by 1  $\mu$ m of gold.

(12) The photoresist was then removed in warmed hydrogen sulfide.

(13) The U-shaped groove was filled with heated agarose gel containing a 0.1 M KCl solution using a microsyringe. Then the

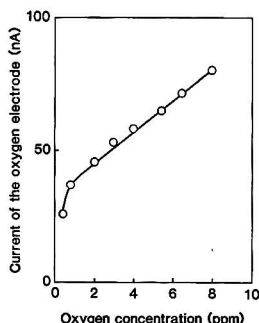


**Figure 2.** Calibration curve for the 2-mm-wide oxygen electrode. The terminal voltage was 0.8 V. The experiment was performed in a 10 mM phosphate buffer (27  $^{\circ}$ C, pH 7.0).

gel was cooled. The agarose gel concentration was 1%.

(14) A hydrophobic polymer was applied, followed by a photochemical reaction. In this case, the same photoresist (OMR-83) as was used to fabricate the oxygen electrode was used as the gas-permeable membrane and for insulation. The photoresist was spin-coated at 500 rpm for 5 s and 1500 rpm for 20 s, followed by exposure to ultraviolet light; 1500 rpm may be the speed at which the photoresist can be applied homogeneously. A photoresist membrane capable of functioning as a gas-permeable membrane was obtained at lower speeds, for example, less than 3000 rpm. The higher the speed however, the lower the yield of the perfect gas-permeable membrane. At such a speed, the gel is firmly supported by the side walls of the groove and remains after application of the photoresist.

## RESULTS AND DISCUSSION

**Characteristics of the Oxygen Electrode. Response Curve.** The response time of the oxygen electrode to an oxygen concentration change from saturation to almost zero was measured by adding sodium sulfite to reduce the dissolved oxygen concentration. The response profiles were similar regardless of the electrode's size. It responded as soon as sodium sulfite was added to the buffer solution, a steady-state being achieved 8–10 min later. The 90% response time of the oxygen electrode was approximately 3 min, which is about 3 to 4 times longer than that of conventional oxygen electrodes. This is not considered to be a function of the cathode area but is probably governed mainly by oxygen diffusion through the agarose gel. The distance between the cathode and the gas-permeable membrane can be shortened and will be our next step.

**Calibration Curve.** Figure 2 is the calibration curve for a 2-mm-wide electrode. A linear relationship was obtained for an oxygen concentration between about 1 and 7.9 ppm (saturated) when the terminal voltage between the two gold electrodes was 0.8 V, even though it deviated from linearity at lower concentrations. Similar calibration curves were obtained by using other oxygen electrodes. This confirmed the device's operation as an oxygen sensor.

**Function of the Photoresist Membrane.** To confirm that the photoresist membrane worked as a gas-permeable membrane, the sensitive part of the oxygen electrode and the gold electrodes (without the gas-permeable membrane and the agarose gel, and the same size as the oxygen electrode) were dipped into distilled water. After the initial current-potential curves were obtained, electrochemically active compounds, such as sodium sulfite, potassium ferricyanide, hydroquinone, and L-ascorbic acid were added. Then, the changes in the curve were compared. The potential of one of the two gold electrodes was scanned in both cases at 50 mV/s between -0.5

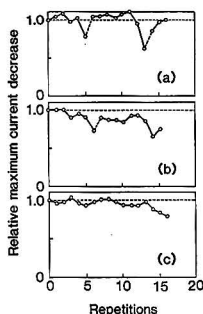


**Figure 3.** Stability of the oxygen electrode. The terminal voltage of each oxygen electrode was 0.8 V. The experiment was performed in a 10 mM phosphate buffer (27 °C, pH 7.0). Data are presented for (a) the 4-mm-wide oxygen electrode, (b) for the 3-mm-wide electrode, and (c) for the 2-mm-wide electrode. The dashed lines in (a) and (b) indicate intervals where no voltage is applied.

and +0.5 V with reference to the other gold electrode. In every experiment, the gold electrodes without the gas-permeable membrane showed a current increase due to the direct electrochemical reaction of the compounds on the gold electrode, while the oxygen electrode showed no current change (for sodium sulfite, a current decrease was observed due to the oxygen concentration reduction). This confirmed the photoresist's action as a gas-permeable membrane and showed that its selectivity to ionic compounds was excellent.

**Stability.** The stability of the oxygen electrode was tested. Figure 3 shows the results. When larger oxygen electrodes were used, their response decreased after they were used successively for a few times in experiments. If they are stored for several hours in a phosphate buffer solution or in distilled water with no voltage applied, however, their sensitivity returns to the initial level as denoted by the dashed lines in Figure 3a,b. The small oxygen electrode could be used more than 15 times, although the response decreased slightly as with the larger oxygen electrodes. In this study, we found that the smaller the oxygen electrode, the more stable it was. Poor stability of the larger oxygen electrode was thought to be due to accumulation of reaction products in the vicinity of each of the two gold electrodes.

**Characteristics of the Glucose Sensor. Response Time.** The glucose sensor responded as soon as the glucose solution was injected into the buffer solution in which the sensitive part of the sensor was dipped, and stabilized 5–10 min after the injection. The time delay of the oxygen electrode seemed to be more important than the thickness of the GOD-immobilized membrane. The response time of the glucose sensor will be shortened once the oxygen electrode is improved.

**Calibration Curve.** Figure 4 shows a calibration curve for the glucose sensor at 30 °C and pH 7.0. As can be seen, the sensor responded almost linearly for glucose concentrations between 0.2 and 2 mM, which is comparable to conventional glucose sensors. The glucose sensor was a little sensitive to glucose at normal blood glucose concentrations (5 mM), but

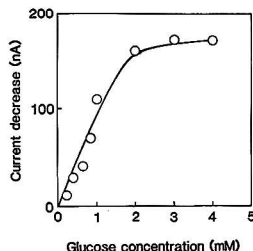


**Figure 4.** Calibration curve for the 3-mm-wide glucose sensor. The experiment was performed in a 10 mM phosphate buffer (30 °C, pH 7.0). The terminal voltage was 0.8 V.

the sensitivity is easily shifted by adjusting the amount of immobilized enzyme.

**Stability.** The stability of the glucose sensor was evaluated by performing the same experiments as were done to obtain the response curve. In this experiment, the stability of the 3-mm-wide glucose sensor was evaluated. In subsequent experiments at 30 °C, its response gradually decreased, but it returned to the initial level when the sensor was stored with no voltage applied, as can be seen in the case of the oxygen electrodes. The stability seems to be mainly dependent on the stability of the oxygen electrode used as the transducer.

#### ACKNOWLEDGMENT

We thank Professor S. Nakahama and Mr. Mark Downs for their helpful discussion in compiling this report.

**Registry No.** GOD, 9001-37-0; GA, 111-30-8; agarose, 9012-36-6; glucose, 50-99-7; oxygen, 7782-44-7.

#### LITERATURE CITED

- (1) Karube, I.; Suzuki, S. *Ion-Selective Electrode Reviews*; Pergamon: Oxford, 1984; Vol. 6, p 15.
- (2) Karube, I.; Suzuki, S. *Enzymes and Immobilized Cells in Biotechnology*; Benjamin/Cummings Publishing: 1985; p 209.
- (3) Eden, G.; Inbar, G. I.; Timor-Tritch, I.; Bicher, H. I. *IEEE Trans. Biomed. Eng.* 1975, BME-22(No. 4), 275.
- (4) Esashi, M.; Kozu, J.; Matsuo, T. *Jpn. J. Med. Electron. Biol. Eng.* 1980, 18, 968.
- (5) Miyahara, Y.; Matsuo, F.; Shiohara, S.; Morizumi, T.; Matsuoka, H.; Karube, I.; Suzuki, S. *Proceedings of the 3rd Sensor Symposium*; Institute of Electrical Engineers of Japan 1983; p 21.
- (6) Karube, I. *Biosensors—Fundamentals and Applications*; Oxford University Press: Oxford, 1987; p 471.
- (7) Karube, I.; Tamiya, E.; Murakami, T. *Enzyme Engineering*; The New York Academy of Sciences: New York, 1987; Vol. 8, p 256.

Hiroaki Suzuki

Fujitsu Laboratories, Ltd.  
10-1 Morinosato-Wakamiya  
Atsugi 243-01, Japan

Eiichi Tamiya  
Isao Karube\*

Research Laboratory of Resources Utilization  
Tokyo Institute of Technology  
4259 Nagatsuta-cho, Midori-ku  
Yokohama 227, Japan

RECEIVED for review June 22, 1987. Resubmitted December 9, 1987. Accepted January 4, 1988.

## Fiber-Optic Biosensors Based on the Fluorometric Detection of Reduced Nicotinamide Adenine Dinucleotide

Sir: Biosensors based on the immobilization of a biocatalyst at the tip of either a potentiometric or amperometric electrode

have been developed (1, 2). More recently, biosensors based on a biocatalytic layer at the tip of a fiber-optic device have

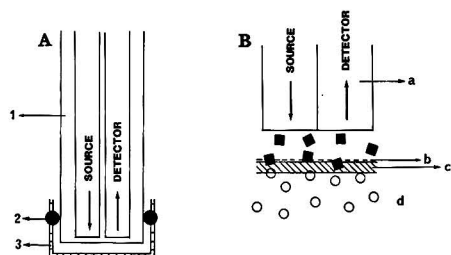


**Figure 1.** Schematic diagrams of the NADH-based fiber-optic biosensor (A) and of the various membrane phases involved in the sensor response (B): (1) common end of the bifurcated fiber-optic probe; (2) O-ring; (3) nylon membrane with immobilized enzyme; (4) fiber-optic probe; (5) nylon membrane; (6) biocatalytic layer; (7) bulk solution; (8) enzymatic substrate; (9) fluorometrically detectable product (NADH).

been introduced. These fiber optic biosensors are based on either the generation of light from a chemiluminescence reaction (3) or the production of a chromophoric species from an enzymatic reaction (4). We report here a new class of biosensors. This new class of sensors is based on both the immobilization of a dehydrogenase enzyme at the sensing tip of a fiber optic probe and the fluorometric detection of consumed or generated reduced nicotinamide adenine dinucleotide (NADH). The concept is demonstrated for the first time with biosensors for lactate and pyruvate. Both sensors employ a layer of covalently immobilized lactate dehydrogenase (LDH, EC 1.1.1.27) at the tip of a bifurcated fiber-optic probe. By combination of this innovative biosensor concept with the many available NADH-based biocatalyzed reactions, a wide variety of new biosensors are possible.

## EXPERIMENTAL SECTION

**Apparatus and Reagents.** Excitation radiation was provided by a 100-W quartz halogen tungsten lamp in conjunction with a constant voltage transformer (Oriol Model 6393). The radiation passed through a 50-nm band-pass filter centered at 360 nm (SLM-Aminco, UG1). NADH fluorescence was measured through a fused-silica bifurcated fiber-optic probe (Oriol Model 77550). This probe tip consisted of two separate fiber bundles with an overall probe diameter of 8 mm at the common end. The fiber-optic bundle has a numerical aperture of 0.19 at 254 nm. The excitation radiation was directed to the biocatalytic layer at the common end of the probe through one of the fiber bundles. A portion of the emitted radiation from NADH at the probe tip was collected by the second fiber bundle and was directed to a photomultiplier tube (PMT) detector (Oriol Model 77761). A 450 nm cutoff long wavelength pass filter (SLM-Aminco, KV470) served to isolate the emitted radiation before it reached the detector. The PMT was operated at -500 V with a common photometer (Oriol Model 7070) and the fluorescence intensities were measured as the resulting currents. The PMT output was recorded on a Sargent-Welch XKR strip chart recorder. All measurements were carried out in thermostated, glass-jacketed cells. A Fisher Model 80 water bath was employed to maintain a constant temperature of  $25.0 \pm 0.5^\circ\text{C}$ .

L-(+)-Lactic acid (lithium salt), L-(+)-pyruvic acid (sodium salt), DL-dithiothreitol (DL-DTT), and  $\beta$ -NADH and  $\beta$ -NAD<sup>+</sup> from yeast were purchased from Sigma Chemical Co., St. Louis, MO. The nylon mesh was from Small Parts, Inc., Miami, FL.

**Procedures.** Figure 1A shows the sensor design. The sensor is composed of a nylon membrane onto which the enzyme lactate dehydrogenase (LDH) is immobilized. Lactate dehydrogenase was covalently immobilized onto a 44- $\mu\text{m}$  mesh of nylon according to the procedure of Mascini and co-workers (5). The resulting LDH-nylon membrane was held at the common end of the bifurcated fiber-optic probe by an O-ring.

Response curves were obtained by first placing the sensor tip in a 10-mL buffer volume. The steady-state background intensity was recorded. A known volume of the appropriate standard was

**Table I.** Effect of Sample Turbidity on Sensor Response

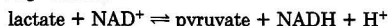
amt of silica, mg/mL	effective absorbance	sensor signal, <sup>a</sup> pA	% response
0.00	0.000	55.0	100.0
0.015	0.046	55.9	101.7
0.030	0.092	54.7	99.4
0.060	0.166	54.1	98.3
0.090	0.237	53.1	96.6
0.120	0.329	53.0	96.3
0.240	0.635	48.0	87.3
0.360	0.773	47.0	85.5

<sup>a</sup> For 125  $\mu\text{M}$  lactate.

then added to the buffer and the resulting final steady-state intensity was measured. Standard additions were continued until the steady-state intensity levels were recorded until the entire concentration range was covered. The buffer solution for the lactate sensor was composed of 0.05 M Tris-HCl with 1 mM DL-dithiothreitol and 0.2 M NaCl at pH 8.6. The same buffer composition at pH 7.4 was employed for the pyruvate sensor. The buffer solution was stirred continuously at a moderated rate by using a small magnetic stir bar. Some stirring was required for the sensor response.

## RESULTS AND DISCUSSION

Figure 1B shows schematically the various membrane phases involved in the sensor response. LDH catalyzes the following reaction:



The equilibrium position of this reaction can be controlled in either direction by proper adjustment of solution conditions. In a solution of high pH, pyruvate is the favored product. By addition of an appropriate amount of NAD<sup>+</sup> to the sample solution, this biosensor can be used for lactate concentration measurements. Sensor operation, in this case, involves diffusion of lactate to the biocatalytic layer where the biocatalyzed reaction takes place. As the reaction proceeds, NADH is generated at the tip of the fiber-optic probe. A steady-state NADH concentration is established when the rate of NADH generation is exactly counterbalanced by the diffusion of NADH away from the sensor tip. This steady-state NADH level is monitored fluorometrically through the fiber-optic probe. This fluorescent signal can be related to the sample lactate concentration through a calibration curve. The pyruvate biosensor works by a similar mechanism, but the consumption of NADH during the biocatalyzed reaction is monitored. A decrease in fluorescence is measured in response to an increase in pyruvate concentration.

Figure 2 shows a response curve for the first NADH-based fiber-optic biosensor for lactate. The lactate concentration range used to obtain the response curve was from 0 to 60  $\mu\text{M}$ . Sensor response was obtained in a pH 8.6, 0.05 M Tris-HCl buffer with 1 mM DTT and 0.2 M NaCl. An increase in the sample lactate concentration results in an increase in the measured steady-state fluorescence intensity. Higher lactate concentrations correspond to faster rates of NADH production which result in higher steady-state NADH concentrations at the probe tip. The dynamic range for the lactate sensor is from the detection limit of 2–50  $\mu\text{M}$ . This detection limit has been calculated as the lactate concentration that gives a response which is 3 times the noise level of the base-line signal. Relative standard deviations range from 5% to 9% with higher percentage of error at lower concentrations of lactate. Response times range from 5 to 12 min during calibration with the faster response times at higher lactate concentrations. Recovery to the base line when the sensor is placed in fresh buffer without lactate present is instantaneous. Reproducible sensor response is obtained for at least 7 days.

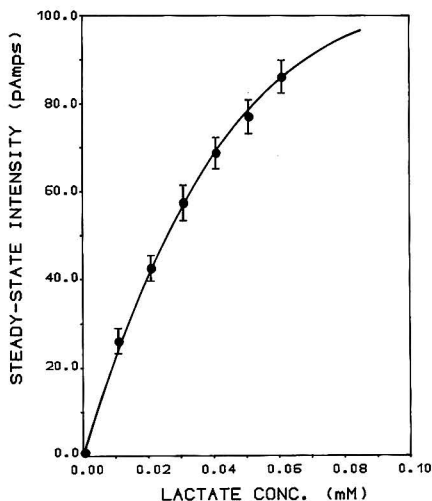


Figure 2. Response curve of lactate using the lactate dehydrogenase based fiber-optic biosensor.

Because  $\text{NAD}^+$  is required for the biocatalyzed reaction, the effect of  $\text{NAD}^+$  concentration on the response of the lactate biosensor has been established. Sensor responses have been monitored for 100  $\mu\text{M}$  lactate solutions with various concentrations of  $\text{NAD}^+$ . Maximum signals are obtained with  $\text{NAD}^+$  concentrations above 2.5 mM. The  $K_M$  value for  $\text{NAD}^+$  with LDH is 0.1 mM (6). As expected,  $\text{NAD}^+$  concentrations well above the  $K_M$  value render the reaction rate independent of the  $\text{NAD}^+$  concentration and provide the the greatest signal. A  $\text{NAD}^+$  concentration of 3 mM has been used in subsequent experiments.

Figure 3 shows a typical response curve for the pyruvate biosensor. In this case, the pH of the 0.05 M Tris-HCl buffer with 1 mM DTT and 0.2 M NaCl has been decreased to 7.4 at which lactate is the favored product. In addition, 1 mM NADH has been added to the sample solution. The expected inverse relationship between sample pyruvate concentration and fluorescence intensity is obtained. A detection limit of 0.2 mM is obtained under these conditions. Higher detection limits are observed for the pyruvate sensor in comparison to the lactate sensor because a change in intensity superimposed on a high initial intensity is required for the pyruvate system. In contrast, the generation of light on a dark background provides superior detection limits in the lactate system. Pyruvate detection limits can be enhanced by lowering the initial NADH concentration. Relative standard deviations for pyruvate sensor range from 1% to 8% with higher percentage of error at higher levels of pyruvate or lower fluorescent intensities.

Interference from sample turbidity has been evaluated by comparing the response of a lactate biosensor in turbid and nonturbid solutions. Turbidity has been generated by adding silica particles with diameters from 1 to 5  $\mu\text{m}$  to a 125  $\mu\text{M}$  lactate standard. Effective absorbance units have been used to express the resulting turbidity levels. Table I summarizes the results of these experiments. Minimal effect on the sensor response is observed at turbidity levels as high as 0.33 absorbance units. Higher levels of turbidity cause a decrease in signal. Calibration of the sensor with standards that possess the same level of turbidity as the sample can be used to account for the effects of high turbidity.

The results in Table I indicate that the sensor response is primarily dependent on the fluorescence generated immedi-

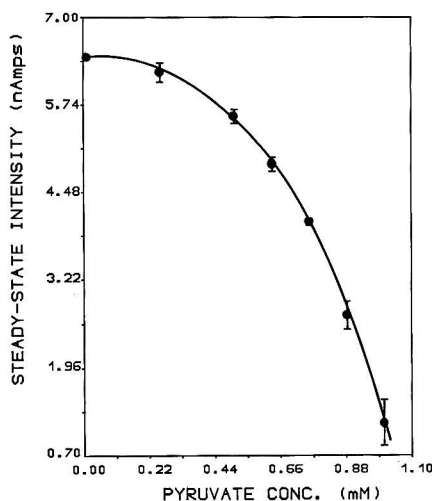


Figure 3. Calibration curve for pyruvate based on the fluorometric detection of NADH consumption.

ately at the sensor tip. Reflected or scattered light from within the bulk solution apparently does not contribute to the measured signal at low to moderate turbidity levels. The effect of the reflectivity at the sensor/solution interface must be considered, however. The nylon support used in this sensor for enzyme immobilization is an effective scattering agent. Other sensor configurations that employ a less effective scattering material at this interface will most likely suffer stronger effects from sample turbidity.

The demonstrated feasibility of NADH-based fiber-optic biosensors for lactate and pyruvate opens the way for the development of an entire new class of biosensing probes. The biosensor strategy demonstrated here can be coupled with a large number of selective NADH- and NADPH-based biocatalyzed reactions. Such reactions are widely available which make possible a wide variety of selective biosensing probes.

#### ACKNOWLEDGMENT

We thank the Petroleum Research Fund, administered by the American Chemical Society, for partial support of this research. Also, financial support from the National Institutes of Health (GM-35487) is acknowledged.

Registry No. NADH, 58-68-4; LDH, 9001-60-9; pyruvic acid, 127-17-3; lactic acid, 50-21-5.

#### LITERATURE CITED

- Rechnitz, G. A. *Science* (Washington, D.C.) **1975**, *190*, 234-238.
- Turner, A. P. F.; Karube, I.; Wilson, G. S. *Biosensor: Fundamentals and Applications*; Oxford University Press: New York, 1987.
- Freeman, T. M.; Seltz, W. R. *Anal. Chem.* **1978**, *50*, 1242-1246.
- Arnold, M. A. *Anal. Chem.* **1985**, *57*, 565-566.
- Maschini, M.; Iannello, M.; Palleschi, G. *Anal. Chim. Acta* **1983**, *146*, 135-148.
- Barman, T. E. *Enzyme Handbook*; Springer-Verlag: New York, 1969; Vol. 1.

\* Author to whom correspondence should be directed.

Julie Wangsa  
Mark A. Arnold\*

Department of Chemistry  
University of Iowa  
Iowa City, Iowa 52242

RECEIVED for review October 29, 1987. Accepted February 1, 1988.



# Comment on Rigorous Convergence Algorithm for Fitting a Monoexponential Function with a Background Term Using the Least-Squares Method

Sir: Recently, Smith et al. (1) described an algorithm for analyzing data that can be described by a single exponential  $ae^{-kt}$  plus a background term  $b$ , claiming among others guaranteed convergence to the global minimum according to the least-squares criterion

$$s = \sum_{i=1}^n \delta_i^2 = \text{Min}; \delta_i = y_i - b - ae^{-kt_i} \quad (1)$$

In eq 1,  $n$  is the number of data pairs  $y_i, t_i$  and  $b, a$ , and  $k$  are adjustable parameters. Weights are omitted throughout this comment for simplicity. The algorithm proposed in ref 1 seems to be fast, new, and attractive. Because this might induce widespread application, it is mandatory to point out that the underlying mathematics are incorrect in a nonobvious way and will not yield the global minimum as postulated by the authors, who propose to find this minimum by solving the equations

$$0 = \sum_{i=1}^n (y_i - b - ae^{-kt_i})e^{-kt_i} = \sum_{i=1}^n \delta_i e^{-kt_i} \quad (2)$$

$$0 = \sum_{i=1}^n (y_i - b - ae^{-kt_i}) = \sum_{i=1}^n \delta_i \quad (3)$$

$$0 = \sum_{i=1}^n (y_i - b - ae^{-kt_i})t_i = \sum_{i=1}^n \delta_i t_i \quad (4)$$

Equations 2 and 3 are the derivatives of eq 1 with respect to  $a$  and  $b$ , respectively, and eq 4 pertains to a hypothetical second exponential term  $be^{-k_0 t}$  where  $k_0$  is zero. In eq 2-4  $a$  and  $b$  are linear parameters and therefore may be eliminated, leaving a single equation  $f(k) = 0$  with  $k$  as the only adjustable parameter. The optimum value of  $k$  is found iteratively by the Newton-Raphson method

$$k_n = k - f(k)/f'(k) \quad (5)$$

According to the authors, cf. ref 1, this algorithm is about 20 times faster than a classical least-squares approach as described by Wentworth (2). As already stated, the use of eq 2-4 does not yield the global minimum, however. The global minimum is uniquely defined by eq 2, 3, and 6 where eq 6 is

$$0 = \sum_{i=1}^n (y_i - b - ae^{-kt_i})t_i e^{-kt_i} = \sum_{i=1}^n \delta_i t_i e^{-kt_i} \quad (6)$$

the derivative of eq 1 with respect to  $k$ . Obviously, eq 4 and 6 are not identical and therefore their roots will be different in the general case. In order to clarify the difference between the two approaches, eq 10 of (1) and its correct analogue can be reformulated as 7 and 8, respectively. Equation 7 is slightly

$$f(k) = \sum_{i=1}^n A_i t_i \quad (7)$$

$$g(k) = \sum_{i=1}^n A_i t_i e^{-kt_i} \quad (8)$$

$$A_i = ((\sum_{j=1}^n e^{-kt_j})^2 - n \sum_{j=1}^n e^{-2kt_j}) (\sum_{j=1}^n y_j - n y_i) - (\sum_{j=1}^n y_j \sum_{j=1}^n e^{-kt_j} - n \sum_{j=1}^n y_j e^{-kt_i}) (\sum_{j=1}^n e^{-kt_j} - n e^{-kt_i}) \quad (9)$$

simpler than 8 but the residuals are not properly weighted; the use of  $t_i$  instead of  $t_i e^{-kt_i}$  overweights the residuals near the end of the measurement relative to the least-squares solution.

Unfortunately, the authors have been misled by an invalid test to believe that the global minimum can be reached this way. Rather than discussing the errors in the involved test, we present the results of some calculations that show that the incriminated algorithm, while giving rather close estimates, never actually reaches the global minimum. Computer data were generated at 20 equidistant times  $t_i = 1, 2, \dots, 20$  with  $a = 1, b = 0.5$ , and  $k = 0.2$  or  $k = 0.4$ , and random noise (3) of 0.005-0.08 absorbance unit was superimposed. Rate constants were calculated with the algorithm proposed by Smith et al. (1), eq 5, with a program based on the correct normal equations and with the noniterative method of Guggenheim (4). By use of these rate constants, the best estimates of  $a$  and  $b$  were obtained by linear regression and subsequently the sums of squared residuals,  $s$ , were calculated. The results are compiled in Table I.

Several points are obvious. (i) The fit based on the correct normal equations always gives the lowest value of  $s$ , as postulated by theory. (ii) Differences between the results based on a given set of data are generally small, 1% in either  $k$  or  $s$  is observed only at relatively high noise levels. (iii) With small or moderate noise levels the noniterative method of

Table I. Sum of Squared Residuals,  $s$ , and Rate Constants,  $k$ , Obtained with Different Algorithms

entry	model data		least-squares estimates		Smith et al. (1)		Guggenheim (3)	
	$k$	noise <sup>a</sup>	$s_{LS}$	$k_{LS}$	$\Delta s^b$	$\Delta k^b$	$\Delta s^b$	$\Delta k^b$
1	0.2	0.5	$2.43 \times 10^{-4}$	0.200	0.04	0.07	0.01	0.03
2	0.2	1	$9.76 \times 10^{-4}$	0.200	0.04	0.14	0.01	0.06
3	0.2	2	$3.90 \times 10^{-3}$	0.200	0.04	0.27	0.01	0.16
4	0.2	4	$1.56 \times 10^{-2}$	0.201	0.04	0.54	0.03	0.43
5	0.2	8	$6.24 \times 10^{-2}$	0.201	0.05	1.08	0.07	1.34
6	0.4	0.5	$2.43 \times 10^{-4}$	0.399	0.25	0.14	0.13	0.11
7	0.4	1	$9.72 \times 10^{-4}$	0.398	0.25	0.29	0.15	0.22
8	0.4	2	$3.89 \times 10^{-4}$	0.398	0.24	0.57	0.17	0.48
9	0.4	4	$1.56 \times 10^{-3}$	0.393	0.24	1.13	0.24	1.13
10	0.4	8	$6.22 \times 10^{-2}$	0.386	0.23	2.20	0.43	2.96

<sup>a</sup>In percent of total change in absorbance. <sup>b</sup>In percent of least-squares estimates:  $\Delta s = (s - s_{LS})/s_{LS}$ ,  $\Delta k = |k - k_{LS}|/k_{LS}$ .

Guggenheim (4) may be equal to or better than the result based on eq 2-5.

### CONCLUSIONS

The use of the algorithm described in ref 1 should not be advocated, since it does not converge to the global minimum as defined by the least-squares criterion. If for any reason finding the global minimum is thought to be superfluous, noniterative approaches, e.g. the method of Guggenheim (4), will give results of comparable quality in still much less computing time.

If the global minimum is wanted, and we surely support this approach, the elimination of linear parameters and the use of analytical instead of numerical derivatives is indeed the method of choice. An algorithm based on the correct normal equations (eq 2, 3, and 6 in this comment) and otherwise following the ideas presented in ref 1 will find the global minimum in a one-dimensional parameter space. Elimination of linear parameters (5-7) and analytical derivatives (8, 9) have been suggested before, however, and, contrary to an explicit statement in ref 1, have been used in combination (8, 9).

An algorithm based on the correct normal equations combined with the ideas presented in ref 1 then is rather close to the approach described in ref 9. As the main remaining difference the implicit changes of the best estimates for  $a$  and  $b$  as a function of  $k$ , i.e. the partial derivatives  $\partial a/\partial k$  and  $\partial b/\partial k$  are included in ref 9, but not in ref 1. As a consequence, the time needed per iteration is reduced, but the number of it-

erations is increased. More important, a much better initial estimate for  $k$  is needed using eq 2, 3, and 6 rather than following the ideas described in ref 5-9 where any estimate between  $10^{-6}$  and 10 gave unproblematic convergence.

### LITERATURE CITED

- (1) Jericevic, Z.; Benson, D. M.; Bryan, J.; Smith, L. C. *Anal. Chem.* **1987**, *59*, 658-662.
- (2) Wentworth, W. E. *J. Chem. Educ.* **1985**, *62*, 96-103.
- (3) Abramowitz, M.; Stegun, I. A. *Handbook of Mathematical Functions*; NBS Appl. Math. Ser. 55; National Bureau of Standards: Washington, DC, 1964; p 952.
- (4) Guggenheim, E. A. *Philos. Mag.* **1926**, *2*, 538.
- (5) Richards, F. S. *G. J. R. Stat. Soc.* **1961**, *23*, 469-475.
- (6) Lawton, W. H.; Sylvestre, E. A. *Technometrics* **1971**, *15*, 461-467.
- (7) Gamp, H.; Maeder, M.; Zuberbühler, A. D. *Talanta* **1980**, *27*, 1037-1045.
- (8) Golub, G. H.; Pereyra, V. *SIAM J. Numer. Anal.* **1973**, *10*, 413-432.
- (9) Gamp, H.; Maeder, M.; Meyer, C.; Zuberbühler, A. D. *Talanta* **1985**, *32*, 95-101.

Harald Gamp  
Marcel Maeder\*  
Andreas D. Zuberbühler\*

Institute of Inorganic Chemistry  
University of Basel  
CH-4056 Basel, Switzerland

RECEIVED for review April 14, 1987. Accepted December 9, 1987. We thank one of the referees for the suggestion to specifically include 7-9 into this work. The work was supported by the Swiss National Science Foundation, Grant No. 2.851-0.85.

## TECHNICAL NOTES

### Fluorination of Sulfur Tetrafluoride, Pentafluorosulfur Chloride, and Disulfur Decafluoride to Sulfur Hexafluoride for Mass Spectrometric Isotope Ratio Analysis

Swroop K. Bains-Sahota and Mark H. Thiemens\*

Department of Chemistry, B-017, University of California—San Diego, La Jolla, California 92093

Measurements of isotopic ratio variations have been employed to study a wide range of processes, e.g. paleoclimatology, rock formation temperatures, and quantum chemical mechanisms. Hulston and Thode (1) were the first to show how stable isotopic variations in meteoritic material could be used to distinguish nuclear and chemical processes. Since chemical processes were thought to obey mass-dependent fractionations, any departure from this fractionation law would then reflect a nuclear process such as nucleosynthesis, radiogenic decay, or spallation. A mass-dependent isotope effect between species of mass  $M$  and  $(M + 2)$  is approximately twice as large as the effect between species of mass  $M$  and  $(M + 1)$ . Therefore, in order to distinguish between mass-dependent and mass-independent processes, at least three isotopes of the same element must be simultaneously measured.

Clayton et al. (2) observed a non-mass-dependent oxygen isotope distribution in the high-temperature minerals within the carbonaceous chondrite Allende. Since chemical processes were assumed to produce mass-dependent fractionations, the observed effect was attributed to a nuclear process. Since that time, mass-independent isotopic fractionations have been observed in chemical processes (3). For oxygen a chemically produced mass-independent effect has been observed which

produces an isotopic fractionation identical with that observed in Allende. The mass-independent effect has been suggested as involving isotopic symmetry effects in the production of ozone (4). A mass-independent sulfur isotope effect has also been reported in the formation of  $S_2F_{10}$  (5). The study of mass-independent fractionations involving symmetry and quantum effects is of considerable importance and necessitates multiisotopic measurements. Employment of multiisotopic measurements allows the detection of physical-chemical processes which might not be observed by other spectroscopic techniques, such as those reported for oxygen and sulfur (3-5). Development of the analytical capability to simultaneously measure  $^{34}S/^{32}S$ ,  $^{33}S/^{32}S$ , at high precision, may also eventually permit measurement of these ratios in atmospheric samples such as sulfate and  $H_2S$ . These gas-phase reactions may produce mass-independent isotopic fractionations which might ultimately be of interest in identifying specific atmospheric transformations. At present, only  $^{34}S/^{32}S$  ratios have been measured in atmospheric sulfur species.

Isotopic analyses of sulfur minerals and native sulfur were first performed by conversion to sulfur dioxide for mass spectrometric analysis. As discussed by Puchett et al. (6), sulfur hexafluoride is a superior gas for mass spectrometric

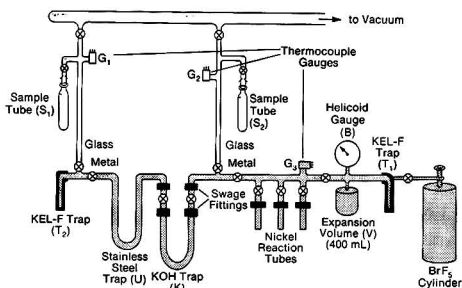


Figure 1. Apparatus for fluorination of sulfur compounds with bromine pentafluoride.

analysis. It is chemically inert, is insensitive to moisture, and does not adsorb on the walls of glass or metal vacuum systems. Fluorine has only one isotope, and no corrections are needed for isobaric interferences.  $\text{SF}_6$  produces a simple mass spectrum on electron impact, and the major ion  $\text{SF}_6^+$  occurs in a mass region free of instrumental background. Hulston and Thode (1) employed  $\text{SF}_6$  for 34/32 and 33/32 isotopic measurements by conversion of sulfur species with fluorine gas. The fluorination products were further purified by gas chromatographic separations. Due to the difficulty in handling  $\text{F}_2$ , Puchett et al. (6) used  $\text{BrF}_3$  as the fluorinating agent. The fluorination products were scrubbed on a KOH trap and  $\text{SF}_6$  was separated from other products on a 5-Å molecular sieve column. Although  $\text{BrF}_3$  is less dangerous than  $\text{F}_2$  or  $\text{BrF}_5$ , it is inconvenient to dispense into the nickel reaction tubes (6). Thode and Rees (7) extracted sulfur from sulfides by reaction with  $\text{BrF}_5$ . The product  $\text{SF}_6$  was subsequently cryogenically separated from unreacted  $\text{BrF}_5$  and other products. The final cleanup was then achieved gas chromatographically with a molecular sieve (5 Å) column.

To obtain ultrapure samples, separation on a gas chromatographic column is essential. A column capable of separating  $\text{SF}_6$  from other fluorinated compounds ( $\text{SiF}_4$ ,  $\text{CF}_4$  and  $\text{SF}_4$ ) is required, since separation between these compounds on molecular sieve 5 Å, as reported in previous work, is inadequate (8). In this paper, we report a procedure for the fluorination of gaseous sulfur compounds, which have previously not been studied, to  $\text{SF}_6$  for sulfur isotopic measurement of both  $^{34}\text{S}/^{32}\text{S}$  and  $^{33}\text{S}/^{32}\text{S}$  ratios. Since the fluorination process is phase and molecule specific (1, 6, 7), such results are important if different species are to be studied.

## EXPERIMENTAL SECTION

The apparatus for fluorination and purification is similar to that described by Clayton and Mayeda (9) and Puchett et al. (6).

**Fluorination.** Figure 1 is a diagram of the fluorination line used in the reported experiments.  $\text{BrF}_5$  is the fluorinating agent (SCM Chemicals) since it can conveniently be used in a metal vacuum system (vapor pressure at 298 K  $\approx$  390 mm). The procedure is as follows:  $\text{BrF}_5$  is aliquoted (30:1 ratio of  $\text{BrF}_5$ -sample) into the expansion volume V ( $\approx$  1 in. pressure on the Helioid gauge) from the reservoir of  $\text{BrF}_5$  in the Kel-F tube, and condensed into an all-nickel reaction tube at 77 K for  $\sim$ 20 min. Small amounts of residual noncondensables are removed, and the sample to be fluorinated is condensed, along with  $\text{BrF}_5$ . The reaction tube valve is closed and the reaction tube subsequently heated to 400 °C for  $\sim$ 15 h. After reaction, the nickel tube is chilled to 77 K for  $\sim$ 20 min and the noncondensables are again removed. The fluorination products are transferred through the removable KOH trap (K) to the stainless steel U-trap which is maintained at liquid nitrogen temperature for approximately 1 h. The trap containing KOH pellets serves to adsorb  $\text{HF}$ ,  $\text{Br}_2$ , and other corrosive byproducts, resulting in a preliminary cleanup. The KOH pellets are replaced after  $\sim$ 10 transfers to prevent clogging, presumably as a result of formation of solid phase KBr. The

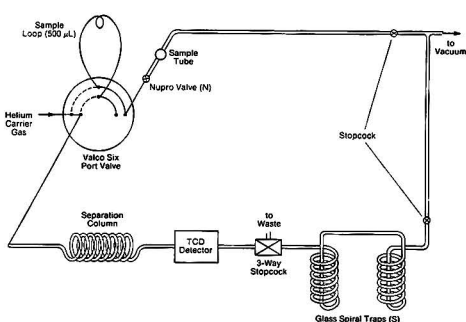


Figure 2. Schematic of gas chromatographic injection and peak collection system.

U-trap is then isolated from the KOH trap and the sample condensed at 77 K into an evacuated sample tube ( $S_1$ ) as shown in Figure 1. Finally, the sample tube is transferred to the gas chromatograph for final purification.

**Gas Chromatography.** The injection port of the gas chromatograph (HP5890A) was modified by incorporating a Valco six-port external volume gas sampling valve (Model 9105) between the gas chromatograph and the vacuum line. The detector vent was connected to a three-way valve which allowed collection of the eluted fractions. The gas chromatographic injection and collection system is shown schematically in Figure 2. A temperature program is used to obtain the desired separation between peaks. The gas chromatograph was equipped with a thermal conductivity detector maintained at 150 °C. A helium carrier gas (flow rate 30 mL/min) was used through a 12 ft,  $1/8$  in. o.d., Porapak QS (80–100 mesh) column. The column temperature was initially held at 27 °C for 5 min and then heated at a rate of 30 °C/min to a final temperature of 100 °C. The total separation time is less than 30 min. The sample to be separated is cryogenically transferred to the sample loop of the sampling valve by condensing at 77 K, isolating the loop with the Nupro valve (N), and subsequently warming the loop to room temperature. The sample is injected by diverting the flow of the He carrier gas through the loop and to the column. When the eluted  $\text{SF}_6$  is detected on the integrator (HP3390A), the output flow of He +  $\text{SF}_6$  is diverted through the glass spiral traps (S) at 77 K, to collect the  $\text{SF}_6$ . After the  $\text{SF}_6$  passes, the He flow is again diverted so that the other components are vented as waste. With the spiral traps (S) at liquid nitrogen temperature, the He is slowly evacuated. The traps are then allowed to come to room temperature and the  $\text{SF}_6$  subsequently transferred to a sample tube for mass spectrometric analysis. Sample sizes in the range 0.1–30  $\mu\text{mol}$  exhibited good separation. Larger sized samples overloaded the column and the separation between peaks was poor.

The gas chromatographic separations should be reproducible and minimize fractionation. The possible extent of isotopic fractionation on the gas chromatographic separation system was determined by control experiments. A sample of pure, isotopically predetermined  $\text{SF}_6$  was injected onto the column and collected as described. The collected sample was analyzed mass spectrometrically and its isotopic composition compared to the starting  $\text{SF}_6$ . Samples of various sizes were used to determine the effect of size on fractionation in the chromatographic separation process.

**Mass Spectrometer.** Isotopic analyses were performed on a Finnigan MAT 251 mass spectrometer which employs a triple ion beam collectors for simultaneous measurement of  $m/e$  127, 128, and 129 for  $^{32}\text{SF}_6^+$ ,  $^{33}\text{SF}_6^+$ , and  $^{34}\text{SF}_6^+$ , respectively. Isotopic ratios are reported in the conventional delta notation where

$$\delta^{34}\text{S}(\text{‰}) = \left[ \frac{(^{34}\text{S}/^{32}\text{S})_{\text{sample}}}{(^{34}\text{S}/^{32}\text{S})_{\text{std}}} - 1 \right] \times 1000$$

Similarly,  $\delta^{33}\text{S}(\text{‰})$  expresses the  $^{33}\text{S}/^{32}\text{S}$  isotope ratio (in per mil) with respect to a standard. The isotopic uncertainty in the measurements ( $\delta^{34}\text{S} \approx \delta^{33}\text{S} \approx \pm 0.03\text{‰}$ ) was determined by repeat analysis of standards. Various sized samples were analyzed for

**Table I. Results of Control Experiments To Determine Extent of Fractionation of SF<sub>6</sub> on the Gas Chromatographic Column**

expt no.	sample size, $\mu\text{mol}$	$\delta^{33}\text{S}, \%$	$\delta^{34}\text{S}, \%$	$\delta^{34}\text{S}/\delta^{33}\text{S} - \delta^{33}\text{S}, \%$
1	5	-0.22	-0.41	0.01
2	8	-0.17	-0.25	0.04
3	10	-0.16	-0.37	0.02
4	19	-0.18	-0.25	0.05

**Table II. Isotopic Results of Fluorination of Various Sulfur Species**

molecule	sample size, $\mu\text{mol}$	$\delta^{33}\text{S}, \%$	$\delta^{34}\text{S}, \%$	$\delta^{33}\text{S}/\delta^{34}\text{S}$
SF <sub>4</sub>	15	5.15	10.01	0.514
SF <sub>4</sub>	5	5.08	9.82	0.518
SF <sub>4</sub>	20	5.26	10.32	0.510
SF <sub>4</sub>	10	5.39	10.50	0.513
S <sub>2</sub> F <sub>10</sub>	25	10.30	20.07	0.513
S <sub>2</sub> F <sub>10</sub>	30	10.52	20.51	0.513
SF <sub>5</sub> Cl	25	8.21	16.03	0.512
SF <sub>5</sub> Cl	30	8.47	16.48	0.514

\* Against standard SF<sub>6</sub> defined as  $\delta^{34}\text{S} = \delta^{33}\text{S} = 0.00\%$ .

reproducibility of the mass spectrometer. Fractionated SF<sub>6</sub> samples were prepared, ranging from +5‰ to +40‰. These fractionated samples then define the isotopic mass fractionation line.

## RESULTS AND DISCUSSION

The data for the control gas chromatographic fractionation experiments are given in Table I. There is a slight isotopic fractionation which occurs on the chromatograph and is consistent with the relationship  $\delta^{33}\text{S} = 0.505(\delta^{34}\text{S})$ , as derived for SF<sub>6</sub> by Hulston and Thode (1). This fractionation ratio for  $\delta^{33}\text{S}/\delta^{34}\text{S}$  depends on the specific molecule and its mass. The ratio derives from the dependency of the molecular partition function ratios upon the normal vibrational frequencies which are a function (in part) of the molecular mass (10). For both diatomic and polyatomic sulfur molecules, the relationship  $\delta^{33}\text{S} = (0.505 \pm 0.01)\delta^{34}\text{S}$  holds, provided the extent of fractionation is not large (1). The magnitude of fractionation, due to the entire transfer and collection process on the fluorination line and gas chromatographic separation, was determined by a control experiment. The control SF<sub>6</sub> sample yielded  $\delta^{33}\text{S} = -0.201\%$  and  $\delta^{34}\text{S} = -0.305\%$ , which is similar to the fractionation on the column. This implies that the isotopic fractionation due to the transfer and col-

lection processes is negligible, and the column is the major source of sample fractionation. Although the gas chromatographic separations can introduce scatter of up to  $\pm 0.4\%$ , in  $\delta^{34}\text{S}$ , the separation is essential for obtaining pure samples for mass spectrometric analysis. The gas chromatogram is useful in that it provides an indication of other possible sulfur species which may be present due to incompleteness of the fluorination process.

Isotopic composition data for the fluorination of SF<sub>4</sub>, SF<sub>5</sub>Cl, and S<sub>2</sub>F<sub>10</sub> are shown in Table II. The sample sizes and  $\delta^{33}\text{S}/\delta^{34}\text{S}$  ratios are included. The  $\delta^{33}\text{S}/\delta^{34}\text{S}$  ratio for SF<sub>4</sub>, SF<sub>5</sub>Cl, and S<sub>2</sub>F<sub>10</sub> falls within the range  $\delta^{33}\text{S} = (0.505 \pm 0.01)\delta^{34}\text{S}$  as predicted. The average value of the sulfur isotopic composition for SF<sub>4</sub> is  $\delta^{34}\text{S} = 10.2 \pm 0.2\%$ , S<sub>2</sub>F<sub>10</sub>  $\delta^{34}\text{S} = 20.3 \pm 0.2\%$ , SF<sub>5</sub>Cl  $\delta^{34}\text{S} = 16.2 \pm 0.2\%$ . The reproducibility of the entire fluorination and separation, therefore, is  $\sim \pm 0.2\%$  for  $\delta^{34}\text{S}$ , similar to that obtained by Puchett et al. (6) for meteoritic mineral fluorination and purification. The chromatographic procedure reported in this paper differs from ref 6 in the use of Porapak QS as the column packing material which is required for these particular separations involving different S<sub>x</sub>-F<sub>y</sub> molecules from SF<sub>6</sub> and to permit determination of the fluorination yields. A molecular sieve column would be more suitable for fluorination and quantitative separation of sulfur-bearing minerals. The technique described here is preferred for fluorination of gaseous sulfur-fluorine molecules and their subsequent purification and mass spectrometric analysis.

**Registry No.** SF<sub>4</sub>, 7783-60-0; SF<sub>5</sub>Cl, 13780-57-9; S<sub>2</sub>F<sub>10</sub>, 5714-22-7; BrF<sub>3</sub>, 7789-30-2; <sup>33</sup>S, 14257-58-0; <sup>34</sup>S, 13965-97-4; <sup>32</sup>S, 13981-57-2.

## LITERATURE CITED

- Hulston, J. R.; Thode, H. G. *J. Geophys. Res.* **1965**, *70*, 3475-3484.
- Clayton, R. N.; Grossman, L.; Mayeda, T. K. *Science (Washington, D.C.)* **1973**, *182*, 485-488.
- Thiemens, M. H.; Heidenreich, J. E. *Science* **1983**, *219*, 1073-1075.
- Heidenreich, J. E.; Thiemens, M. H. *J. Chem. Phys.* **1985**, *84*, 2129-2136.
- Bains-Sahota, S. K.; Thiemens, M. H. *Meteoritics* **1987**, *22*(4), 7.
- Puchett, H.; Sabels, B. R.; Hoering, T. *Geochim. Cosmochim. Acta* **1973**, *35*, 625-628.
- Thode, H. G.; Rees, C. E. *Lunar Planet. Sci.* **1979**, *10*, 1629-1636.
- Janssen, F. J. G. *Kern Sci. Tech. Rep.* **1984**, *2*(2), 9-18.
- Clayton, R. N.; Mayeda, T. K. *Geochim. Cosmochim. Acta* **1963**, *27*, 43-52.
- Matsuhisa, Y.; Goldsmith, J. R.; Clayton, R. N. *Geochim. Cosmochim. Acta* **1978**, *42*, 173-182.

RECEIVED for review September 25, 1987. Accepted January 14, 1988. NASA (Swroop Bains-GSRP#23376) and the donors of the Petroleum Research Fund, administered by the American Chemical Society, (18189-AC2,5) are thanked for financial support.

## Plasma Desorption Mass Spectrometry of Peptides Adsorbed on Nitrocellulose from a Glutathione Matrix

Ian Jardine,\* Gale F. Scanlan, and Anthony Tsaropoulos

Department of Pharmacology, Mayo Clinic, Rochester, Minnesota 55905

Daniel J. Liberato

Department of Drug Metabolism, Hoffmann-La Roche, Inc., Nutley, New Jersey 07110

Two significant advances in peptide sample preparation for analysis by plasma desorption time-of-flight mass spectrometry (PDMS) (1-3) were recently reported (4, 5).

In the first advance, nitrocellulose films were used as sample stage backings to adsorb peptides and proteins for subsequent PDMS analysis. This method conveniently allows the ap-

plication of very small peptide sample sizes from aqueous solutions (picomole to nanomole amounts of sample in 1–5  $\mu\text{L}$ ); allows for effective elimination of salt contaminants in the biomolecular film by washing, thus improving the molecular ion yields; produces relatively narrow and sharp peaks in the mass spectrum; and, finally, generates useful multiply charged molecular ions.

In the second advance, peptides were dissolved and electrosprayed (6) in solutions containing reduced glutathione (1:1, mole:mole) onto PDMS sample targets. Relative to electrospraying without glutathione, this procedure produced increased molecular ion signal, reduction of base-line noise, narrowing of peak widths, and an increase in multiply charged ions. It was suggested that these effects may be caused by enhanced peptide folding and aggregation in glutathione solution, as well as by the possibility of lowering the sample-substrate binding energy during desorption.

Attempts to use the more convenient nitrocellulose technique in our laboratory for the PDMS analysis of peptides were often successful; but often failure resulted, particularly for peptides of >5000 molecular weight. We, therefore, decided to try and combine the nitrocellulose and the glutathione approaches described above. We have found that applying peptides in a 1:1 solution of reduced glutathione directly to nitrocellulose targets, with subsequent washing of the adsorbed sample with 0.1% trifluoroacetic acid solution, results in a higher success rate of peptide analysis by PDMS.

#### EXPERIMENTAL SECTION

**Instrument.** Plasma desorption mass spectra were recorded with a BIO-ION Nordic (Uppsala, Sweden), BIN-10K californium-252 time-of-flight mass spectrometer using an accelerating voltage of 20 kV and a flight tube length of 15 cm. This instrument has been described in ref 7. The spectra of peptides of >10000 molecular weight were accumulated over a 6–9 h period. Spectra for peptides of lower molecular weight were generally acquired over much shorter time periods of less than 1 h.

**Peptides.** Synthetic growth hormone releasing factor and recombinant interleukin-2 from *E. coli* were obtained from Hoffmann-La Roche, Inc. (Nutley, NJ). Recombinant human C5a complement proteins were obtained from Abbott Laboratories (Abbott Park, IL). Recombinant thioredoxin from *E. coli* was purchased from Calbiochem (San Diego, CA). Recombinant human growth hormone from *E. coli* was from Lilly Research Laboratories (Indianapolis, IN). All disulfide-containing peptides were obtained and used in the oxidized form.

**Sample Preparation.** Aluminum sample foils were coated with a nitrocellulose film by using the electrospray method (6, 8). Peptide samples were prepared as a 1:1 (mole:mole) aqueous solution in reduced glutathione (5). One to five microliters of solution was applied to the center of the nitrocellulose-coated sample foil and allowed to stand for 5 min to allow peptide adsorption to the nitrocellulose. The solvent was then removed by rapidly spinning the sample foil at approximately 2000 rpm on a bench top laboratory centrifuge fitted with a sample foil holder. The sample on the nitrocellulose was then washed by applying approximately 0.1–1.0 mL of a 0.1% trifluoroacetic acid solution to the surface, followed by removal of the wash solution by centrifugation, and then insertion in the mass spectrometer.

#### RESULTS AND DISCUSSION

Among the peptides which could not be successfully analyzed by applying them to nitrocellulose targets without glutathione, but which were subsequently successfully analyzed after adsorption to the nitrocellulose target from a glutathione solution, were growth hormone releasing factor (MW 5041) (9), human C5a complement proteins (MWs approximately 8500) (10), thioredoxin from *Escherichia coli* (MW 11 673) (11, 12), interleukin-2 (MW 15 547) (13), and human growth hormone (MW 22 125) (14). The PDMS spectra of growth hormone releasing factor, thioredoxin, and interleukin-2 are shown in the attached figure. All spectra

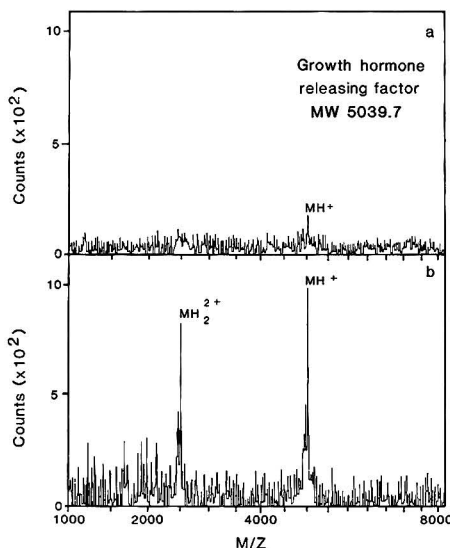


**Figure 1.** Positive ion californium-252 plasma desorption time-of-flight mass spectra of 800-pmol samples of growth hormone releasing factor. (a) The sample was prepared in aqueous solution, applied to a nitrocellulose-coated target, washed with 0.1% trifluoroacetic acid, and dried before PDMS analysis. (b) The sample was prepared as a 1:1 (mole:mole) aqueous solution with reduced glutathione, applied to a nitrocellulose-coated target, washed with 0.1% trifluoroacetic acid, and dried before PDMS analysis.

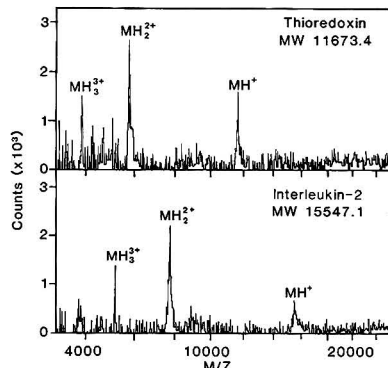


**Figure 2.** Positive ion californium-252 plasma desorption time-of-flight mass spectra of thioredoxin and interleukin-2. Peptide samples were prepared as 1:1 (mole:mole) aqueous solutions with reduced glutathione, applied to nitrocellulose-coated targets, washed with 0.1% trifluoroacetic acid, and dried before PDMS analysis.

have been automatically background subtracted by the data system.

The PDMS spectra of 800-pmol samples of growth hormone releasing factor obtained by desorption from nitrocellulose both without and with application to the target in a 1:1 glutathione solution are presented in parts a and b of Figure 1 for comparison. The enhancement of the PDMS spectrum of this peptide when reduced glutathione is included in the analysis is clear from these spectra. Similar enhancements were observed for the PDMS analysis of the other peptides reported. That is, essentially no peaks were observed above background before glutathione treatment.

Table I

	MH <sup>+</sup> obsd (calcd)	MH <sub>2</sub> <sup>2+</sup> obsd (calcd)	MH <sub>3</sub> <sup>3+</sup> obsd (calcd)
growth hormone releasing factor	5040.9 (5040.7)	2520.8 (2520.9)	— (1680.9)
thioredoxin	11671.0 (11674.4)	5833.4 (5827.7)	3893.7 (3892.1)
interleukin-2	15531.4 (15548.1)	7755.1 (7774.6)	5174.9 (5183.4)

The spectrum of thioredoxin shown in Figure 2 was obtained on 100 pmol of peptide. Spectra of interleukin-2 obtained by using 200 pmol, 2 nmol, and 20 nmol were essentially identical with each other, including the absolute as well as relative intensities of the MH<sup>+</sup>, MH<sub>2</sub><sup>2+</sup>, and MH<sub>3</sub><sup>3+</sup> ions. The spectrum shown is of the 2-nmol sample which had a slightly more clearly defined MH<sup>+</sup> ion than that of the 200-pmol spectrum.

The mass measurement accuracy for the observed ions of these peptides as determined by PDMS is shown in Table I and is generally always better than 0.2%. This is an acceptable level of accuracy at these masses for the simple time-of-flight mass spectrometer of short flight path (15 cm) used in these experiments.

In conclusion, for PDMS analysis of peptides at the 1-nmol level, we recommend preparing peptide samples in a 1:1 (mole:mole) aqueous solution of reduced glutathione, applying this solution to nitrocellulose coated targets, washing the adsorbed peptide with a 0.1% trifluoroacetic acid solution, and drying, before PDMS analysis.

#### ACKNOWLEDGMENT

We thank George Carter of Abbott Labs for the samples

of recombinant human C5a complement proteins, John Oc-colowitz of the Lilly Research Laboratories for the sample of recombinant human growth hormone, and Ronald D. Macfarlane of Texas A&M University for the suggestion of spin-drying the PDMS samples.

**Registry No.** Glutathione, 70-18-8; nitrocellulose, 9004-70-0; growth hormone-releasing factor, 9034-39-3.

#### LITERATURE CITED

- (1) Torgerson, D. F.; Skowronski, R. P.; Macfarlane, R. D. *Biochem. Biophys. Res. Commun.* **1974**, *60*, 616.
- (2) Macfarlane, R. D.; Torgerson, D. F. *Science (Washington, D.C.)* **1976**, *191*, 920.
- (3) Sundqvist, B. V. R.; Macfarlane, R. D. *Mass Spectrom. Rev.* **1985**, *4*, 421.
- (4) Jonsson, G. P.; Hedin, A. B.; Håkansson, P. L.; Sundqvist, B. V. R.; Sæve, B. G. S.; Nielson, P. F.; Roepstorff, P.; Johansson, K.-E.; Kamensky, I.; Lindberg, M. S. L. *Anal. Chem.* **1986**, *58*, 1084.
- (5) Alai, M.; Demirev, P.; Fenselau, C.; Cotter, R. J. *Anal. Chem.* **1986**, *58*, 1303.
- (6) McNeal, C. J.; Macfarlane, R. F.; Thurston, E. L. *Anal. Chem.* **1979**, *51*, 2036.
- (7) Sundqvist, B.; Kamensky, I.; Håkansson, J.; Kjellberg, J.; Salehpour, M.; Widdiyasekera, S.; Fohlman, J.; Peterson, P. A.; Roepstorff, P. *Anal. Chem.* **1984**, *56*, 242.
- (8) Chait, B. T.; Field, F. H. *Biochem. Biophys. Res. Commun.* **1986**, *134*, 420.
- (9) Guillemin, R.; Brazeau, P.; Böhlen, P.; Esch, F.; Ling, F.; Wehrenberg, W. B. *Science (Washington, D.C.)* **1982**, *218*, 585.
- (10) Fernandez, H. N.; Hugli, T. E. *J. Biol. Chem.* **1978**, *253*, 6955.
- (11) Holmgren, A. *Eur. J. Biochem.* **1986**, *156*, 475.
- (12) Höög, J.-O.; Von Bahr-Lindström, H.; Josephson, S.; Wallace, B. J.; Kushner, S. R.; Jörnvall, H.; Holmgren, A. *Biosci. Rep.* **1984**, *4*, 917.
- (13) Robb, R. J. *Methods Enzymol.* **1985**, *116*, 493.
- (14) Niall, H. D. *Nature (London), New Biol.* **1971**, *230*, 90.

RECEIVED for review May 11, 1987. Accepted February 1, 1988. This work was supported by NIH Grants GM 32928 and RR 02682.



# For Over Six Decades...



## The Leader in the Field.

*Now twice a month!*

**ANALYTICAL CHEMISTRY** the world's foremost publication in the vital field of measurement science is now coming to you semi-monthly.

Keeping pace with these changes has continued to make **ANALYTICAL CHEMISTRY** the pinnacle of publications in the field . . . for over 6 decades.

Call now for your own personal subscription

**CALL TOLL FREE (800) 227-5558**



American Chemical Society  
1155 16th St., NW  
Washington, DC 20036

# Inject new life into your old LC.

## Introducing the HP 1050 Series of HPLC modules

The next time you add LC capabilities or replace an aging HPLC component, consider Hewlett-Packard. Our new HP 1050 Series of HPLC modules lets you upgrade to the HP quality you always wanted but thought was out of reach.

Grown out of the same innovative technology that produced the renowned, top-of-the-line HP 1090 family of HPLC systems, the HP 1050 Series brings you all the performance and reliability you've been missing — at a price you can afford.

### Add capabilities a piece at a time

Select from a range of compact, stackable, easy-to-use modules for solvent delivery, autosampling and UV-Visible detection. Available now are both isocratic and quaternary pump modules, variable and multiple wavelength detectors, and 21- and 121-vial autosampler modules. And more are on the way.

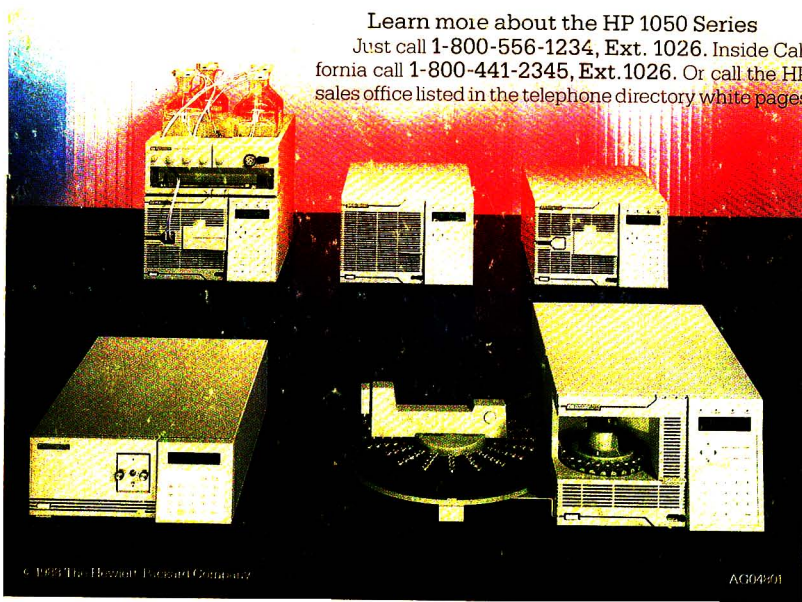
### Boost productivity with superior performance and uptime

The advanced HP 1050 Series gives you the sensitivity, accuracy and precision you need. What's more, it gives you superb results without the usual hassles. That's because it eliminates most set-up, running and maintenance problems. And self diagnostics prevent wasted or lost samples.

Trouble shooting, repair and parts exchange are extremely easy, too. Add to that HP quality, reliability and support, and downtime becomes almost nonexistent. In fact, reliability is so high, we offer a 99% uptime guarantee.

### Learn more about the HP 1050 Series

Just call 1-800-556-1234, Ext. 1026. Inside California call 1-800-441-2345, Ext. 1026. Or call the HP sales office listed in the telephone directory white pages.



© 1993 The Hewlett-Packard Company

AG04901



HEWLETT  
PACKARD

CIRCLE 64 ON READER SERVICE CARD